Analysis of the Structure, Function and Protein-Protein Interactions of the Popeye Domain Containing Proteins

Thesis submitted for the degree of Doctor of Philosophy

Alexander H. Swan

Department of Chemistry,

Imperial College London

2022

Abstract

The Popeye domain containing (POPDC) proteins are a family of three transmembrane proteins. Dysfunction of these proteins is associated with muscular dystrophy and cardiac dysrhythmias. The Popeye domain, unique to this family, is known to bind to cAMP. The structure of the Popeye domain and the mechanism of cAMP binding has not been directly determined. In addition, there is a lack of pharmacological tools to target the cAMP binding site of the POPDC proteins.

Attempts were made to produce a protein construct based on the Popeye domain for structural characterisation and the design of ligand binding assays. A novel construct was produced although, while preliminary structural analysis was initiated, it did not possess robust cAMP binding properties. This meant that the construct was unsuitable for further study. Attempts to develop cell-based assays to detect cAMP and other compound binding to the Popeye domain were also unsuccessful.

An interaction between POPDC1 and POPDC2 is thought to occur. Changes in normal subcellular expression of both POPDC1 and POPDC2 within tissue have been found in the presence of mutations in either of these proteins. Here, analysis of skeletal muscle biopsies from patients found this to be the case in two recently identified mutations in POPDC1. Furthermore, it was discovered that plasma membrane localisation of POPDC1 and POPDC2 in HEK293 cells is dependent on the co-expression of both proteins. This finding was exploited to design an assay in HEK293 cells modelling the effect of known mutations on POPDC expression in tissue. The nature of POPDC1-POPDC2 interactions was investigated and a novel interface was proposed to form through a helix-helix interaction within the Popeye domain of each protein. It was found that residues in this putative interface are required for proper POPDC1 and POPDC2 protein subcellular expression.

Statement of Originality

I declare that all work included in this thesis was performed by myself unless stated otherwise. All work that is not my own is cited, with full references provided in the references section.

Copyright Declaration

The copyright of this thesis rests with the author. Unless otherwise indicated, its contents are licensed under a Creative Commons Attribution-NonCommercial 4.0 International Licence (CC BY-NC).

Under this licence, you may copy and redistribute the material in any medium or format. You may also create and distribute modified versions of the work. This is on the condition that: you credit the author and do not use it, or any derivative works, for a commercial purpose.

When reusing or sharing this work, ensure you make the licence terms clear to others by naming the licence and linking to the licence text. Where a work has been adapted, you should indicate that the work has been changed and describe those changes.

Please seek permission from the copyright holder for uses of this work that are not included in this licence or permitted under UK Copyright Law.

Acknowledgements

Firstly, my deep thanks must go to my supervisors Dr Katie Chapman, Dr Mark Pfuhl, Prof Alan Spivey and Prof Thomas Brand. Despite the many setbacks that I faced during this project, they were unfailingly supportive and ever willing to discuss ideas. Thank you for hosting me in your labs and mentoring me throughout the duration of this work.

Without Ursula Herbort-Brand I would not have been able to begin to learn the majority of the skills I used to complete much of the work described here. From my first days in the lab to the last you were always willing to help and provide your advice. It has been a pleasure to work with you. Moving forward I hope to always match your levels of attention to detail, work ethic and integrity.

Thank you to the other members of the Brand, Spivey and Pfuhl groups for your assistance and for making my time in the lab enjoyable. In addition, Stephen Rothery was hugely generous with his time and expertise when helping me design the imaging experiments.

My funding bodies, the British Heart Foundation and EPSRC, provided the means for me to conduct this research. I hope that others in the field will use this work to further advance our understanding of the POPDC proteins and ultimately use the information contained below to provide some benefit to the world.

My friends and family were always there to provide words of encouragement when needed. I certainly would not be in this position if it were not for the unfailing and continuous support my parents have given me throughout my education and all of my other endeavours.

Lastly, I must express my deepest thanks to my partner Becky. I am sure you will be as glad as I am when this is completed. You are the best teammate I will ever have, and I can't wait for what comes next because, whatever it is, it will be with you.

"Science is not a body of knowledge nor a system of belief; it is just a term which describes humankind's incremental acquisition of understanding through observation. Science is awesome." — **Tim Minchin**

Table of Contents

Abstract ***2***

Statement of Originality ***3***

Copyright Declaration ***3***

Acknowledgements ***4***

List of Figures ***10***

List of Tables ***13***

Abbreviations ***18***

1 Introduction ***20***

1.1 Protein Constructs for use in Structural and Activity Studies **20**

1.2 Protein Structure Prediction **22**

1.3 Protein-Protein Interactions **23**

1.3.1 The Nature of Protein-Protein Interactions 23

1.3.2 Cell-Based Methods for Studying Protein-Protein Interactions 24

1.4 Processing of Integral Membrane Proteins **26**

1.5 The *POPDC* Genes **27**

1.6 Features of the POPDC Proteins **28**

1.7 Structural Studies of the POPDC Proteins **29**

1.8 Oligomerisation of the POPDC Proteins **30**

1.9 The POPDC Proteins and the cAMP Pathway **31**

1.9.1 The cAMP Pathway 31

1.9.2 POPDC Proteins Bind cAMP 33

1.9.3 Protein-Protein Interactions of POPDC Proteins within the cAMP Pathway 36

1.9.4 Summary of Possible Roles of POPDC Proteins within the cAMP Pathway 38

1.10 POPDC Proteins in Disease **39**

1.10.1 Overview of Striated Muscle 39

1.10.2 POPDC Protein-Protein Interactions in Striated Muscle 40

1.10.3 POPDC Proteins in Cardiac and Skeletal Muscle Disease 41

1.10.4 Cancer 44

1.11 Attempts to Develop Selective Small Molecule Popeye Domain Ligands **45**

1.12 Main Hypotheses and Aims of this Work **45**

1.12.1 Hypotheses and Context of this Work 45

1.12.2 Aims 47

2 Methods and Materials ***48***

2.1 General Laboratory Practice **48**

2.2 Reagents and Equipment **48**

2.3 Composition of Non-Commercial Buffers and Media 53

2.4 Molecular Cloning 54

2.4.1 General PCR Procedure 54
2.4.2 General Restriction Reaction Procedure 55
2.4.3 General Ligation Reaction Procedure 56
2.4.4 General Site Directed Mutagenesis Procedure 57
2.4.5 Transformation of Chemically Competent *E. coli* 58
2.4.6 Preparation of Chemically Competent *E. coli* 59
2.4.7 Preparation of Plasmid DNA from *E. coli* Liquid Cultures 59
2.4.8 Measurement of DNA Concentration and Purity 59
2.4.9 Preparation of glycerol stocks 60
2.4.10 Oligonucleotide Sequencing 60
2.4.11 Cloning of Popeye Domain Constructs for Expression Trials 60
2.4.12 PKA and EPAC1 cAMP Sensors 61
2.4.13 Unimolecular Popeye Domain BRET Sensors 62
2.4.14 *POPDC1*-ECFP and *POPDC2*-EYFP Constructs for use in Trafficking Studies in HEK293 Cells 62
2.4.15 Cloning of POPDC NanoBRET Constructs 64
2.4.16 Cloning of POPDC AP-FRET Constructs 64
2.4.17 Cloning of POPDC BiFC Constructs 65

2.5 Expression, Purification and Analysis of Popeye Domain Constructs 66

2.5.1 Expression of Popeye Domain Protein Constructs in *E. coli* 66
2.5.2 Fast Protein Liquid Chromatography 66
2.5.3 Size Exclusion Chromatography 67
2.5.4 Dialysis 67

2.6 Analysis of Purified Popeye Domain Constructs 67

2.6.1 Protein Concentration Measurements 67
2.6.2 SDS-PAGE (Popeye Domain Construct Analysis Only) 67
2.6.3 Size Exclusion Chromatography-Multi Angle Laser Lights Scattering 67
2.6.4 Circular Dichroism 68
2.6.5 Protein-NMR 68
2.6.6 Differential Scanning Fluorimetry 69
2.6.7 Microscale Thermophoresis 70
2.6.8 cAMP Agarose Precipitation 71

2.7 Expression and Analysis of Full-Length POPDC Protein Constructs in HEK293 Cells 71

2.7.1 General HEK293 Cell Culture Procedure 71
2.7.2 General HEK293 Transfection Procedure 72
2.7.3 POPDC Expression and Trafficking Assay in HEK293 Cells 72
2.7.4 Type-1 Quantitative BRET Assay 75
2.7.5 Acceptor-Photobleaching FRET 78
2.7.6 Bimolecular Fluorescence Complementation 79
2.7.7 Co-Immunoprecipitation 81

2.8 BRET Assays for the Detection of cAMP or Hit Compound Dependent Changes in POPDC Protein, Popeye Domain, or Canonical cAMP Effectors 82

2.8.1 POPDC1-POPDC2 cAMP Response NanoBRET Assay 82
2.8.2 Popeye Domain cAMP Sensor Trials 83

2.9 PKA and EPAC1 cAMP Sensor Assays 84

2.10 Skeletal Muscle Biopsy Sections Staining and Imaging....85
2.10.1 Determining the Ratio of POPDC Protein Expression within the Plasma Membrane and Cytoplasm of Skeletal Muscle Fibres....86
2.10.2 Genetic Analysis of cJET Patients....87
2.11 Protein Sequence Alignments....87
2.12 Structural Models of POPDC Proteins....87
2.13 Software....87
2.14 Microscopy Acquisition Settings....88
2.15 FIJI Macros used in Image Processing....89
3 Attempts to Develop Popeye Domain Protein Constructs for use in Structural and Ligand Binding Studies....91
3.1 Introduction....91
3.1.1 Development of Recombinant POPDC Constructs for Structural Studies....91
3.1.2 Attempts to Develop Selective Small Molecule Popeye Domain Ligands....92
3.2 Outline of Work and Aims....95
3.2.1 Description of this Work....95
3.2.2 Aims....95
3.3 Results....95
3.3.1 Search for a Novel Popeye Domain Construct....95
3.3.2 Purification of the Novel S109-K272 Popeye Domain Construct....100
3.3.3 Structural Characterisation of the S109-K272 Popeye Domain Construct....104
3.3.4 Assessing cAMP binding to the novel Popeye domain construct....112
3.3.5 Co-Expression of POPDC1 and POPDC2 Popeye Domain Constructs....119
3.4 Discussion....121
3.4.1 The Properties of the Novel Popeye Domain Construct....121
3.4.2 The Lack of cAMP Affinity to Novel and Known POPDC Constructs....122
3.4.3 Future Attempts at Studying POPDC Structure and Ligand Binding....123
4 Attempts to Develop Popeye Domain-Based cAMP Sensitive BRET Sensors for use in Ligand Binding Studies....125
4.1 Introduction....125
4.1.1 The Optical Sensing of cAMP in Cells....125
4.1.2 Previous Attempts to use POPDC Proteins in Optical cAMP Sensing....126
4.2 Outline of Work and Aims....129
4.2.1 Description of this Work....129
4.2.2 Aims....129
4.3 Results....129
4.3.1 Examining cAMP Induced Changes in POPDC1-POPDC2 Interaction by NanoBRET....129
4.3.2 Popeye Domain BRET Constructs....132
4.3.3 Hit Compound Off Target Screening....134
4.4 Discussion....136

5 Investigations into the Expression of Wildtype and Mutant POPDC1 and POPDC2 in Skeletal Muscle and HEK293 Cells 139

5.1 Introduction 139

5.1.1 POPDC Mutations are Associated with Mislocalisation of POPDC1 and POPDC2 in Patients 139

5.2 Outline of this Work and Aims 142

5.2.1 Description of this Work 142

5.2.2 Aims 143

5.3 Results 143

5.3.1 Analysis of POPDC1 and POPDC2 Plasma Membrane Localisation in Skeletal Muscle in the Presence of a Selection of POPDC Mutations 143

5.3.2 Development of a HEK293 Cell Model to Study the Subcellular Expression of POPDC Proteins 156

5.4 Discussion 168

5.4.1 The Changes in POPDC Expression in Skeletal Muscle Fibres and Fibre Morphology in the Presence of Various POPDC Variants 168

5.4.2 Insights into the Mechanism of POPDC Mislocalisation 169

6 Investigations into the Mechanism and Function of the Interaction between POPDC1 and POPDC2 174

6.1 Introduction 174

6.1.1 POPDC1 Forms Homomeric Complexes 174

6.1.2 POPDC1 and POPDC2 Form Heteromeric Complexes 174

6.2 Outline of this Work and Aims 175

6.2.1 Description of this Work 175

6.2.2 Aims 176

6.3 Results 176

6.3.1 Investigations into the Stoichiometry of the Interaction Between POPDC1 and POPDC2 with Quantitative BRET 176

6.3.2 Changes in the POPDC1-POPDC2 Interaction in the Presence of Clinically Relevant POPDC Variants 181

6.3.3 Investigations into a Putative Site of Interaction Between POPDC1 and POPDC2 190

6.3.4 Assessing the Importance of Conserved Hydrophobic Residues in the Popeye Domain for POPDC1 and POPDC2 Subcellular Expression in HEK293 Cells 194

6.3.5 A Possible Mechanism for how POPDC1-POPDC2 Complexation Controls Expression and Trafficking 198

6.3.6 The Putative αC-helix may also be involved in Popeye Domain cAMP Binding 199

6.4 Discussion 202

6.4.1 POPDC1 and POPDC2 Form Heteromeric Complexes 202

6.4.2 POPDC Proteins may Interact through their αC-Helix which could be required for Correct Subcellular Expression 202

6.4.3 Some POPDC Mutations Identified in Patients may cause Partial Disruption of POPDC1-POPDC2 Complexes 206

7 POPDC2 is a Candidate Gene for Congenital Ectopic Tachycardia 209

7.1 Introduction 209

7.2 Outline of Work and Aims 210
7.2.1 Description of this Work 210
7.2.2 Aims 210
7.3 Results 211
7.3.1 Initial Assessment from Previous Investigations into POPDC2 211
7.3.2 The Effect of the *POPDC2* p.L245P Mutation on POPDC1 and POPDC2 Protein Trafficking in HEK293 Cells 212
7.3.3 The Impact of the POPDC2 p.L245P Mutation on POPDC1-POPDC2 Interactions 214
7.4 Discussion 216
7.4.1 POPDC2 p.L245P Resembles the Effect of POPDC Variants known to be Pathogenic, Supporting its Classification as a Candidate Gene for cJET 216
7.4.2 The Possible Mechanism of POPDC2 Functional Changes Caused by the L245P Mutation 217
8 Final Discussion 219
8.1 The Context of the Findings of this Work 219
8.2 Summary of the Main Findings of this Work 220
8.2.1 Attempts to Produce a Novel Popeye Domain Construct were Unsuccessful 220
8.2.2 POPDC1 and POPDC2 Subcellular Expression is Dependent on Co-Expression 220
8.2.3 An Interaction through the αC-helix of the Popeye Domain may Modulate POPDC1-POPDC Subcellular Expression 221
8.3 Outlook and Future Work 222
8.3.1 Determining the Structure of the POPDC Proteins and Mode of cAMP Binding 222
8.3.2 The Importance of POPDC1-POPDC2 Interactions 223
8.3.3 Further Testing of the Effects of POPDC Mutations 225
9 References 227
10 Appendix 242
10.1 Popeye Domain-Based cAMP BRET Sensor Data 242
10.2 Skeletal Muscle Biopsy Image Analysis Supplementary Results 243
10.3 HEK293 POPDC1 and POPDC2 HEK293 Cells Co-Expression Supplementary Results 246
10.4 Quantitative BRET Summary Data 256
10.5 POPDC1 + POPDC2 Clinical Mutant Co-Immunoprecipitation Full Blots 257
10.6 POPDC1 + POPDC2 Clinical Mutants Bimolecular Fluorescence Complementation Summary Data 258
10.7 POPDC1 + POPDC2 Clinical Mutants Acceptor Photobleaching FRET Summary Data 258
10.8 Summary of Assays used to Characterise the POPDC2p.L245P Variant 259
10.9 Full Oligonucleotide Sequences of Protein Constructs 260
10.9.1 Site Directed Mutagenesis Sanger Sequencing Results 265

List of Figures

Figure 1.1: The Subcellular Localisation of Popdc1 and Popdc2 in Mouse Skeletal Muscle and Heart.....28

Figure 1.2: Structural Predictions of POPDC1, POPDC2 and POPDC3.....29

Figure 1.3: A simplified model of the cAMP pathway including POPDC1 and POPDC2.....33

Figure 1.4: The Structure of Classical CNBDs and the Popeye Domain.....34

Figure 1.5: Models of POPDC Function within the cAMP Pathway.....39

Figure 1.6: Changes in Subcellular Expression and Localisation of POPDC1 and POPDC2 in the Skeletal Muscle of a Patient Possessing the *POPDC1* (c.602C>T, p.S201F) Mutation.....44

Figure 2.1: Macro for Measuring POPDC1-ECFP and POPDC2-EYFP Expression in Different Regions of HEK293 Cells.....89

Figure 2.2: Macro for Measuring Protein Expression Levels in the Plasma membrane and Sarcoplasm of Muscle Fibres.....90

Figure 3.1: The Structures of Potential Popeye Domain Ligands identified in a Compound Screening Project.....94

Figure 3.2: An Initial Expression Trial of Novel GB1-Popeye Domain Constructs in *E. coli*.....97

Figure 3.3: Schematic of the Novel GB1-S109-K272 and Un-tagged S109-K272 Constructs compared to the GB1-E123-D266 Construct.....99

Figure 3.4: GB1 Tag Cleavage from and Purification of the S109-K272 Popeye Domain Construct.....101

Figure 3.5: FPLC Purification of the GB1-S109-K272 and Digested S109-K272 Constructs.....103

Figure 3.6: SEC-MALS of the S109-K272 and GB1-E123-D266 Constructs.....104

Figure 3.7: Circular Dichroism Spectra of the S109-K272 and GB1-E123-D266 Constructs.....107

Figure 3.8: Circular Dichroism Derived Secondary Structure Predictions of the S109-K272 and GB1-E123-D266 Constructs.....109

Figure 3.9: Protein-NMR ^{1}H-^{15}N HSQC-TROSY of S109-K272 Construct.....111

Figure 3.10: Differential Scanning Fluorimetry Spectra of the S109-K272 and GB1-E123-D266 Constructs at different Protein Concentrations.....114

Figure 3.11: Differential Scanning Fluorimetry titration of cAMP with the S109-K272 and GB1-E123-K272 constructs.....115

Figure 3.12: Microscale Thermophoresis Titration of cAMP with the S109-K272 and GST-BVES Constructs.....117

Figure 3.13: cAMP-Agarose Precipitation of the GB1-E123-D266 and GST-BVES Constructs.....119

Figure 3.14: Expression Levels in *E. coli* of the GB1-S109-K272 Construct alone and with a POPDC2 derived Analogue GB1-Q94-K255.....120

Figure 4.1: The Emission and Absorption Spectra of a BRET Donor and Acceptor Pair.....127

Figure 4.2: Schematic of the POPDC1-TREK-1 and POPDC1-POPDC1 NanoBRET Pairs Previously Trialled as cAMP Responsive BRET Reporters.....128

Figure 4.3: Schematic of the POPDC1 and POPDC2 NanoBRET Pairs Trialled as cAMP Responsive BRET Reporters.....130

Figure 4.4: The Change in BRET between POPDC1 and POPDC2 NanoBRET Constructs after the Addition of Forskolin.....131

Figure 4.5: Schematic of the General Structure of the Proposed Unimolecular Popeye domain BRET cAMP Sensors.....133

Figure 4.6: The Change in BRET Signal from a Series of Popeye Domain-Based cAMP Reporter Constructs within HEK293 Cells.....134

Figure 4.7: The Change in BRET Signal from a PKA and EPAC1 based BRET cAMP Reporter in Response to cAMP Analogues and the Popeye Domain Hit Compounds.....136

Figure 5.1: Outlines of Skeletal Muscle Fibres to allow Quantification of POPDC and α-Sarcoglycan Expression in the Sarcolemma and Sarcoplasm.....144

Figure 5.2: Immunostaining of POPDC1 and POPDC2 within Skeletal Muscle Fibres from a Patient possessing the POPDC1 p.Q153X Variant and a Control.....145

Figure 5.3: Quantification of the Changes in POPDC1 and POPDC2 Expression at the Plasma Membrane and Cytoplasm of Skeletal Muscle fibres of a Patient possessing the *POPDC1* p.Q153X Mutation.....146

Figure 5.4: The Change in Cross-Sectional Area of Skeletal Muscle Fibres between a Patient Possessing the *POPDC1* p.Q153X Mutation and a Control.....147

Figure 5.5: The Changes in POPDC1 and POPDC2 Subcellular Expression Plotted against the Cross-Sectional Area of Individual Skeletal Muscle Fibres of a patient possessing the *POPDC1* p.Q153X Variant and a Control.....148

Figure 5.6: Immunostaining of POPDC1 and POPDC2 within Skeletal Muscle Fibres from a Patient possessing the *POPDC1* p.V183F Variant and a Control.....149

Figure 5.7: Quantification of the Changes in POPDC1 and POPDC2 Expression at the Plasma Membrane and Cytoplasm of Skeletal Muscle Fibres of a Patient possessing the *POPDC1* p.V183F Mutation.....150

Figure 5.8: The Change in Cross-Sectional Area of Skeletal Muscle Fibres between a Patient possessing the *POPDC1* p.V183F Mutation and a Control.....151

Figure 5.9: The Changes in POPDC1 And POPDC2 Expression Levels at the Plasma Membrane and Cytoplasm Plotted against the Cross-Sectional Area of Individual Skeletal Muscle Fibres of a Patient possessing The *POPDC1* P.V183F Variant and a Control.....152

Figure 5.10: Immunostaining of POPDC1 and POPDC2 within Skeletal Muscle Fibres from a Homozygous *Popdc1* p.S201F Mouse and a Control.....153

Figure 5.11: Quantification of the Changes in POPDC1 and POPDC2 Expression at the Plasma Membrane and Cytoplasm of Skeletal Muscle Fibres of a Homozygous *Popdc1* p.S201F Mouse Mutant.....154

Figure 5.12: The Change in Cross-Sectional Area of Skeletal Muscle fibres between a Homozygous *Popdc1* p.S201F Mouse and a Control.....155

Figure 5.13: The Changes in POPDC1 and POPDC2 Expression Levels at the Plasma Membrane and Cytoplasm Plotted against the Cross-Sectional Area of Individual Skeletal Muscle Fibres of a Homozygous *Popdc1* p.S201F Mouse and a Control.....155

Figure 5.14: The Plasma Membrane and Cytoplasmic Expression of POPDC1 and POPDC2 when Transiently Expressed alone or Co-expressed in HEK293 Cells.....158

Figure 5.15: The Normalised Expression Profile of POPDC1 and POPDC2 Relative to Position of the Plasma Membrane of HEK293 Cells when Co-expressed or Expressed Alone.....161

Figure 5.16: The Plasma Membrane and Cytoplasmic Expression of POPDC1 and POPDC2 in the Presence of Various POPDC Variants when Transiently Expressed in HEK293 Cells.....163

Figure 5.17: The Normalised Expression Profile of POPDC1 and POPDC2 Relative to the Position of the Plasma Membrane of HEK293 Cells in Presence of Various POPDC Variants.....167

Figure 6.1: The Mechanism of a Type 1 Quantitative BRET Assay.....177

Figure 6.2: The Quantitative BRET Analysis of Homomeric and Heteromeric Interactions between POPDC1 and POPDC2…179

Figure 6.3: Acceptor-photobleaching FRET between POPDC1 and POPDC2 in the Presence of Various POPDC Mutants in HEK293 Cells……183

Figure 6.4: The Changes in BiFC Signal from the Co-expression of POPDC1 and POPDC2 Variants in HEK293 Cells……187

Figure 6.5: Co-Immunoprecipitation of POPDC2 with POPDC1 from HEK293 Cells in the Presence of Various POPDC Variants……189

Figure 6.6: POPDC1, POPDC2 and POPDC3 all contain a Sequence of Highly Conserved Hydrophobic Residues with the Predicted αC-helix at the C-terminus of the Popeye Domain……191

Figure 6.7: A Model POPDC1-POPDC2 Popeye Domain Dimer based on the Structure of CAP……193

Figure 6.8: The Subcellular Expression of POPDC1 αC-helix Mutants and POPDC2 in HEK293 Cells……195

Figure 6.9: The Subcellular Expression of POPDC1 and POPDC2 αC-helix Mutants in HEK293 Cells……197

Figure 6.10: POPDC Protein Trafficking to the Plasma Membrane may be controlled by Endoplasmic Reticulum Retention and Adaptor Protein Interaction Signals……199

Figure 6.11: The Mode of cAMP Binding to CAP and a Possible Interactions between cAMP and the αC-helix of the Popeye Domain……201

Figure 6.12: A Working Model for POPDC Protein Interactions……204

Figure 6.13: The Modified AlphaFold Structures of the Clinically Identified POPDC Mutations and their Relation to the αC-helix……207

Figure 7.1: A Family Pedigree of a Family with Members who have displayed a cJET Phenotype, with respect to the *POPDC2* p.L245P Variant……209

Figure 7.2: The Conservation of Residue L245 in POPDC2 and its Position in POPDC2……212

Figure 7.3: The Co-Expression of POPDC1 and POPDC2 p.L245P in HEK293 Cells……213

Figure 7.4: The Normalised Cellular Cross-Sectional Expression Profile of POPDC1 and POPDC2 Relative to the Position of the Plasma Membrane of HEK293 Cells in Presence of the POPDC2 p.L245P Variant……214

Figure 7.5: BiFC, AP-FRET and Co-IP Assays suggest the Interaction between POPDC1 and POPDC2 p.L245P is Impaired……216

Figures Included in the Appendix

Figure 10.1: The plasma Membrane Localisation of POPDC1 and POPDC2 in HEK293 cells when Co-Transfected at differing Ratios……246

Figure 10.2: The Normalised Expression Profile of POPDC1 and POPDC2 Relative to Position of the Plasma Membrane of HEK293 Cells when Transfected a different Ratios……246

Figure 10.3: Plots showing the Total Expression Level of POPDC-NL and POPDC-HT at different Expression Ratios……256

Figure 10.4: Co-Immunoprecipitation of POPDC2 with POPDC1 from HEK293 Cells in the Presence of Various POPDC Variants Full Blots……257

Figure 10.5: The cDNA Oligonucleotide Sequence of the GB1-S109-K272 Popeye Domain Construct……260

Figure 10.6: The cDNA Oligonucleotide Sequence of the GB1-E123-D266 Popeye Domain Construct……260

Figure 10.7: The cDNA Oligonucleotide Sequence of the GST-BVES Popeye Domain Construct……260

Figure 10.8: The cDNA Oligonucleotide Sequence of the GB1-Q94-K255 POPDC2 Popeye Domain Construct.....261

Figure 10.9: The cDNA Oligonucleotide Sequence of the POPDC1-ECFP Construct.....261

Figure 10.11: The cDNA Oligonucleotide Sequence of the POPDC1p.Q153X-ECFP Construct.....261

Figure 10.12: The cDNA Oligonucleotide Sequence of the POPDC1p.R172H/p.V183F/p.S201F-ECFP Constructs.....262

Figure 10.13: The cDNA Oligonucleotide Sequence of the POPDC2p.W188X-EYFP Construct.....262

Figure 10.14: The cDNA Oligonucleotide Sequence of the POPDC2p.L245P-EYFP Construct. 262

Figure 10.15: The cDNA Oligonucleotide Sequence of the αC-helix Mutant POPDC1-ECFP Constructs.....263

Figure 10.16: The cDNA Oligonucleotide Sequence of the αC-helix Mutant POPDC2-EYFP Constructs.....263

Figure 10.17: The cDNA Oligonucleotide Sequence of the ECFP-EYFP AP-FRET Positive Control Construct.....263

Figure 10.18: The cDNA Oligonucleotide Sequence of the POPDC1-VC155 Construct.....264

Figure 10.19: The cDNA Oligonucleotide Sequence of the POPDC2-VN155 Construct.....264

Figure 10.20: The cDNA Oligonucleotide Sequence of the POPDC1p.Q153X-VC155 Construct.....264

Figure 10.21: The cDNA Oligonucleotide Sequence of the POPDC1p.R172H/p.V183F/p.S201F-VC155 Constructs.....264

Figure 10.22: The cDNA Oligonucleotide Sequence of the POPDC2p.W188X-VN155 Construct.....264

Figure 10.23: The cDNA Oligonucleotide Sequence of the POPDC2p.L245P-VN155 Construct.....265

Figure 10.24: The Forward Sanger Sequencing Chromatograms of Site Directed Mutagenesis of POPDC1 and POPDC2 to Introduce Clinically Identified Mutations.....265

Figure 10.25: The Forward Sanger Sequencing Chromatograms of Site Directed Mutagenesis of αC-helix POPDC1 Mutants.....265

Figure 10.26: The Forward Sanger Sequencing Chromatograms of Site Directed Mutagenesis of αC-helix POPDC2 Mutants.....266

List of Tables

Table 1.1: A table showing the mutations in POPDC genes identified in patients, as well as POPDC gene knock-out or knock-down animal, and their general skeletal muscle and cardiac phenotype.....42

Table 2.1: A table listing the reagents utilised in this work, with their respective supplier and product codes.....48-50

Table 2.2: A table listing the commercial buffers and media utilised in this work, with their respective supplier and product codes.....50

Table 2.3: A table listing the enzymes utilised in this work, with their respective supplier and product codes.....50

Table 2.4: A table listing the plasmids and other oligonucleotides utilised in this work, with their respective supplier and product codes.....51

Table 2.5: A table listing the antibodies utilised in this work, with their respective supplier and product codes.....51

Table 2.6: A table listing eukaryotic cell lines and bacterial cells utilised in this work, with their respective supplier and product codes.....51

Table 2.7: A table listing the equipment utilised in this work, with their respective supplier and product codes (where available).....51-52

Table 2.8: A table listing the components of non-commercial buffers and media with their respective proportions, amounts or concentration.....53-54

Table 2.9: A table listing the standard components of regular PCR reactions.....55

Table 2.10: A table showing the general thermocycler steps performed during standard PCR reactions.....55

Table 2.11: A table listing the standard components of restriction reactions.....56

Table 2.12: A table listing the standard components of dephosphorylation reactions.....56

Table 2.13: A table listing the standard components of ligation reactions.....57

Table 2.14: A table listing the standard components of site directed mutagenesis PCR reactions.....57

Table 2.15: A table showing the general thermocycler steps performed during standard site directed mutagenesis PCR reactions.....58

Table 2.16: A table showing the standard components of the phosphorylation, ligation and DpnI (KLD) reaction.....58

Table 2.17: A table showing the primers used to produce sequences of mouse Popeye domain by PCR with mouse *Popdc1* as a template, for use in constructing initial Popeye domain constructs for structural studies.....60

Table 2.18: A table showing the primers used to produce a set of Popeye domain constructs by site directed deletion PCR using the GB1-S109-S288 construct as a template.....61

Table 2.19: A table showing the primers used to introduce the H188Q substitution into the GB1-S109-K272 Popeye domain construct.....61

Table 2.20: A table showing the primers used to produce sequences of mouse Popeye domain by PCR, for use in constructing an initial set of Popeye domain-based BRET2 cAMP sensors.....62

Table 2.21: A table showing the primers used in site directed mutagenesis of *POPDC1*-ECFP or *POPDC2*-EYFP construct sequences to introduce a set of clinically identified mutations.....63

Table 2.22: A table showing the primers used in site directed mutagenesis of the *POPDC1*-ECFP construct sequence to introduce a set αC-helix aspartic acid scanning mutations.....63

Table 2.23: A table showing the primers used in site directed mutagenesis of the *POPDC2*-EYFP construct sequence to introduce a set αC-helix aspartic acid scanning mutations.....63

Table 2.24: A table listing the standard components of Flexi restriction reactions used in the production of POPDC NanoBRET constructs.....64

Table 2.25: A table showing the primers used in site directed mutagenesis of the *POPDC1*-ECFP and *POPDC2*-EYFP construct sequences to introduce A206K mutations into the ECFP and EYFP domains.....65

Table 2.26: A table showing the primers used in the PCR reaction to amplify the ECFP sequence to produce the ECFP-EYFP fusion construct.....65

Table 2.27: A table showing the Protein-NMR ^{1}H-^{15}N HSQC-TROSY acquisition parameters.....69

Table 2.28: A table showing the components of the transfection of *POPDC1*-ECFP and *POPDC2*-EYFP constructs, and various mutant variants, into HEK293 cells for trafficking and expression studies.....73

Table 2.29: A table showing the components of the transfection of *POPDC1*-ECFP and *POPDC2*-EYFP constructs, and various mutant variants, into HEK293 cells for AP-FRET assays.....78

Table 2.30: A table showing the components of the calcium phosphate based transfection of *POPDC1*-VC155 and *POPDC2*-VN155 containing plasmids, and various mutant variants, into HEK293 cells for BiFC studies.....80

Table 2.31: A table showing the components of each 10% SDS-PAGE resolving gel.....81

Table 2.32: A table showing the components of the SDS-PAGE stacking gel.....81

Table 2.33: A table showing the image acquisition settings used for the different imaging based studies completed in this work.....88

Table 3.1: A table summarising of all expression trials of novel Popdc1 Popeye domain constructs.....99

Table 5.1: A table listing the known POPDC mutations identified in patients, as well as various animal models, and the effect of the mutation or knock out on the expression pattern or subcellular localisation of POPDC1 and POPDC2 in skeletal muscle fibres.....140

Tables Included in the Appendix

Table 10.1: Table summarising the cAMP dependent change in BRET signal from the Popeye domain sensors.....242

Table 10.2: Table summarising the data for skeletal muscle biopsy Staining for POPDC1, POPDC2 and α-sarcoglycan in control and POPDC1 p.Q153X patient.....243

Table 10.3: Table summarising the data for skeletal muscle biopsy staining for POPDC1, POPDC2 and α-sarcoglycan in control and POPDC1 p.V183F patient.....244

Table 10.4: Table summarising the data for skeletal muscle biopsy staining for POPDC1, POPDC2 and α-sarcoglycan in control and POPDC1 p.S201F mouse.....245

Table 10.5: Table summarising the normalised POPDC1 plasma membrane expression in HEK293 cells in the presence of the clinical POPDC mutations. 247

Table 10.6: ANOVA table summarising the comparisons of the normalised POPDC1 plasma membrane expression in HEK293 cells in the presence of the clinical POPDC mutations.....247

Table 10.7: Table summarising the normalised POPDC2 plasma membrane expression in HEK293 cells in the presence of the clinical POPDC mutations.....247

Table 10.8: ANOVA table summarising the comparisons of the normalised POPDC2 plasma membrane expression in HEK293 cells in the presence of the clinical POPDC mutations.....247

Table 10.9: Table summarising the normalised POPDC1 cytoplasm expression in HEK293 cells in the presence of the clinical POPDC mutations.....248

Table 10.10: ANOVA table summarising the comparisons of the normalised POPDC1 cytoplasm expression in HEK293 cells in the presence of the clinical POPDC mutations.....248

Table 10.11: Table summarising the normalised POPDC2 cytoplasm expression in HEK293 cells in the presence of the clinical POPDC mutations.... 248

Table 10.12: ANOVA table summarising the comparisons of the normalised POPDC2 cytoplasm expression in HEK293 cells in the presence of the clinical POPDC mutations.....248

Table 10.13: Table summarising the normalised ratio of POPDC1 in the plasma membrane and cytoplasm in HEK293 cells in the presence of the clinical POPDC mutations.....249

Table 10.14: ANOVA table summarising the comparisons of the normalised POPDC1 ratio in the plasma membrane and cytoplasm in HEK293 cells in the presence of the clinical POPDC mutations.....249

Table 10.15: Table summarising the normalised ratio of POPDC2 in the plasma membrane and cytoplasm in HEK293 cells in the presence of the clinical POPDC mutations.....249

Table 10.16: ANOVA table summarising the comparisons of the normalised POPDC1 ratio in the plasma membrane and cytoplasm in HEK293 cells in the presence of the clinical POPDC mutations.....249

Table 10.17: Table summarising the normalised POPDC1 plasma membrane expression in HEK293 cells in the presence of the αC-helix POPDC1 mutations.....250

Table 10.18: ANOVA table summarising the comparisons of the normalised POPDC1 plasma membrane expression in HEK293 cells in the presence of the αC-helix POPDC1 mutations.....250

Table 10.19: Table summarising the normalised POPDC2 plasma membrane expression in HEK293 cells in the presence of the αC-helix POPDC1 mutations.....250

Table 10.20: ANOVA table summarising the comparisons of the normalised POPDC2 plasma membrane expression in HEK293 cells in the presence of the αC-helix POPDC1 mutations.....250

Table 10.21: Table summarising the normalised POPDC1 cytoplasm expression in HEK293 cells in the presence of the αC-helix POPDC1 mutations.....251

Table 10.22: ANOVA table summarising the comparisons of the normalised POPDC1 cytoplasm expression in HEK293 cells in the presence of the αC-helix POPDC1 mutations.....251

Table 10.23: Table summarising the normalised POPDC2 cytoplasm expression in HEK293 cells in the presence of the αC-helix POPDC1 mutations.....251

Table 10.24: ANOVA table summarising the comparisons of the normalised POPDC2 cytoplasm expression in HEK293 cells in the presence of the αC-helix POPDC1 mutations.....251

Table 10.25: Table summarising the normalised ratio of POPDC1 in the plasma membrane and cytoplasm in HEK293 cells in the presence of the αC-helix POPDC1 mutations.....252

Table 10.26: ANOVA table summarising the comparisons of the normalised POPDC1 ratio in the plasma membrane and cytoplasm in HEK293 cells in the presence of the αC-helix POPDC1 mutations.....252

Table 10.27: Table summarising the normalised ratio of POPDC2 in the plasma membrane and cytoplasm in HEK293 cells in the presence of the αC-helix POPDC1 mutations.....252

Table 10.28: ANOVA table summarising the comparisons of the normalised POPDC2 ratio in the plasma membrane and cytoplasm in HEK293 cells in the presence of the αC-helix POPDC1 mutations.....252

Table 10.29: Table summarising the normalised POPDC1 plasma membrane expression in HEK293 cells in the presence of the αC-helix POPDC2 mutations.....253

Table 10.30: ANOVA table summarising the comparisons of the normalised POPDC1 plasma membrane expression in HEK293 cells in the presence of the αC-helix POPDC2 mutations.....253

Table 10.31: Table summarising the normalised POPDC2 plasma membrane expression in HEK293 cells in the presence of the αC-helix POPDC2 mutations.....253

Table 10.32: ANOVA table summarising the comparisons of the normalised POPDC2 plasma membrane expression in HEK293 cells in the presence of the αC-helix POPDC2 mutations.....253

Table 10.33: Table summarising the normalised POPDC1 cytoplasm expression in HEK293 cells in the presence of the αC-helix POPDC2 mutations.....254

Table 10.34: ANOVA table summarising the comparisons of the normalised POPDC1 cytoplasm expression in HEK293 cells in the presence of the αC-helix POPDC2 mutations.....254

Table 10.35: Table summarising the normalised POPDC2 cytoplasm expression in HEK293 cells in the presence of the αC-helix POPDC2 mutations.....254

Table 10.36: ANOVA table summarising the comparisons of the normalised POPDC2 cytoplasm expression in HEK293 cells in the presence of the αC-helix POPDC2 mutations.....254

Table 10.37: Table summarising the normalised ratio of POPDC1 in the plasma membrane and cytoplasm in HEK293 cells in the presence of the αC-helix POPDC2 mutations.....255

Table 10.38: ANOVA table summarising the comparisons of the normalised POPDC1 ratio in the plasma membrane and cytoplasm in HEK293 cells in the presence of the αC-helix POPDC2 mutations.....255

Table 10.39: Table summarising the normalised ratio of POPDC2 in the plasma membrane and cytoplasm in HEK293 cells in the presence of the αC-helix POPDC2 mutations……255

Table 10.40: ANOVA table summarising the comparisons of the normalised POPDC2 ratio in the plasma membrane and cytoplasm in HEK293 cells in the presence of the αC-helix POPDC2 mutations……255

Table 10.41: Table summarising the parameters determined for the different POPDC combinations in the qBRET assay…..256

Table 10.42: Table summarising the normalised BiFC signal produced by co-expression of POPDC1 and POPDC2 with different clinically identified mutations……258

Table 10.43: ANOVA table summarising the comparisons of the normalised BiFC signal produced by co-expression of POPDC1 and POPDC2 with different clinically identified mutations……258

Table 10.44: Table summarising the normalised AP-FRET signal produced by co-expression of POPDC1 and POPDC2 with different clinically identified mutations……258

Table 10.45: ANOVA table summarising the comparisons of the normalised AP-FRET signal produced by co-expression of POPDC1 and POPDC2 with different clinically identified mutations……259

Table 10.46: Table summarising the normalised expression and plasma membrane localisation of POPDC1 and POPDC2 in HEK293 cells in the presence of the POPDC1 p.L245P mutation……259

Table 10.47: Table summarising the normalised BiFC signal produced by co-expression of POPDC1/POPDC1 p.L245P and POPDC2……260

Table 10.48: Table summarising the normalised AP-FRET signal produced by co-expression of POPDC1/POPDC1 p.L245P and POPDC2……260

Abbreviations

Abbreviation	Full Term
6XHis	Hexa histidine
AC	Adenylyl cyclase
AC9	Adenylyl cyclase 9
AKAPs	A-kinase anchoring proteins
AMP	Adenosine 5’-monophosphate
AP-FRET	Acceptor photobleaching fluorescence resonance energy transfer
ATP	Adenosine-5’-triphosphate
AVN	Atrioventricular node
BiFC	Bimolecular fluorescence complementation
BRET	Bioluminescence resonance energy transfer
cAMP	3’,5’-cyclic adenosine monophosphate
CAP	Catabolite activator protein
CD	Circular dichroism
cDMEM	Complete Dulbecco’s modified eagle’s medium
cDNA	Complementary DNA
cJET	Congenital junctional ectopic tachycardia
CNBD	Cyclic nucleotide binding domain
Co-IP	Co-immunoprecipitation
CRP	Cyclic AMP receptor protein
DAPI	4’,6-diamidino-2-phenylindole
DiD	1,1-Dioctadecyl-3,3,3,3-tetramethylindodicarbocyanine
DMEM	Dulbecco’s modified eagle’s medium
DMSO	Dimethyl sulfoxide
DSF	Differential scanning fluorimetry
ECFP	Enhanced cyan fluorescent protein
EGTA	Ethylene glycol-bis(β-aminoethyl ether)-N,N,N,’N’-tetraacetic acid
ELISA	Enzyme linked immunosorbent assay
EPAC	Exchange factor directly activated by cAMP
ER	Endoplasmic reticulum
EYFP	Enhanced yellow fluorescent protein
FBS	Foetal bovine serum
FPLC	Fast protein liquid chromatography
FRET	Fluorescence resonance energy transfer
GFP	Green fluorescent protein
GFP2	Green fluorescent protein 2
GPCR	G-protein coupled receptor
GST	Glutathione S-transferase
GTP	Guanosine 3',5'-cyclic monophosphate
GTP	Guanosine-5’-triphosphate
H-bond	Hydrogen bond
HA	Human influenza haemagglutinin
HEK293	Human embryonic kidney 293
HRP	Horse radish peroxidase
HSQC-TROSY	Heteronuclear single quantum coherence transverse relaxation optimized spectroscopy
ITC	Isothermal calorimetry
JET	Junctional ectopic tachycardia
LB	Luria broth
mECFP	Monomerised enhanced cyan fluorescent protein
mEYFP	Monomerised enhanced yellow fluorescent protein
MST	Microscale thermophoresis
Ni-NTA	Ni^{2+} charged nitriloacetic acid (Ni-NTA)
NMD	Nonsense mediated decay
NMR	Nuclear magnetic resonance
NusA	N-utilization substance A
PBS	Phosphate buffered saline
PCR	Polymerase chain reaction

PDB	Protein Data Bank
PDE	Phosphodiesterase
PDE4A	Phosphodiesterase 4A
PFA	Paraformaldehyde
PKA	Protein kinase A
PLA	Proximity ligation assay
POPDC	Popeye domain containing
PPI	Protein-protein interactions
qBRET	Quantitative BRET
RET	Resonance energy transfer
SAN	Sinoatrial node
SDS-PAGE	Sodium dodecyl sulfate polyacrylamide gel electrophoresis
SEC	Size exclusion chromatography
SEC-MALS	Size exclusion chromatography multi angle light scattering
UV	Ultraviolet
VC155	Split Venus C-terminal tag
VN155	Split Venus N-terminal tag

Nomenclature of the Popeye domain containing proteins and genes

The Popeye domain containing proteins are referred to as follows:

POPDC1, POPDC2, POPDC3 refer to the human protein of each isoform. Popdc1, Popdc2 and Popdc3 refer to the mouse forms of these proteins, while popdc1, popdc2 and popdc3 are applied to the zebrafish variants.

The *POPDC* genes are referred to as:

POPDC1, POPDC2, *POPDC3* refer to human genes, *Popdc1*, *Popdc2* and *Popdc3* refer to the mouse forms, while *popdc1*, *popdc2* and *popdc3* are applied to the zebrafish variants.

POPDC is used as an abbreviation of 'Popeye domain containing' and is applied to both the gene and protein families.

1 Introduction

1.1 Protein Constructs for use in Structural and Activity Studies

Given that a protein's function is determined by its shape, much effort has been applied to the study of protein structures. A number of biophysical techniques have been developed to determine the structure of proteins. Perhaps the most well-known is x-ray crystallography, in which analysis of the diffraction pattern of x-rays after interacting with protein crystals provides information about the distribution of electron density within, and so structure of, a protein molecule.[1] An alternative method is cryo-electron microscopy, which uses a transmission electron microscope to take many images of a protein particle, which are combined to build a three dimensional image of the protein structure.[2] Protein nuclear magnetic resonance (NMR), discussed further in Chapter 3, utilises the absorption of radio waves by specific, spin active, nuclei within a protein.[3] Proteins are exposed to a strong magnetic field, which leads to a uniform orientation of the spin of the nuclei present. Nuclei will absorb electromagnetic radiation at specific frequency, depending on their electronic environment, which can subsequently be detected. The frequency of radiation absorbed is influenced by the chemical bonding of a nuclei's atom, and its neighbours, as well as the spatial distribution of electron density in its vicinity. As such, by identifying the signals from nuclei within each amino acid, the spatial arrangement of residues in the three dimensional structure of the protein can be determined.[4] Structure determination can be performed in solution and the conformational dynamics of proteins can also be observed, allowing observation of proteins in a state close to their natural environment.[5] The atomic level resolution that can be achieved with protein-NMR can be applied to determining the residues involved in protein-protein interfaces, with the contacts and conformational changes involved in protein-protein interactions (PPIs) able to elicit changes in the chemical shift of atoms. Other techniques can provide other information about protein structure. Circular dichroism (CD) can be used to investigate the secondary structure features within a protein *via* the disparate absorption of right and left circularly polarised light by chiral protein particles.[6] Furthermore, light scattering methods are able to determine the size and molecular weight of a protein in solution.[7]

A requirement of all these techniques is to be in possession of a suitable version of the target protein. Each experimental technique has its own requirements for an ideal protein construct, but generally a protein construct intended for use in structural or activity studies should be able to be expressed at a high level in the chosen expression system, purified effectively and retain its native conformation and function during the experiment.[8] The data yielded from structural techniques such as x-ray crystallography and protein-NMR will represent the average structure of proteins in the sample, meaning the sample should also be homogenous. While conformational exchange in proteins can be exploited during protein-NMR experiments to provide information on protein dynamics, it can also

prevent the running of other protein-NMR experiments and should be reduced in initial structural studies.[9] This means a conformationally stable protein is generally desirable. Before a construct is used in structural studies, it should be confirmed that it possesses activity comparable to the native protein.[10] For example, if a protein is known to bind a ligand, the binding affinity of the recombinant construct should be assessed, with any loss of binding activity indicative of misfolding or other issues with the protein. Techniques such as circular dichroism can provide rapid indications of whether the construct is folded before investment in time and financially costly experiments.[6]

The residues from the native protein included in a recombinant construct is an important consideration.[8] For smaller, globular proteins it may be possible to express the entire protein. However, for larger, multidomain proteins it may be advantageous to remove parts of the protein, focusing on the domain of interest. This is because interdomain flexibility and disordered areas of the protein will hinder structure determination. The designation of domain boundaries is not always clear, and sequence alignments to known structures and secondary structure predictions can be used to guide the choice of terminal residues.[8] Regions with a high density of surface exposed hydrophobic residues, particularly transmembrane domains, will likely inhibit construct solubility and are usually removed, unless special conditions are used.[11]

The expression system is also a key choice, such as bacteria, yeast, insect, or mammalian cells. Mammalian cell lines tend to be used when post-translational modifications, such as phosphorylation and glycosylation, are required for the production of fully functional protein.[12] Bacterial cells possess the advantage of being able to be cultured at large scale with high levels of protein production.[13] While smaller, globular proteins tend to be more amenable to expression and purification, the behaviour of recombinant proteins can be unpredictable, with low expression, inclusion body formation, misfolding, low solubility, low stability and poor activity all possible.[13] As well as the expression system, the pH and salinity of the buffer the proteins are dissolved in, as well the addition of ligands or other compounds, can be altered to improve the physical properties of the protein.[10]

The addition of affinity tags, either short polypeptide sequences, such as the hexa histidine (6XHis) tag, or larger protein domains, for use in the purification of a construct from the expression system's own proteome, is a common strategy.[14] This can also have a beneficial effect on the construct's solubility. Larger tags such as N-utilization substance A (NusA) or glutathione S-transferase (GST) tend to have greater effects on solubility although it is sometimes unclear why this is the case.[15,16] However, if these tags remain in place during analysis of the construct, they may interfere with the physical and functional properties of the target protein.[17] It is usually desirable to remove such appendages, often

through the use of enzymatic cleavage sites.[13] As such, the target protein itself should ideally remain soluble and stably folded in the absence of the fusion tag.

The amount of protein that can be expressed and purified must be sufficient for the intended use, without requiring impractical scale-up or costs.[10] Improving the level of expression of the protein construct, and so the ratio of target protein to contaminants, can also help improve the purity of the final sample.[8] Batch to batch repeatability must be established if multiple preparations of protein will be required. If any of these criteria are not met, then the protein construct may not be suitable for use in structural studies and modification may be required. Similar standards should also be met in the development of recombinant proteins for use in ligand binding experiments.

1.2 Protein Structure Prediction

In the absence of, or in addition to, empirical data, information about protein structures can be obtained through computational modelling techniques. Two main types of modelling have been employed: template-based and template-free.[18] Template-based methods use a known structure of a related protein, previously determined empirically, as a starting point for the structure of the target protein. This is often referred to as homology modelling. The more similar in amino acid sequence and evolutionary relatedness, the closer the template is likely to be to the true structure of the unknown protein.[19] It is important to choose the most appropriate templates when conducting homology modelling, with multiple templates usually selected through sequence alignments with the target protein. Therefore, this approach is limited if no structures of closely related proteins are available. If a sequence identity of a target protein is less than around 25% of a template protein, the results of the homology modelling are much less likely to be accurate.[18] Many proteins do not have high sequence similarity with any other proteins whose structures have been deposited in the Protein Data Bank (PDB). As such, template-based methods are not able to provide high confidence, accurate structure prediction. In these cases, template-free, or *ab initio*, methods are more suitable. Purely *ab initio* methods use molecular dynamics force fields to find the lowest energy conformation of an amino acid sequence.[20] The huge conformational space that polypeptide chains can occupy can make these techniques computationally expensive, and limits its use on full length proteins. For larger proteins, these molecular dynamics based methods are usually combined with fragment based approaches.[19] These use small structural fragments from known structures, which may correlate with similar sequences in the target protein. The fragments used are taken from known structures which, being found in nature are already stable, reducing the number of conformations that need to be sampled. The use of pairwise spatial constraints, in combination with machine learning, has further improved protein structure prediction. Predictions of which amino acids within a protein sequence are likely to be found in close proximity in space can be made, which can then be used to guide model construction,

reducing the number of possible conformations that must be sampled.[19] The basic principle behind this technique is that residues that are co-conserved in related protein sequences are likely to be involved in similar roles, and so may be found in the same domain of the protein. Recently, neural network programs, such as AlphaFold and RoseTTAFold, have incorporated biological and physical inputs to be able to make protein models with unprecedented accuracy.[21,22] Databases containing predicted structures for entire proteomes, built using AlphaFold, have been released.[23,24] While this provides great opportunities for researching proteins with no solved structure and/or with only poor templates available for homology modelling, caution should still be applied when interpreting results using these models.

1.3 Protein-Protein Interactions

1.3.1 The Nature of Protein-Protein Interactions

Many proteins only function fully in the presence of other proteins, with only a minority of proteins existing in isolation.[25] Direct PPIs are essential for many cellular processes, with highly complex protein interaction networks present in all cells, while disruption of these networks underpins many disease states. Proteins of the same type can interact to form homo-oligomers, where all constituent proteins of a complex are identical. Homo-oligomers tend to show some form of symmetry, sometimes using the equivalent surface on each monomer to form the interface.[26] Alternatively, multiple types of protein can coalesce to form hetero-oligomers. The proteins contained in hetero-oligomers may still display similarities at the interface, helping to form complementary contacts with some degree of symmetry. It is also possible for homo-oligomers to exist as part of larger hetero-oligomeric structures. PPIs may lead to formation of stable complexes that exist almost as a single entity, with minimal alterations in subunit composition.[27] Some proteins are even destabilised in the monomeric form, only attaining their ideal folded structure when complexed with other molecules. Alternatively, other proteins will continuously associate and dissociate with PPI partners, remaining properly folded in the absence of any interactions. The ability of PPIs to rapidly shift is important in cells being able to quickly respond to different stimuli, as PPIs often form key functions in signalling pathways.[25] PPIs may respond to their environment, being favoured at one time but inhibited at another. A number of forces drive the formation of PPIs, with electrostatic interactions, hydrogen bonds (H-bonds), hydrophobic interactions, disulfide bonds all found at interfaces in various combinations.[27]

The properties of the interface between two proteins such as the size, the types of amino acid involved, secondary structure, H-bonding, hydrophobic interactions, and complementarity of the shape all influence the nature of the interaction.[27] It should be noted that in many complexes there will be proteins that do not directly interact with each other, but their association with the overall complex is necessary for function. In such a way proteins may rely on other proteins without making

direct contact. On the other hand, proteins may form temporary contacts with no functional relevance as result of diffusion alone. Many combinations of domains may combine to form PPI interfaces. α-helix-α-helix pairs, bundles of α-helices, and coiled-coils are examples of types of interfaces dominated by α-helices.[28] In addition, α-helices may interact with β-sheets or disordered areas of partner proteins. β-sheets can form interfaces with each other, as well as non-ordered regions, while interfaces can also be formed only from disordered loops. It has been suggested that symmetric interfaces, such as helix-helix interfaces, are more commonly found in homo-oligomers, with mixed interfaces more prevalent in hetero-oligomers.[28] More widely, proteins with a close evolutionary relationship are more likely to interact through similar domains, and this can inform predictions of interface sites between related proteins.[26] Areas of proteins involved in important PPIs will often show a high degree of sequence conservation, which can provide further insights into the location of interaction sites in the absence of detailed structural information.[29]

1.3.2 Cell-Based Methods for Studying Protein-Protein Interactions

It is highly desirable to detect PPIs within cellular environments and is one of the aims of this work. The subcellular location of fluorescently labelled proteins can be analysed within cells, or even in whole organisms.[30,31] The use of proteins whose sequence has been modified to append a fluorescent protein is well established and allows the visualisation of proteins within cells.[30] One drawback with this method is the large size of the fluorescent protein domain, around 27 kDa for green fluorescence proteins (GFP) variants, which may alter the function of the tagged protein.[32] When the signal from two proteins that are fluorescently labelled overlap within the cell, they are said to colocalize. While colocalization can provide useful guidance about protein-protein interactions, colocalization does not necessarily mean an interaction between two tagged proteins is occurring.[33] The resolution of optical microscopes is not sufficient to isolate emission from single protein complexes. Therefore, signals may appear in the same pixel of an image but originate from non-interacting molecules. Some super-resolution single molecule fluorescence techniques may be able to directly detect PPIs.[34]

Fluorescence resonance energy transfer (FRET) and bioluminescence resonance energy transfer (BRET), which are discussed in more detail in Chapters 4 and 6, exploit the phenomenon of resonance energy transfer (RET).[35] This is the non-radiative transfer of energy between an electronically excited donor and fluorescent acceptor group. These are normally each fused to a protein of interest, which can be expressed in cells.[36] In FRET the donor is a fluorophore excited by incident light, while BRET uses an *in situ* reaction catalysed by a luciferase enzyme to produce a bioluminescent donor.[37] FRET donors and acceptors are typically either fluorescent proteins that have been genetically fused to the protein of interest, or covalently bound small molecule dyes. BRET can use the same types of acceptors as FRET but will have a genetically appended luciferase attached to one protein acting as the donor.

RET is highly distance dependent, being inversely proportional to the distance between the donor and acceptor groups to the power of six.[35] Therefore, the fluorescent acceptor will only emit light if the two proteins are close enough, within a few nanometres, for RET to occur. While RET is a non-radiative process, the emission spectrum of the donor and the absorption spectra of the acceptor must overlap for RET to occur. The proportion of the energy from the electronically excited donor that is transferred to the acceptor depends on the distance between them, the extent of the overlap of their emission and absorption spectra, their relative orientations, and the nature of the solvent.[36] Note that the dependency on factors other than distance means that greater efficiency of RET does not always mean a tighter interaction between the tagged proteins is occurring. The remainder of the donor energy is lost to other non-radiative decay processes. After RET has occurred, the electronically excited acceptor will emit some of acquired energy as light. The ratio of emission from the donor and acceptor species is used to determine the efficiency of FRET/BRET, with increased signal associated with the presence of a PPI.

Fluorescence complementation assays, of which the most common format is bimolecular fluorescence complementation (BiFC) and is discussed in Chapter 6, use the reformation of a split, non-functional protein fluorophore to detect PPIs.[38] Like FRET and BRET these protein domains are genetically fused to two different proteins of interest, such that when the two fragments are brought together as a result of a PPI they reform a functional fluorophore. A similar assay has been developed using split luciferase enzymes, that are only capable of generating bioluminescence when reformed as a result of a PPI.[39]

Antibodies can be used to isolate interacting proteins using co-immunoprecipitation (Co-IP).[40] A mixture containing proteins, such as cell lysate, can be incubated with antibodies, targeted to a bait protein, that are conjugated to a bead. Washing of the beads will leave behind the bait protein, bound to the antibodies, along with any proteins that are in a complex with the bait protein. Denaturing of the beads and antibodies releases the individual proteins that can be detected using sodium dodecyl sulfate polyacrylamide gel electrophoresis (SDS-PAGE) followed by Western blotting, or other methods. The co-immunoprecipitated proteins can then be identified as those which were interacting with the bait protein.[40]

Many other techniques such as the proximity ligation assay (PLA) and cross-linking mass spectrometry have been developed to identify PPIs within cells.[41,42] Biophysical techniques such as surface plasmon resonance, isothermal calorimetry and microscale thermophoresis can be used to determine kinetic and thermodynamic parameters of PPIs *in vitro*.[43]

1.4 Processing of Integral Membrane Proteins

This work will investigate the expression and subcellular localisation of transmembrane proteins within skeletal muscle fibres and the HEK293 cell line. As such, a brief description of these processes is given below. Transmembrane proteins are a form of integral membrane protein and are one of the most common classes of proteins in eukaryotes, comprising around 30% of known proteins.[44] Such proteins typically interact with lipid membranes through hydrophobic α-helical domains, anchoring them to the membrane. Membrane proteins must go through several processing steps before becoming fully functional.[45] They must be translocated to the endoplasmic reticulum (ER) membrane, followed by membrane insertion and any additional folding that is required, as well as any complexation with other proteins. Folding of transmembrane domains is often required to shield polar residues from the lipophilic membrane, particularly with multiple pass transmembrane regions. This can then be followed by transportation to the correct destination within the cell. Targeting of membrane proteins to the ER for initial processing can often happen in a co-translational manner *via* the signal recognition particle or other pathways, which utilise N-terminal signal motifs on the protein to identify transmembrane proteins during translation.[46]

Membrane proteins must reach their correct subcellular localisation if they are to perform their function, with multiple membrane compartments present within the cell.[45] Amino acid motifs, usually within the cytoplasmic domain of the protein, often play a role in subcellular targeting of transmembrane proteins. The nature of transmembrane domains themselves also play a part in determining the location of membrane proteins.[47,48] Proteins are secreted from the ER *via* the Golgi to the plasma membrane, or other membrane targets through the anterograde secretory pathway.[49] Transport of proteins occurs within specific vesicles, which can be transported to the plasma membrane *via* interactions with the cytoskeleton of the cell. Targeting and fusion of the vesicle to the destination membrane is influenced by the cargo protein, as well as vesicle and target membrane proteins.[50] Once in the target membrane, such as the plasma membrane, proteins are routinely recycled or internalised through the retrograde pathway. Proteins can be prevented from leaving the ER by the action of ER retention motifs within the amino acid sequence of the protein. Examples include the KKXX, RXR, KDEL and HDEL motifs.[51] Often found on the cytoplasmic domains of proteins, these various motifs differ in their regulatory purpose in a protein specific manner. Masking of these motifs, often through the formation of protein complexes or interactions with trafficking proteins, can allow exit from the ER and progression along the anterograde pathway.[52,53]

Many transmembrane proteins form complexes when associated with the lipid bilayer.[54] This could be due to diffusion-controlled interactions or specific interaction pathways bringing the various protein subunits together. Protein subunits that are not incorporated into their usual complex,

referred to as orphans, are prone to aggregation and subsequent degradation within the ER.[55] Proteins might not enter their normal complex because of the absence or reduced expression of a partner protein, or a premature interaction with another protein before the reaching the target complex. There are many cases of proteins that are degraded when not co-expressed with partner subunits. An example is the α subunit of the T cell antigen receptor, which is rapidly removed when not expressed with the other subunits that make up the functional receptor complex.[56] The degradation of orphan proteins can be due to inherent instability of the monomer. Exposure of polar side chains in the monomer transmembrane domains or cytoplasmic retention motifs are known triggers for degradation.[55] Alternatively, motifs normally shielded in the complex can lead to retention and degradation in the ER. An example of this phenomenon is the $GABA_B$ receptor, which is formed of the $GABA_B$ receptor 1 and $GABA_B$ receptor 2 subunits.[57,58] The interaction of the two subunits through a cytoplasmic coiled-coil interaction domain, while in the ER, leads to the masking of an ER retention motif (RSRR) within the $GABA_B$ receptor 1, permitting trafficking to the plasma membrane.[59,60] In the absence of the interaction with $GABA_B$ receptor 2, $GABA_B$ receptor 1 is retained in the ER and degraded. In the ER, embedded ubiquitin ligase complexes can target misfolded or orphaned transmembrane proteins for degradation before trafficking.[61] An alternative is that orphaned proteins are translocated into the ER lumen, due to exposed transmembrane domain polar residues disfavouring insertion into the lipid membrane, and are then subsequently degraded.[62] If transmembrane proteins are mislocalised to the cytoplasm they are degraded, including *via* ubiquitin-ligase pathways, after recognition of their transmembrane domains or other signalling motifs.[63]

1.5 The *POPDC* Genes

The Popeye domain containing (POPDC*)* gene family is comprised of three isoforms encoding *POPDC1* (also known as *BVES*), *POPDC2* and *POPDC3*. The members of this family were first identified by Reese *et al.* and Andreé *et al*.[64,65] The POPDC genes are highly conserved throughout nature, with vertebrates possessing all three members of the family. *POPDC2* and *POPDC3* display the greatest sequence similarity, with *POPDC1* being more distinct. The high conservation of the POPDC genes across species, including protozoa, suggests that there is a strong evolutionary pressure for their maintenance. Expression of these genes is most prominent in striated and cardiac muscle, with the muscular expression pattern inspiring the Popeye name.[65,66] *POPDC1* is expressed in both cardiac and skeletal muscle, *POPDC2* predominantly in cardiac tissue with a lesser skeletal presence, while *POPDC3* is mostly skeletal muscle specific.[67] Expression of the POPDC family is also observed in other tissues such as the smooth muscle of the gastrointestinal tract and bladder,[68] epithelial cells,[69] as well as the nervous system.[70] Within cardiomyocytes and skeletal muscle fibres, the POPDC proteins are localised to the plasma membrane, as well as t-tubules, intercalated disks and caveolae within

cardiomyocytes.[71,72] The plasma membrane localisation of Popdc1 and Popdc2 in mouse skeletal muscle, atrial and ventricular myocytes can be seen in Figure 1.1A, B and C, respectively.

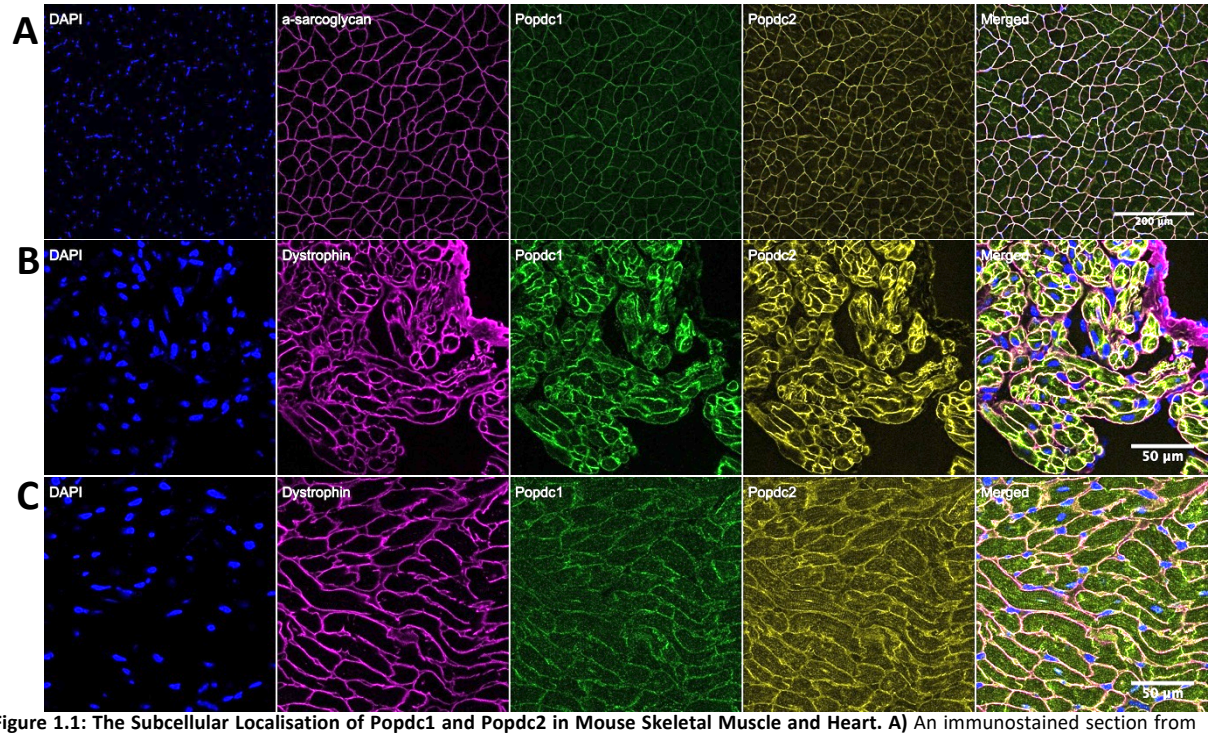


Figure 1.1: The Subcellular Localisation of Popdc1 and Popdc2 in Mouse Skeletal Muscle and Heart. A) An immunostained section from mouse skeletal muscle showing α-sarcoglycan as a sarcolemma marker, and also Popdc1 and Popdc2. All proteins are clearly localised to the sarcolemma, with minimal expression in the sarcoplasm. Sections from mouse heart atrium **(B)** and ventricle **(C)** immunostained to show dystrophin as a plasma membrane marker, as well as Popdc1 and Popdc2. Reasonable localisation to the plasma membrane is apparent, with expression of both Popdc1 and Popdc2 also seen in ventricular cardiomyocyte t-tubules. All images were kindly provided by Ursula Herbort-Brand.

1.6 Features of the POPDC Proteins

The POPDC proteins display a high degree of structural similarity across the family. POPDC1 and POPDC2 both possess around 360 amino acids, while POPDC3 is shorter at approximately 290 residues, while their theoretical masses are 41.5 kDa, 40.5 kDa and 33.9 kDa, respectively.[73] A fully empirical structure based on direct observations from x-ray crystallography, protein-NMR or cryogenic electron microscopy has not been determined for any member of the POPDC family.[74] However, a significant amount is known about their overall structure through biochemical investigations and modelling.[68,73] The models of human POPDC1, POPDC2 and POPDC3 deposited in the AlphaFold human proteome database are shown in Figure 1.2A-C. The POPDC proteins possess three transmembrane domains, which are preceded by an extracellular N-terminus of around 27-39 amino acids. All residues downstream of the transmembrane domains are found within the cytoplasm. This intracellular region contains the Popeye domain, a globular domain that is highly conserved between the different isoforms and is the defining feature of the POPDC protein family.[75] Each protein also contains a cytoplasmic C-terminal tail which shows reduced conservation within the POPDC family compared to other regions; indeed, a shortened C-terminal domain is the primary reason for POPDC3's

reduced length compared to POPDC1 and POPDC2. The structure of this C-terminal tail is predicted to be highly disordered, as seen in Figure 1.2D.

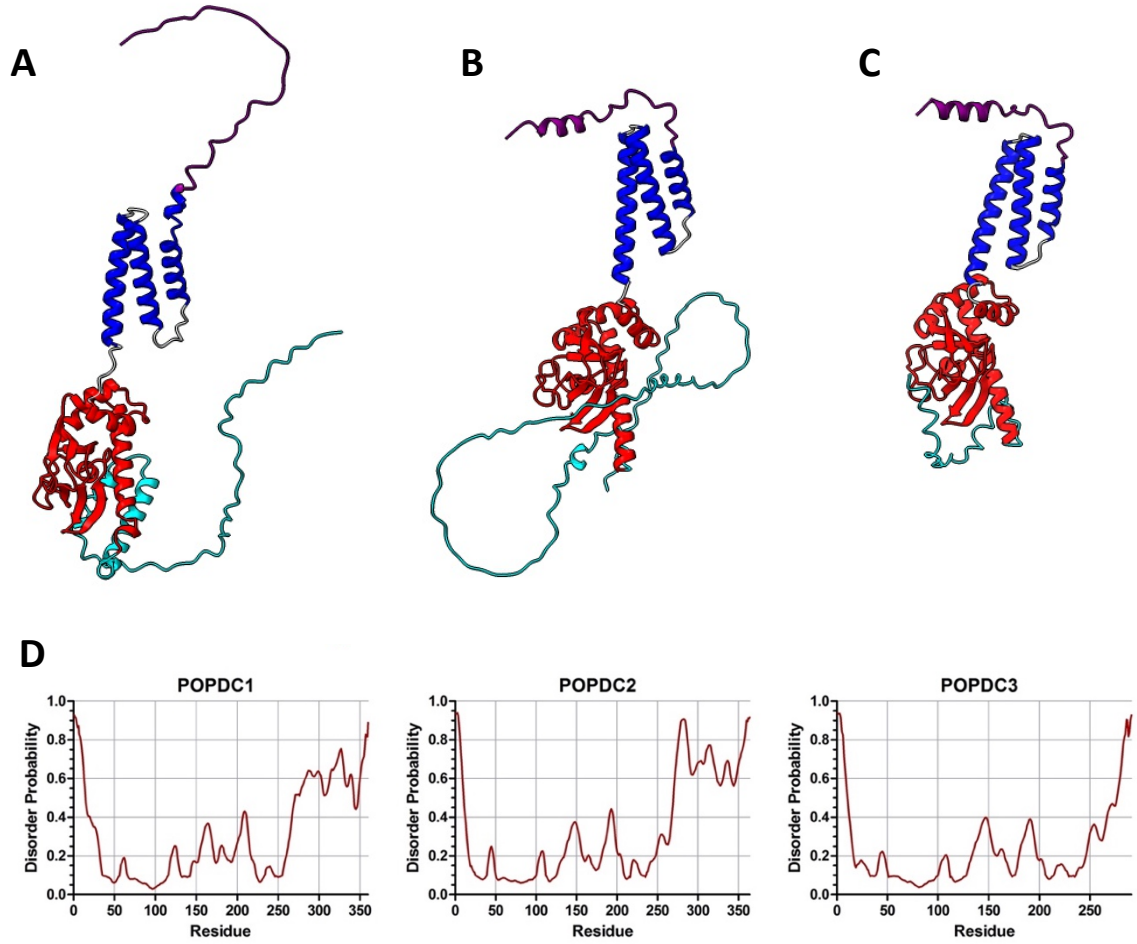


Figure 1.2: Structural Predictions of POPDC1, POPDC2 and POPDC3. The AlphaFold models of human POPDC1 (**A**), POPDC2 (**B**) and POPDC3 (**C**). The extracellular N-terminus is coloured purple, the transmembrane domains in blue, the Popeye domain in red and the C-terminal tail in cyan. **D**) Predictions of the level of disorder across human POPDC1, POPDC2 and POPDC3. The extracellular N-terminus and cytoplasmic C-terminus are predicted to display the greatest disorder, while the transmembrane and Popeye domains are likely to be highly structured. Predictions were made using the PrDOS server.[76]

The POPDC proteins are subject to post-translational modification, with two N-glycosylation sites identified in the extracellular N-terminal domain of POPDC1. [73,77] The role of glycosylation on the function of POPDC proteins is unknown, although the extent of glycosylation appears to be tissue specific. It has also been suggested that serine/threonine phosphorylation can occur within the cytoplasmic portion of the POPDC proteins.[78]

1.7 Structural Studies of the POPDC Proteins

The structure of POPDC proteins has been determined predominantly from modelling, as well as biochemical studies,[68,73] and this lack of an empirical structure has inhibited understanding of POPDC function and behaviour.[74] As a transmembrane protein, POPDC proteins are difficult to isolate in their native form meaning that structural studies to date have utilised isolated Popeye domain or

cytoplasmic sequences. Attempts to produce forms of the Popeye domain that would be suitable for x-ray crystallography studies have failed, despite a wide range of constructs being trialled.[79] This was due to the poor expression, purification or stability of the various constructs that were tested. Protein-NMR trials have also been conducted using a construct based upon the Popeye domain of mouse Popdc1.[80] Again, it was found that poor stability of the construct meant that it was not suitable for detailed structure analysis of the Popeye domain, with likely conformational exchange occurring in solution. Attempts to produce constructs suitable for empirical structural studies of the Popeye domain are discussed in more detail in Chapter 3.

1.8 Oligomerisation of the POPDC Proteins

Homo-oligomerisation of the POPDC proteins was first identified by Knight *et al*.[73] FLAG-tagged mouse Popdc1 was expressed in COS-7 cells and analysed using Western Blots. It was found that, as well as the monomeric form, a significant amount of the Popdc1 construct ran as higher order oligomers. The determination of stoichiometry was complicated by the presence of glycosylation, leading to species of varying molecular weight, but it was estimated that only 20% of Popdc1 was present in the monomeric form. Exposing the samples to reducing conditions caused the monomeric form to dominate, due to presumptive dissociation of the higher order oligomers. The sensitivity of Popdc1 oligomers to reducing conditions was confirmed by Vasavada *et al*.[77]

Co-immunoprecipitation of full-length Popdc1 with a series of truncation mutants was used to localise the interface between Popdc1 monomers.[73] It was found that co-immunoprecipitation of Popdc1 was possible when using a construct containing only the residues of the Popeye domain and C-terminal tail of Popdc1. Further work has suggested that residues 268-274, immediately C-terminal to the Popeye domain, are particularly important for Popdc1-Popdc1 complex formation.[81]

It has been found that after co-expressing Popdc1 and Popdc2 in COS-7 cells and analysing lysates by Western blot that probable Popdc1-Popdc2 heterodimers were present.[82] Bands corresponding to the mass expected of a Popdc1-Popdc2 tetramer, formed of two Popdc1 units and two Popdc2 units, were also present. This possible tetramer did not survive reducing conditions; however, the Popdc1-Popdc2 heterodimer remained and even increased in relative intensity. Heterodimers and possible heterotetramers of Popdc1 and Popdc3 were also observed, although not between Popdc2 and Popdc3. Deletion mutants were used to determine that interactions between POPDC proteins could occur within the N-terminal region and/or transmembrane domains, as well as the cytoplasmic region containing the Popeye domain. It was also found that POPDC2 truncated to residue W188, matching a mutant identified in patients that lacks the majority of the cytoplasmic region of the protein, is able to homodimerize, as well as interact with wildtype Popdc2 and Popdc1.[82] It appears that the removal

of either the N-terminus/transmembrane domains or cytoplasmic part of the protein does not completely prevent oligomer formation.[81,82] The role of each of the putative interaction sites identified is not known and, while oligomerisation may be possible in the absence of one interface, differences within the resulting complex may lead to POPDC dysfunction.

1.9 The POPDC Proteins and the cAMP Pathway

1.9.1 The cAMP Pathway

3',5'-cyclic adenosine monophosphate (cAMP) is a ubiquitous second messenger molecule involved in many cellular processes. cAMP is synthesised by adenylyl cyclases (AC) from adenosine-5'-triphosphate (ATP), with pyrophosphate produced as a by-product.[83] ACs are stimulated in response to the activation of G-protein coupled receptors (GPCRs), such as the β-adrenoceptors. GPCRs are transmembrane receptors that are intracellularly coupled to heterotrimeric G proteins, formed of α, β and γ subunits.[84] When the GPCR is activated by an extracellular ligand it releases the Gα protein, dependent on the binding of GTP to the Gα protein. Gα proteins can be classed as $G\alpha_s$ or $G\alpha_i$, which bind to and then activate or inhibit AC, respectively.[84] $G\alpha_q$ proteins are also present but generally work independently of the cAMP pathway. When $G\alpha_s$ couples to an AC the rate of cAMP production is increased. cAMP is then able to bind to the various cAMP effector proteins, such as protein kinase A (PKA) and exchange factor directly activated by cAMP (EPAC), and so initiate further signalling events. PKA, the first cAMP protein to be identified, phosphorylates target proteins in response to cAMP binding. PKA is a tetrameric holoenzyme, consisting of two regulatory and two catalytic subunits. Binding of cAMP to its regulatory subunits disinhibits the catalytic domains, possibly through dissociation, which can then phosphorylate other proteins.[85] cAMP is hydrolysed by the phosphodiesterase (PDE) enzymes to adenosine 5'-monophosphate (AMP), which limits cAMP signalling by lowering the concentration of cAMP.[86]

The activation of a wide range of GPCRs can lead to the production of cAMP within the cell. Despite their common cAMP-based signalling mechanism, stimulation of the different receptors leads to specific downstream responses. Several factors have been used to explain the apparent disparity between cAMP's ubiquity as a signalling molecule, and the many discrete responses it can specifically elicit, even within a single cell. There are ten known AC isoforms, and eleven families of PDE enzymes.[86,87] These isoforms display varying tissue and subcellular localisation, and their specific activation or inhibition leads to different effects, demonstrating their unique roles. However, the different members of the AC and PDE family perform the same basic functions as each other, necessitating further mechanisms to explain their disparate activation by specific GPCRs and subsequent effects on the cell. This has been partially explained by the complexation of components of the cAMP pathway.[88] The formation of signalling complexes containing AC, PDE and cAMP effectors,

such as PKA, allows each member of the complex to have a disproportionate impact on its neighbours compared to other proteins throughout the cell. These complexes are usually dependent on the role of A-kinase anchoring proteins (AKAPs), which act as a membrane associated scaffold for the complexes.[88] These complexes can also be associated with individual GPCR receptors, providing a means of signalling specificity downstream of the various $G\alpha_{s/i}$ linked GPCRs.[89] Therefore a particular combination of GPCR, AC, PDE, PKA (or other cAMP effector) can be constructed at a specific subcellular location, providing a unique signalling module that will lead to only a specific downstream effect, despite relying on cAMP signalling. The increases in cAMP concentration after GPCR stimulation are usually confined to the region around the receptor and associated signalling complex, which is necessary to avoid stimulation of cAMP pathway members in other complexes.[90] To limit the spread of cAMP from sites containing activated AC, which as a small molecule should efficiently diffuse through the cytosol, a number of mechanisms may be employed. PDE mediated hydrolysis of cAMP has been shown to be essential for the spatiotemporal control of intracellular cAMP concentrations, where cAMP is locally degraded before diffusing into the wider cell.[86] However, this effect may not be sufficient to control cAMP diffusion by itself.[90] The sequestering of cAMP in the binding sites of PKA, or other proteins, may act as local cAMP sinks, greatly reducing the levels of freely diffusible cAMP emanating from cAMP signalling nanodomains.[90,91] This would then allow the action of PDEs to control the spread of the remaining free cAMP. The liquid-liquid phase separation of PKA has also been shown to influence compartmentation of cAMP.[92] This need to contain cAMP to discrete regions within cells makes the interactions and spatial organisation of proteins within the various controlled cAMP pathways highly important, with disruption of cAMP signalling complexes associated with pathway dysfunction.

A simplified schematic of the cAMP pathway is shown in Figure 1.3. This includes some examples of the proteins involved in cAMP signalling. POPDC proteins are included, although their exact role in cAMP signalling is still under investigation, as discussed below. In addition, some of the specific cAMP pathway proteins found to interact with POPDC proteins, also discussed below, are included.

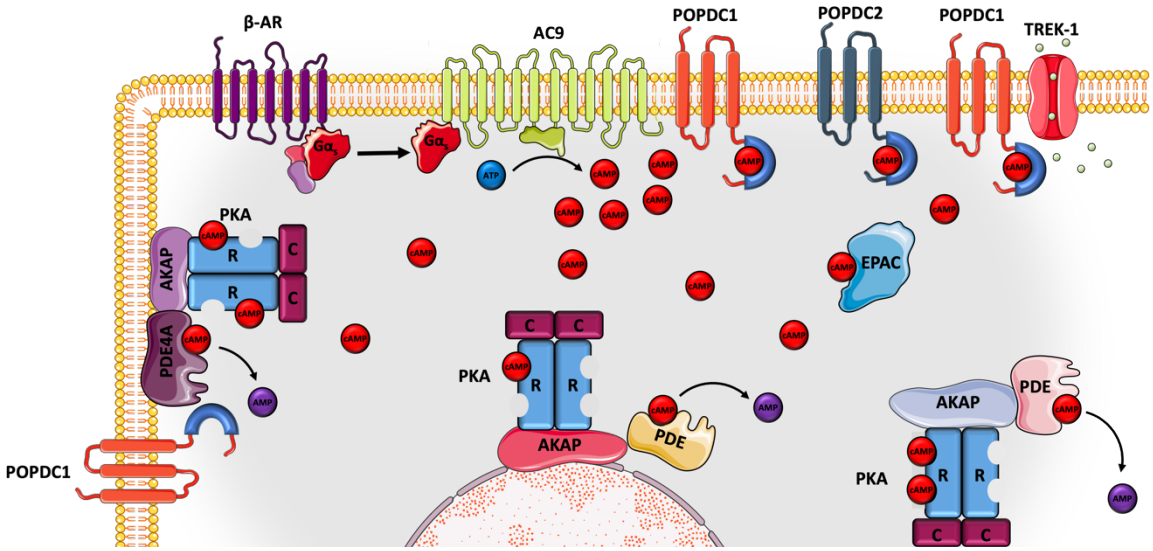


Figure 1.3: A simplified model of the cAMP pathway including POPDC1 and POPDC2. cAMP is generated by AC (such as AC9) in response to $G\alpha_s$ signalling downstream of GPCR activation (such as the β-AR receptors). cAMP can diffuse to bind to cAMP effector proteins, but spatial control occurs so that cAMP nanodomains form (grey area) containing locally increased cAMP concentrations. cAMP diffusion is at least partially controlled by hydrolysis to AMP by PDEs. cAMP stimulates cAMP effectors such as PKA or EPAC, leading to activation of various downstream pathways. The regulatory and catalytic subunits of PKA are labelled as R and C, respectively. AKAPs anchor members of the cAMP pathway allowing for further spatial control of signalling. The POPDC proteins are known to interact with AC9 and PDE4A, modulating the cAMP pathway. Other proteins, such as TREK-1, seem to be influenced by the activity of POPDC proteins in a cAMP responsive manner. The full role of POPDC proteins within the cAMP pathway is unknown, and the make-up of various protein complexes are still uncertain. This figure only provides an approximate model and is not an exhaustive representation of cAMP signalling pathways, including or separate to the POPDC proteins. This figure was adapted from Swan *et al*.[74] under a Creative Commons CC BY license.

1.9.2 POPDC Proteins Bind cAMP

POPDC proteins are predicted to contain a cyclic nucleotide binding domain (CNBD) within the Popeye domain, and indeed were found to bind to cAMP, despite the Popeye domain having low sequence homology to other known CNBDs.[71] A model of the Popeye domain is shown in Figure 1.4A, with the features predicted to resemble those found in classical CNBDs highlighted. The most closely related CNBD is that of the prokaryotic cyclic AMP receptor proteins (CRP, also known as catabolite activator protein, CAP), which has approximately 20% sequence homology to the Popeye domain.[71] The divergent consensus sequences of the cAMP binding sites in the Popeye domain and canonical CNBDs are shown in Figure1.4C and D. This suggests a distinct evolution of the POPDC proteins compared to other CNBDs containing proteins, such as PKA and EPAC. Despite this lack of sequence homology, secondary structure predictions of the Popeye domain show a high degree of similarity to established CNBDs, as shown by the overlays in Figure 1.4B.[71] Early homology modelling of the Popeye domain was performed using a CRP protein from *Streptomyces coelicolor* (PDB: 2PQQ) as a template, with further refinement carried out using the CNBD of regulatory II subunit of PKA (PDB: 1CX4).[71] This identified a putative phosphate binding cassette within the Popeye domain, a key feature of CNBDs. However, like all of the Popeye domain, this PBC was highly divergent in sequence from those seen in classical CNBDs. This putative PBC contained two motifs super-conserved across the POPDC family: FL/IDSPEW/F and FQVT/S. To examine the potential cyclic nucleotide binding of the Popeye domain a number of experiments were performed. Full-length murine Popdc1, Popdc2 and Popdc3

protein were shown to bind to cAMP-conjugated agarose, with specific elution achieved through addition of cAMP in the eluent.[71] To investigate the role of the putative PBC motifs on the binding of cAMP, Popdc1 was expressed with a number of point mutations and binding to the cAMP-agarose re-examined. Within the FL/IDSPEW/F motif, a D200A point mutant showed a 90% reduction in cAMP binding, while a E203A variant showed an intermediate effect. A P202A mutant showed no reduction in cAMP binding affinity. It was subsequently shown that a S201F mutant, which has been found in patients, shows approximately 50% lower cAMP affinity compared to wildtype Popdc1.[93] In Popdc2, a D184A mutant, equivalent to the D200A mutant in Popdc1, also showed a large drop in cAMP affinity.[71] Within the FQVT/S motif of Popdc1, a V217A mutant showed a modest drop in cAMP affinity. To further confirm cAMP binding to the Popeye domain, a radioligand assay was performed using a recombinant construct of Popdc1 containing the cytoplasmic region (the Popeye domain and C-terminal tail). This assay yielded an affinity for cAMP of 118 nM, with around a 40-fold selectivity over guanosine 3',5'-cyclic monophosphate (cGMP).[71]

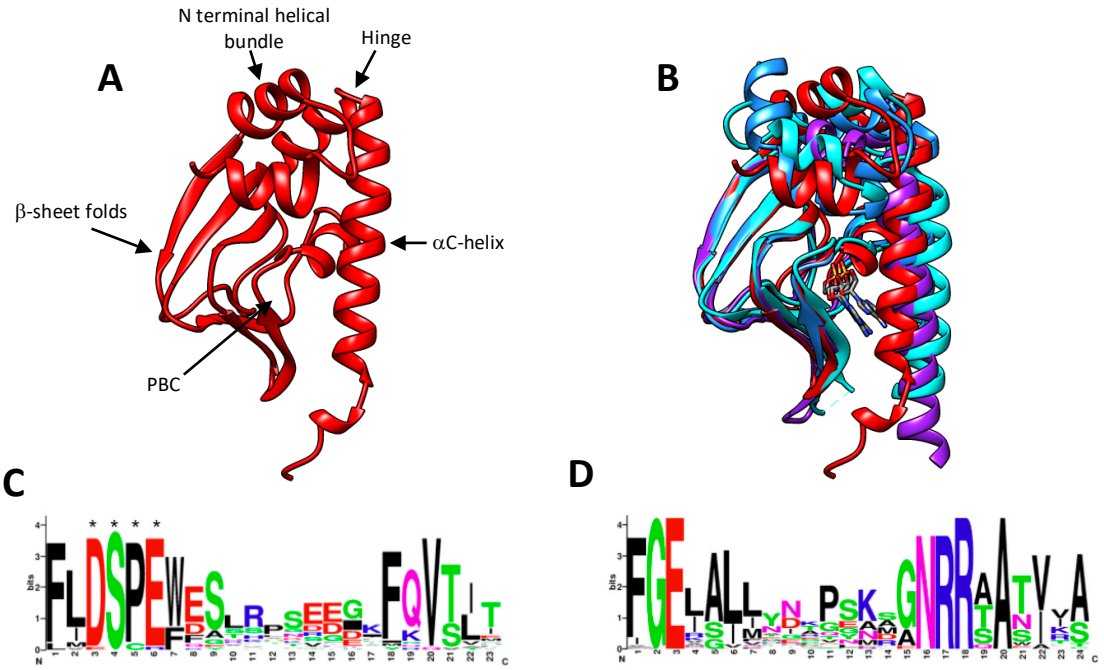


Figure 1.4: The Structure of Classical CNBDs and the Popeye Domain. A) A model of the Popeye domain from the AlphaFold model of full length POPDC1. The areas of the Popeye domain structure that are thought to correspond to the features of canonical CNBDs are labelled. **B)** An overlay of the Popeye domain model with the known structures of the CNBDs of PKA RIIβ (cyan, PDB: 1CX4), CAP (purple, PDB: 2CGP), HCN4 (blue, PDB: 1Q43). cAMP bound to the non-Popeye domain structures is shown, with the cAMP binding pocket likely to be found in a similar position within the Popeye domain. The consensus sequences logos of the PBC of the Popeye domain **(C)** and canonical CNBDs **(D)** are shown, highlighting the low sequence homology between them. The Popeye domain's characteristic FL/IDSPEW/F and FQVT/S motifs are not present in canonical CNBDs. The canonical CNBD consensus sequence logo was retrieved from: https://prosite.expasy.org/PDOC00691, while the Popeye domain logo was generated using the https://prosite.expasy.org/scanprosite/ tool using the 'Popeye' identifier.

Froese *et al.* performed docking experiments of cAMP to the homology model of the Popeye domain.[71] In agreement with the mutagenesis results, it predicted close contacts between bound cAMP and the FL/IDSPEW/F and FQVT motifs of the Popeye domain giving further evidence that the FL/IDSPEW/F

and FQVT/S motifs form part of the PBC. The exact mode of cAMP binding to the Popeye domain has not been empirically confirmed with protein-NMR or related techniques, with the sequence differences between canonical CNBDs making predictions more uncertain. Canonical CNBDs in cAMP effectors such as PKA and EPAC have a highly characteristic structure, examples of which are shown in Figure 1.4B. CNBDs typically contain a PBC, a helical bundle towards the N-terminus of the domain, a jelly-roll β-barrel fold and a hinge followed by a lid formed of an α-helix known as the C-helix.[94,95] The PBC is usually formed of a short loop, an α-helix and two β-sheets, which each form an interaction with the bound cyclic nucleotide. A change in conformation of the PBC upon binding of a cyclic nucleotide releases steric strain which leads to a reorientation of the hinge and C-helix. The reoriented C-helix interacts with the base of the nucleotide, shields the binding pocket from solvent, and leads to allosteric effects on the protein, which results in activation.[94,95] In PKA, cAMP leads to the partial or full dissociation of the catalytic subunits from the holoenzyme resulting in their activation.[85] In EPAC, cAMP binding relieves autoinhibition of the catalytic domain as a result of its interaction with the CNBD containing regulatory domain.[96,97]

The acute structural and functional effects of cAMP binding on the Popeye domain have not yet been determined, mainly due to the absence of crystallographic or NMR-derived structures of the Popeye domain.[74] The homology model of the Popeye domain of Popdc1 built by Froese *et al.*, and subsequent models, predict the presence of an α-helix towards the C-terminal region of the Popeye domain, known as the αC-helix, which is labelled in Figure 4.1A.[71] This could act in an analogous fashion to the C-helix found in classical CNBDs. β-sheets, resembling those found in canonical CNBDs, are also predicted. However, the detailed structure of the Popeye domain is still unknown given the reliance of homology modelling. The low sequence homology of the Popeye domain and the template sequences used to construct the models reduces confidence in the predicted secondary structure. The templates on which Popeye domain models are built usually consist of canonical CNBDs, despite their low sequence similarity, which may lead predictions biased towards known CNBD structures, although more recent *ab initio* modelling methods may reduce this effect. There is, therefore, a need for an empirically derived structure of the Popeye domain.[74,98]

The study of cAMP binding and phenotyping of full-length POPDC proteins containing mutations within the Popeye domain has provided some information on the binding mode of cAMP. The alanine substitutions carried out by Froese *et al.*, as described above, demonstrated the importance of the putative PBC containing the FL/IDSPEW/F and FQVT/S motifs.[71] Further evidence was demonstrated by the reduced cAMP binding affinity of a pathological p.S201F mutation identified in a small number of patients.[93] Modelling of the S201F variant of POPDC1 suggested the loss of a H-bond between the

hydroxyl group of the serine side chain and the 2'-OH group of cAMP.[96] The loss of this possible interaction, along with the increased steric hindrance of the larger phenylalanine residue, may explain the reduction in cAMP binding affinity of the S201F mutant. A recently reported pathological mutation in POPDC3 (c.464T>A, p.L155H), was shown to be insensitive to cAMP.[99] L155 is not within the highly conserved FL/IDSPEW/F and FQVT/S motifs of the Popeye domain that have been identified as being particularly important in the mechanism of cAMP binding. There is uncertainty in how this substitution negatively impacts cAMP binding affinity, given the lack of knowledge regarding the position of L155 within the Popeye domain, but may be due to allosteric effects.

1.9.3 Protein-Protein Interactions of POPDC Proteins within the cAMP Pathway

The POPDC proteins have been reported to directly interact with multiple proteins, including members of the cAMP pathway. These provide an insight into the possible roles of the POPDC proteins in cAMP signalling. Some of these interactions are discussed below.

1.9.3.1 POPDC1 and PDE4A

It was recently reported that POPDC1 directly interacts with phosphodiesterase 4A (PDE4A).[100] POPDC1 and PDE4A were found to colocalise in rat cardiomyocytes through a PLA. A further Co-IP experiment confirmed a direct interaction between the two proteins. POPDC1 showed a high degree of selectivity for PDE4A compared to other PDE4 isoforms. The interaction site between the two proteins was mapped using peptide array techniques, which suggested a RLSILLK motif between R172 and K178 of POPDC1 was essential for the interaction. A POPDC1 binding site in the UCR1 region of PDE4A was found using the same method.

Inhibition of PDE4A with rolipram led to a reduction in the known interaction between POPDC1 and TREK-1 (a two pore domain potassium channel, see below).[100] To further investigate the function of the POPDC1-PDE4A interaction a cell-permeable disrupting peptide was developed, targeted to the RLSILLK motif of POPDC1. Disruption of the interaction did not alter the cAMP hydrolysis activity or PKA-mediated phosphorylation of PDE4A *in vitro*. This suggests that PDE4A may be able to modulate POPDC1 function by reducing the local concentration of free cAMP that can bind to the Popeye domain. In addition, an elongation of the repolarisation of isolated atrial rat cardiomyocytes was observed in response to the addition of the disrupting peptide suggesting the POPDC1-PDE4A interaction is involved in modulating the cardiac conduction cycle.

1.9.3.2 POPDC1 and Adenylyl Cyclase 9

POPDC1 has also been found to interact with adenylyl cyclase 9 (AC9).[101] AC9 is expressed in the sinoatrial node (SAN) and, although its full role is not clear, it has been shown to influence the resting heart rate of mice.[102] PLA, BiFC and Co-IP assays showed the presence of an interaction between

recombinant POPDC1 and AC9 in human embryonic kidney 293 (HEK293) cells. TREK-1 was also found to interact with AC9. It appears likely that POPDC1, TREK-1 and AC9 form a whole or partial complex that is involved in cAMP signalling.[101] Using FRET and BiFC techniques it was found that TREK-1 dissociates from this complex in a cAMP responsive manner, and that this response requires the presence of active AC9 and POPDC1. It was concluded that POPDC1 acts as a scaffold for AC9, ensuring correct localisation and function within specific cAMP nanodomains. As such, POPDC1 may modulate TREK-1 currents in response the β-adrenergic signalling and subsequent AC9 stimulation.

1.9.3.3 POPDC Proteins and TREK-1

POPDC1 has been found to interact with the two-pore domain potassium channel TREK-1,[71] which is expressed in cardiomyocytes.[103] POPDC2 and POPDC3 may also interact with TREK-1. TREK-1 is expressed in the SAN and likely plays a role in cardiac pace-making through regulation of SAN excitability.[104] When Popdc1, Popdc2 or Popdc3 are co-expressed with TREK-1 in *Xenopus* oocytes, the outward current of TREK-1 increases above levels observed in the presence of TREK-1 alone.[71] It is thought that this increase in current is due to the enhanced surface expression of TREK-1, suggesting that the POPDC proteins promote the trafficking of TREK-1 to the plasma membrane. It was found that an increase in cAMP concentrations within the *Xenopus* oocytes abolished the POPDC-mediated TREK-1 current increase.[71,93] This is likely to be due to cAMP binding to the POPDC protein, as it was found that the TREK-1 current was not reduced in response to a raised cAMP concentration when co-expressed with the POPDC1 p.S201F variant, which shows reduced cAMP binding affinity.[93] However, the TREK-1 current at basal cAMP concentrations was significantly increased in the presence of POPDC1 p.S201F compared to wildtype POPDC1. This suggested that cAMP binding to POPDC1 has an inhibitory effect on TREK-1 current. In contrast, it was found that when TREK-1 was co-expressed with the POPDC2 p.W188X truncation mutant no increase in current compared to TREK-1 alone occurred.[105] A cAMP-responsive interaction between Popdc1 and TREK-1 was demonstrated through the use of a bimolecular FRET assay within HEK293 cells.[71,93] The FRET signal recorded after co-expression of Popdc1-CFP with YFP-TREK-1 showed a small, acute, dose-dependent reduction upon application of isoproterenol or forskolin. This cAMP dependent change in FRET signal was reduced in the presence of the Popdc1 p.D200A and p.S201F variants. This suggests that POPDC proteins are required for efficient trafficking of TREK-1 to plasma membranes, but that cAMP induces a change in the Popdc1-TREK-1 interaction, which leads to an inhibition of TREK-1 current.

The interactions between POPDC proteins, PDE4A, AC9 and TREK-1 may be part of a common signalling complex, demonstrating the importance of the spatial distribution of the components of the cAMP pathway. However, the true nature of such a complex is unknown. TREK-1 is also known to

interact with the AKAP79 and be a target of PKA, suggesting the involvement of other proteins in this putative signalosome.[106]

1.9.4 Summary of Possible Roles of POPDC Proteins within the cAMP Pathway

A number of models have been proposed to describe the role of the POPDC proteins within the cAMP pathway, which are visualised in Figure 1.5.[74] The switch model suggests that the interaction of POPDC proteins with proteins such as TREK-1 could lead to their direct activation or inactivation, perhaps in a cAMP-dependent manner. As such, cAMP binding to POPDC proteins may act as a trigger for the activity of other proteins. If this is the case, the suggestion that PDE4A mediates the level of cAMP binding to POPDC proteins adds a further layer of regulation.[100] The sponge model states that POPDC proteins may be involved in the modulation of cAMP signalling by acting as a cAMP buffer within the cell, in a similar way as has been proposed for PKA. This would contribute to the spatial and temporal control of cAMP concentrations known to be required for specific signalling. The cargo model places the importance of POPDC proteins towards their role in trafficking proteins involved in the cAMP pathway to the correct subcellular location, mostly the plasma membrane. An example would be TREK-1, whose POPDC dependent increase in current in *Xenopus* oocytes is thought to be, at least in part, due to greater surface expression of the channel as a result of POPDC activity.[71] This could also be extended to other known protein partners of the POPDC proteins outside of the cAMP pathway. The recent finding that POPDC1 controls the association of TREK-1 and AC9, in addition to interactions with PDE4A, means that POPDC proteins may be acting as a scaffold, bringing together members of the cAMP pathway into complexes required for normal signalling.[101] Loss of POPDC proteins may lead to the disruption of such signalosomes, which are required for the strict spatial control of cAMP signalling. While the true nature of the POPDC protein's role remains unclear, these models provide a starting point for considering the phenotypes seen in animals and patients when POPDC proteins are lost or mutated.

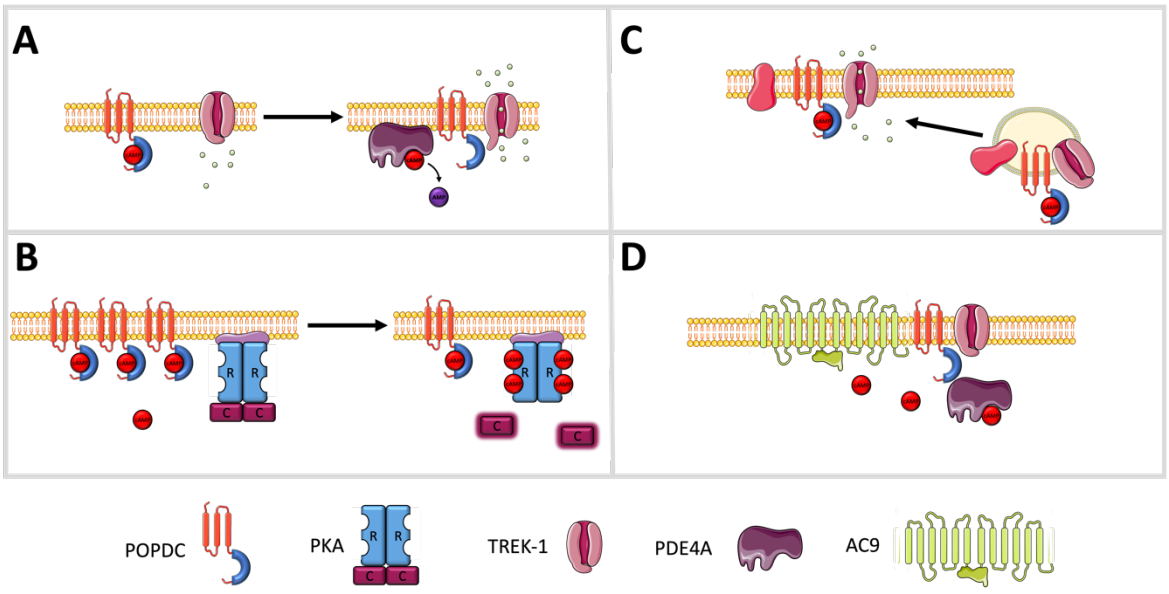


Figure 1.5: Models of POPDC Function within the cAMP Pathway. Simplified schematics of some of the proposed models of POPDC protein function within the cAMP pathway: the switch **(A)** model, sponge model **(B)**, cargo model **(C)** and scaffold model **(D)**. The partner proteins shown are not exhaustive and are shown as possible examples. This figure was adapted from Swan *et al.* [74] under a Creative Commons CC BY license.

1.10 POPDC Proteins in Disease

1.10.1 Overview of Striated Muscle

POPDC dysfunction is linked to problems in skeletal muscle and cardiac dysrhythmias, as described below. Skeletal muscle is formed of bundles of multinuclear muscle fibres, arranged longitudinally along the muscle. Within the muscle fibres are many myofibrils, formed primarily of actin and myosin, which form the basic contractile units of muscle.[107] Contraction of muscle is stimulated by depolarisation, propagated by action potentials along membrane surfaces. Muscle fibres are around 100 nm in diameter and up to 1 cm in length. They are surrounded by their plasma membrane, known as the sarcolemma. The cytoplasm of muscle fibres is referred to as the sarcoplasm. Plasma membrane and cytoplasm are used interchangeably with sarcolemma and sarcoplasm, respectively, in this work. Many proteins are found in complexes at the sarcolemma, which provide the connection between intracellular and extracellular proteins that is essential for muscle fibre contraction.[107] Loss of a member of these complexes can lead to the development of muscular dystrophies, which are associated with the progressive onset of muscle weakness caused by the degeneration of muscle fibres.[108] Limb girdle muscular dystrophy (LGMD), has been linked to mutations in the sarcoglycan proteins. These consist of α-, β-, γ-, and δ-sarcoglycan and form the sarcoglycan complex, which resides at the plasma membrane, and is essential for transduction of mechanical information and regulation of muscle contractions.[109] Interestingly, if one member of the sarcoglycan family is absent, or mutated, the entire sarcoglycan complex will be lost from the sarcolemma.[110] α-Sarcoglycan is used

as a marker for the sarcolemma in skeletal muscle biopsy section staining in this work. Many more proteins are present at the plasma membrane of muscle fibres, some of which will be mentioned briefly below.

Cardiac muscle is also a form of striated muscle, although the constituent cells, cardiomyocytes, differ to muscle fibres.[111] Cellular membrane surfaces known as t-tubules, which appear as striations along cells, are important for propagation of action potentials.[112] Initial depolarisation of the heart occurs in the SAN, followed by conduction of the action potential across the atria, then to the ventricles *via* the atrioventricular node (AVN). The changes in charge involved in the spread of action potential are mediated by the influx and efflux of ions including Na^+, K^+ and Ca^{2+}.[111] This means that ion channels in the plasma membrane of cardiomyocytes play a key role in cardiac physiology. Dysfunction of these channels may lead to cardiac dysrhythmias, where the normal depolarisation and repolarisation events involved in the control of heartbeats are altered.

cAMP signalling is a key pathway for the control of heart function, most notably downstream of the β-adrenoceptor GPCRs. Activation of β-adrenoceptors in the heart, and subsequent cAMP signalling, influences heart rate, with dysregulation linked to cardiac hypertrophy and changes in the response to stress and hypoxia.[113] The activity of skeletal muscle is also mediated by cAMP signalling, problems with which have been associated with muscular dystrophy.[114]

1.10.2 POPDC Protein-Protein Interactions in Striated Muscle

Caveolae are invaginations found on the surface of cardiomyocytes and skeletal muscle, which are implicated in a number of cellular processes.[115] They are involved in vesicular trafficking, mechanotransduction and cAMP signalling via β-adrenergic receptors. Popdc1 was found to interact with caveolin-3, a key component of caveolae.[72] Loss of Popdc1 in mice led to a decrease in the number of caveolae and changes in the size of the heart. Greater sensitivity to oxidative stress, reduced heart recovery after ischaemia and impaired Ca^{2+} signalling were also observed. This suggests that the presence of POPDC proteins at the surface of cardiomyocytes and skeletal muscle fibres, particularly within caveolae, is essential for normal function and recovery.

Dysferlin, a plasma membrane protein involved in sarcolemma repair and skeletal muscle regeneration, which is linked to LGMD,[116] has been found to interact with POPDC1.[71] The loss of dyferslin sarcolemma localisation was observed in the skeletal muscle of patients possessing two different *POPDC1* mutations.[117] POPDC1 has been reported to interact with anoctamin-5, which is involved in the repair of the plasma membrane of skeletal muscle.[118] POPDC1 has been found to directly interact with VAMP3, which is involved in mediating vesicular transport.[119] VAMP3 is involved with β-1-integrin recycling from the plasma membrane, which was found to be impaired in the

absence of POPDC1.[119] This further indicates the importance of POPDC for normal function of the skeletal muscle plasma membrane. In addition, XIRP1, a protein involved in the function of intercalated disks in cardiomyocytes, was found to be a partner of POPDC1 and POPDC2.[120] The relevance of POPDC protein's involvement in cAMP signalling in the mediation of the function of these protein partners is not fully understood.

1.10.3 POPDC Proteins in Cardiac and Skeletal Muscle Disease

To help determine the function of the POPDC proteins both, *Popdc1*$^{-/-}$ and *Popdc2*$^{-/-}$ null mice models were created.[71] While both knock-out models are viable they each display an age-dependent stress-induced sinus bradycardia dysrhythmia. Skeletal muscle and cardiac effects are also seen in zebrafish after *popdc* gene mutation or knock-down.[93,121] In addition, *Popdc1*$^{-/-}$ mice display an increased intolerance to ischaemia reperfusion in the heart compared to wildtype mice.[72] A number of mutations in *POPDC1*, *POPDC2* and *POPDC3* have been identified in patients, shown in Table 1.1. The range of symptoms exhibited by these patients provide further evidence for the physiological role of the POPDC proteins. In general, mutations identified in *POPDC1* lead to both a cardiac dysrhythmia, usually an AV-block, in addition to LGMD.[93,117,122,123] The only currently identified mutation in *POPDC2* (c.563G>A, p.W188X), led to an AV-block but no major skeletal muscular phenotype.[105] In contrast, all patients found to possess a *POPDC3* mutation display only LGMD but no clear cardiac arrythmia.[99,124] Raised creatine kinase (CK) levels in serum in patients further indicates muscle damage. The range of phenotypes between the three isoforms likely reflects their differential expression in cardiac and skeletal muscle.[67] A variety of mutation types in POPDC genes have been identified, including missense, nonsense and deletions. The effect of these mutations appears to be broadly consistent, suggesting that a common pathological mechanism is initiated in the presence of the different types of mutation. Furthermore, the knock-out animal models show similar phenotypes to patients with single residue missense mutations. This indicates that the loss of specific, single residues is enough to prevent POPDC function, mimicking a situation where no protein is present. The position of such missense mutations may provide evidence for the role of particular domains within the POPDC proteins. The POPDC1 (c.602C>T, p.S201F) mutation, discussed above, which is known to display a reduced cAMP binding affinity, is one of the known mutations found in patients.[93] Patients display a similar phenotype to those with other mutations, suggesting that the loss of cAMP binding to POPDC1 is sufficient to lead to disease. The downregulation of POPDC1 has been linked to heart failure, as well as being linked to changes in the duration of the cardiac conduction cycle.[125-127]

Table 1.1: A table showing the mutations in POPDC genes identified in patients, as well as POPDC gene knock-out or knock-down animal, and their general skeletal muscle and cardiac phenotype.

	Species	POPDC Mutation	Cardiac Phenotype	Skeletal Muscle Phenotype	Reference
Animal Models	Mouse	*Popdc1*$^{-/-}$	Stress-induced sinus bradycardia	Reduced regeneration	71
	Mouse	*Popdc2*$^{-/-}$	Stress-induced sinus bradycardia	None	71
	Mouse	*Popdc2* (c.563G>A, p.W188X)	Stress-induced sinus bradycardia	None	105
	Zebrafish	*Popdc1* morpholino knock down	AV-block	Muscular dystrophy	93
	Zebrafish	*Popdc1* (c.572CT>TC, p.S191F)	AV-block	Muscular dystrophy	93
	Zebrafish	*popdc2* morpholino knock down	AV-block	Impaired development	121
Patients	Human	*POPDC1* (c.1A>G, p.X)	AV-block	Myalgia, raised CK	122
	Human	POPDC1 (c.262C>T, p.R88X)	AV-block	LGMD, raised CK	122
	Human	POPDC1 (c.275A>G, p.D92G)	None	EDMD	128
	Human	POPDC1 (c.427A>T, p.R143X)	AV-block	LGMD, raised CK	129
	Human	POPDC1 (c.457C>T, p.Q153X)	AV-block	Myopathy, raised CK	117
	Human	POPDC1 (c.578T>G, p.I193S)	Sinus bradycardia	Raised CK	117
	Human	POPDC1 (c.602C>T, p.S201F)	AV-block	LGMD, raised CK	93
	Human	POPDC1 (c.816+2T>C, p.V217-K272del)	AV-block	LGMD, raised CK	122
	Human	POPDC1 (c.788C>A, p.S263X)	AV-block	LGMD, raised CK	123
	Human	POPDC2 (c.563G>A, p.W188X)	AV-block	Possible raised CK	105
	Human	POPDC3 (c.460A>G, p.K154E)	None	LGMD, raised CK	124
	Human	POPDC3 (c.464T>A, p.L155H)	None	LGMD, raised CK	99
	Human	POPDC3 (c.651A>T, p.L217F)	None	LGMD, raised CK	99
	Human	POPDC3 (c.782>A, p.R261Q)	None	LGMD, raised CK	99

The cardiac arrythmias seen in animal model and patients are likely caused, in part, by cAMP pathway dysfunction. This is a plausible effect of POPDC dysfunction given the known interactions with PDE4A, AC9, the changes in cAMP-dependent TREK-1 modulation, as well as the POPDC protein's own cAMP binding behaviour. If POPDC proteins are acting as a scaffold for cAMP signalosomes, or in any other of the proposed roles in the cAMP pathway, then their dysfunction could have wide effects on cAMP

signalling. The role of the known POPDC1 interaction partner XIRP1 at intercalated disks in the heart provides an additional possible mechanism for POPDC mutation induced cardiac arrythmia.[120] Changes in the muscular dystrophy and/or poor muscle repair after injury fit with the POPDC protein's interactions with dysferlin, anoctamine-5 and caveolin-3.[71,72,118]

A feature of these mutations is that the loss of, or mutations in, a single POPDC gene leads to a joint loss of other POPDC isoforms from the plasma membrane of cells as well as the affected protein, as determined by histochemical analysis of muscle biopsy sections.[71,93,122,123] This effect is seen in patients and knock-out animal models. The reason for this dual effect on multiple members of the POPDC family is not understood and could be due to a number of mechanisms. One hypothesis is that it is due to the loss, or change in, an interaction between POPDC1 and POPDC2. It does suggest a role for the disruption of POPDC protein expression or localisation at the plasma membrane of cells in the pathologies observed in patients. An example of this phenomenon can be seen in muscle biopsy sections taken from a patient possessing the *POPDC1* (c.602C>T, p.S201F) mutation,[93] shown in Figure 1.6. Here, despite only the *POPDC1* gene containing a mutation, both POPDC1 and POPDC2 expression at the sarcolemma of skeletal muscle was greatly reduced compared to a matched control. In this case, Western blot analysis suggested that both proteins were still present meaning that a defect in trafficking was the likely cause of the reduced membrane expression, not degradation. It could be that an interaction between POPDC1 and POPDC2 is altered, or lost, when a mutation is present in a single isoform, which leads to this joint change in localisation. Given the multiple PPIs between proteins involved in muscle function and the POPDC proteins, this loss in POPDC1 and POPDC2 from the plasma membrane of muscle fibres is likely a key feature in the pathology of POPDC linked muscular dystrophy. The loss of POPDC proteins at the plasma membrane may have additional effects given its suggested role in the trafficking of other proteins to the plasma membrane, as evidenced by its interaction with VAMP3.[119] Similar effects could be seen in the heart of patients, although this has not yet been confirmed. This feature of POPDC mutations is investigated in Chapter 5, with its link to interactions between POPDC1 and POPDC2 examined in Chapter 6.

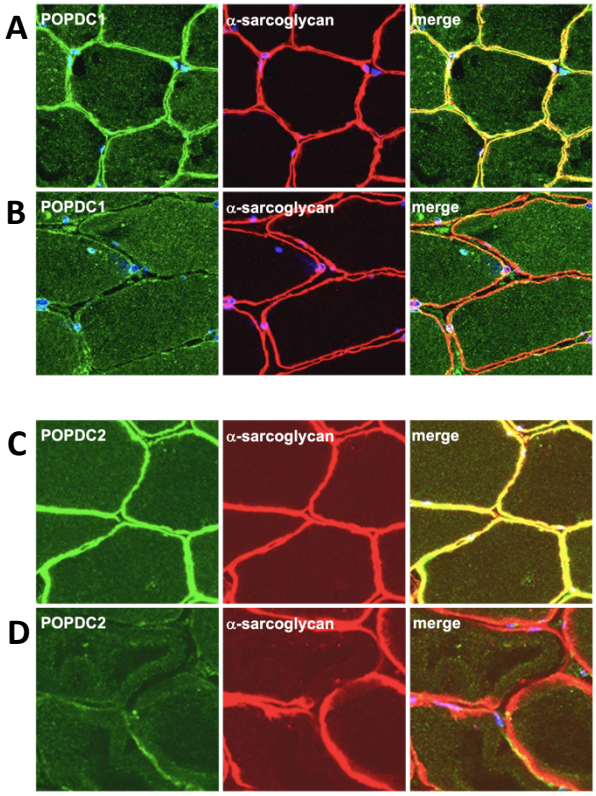


Figure 1.6: Changes in Subcellular Expression and Localisation of POPDC1 and POPDC2 in the Skeletal Muscle of a Patient Possessing the *POPDC1* (c.602C>T, p.S201F) Mutation. Skeletal muscle biopsy sections taken from a control **(A, C)** and a patient possessing the *POPDC1* (c.602C>T, p.S201F) mutation **(B, D)**. The sections were immunostained for POPDC1/POPDC2 and the sarcoplasm marker α-sarcoglycan. In the control biopsies POPDC1 and POPDC2 are clearly localised the sarcolemma, however sarcolemma expression levels of POPDC1 and POPDC2 are both reduced in the patient despite only the *POPDC1* gene containing a mutation. This figure was adapted from Schindler *et al*,[93] under licence (CCC ID: 1240285-1).

1.10.4 Cancer

In addition to the function of striated muscle, POPDC proteins have also been linked to the control of cell proliferation and may be involved in the formation of tumour cells. Downregulation of *POPDC1* expression has been linked to the progression of multiple tumour types, whereas *POPDC2* and *POPDC3* were found to be upregulated in breast cancer cells.[130-132] In addition, increased *POPDC3* expression was found to be related to poor prognosis in head and neck squamous cell carcinoma.[133] While the exact mechanism behind its function as a tumour suppression gene is not known, POPDC1 has been found to interact with and modulate a number of proteins involved in cell proliferation pathways, such as wnt and c-myc.[134] Dysregulation of the cAMP pathway has been linked to tumour cell proliferation and it has been found that the POPDC1-dependent modulation of tumour cell proliferation is altered after application of cAMP to cells, possibly providing a link between POPDC1's role in the cAMP pathway and cancer.[132] It has also been suggested that the function of POPDC1 as a tumour suppressor relies on its localisation to the plasma membrane.[74] As such, a loss of POPDC1 at the plasma membrane, such as those observed in muscle fibres of *POPDC1* mutant possessing patients and *Popdc1*$^{-/-}$mice, could contribute to cancer progression in other tissue types. Given their potential role

in tumour progression the POPDC proteins have been suggested as possible targets for anti-cancer treatments.[135]

1.11 Attempts to Develop Selective Small Molecule Popeye Domain Ligands

The poorly understood, and likely highly complex, role of the POPDC proteins in the cAMP pathway means that it is difficult to isolate the effect of POPDC proteins during non-specific modulation of the cAMP pathway. Likewise, the removal of POPDC proteins, such as in knock-out animal models, likely has multiple downstream effects. The divergent sequence of the CNBD of the Popeye domain makes the POPDC proteins interesting targets for pharmacological modulation of the cAMP pathway.[74] Being able to mimic or inhibit the binding of cAMP to the Popeye domain of POPDC proteins, without perturbing their other functions, would help provide evidence on what the role of cAMP binding to the POPDC proteins is. Their association with muscular dystrophies, cardiac dysrhythmias and tumorigenesis also make them potential clinical targets.[135,136] At present, no small molecules are known to selectively bind to the POPDC proteins. It has been thought that cAMP mimics may be able to bind selectively to the Popeye domain and at least one project was previously launched in an attempt to develop such ligands, which is discussed in Chapter 3.[137,138] While a set of hit compounds, initially selected as pharmacophore analogues of cAMP, were identified as potential Popeye domain binders, efforts were hampered by the lack of an empirical structure of the CNBD of the Popeye domain and uncertainty about the binding mode of cAMP. In addition, the same issues faced during the attempts to develop constructs containing the Popeye domain for structural studies were faced during compound binding assay development. The same construct that failed to produce high-quality protein-NMR results (see Section 1.7) was used, leading to persistent problems with construct stability. As a result, some of the assays used in hit compound identification showed relatively low signal-noise output and required significant optimisation to produce acceptable results.[138] While the data obtained do provide evidence of possible binding of these compounds to the Popeye domain, the issues highlighted make it harder to draw firm conclusions. Future compound development efforts would greatly benefit from a higher performing Popeye domain construct. These issues and efforts to develop such a Popeye domain construct and use it to optimise the previously identified hit compounds are discussed in Chapter 3.

1.12 Main Hypotheses and Aims of this Work

1.12.1 Hypotheses and Context of this Work

This project aimed to conduct further research on the use of POPDC protein derived constructs for use in structural and ligand binding studies. The main motivation for focusing on this area of research is the lack of structural and mechanistic understanding of the Popeye domain, alongside the absence of any pharmacological tools that are able to selectively target POPDC proteins. Attempts to address

these issues have been hindered by the poor performance of Popeye domain-based constructs, such as suboptimal solubility and stability in solution.[138] The Popeye domain of POPDC1 was selected as the target on which to focus efforts, building on previous work that had examined the use of Popeye domain constructs. It was hypothesised that modifications to the previously developed constructs, specifically extensions and/or truncations to the Popeye domain sequences used, would yield improvements in the performance of the constructs. A construct that displayed suitable solubility and stability could then be employed in protein-NMR experiments to allow direct analysis of the structure of the Popeye domain. The binding of cAMP to the Popeye domain could also be studied, with the results being used to inform future Popeye domain ligand development. Optimisation of the previously identified hit compounds could then be carried out in a rational fashion. Existing and novel candidate compounds could be assessed using protein-observed and/or ligand-observed protein-NMR methods with the Popeye domain construct. Other ligand screening methods, also dependent on the Popeye domain construct, could also be employed, such as differential scanning fluorimetry (DSF) and microscale thermophoresis (MST), to enable the characterisation of the binding parameters of compounds of interest. The findings from this part of the project are described in Chapter 3.

It was also wished to develop a cell-based assay in which the functional effect of any compounds of interest could be assessed with respect to changes in POPDC protein function. Given the established use of FRET and BRET assays in monitoring the activity of cAMP binding proteins,[139] as well as the use of FRET in studying the cAMP-responsive interaction of POPDC1 and TREK-1,[71] this assay type was chosen as the basis for this area of the project. The interaction of POPDC proteins and conformational changes within the Popeye domain were selected as possible processes that could be exploited in the development of cAMP-sensitive optical BRET sensors, the results of which are outlined in Chapter 4.

In addition, the phenomenon of the dual loss of POPDC1 and POPDC2 expression and/or plasma membrane localisation in patient and animal tissue expressing a single POPDC mutant,[71,93,122,123] along with the recent discovery of an interaction between POPDC1 and POPDC2,[82] meant that investigations into the features of POPDC complex formation were also conducted. It was hypothesised that the loss of, or change in, the interaction between POPDC1 and POPDC2 was contributing to the changes in POPDC protein behaviour in the presence of POPDC mutations. It was desired to characterise the changes in subcellular POPDC protein expression in patient and animal tissue in more detail than previously attempted through the visualisation of POPDC proteins in skeletal muscle sections followed by image analysis. Extending this area of research into cell line-based assays was identified as a possible method of removing barriers to the study of changes in subcellular POPDC expression. Chapter 5 provides an account of this part of the project.

In Chapter 6, investigations into the mechanism underlying the POPDC1-POPDC2 interaction were performed. The possible link between POPDC1-POPDC2 interactions and subcellular expression and localisation was also briefly explored, as it was thought that this may aid the understanding of the effects of POPDC mutants in tissue.

The methods developed in Chapter 5 and 6 were also applied to the study of a novel *POPDC2* variant implicated in cardiac arrythmia, to allow characterisation of the mutant without access to patient biopsy material, as described in Chapter 7.

1.12.2 Aims

The aims of this work can be summarised as the following:

- Produce a novel Popeye domain-based construct with enhanced expression, stability, and solubility properties.
- Use such a construct in protein-NMR experiments to provide structural information regarding the Popeye domain.
- Conduct protein-NMR, as well as other biophysical compound binding assays, to characterise cAMP and hit compound binding to the Popeye domain.
- Develop cell-based BRET assays to investigate the functional changes in POPDC proteins upon cAMP, or hit compound binding, within cells.
- Investigate the changes in POPDC1 and POPDC2 subcellular expression in the skeletal muscle tissue of patients and mice expressing recently identified pathogenic POPDC variants.
- Develop a cell line-based model for studying the subcellular expression of POPDC proteins, which can be used to further understand findings from native tissue.
- Investigate the direct interaction of POPDC1 and POPDC2 in a cellular environment and begin to study a possible mechanism of complexation.
- Use a combination of the assays used throughout the project to enable the characterisation of known and novel POPDC mutations on the function of POPDC proteins within cell lines, which can be used to aid interpretation of clinical investigations.

2 Methods and Materials

2.1 General Laboratory Practice

All activities were performed according to general laboratory safety guidelines, as well as any local regulations, using appropriate personal protective equipment.

Liquid volume measurements were made using Eppendorf Research Plus pipettes or Greiner serological pipettes. The mass of reagents were measured using a Denver Instruments SI-2002 balance or Sartorius CP1245 analytical balance. All solutions were prepared with water purified using a Milli-Q Integral 3 water purification system equipped with a Biopak Polisher ultrafilter. Water was additionally sterilised through autoclaving if required. Temperature controlled processes were performed in an Eppendorf Thermomixer Comfort heating block or Grant OLS200 water bath. The pH of solutions were determined using an appropriately calibrated Hanna Edge pH meter. General glassware was cleaned using a Miele Professional dishwasher before drying in a heating cabinet. Other processes were conducted using single use, sterile micro tubes or conical centrifuge tubes unless otherwise stated. Equipment and reagents were sterilised using Priorclave Tactrol 2 autoclave. Centrifugation steps were conducted using an Eppendorf 5424 or 5415 R (for temperature sensitive samples) benchtop centrifuge.

2.2 Reagents and Equipment

The identity and source of the reagents (Table 2.1), commercial buffers and media (Table 2.2), enzymes (Table 2.3), oligonucleotides (Table 2.4), antibodies (Table 2.5), cell lines (Table 2.6) and equipment (Table 2.7) used in this work are shown below.

Table 2.1: A table listing the reagents utilised in this work, with their respective supplier and product codes.

Reagent	Supplier	Product Code
$^{15}NH_4Cl$	CortecNet	CN80P1
30% acrylamide/bis solution	Bio Rad	1610154
8-Br-cAMP	BioLog	B007-100
8-CPT-cAMP	BioLog	C010-100
Agar	Sigma Aldrich	A5306
Agarose	Sigma Aldrich	A9539
Alexa Fluor 647 NHS Ester	Invitrogen	A20006
Ampicillin	Sigma Aldrich	A9518
APS	Sigma Aldrich	A3678
Arginine	Sigma Aldrich	A5006
BME	Sigma Aldrich	M7522
C8-conjugated cAMP-agarose	Sigma Aldrich	A0144
$CaCl_2$	Sigma Aldrich	C5670
$CaCl_2$ (for transfection)	Promega	E109A
$CaCl_2 \cdot 2H_2O$	Sigma Aldrich	C8106
cAMP	BioLog	A0001S
coelenterazine-400a	Biotum	BT10125-2
cOmplete EDTA-free Protease inhibitor cocktail	Roche	11836170001

D_2O	CortecNet	CD5251P1000
DAPI	Calbiochem	268298
DiD	Biotum	30023
DMSO	Sigma Aldrich	D2650
DMX0006151	Enamine	Z168720550
DMX0006224	Enamine	Z1012507986
DMX0006343	Enamine	Z1397205302
DMX0006345	Enamine	Z912219494
DMX0006517	Enamine	Z1618174745
DMX0006565	Enamine	Z1461498316
DMX0006593	Enamine	Z406350666
dNTPs	Roche	11969064001
DTT	Molelula	M10166694
EDTA	Sigma Aldrich	EDS
EGTA	Sigma Aldrich	E3889
Forskolin	Sigma Aldrich	F6886
Furimazine	Promega	N157A
Gelatine (bovine)	Sigma Aldrich	G9391
GeneRuler	Thermo Scientific	SM0331
Glucose	Sigma Aldrich	G7528
Glutamic acid	Sigma Aldrich	G1251
Glycerol	Sigma Aldrich	G5516
Glycine	Sigma Aldrich	G7126
HaloTag-618	Promega	G9801
HBS (for transfection)	Promega	E110A
HEPES	VWR	441485H
Hoechst-33342	Sigma Aldrich	14533
IBMX	Abcam	ab120840
Imidazole	Sigma Aldrich	I5513
Immobilon Western Chemiluminescence Kit Reagents	Millipore	WBKLSO500
InstantBlue Coomassie Protein Stain	Abcam	ab119211
IPTG	FluoroChem	367-93-1
Isopropanol	VWR	20842.330
Kanamycin	Sigma Aldrich	11815024
KCl	Sigma Aldrich	P5405
KH_2PO_4	Sigma Aldrich	P9791
L-glutamine	Sigma Aldrich	G7513
Lipofectamine 2000	Invitrogen	11668027
Mark 12 unstained protein standard	Invitrogen	LC5677
Methanol	VWR	20837.320
$MgCl_2$	Sigma Aldrich	M8266
$MgCl_2 \cdot 6H_2O$	Sigma Aldrich	M9272
$MgSO_2$	Sigma Aldrich	M7506
Milk powder	Fluka	70166
$MnCl_2 \cdot 4H_2O$	Sigma Aldrich	203734
MOWIOL 4-88	Cabiochem	475904
Na_2HPO_4	Acros Organics	424375000
NaCl	Sigma Aldrich	S7653
$NaH_2PO_4 \cdot 2H_2O$	Sigma Aldrich	100952000
NaN_3	Sigma Aldrich	S2002
Paraformaldehyde	Merck	S5406815
Penicillin/Streptomycin	Sigma Aldrich	P0781
Peptone	BD	211677
Poly-L-lysine	Sigma Aldrich	P4832
Potassium acetate	Sigma Aldrich	P1190
Potassium phosphate monobasic	ACROS Organics	424205000
SDS	Sigma Aldrich	05030
SYBR Safe DNA Gel Stain	Life Technologies	S33102
SYPRO Orange	Sigma Aldrich	S5692
TEMED	Merck	1.10732.0100

Tris Base	Sigma Aldrich	T1503
Tris-Cl	Sigma Aldrich	T3253
Triton-X-100	Sigma Aldrich	T8787
Trypan blue	Sigma Aldrich	T8154
Trypsin-EDTA	Sigma Aldrich	T4174
Tween-20	Electran	437082Q
Yeast Extract	BD	212750

Table 2.2: A table listing the commercial buffers and media utilised in this work, with their respective supplier and product codes.

Buffer / Media	Supplier	Product Code
Buffer EB	Qiagen	19086
Buffer N3	Qiagen	19064
Buffer P1	Qiagen	19051
Buffer P2	Qiagen	19052
Buffer PB	Qiagen	19066
Buffer PE	Qiagen	19065
CutSmart buffer	NEB	B6004SVIAL
Dephosphorylation buffer	Roche	11596820
DMEM	Sigma Aldrich	D6429
DNA Loading Dye	NEB	B7024S
FBS	Merck	F2442
Flexi Digest Buffer	Promega	R186A
HBS	Promega	E110A
KLD reaction buffer	NEB	B0554AVIAL
OptiMEM I	(Gibco	11058021
PAGE Ruler	Thermo Scientific	26616
Passive lysis buffer	Promega	E1941
Phusion HF buffer	Thermo Scientific	F-520L
T4 DNA Ligase buffer	Promega	C126B

Table 2.3: A table listing the enzymes utilised in this work, with their respective supplier and product codes.

Enzyme	Supplier	Product Code
BamHI-HF	NEB	R3136S
Calf alkaline phosphatase	Roche	10713023001
Carboxy flexi enzyme blend	Promega	R1901
EcoRI	NEB	R0101S
Flexi Enzyme blend (SgfI + PmeI)	Promega	R1851
KLD enzyme mix	NEB	M0554AVIAL
NotI-HF	NEB	R3189S
Phusion High Fidelity DNA polymerase	ThermoFisher	F530S
Q5 Hot start high fidelity master mix	NEB	M0494AVIAL
SacI	NEB	R0156S
SacII	NEB	R0157S
T4 DNA Ligase	Promega	M1794
TEV protease	Pfuhl Lab, Kings College London	-
Trypsin-EDTA	Sigma Aldrich	T4174
XhoI	NEB	R0146S

Table 2.4: A table listing the plasmids and other oligonucleotides utilised in this work, with their respective supplier and product codes (where available).

Plasmid / Oligonucleotide	Supplier	Product Code
GEV2	John Louis (Addgene)	12616
mRFP-N1	Robert Campbell & Michael Davidson & Roger Tsien (Addgene)	54635
pECFP-N1	Clontech	6900-1
pEGFP-N1	Clontech	6085-1
pEYFP-N1	Clontech	6006-1
pFC14K	Promega	G9961
pFC32K	Promega	N1341
pFN21A	Promega	G2821
pFN31K	Promega	N1321
pGFP2-C1	Friedrich Herberg, University of Kassel	-
pGFP2-C3	Friedrich Herberg, University of Kassel	-
pLEICS-91	Protein Expression Laboratory, Department of Molecular and Cell Biology, University of Leicester	pLEICS-91
Primer oligonucleotides	Invitrogen	-
pRluc8-N3	Friedrich Herberg	-
pUC18	Thermo Fisher	SD0051

Table 2.5: A table listing the antibodies utilised in this work, with their respective supplier and product codes.

Antibody	Species	Primary / Secondary	Conjugate	Supplier	Product Code
Anti-α-sarcoglycan	Mouse	Primary	N/A	Leica Biosystems	NCL-a-SARC-mouse
Anti-POPDC1	Rabbit	Primary	N/A	Sigma Aldrich	HPA018176
Anti-POPDC2	Rabbit	Primary	N/A	Sigma Aldrich	HPA02224255
Anti-rabbit	Donkey	Secondary	Alexa Fluor 488	Invitrogen	A21206
Anti-mouse	Donkey	Secondary	Alexa Fluor 555	Invitrogen	A31570
Anti-HA	Mouse	Primary	N/A	Covance	MMS-101R
Anti-mouse	Horse	Secondary	HRP	Vector Laboratories	PI-2000
Anti-rabbit	Goat	Secondary	HRP	Vector Laboratories	PI-1000

Table 2.6: A table listing eukaryotic cell lines and bacterial cells utilised in this work, with their respective supplier and product codes.

Cell Lines	Supplier	Product Code
Arctic Express (DE3) *E. coli*	Agilent	230192
BL21 Star (DE3) *E. coli*	Invitrogen	C601003
HEK293	DSMZ	ACC305
Top10 *E. coli*	Thermo Fisher	C404003
XL1 Blue *E. coli*	Stratagene	200268

Table 2.7: A table listing the equipment utilised in this work, with their respective supplier and product codes (where available).

Equipment	Supplier	Product Code
1.5 ml micro tubes	Sarstedt	72.706.400
10 cm tissue culture plate	Sarstedt	83.3902.300
10 ml serological pipette	Greiner Bio-One	607180
12-well tissue culture plate	Greiner Bio-One	665180
14 ml polypropylene round-bottom sterile tube	Falcon	352059
15 ml Conical centrifuge tubes	Sarstedt	62.554.502
15 well microscope slide	Ibidi	81506
24-well tissue culture plate	Greiner Bio-One	662160

25 ml serological pipette	Greiner Bio-One	760160
384-well Adhesive Cover	Life Technologies	4360954
5 ml serological pipette	Greiner Bio-One	606180
50 ml Conical centrifuge tubes	Sarstedt	62.547.254
6-well tissue culture plate	Greiner Bio-One	657160
700 MHz NMR Spectrometer	Bruker	-
8-well microscope slide	Ibidi	80807
96-well white tissue culture plate	Corning Life Sciences	3917
AKTA Pure FPLC	GE Healthcare	-
Benchtop Centrifuge 5415 R	Eppendorf	Z605212
Benchtop Centrifuge 5424	Eppendorf	EP6505000537
Biopak Polisher ultrafilter	Millipore	CDUFBI001
ChemiDoc MP Imaging System	Bio-Rad	ChemiDoc MP Imaging System
Chirascan Plus spectrometer	Applied Photophysics	-
CP124S analytical balance	Sartorius	CP124S
EC Plan-Neofluar 10x/0.30 M27 Objective	Zeiss	420340-9901
Edge pH meter	Hanna	-
Eppendorf Research Plus p10	Eppendorf	3123000020
Eppendorf Research Plus p100	Eppendorf	3123000047
Eppendorf Research Plus p1000	Eppendorf	3123000063
Eppendorf Research Plus p20	Eppendorf	3123000039
HisTrap FF column	GE Life Sciences	17-5255
LSM 780 Axio Observer Confocal microscope	Zeiss	-
LUMIstar Optima microplate reader	BMG Labtech	-
MicroAmp Optical 384-well Reaction Plate	Applied Biosystems	4309849
Milli-Q Integral 3 water purification system	Millipore	-
miniDAWN MALS detector	Wyatt Technology	-
Monolith NT.115	NanoTemper	-
Monolith premium glass capillaries	NanoTemper	MO-K025
Monolith Protein Labelling kit	NanoTemper	MO-L001
ND-8000 UV/Vis photospectrometer	NanoDrop	-
Nitrocellulose membranes	Bio Trace	VWR732-3031
Shigemi NMR tubes	Bruker	-
NuPAGE 12% Bis-Tris Gel	Invitrogen	NP0323
OLS200 Water Bath	Grant	-
Optical 410-80 nm filter	BMG Labtech	-
Optical 515-30 nm filter	BMG Labtech	-
Optical LWP-610 nm filter	BMG Labtech	-
Optical SWP-460 nm filter	BMG Labtech	-
OWL HEP-1 Semi Dry Blotter	Thermo Scientific	HEP-1
PCR tubes	Sarstedt	72.737.002
Plan-apochromat 20X/0.8 M27 Objective	Zeiss	420650-9901
Plan-apochromat 63X/1.40 oil DIC M27 Objective	Zeiss	420782-9900-720
PowerPac Basic power source	Bio-Rad	1645050
ProFound Pierce c-myc-tag IP/Co-IP Kit	Thermo Scientific	23620
ProSEC 16/60 3-70 HR SEC column	Generon	SEC-16/60-3-70
Q5 Site Directed Mutagenesis Kit	NEB	E0554S
QIAprep Spin Miniprep Kit	Qiagen	27106
QIAquick Gel Extraction Kit	Qiagen	28706
QIAquick PCR Purification kit	Qiagen	28104
QuantStudio 6 flex real time PCR thermocycler	Applied Biosystems	4485691
Quartz Suprasil rectangular cuvettes	Starna Scientific Ltd	-
Safe Imager 2.0 Blue-Light Transmitter	Invitrogen	G6600
SI-2002 balance	Denver Instrument	10639474
Spectra/Por Dialysis Membrane	Repligen	132655
Superdex 75 5/150 GL column	Cytiva	GE28-9205-04
T3000 Thermocycler	Biometra	050-723
Tactrol 2 autoclave	Priorclave	-
Thermomixer Comfort Heating Block	Eppendorf	-
Zeiss AxioObserver Inverted Widefield Microscope	Zeiss	-

2.3 Composition of Non-Commercial Buffers and Media

The components of buffers and media that were produced locally are shown below in Table 2.8.

Table 2.8: A table listing the components of non-commercial buffers and media with their respective proportions, amounts or concentration.

Buffer / Media	Component	Proportion / Amount / Concentration	Notes
cDMEM	DMEM	90% (v/v)	
	FBS	10% (v/v)	
	L-glutamine	2 mM	
	Streptomycin	100 mg/ml	
	Penicillin	100 U/ml	
LB	Deionised Water	-	† LB-agar culture plates only pH adjusted to 7. Autoclave sterilised.
	Bacto peptone	1% (w/v)	
	Yeast extract	0.5% (w/v)	
	NaCl	1% (w/v)	
	Agar†	1.5% (w/v)	
CCMB80 Buffer	Potassium acetate	10 mM	pH adjusted to 6.4. Sterile filtered.
	$CaCl_2 \cdot 2H_2O$	80 mM	
	$MnCl_2 \cdot 4H_2O$	20 mM	
	$MgCl_2 \cdot 6H_2O$	10 mM	
	Glycerol	10% (v/v)	
PBS	Deionised Water	-	pH adjusted to 7.3. Autoclave sterilised for tissue culture applications.
	KCl	2.7 mM	
	Na_2HPO_4	10 mM	
	KH_2PO_4	2 mM	
	NaCl	137 mM	
FF6 wash / elution buffer	Deionised Water	-	† FF6 elution buffer only pH adjusted to 7.5. Filtered to remove particles.
	Na_2HPO_4	10 mM	
	NaH_2PO_4	10 mM	
	NaCl	500 mM	
	Imidazole†	500 mM	
	NaN_3	0.02% (w/v)	
M9 media	Deionised Water	-	pH adjusted to 7-7.4. Autoclaved sterilised.
	Na_2HPO_4	42 mM	
	KH_2PO_4	44 mM	
	NaCl	8.5 mM	
Complete M9 Media	Deionised Water	-	† M9 micronutrients includes 730 ng $NaMoO_4$, 24.7 μg H_3BO_3, 7.1 μg $CoCl_2$, 2.5 μg $CuSO_4$, 15.8 μg $MnCl_2$ and 2.9 μg $ZnSO_4$ per litre of complete M9 media. * M9 vitamins includes 400 μg choline chloride, 500 μg folic acid, 500 μg pantothenic acid, 500 μg nicotinamide, 1 mg myo-inositol, 500 μg pyridoxal hydrochloride, 500 μg thiamine hydrochloride, 50 μg riboflavin and 1 mg biotin per litre of complete M9 media. pH adjusted to 7-7.4. Autoclaved sterilised.
	Na_2HPO_4	42 mM	
	KH_2PO_4	44 mM	
	NaCl	8.5 mM	
	$MgSO_2$	2 mM	
	$CaCl_2$	10 μM	
	M9 micronutrients† and vitamins*	-	
	Glucose	33.3 mM	
	$^{15}NH_4Cl$	18.7 mM	
Arginine/Glutamic acid Protein-NMR buffer	Deionised Water	-	pH adjusted to 7.25. Filtered to remove particles.
	Na_2HPO_4	10 mM	
	NaH_2PO_4	10 mM	
	Glutamic acid	300 mM	
	Arginine	300 mM	
	DTT	2 mM	
	NaN_3	0.02% (w/v)	
DSF Buffer A	Deionised Water	-	pH adjusted to 6.5.
	HEPES	10 mM	

	NaCl	150 mM	
DSF Buffer B	Deionised Water	-	pH adjusted to 7.5.
	Tris-Cl	50 mM	
	$MgCl_2$	10 mM	
	NaCl	500 mM	
Co-IP Lysis Buffer	Deionised water	-	pH adjusted to 8.0. One tablet of cOmplete Mini Protease Inhibitor Cocktail was added per 10 ml of lysis buffer immediately before use.
	Tris-Cl	50 mM	
	Triton-X-100	150 mM	
	EDTA	1% (v/v)	
	Gelatine (bovine)	0.25% (w/v)	
SDS-PAGE Sample Buffer	Glycerol	90% (v/v)	
	Deionised Water	10% (v/v)	
	SDS	2% (w/v)	
	Tris-Cl	50 mM	
	Bromophenol blue	0.2 mg/ml	
	DTT	100 mM	
Transfer Buffer	Deionised Water	-	pH adjusted to 8.3.
	Methanol	10% (v/v)	
	Tris	25 mM	
	Glycine	150 mM	
Membrane Blocking Solution	TBS-T	-	
	Milk powder	5% (w/v)	
TBS	Deionised Water	-	pH adjusted to 7.4.
	NaCl	150 mM	
	Tris-Cl	50 mM	
TBS-T	TBS	-	
	Tween-20	0.1% (v/v)	
Section Blocking Buffer	PBS	-	
	BSA	1% (w/v)	
	FBS	5% (v/v)	
	Triton X-100	0.25% (v/v)	
MOWIOL Mounting Medium	Glycerol	25% (w/v)	pH adjusted to 8.5.
	Deionised water	-	
	MOWIOL 4-88	10% (w/v)	
	Tris	200 mM	

2.4 Molecular Cloning

DNA sequences coding for protein constructs expressed in bacterial or mammalian cells were constructed using a conventional molecular cloning protocol. This consisted of PCR amplification of the desired sequence with primers containing the appropriate restriction sites for subcloning at their 5' and 3' end, followed by restriction and ligation reactions to insert the PCR product into the desired plasmid. All PCR reactions were performed using a T300 thermocycler (Biometra). Alternatively, site-directed mutagenesis was performed to introduce desired modifications to a template sequence. The protocol of each step is described below.

2.4.1 General PCR Procedure

Standard PCR reactions contained the reagents shown in Table 2.9. The reaction mixture was compiled in sterile PCR tubes on ice and contained Phusion High-Fidelity DNA polymerase (Thermo Fisher).

Primers were manually designed using the SnapGene software (Insightful Science) and produced by Invitrogen. All primers were purified by desalting before delivery.

Table 2.9: A table listing the standard components of regular PCR reactions.

Reagent	Volume / µl	Final Concentration
Phusion HF Buffer (5X)	4	1X
Forward primer	2	0.5 µM
Reverse primer	2	0.5 µM
dNTPs	0.4	200 µM per nucleotide
DMSO	0.6	3% (v/v)
Template DNA	0.5	1-5 ng/µl
Phusion High-Fidelity DNA Polymerase	0.2	0.4 U
Total	**20**	

The PCR reaction mixture was subjected to the standard thermocycler protocol shown in Table 2.10. Specific annealing temperatures for each set of primers were determined using the NEB Tm Calculator (https://tmcalculator.neb.com).

Table 2.10: A table showing the general thermocycler steps performed during standard PCR reactions.

Step	Temperature / °C	Time / s	Cycles
Initial denaturation	98	30	
Denature	98	15	X25-35
Annealing	*	30	
Extension	72	†	
Hold	4	∞	

† The extension time was set to 30 s per kb of DNA.
*Dependent on primer sequence.

The PCR reaction mixture was then purified using the QIAquick PCR purification kit (Qiagen) following the provided protocol. Briefly, the PCR reaction was transferred to a 1.5 ml micro tube and mixed with five volumes of Buffer PB. This mixture was passed through the provided QIAquick spin column by centrifugation at 17,900 rcf for 1 minute and the flowthrough discarded. The column was washed with 750 µl Buffer PE and centrifuged as before. The PCR product was eluted from the column by application of 50 µl Buffer EB. PCR products were separated and imaged using agarose gel (0.4-1.2% (w/v)) electrophoresis to ensure the product molecular weight corresponded to the predicted size and to assess the purity of the reaction products.

2.4.2 General Restriction Reaction Procedure

Purified PCR product, or previously isolated plasmid DNA, containing the target sequence was subjected to a restriction reaction to enable ligation into the desired destination plasmid, which also underwent parallel restriction digestion. Reactions were performed in sterile 1.5 ml micro tubes and

were incubated at 37 °C for 30-60 mins. The standard components of each restriction reaction are shown in Table 2.11.

Table 2.11: A table listing the standard components of restriction reactions.

Reagent	Volume / µl	Final Concentration or Amount
Cut Smart Buffer	4.5	1X
Restriction enzyme 1	1	20 U
Restriction enzyme 2	1	20 U
PCR product / plasmid	*	1500 ng / 3000 ng
Water	†	-
Total	**20**	

*Dependent on PCR product/plasmid concentration.
† As required to yield total reaction mixture volume of 20 µl.

The restriction reaction mixture was then subjected to electrophoresis using an agarose gel (0.4-1.2% (w/v)) to separate the products of the reaction according to their molecular weight. Product bands were imaged using SYBR Safe dye (Life Technologies) added to the agarose gel and a blue light transilluminator (Invitrogen). Bands corresponding to the expected product size were excised from the gel and purified using the QIAquick Gel Extraction kit (Qiagen). Briefly, 3 volumes of Buffer QG were added to a 1.5 ml micro tube containing the excised gel fragment and incubated at 50 °C for 10 minutes with occasional shaking. One volume of isopropanol was then added to the tube and mixed through inversion. The resulting solution was applied to a QIAquick spin column and centrifuged at 17,900 rcf for 1 minute. The column was washed with 750 µl Buffer PE using a one minute centrifugation step at 17,900 rcf. The restriction reaction products were eluted from the column through addition of 30-50 µl Buffer EB.

2.4.3 General Ligation Reaction Procedure

Before ligation reactions were performed the restricted destination plasmids were de-phosphorylated at the 5' end to reduce self-ligation. The phosphatase reaction was constructed as shown in Table 2.12. Calf alkaline phosphatase (Roche) and dephosphorylation buffer (Roche) were added directly to the restriction reaction tube and incubated at 37 °C for 60 minutes.

Table 2.12: A table listing the standard components of dephosphorylation reactions.

Reagent	Volume / µl	Final Concentration or Amount
10X Dephosphorylation buffer	3	1X
Water	4	-
Calf Alkaline Phosphatase	0.5	0.5 U
Plasmid Restriction Reaction Product	20	3000 ng
Total	**30**	

The reaction was quenched through the addition of ethylene glycol-bis(β-aminoethyl ether)-N,N,N,'N'-tetraacetic acid (EGTA) (Sigma Aldrich) to a final concentration of 20 mM, followed by heating to 65 °C for 10 minutes to denature the calf alkaline phosphatase. The restricted and dephosphorylated plasmid was then ligated with the restricted PCR product or other target DNA sequence using T4 DNA ligase (Promega). The ligation reaction was performed at 16 °C overnight and contained the reagents shown in Table 2.13.

Table 2.13: A table listing the standard components of ligation reactions.

Reagent	Volume / µl	Final Concentration or Amount
10X T4 DNA Ligase Buffer	2	1X
Digested Vector	*	25 ng
Digested PCR Product	*	100 ng
T4 DNA Ligase	1	10 U
Water	†	-
Total	**20**	

*Dependent on digested vector and PCR product concentration.
† As required to yield total reaction mixture volume of 20 µl.

Ligation reaction products were then used in the transformation of chemically competent cells without further purification, as detailed below.

2.4.4 General Site Directed Mutagenesis Procedure

Modification of DNA sequences was performed using the Q5 Site-Directed Mutagenesis Kit (NEB). Mutagenesis reactions were performed following the standard protocol. Primers used for mutagenesis were designed using the NEBaseChanger tool (https://nebasechanger.neb.com/). The mutagenesis PCR reaction contained the reagents shown in Table 2.14 or was performed on a smaller scale by reducing all volumes by half.

Table 2.14: A table listing the standard components of site directed mutagenesis PCR reactions.

Reagent	Volume / µl	Final Concentration or Amount
Q5 2X Master Mix	12.5	1X
10µM Forward primer	1.25	0.5 µM
10µM Reverse primer	1.25	0.5 µM
Template	0.5	1-5 ng/µl
Water	9.5	-
Total	**25**	

The PCR reaction mixture was subjected to the thermocycler protocol shown in Table 2.15. Annealing temperatures were determined by subtracting 6-8 °C from the annealing temperature recommended by the NEBaseChanger tool, which was found to give more reliable results.

Table 2.15: A table showing the general thermocycler steps performed during standard site directed mutagenesis PCR reactions.

Step	Temperature / °C	Time / s	Cycles
Initial denature	98	30	
Denature	98	10	X25
Annealing	*	30	
Extension	72	†	
Final Extension	72	120	
Hold	4	∞	

† The extension time was set to 30 s per kb of DNA.
*Dependent on primer sequence.

The linear PCR product was then phosphorylated and ligated to form circularised plasmids, as well as template DNA being digested with DpnI in the same tube using the KLD enzyme mix (NEB). The phosphorylation, ligation and DpnI (KLD) reaction mix was constructed as shown in Table 2.16 and incubated at room temperature for 30 minutes.

Table 2.16: A table showing the standard components of the phosphorylation, ligation and DpnI (KLD) reaction.

Reagent	Volume / μl	Final Concentration or Amount
PCR product	1	-
2X KLD Reaction Buffer	5	1X
10X KLD Enzyme Mix	1	1X
Water	3	-
Total	**10**	

The product of this one-pot reaction was used to transform chemically competent cells, as described below, without further purification.

2.4.5 Transformation of Chemically Competent *E. coli*

All transformations were performed using a heat shock protocol. 4-8 μl of previously constructed plasmid DNA, ligation reaction product or KLD reaction mix, containing 50-100 ng/μl of plasmid DNA, was placed onto the bottom of ice cold, sterile 14 ml polypropylene round-bottom tubes (Falcon). Chemically competent Top10 (Thermo Fisher) or XL-1 blue (Stratagene) *E. coli* cells were carefully added on top of the DNA solution. The cells and DNA were incubated on ice for 20 minutes. Cells were placed into a water bath or heating block set to 42 °C for 45 seconds followed by immediate immersion in an ice bath for 2 minutes. 300 μl of Luria broth (LB) media, pre-warmed to 37 °C, was added to the DNA-cell mix. Tubes were incubated at 37 °C and subjected to shaking at 150 RPM for 60-90 mins. 50-200 μl of the cell suspension was then plated onto LB-agar plates containing appropriate selection antibiotic and distributed using sterile spreaders or beads. Plates were incubated overnight at 37 °C.

2.4.6 Preparation of Chemically Competent *E. coli*

LB media was inoculated with a commercial stock of the chosen cell strain and progressively cultured up to a volume of 100 ml. Selection antibiotic was used in the LB media if the cell strain contained intrinsic plasmids which required maintenance. Cells were harvested through centrifugation of the cell suspension at approximately 5000 rcf at 4 °C. The supernatant was removed, and the cells were resuspended in 15 ml of ice cold CCMB80 buffer and incubated on ice for 30 minutes. Cells were recovered by centrifugation at approximately 2500 rcf for 30 minutes at 4 °C. Cells were gently resuspended in 4 ml CCMB80 buffer and incubated on ice for a further 30 minutes. The cell suspension was mixed with 1 ml pre-cooled 50% (v/v) aqueous glycerol solution. The cells were aliquoted and flash frozen in liquid nitrogen before long term storage at -80 °C.

2.4.7 Preparation of Plasmid DNA from *E. coli* Liquid Cultures

Single colonies from LB-agar plates, or aliquots of glycerol stocks, were extracted using a sterile pipette tip which was washed in antibiotic supplemented LB media in sterile 14 ml polypropylene round-bottom tubes. Inoculated LB media was then incubated overnight at 37 °C, while being shaken at approximately 300 RPM. The following day bacterial cultures were split into aliquots in 1.5 ml micro tubes. Aliquots were then centrifuged at 6,800 rcf to pellet the bacterial cells. The supernatant was then removed.

Plasmid DNA was isolated using the QIAprep Spin Miniprep Kit (Qiagen). The bacterial pellet was re-suspended in 250 μl P1 buffer. Lysis of the cells was achieved by the addition of 250 μl P2 buffer to the cell suspension which was mixed by vigorous inversion of the 1.5 ml micro tube and incubated at room temperature for 5 mins. The lysis reaction was quenched, and unwanted cell material precipitated, through the addition of 350 μl N3 buffer. The reaction mixture was centrifuged at 17,900 rcf for 10 minutes and the supernatant collected and loaded onto the provided spin-columns. The supernatant was passed through the column by a 1 min centrifugation at 17,900 rcf. The column was washed with 500 μl of PB buffer, followed by 750 μl PE buffer each using a 1 min centrifugation step at 17,900 rcf. Plasmid DNA was eluted from the column using 30-50 μl EB buffer and a final centrifugation as before.

2.4.8 Measurement of DNA Concentration and Purity

The concentration and purity of DNA containing solutions were analysed using a Nanodrop ultraviolet (UV) spectrophotometer. Solutions displaying 260/280 nm and 260/230 nm ratios of 1.7-2.0 and 1.8-2.2 were considered to be of sufficient purity.

2.4.9 Preparation of glycerol stocks

Glycerol stocks were produced for medium-term storage of transformed *E. coli*. 420 μl of sterile 80% (v/v) glycerol in water was added to 120 μl of fresh liquid bacterial culture in a sterile 1.5 ml micro tube. The tube was immediately placed on dry ice or immersed in liquid N_2. Glycerol stocks were stored at -80 °C.

2.4.10 Oligonucleotide Sequencing

Plasmid DNA was sequenced using single or bi-directional Sanger sequencing, which was performed by GeneWiz (https://www.genewiz.com/en-GB/Public/Services/Sanger-Sequencing).

2.4.11 Cloning of Popeye Domain Constructs for Expression Trials

Murine *Popdc1* was used to construct the Popeye domain constructs. The original set of constructs were produced by PCR using the full length *Popdc1* complementary DNA (cDNA) sequence in the pEGFP-N1 vector (Clontech) as a template. The PCR was conducted using the standard PCR protocol outlined above. A set of primers were designed to append BamHI and XhoI restriction sites at the 5' and 3' ends of the PCR products, respectively. The primers used to produce the set of PCR products for each construct are shown in Table 2.17.

Table 2.17: A table showing the primers used to produce sequences of mouse Popeye domain by PCR with mouse *Popdc1* as a template, for use in constructing initial Popeye domain constructs for structural studies.

Template	Product	Forward	Reverse
Murine *Popdc1*	GB1-E123-D266	CCCGGATCCGAGCTGGGTGGTGTCTACCAT	CCTCTCGAGGTCATTCAGTGAGTACAGCTT
	GB1-E123-K272	CCCGGATCCGAGCTGGGTGGTGTCTACCAT	GGCCTCGAGCTTATCATTTAAAGTAGGGTCATTCAG
	GB1-E123-Q280	CCCGGATCCGAGCTGGGTGGTGTCTACCAT	CTCCTCGAGCTGGGGCTCCAGCTTCTTAA
	GB1-E123-S288	CCCGGATCCGAGCTGGGTGGTGTCTACCAT	TTACTCGAGGGAGATCTGTGTGCAGAGG
	GB1-S109-D266	GGAGGATCCTCATATCTTTTGTACAAGAAAAGACC	CCTCTCGAGGTCATTCAGTGAGTACAGCTT
	GB1-K114-D266	GCCGGATCCAAGAAAAGACCGGTCAAAA	CCTCTCGAGGTCATTCAGTGAGTACAGCTT
	GB1-K119-D266	GTTGGATCCAAAATTGAAAAGGAGCTGG	CCTCTCGAGGTCATTCAGTGAGTACAGCTT

These restriction sites were then used to ligate the PCR products into the GEV2 expression vector (gifted by John Louis, Addgene plasmid 12616),[140] which appended an N-terminal GB1 tag and a 6XHis tag at the C-terminus of the construct. Plasmids were transformed into Top10 *E. coli* using the heat-shock method and cultured on ampicillin containing LB-agar plates. Colonies were selected and used to inoculate liquid LB cultures. Plasmid DNA was isolated from the liquid cultures and the presence of the desired sequences was confirmed by bi-directional Sanger sequencing.

Two additional Popeye domain constructs containing the cDNA sequence of residues S109-S288 of *Popdc1* were produced by the Protein Expression Laboratory at Kings College London. One used the pAG108-pET28a vector to append an N-terminal NusA tag to the Popeye domain sequence. The other

utilised the pLEICS-91 plasmid (Protein Expression Laboratory, Department of Molecular and Cell Biology, University of Leicester), which fused an N-terminal GB1 tag *via* a tobacco etch virus (TEV) protease cleavage and 6XHis tag sequence to the Popeye domain sequence (GB1-S109-S288).

Further constructs were produced through site directed mutagenesis of the GB1-S109-S288 sequence in the pLEICS-91 plasmid. Mutagenesis reactions were carried out using the Q5 Site-Directed Mutagenesis Kit, as described above. Primers were designed to produce the following constructs GB1-S109-D266, GB1-S109-K272 and GB1-S109-Q280 through a deletion mutagenesis reaction and are shown in Table 2.18.

Table 2.18: A table showing the primers used to produce a set of Popeye domain constructs by site directed deletion PCR using the GB1-S109-S288 construct as a template.

Template	Product	Forward Primer	Reverse Primer
GB1-S109-S288	GB1-S109-D266	5'-TAACTCCTGAGTAGGACAAATCCG-3'	5'-GTCATTCAGTGAGTACAGCTTATTTGTAATG-3'
	GB1-S109-K272		5'-CTTATCATTTAAAGTAGGGTCATTCAGTGAGTAC-3'
	GB1-S109-Q280		5'-CTGGGGCTCCAGCTTCTTAAC-3'

To test the influence of H188 on the affinity of the cleaved S109-K272 Popeye domain construct for the Ni^{2+} charged nitriloacetic acid (Ni-NTA) column the GB1-S109-K272[H188Q] construct was produced through site-directed mutagenesis. The primers used are shown below in Table 2.19.

Table 2.19: A table showing the primers used to introduce the H188Q substitution into the GB1-S109-K272 Popeye domain construct.

Template	Product	Forward Primer	Reverse Primer
GB1-S109-K272	GB1-S109-K272[H188Q]	5'-CTATCGAGGACAGTTTCTGCATAAC-3'	5'-GAGACCTTCATTCTTCCTTTTAG-3'

2.4.12 PKA and EPAC1 cAMP Sensors

The PKAI and EPAC-1 based cAMP sensors sequences, within their respective plasmids, were a gift from Prof Friedrich Herberg, University of Kassel. The PKAI sensor was comprised of the human RIα subunit and the human Cα subunit of PKA, each in separate plasmids. The sensor had been created by the Herberg group through the cloning of the RIα subunit into the pRluc8-N3 vector using the XhoI and HindIII restriction sites to append a C-terminal Rluc8 group. The Cα subunit was cloned into the pGFP2-C3 vector using the HindIII and BamHI restriction sites to introduce an N-terminal GFP2 tag.

The EPAC-1 construct contained residues E157-P881 of human EPAC1 ΔDEP. The sequence had been cloned into the pGFP2-C1 vector using the SacI (5') and SacII (3') restriction sites, which appends a N-terminal green fluorescent protein 2 (GFP2) domain and a C-terminal Renilla luciferase 8 (Rluc8) tag to the EPAC sequence.

2.4.13 Unimolecular Popeye Domain BRET Sensors

The Popeye domain-based cAMP sensors were created through a standard cloning protocol as described above. Sequences containing the cDNA of *Popdc1* Popeye domain of differing length were inserted into the pGFP2-C1 plasmid (gifted by Friedrich Herberg) that previously contained the EPAC-1 sensor, described above, to append sequences for GFP2 and Rluc8 at the N- and C-terminal of the Popeye domain sequences, respectively. Full length murine *Popdc1* cDNA was used for the PCR template as before. Primers, shown in Table 2.20, were used to append SacI and SacII restriction sites to the Popeye domain PCR products to allow ligation into the pGFP2-C1. After completion of the standard cloning procedure, product sequences were confirmed by bi-directional Sanger sequencing.

Table 2.20: A table showing the primers used to produce sequences of mouse Popeye domain by PCR, for use in constructing an initial set of Popeye domain-based BRET2 cAMP sensors.

Template	Final Product	Forward Primer	Reverse Primer
Murine *Popdc1*	GFP2-E123-D266-Rluc8	5'-GAGCTGGGTGGTGTCTACC-3'	5'-GTCATTCAGTGAGTACAGCTTATT-3'
	GFP2-E123-K272-Rluc8	5'-GAGCTGGGTGGTGTCTACC-3'	5'-CTTATCATTTAAAGTAGGGTCATTCAG-3'
	GFP2-E123-Q280-Rluc8	5'-GAGCTGGGTGGTGTCTACC-3'	5'-CTGGGGCTCCAGCTTCTTAA-3'
	GFP2-E123-S288-Rluc8	5'-GAGCTGGGTGGTGTCTACC-3'	5'-GGAGATCTGTGTGCAGAGG-3'
	GFP2-S109-D266-Rluc8	5'-TCAAAATTGAAAAGGAGCTGG-3'	5'-GTCATTCAGTGAGTACAGCTTATT-3'
	GFP2-K114-D266-Rluc8	5'-CAAGAAAAGACCGGTCAAAAT-3'	5'-GTCATTCAGTGAGTACAGCTTATT-3'
	GFP2-K119-D266-Rluc8	5'-TCATATCTTTTGTACAAGAAAAGACC-3'	5'-GTCATTCAGTGAGTACAGCTTATT-3'

2.4.14 *POPDC1*-ECFP and *POPDC2*-EYFP Constructs for use in Trafficking Studies in HEK293 Cells

Existing full-length cDNA sequences of human *POPDC1* and *POPDC2* within the pECFP-N1/pEYFP-N1 plasmids, which appended the sequences for C-terminus enhanced cyan fluorescent protein (ECFP) or enhanced yellow fluorescent protein (EYFP) tags, respectively, were used for POPDC protein expression and trafficking studies in HEK293 cells. The ECFP and EYFP sequences had also been previously modified to contain a C-terminus myc or human influenza haemagglutinin (HA) epitope tag, respectively. The wildtype *POPDC1* and *POPDC2* construct sequences were used as templates for the production of the modified *POPDC1*-ECFP and *POPDC2*-EYFP constructs containing the clinically identified mutations, and the αC-helix aspartic acid scanning mutations, through site-directed mutagenesis. The primers used in these reactions are shown in Table 2.21, Table 2.22, and Table 2.23, respectively, along with the specific mutation found within each construct. The oligonucleotide sequences of the constructs are shown in Appendix 10.9, Figure 10.9-16.

Table 2.21: A table showing the primers used in site directed mutagenesis of *POPDC1*-ECFP or *POPDC2*-EYFP construct sequences to introduce a set of clinically identified mutations.

Template	Product	Forward Primer	Reverse Primer
POPDC1-ECFP	*POPDC1-ECFP* (c.456_1081del; p.Q153X)	5'-CGGGATCCACCGGTCGCC-3'	5'-GATCATGCAAAACTGTCCAGTTAGTCTTCTGAAC-3'
	POPDC1-ECFP (c.515G>A; p.R172H)	5'-GTTGATGACCATCTGAGTATTC-3	5'-TGAGGTTTTATCCTCTGC-3'
	POPDC1-ECFP (c.547G>T; p.V183F)	5'-AAAAATGAAGTTCTCCTATCGAG-3'	5'-CCCTTCAAGAGAATACTC-3'
	POPDC1-ECFP (c.602C>T; p.S201F)	5'-TTTATAGATTTTCCTGAATTTAGATCAACTC-3'	5'-GGCACAGGGGTAAATGTT-3'
POPDC2-EYFP	*POPDC2-EYFP* (c.561_1093del; p.W188X)	5'-CGGGATCCACCGGTCGCC-3'	5'-CTCAGGAGAGTCCATGAACTGGTATGG-3'
	POPDC2-EYFP (c.734T>C; p.L245P)	5'-TCGGAGAAGCCCTACACTCTC-3'	5'-GATGTCATATCCCAGCAG-3'

Table 2.22: A table showing the primers used in site directed mutagenesis of the *POPDC1*-ECFP construct sequence to introduce a set αC-helix aspartic acid scanning mutations.

Template	Product	Forward Primer	Reverse Primer
POPDC1-ECFP	*POPDC1-ECFP* (c.733TTG>GAC; p.L245D)	5'-AGAACCTTTCGACTATGAAATCTTTAGGTATCTTATTG-3'	5'-GATTCCAGAAAGTATGTTAATC-3'
	POPDC1-ECFP (c.745TTT>GAC; p.F249D)	5'-GTATGAAATCGACAGGTATCTTATTGGAAAAG-3'	5'-AAGAAAGGTTCTGATTCC-3'
	POPDC1-ECFP (c.757ATT>GAC; p.I253D)	5'-TAGGTATCTTGACGGAAAAGACATCACAAATAAG-3'	5'-AAGATTTCATACAAGAAAGGTTC-3'
	POPDC1-ECFP (c.769ATC>GAC; p.I257D)	5'-TGGAAAAGACGACACAAATAAGCTC-3'	5'-ATAAGATACCTAAAGATTTCATAC-3'
	POPDC1-ECFP (c.781CTC>GAC; p.L261D)	5'-CACAAATAAGGACTACTCATTGAATGATC-3'	5'-ATGTCTTTTCCAATAAGATAC-3'
	POPDC1-ECFP (c.790TTG>GAC; p.L264D)	5'-GCTCTACTCAGACAATGATCCCAC-3'	5'-TTATTTGTGATGTCTTTTCC-3'

Table 2.23: A table showing the primers used in site directed mutagenesis of the *POPDC2*-EYFP construct sequence to introduce a set αC-helix aspartic acid scanning mutations.

Template	Product	Forward Primer	Reverse Primer
POPDC2-EYFP	*POPDC2-EYFP* (c.685ATC>GAC; p.I229D)	5'-AGAACCTTTCGACTATGAAATCTTTAGGTATCTTATTG-3'	5'-GATTCCAGAAAGTATGTTAATC-3'
	POPDC2-EYFP (c.697TTC>GAC; p.F233D)	5'-GTATGAAATCGACAGGTATCTTATTGGAAAAG-3'	5'-AAGAAAGGTTCTGATTCC-3'
	POPDC2-EYFP (c.709CTG>GAC; p.L237D)	5'-TAGGTATCTTGACGGAAAAGACATCACAAATAAG-3'	5'-AAGATTTCATACAAGAAAGGTTC-3'
	POPDC2-EYFP (c.721ATC>GAC; p.I241D)	5'-TGGAAAAGACGACACAAATAAGCTC-3'	5'-ATAAGATACCTAAAGATTTCATAC-3'
	POPDC2-EYFP (c.733CTC>GAC; p.L245D)	5'-CACAAATAAGGACTACTCATTGAATGATC-3'	5'-ATGTCTTTTCCAATAAGATAC-3'
	POPDC2-EYFP (c.742CTC>GAC; p.L248D)	5'-GCTCTACTCAGACAATGATCCCAC-3'	5'-TTATTTGTGATGTCTTTTCC-3'

2.4.15 Cloning of POPDC NanoBRET Constructs

A standard cloning protocol, as described above, was used to produce the NanoBRET constructs. Human *POPDC1* and *POPDC2* cDNA sequences, contained in pECFP-N1/pEYFP-N1 plasmids (Clontech), were used as templates. The POPDC sequences were cloned into the pFC14K or pFC32K plasmids (Promega), which contain C-terminus sequences for HaloTag and NanoLuc tags, respectively. The *POPDC1* and *POPDC2* cDNA sequences were amplified by PCR. The PCR products and destination plasmids underwent restriction digestion using the Flexi Enzyme Blend (Promega) containing SgfI and PmeI or the Carboxy Flexi Enzyme Blend (Promega), containing SgfI and EcoICRI, as appropriate. The components of the restriction digestion reactions are shown in Table 2.24. Standard ligation and amplification procedures were followed, with final products being sequenced through bi-directional Sanger sequencing.

Table 2.24: A table listing the standard components of Flexi restriction reactions used in the production of POPDC NanoBRET constructs.

Reagent	Volume / µl	Final Concentration
Flexi Digest Buffer (5X)	4	1X
PCR product / plasmid (pFC14K or pFC32K)	6 / 2	1-5 ng/µl
(Carboxy) Flexi Enzyme Blend	2	*
Water	8 / 12	-
Total	**20**	

*Stock enzyme concentration not provided.

2.4.16 Cloning of POPDC AP-FRET Constructs

The constructs previously produced to study the trafficking of the clinical POPDC mutants were subjected to site directed mutagenesis to produce the AP-FRET constructs. This was performed to produce monomerised ECFP/EYFP (mECFP/mEYFP) sequences within each construct. The wildtype and clinical mutant *POPDC1*-ECFP and *POPDC2*-EYFP construct sequences within the pECFP-N1 or pEYFP-N1 plasmids, respectively, were used as templates for the mutagenesis PCR reaction. The codon for A206 within the ECFP/EYFP tags was mutated to lysine (c.619GCC>AAG, p.A206K; numbered from the start codon of the ECFP/EYFP sequence) to obstruct endogenous dimerization of the ECFP and EYFP protein tags.[162,163] The primers shown in Table 2.25 were used for the site directed mutagenesis PCR reaction. Identical reactions were also performed with the pECFP-N1 and pEYFP-N1 plasmids to produce the mECFP and mEYFP negative control AP-FRET constructs.

Table 2.25: A table showing the primers used in site directed mutagenesis of the *POPDC1*-ECFP and *POPDC2*-EYFP construct sequences to introduce A206K mutations into the ECFP and EYFP domains.

Template	Product	Forward Primer	Reverse Primer
POPDC1-ECFP and mutant variants	mECFP (c.619GCC>AAG; p.A206K) within *POPDC1*-mECFP construct and *POPDC1* mutant variants	5'-CACCCAGTCCAAGCTGAGCAAAGAC-3'	5'-CTCAGGTAGTGGTTGTCG-3'
POPDC2-EYFP and mutant variants	mEYFP(c.619GCC>AAG; p.A206K) within *POPDC2*-mEYFP construct and *POPDC2* mutant variants	5'-CTACCAGTCCAAGCTGAGCAAAGACC-3'	5'-CTCAGGTAGTGGTTGTCG-3'

The ECFP-EYFP fusion construct, which was used as a positive control for AP-FRET experiments, was constructed using a standard cloning protocol in which the ECFP sequence was amplified by PCR and ligated into a plasmid containing the EYFP sequence. The primers used in the PCR reaction (Table 2.26) appended EcoRI and BamHI restriction sites at the 5' and 3' end of the PCR product, respectively. Bases coding for the amino acid sequence GGSG were added *via* the reverse primers to extend the final linker between the two domains to GGSGMDPPVAT. A restriction digestion of the PCR product and pEYFP-N1 plasmid using the EcoRI and BamHI enzymes, followed by ligation of the two sequences, appended the ECFP sequence to the N-terminus of EYFP within the pEYFP-N1 plasmid. The full nucleotide sequence of the construct is shown in Appendix 10.9, Figure 10.17.

Table 2.26: A table showing the primers used in the PCR reaction to amplify the ECFP sequence to produce the ECFP-EYFP fusion construct.

Template	Product	Forward Primer	Reverse Primer
pECFP-N1	*ECFP* (for ECFP-EYFP fusion construct)	5'-GATGAATTCATGGTGAGCAAGGGCGAG-3'	5'-CTCGGATCCATTCCGCTTCCTCCCTTGTACAGCTCGTCCATGCC-3'

2.4.17 Cloning of POPDC BiFC Constructs

The BiFC POPDC constructs were created using a standard cloning protocol in which the sequences for the split Venus N-terminal (VN155) and C-terminal (VC155) tags (originally provided by Carmen Dessauer, University of Texas) were inserted into plasmids containing the wildtype and clinical mutant POPDC sequences produced for the HEK293 trafficking studies. pECFP-N1 or pEYFP-N1 plasmids containing full-length wildtype and mutant *POPDC* sequences, shown above, were digested using NotI and BamHI to remove the C-terminus ECFP/EYFP tags. Concurrent digestion of plasmids containing the VN155 and VC155 tags, which also contained C-terminal myc and HA tags, respectively, yielded sequences which were ligated into the digested *POPDC1* or *POPDC2* plasmids. The full nucleotide sequences of each construct are shown in Appendix 10.9, Figures 10.18-23.

2.5 Expression, Purification and Analysis of Popeye Domain Constructs

2.5.1 Expression of Popeye Domain Protein Constructs in *E. coli*

After trials with other cell strains, the Popeye domain constructs were expressed in BL21 Star (DE3) chemically competent *E. coli* cells (Invitrogen). Cells were cultured after purchase and subjected to competency inducing reaction, as described above, before flash freezing.

Glycerol stocks or single colonies from LB-agar plates containing transformed BL21 Star (DE3) were used to inoculate 5 ml of antibiotic containing LB media (50 μg/ml ampicillin/carbenicillin or 40 μg/ml kanamycin as appropriate) in 50 ml sterile, polypropylene tubes (Falcon). These were incubated for 5-6 hours at 37 °C with shaking at 200 RPM. 1 ml of this culture was then used in inoculate 100 ml of antibiotic containing LB media in a 250 ml capacity, sterile Erlenmeyer flask, which was incubated overnight at 37 °C with shaking at 200 RPM. 20 ml of overnight culture was used to inoculate 1 L of antibiotic containing LB media in a 2 L capacity Erlenmeyer flask. These were incubated for approximately 4 hours at 37 °C with shaking at 200 RPM while the OD_{600} was measured at regular intervals. When the OD_{600} = 0.6-0.8 the cultures were cooled to 18 °C before IPTG (FluoroChem) was added to a final concentration of 750 μM. When making ^{15}N labelled protein, cultures were pelleted before addition of IPTG and washed twice in approximately 200 ml M9 salt solution. The cultures were combined and re-suspended in 1 L complete M9 medium, supplemented with 750 μM IPTG. The cultures were incubated at 18 °C overnight with continuous shaking at 200 RPM. Media was removed through centrifugation and the cell pellet resuspended in FF6 wash buffer. Cells were lysed using three runs of a French Press set to 18 kPa. The cell lysate was centrifuged for 120 minutes at 13840 rcf at 4 °C to remove cell debris and insoluble protein.

2.5.2 Fast Protein Liquid Chromatography

The AKTA Pure Protein Purification system (GE Healthcare) was used for all fast protein liquid chromatography (FPLC) purifications. 5 ml HisTrap FF Ni-NTA columns (GE Life Sciences) were used in the purification of His-tagged Popeye domain constructs. FF6 wash buffer was used to prime all system lines and equilibrate the column before sample loading. The sample was loaded onto the column at a rate of 2.5 ml/min. The column was washed with 50 ml (10 column volumes) of FF6 wash buffer at a rate of 2.5 ml/min. Elution was achieved through increasing the proportion of FF6 elution buffer in the eluent, which contained 500 mM imidazole (Sigma Aldrich). Firstly, 10 ml of a 95:5 (v/v) FF6 wash buffer to elution buffer mix was passed over the column, followed by the same volume of a 90:10 (v/v) mixture. The proportion of FF6 elution buffer was then increased to 55% (v/v) lineally over 15 ml, with a further 15 ml of this mixture passed through the column. The proportion of FF6 wash buffer was raised to 100% in a linear fashion over 20 ml, with a final 20 ml elution with pure FF6 elution buffer.

Fractions of 2 ml were collected in a cooled 96-well plate. The system was washed with FF6 wash buffer between all samples. A UV chromatogram was used to detect protein elution and to target fractions for SDS-PAGE analysis to confirm the presence of the target construct.

2.5.3 Size Exclusion Chromatography

Size exclusion chromatography was performed by passing the solution containing the FPLC purified Popeye domain construct through a ProSEC 16/60 3-70 kDa HR resin column (Generon). An AKTA Prime pump was used with a flow rate of 0.5 ml/min. The sample was loaded in FF6 wash buffer, with a reduced NaCl concentration of 250 mM, after column equilibration with identical buffer. After 80 ml of flow, 5 ml fractions were collected until all protein had passed through the column. A UV chromatogram was used to detect protein elution and to target fractions for SDS-PAGE analysis to confirm the presence of the target construct.

2.5.4 Dialysis

Solvent exchange, where required, was performed using dialysis tubing with a 6-8 kDa molecular weight cut-off (Repligen). Protein solutions of about 10-20 ml were exchanged with 1 L of buffer three times for at least 4 hours each. Continuous stirring of the exchange buffer was employed, and the samples kept at 4 °C throughout.

2.6 Analysis of Purified Popeye Domain Constructs

2.6.1 Protein Concentration Measurements

Samples containing protein were measured using a NanoDrop ND-8000 spectrophotometer. The absorption of 280 nm light was used to measure protein concentration, with the extinction coefficient for each construct estimated using the Expasy ProtParam tool (https://web.expasy.org/protparam/)

2.6.2 SDS-PAGE (Popeye Domain Construct Analysis Only)

Protein construct containing samples were analysed throughout the purification and analysis process using 1.0 mm, 8 cm x 8 cm NuPAGE 12% Bis-Tris Protein Gels (Invitrogen). Samples were mixed with loading buffer in a ratio of 4:1 (v/v) and heated at 95 °C for 3 minutes before loading. Protein size calibration was achieved using a Mark 12 unstained protein standard (Invitrogen). Protein bands were imaged using InstantBlue Coomassie protein stain (Abcam).

2.6.3 Size Exclusion Chromatography-Multi Angle Laser Lights Scattering

The protein constructs were dissolved in FF6 wash buffer with a reduced NaCl concentration of 100 mM. 50 μl of sample was manually loaded onto a Superdex 75 5/150 GL column (Cytiva). Samples were loaded at a concentration of 2.13 mg/ml (108 μM) for the S109-K272 construct and 2.6 mg/ml (105 μM) for the GB1-123-266 construct. A flow rate of 0.3 ml/min was used at a pressure of 21 bar.

The eluent was run through at Shimadzu DGU-20A5 degasser before entering the column. A Shimadzu LC-20AD pump with pulse correction was used along with an SPD-20A UV/Vis detector which recorded absorbance at 280 nm. A miniDAWN MALS detector (Wyatt) was used to measure light scattering of 690 nm light at angles of 41.5°, 90.0° and 138.5°. A Zimm fit method was applied. Curves were produced and processed in the ASTRA software package, along with the particle mass determination calculations.

2.6.4 Circular Dichroism

Circular dichroism analysis was performed by Dr Tam Bui of Kings College London. Protein samples were supplied in FF6 wash buffer with a reduced NaCl concentration of 100 mM. Each construct was at a concentration of 0.2 mg/ml.

UV & CD spectra of proteins were acquired on an Chirascan Plus spectrometer (Applied Photophysics) using 10 mm Quartz Suprasil rectangular cuvettes (Starna Scientific). The instrument was flushed continuously with nitrogen throughout the experiment. The following parameters were employed: 1 nm & 2 nm spectral bandwidth, 1 nm step-size and 1.0 s (400-230 nm) & 1.5 s (260-195 nm) sampling time per point. Background subtraction of the buffer UV & CD spectra was applied. Unless otherwise stated, all spectra were measured at 23 °C. Light scattering correction was applied on the protein near-UV absorption spectrum prior to protein concentration determination. The far-UV CD spectra were smoothed with a window factor of 4 & 8 using a Savitzky-Golay filter. Data processing was completed using APL Prodata Viewer v4.2.15 & spectra produced using Origin V6. The far-UV CD spectra of each protein were recorded at 23 °C, cooled to 6 °C, then heated to 94 °C at a rate of 1 °C/min with a 2 °C step size, and then re-cooled to 23 °C after heating. The multi–wavelength melting profiles monitored at 260-195 nm were recorded during the heating process. A 1.5 s time-per-point CD measurement time (total scan time = 2 minutes per spectrum) and 1 nm step-size were employed in the 260-195 nm with a 2 nm spectral bandwidth. A 0.5 mm rectangular cell pathlength was used. Melting temperatures were determined from the derivative CD-temperature spectra and fitted using a Levenberg–Marquardt algorithm to the van't Hoff isochore. Secondary structure predictions were made using the BeStSel web server (https://bestsel.elte.hu/index.php).[141]

2.6.5 Protein-NMR

^{1}H-^{15}N heteronuclear single quantum coherence transverse relaxation optimized spectroscopy (HSQC-TROSY) spectra were acquired on a 700 MHz spectrometer (Bruker) equipped with a QCI helium cooled cryoprobe. The GB1-S109-K272 and cleaved S109-K272 POPDC1 Popeye domain constructs were analysed at a concentration of 115 μM at 303K in arginine/glutamic acid protein-NMR buffer supplemented with 10% (v/v) D_2O (CortecNet). Samples were loaded into Shigemi NMR tubes.

Spectral widths of 38 ppm (^{15}N, direct) and 6 ppm (^{1}H, indirect) were used. Acquisition times of 47.4 ms and 69.8 ms were utilised for the ^{15}N and ^{1}H dimensions, respectively, with a total of 512 scans. Full acquisition parameters are shown below in Table 2.27.

Table 2.27: A table showing the Protein-NMR ^{1}H-^{15}N HSQC-TROSY acquisition parameters

F2 - Acquisition parameters		CHANNEL f1		CHANNEL f2		CHANNEL f3		G RADIENT CHANNEL	
Date_	20191001	SFO1	700.203348 MHz	SFO2	176.0830365 MHz	SFO3	70.9590222 MHz	GPNAM[1]	SMSQ10.100
Time	19.36	NUC1	1H	NUC2	13C	NUC3	15N	GPNAM[2]	SMSQ10.100
INSTRUM	spect	P42	1384.3 usec	P8	500 usec	P21	35 usec	GPNAM[3]	SMSQ10.100
PROBHD	5 mm CPQCI 1H-	P43	1179.05 usec	PLW2	151.0099945 W	PLW3	118.5800018 W	GPNAM[4]	SMSQ10.32
PULPROG	K_b_trosyetf3gpsi.2	PLW0	0 W	SPNAM[13	Crp80,0.5,20.1			GPNAM[5]	SMSQ10.100
TD	1574	PLW1	10.71500015 W	SPOAL13	0.5			GPNAM[6]	SMSQ10.100
SOLVENT	H2O+D2O	SPNAM[26	Reburp.1000	spoffs13	0.04 Hz			GPNAM[7]	SMSQ10.100
NS	512	SPOAL26	0.5	SPW13	44.29899979 W			GPZ1	2%
DS	8	spoffs26	2708.73 Hz					GPZ2	21%
SWH	11261.262 Hz	SPW26	0.85672998 W						
FIDRES	7.15455 Hz	SPNAM[28	Eburp2.1000						
AQ	0.0698856 sec	SPOAL28	1						
RG	256	spoffs28	2708.73 Hz						
DW	44.4 usec	SPW28	0.50490999 W						
DE	32.75 usec	SPNAM[29	Eburp2tr.1000						
TE	303 K	SPOAL29	0						
CNST19	8.6499996	spoffs29	2708.73 Hz						
CNST26	100	SPW29	0.50490999 W						
CNST43	0.69								
D0	0.000003 sec								
D1	0.27500001 sec								
D11	0.03 sec								
D12	0.00002 sec								
D13	0.000004 sec								
D16	0.0002 sec								
D25	0.0027 sec								
D26	0.0027 sec								
IN0	0.0001854 sec								
ZGOPTNS	-DLABEL_CN								

2.6.6 Differential Scanning Fluorimetry

DSF experiments were run using a QuantStudio 6 Flex Real Time PCR Thermocycler (Applied Biosystems) in MicroAmp Optical 384-well reaction plates (Life Technologies), with a total sample volume of 20 μl per well. At least 6 well replicates were run per group in each experiment. The plate was sealed with an optical adhesive cover. SYPRO orange (Sigma Aldrich) was used as the reporter dye at a final concentration of 4X (from 5000X commercial stock, actual concentration not provided). SYPRO orange fluorescence was detected using the x4-m4 filter set (as used for the ROX rtPCR

reference dye) with excitation wavelengths of 580 ± 10 nm and an emission range of 623 ± 14 nm. The plate was centrifuged before running to ensure the sample was at the bottom of the well and all bubbles had been removed. The plate was equilibrated to 25 °C for 2 minutes prior to a linear ramp from 25 °C to 95 °C at 0.05 °C/s and the change in SYPRO orange emission observed. Changes in fluorescence were sampled at 0.1 °C intervals. The first derivative of the fluorescence versus temperature was plotted, averaged, and normalised for each set of replicates. These plots were smoothed by performing averaging of 10 adjacent points with a second order smoothing function. The resulting inflection point of the smoothed derivative plot (i.e. where the rate of SYPRO fluorescence increase was at its greatest) was taken as the T_m of the protein construct.

Changes in the T_m of protein constructs as a function of the protein concentration was assessed between 0.5-25 μM. cAMP titrations (BioLog) were performed between 0-100 mM. Two sets of buffer conditions were trialled across DSF experiments. Reactions run in DSF Buffer A contained 10 mM HEPES pH 6.5 buffer, 150 mM NaCl, 4X SYPRO Orange; while reactions in DSF Buffer B contained 50 mM Tris-Cl pH 7.5 buffer, 500 mM NaCl, 10 mM $MgCl_2$, 4X SYPRO Orange. Unless otherwise stated all experiments used 10 μM protein concentration. All samples were prepared freshly on ice before analysis by combining the necessary components with recently thawed protein aliquots being added last. Residual phosphate buffer from protein purification was present resulting in approximate 1 mM Na_2HPO_4 and NaH_2PO_4 concentrations in all samples.

2.6.7 Microscale Thermophoresis

MST experiments were conducted using a Monolith NT.115 (NanoTemper). Constructs were labelled with Alexa Fluor 647 NHS Ester (Invitrogen). 10 μM protein construct were combined with 20 μM Alexa Fluor 647 NHS Ester in 200 μl of Tris-Cl buffer containing 250 mM NaCl, pH 8.5 and incubated while protected from light for 80 minutes at 25 °C. The labelling reaction mixture was applied to a solvent exchange column, as supplied with the Monolith Protein Labelling kit (NanoTemper) and equilibrated in SEC buffer. The sample was washed with 400 μl SEC buffer and the flowthrough discarded. A further 600 μl of SEC buffer was added to the column and the flowthrough collected in 100 μl fractions. The fluorescence of the sample at 280 nm and 650 nm was used to determine the total protein and Alex Fluor 647 concentration, respectively. Labelling efficiency of the protein constructs was routinely approximately 0.5. The samples were diluted in SEC buffer to yield a final concentration of 100-200 nM and cAMP was titrated into the sample. Samples were loaded into Monolith premium glass capillaries (NanoTemper). Capillary scans were conducted to ensure sufficient dye emission and locate the midpoint of each capillary for optimum MST measurement. The LED power was set to 40-60% and an infrared laser was used for 30 s while Alexa Fluor 647 emission

at the measurement point was monitored. The normalised change in fluorescence as a result of the dye temperature shift and thermophoresis were used to analyse cAMP dependent changes, determined by the change in fluorescence from pre-light application to 30 s post exposure.

2.6.8 cAMP Agarose Precipitation

Protein constructs in SEC buffer were incubated with C-8 conjugated cAMP agarose beads (Sigma Aldrich). The agarose beads were pre-equilibrated in SEC buffer. Approximately 500 nmol of conjugated cAMP was present and incubated with 1-10 nmol of protein construct in a total buffer volume of 150 μl. After a 2 hour incubation at 4 °C with continuous rolling, the column was centrifuged to pellet the cAMP conjugated agarose and the supernatant was removed. 400 μl of SEC buffer was added to the agarose pellet, which was re-suspended, and incubated with continuous rolling for 30 minutes. The suspension was again centrifuged, and the supernatant collected. A quick wash with 300 μl SEC buffer was conducted, and the buffer collected. 300 μl of SEC buffer containing 50 mM cAMP was then added to the agarose pellet and incubated for 2 hours with continuous rolling. A final centrifugation step was conducted to recover any cAMP eluted protein in the supernatant. The supernatant from each step, alongside the original protein stock was analysed by SDS-PAGE to assess any changes in Popeye domain construct.

2.7 Expression and Analysis of Full-Length POPDC Protein Constructs in HEK293 Cells

2.7.1 General HEK293 Cell Culture Procedure

All cell culture procedures were conducted in a sterile class II laminar flow cabinet. All media, reagents and equipment used was sterilised before use, and only exposed to air within the laminar flow cabinet. Cells were stored at -80 °C until thawing, and all cells that were used were between passage number 5-25. After the maximum passage number was reached, new cell cultures were established from cryo-preserved stocks. Vials containing the cells were removed from liquid N_2 immersed storage and immediately thawed in a 37 °C water bath. Cells were suspended in complete Dulbecco's modified Eagle's medium (cDMEM) and centrifuged at 125 rcf for 5 minutes. After removal of the supernatant the cell pellet was re-suspended and seeded into tissue culture plates at the desired density.

The HEK293 cell line (DSMZ) was maintained at 37 °C with 5% atmospheric CO_2 in a humidified incubator, plated in 10 cm polystyrene tissue culture plates (Sarstedt) immersed in cDMEM. When at approximately 90% confluency, cells were passaged by washing with around 10 ml phosphate buffered saline (PBS), before a brief incubation with 1 ml of trypsin-EDTA solution (Sigma Aldrich) followed by quenching of the trypsin with cDMEM after cell detachment. The cell suspension was centrifuged for

5 minutes at 125 rcf before washing with 5 ml cDMEM before an aliquot of the re-suspended cells (typically 8-15% of the total number of cells) was re-seeded in a fresh tissue culture plate.

2.7.2 General HEK293 Transfection Procedure

Cells were transferred from the starting culture dish through trypsin-EDTA detachment and seeded in 6-, 12- or 24- well tissue culture plates (Greiner Bio-One). Cells were seeded at a density of approximately 800,000, 400,000 or 200,000 per well in 2 ml, 1 ml, or 0.5 ml of cDMEM, respectively, depending on the size of the well plate used. Cells were then incubated for 24 hours to allow attachment of the cells to the plate surface and for a cell confluency of 50-60% to be achieved. Cells were then washed with PBS and fresh cDMEM was added to the wells. The protocol continued either through the use of the Lipofectamine 2000 or calcium phosphate transfection methods, as detailed below.

2.7.2.1 Lipofectamine 2000

Lipofectamine 2000 stock (Invitrogen) was diluted 20-fold in a total of 250 μl, 125 μl or 75 μl non-supplemented Dulbecco's modified Eagles medium (DMEM) or OptiMEM I (Gibco) in a sterile 1.5 ml micro tube. Plasmid DNA was separately diluted in an equal volume of DMEM or OptiMEM I. The total amount of plasmid DNA that was used depended on the size of the culture plate with 2 μg, 1 μg and 0.5 μg added per well for 6-, 12- and 24- well plates, respectively. The Lipofectamine 2000 and DNA containing solutions were combined in a 1:1 (v/v) ratio and mixed through pipetting, before incubating at room temperature for 20 minutes. Fresh cDMEM was added to the cells before the mixture containing the Lipofectamine 2000 and DNA was added dropwise to the culture plates. Cells were incubated at 37 °C with 5% atmospheric CO_2 in a humidified incubator for 24-48 hours to allow protein expression before use in the desired assay.

2.7.2.2 Calcium Phosphate

The desired amount of each plasmid was mixed with water, followed by the addition of 200 mM $CaCl_2$ (Promega) to yield a solution of total volume of 100 μl or 50 μl for 6- and 12-well culture plates, respectively. After thorough mixing, the solution was slowly added dropwise into a 1.5 ml micro tube containing an equal volume of 2X HBS (Promega), while under constant agitation. The mixture was incubated for 30 minutes with occasional mixing at room temperature before being added dropwise to the wells containing the cells. Cells were incubated at 37 °C with 5% atmospheric CO_2 in a humidified incubator for 24-48 hours to allow protein expression before use in the desired assay.

2.7.3 POPDC Expression and Trafficking Assay in HEK293 Cells

HEK293 cells were transfected in 6-well plates using the calcium phosphate method described in Section 2.7.2.2. A total of 2000 ng of plasmid DNA, with a combined total of 1200 ng of *POPDC1* and

POPDC2 cDNA coding plasmid, was used in each transfection. Empty pUC18 plasmid DNA (Thermo Fisher) was used to increase the total amount of DNA present without necessitating an increase in POPDC construct expression. Human *POPDC1* sequence containing constructs possessed C-terminal ECFP tags, while human *POPDC2* sequences were fused at the C-terminus to EYFP. See Section 2.4.14 for construct cloning details. A 5-fold excess of plasmid containing *POPDC1* cDNA was used relative to *POPDC2* in all assays of this type, including for wildtype, clinical mutants, and site directed mutants of the αC-helix. 2-3 separate transfections were performed for each experimental group. The amounts of plasmid DNA, and other reagents, used in each transfection are shown in Table 2.28.

Table 2.28: A table showing the components of the transfection of *POPDC1*-ECFP and *POPDC2*-EYFP constructs, and various mutant variants, into HEK293 cells for trafficking and expression studies.

***POPDC1*-ECFP (or mutant variant) Plasmid/ ng DNA**	***POPDC2*-EYFP (or mutant variant) Plasmid / ng DNA**	**pUC18 / ng**	**Total POPDC Coding DNA / ng**	**Total DNA / ng**	**2M $CaCl_2$ / µl**	**Water / µl**	**Total Volume / µl**
1000	200	800	1200	2000	10	Up to 100	100

Approximately 24 hours after transfection cells were seeded at a density of 120,000 cells per well into an 8-well microscope slide with a D263 M Schott glass, No. 1.5H, 170 µm ± 5 µm glass coverslip base (Ibidi). Prior to cell plating the surface of the coverslip was coated in 0.01% (w/v) sterile-filtered poly-L-lysine solution (Sigma Aldrich) for 15 minutes, followed by three washes with sterile water. Cells were incubated at 37 °C, 5% CO_2 immersed in cDMEM for approximately 24 hours. The following day the cDMEM was removed and replaced with fresh cDMEM supplemented with 1,1-dioctadecyl-3,3,3,3-tetramethylindodicarbocyanine (DiD) (Biotum) diluted 200-fold from commercial stock (actual concentration not provided). Cells were incubated with the DiD containing cDMEM for 12 minutes at 37 °C, 5% CO_2 while protected from light. Cells were then washed once with 200 µl of warm PBS before addition of 3% (w/v) paraformaldehyde (PFA) (Merck) solution for 10 minutes on ice. Cells were washed in triplicate with PBS to remove the remaining PFA before incubation with 2 µg/ml Hoechst-33342 (Sigma Aldrich) solution in PBS at room temperature for approximately 1 hour, followed by an additional wash with PBS. Cells were stored in PBS at 4 °C, protected from light for 0-2 days before imaging.

The fixed cells were imaged using a Zeiss LSM 780 AxioObserver inverted confocal laser scanning microscope, with a plan-apochromat 63X/1.40 oil objective (Zeiss). Cells were immersed in PBS during imaging. Four channels were used during image acquisition to detect the four fluorophores present: 405_{ex}/410-452_{em} nm for Hoechst-33342 (nuclei), 633_{ex}/636-735_{em} nm for DiD (plasma membrane), 458_{ex}/463-516_{em} nm for ECFP (POPDC1 constructs) and 514_{ex}/519-621_{em} nm for EYFP (POPDC2

constructs). Image acquisition settings were maintained for all images and are shown in full in Section 2.14, Table 2.32.

2.7.3.1 Determining the Ratio of POPDC Protein Expression within the Plasma Membrane and Cytoplasm of HEK293 Cells

Images of the HEK293 cells expressing POPDC proteins tagged with ECFP/EYFP were processed using FIJI.[142] To determine changes in POPDC1 and POPDC2 construct expression within the plasma membrane and cytoplasm of the cells, firstly outlines of transfected cells were manually created using the DiD dye channel as a plasma membrane marker. The nuclear stain (Hoechst-33342) was used to produce a mask containing the nuclei within the image through applying a threshold. Each cell outline was then contracted and dilated by 0.4 μm each way, which was empirically found to provide the best encapsulation of the plasma membrane accounting for imperfect outlining of cells, using a custom FIJI macro (shown in Methods section 2.15, Figure 2.1 below) to produce regions containing the plasma membrane of each cell of interest. The cytoplasm of the cells was defined as the area between the internal plasma membrane region boundary and the nucleus, as defined by the Hoechst-33342 threshold mask. An example of these analysis segments are shown in Figure 5.14 in Chapter 5. Other cell areas were defined and measured but were not used in the analysis. Background fluorescence was subtracted before measurements of ECFP and EYFP fluorescence were taken from within the plasma membrane and cytoplasmic segments. Raw ECFP and EYFP emission within the two compartments were normalised to the average value measured from HEK293 cells expressing the wildtype POPDC1-ECFP and POPDC2-EYFP pair of constructs. The ratio of emission of each fluorophore from the plasma membrane compared to the cytoplasm was used to determine the efficiency of POPDC protein trafficking/localisation to the plasma membrane of cells. Differences in the normalised emission levels of each POPDC isoform within the plasma membrane and cytoplasm, as well as the level of plasma membrane localisation, was analysed using a one-way ANOVA followed by Dunnett's post hoc test comparing values to the wildtype POPDC1-ECFP and POPDC2-EYFP group.

2.7.3.2 Cross-sectional Plots of Average POPDC Concentration across HEK293 Cells

To determine the distribution of POPDC1 and POPDC2 constructs along partial cross-sections of HEK293 cells, 10 pixel wide lines intersecting the plasma membrane in a perpendicular fashion were drawn from outside the cell to the nucleus. An example is shown in Figure 5.15A. Typically, twelve sample lines were placed within each cell, unless the size of the cell prohibited this. The level of ECFP and/or EYFP emission along each line, was recorded and normalised to their most intense point to yield peaks where the highest concentration of POPDC1-ECFP and POPDC2-EYFP was found along each partial cross-section. The level of DiD emission was also determined and the position of the plasma membrane was set to the point of maximum DiD fluorescence along each cross-section. Each partial

cross-section from cells expressing the same construct pair were aligned using the position of the plasma membrane. Each cross-sectional emission profile across all cells within each group were then combined to allow the creation of an average cross-sectional expression profile of POPDC1 and POPDC2. The peak of each emission profile represents the position, relative to the plasma membrane, where the highest concentration of POPDC1 or POPDC2 is most likely to be found within any cell expressing the particular combination of POPDC constructs. The height of the peak, relative to the rest of the profile, indicates the average enrichment of POPDC1 or POPDC2 at this favoured position compared to the rest of the cell (excluding nucleus). The cross-sectional emission profiles were plotted from 0.5 μm outside the cell to 2 μm within the plasma membrane for clarity.

The correlation between the plasma membrane and each POPDC construct was determined by finding the Pearson correlation score between DiD fluorescence and ECFP and EYFP along the averaged cross-sectional profile. Higher scores indicate that the POPDC construct is more specifically confined to the plasma membrane. A negative score shows that the localisation of the proteins to the plasma membrane is disfavoured, instead showing preferential cytoplasmic expression.

2.7.4 Type-1 Quantitative BRET Assay

The type-1 quantitative BRET assay was performed using the NanoBRET platform (Promega).[143] HEK293 cells were transfected in 12-well plates, using the Lipofectamine 2000 method described in Section 2.7.2.1. Plasmids containing cDNA sequences of human *POPDC1* and *POPDC2* fused at the C-terminus to NanoLuc (POPDC-NL) or HaloTag (POPDC-HT) sequences were used. See Section 2.4.15 for details of the cloning of these constructs. The pFC32K and pFC14K expression vectors (Promega) were used for NanoLuc and HaloTag containing constructs, respectively. The concept of the qBRET assay is described in Section 6.3.1 and Figure 6.1. To induce the range of expression ratios of POPDC-NL and POPDC-HT constructs, the ratio of plasmids containing their respective sequences was varied during the transfection. The ratios of POPDC-NL to POPDC-HT sequence containing plasmids used were: 1:1, 1:5, 1:10, 1:25, 1:50, 1:100 and 1:250. A total of 1000 ng of plasmid DNA was used when POPDC1 and POPDC2 homomeric interactions were probed, whereas a total of 500 ng was used for the co-expression of POPDC1 and POPDC2 NanoBRET constructs.

24 hours post-transfection cells were washed with PBS and cDMEM before detachment using trypsin-EDTA followed by quenching in cDMEM. The cell suspension was centrifuged at 125 rcf for 5 minutes and the cell pellet was resuspended in OptiMEM I reduced serum media supplemented with 4% (v/v) foetal bovine serum (FBS). Cells were split into two equal pools. To one group HaloTag-618 ligand stock (Promega) was added at 1 μl/ml of cell suspension to give a final concentration of 100 nM HaloTag-618. To the other cell pool 1 μl/ml of dimethyl sulfoxide (DMSO) was added. Each set of cells

were lightly vortexed and then cells were seeded into a white, flat-bottom polystyrene, tissue-culture treated 96-well plate (Corning) at a density of 20,000 cells per well in 100 μl of media, with 6 replicate wells seeded each for the HaloTag-618 and DMSO (Sigma Aldrich) aliquots in each transfection group. Cells were incubated for 24 hours at 37 °C with 5% CO_2 in a humidified incubator. An additional aliquot of HaloTag-618 supplemented cells were set aside for POPDC-HT concentration determination and seeded in a 15-well μ-slide (Ibidi) at a density of 20,000 cells per well, with two wells seeded per transfection group. Cells were incubated overnight at 37°C and 5% CO_2.

The following day, a 100-fold dilution of the commercial furimazine stock (Promega, actual concentration not provided) was made in OptiMEM I. 25 μl of the diluted furimazine was added to each well of the 96-well plate and incubated for approximately 5 minutes at room temperature. The plate was loaded into a Lumistar Optima luminometer (BMG Labtech) and shaken for 30 s. The total luminescence from each well was measured 5 minutes after furimazine addition with no optical filters in place, only the preinstalled lens. This was to provide a BRET independent measure of the expression level of POPDC-NL constructs in the cell. The specific NanoLuc luminescence and BRET-dependent HaloTag-618 ligand emission were measured immediately after using a SWP-460nm and LWP-610nm filter (both BMG Labtech), respectively. The BRET signal from each well was determined by dividing the HaloTag-618 signal by the NanoLuc luminescence and the average across the wells for each test group calculated. The background BRET was determined from the control cell wells within each group (containing no HaloTag-618 ligand) and was subtracted to give the mean corrected BRET response. For all experiments orbital averaging reading of the wells over 0.4s was used. The gain was kept constant between the two filter channels.

The aliquot of cells set aside for measuring the POPDC-HT expression level *via* direct HaloTag-618 fluorescence intensity determination were fixed in 4% (v/v) PFA for 10 minutes within the 15-well μ-slide, washed in PBS, followed by staining with 4',6-diamidino-2-phenylindole (DAPI) (Calbiochem) at a concentration of 25 μg/ml for 1 hour. Cells were imaged with a widefield Zeiss Axio Observer microscope with a X10 objective lens. When measuring HaloTag-618 fluorescence, a 593 nm laser was used with an emission filter of range 597-695 nm. When measuring DAPI emission, a 405 nm laser was used with a 410-495 nm emission filter. The entire well surface was imaged, and each image was stitched to form a single image containing all cells within the well. The DAPI channel was used to create an expanded template within FIJI which contained all the cells in the image. The template was then superimposed onto the HaloTag-618 ligand channel image. The total HaloTag-618 ligand fluorescence intensity was then measured within the template, therefore excluding empty spaces on the plate and

removing the effects of any changes in cell density. The average signal from non-transfected cells was subtracted to remove background fluorescence.

The total luminescence, as recorded from the luminometer, and the HaloTag-618 fluorescence measurements, from the widefield microscope images, were used to determine the relative cellular expression levels of POPDC-NL and POPDC-HT constructs, respectively, within each transfection group. The values of each measurement were in terms of relative luminescence units (RLU) and relative fluorescence units (RFU), respectively. A factor that allowed conversion between the two sets of units was determined through the use of a fused NanoLuc-HaloTag construct (Promega). This fusion construct was expressed in HEK293 cells and analysed in an identical manner to the POPDC containing constructs, with the total luminescence and HaloTag-618 fluorescence determined. The known one-to-one stoichiometry of the NanoLuc and HaloTag domains in this construct provided the relationship between RLU and RFU. After conversion of the total luminescence value to RFU, division of the HaloTag-618 fluorescence value by the total luminescence value (now in RFU) provided the expression ratio between the POPDC-HT and POPDC-NL constructs in each set of cells, which was used to construct the saturating BRET curves.

Analysis of the BRET saturation curves was carried out as previously reported by Felce *et al*.[144] Data points from at least three sperate transfections per group were combined. The points were fitted to a hyperbolic curve to find $BRET_{max}$. The BRET curves were then used to determine the likely stoichiometry of the any complexes formed between POPDC-NL and POPDC-HT constructs in the cells. The stoichiometry (*n*) was determined by fitting the relative expression ratio of the POPDC-HT and POPDC-NL constructs (*f*) and the BRET signal (normalised to the maximum BRET signal observed at saturating acceptor levels), to Equation 2.1.

Equation 2.1

$$\frac{BRET_{eff}}{BRET_{max}} = 1 - \frac{1}{(1+f)^{n-1}}$$

Points where *f* = 2-15 were included in the analysis. This is because the high rate of increase in diffusion mediated interactions from very low *f* ratios may lead to false oligomer signals. The points included in the analysis were either fitted to Equation 2.1 with *n* = 2, a dimer model, or *n* = 1 for a monomer model where Equation 2.1 simplifies to a linear, horizontal line at y = $BRET_{max}$. Non-linear least-squares regression was applied to the points to generate optimal curve fits for the two models. The absolute sum of squares for the dimer (SS_{dimer}) and the monomer model ($SS_{monomer}$) were determined. The ratio of these two values (SS_{dimer} / $SS_{monomer}$) was found. This ratio was then subtracted from 1 to give an R^2

value, as shown in Equation 2.2. If R^2 was positive a dimer model was preferred, whereas a negative R^2 value indicated monomers.

Equation 2.2

$$R^2 = 1 - \frac{SS_{dimer}}{SS_{monomer}}$$

It is important to have consistent total protein expression in type-1 BRET assays to reduce the effect of non-specific, diffusion-controlled interactions on the BRET signal. The total expression of POPDC-NL and POPDC-HT in each experiment were determined by summing the total luminescence, now in RFU, and HaloTag-618 fluorescence intensity, also in RFU, for each point on the BRET curve. Total emission was plotted against *f*. An F test was used to compare the fit of a horizontal line at the mean expression value for all points versus fitting using linear regression. p >0.05 indicated that there was not a statistically significant change in total expression levels as the POPDC-NL to POPDC-HT ratio was varied, i.e. the fit of the horizontal line was not significantly better than the linear regression line.

2.7.5 Acceptor-Photobleaching FRET

HEK293 cells were transfected in 6-well plates using the calcium phosphate method described in Section 2.7.2.2. A total of 2000 ng of plasmid DNA, with a combined total of 1200 ng of *POPDC1* and *POPDC2* cDNA coding plasmid, was used in each transfection. Empty pUC18 plasmid DNA (Thermo Fisher) was used to increase the total amount of DNA present without necessitating an increase in POPDC construct expression. Human *POPDC1* sequence containing constructs possessed C-terminal mECFP tags, while human *POPDC2* sequences were fused at the C-terminus to mEYFP. See Section 2.4.14 and 2.4.16 for construct cloning details. A 5-fold excess of plasmid containing *POPDC1* cDNA was used relative to *POPDC2* in all assays. 2-3 separate transfections were performed for each experimental group. The amounts of plasmid DNA, and other reagents, used in each transfection are shown in Table 2.29.

Table 2.29: A table showing the components of the transfection of *POPDC1*-ECFP and *POPDC2*-EYFP constructs, and various mutant variants, into HEK293 cells for AP-FRET assays.

***POPDC1*-*m*ECFP (or mutant variant) Plasmid/ ng DNA**	***POPDC2*-mEYFP (or mutant variant) Plasmid / ng DNA**	**pUC18 / ng**	**Total POPDC Coding DNA / ng**	**Total DNA / ng**	**2M $CaCl_2$ / µl**	**Water / µl**	**Total Volume /µl**
1000	200	800	1200	2000	10	Up to 100	100

Approximately 24 hours after transfection cells were seeded at a density of 120,000 cells per well into an 8-well microscope slide with a D263 M Schott glass, No. 1.5H, 170 µm ± 5 µm glass coverslip base (Ibidi). Prior to cell plating the surface of the coverslip was coated in 0.01% (w/v) sterile-filtered poly-L-lysine solution (Sigma Aldrich) for 15 minutes, followed by three washes with sterile water. Cells

were incubated at 37 °C, 5% CO_2 immersed in cDMEM for approximately 24 hours. The following day the cDMEM was removed and replaced with fresh cDMEM supplemented with 1,1-dioctadecyl-3,3,3,3-tetramethylindodicarbocyanine (DiD) (Biotum) diluted 200-fold from commercial stock (actual concentration not provided). Cells were incubated with the DiD containing cDMEM for 12 minutes at 37 °C, 5% CO_2 while protected from light. Cells were then washed once with 200 μl of warm PBS before addition of 3% (w/v) paraformaldehyde (PFA) (Merck) solution for 10 minutes on ice. Cells were washed in triplicate with PBS to remove the remaining PFA before incubation with 2 μg/ml Hoechst-33342 (Sigma Aldrich) solution in PBS at room temperature for approximately 1 hour, followed by an additional wash with PBS. Cells were stored in PBS at 4 °C, protected from light for 0-2 days before imaging.

The fixed cells were imaged using a Zeiss LSM 780 AxioObserver inverted confocal laser scanning microscope, with a plan-apochromat 63X/1.40 oil objective (Zeiss). Cells were immersed in PBS during imaging. ECFP was excited and detected using 458_{ex}/463-516_{em} nm channels, while EYFP FRET dependent emission was monitored using a 519-621 nm emission channel. EYFP was then photobleached using a 514 nm laser, and the ECFP emission remeasured. Any residual EYFP fluorescence was measured after photobleaching. Image acquisition settings were maintained for all images and are shown in full in Section 2.14, Table 2.32.

The efficiency of FRET between the ECFP and EYFP groups was determined using Equation 2.3, where I_{pre} is the ECFP emission before EYFP photobleaching and I_{post} is the ECFP emission after EYFP photobleaching. I_{post} was normalised to account for any remaining non-photobleached EYFP so that all values were extrapolated to the expected value for when no active EYFP was present. Results were excluded from samples where more than 70% of the initial EYFP signal remained. The difference between the POPDC groups and the negative control mECFP + mEYFP co-transfection group were analysed using one-way ANOVA followed by Dunnett's method. A schematic of the assay is provided in Figure 6.3.

Equation 2.3

$$E = \frac{I_{post} + I_{pre}}{I_{post}}$$

2.7.6 Bimolecular Fluorescence Complementation

HEK293 cells were transfected using the calcium phosphate method, as described in Section 2.7.2.2, in 6-well tissue culture plates. pECFP-N1 plasmids containing the cDNA sequences of full-length human *POPDC1* and *POPDC2* constructs fused at the C-terminus with VC155 or VN155 sequences,

respectively, were used for transfection. The production of these constructs by molecular cloning is described in Section 2.4.17. A 5:1 ratio of *POPDC1*-VC155 to *POPDC2*-VN155 sequence containing plasmid was used in all transfections. Co-transfection of *POPDC1*-VN155 and *POPDC2*-VN155 was used as negative control. A total of 1200 ng of POPDC containing plasmid was used in all transfections. All cells were also transfected with 400 ng of the pmRFP-N1 plasmid (gifted by Robert Campbell & Michael Davidson & Roger Tsien, Addgene plasmid 54635) to act as an internal control for transfection efficiency, as well as the pUC18 plasmid to bring the total DNA amount used to 2000 ng. The components of the transfection reaction are shown in Table 2.30.

Table 2.30: A table showing the components of the calcium phosphate-based transfection of *POPDC1*-VC155 and *POPDC2*-VN155 containing plasmids, and various mutant variants, into HEK293 cells for BiFC studies.

POPDC1-VC155 Plasmid DNA/ ng	POPDC2-VN155 Plasmid DNA/ ng	mRFP Plasmid DNA / ng	pUC18 / ng	Total POPDC Coding DNA / ng	Total DNA / ng	2M $CaCl_2$ / µl	Water / µl	Total Volume /µl
1000	200	400	400	1200	2000	10	Up to 100	100

Approximately 24 hours post-transfection, cells were washed with PBS and detached using trypsin-EDTA solution. Cells were pelleted through centrifugation at 125 rcf for 5 minutes, followed by re-suspension in cDMEM. 300ml of cell suspension was added to a well of an 8-well microscope slide, freshly coated in poly-L-lysine, and incubated for a further 24 hours. The following day cells were washed once with PBS before fixation with 4% (w/v) PFA on ice, which was removed with three further washes with PBS. Incubation with 2 µg/ml Hoechst-33342 in PBS at room temperature was performed, and the cells were stored for 0-2 days in PBS at 4 °C, protected from light.

The cells were imaged using a Zeiss Axio Observer confocal microscope using a 10X objective (Zeiss). Three channels were used during image acquisition to detect the three fluorophores present: 405_{ex}/410-503_{em} nm for Hoechst-33342 (nuclei), 514_{ex}/516-587_{em} nm for reformed Venus (interacting POPDC constructs) and 543_{ex}/582-754_{em} nm for the mRFP (internal control). Images were analysed using FIJI. The Hoechst-33342 channel was used to create a threshold mask to allow subtraction of the nuclear area of cells. To further control for transfection efficiency, protein expression and cell density differences a mask containing only transfected cells was created using a combined projection of the Venus and mRFP channels, with areas below background fluorescence excluded. Background fluorescence was subtracted before measurement. The median Venus intensity within the area containing transfected cells was divided by the median mRFP emission. The Venus:mRFP ratio (the normalised BiFC signal) from each group was further normalised to the wildtype POPDC1-VC155 and POPDC2-VN155 pair. Difference in the normalised BiFC signal were analysed using a one-way ANOVA

followed by Dunnett's post hoc test comparing values to the wildtype POPDC1-VC155 and POPDC2-VN155 group

2.7.7 Co-Immunoprecipitation

Co-IP was performed using the ProFound Pierce c-myc-tag IP/Co-IP Kit (Thermo Scientific). HEK293 cells in a 6-well plate expressing wildtype or clinical mutant POPDC1-ECFP (containing a C-terminal myc epitope tag) and POPDC2-EYFP (containing a C-terminal HA epitope tag) constructs were incubated with 700 μl Co-IP lysis buffer for 30 minutes on ice. Cells were scraped from the surface of the well and passed through a 25G needle five times using a 1 ml syringe and transferred to a 1.5 ml micro tube on ice. Lysates were sonicated at 20 mA on ice using three rounds of 15 s between 15 s pauses. The sonicated lysates were centrifuged at 16,000 rcf for 30 mins at 4 °C. The supernatant was recovered, and a second round of centrifugation was performed as before. The supernatant was transferred to the provided sealed spin column. A 30 μl aliquot was removed and stored at 4 °C overnight as a control. Meanwhile, 9.8 μl of the provided anti-myc agarose was added to the spin column and incubated with continuous rotation overnight at 4 °C. The following day the spin column was centrifuged at 2500 rcf for 10 s and the flowthrough discarded. The remaining agarose was washed in 500 μl of the provided BuPH-TBS solution five times. 30 μl of the provided non-reducing sample buffer, diluted to 2X from 5X stock using water, was added to the re-sealed spin column. The agarose and non-reducing sample buffer were mixed by pipetting and then boiled at 96 °C for 5 minutes. The spin column was briefly centrifuged, and the flowthrough collected. 3 μl of β-mercaptoethanol was added to each sample before loading onto an SDS-PAGE gel.

SDS-PAGE gels were constructed using combined resolving and stacking gels, with their components shown in Table 2.31 and Table 2.32, respectively.

Table 2.31: A table showing the components of each 10% SDS-PAGE resolving gel.

Component	Volume
Deionised water	3.3 ml
30% acrylamide/bis solution	2.8 ml
1.5 M Tris-Cl pH 8.8	2.1 μl
20% (w/v) SDS	42 μl
10% APS	83 μl
TEMED	3.3 μl

Table 2.32: A table showing the components of the SDS-PAGE stacking gel.

Component	Volume
Deionised water	1.4 ml
30% acrylamide/bis solution	333 μl
1 M Tris-Cl pH 6.8	250 μl
20% (w/v) SDS	10 μl
10% APS	20 μl
TEMED	2 μl

APS (Sigma Aldrich) and TEMED (Merck) were added immediately before the pouring of each gel and thoroughly mixed. The resolving gel was poured between two glass plates, using a 1.5 mm spacer plate, and left to solidify for approximately 45 minutes. After the resolving gel had set, the stacking gel was added on top and the well comb inserted. The SDS-PAGE was stored at 4 °C until use within two days. The glass plates containing the gel was placed in the electrophoresis chamber, which was filled with SDS-PAGE running buffer. 50 μl of each sample was added to each well, along with a protein marker in terminal wells. Electrophoresis was performed by the application of 110-150 V using a PowerPac Basic (Bio-Rad).

Following completion of SDS-PAGE, the gel was removed from the glass plates and was equilibrated in transfer buffer for 10 minutes, along with size-matched 3M filter paper sheets (Whatman) and nitrocellulose membrane (Bio Trace). The gel, membrane, and filter paper sheets (three below, three above the gel and membrane) were stacked onto a semi-dry blotter. Air bubbles were removed from the stack by compression. Blotting was performed with a set current of 0.07 A per stack for 90 minutes. After transfer of the protein to the nitrocellulose membrane, the membrane was blocked with blocking buffer for 60 minutes with gentle shaking. The membrane was incubated with the primary antibody at the desired concentration in blocking buffer overnight at 4 °C with continuous rotation. The following day the membrane was washed with TBS-T using three quick washes and a further three washes of 15 minutes each. The horse radish peroxidase (HRP) conjugated secondary antibody (1:1000 (v/v) dilution from commercial stock, Vector Laboratories) was added in blocking buffer and incubated with the membrane for 60 minutes at room temperature. The membrane was washed with TBS-T as before. The blot was imaged using the Immobilon Western chemiluminescence kit (Millipore). The chemiluminescence solution was prepared immediately before imaging and incubated with the membrane for 5 minutes before exposure using a ChemiDoc MP Imaging System (Bio-Rad).

2.8 BRET Assays for the Detection of cAMP or Hit Compound Dependent Changes in POPDC Protein, Popeye Domain, or Canonical cAMP Effectors

2.8.1 POPDC1-POPDC2 cAMP Response NanoBRET Assay

The NanoBRET platform was utilised to try to detect cAMP-dependent changes in the interaction between POPDC1 and POPDC2.[166] HEK293 cells were transfected with POPDC-NL and POPDC-HT constructs using Lipofectamine 2000. See Section 2.4.15 for details of NanoBRET construct cloning. A total of 2200 ng of plasmid DNA was used, with a 100-fold excess of *POPDC2* sequence containing plasmid. 24 hours post-transfection cells were washed with PBS and cDMEM before detachment using trypsin-EDTA followed by quenching in cDMEM. The cell suspension was centrifuged at 125 rcf for 5 minutes and the cell pellet was resuspended in OptiMEM I reduced serum media supplemented with 4% (v/v) FBS. Cells were split into two equal pools. To one group HaloTag-618 ligand stock was added

at a ratio of 1 μl/ml of cell suspension to give a final concentration of 100 nM HaloTag-618. To the other cells pool 1 μl/ml of DMSO was added. Each set of cells were lightly vortexed and then cells were seeded into a white, flat-bottom polystyrene, tissue-culture treated 96-well plate at a density of 20,000 cells per well in 100 μl of media, with 4-6 wells seeded for both the HaloTag-618 and DMSO aliquots in each transfection group. Cells were incubated for 24 hours at 37 °C with 5% CO_2 in a humidified incubator.

The following day, 50 μM forskolin (Sigma Aldrich) was added to the wells and incubated for 15 minutes. A 100-fold dilution of the commercial furimazine stock was made in OptiMEM I. 25 μl of the diluted furimazine was added to each well of the 96-well plate and incubated for a further 5 minutes at room temperature. The plate was loaded into a Lumistar Optima luminometer and shaken for 30 s. The NanoLuc luminescence and BRET-dependent HaloTag-618 ligand emission were immediately measured using a SWP-460 nm filter and LWP-610 nm filter, respectively. The BRET signal from each well was determined by dividing the HaloTag-618 signal by the NanoLuc luminescence and the average for each test group calculated (minimum 6 wells per test group). The background BRET was determined from the DMSO only cell wells within each group (containing no HaloTag-618 ligand). The background BRET was subtracted for each group to give the mean corrected BRET response. For all experiments orbital averaging reading of the wells over 0.4 s was used. The gain was kept constant between the two filter channels. The difference in the BRET signal from control and 50 μM forskolin supplemented cells was analysed by a student's t-test.

2.8.2 Popeye Domain cAMP Sensor Trials

The Popeye domain cAMP sensors utilised the BRET2 platform. HEK293 cells were transfected with one of the series of Popeye domain containing sequences contained within the pGFP2-C1 plasmid. See Section 2.4.13 for details on the cloning of the constructs. The Popeye domain sequences were fused at the N-terminus to a GFP2 sequence and at the C-terminus to Rluc8. The Lipofectamine 2000 method of transfection (as described in Section 2.7.2.1) was employed with the cells seeded into a 12-well plate. 1000 ng of Popeye domain sequence containing plasmid DNA was used in each transfection. 24 hours post-transfection cells were washed with PBS and cDMEM before detachment using trypsin-EDTA followed by quenching in cDMEM. The cell suspension was centrifuged at 125 rcf for 5 minutes and the cell pellet resuspended in OptiMEM I supplemented with 4% (v/v) FBS. Cells were then seeded into a white, flat-bottom polystyrene, tissue-culture treated 96 well plate at a density of 20,000 cells per well in 100 μl of media. Cells were incubated for a further 24 hours at 37 °C with 5% atmospheric CO_2 in a humidified incubator. The following day forskolin was added to wells to a final concentration of 50 μM and the cells were incubated for a further 20 minutes. Vehicle was added to control cells

instead of forskolin. 5 minutes before measurement 5 μM coelenterazine-400a (Biotum) was added to the wells. The well plate was inserted into a Lumistar Optima luminometer and shaken for 20 s before immediately recording the BRET signal. The Rluc8 luminescence was recorded using a 410-80 nm filter, and the BRET dependent GFP2 emission was measured with a 515-30 nm filter (both BMG Labtech). The BRET signal from each well was determined by dividing the Rluc8 emission by the GFP2 signal, which was averaged across each test group (minimum 5 wells per test group). The difference in the BRET signal from control and 50 μM forskolin supplemented cells was analysed by a student's t-test.

2.9 PKA and EPAC1 cAMP Sensor Assays

HEK293 cells were transfected with either sensor, both using the BRET2 platform, using the Lipofectamine 2000 method of transfection (as described in Section 2.7.2.1) in 6-well plates. Details of the plasmids used in the transfections of both sensors are provided in Section 2.4.12. 2000 ng of plasmid containing the EPAC-1 sensor was used in each well, while 1000 ng of each PKA sequence containing plasmid (one containing the RIα-Rluc8 sequence, and the other plasmid with GFP2-Cα) was used for each well. 24 hours post-transfection the cells were washed with PBS and cDMEM before detachment using trypsin-EDTA followed by quenching in cDMEM. The cell suspension was centrifuged at 125 rcf for 5 minutes and the cell pellet resuspended in OptiMEM I supplemented with 4% (v/v) FBS. Cells were then seeded into a white, flat-bottom polystyrene, tissue-culture treated 96-well plate at a density of 20,000 cells per well in 90 μl of media. Cells were incubated for a further 24 hours at 37°C with 5% atmospheric CO_2 in a humidified incubator. The following day 20 μl of passive lysis buffer (Promega) was added directly to each well and incubated at room temperature for 15 minutes on a plate rocker. 30 μl of PBS containing the 8-CPT-cAMP, 8-Br-cAMP (both BioLog) or Popeye domain hit compound (Enamine) to give the desired final concentration in the well, along with 5μM coelenterazine-400a (Biotum), was added to each well and mixed using a pipette. Each concentration of Popeye domain hit compounds was tested in triplicate wells per experiment, while each concentration of cAMP analogue was added to 6-7 wells. The plate was incubated for a further 5 minutes before the well plate was inserted into the luminometer and shaken for 20 s before immediately recording the BRET signal. The Rluc8 luminescence was recorded using a 410-80 nm filter, and the BRET dependent GFP2 emission was measured with a 515-30 nm filter. The BRET signal from each well was determined by dividing the Rluc8 emission by the GFP2 signal. The level of recorded BRET from each well was normalised to maximal BRET for each reporter and the relative BRET change used to find the EC_{50} of each compound where possible. Three full repeats of the assay were performed.

2.10 Skeletal Muscle Biopsy Sections Staining and Imaging

All processing and staining of human and mouse tissue sections was performed by Ursula Herbort-Brand. Activities involving animals were completed by Ursula Herbort-Brand in compliance with United Kingdom Home Office Animals (Scientific Procedures) Act 1986. Anaesthetised 16-week male and female C57BL/6OlaHsd mice were euthanised by decapitation before dissection. Mouse skeletal muscle was taken from the gastrocnemius. Tissue was fixed in 2% (w/v) PFA in PBS for 10 minutes. The fixed tissue was transferred to a solution of 10% (w/v) sucrose in PBS until it was no longer buoyant, before the same procedure was carried out using 20% (w/v) sucrose in PBS. A further incubation overnight in 30% (w/v) sucrose in PBS was performed. A 1:1 mixture of 30% (w/v) sucrose in PBS and polyfreeze tissue freezing medium was made and used to incubate the tissue for 2 hours. Two further incubations with only polyfreeze tissue freezing medium, each for 2 hours, were completed before storing the tissue at -80 °C before sectioning using a cryo-microtome.

Skeletal muscle biopsies were taken from the leg of patients in accordance with all local regulations. Sections mounted on coverslips from the *POPDC1* (c.547G>T, p.V183F) supplied by Giorgio Tasca (Gemilli University Hospital, Rome), and the *POPDC1* (c.457C>T, p.Q153X) patient from Anne Schänzer (Justus Liebig University, Giessen). Unfixed cryosections from patient biopsies mounted on slides were thawed while immersed in PBS, followed by fixation using a 2% (w/v) PFA solution in PBS for 10 minutes at room temperature. The PFA was removed by three washes with PBS, each with a 5 minute incubation.

Both human and mouse samples were then permeabilised through three 5 minute incubations with 0.25% (v/v) Triton X-100 solution (Sigma Aldrich) in PBS. The sections were subsequently blocked through a 60 minute incubation with section blocking buffer at room temperature. An overnight incubation with a 50-fold dilution of anti-POPDC1/POPDC2 primary antibody (both Sigma Aldrich) and a 100-fold dilution of anti-α-sarcoglycan primary antibody (Lecia Biosystems) in section blocking buffer was performed at 4 °C. The following day three 5 minute washes with PBS were carried out before application of the respective secondary antibodies, also in section blocking buffer, for a 60 minute incubation at room temperature, protected from light. An Alexa Fluor 488 conjugated anti-rabbit secondary antibody (Invitrogen) was used for POPDC1 or POPDC2 staining, while an Alexa Fluor 555 conjugated anti-mouse secondary antibody was utilised for α-sarcoglycan staining (Invitrogen). Both secondary antibodies were diluted 200-fold from the commercial stock and were centrifuged for 5 minutes before use. After a double 5 minute wash with PBS a third 5 minute incubation with PBS containing 1 μg/ml DAPI was performed. Sections were mounted using MOWIOL (Calbiochem) and stored at 4 °C, protected from light, until fully set.

The fixed cells were imaged using a Zeiss LSM 780 AxioObserver inverted confocal laser scanning microscope, with a plan-apochromat 20X/0.8 M27 objective (Zeiss). Four channels were used during image acquisition: 405_{ex}/410-495_{em} nm for DAPI (nuclei), 488_{ex}/489-552_{em} nm for Alexa Fluor 488 (POPDC1 or POPDC2), 543_{ex}/548-697_{em} nm for Alexa Fluor 544 (α-sarcoglycan) and a brightfield channel. Detailed image acquisition settings were maintained for all images and are shown in Table 2.32. 4-6 images were taken for each analysis group.

2.10.1 Determining the Ratio of POPDC Protein Expression within the Plasma Membrane and Cytoplasm of Skeletal Muscle Fibres

Images of the skeletal muscle fibres were processed using FIJI. To determine changes in the expression of POPDC1 and POPDC2 within the plasma membrane and cytoplasm of the cells the α-sarcoglycan channel was used to define the outline of the muscle fibres. Control sections from age and sex-matched patient, or wildtype mouse, were prepared and analysed simultaneously within each analysis group. POPDC1 and POPDC2 stainings were assigned separate control sections to ensure consistent comparisons.

Background fluorescence was subtracted before analysis. A custom macro in FIJI was used to analyse the images, which is shown in full in Section 2.15, Figure 2.2. A threshold was applied to the α-sarcoglycan channel to produce outlines of each complete, individual muscle fibre cross-section within each image. The outlines created were manually inspected to remove any erroneous fibre outlines. Any remaining outlines smaller than 200 μm^2 were excluded. The cell outlines were then contracted and dilated by 0.8 μm each way, which was empirically found to provide the best encapsulation of the plasma membrane accounting for imperfect outlining of cells, to produce a region containing the plasma membrane and the cytoplasm of the cell of interest. Measurements of the mean Alexa Fluor 488 and Alexa Fluor 544 fluorescence from within the plasma membrane region and cytoplasmic region of each identified fibre were then taken. These measurements were used to determine the expression level of POPDC1/POPDC2 and α-sarcoglycan within each subcellular location, and the expression level of POPDC1/POPDC2 relative to the level of α-sarcoglycan in the plasma membrane. These values were normalised to each respective control sample. The ratio of Alex Fluor 488 fluorescence from the plasma membrane and cytoplasm was used to determine the efficiency of POPDC protein trafficking/localisation to the plasma membrane of each fibre. In addition, the cross-sectional area of each muscle fibre was also determined from each group of images. The α-sarcoglycan channel was used for determination of muscle fibre area meaning that images for POPDC1 and POPDC2 were combined for this analysis. The values from individual fibres were combined across multiple images within each group, and comparisons were made between each patient/mutant mouse and their respective controls using a student's t-test.

2.10.2 Genetic Analysis of cJET Patients

Genetic analysis of patients was performed by Benjamin Helm.[145] Whole exome genetic sequences were analysed using the Exomiser variant prioritization program,[146] based on gene-phenotype associations, expected protein impact, and other parameters. Variants with Exomiser scores of greater than 0.80 and reasonable biological plausibility were prioritised. Further filtering to favour variants likely to act in an autosomal dominant manner and which were found in all symptomatic members of the family was also performed.

2.11 Protein Sequence Alignments

All alignments of POPDC amino acid residue sequences were performed using the Clustal Omega algorithm within the online server (https://www.ebi.ac.uk/Tools/msa/clustalo/) or the JalView application.[147,148]

2.12 Structural Models of POPDC Proteins

Full-length structural models of the POPDC proteins were taken from the AlphaFold Protein Structure Database.[23,24] Models and empirical protein structures were examined and analysed using Chimera X.[149] Overlays of protein structures were created using the Matchmaker tool in ChimeraX. Additional models of the Popeye domain were constructed using the Phyre2 server.[150] Secondary structure predictions were made using the JPred4 program.[151]

2.13 Software

Oligonucleotide sequence inspection and primer design was performed in SnapGene Viewer. Confocal images of muscle fibres and HEK293 cells were obtained using the inbuilt Zeiss Zen Black control software and images processed using FIJI.[142] Data produced by FIJI analysis was further processed using Python3. Graphs were plotted in GraphPad Prism. Figures were constructed using the Microsoft PowerPoint, BioRender and Servier Medical Art packages. BRET data was processed using the in-built BMG Labtech MARS Data Analysis Software. Further data analysis was performed in Microsoft Excel.

2.14 Microscopy Acquisition Settings

The settings used during acquisition of images using the confocal microscope are shown in Table 2.33.

Table 2.33: A table showing the image acquisition settings used for the different imaging-based studies completed in this work.

	HEK293 POPDC Trafficking	Muscle Biopsy Sections	HEK293 AP-FRET	HEK293 BiFC
Channels	4	4	2	3
Scaling (per Pixel)	0.07 X 0.07μm	0.42 X 0.42μm	0.13 X 0.13 μm	0.83 X 0.83 μm
Image Size (Pixels)	1024 X 1024	1024 X 1024	512 X 512	1024 X 1024
Image Size (Scaled)	67.48 x 67.48μm	425.10 x 425.10 μm	67.48 x 67.48 μm	850.19 x 850.19 μm
Bit Depth	16 bit	16 bit	16 bit	16 bit
Scan Zoom	X: 2, Y 2	X: 1, Y 1	X: 2, Y 2	X: 1, Y 1
Pixel Time	3.15μs	1.27. μs	0.79 μs	1.27 μs
Line Time	0.35 ms	0.03 ms	0.42 ms	0.03 ms
Frame Time	15.49s	37.53 s	1.94s	12.51 s
Averaging	4	4	4	4
Microscope	Zeiss LSM 780 AxioObserver	Zeiss LSM 780 AxioObserver	Zeiss LSM 780 AxioObserver	Zeiss LSM 780 AxioObserver
Objective	Plan-apochromat 63X/1.40 oil DIC M27	Plan-apochromat 20X/0.8 M27	Plan-apochromat 63X/1.40 oil DIC M27	EC Plan-Neofluar 10x/0.30 M27
Beam Splitter	MBS: 488/543/633 MBS_InVis: -405	MBS: Plate MBS_InVis: MBS -405	MBS: 488/543/633 MBS_InVis: -405	MBS: 488/543/633 MBS_InVis: -405
Lasers	405nm: 2.00% 458nm: 12.6% 514nm: 2.00% 633nm: 1.90%	405 nm: 0.89% 488 nm: 0.96% 543 nm: 0.87%	458nm: 29.1%	405nm: 0.97% 514nm: 0.98% 543nm: 0.82%
Excitation Wavelength	Hoechst-33342: 405 nm ECFP: 458 nm EYFP: 514 nm DiD: 633 nm	DAPI: 405nm Alex Fluor 488: 488 nm Alex Fluor 544: 543 nm Brightfield	ECFP: 458 nm	Hoechst-33342: 405nm Venus: 514nm mRFP: 543nm
Emission Wavelengths	Hoechst-33342: 410-452 nm ECFP: 463-516 nm EYFP: 519-621 nm DiD: 636-735 nm	DAPI: 410-495 nm Alex Fluor 488: 489-552 nm Alex Fluor 544: 548-697 nm Brightfield	ECFP: 463-516 nm EYFP: 519-621 nm	Hoechst-33342: 410-503nm Venus: 516-587nm mRFP: 582-754nm
Binning Mode	1X1	1X1	1X1	1X1
Detector	PMT	PMT	PMT	PMT
Detector Gain	Hoechst-33342: 636.2 ECFP: 789.0 EYFP: 759.7 DiD: 694.4	DAPI: 401 Alex Fluor 488: 795 Alex Fluor 544: 727 Brightfield: 245	ECFP: 779.3 EYFP: 774.1	Hoechst-33342: 738.4 Venus: 784.3 mRFP: 657.6
Detector Offset	Hoechst-33342: 100 ECFP: 100 EYFP: 256 DiD: 256	DAPI: 800 Alex Fluor 488: 36 Alex Fluor 544: 200 Brightfield: -9368	ECFP: 256 EYFP: 200	Hoechst-33342: 200 Venus: 100 mRFP: 200
Detector Digital Gain	All channels: 1.0	DAPI: 1.4 Alex Fluor 488: 0.7 Alex Fluor 544: 1.0 Brightfield: 0.3	All channels: 1.0	All channels: 1.0

2.15 FIJI Macros used in Image Processing

The macros used to define subcellular segments in HEK293 cells and skeletal muscle sections and measure POPDC expression levels are shown in Figure 2.1 and 2.2, respectively.

```
//initialise
fn=getTitle();
getDimensions(ImageWidth, ImageHeight, ImageChannels, ImageSlices, ImageFrames);
getVoxelSize(px, py, pz, unit);
n=roiManager("Count");
roiManager("Show All with labels");
Pix="";
keep_int=5;

//creat nuclear mask
run("Select None");
run("Duplicate...", "title=[nuclear mask] duplicate channels=1");
run("Gaussian Blur...", "sigma=2");
run("Threshold...");
setAutoThreshold("Default dark");
waitForUser("Check threshold for nuclei /n then press OK");
setOption("BlackBackground", false);
run("Convert to Mask");
run("Fill Holes");

//rename original rois
for (roi=0;roi<n;roi++){
    i. roiManager("select", roi);
    ii. roiManager("rename", "original ROI "+roi+1);
b. }

//size values
enlarge_value=0.4;
reduce_value=0.4;
reduce_value=reduce_value*-1;
In_Pixels=false;

if (In_Pixels==true){
Pix=" pixel";
}

for (roi=0;roi<n;roi++){
//reduce
roiManager("select", roi)
run("Enlarge...", "enlarge=reduce_value"+Pix);
roiManager("Add");

//cytoplasmic ring
roiManager("select", n+(roi*keep_int));
run("Analyze Particles...", "size=10.00-Infinity add");
roiManager("Select", newArray(n+(roi*keep_int),n+(roi*keep_int)+1));
roiManager("XOR");
roiManager("Add");

//enlarge
roiManager("select", roi);
run("Enlarge...", "enlarge=enlarge_value"+Pix);
roiManager("Add");

//membrane ring
roiManager("Select", newArray(n+(roi*keep_int),n+(roi*keep_int)+3));
roiManager("XOR");
roiManager("Add");
roiManager("deselect");
roiManager("select", n+(roi*keep_int));
roiManager("rename", "New Reduced ROI "+roi+1);
roiManager("select", n+(roi*keep_int)+1);
roiManager("rename", "Nucleus "+roi+1);
roiManager("select", n+(roi*keep_int)+2);
roiManager("rename", "Cytoplasmic Roi "+roi+1);
roiManager("select", n+(roi*keep_int)+3);
roiManager("rename", "New Enlarged Roi "+roi+1);
roiManager("select", n+(roi*keep_int)+4);
roiManager("rename", "Membrane Roi "+roi+1);
roiManager("deselect");
}

selectWindow("nuclear mask");
close();

selectWindow(fn);
roiManager("Show All with labels");
run("Subtract Background...", "rolling=50");
run("Subtract Background...", "rolling=50");
roiManager("multi-measure measure_all");
```

Figure 2.1: Macro for Measuring POPDC1-ECFP and POPDC2-EYFP Expression in Different Regions of HEK293 Cells

```
1.  //initialise
2.  fn=getTitle();
3.  getDimensions(ImageWidth, ImageHeight,
    ImageChannels, ImageSlices, ImageFrames);
4.  getVoxelSize(px, py, pz, unit);
5.  run("Options...", "iterations=1 count=1 black");

6.  roiManager("Show All with labels");
7.  Pix="";
8.  keep_int=3;


9.  //size values
10. enlarge_value=0.8;
11. reduce_value=0.8;
12. reduce_value=reduce_value*-1;
13. In_Pixels=false;

14. if (In_Pixels==true){
15. Pix=" pixel";
16. }

17. //clears roi manager
18. roiManager("reset");

19. //creates mask
20. run("Select None");
21. run("Duplicate...", "title=mask duplicate
    channels=ImageChannels");
22. run("Enhance Local Contrast (CLAHE)", "blocksize=127
    histogram=256 maximum=6 mask=*None*");
23. run("Despeckle");
24. //run("Median...", "radius=2");
25. run("Threshold...");
26. setAutoThreshold("Default dark");

27. waitForUser("Check threshold \n then press ok");

28. run("Convert to Mask");
29. //run("Dilate");
30. run("Skeletonize");
31. run("Dilate");
32. setAutoThreshold("Huang");
33. run("Analyze Particles...", "size=200-Infinity exclude
    add");
34. close();

35. roiManager("Show All without labels");
36. waitForUser("Edit Originl list of ROI's \n then press
    OK");
37. n=roiManager("Count");

38. //rename original rois
39. for (roi=0;roi<n;roi++){
        i. roiManager("select", roi);
        ii. roiManager("rename", "original
        ROI "+roi+1);
40. }


41. //create region rois
42. for (roi=0;roi<n;roi++){
43. //reduce
44. roiManager("select", roi)
45. run("Enlarge...", "enlarge=reduce_value"+Pix);
46. roiManager("Add");

47. //enlarge
48. roiManager("select", roi);
49. run("Enlarge...", "enlarge=enlarge_value"+Pix);
50. roiManager("Add");

51. //cytoplasmic ring
52. roiManager("Select",
    newArray(n+(roi*keep_int),n+(roi*keep_int)+1));
53. roiManager("XOR");
54. roiManager("Add");

55. //rename
56. roiManager("select", n+(roi*keep_int));
57. roiManager("rename", "Cytoplasmic Roi "+roi+1);
58. roiManager("select", n+(roi*keep_int)+1);
59. roiManager("rename", "New Enlarged Roi "+roi+1);
60. roiManager("select", n+(roi*keep_int)+2);
61. roiManager("rename", "Membrane Roi "+roi+1);
62. roiManager("deselect");
63. }
```

Figure 2.2: Macro for Measuring Protein Expression Levels in the Plasma membrane and Sarcoplasm of Muscle Fibres

3 Attempts to Develop Popeye Domain Protein Constructs for use in Structural and Ligand Binding Studies

3.1 Introduction

3.1.1 Development of Recombinant POPDC Constructs for Structural Studies

The lack of an empirically determined structure of the POPDC proteins, particularly the Popeye domain, has been a persistent issue in the field since the discovery of the POPDC proteins.[74] The POPDC proteins have relatively low sequence homology to other proteins, including in the predicted CNBD of the Popeye domain, making homology modelling difficult. While newer modelling methods such as AlphaFold may improve the confidence with which models can be interpreted, they still suffer from the uncertainties that come with using models instead of experimental data. The mode of binding of cAMP is still uncertain, given the high divergence of the Popeye domain sequence from canonical CNBDS, although mutagenesis data has provided some insight.[71] This has held back attempts to produce small molecules that could mimic the binding of cAMP to the Popeye domain. It has also meant that there is a poor understanding of any allosteric changes that occur in the POPDC proteins after cAMP binding. The interactions of the Popeye domain with other proteins, both between POPDC proteins, and other interaction partners such as PDE4A and AC9, could also be studied in more detail if the structure of potential interfaces were known.

As transmembrane proteins, POPDC proteins are difficult to isolate in their native form and there have been several attempts to produce truncated, soluble POPDC constructs that could be used in structural studies.[71,79,138] These have mostly been based on the isolated Popeye domain or the entire cytoplasmic portion of POPDC1. An attempt to express and purify isolated Popeye domain from *E. coli*, and full-length protein from insect cells, in a form suitable for x-ray crystallography studies was previously undertaken.[79] A large number of truncations of POPDC1 alongside a wide variety of peptide tags were trialled. However, none of the designed constructs were found to be suitable for structural studies due to a combination of low expression levels, poor purification, construct instability and insolubility.

A Popeye domain-based construct was separately developed that contained the residues E123-D266 of mouse Popdc1 fused at the N-terminus to an immunoglobulin-binding domain of *Streptococcal* protein G (GB1) *via* a TEV protease cleavage site and 6XHis tag.[80,138] GB1 is a 6.2 kDa protein tag that is known to enhance the solubility of protein constructs.[140,152] After expression of the construct in *E. coli,* it was found that the Popeye domain region of the construct precipitated after cleavage of the GB1 tag. The full, tagged construct (referred to as GB1-E123-D266) underwent initial protein-NMR trials to determine if it would be possible to use this construct for structural studies of the Popeye domain. Protein-NMR is heavily influenced by the size of the protein analysed, with signals suffering

from line broadening and reduction in strength due to a greater rate in transverse magnetization decay.[153] It was thought that the GB1-E123-D266 construct was dimerising in standard conditions, based on gel filtration results. The theoretical mass of the dimeric construct was 50.7 kDa, which is large with respect to NMR. Optimisation of buffer conditions led to improvements of the 2D ^{1}H-^{15}N HSQC-TROSY spectra obtained, which confirmed the presence of folded protein. However, it was not possible to obtain high quality spectra, with many Popeye domain residues not visible, as well as indications that conformational exchange within the Popeye domain was occurring. Peak intensities were improved using high pressure NMR, with Popeye domain residue peaks increasing in intensity by an average of around 3.2-fold under the high-pressure conditions, compared to 1.1-fold for the known GB1 signals correlating with previous findings of GB1 behaviour under high pressure. This suggested that the GB1 domain was more stably folded at standard pressure compared to the Popeye domain. It was decided that the GB1-E123-D266 was not suitable for detailed structural analysis of the Popeye domain.

In addition, a construct named GST-BVES has also been used in pull-down and cAMP binding studies.[71,154] This construct contains the entire cytoplasmic region of mouse Popdc1, fused at the N-terminus to a GST tag. This was used in a ^{3}H-cAMP binding study to determine that the Popeye domain has high affinity for cAMP.[71] However, the large size of this construct (57 kDa) makes it non-ideal for use in protein-NMR structural studies. The N-terminal GST tag must remain in place to avoid precipitation of the Popdc1 residues. In addition, it has been reported that this construct is prone to fragmentation, which can cause complications during purification and subsequent assays.

3.1.2 Attempts to Develop Selective Small Molecule Popeye Domain Ligands

At present there are no small molecules known to selectively bind to the CNBD of the Popeye domain. Studies investigating POPDC protein function are highly reliant on genetically modified animal models, or the study of patients found to possess mutations in the POPDC genes. A specific small molecule agonist or antagonist could be used to pharmacologically modulate the activity of the Popeye domain, by mimicking cAMP binding, helping to elucidate the role of the POPDC proteins. It is also possible that the POPDC proteins could be targets for the treatment of cardiac arrythmias and muscular diseases making Popeye domain ligands potential therapeutics.[135,136] To try and produce a set of small molecule ligands which would specifically bind to Popeye domains a screening project was launched through a collaboration between Imperial College London and Domainex.[137,138] Compounds were initially selected using pharmacophore models of cAMP binding, based on known cAMP-bound CNBD structures. These compounds were then docked into a homology model of the Popeye domain of POPDC1. The top 500 molecules from the docking screen were taken forward to *in vitro* assays which used the GB1-E123-D266 Popeye domain construct. As discussed above, this construct had been

found to be unsuitable for structural studies, in part due to probable conformational instability of the Popeye domain. It was found that fluorescent analogues of cAMP, such as 8-NBD-cAMP, did not show a change in fluorescence in the presence of GB1-E123-D266 in contrast to EPAC1 and EPAC2 which showed significant changes in cAMP analogue fluorescence upon binding.[138] This suggested a lack of cAMP analogue binding to the GB1-E123-D266 construct, or perhaps a different mechanism of cAMP binding that is distinct to canonical CNBDs leading to a lower cAMP analogue affinity or fluorescence change. Attempts to develop an assay utilising elution of this construct from cAMP conjugated agarose found an EC_{50} of 561 μM, several orders of magnitude higher than the 118 nM reported by Froese *et al* using the GST-BVES construct in a radioligand binding assay.[71] This suggested that the cAMP binding activity of the GB1-E123-D266 construct is impaired compared to full-length POPDC1 and the GST-BVES construct. An enzyme linked immunosorbent assay (ELISA) using fixed GB1-E123-D266 and AHA-conjugated cAMP in competition with cAMP was then developed.[138] While the sensitivity of this assay to cAMP binding was low it was deemed acceptable for compound screening and was used to identify a set of potential Popeye domain binding small molecules alongside a DSF assay also utilising the GB1-E123-D266 construct. However, the DSF assay gave biphasic melt curves as a result of the differing melt profiles of the Popeye domain and GB1 domains within the GB1-E123-D266 construct. It was found that the presence of cAMP lowered the DSF derived T_m of the GB1-E123-D266 construct by up to 4 °C, which is unusual for a specific binding interaction which would be expected to thermally stabilise the target protein.[155] This negative shift in T_m was also observed for some of the compounds identified as binders in the ELISA assay, while some others led to a positive shift. In total the *in silico* and *in vitro* screening identified seven compounds (DMX0006151, DMX0006593, DMX0006345, DMX0006517, DMX0006342, DMX0006565 and DMX0006224) as hits, which inhibited binding of a cAMP analogue in the ELISA with an IC_{50} of 0.42-6.83 μM, and also showed activity in the other assays used.[138] The structures of these compounds are shown in Figure 3.1.

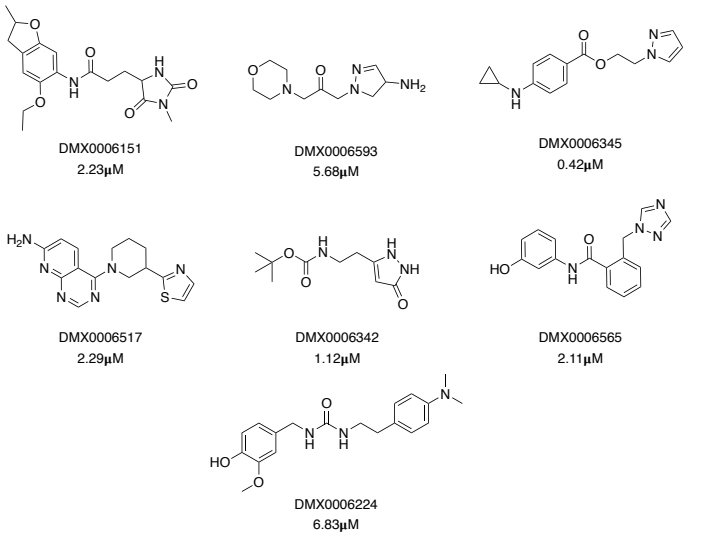


Figure 3.1: The Structures of Potential Popeye Domain Ligands identified in a Compound Screening Project. The structures of the seven hit compounds identified in the previous compound screen run in collaboration between Imperial College London and Domainex. The affinities for the GB1-E123-D266 construct of each compound according to an ELISA are shown. It was planned to use these compounds as templates to develop optimised Popeye domain specific binders.

The GB1-E123-D266 construct's poor physical properties and cAMP binding affinity were a recurrent problem throughout the compound screen. Some of the assays showed relatively poor signal-to-noise and required significant optimisation before use. The unusual negative shift in T_m observed in the DSF assays, along with the non-ideal melting profile, make these results difficult to interpret. The data obtained from the multiple assays do provide evidence of possible binding of these compounds to the Popeye domain, although the issues highlighted make it difficult to draw firm conclusions. Throughout the assay development process, constructs of EPAC1 and EPAC2 were used as positive controls for identification of cAMP binding. High quality signals were observed from the EPAC constructs. It is, therefore, highly likely that many of the issues faced in the *in vitro* compound screen were due to the non-ideal properties of the GB1-E123-D266 construct.

A higher performing recombinant construct of the Popeye domain of one of the POPDC isoforms would provide much greater confidence in compound screening efforts. It may also facilitate the determination of an empirical structure of the Popeye domain using protein-NMR or x-ray crystallography. A structure of the Popeye domain, and subsequent experiments, could be used to provide details on the mechanism of cAMP binding. This could permit a more structure-based rational design of Popeye domain ligands. An empirical Popeye domain structure could also be of use in the efforts to understand POPDC protein intermolecular protein-protein interactions *via* the Popeye domain. As such, the development of an optimised recombinant construct derived from a POPDC protein is a major goal in the study of the POPDC proteins.

3.2 Outline of Work and Aims

3.2.1 Description of this Work

Attempts were made to produce a novel protein construct containing the Popeye domain of Popdc1, which could be used for improved structural and compound binding studies. Starting from the previously developed GB1-E123-D266 construct, which had shown moderate but non-optimal activity, a set of extensions and truncations were made to the Popeye domain sequence. The resulting constructs were expressed in *E. coli* and tested for their level of expression and, where applicable, solubility without a protein fusion tag. A novel Popeye domain sequence that showed an unprecedented ability to remain in solution with no exogenous tag was identified. After the development of an acceptable purification protocol, preliminary investigations into its structure and stability using circular dichroism and multi-angle light scattering were performed. Initial 2D protein-NMR experiments showed mild improvements compared to previous constructs. Attempts were then made to detect cAMP binding to the construct using DSF and MST to confirm normal activity of the Popeye domain. cAMP binding was not found, meaning further work with this construct was not continued.

3.2.2 Aims

1. To develop an improved recombinant Popeye domain construct displaying satisfactory conformational stability and solubility (preferably without the requirement for the presence of an exogenous protein tag), while possessing a strong affinity for cAMP.

2. Use the improved Popeye domain construct in protein-NMR studies to empirically determine structural features of the Popeye domain. The binding mode of cAMP to the Popeye could also be investigated.

3. Develop improved compound bindings assays utilising the optimised Popeye domain construct to allow efficient screening of small molecule compounds.

4. Utilise the newly developed Popeye domain constructs to optimise the hit compounds identified in the previous screen and develop specific Popeye domain small molecule ligands capable of mimicking cAMP binding to the POPDC proteins.

3.3 Results

3.3.1 Search for a Novel Popeye Domain Construct

The GB1-E123-D266 construct previously developed was used as a starting point for the development of a new construct based on the Popeye domain of mouse Popdc1. While this construct has several

issues it was shown to be well expressed in and purified from *E. coli*, as well as perhaps showing some cAMP affinity. Preliminary protein-NMR studies had also confirmed folding of the Popeye domain sequence. Modelling of the Popeye domain, firstly using the Phyre2 server followed by AlphaFold structures, predicted that the αC-helix of the Popeye domain could extend to approximately L269-V274. If so, this would mean that this helix is truncated in the GB1-E123-D266 construct, as shown in Figure 3.2A. A conserved lysine pair, K272 and K273, which are not present in the GB1-E123-D266 construct, have also been implicated in the oligomerisation of full-length POPDC1.[81] Similarly, the cytoplasmic region of POPDC1 was predicted to begin at around K115. It could have been that residues present in the globular cytoplasmic region of the protein, which may improve solubility, were excluded in the previous construct. It was hypothesised that extending the constructs to ensure full formation of the αC-helix, plus other extensions, may help stabilise the Popeye domain construct. Particularly if the addition of extra residues promoted the formation of stabilising intermolecular interactions.

A series of extensions to GB1-E123-D266 were designed and the novel Popeye domain constructs were created by PCR using full-length mouse *Popdc1* as a template, Figure 3.2B. In a previous study it was found that small changes to the position of truncations to the Popeye domain could lead to large and unpredictable changes in the expression levels of constructs in *E. coli*.[79] It was also found that expression levels often depended on both the position of the N- and C-terminal ends of the Popeye domain sequence. As such it was important to test the effect of the proposed extensions to the GB1-E123-D266 construct on the expression of each new construct. To first assess the impact of these extensions of the Popeye domain sequence on expression in *E. coli*, each sequence was cloned into the GEV2 plasmid, which appends an N-terminal GB1 tag, *via* a thrombin cleavage site linker. A C-terminus 6XHis tag was also fused to the constructs. Each construct was expressed in transformed BL21 (DE3) *E. coli*. The GEV2 plasmid contains a T7 promoter and expression was induced through addition of IPTG to the cultures. Lysates of the transformed *E. coli* were assessed for construct expression using a Western blot with anti-6XHis tag antibody (Figure 3.2C). Strong expression of all novel constructs, except GB1-S109-D266, was detected in crude cell lysate and supernatant suggesting the addition of additional residues had not impacted expression and solubility of the GB1-tagged constructs.

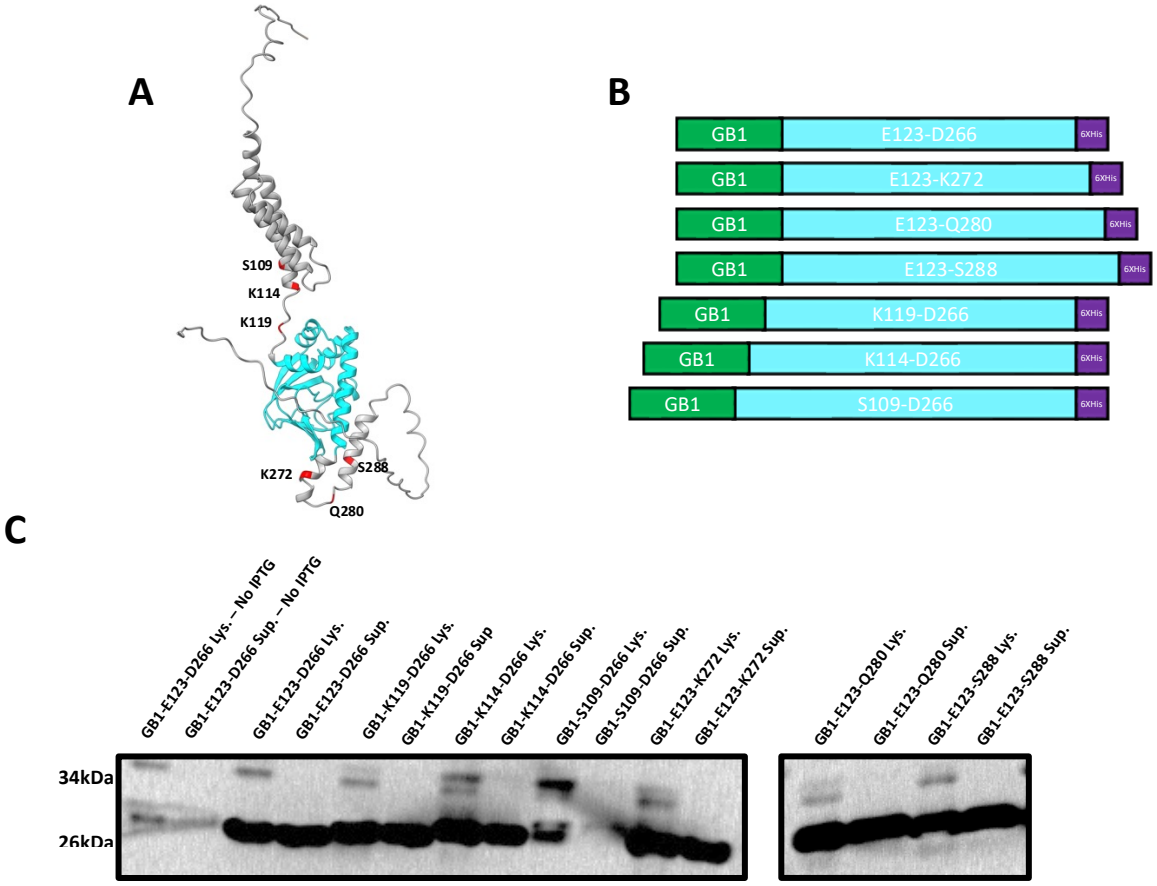


Figure 3.2: An Initial Expression Trial of Novel GB1-Popeye Domain Constructs in *E. coli*. A) AlphaFold structure of mouse Popdc1 with the residues contained in the GB1-E123-D266 construct coloured cyan. It was proposed to extend the N- and/or C-terminus of the Popeye domain to the positions highlighted in red, to form novel Popeye domain constructs . **B)** Schematic of the series of Popdc1 Popeye domain constructs tested in the initial expression trial. Each construct contains an N-terminus GB1 tag linked *via* a thrombin cleavage site (not shown) to a Popdc1 sequence-centred on the Popeye domain, followed by a C-terminus 6XHis affinity tag. **C)** Each new construct was expressed in BL21(DE3). Cells were lysed, centrifuged and the supernatant collected. Expression was assessed by Western blot of the crude lysate (lys) and supernatant (sup) of each group to detect insoluble constructs. An anti-His tag primary antibody was used for detection. A control group with no IPTG was used as a negative control.

It was not known if the previous issues with the GB1-E123-D266 construct were caused by a suboptimal N- or C-terminus position, if either. Therefore, after the initial expression screen, it was decided to investigate whether combining the extensions to the N- and C-termini of the Popeye domain would result in differing construct behaviour compared to single extensions. At this point a slight change in the format of the construct was made, with the GB1 tag now linked to the Popeye domain residues *via* a TEV cleavage site and 6XHis tag linker. The C-terminus of the Popeye domain was now untagged. This change was made to match the exact layout of the original GB1-E123-D266 construct and was achieved through the insertion of the construct sequence into the pLEICS-91 plasmid. This plasmid had been unavailable at the time of the initial expression described above.

It was also desired to attempt the expression of the constructs in more advanced *E. coli* expression strains, which may have positive effects on the folding, stability and expression level of protein

constructs. The expression of subsequent Popeye domain constructs were trialled in BL21 Star (DE3) (Invitrogen) and Arctic Express (Agilent) *E. coli* strains.

At first the maximum extensions made to either end of the protein, to S109 and S288 respectively, were combined to produce a GB1-S109-S288 construct. The level of expression of this construct in both BL21 Star (DE3) and Arctic Express cells was determined as above. In both cases, no clear expression of the protein was observed in the bulk or soluble fractions of the cell cultures using SDS-PAGE analysis. To assess if the expression of this doubly extended construct could be rescued by a change of protein tag, the construct sequence was cloned into the pAG108-pET28a plasmid, which appended an N-terminal NusA tag in place of GB1. The expression trial was repeated in both cell strains but once again no expression was observed. Expression of both novel constructs, as well as the original GB1-E123-D266, was also unsuccessful in the SoluBL21 *E. coli* strain. This suggested that the dual extension of the Popeye domain to S109 and S288 at the N- and C-termini, respectively, prohibited expression of the construct, although the mechanism underlying this effect is unknown. A previous project that aimed to produce Popeye domain-based constructs also found an unpredictable interplay between N- and C-terminus truncations of the Popeye domain on expression levels.[79] Generally, it has also been found that residues at the N- and C-termini generally have a disproportionate impact on protein behaviour and solubility.[156]

To determine the residues that were causing of the loss of expression of the constructs containing residues S109-S288 of the Popeye domain truncations of either the N- or C-termini were planned. The GB1-tagged constructs within the pLEICS-91 plasmid were once again used. Firstly, the C-terminus of the construct was positioned at D266, K272 and Q280, while the placement of the N-terminus at S109 remained unchanged. This yielded constructs of GB1-S109-D266, GB1-S109-K272 and GB1-S109-Q280. Expression of all three constructs was seen in BL21 Star (DE3) cells but not Arctic Express. A construct containing residues S109-D266 was tested in the initial expression screen using standard BL21 (DE3) and was found to show low or no expression (Figure 3.2C). These results demonstrate that the expression of Popeye domain constructs show some *E. coli* strain dependency. It also suggests that the residues between Q280-S288, in combination with a N-terminus at S109, were inhibiting expression of the GB1-S109-S288 construct within the BL21 Star (DE3) *E. coli*.

The GB1-S109-D266, GB1-S109-K272 and GB1-S109-Q280 constructs, which contain both a TEV cleavage site and 6XHis tag linker, were crudely purified using FPLC with a Ni-NTA column before undergoing digestion with TEV protease to yield free GB1 and untagged Popeye domain. The phosphate-based FF6 wash and elution buffers, containing 500 mM NaCl and set to pH 7.5, were used during FPLC. The elution fractions underwent dialysis overnight using a 6-8 kDa molecular cut-off

membrane to remove the imidazole used in the elution of the proteins in FPLC. The following morning, significant levels of precipitate were visible in the dialysis membranes containing the products of the digestion of the GB1-S109-Q280 and GB1-S109-D266 constructs. In contrast, minimal precipitation had occurred after digestion of the GB1-S109-K272 construct. The now untagged GB1-S109-K272 construct, herein referred to as the S109-K272 construct, was chosen for further study as this was the first known example of an untagged Popeye domain construct remaining in solution without the presence of a protein tag. It was hoped that this improvement in solubility could also indicate an improvement in other properties of the construct. The basic structure of the GB1-S109-K272 construct, and the un-tagged S109-K272 form, are shown in Figure 3.3 alongside the previously developed GB1-E123-D266 construct.



Figure 3.3: Schematic of the Novel GB1-S109-K272 and Un-Tagged S109-K272 Constructs compared to the GB1-E123-D266 Construct. Schematic of the original GB1-E123-D266 Popdc1 Popeye domain construct **(A)** and the extended GB1-S109-K272 **(B)**. Both contain an N terminal GB1 tag linked *via* a 6XHis tag and a TEV cleavage site (not shown) to a Popdc1 sequence centred on the Popeye domain. The GB1-S109-K272 was digested with TEV protease to remove the GB1 and 6XHis tag and yield a soluble Popeye domain sequence with no additional tags **(C)**.

All Popeye domain constructs tested for expression, and solubility where applicable, are summarised in Table 3.1.

Table 3.1: A table summarising the expression trials of the novel Popdc1 Popeye domain constructs.

Plasmid	N-Terminus	C-Terminus	N-terminus Tag	Purification Tag	Cleavage Site Linker	*E. coli* Strain	Expression	Soluble	Soluble without tag
GEV2	S109	D266	GB1	6XHis	Thrombin	BL21(DE3)	N	-	-
GEV2	S109	D266	GB1	6XHis	Thrombin	Arctic Express	N	-	-
GEV2	K114	D266	GB1	6XHis	Thrombin	BL21(DE3)	Y	Y	-
GEV2	K119	D266	GB1	6XHis	Thrombin	BL21(DE3)	Y	Y	-
GEV2	E123	D266	GB1	6XHis	Thrombin	BL21(DE3)	Y	Y	-
GEV2	E123	K272	GB1	6XHis	Thrombin	BL21(DE3)	Y	Y	-
GEV2	E123	Q280	GB1	6XHis	Thrombin	BL21(DE3)	Y	Y	-
GEV2	E123	S288	GB1	6XHis	Thrombin	BL21(DE3)	Y	Y	-
pAG108-pET28a	S109	S288	NusA	2X 6XHis	TEV	SoluBL21	N	-	-
pAG108-pET28a	S109	S288	NusA	2X 6XHis	TEV	Arctic Express	N	-	-
pAG108-pET28a	S109	S288	NusA	2X 6XHis	TEV	BL21 Star	N	-	-
pLEICS-91	S109	S288	GB1	6XHis	TEV	SoluBL21	N	-	-
pLEICS-91	S109	S288	GB1	6XHis	TEV	Arctic Express	N	-	-
pLEICS-91	E123	D266	GB1	6XHis	TEV	SoluBL21	N	-	-
pLEICS-91	E123	D266	GB1	6XHis	TEV	Arctic Express	N	-	-
pLEICS-91	E123	D266	GB1	6XHis	TEV	BL21 Star	Y	Y	N
pLEICS-91	S109	D266	GB1	6XHis	TEV	BL21 Star	Y	Y	N
pLEICS-91	S109	D266	GB1	6XHis	TEV	Arctic Express	N	-	-
pLEICS-91	S109	K272	GB1	6XHis	TEV	BL21 Star	Y	Y	Y
pLEICS-91	S109	K272	GB1	6XHis	TEV	Arctic Express	N	-	-
pLEICS-91	S109	Q280	GB1	6XHis	TEV	BL21 Star	Y	Y	N
pLEICS-91	S109	Q280	GB1	6XHis	TEV	Arctic Express	N	-	-
pLEICS-91	S109	S288	GB1	6XHis	TEV	BL21 Star	N	-	-
pLEICS-91	S109	S288	GB1	6XHis	TEV	Arctic Express	N	-	-

After the S109-K272 construct was identified as a soluble version of the Popeye domain, efforts were made to optimise its expression. Expression was compared between BL21 Star (DE3) and Arctic Express *E. coli*. It was found that BL21 Star (DE3) cells yielded a relatively low 1.5-3 mg/L of culture. However, no significant expression was observed in Arctic Express cells. Despite the low yield, it was decided to continue to use BL21 Star (DE3) cells to express the S109-K272 construct for initial characterisation. Expression was induced using 0.75 mM IPTG at a temperature of 18 °C and expression run overnight. Standard LB media was used during expression. The OD_{600} at which the IPTG was added was varied between 0.5 and 0.8 but was found to not have a significant influence on the yield of the construct.

3.3.2 Purification of the Novel S109-K272 Popeye Domain Construct

The focus then moved to the optimisation of the purification method of the S109-K272 construct. After expression had been induced in *E. coli*, the cells were collected through centrifugation and resuspended in FF6 wash buffer (20 mM phosphate buffer with 500 mM NaCl and pH 7.3). The cell suspension was lysed using a French Press, followed by centrifugation to remove cell debris and insoluble proteins. The supernatant containing the GB1-tagged GB1-S109-K272 was loaded onto an FPLC Ni-NTA column. At this stage the construct contained a 6XHis tag within the linker between the GB1 tag and the Popeye domain. The construct bound to the column and was eluted by linearly increasing the concentration of imidazole in the elution buffer from 0-500 mM. It was found that the construct eluted at an imidazole concentration of approximately 400 mM. The construct was then digested with TEV protease to remove the GB1 tag followed by removal of imidazole by dialysis overnight. GB1 and 6XHis tag cleavage was confirmed using SDS-PAGE, which can be seen in Figure 3.4A. The digested construct, now lacking the 6XHis tag, was expected to flow through the Ni-NTA column during a second round of FPLC, while the GB1 domain fused to 6XHis tag would remain bound to the column. However, it was found that the cleaved S109-K272 construct was not present in the flow through but bound to the column with a similar affinity to the non-cleaved construct and eluted together with the free GB1-6XHis domain, which is apparent in Figure 3.4B. This meant effective separation of the GB1 tag and Popeye domain was not possible. The TEV protease used also possessed a 6XHis tag, which meant it also partially coeluted with the Popeye domain.

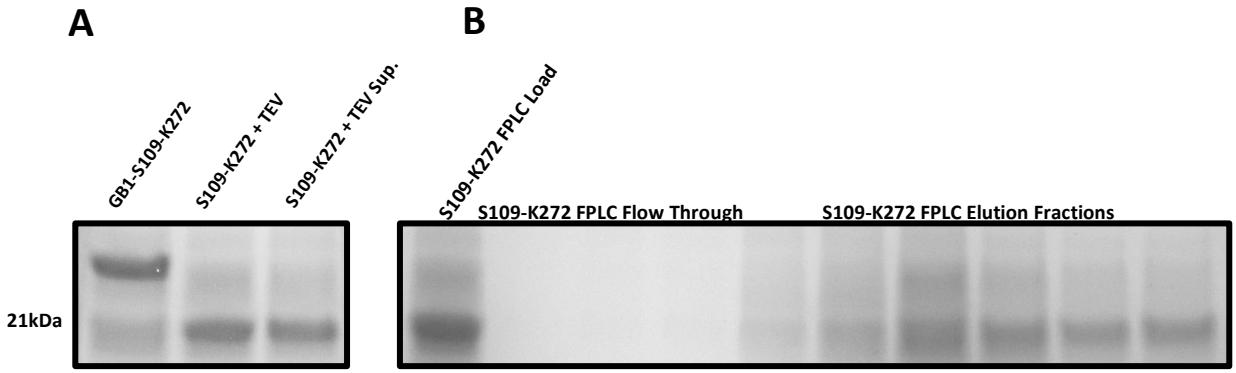


Figure 3.4: GB1 Tag Cleavage from and Purification of the S109-K272 Popeye Domain Construct. A) SDS-PAGE with general protein stain showing FPLC purified GB1-S109-K272, around 25 kDa. This was incubated at room temperature with TEV protease for two hours to remove the GB1 and 6XHis tags and yield the S109-K272, around 19 kDa. Significant levels of S109-K272 were present in the supernatant (sup.) after centrifugation. **B)** The digested S109-K272 construct was run through a second round of FPLC using a Ni-NTA column. The untagged construct was expected to elute in the flow through removing contaminants with affinity to the Ni-NTA column remaining from the first round of FPLC. Instead, the S109-K272 construct was retained on the column and only eluted after addition of imidazole to the eluent.

The origin of the Popeye domain's affinity for the Ni-NTA column is not fully understood. SDS-PAGE showed the major species present was the cleaved S109-K272 product, meaning that incomplete TEV digestion and retention of the GB1-6XHis domain was not the cause of the affinity for the Ni-NTA column. It is interesting to note that the cAMP binding CAP proteins, which are the closest homologues to the Popeye domain and have been used as templates in homology modelling, have also been reported to possess endogenous affinity to Ni-NTA columns.[157] The Popeye domain contains two His residues in close proximity, H188 and H191, which homology modelling predicted to be at the surface of the construct. It was hypothesised that this pair may be interacting the Ni-NTA column, mimicking a 6XHis affinity tag. His188 is not highly conserved between Popeye domains and was mutated to Gln to form the S109-K272[H188Q] construct. It was found that both the GB1-S109-K272[H188Q] and the digested S109-K272[H188Q] construct eluted at lower imidazole concentrations during FPLC compared to the wild type versions, 280 mM and 100 mM respectively. However, S109-K272[H188Q] still showed affinity for the Ni-NTA column. This means that H188 contributed to the observed affinity, possibly as part of a pair with H191, but other interactions were also responsible. In addition, the cleaved Popeye domains constructs, with and without the H188Q point mutation, had broad elution peaks which overlapped with the free GB1-6XHis tag. This meant it was still not possible to effectively separate the cleaved Popeye domain from its GB1 tag.

To overcome this, a new construct was created with an additional TEV protease cleavage site between the 6XHis tag and the GB1 domain. It was hoped that this would mean that after TEV protease digestion the GB1 side product, which would now not contain a 6XHis tag, would show no affinity to the FPLC column meaning that the S109-K272 construct would be the only major eluate during the

second round of FPLC. Indeed, it was found that this method achieved effective separation of the Popeye domain and the GB1 tag, which is shown in Figure 3.5B. However, some other contaminants, including the 6XHis-tagged TEV protease, were present in the collected fraction containing the Popeye domain. Fortunately, through adjustment of the imidazole concentration gradient used during elution it was possible to achieve approximately 90% purity, as judged through non-specific staining of SDS-PAGE gels, with two rounds of FPLC, which can be seen in Figure 3.5C. Size exclusion chromatography could be used instead of a second round of FPLC to remove GB1, although this could lead to co-elution of the TEV protease used in the digestion reaction, as can be seen in Figure 3.5E. For many applications, such as DSF and NMR, 90-95% purity of the target protein is considered acceptable, so this purification protocol was adopted for initial studies of the construct. However, the level of purity was deemed insufficient for a crystallography screen. It was decided that further optimisation of S109-K272 purification could be completed after initial activity studies had been performed. For activity assays two rounds of FPLC only were used during purification of the S109-K272 construct. FPLC and SEC were used to purify samples for protein-NMR.

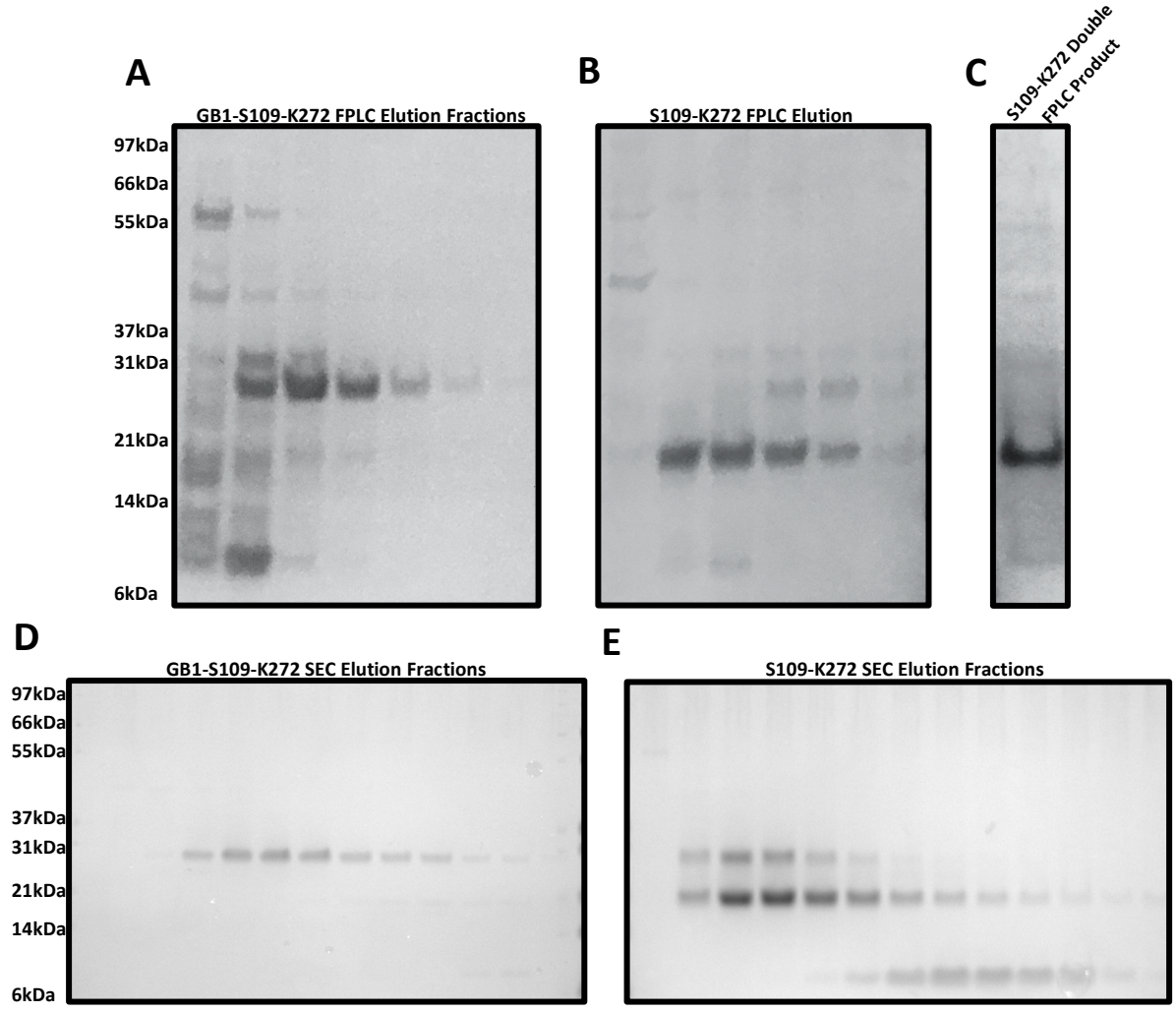


Figure 3.5: FPLC Purification of the GB1-S109-K272 and Digested S109-K272 Constructs. A) SDS-PAGE with general protein stain showing elution fractions from FPLC using a Ni-NTA column for initial purification of the GB1-S109-K272 construct from the supernatant of *E. coli* cell lysate. Reasonable purification of GB1-S109-K272 (25 kDa) was possible. **B)** SDS-PAGE with general protein stain of FPLC elution fractions containing the TEV digested S109-K272. **C)** Pooled fractions from the second round of FPLC containing the S109-K272 construct, purified only using FPLC. **D)** SDS-PAGE with general protein stain showing elution fractions from SEC purification of the GB1-S109-K272 construct. The protein had previously been subjected to one round of FPLC purification. **E)** SDS-PAGE with general protein stain showing elution fractions from SEC purification of the S109-K272 construct (19 kDa). The protein had previously been subjected to one round of FPLC purification and TEV protease (27 kDa) digestion. The cleaved GB1 tag can be seen at approximately 7 kDa.

The GB1-E123-D266 construct, previously used in the Domainex hit compound screen, was also expressed and purified. It was planned to use the GB1-E123-D266 construct as a comparison with the novel S109-K272 construct. The construct was expressed following the same protocol as the S109-K272 construct. As the GB1-E123-D266 construct requires the GB1 tag to remain in solution, no TEV protease digestion was run after the first round of FPLC. Instead, after dialysis, the collected FPLC fractions were run through SEC to further purify the construct. Purities of over 90% were routinely reached using this method. The yields of the purified construct were comparable to the S109-K272 construct at 1.6-2.0 mg/L of bacterial culture. Concentration of both purified constructs routinely produced concentrations of around 110 μM, which was sufficient for the desired applications.

3.3.3 Structural Characterisation of the S109-K272 Popeye Domain Construct

3.3.3.1 SEC-MALS

The purified constructs were analysed using size exclusion chromatography multi angle light scattering (SEC-MALS) to assess their homogeneity and particle size. SEC-MALS uses a column packed with pore containing beads through which a solution containing multiple species is passed.[7] The extent of penetration into the beads of the different species depends on their size, which controls their flow rate through the column.[158] This allows separation of the components of a mixture according to their approximate size. As the particles are eluted from the column, in order of decreasing size, they are passed through a UV beam which allows an estimation of the concentration of the species. The key feature of the technique is MALS which measures the scattering of an incident laser beam to determine the absolute size of eluted particles.[7] The radius of particles can also be estimated by measuring the variation in the scattering intensity at different angles. This allows the distribution of particle sizes in a mixture to be visualised on a chromatogram trace and absolute measurements of each particle size to be made.

The chromatogram of the S109-K272 elution, shown in Figure 3.6A, was dominated by a UV and light scattering (LS) peak from 5.0-5.5 minutes. This peak was analysed and was estimated to contain particles with molar mass moments of 41 kDa, with a low degree of polydispersity with the M_w/M_n and M_z/M_n ratios being 1.010±0.039 and 1.018±0.067, respectively. The theoretical mass of the S109-K272 monomer is 19.6 kDa so it seems highly likely the major species in the sample is a S109-K272 dimer, which would be predicted to be 39.2 kDa. Two small LS peaks can be seen at 2.5 and 3.5 minutes suggesting the presence of some higher order complexes or aggregate. However, the negligible UV absorption at these elution time points shows that these species were present at very low concentrations. The negative UV absorption peak at the end of the trace is probably due to the presence of air in the detector.

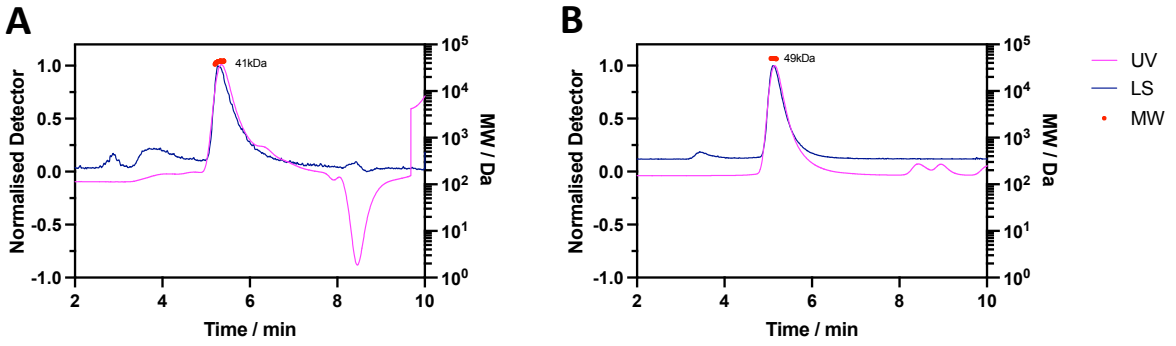


Figure 3.6: SEC-MALS of the S109-K272 and GB1-E123-D266 Constructs. The purified constructs, S109-K272 **(A)** and GB1-E123-D266 **(B)** were separated and analysed using SEC-MALS. The chromatogram shows UV absorption (pink), light scattering (LS) at 90° (blue) and molar mass (MW) of the major peak as determined by MALS. One major peak was present in each chromatogram showing a high degree of monodispersity in both samples. The determined MW in each sample suggests that both constructs exist primarily as a dimer.

The GB1-E123-D266 construct mixture also contained a very small amount of aggregate or high order complex, as shown by minor LS peaks at the start of elution, but with very low UV absorption (Figure 3.6B). The chromatogram was dominated by one major scattering peak estimated to contain particles of mass 49.6 kDa with a very high degree of homogeneity, M_w/M_n and M_z/M_n ratios being 1.000±0.032 and 1.000±0.056 respectively. Again, this correlates with a predicted GB1-E123-D266 dimer mass of 50.7 kDa.

It appears that both constructs predominantly exist in a dimeric state. This correlates with findings in Chapter 6 regarding the ability of Popeye domains to interact with each other. The lack of aggregation and high homogeneity is despite both constructs having undergone a flash-freeze and thaw cycle before SEC-MALS analysis, which suggests that both constructs are resistant to freeze-thaw degradation.

3.3.3.2 Circular Dichroism

Both constructs were subjected to analysis by CD to investigate their secondary structure content. CD uses circularly polarised light, rotating clockwise or anticlockwise perpendicular to the direction of the beam. When this circularly polarised light interacts with an asymmetric molecule the clockwise and anticlockwise rotating components of the beam are absorbed to different extents depending on the secondary structure of the molecule.[6] Structural features of proteins, such as α-helices and β-sheets, have characteristic CD spectra due to the differences in absorption of the circularly polarised light at different wavelengths. By determining the contribution of the characteristic secondary structure patterns to the overall CD spectra the secondary structure content of the target can be determined.[6] CD spectroscopy cannot be used to determine the structural environment of individual residues or atoms, but can be used as a quick way to confirm folding of a protein and determine the proportion of different secondary structural features. In addition, the measurement of the CD spectra over a range of temperatures can be used to follow the unfolding of the protein because the ellipticity will reduce as the protein loses its secondary structure at higher temperatures. This can be used to determine the melting temperature and thermal stability of proteins.

CD spectra for both the S109-K272 and GB1-E123-D266 constructs were first measured at ambient temperature, shown in Figure 3.7A. Clear ellipticity with similar features was observed for both constructs. A positive band was present just below 200 nm, followed by two negative bands at 210 nm and 220nm. This confirmed that the constructs were folded in solution. Next, each construct was cooled to 6 °C and then heated to 94 °C at a rate of 1 °C per minute. Figure 3.7B and D shows the decrease in ellipticity of each construct at different wavelengths over the temperature range. The derivative of the change in CD with temperature at each wavelength was plotted, with peaks in Figure

3.7C and E showing the point of unfolding of the constructs. The melt profile derivative of the S109-K272 construct showed one clear peak indicating a single unfolding event. This was fitted to a one transition model to give a T_m of 46.5±0.1 °C. In contrast, the GB1-E123-D266 construct displayed two clear unfolding events determined to occur at 46.8±0.1 °C and 62.1±0.2 °C. The number of transitions in the melt profiles correlates with the number of distinct protein domains in each construct. The transition observed at 46.5±0.1 °C in S109-K272 can only be due to unfolding of the Popeye domain, being the single domain within the construct. It is assumed that the melting transitions at 46.8±0.1 °C in the GB1-E123-D266 construct also derives from the Popeye domain. The highly similar T_m's indicate that the folding of the Popeye domain sequences are similar in each construct, and the minor extensions in the S109-K272 construct have not significantly altered the thermal stability, despite the difference in construct solubility. This could mean that the S109-K272 construct is subject to the same conformational exchanges that hampered the NMR analysis of the GB1-E123-D266 construct. The transition at 62.1±0.2 °C within the GB1-E123-D266 construct is assumed to derive from the GB1 domain. The T_m of GB1 is often reported to be in the region of 85 °C.[159] However, these values are typically recorded at pH 5.5, which has been found to give the greatest stabilisation of GB1, and also high NaCl concentrations. It has been shown that changes in pH and reductions in NaCl to those used in the CD analysis reduce the T_m of GB1 to levels comparable to the 62.1±0.2 °C observed here, supporting the argument that this transition is due to GB1 unfolding.[159]

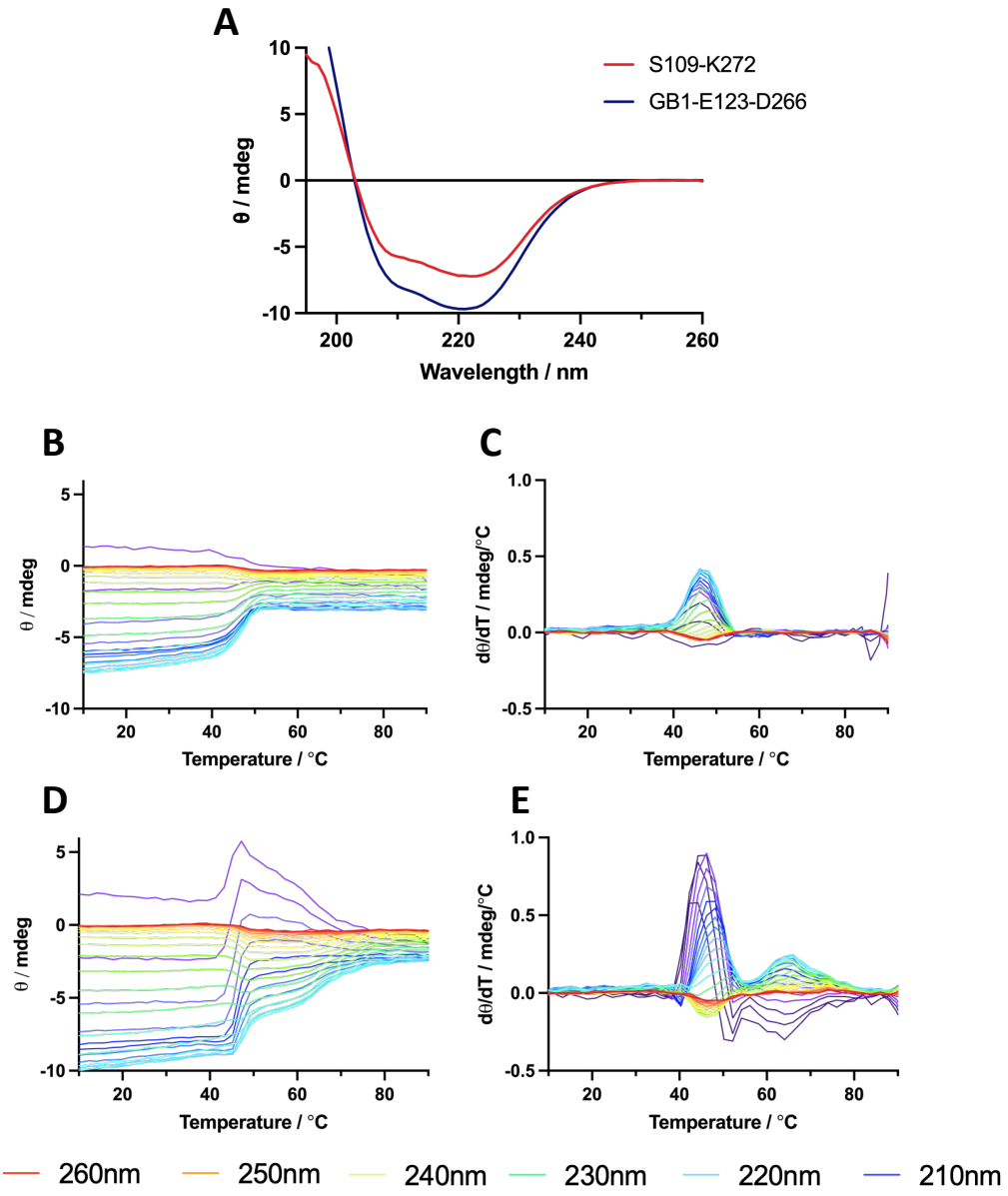


Figure 3.7: Circular Dichroism Spectra of the S109-K272 and GB1-E123-D266 Constructs. A) Circular dichroism spectra of the S109-K272 and GB1-E123-D266 constructs at 23 °C in 20 mM phosphate buffer, 100mM NaCl, pH 7.4. The same sample of S109-K272 **(B)** and GB1-E123-D266 **(D)** were then heated from 6-94 °C and the ellipticity monitored at wavelengths between 260-195 nm. The first derivative of the change in ellipticity against temperature was determined and plotted for the S109-K272 **(C)** and GB1-E123-D266 **(E)** to show the temperature at which the constructs unfolded, shown by the presence of peaks in the derivative plots. One transition at 46.5 °C was observed for the S109-K272 construct, whereas two transitions at 46.8 °C and 62.1 °C are evident during the melting of the GB1-E123-D266 construct.

Secondary structure predictions of each construct were produced based on the ambient temperature CD spectra using the BeStSel web server,[141] with the proportions of each type of secondary structure within each construct shown in Figure 3.8A. While these were not intended to be used for detailed structural analysis, they do provide a good first approximation of the structure of each construct and constitute the first direct, empirical structural determination of the Popeye domain. The constructs were predicted to contain similar proportions of secondary structural features. The main difference between the S109-K272 and GB1-E123-D266 CD derived secondary structure estimations is the

percentage of antiparallel β-sheet present, with 14.5% in the S109-K272 construct and 25.8% in the GB1-E123-D266 construct. The GB1 tag is a highly characterised domain, with structures determined through protein NMR and x-ray crystallography.[160] GB1 contains a 4-strand anti-parallel β-sheet, comprising 37.5% of the whole GB1 domain. The GB1 tag forms 25.6% of the GB1-E123-D266 construct. Therefore, the β-sheet of GB1 will constitute approximately 10% of the total construct, which corresponds to the 10% increase in antiparallel β-sheet in the GB1-E123-D266 construct versus the S109-K272 construct. This supports the conclusion that the S109-K272 and GB1-E123-D266 constructs have similarly folded Popeye domains with comparable proportions of secondary structural features.

A comparison of the S109-K272 construct's predicted secondary structure to that of the S109-K272 region of the AlphaFold model of full-length mouse Popdc1 is shown in Figure 3.8B. The largest difference is the lesser α-helix component in the S109-K272 construct, 31.2% compared to 40.2% in the AlphaFold model. If the AlphaFold model is accurate, the differences between the model and empirical results could be due to the unfolding of the first six residues of S109-K272, which are predicted to be within the C-terminus of the third TM domain in the AlphaFold structure of full-length POPDC1, which may be destabilised in isolation. The most significant α-helix in Popeye domain models comes from the αC-helix. It is possible that the C-terminus of the α-helix, predicted to be less stable in the AlphaFold models, could be unfolded. If this helix is destabilised, it could lead to disruption of Popeye domain activity such as cAMP binding. It should be noted that the AlphaFold models are produced as monomers, whereas the S109-K272 construct was found to be dimeric through SEC-MALS. This could have contributed the differences in secondary structure estimations.

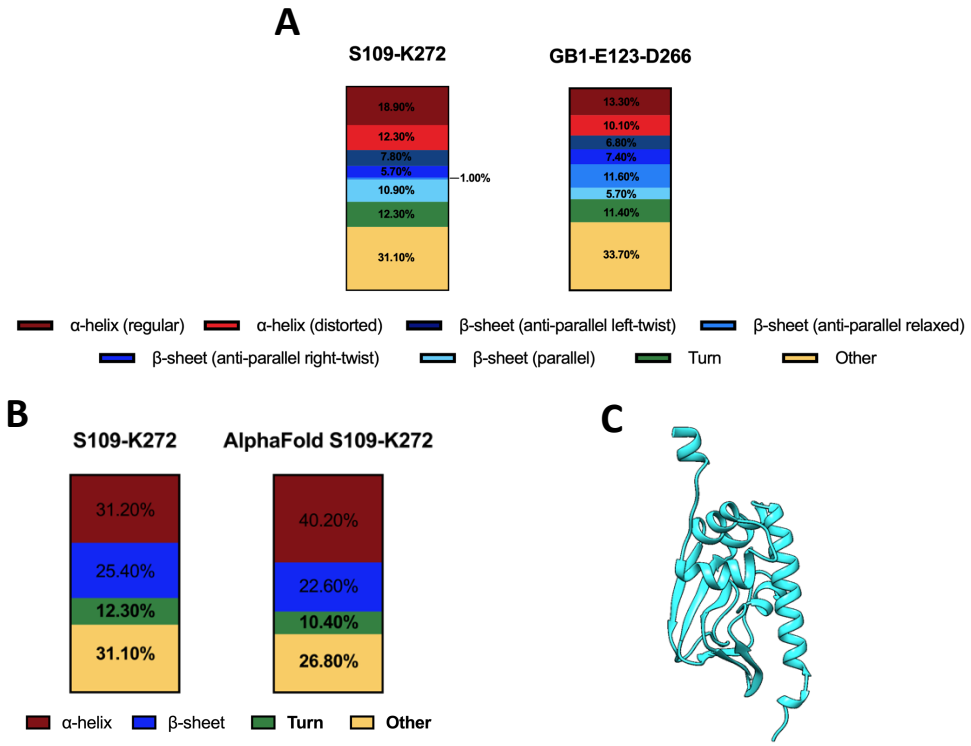


Figure 3.8: Circular Dichroism Derived Secondary Structure Predictions of the S109-K272 and GB1-E123-D266 Constructs. A) The circular dichroism spectra of each construct at 23 °C was used to predict the secondary structure content of both constructs using the BeStSel server. The constructs have similar secondary structure contents, with the difference between the two mostly accounted for by the presence of the GB1 tag in the GB1-E123-D266 construct. **B)** The empirically determined approximate secondary structure of the S109-K272 is compared to the secondary structure of the AlphaFold model of mouse Popdc1 between residues S109 and K272. While both secondary structure contents are similar there is a 9% drop in α-helix in the empirical data as well as 2-5% changes in other structures. **C)** AlphaFold structure of POPDC1 with residues S109-K272 shown. This model may resemble the structure of the S109-K272 construct in solution. The AlphaFold structure is monomeric, whereas the S109-K272 was found to be primarily present as a dimer.

3.3.3.3 Protein-NMR Analysis of the Popeye Domain Constructs

Protein-NMR can be used to study the structure and dynamics of biomolecules. NMR exploits the difference in magnetic spin of nuclei in a protein as a result of their particular environment within the protein.[3] This permits information to be obtained at atomic resolution, at least for nuclei possessing magnetic spin such as ^{1}H, ^{15}N and ^{13}C, meaning fine structural details of a protein can be determined. Proteins are exposed to a strong magnetic field to align the spins of the nuclei in the sample. A pulse of radio waves is used to excite the aligned nuclei and the change in absorption of the radio waves across a range of wavelengths is used to determine the environments of nuclei present.[3] Multidimensional NMR experiments study the correlation between individual nuclei, which can be linked through bonds or space, to allow assignment of NMR peaks to specific residues and determine the three-dimensional structure of a protein.[4]

It was intended to use protein-NMR techniques to empirically determine detailed structural information about the Popeye domain. In addition, it was hoped that protein-NMR may provide a method to investigate cAMP and compound binding to the Popeye domain. Ligand-observed NMR

techniques can be used to study compound binding in the absence of full protein-NMR structure.[161,162] This was the first time a Popeye domain containing only endogenous residues, the S109-K272 construct, had been subjected to protein-NMR analysis. It was hoped that the change in solubility of the construct, compared to the GB1-E123-D266 construct, would correlate with an improvement of the stability and folding of the Popeye domain and so produce higher quality NMR spectra.

Initial 1D ^{1}H-NMR spectra of both the GB1-S109-K272 and un-tagged S109-K272 construct were recorded. Both constructs were found to be folded, indicated by the appearance of a wide range of sharp peaks, including around δ_H = 0 ppm. Next, a heteronuclear ^{1}H-^{15}N 2D HSQC-TROSY NMR experiment was run. HSQC detects ^{1}H-^{15}N correlations and is primarily used to visualise the correlations derived from the amide groups within the protein backbone.[4] While it provides limited structural information, it is useful for assessing the suitability of a protein for further multidimensional, heteronuclear NMR experiments based upon the quality of the HSQC spectrum.[153]

One issue with the previous NMR experiments using the GB1-E123-D266 construct was the large size of the presumably dimeric species. Larger proteins undergo more rapid transverse relaxation leading to broader NMR peaks with lower intensity.[153] Being able to remove the GB1 tag from the S109-K272 construct without precipitation meant there was a 9 kDa reduction in its molecular weight compared to the GB1-E123-D266 construct, assuming a dimer were present. This may help improve peak intensity and spectra quality although the S109-K272 dimer is still large with respect to protein-NMR. To further help improve spectra quality from the large S109-K272 dimer, it was decided to use a HSQC-TROSY experiment. TROSY subpresses the transverse relaxation of the protein by exploiting constructive interference between different relaxation pathways.[163] This leads to the appearance of only a single peak from each NMR active nuclei in the protein, also with reduced line broadening, improving spectra quality.

A ^{1}H-^{15}N HSQC-TROSY experiment was run using a 700 MHz spectrometer using purified ^{15}N-labelled protein. The construct was present at 100 μM in an arginine-glutamic acid buffer, which had previously been found to improve the spectra of the GB1-E123-D266 construct in HSQC-TROSY experiments.[80] A first spectra was recorded for the GB1-S109-K272 construct, shown in red in Figure 3.9B. The GB1 tag was then removed by addition of TEV protease and the cleaved construct re-purified and concentrated to a similar concentration. An identical ^{1}H-^{15}N HSQC-TROSY experiment was then run (Figure 3.9A). An increase in the intensity of almost all peaks derived from Popeye domain residues are evident in the overlay of the two spectra in Figure 3.9B. A number of new peaks not observed in the GB1-S109-K272 spectra are also observed. This improvement in peak visibility and intensity could be due to the decrease in size of the construct from 50 kDa to 41 kDa, presuming dimeric complexes.

Many peaks tentatively assigned to GB1 are removed in the S109-K272 spectra, however some small peaks remain demonstrating the incomplete purification of the S109-K272 complex after the GB1 cleavage. The changes between the two spectra can be clearly seen in the cross-peaks at approximately (ω_1 = 130, ω_2 = 9.75) and (ω_1 = 132, ω_2 = 10.40). Cross-peaks in this area are typical of signals from Hε-Nε within tryptophan side chains. There are two tryptophan residues in the GB1-S109-K272 construct, one in the GB1 tag and the other in the Popeye domain. Therefore, the S109-K272 construct only contains one tryptophan residue after the removal of GB1. The cross-peak at (ω_1 = 130, ω_2 = 9.75) greatly increases in intensity after GB1 cleavage (blue), whereas the peak at (ω_1 = 132, ω_2 = 10.40) is stronger in the GB1-S109-K272 spectra (red). This suggests that the (ω_1 = 130, ω_2 = 9.75) cross-peak is derived from the Popeye domain tryptophan and that it has increased in intensity, similar to many other cross-peaks, as a result of GB1 cleavage. In contrast the presumed GB1 tryptophan cross-peak at (ω_1 = 132, ω_2 = 10.40) has reduced in intensity after GB1 cleavage. Ideally this peak would have been completely removed, and its presence demonstrates incomplete purification of the construct.

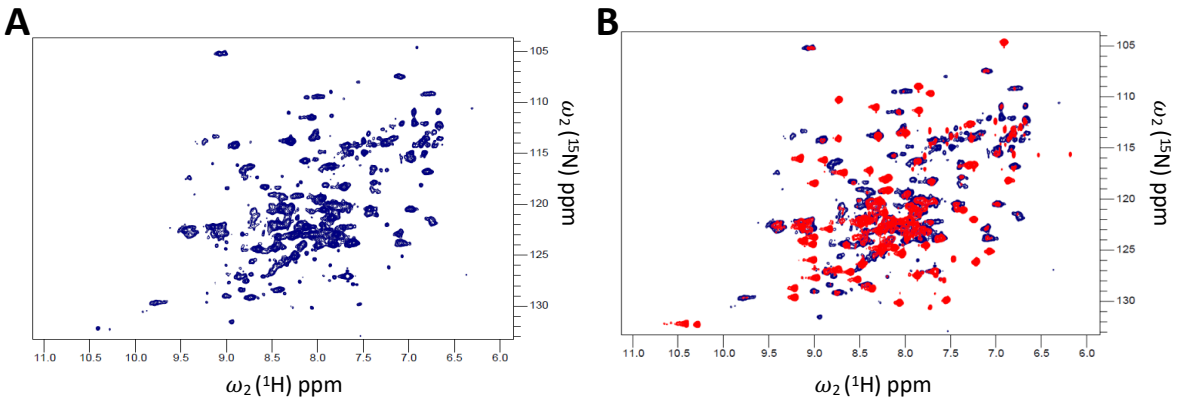


Figure 3.9: Protein-NMR ^{1}H-^{15}N HSQC-TROSY of S109-K272 Construct. A) A HSQC-TROSY of ^{15}N labelled S109-K272 Popeye domain construct. **B)** An overlay of the HSQC-TROSY of ^{15}N S109-K272 (blue) with a spectrum recorded under identical conditions of the same sample before GB1 tag cleavage, GB1-S109-K272 (red). The excess of blue signal compared to red shows the improvement in peak intensity after GB1 cleavage and also the appearance of new peaks previously not visible. Red peaks not found, or highly reduced, in the S109-K272 are derived from GB1 residues. The appearance of some of these peaks in **A** shows that some GB1 remained in the sample, either bound to the Popeye domain or in free. Protein was present at 100 µM in a buffer comprising 300 mM Arg/Glu, 25 mM NaCl, 20 mM NaH_2PO_4, 20 mM Na_2HPO_4, pH 7.24. A temperature of 308 K was used and a 700 MHz spectrometer was used.

The improvement of peak intensities in the spectra of S109-K272 compared to the tagged GB1-S109-K272, demonstrates the benefits of having a Popeye domain sequence that is now able to exist in solution without a protein tag. However, the spectra was not ideal with a high level of overlap between peaks and many Popeye domain residues likely still not visible. The quality of the spectra, compared to those previously obtained for the GB1-E123-D266 construct, was improved but not dramatically. The lack of increase in melting temperature of the Popeye domain within the S109-K272 construct compared to GB1-E123-D266, as shown by CD, suggests no significant increase in thermal stability.

This could mean that the S109-K272 construct is also subject to the conformational exchanges that were proposed to impact the performance of the GB1-E123-D266 construct. It is possible that optimisation of conditions, for example addition of cAMP and increased protein concentration, could have improved the quality of the spectra. Deuteration of the protein could have been performed to allow further experiments that might have improved spectra quality.[163] Further protein-NMR experiments from which detailed structural information could be determined would require double or triple labelling of ^{2}H, ^{13}C and ^{15}N, which would have required a large financial investment. It was decided to assess the activity of the construct, particularly its cAMP affinity, before deciding whether to attempt to optimise the NMR conditions for structural analysis. Initial attempts were also made to use ligand observed NMR techniques to detect cAMP binding to the S109-K272 construct, although results were inconclusive.

3.3.4 Assessing cAMP binding to the novel Popeye domain construct

3.3.4.1 Differential Scanning Fluorimetry

DSF was one of the techniques used to study binding of cAMP to the GB1-E123-D266 construct in the previous hit compounds screen.[138] DSF uses the change in thermal stability induced in a protein upon ligand binding to detect compound binding.[155] The protein is mixed with a fluorescent dye, typically SYPRO-orange, that is quenched in aqueous conditions. When the temperature is increased the protein begins to unfold, exposing core hydrophobic residues previously excluded from the solvent. The dye interacts with the newly exposed hydrophobic side chains, which leads to an unquenching of its fluorescence. The increase in dye fluorescence correlates with the extent of target protein unfolding.[155] The melting temperature of the protein can be determined by finding the point where the rate of increase in fluorescence against temperature is greatest, i.e. the point where the first derivative of the melt curve is at its highest point. If the protein is bound by a ligand it can lead to an increase in the Gibbs free energy of unfolding, due to the enthalpic and entropic contributions of ligand binding, which may result in an increase of the unfolding temperature of the protein.[164] DSF can also be used to determine the impact of other conditions such as optimum buffers, pH, and salt concentrations on the stability of the protein. DSF is a fairly generalisable method that is applicable to most protein ligand binding domains. It also requires low amounts of total protein making it an effective first screening tool.[155]

It was previously reported that cAMP, and some of the hit compounds, gave negative shifts in T_m upon binding to the GB1-E123-D266 construct during DSF.[138] This is an unusual result, with ligand binding in DSF usually leading to increases in T_m.[164] However, this result was found to be specific to cAMP and no change in T_m was seen after addition of ADP, ATP and cGMP. It was reported that the GB1-E123-

D266 Popeye domain construct used in previous DSF screens was difficult to work with and gave non-ideal melt curves.[164] The multiple transitions observed were likely the result of the construct containing both the Popeye domain and the GB1 tag, especially given the results of CD melt curves seen above. It was hoped that the S109-K272 construct would yield single transition melt curves, such as that observed using CD, and allow the clear observation of cAMP induced shifts in melting temperature. The GB1-E123-D266 construct was also tested to allow comparison of the two constructs.

Two buffer conditions were used during DSF experiments. Buffer A comprised of 10 mM HEPES, 150 mM NaCl set to pH 6.5 buffer, based on previous experience with the construct. Buffer B replicated the conditions of the DSF assay used in the previous compound screen and comprised of 50 mM Tris-Cl, 500 mM NaCl, 10 mM $MgCl_2$ with a pH of 7.5. SYPRO orange dye was used to visualise the melting of the protein constructs. Optimisation of conditions showed that approximately 10 μM of Popeye domain construct gave the best signal-to-noise ratio and was used for all experiments. At these conditions a strong transition was observed, centred at about 44.5-47.5 °C for both the S109-K272 and GB1-E123-D266 construct. This closely matches the CD derived T_m of the Popeye domain of each construct which was 46.5±0.1 °C and 46.8±0.1 °C for the S109-K272 and GB1-E123-D266 constructs, respectively.

While investigating the optimum protein concentration for the assay, it was noted that the T_m of the constructs seemed to be inversely related to protein concentration. To explore this effect further, each construct was titrated from 1-20 μM in Buffer A while keeping all other conditions constant (Figure 3.10A and B). It was found 1 μM of protein gave low signal-to-noise and was excluded from the analysis. Figure 3.10C shows that an approximate 5 °C and 3 °C reduction in T_m was observed between 2.5 μM and 20 μM for the S109-K272 and GB1-E123-D266 constructs, respectively. This is a relatively large change over a relatively small concentration range. There is also a change in the shape of the DFS melt curves over the range of protein concentrations. With GB1-E123-D266 a shoulder peak appears around 47 °C followed by another gradual transition at higher protein concentrations. This is masked or absent at lower construct concentrations with an ideal melt curve displayed, with only one clear transition, probably due to the rightward shift of the main transition obscuring the second transition. It was thought that the presence of the second transition may be due to the melting of the GB1 domain, which the CD analysis showed to unfold at higher temperatures compared to the Popeye domain. However, a similar change in the melt curve shape was found the S109-K272, albeit without the presence of a shoulder peak. At low concentrations of construct an ideal melt curve was formed with one single transition. As the concentration was increased it appeared that a second, more

gradual, transition was occurring at high temperatures. This can be seen in an inflection in the main transition around 45-50 °C, depending on the protein concentration.

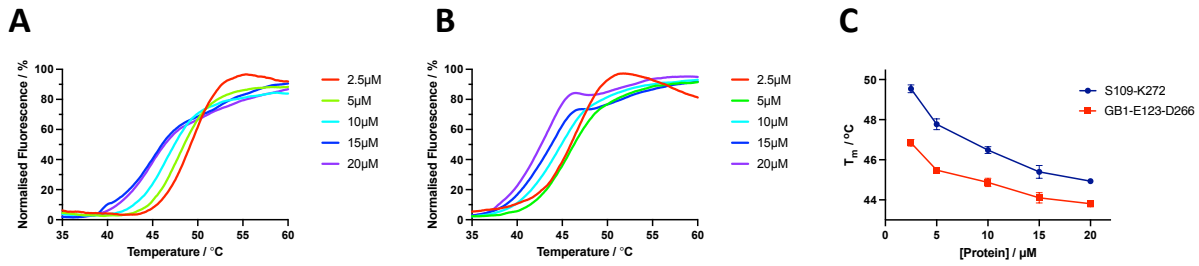


Figure 3.10: Differential Scanning Fluorimetry Spectra of the S109-K272 and GB1-E123-D266 Constructs at different Protein Concentrations. The normalised change in fluorescence of SYPRO orange, indicating protein unfolding, during the heating of S109-K272 **(A)** and GB1-E123-D266 **(B)** at different construct concentrations between 2.5-20 μM in Buffer A. Each curve shown is an average of 7 replicates. A leftward shift in the curves is evident as the protein concentration is raised. A second transition is present in the curves of the GB1-S109-K272 construct at higher concentrations, which could be due to the GB1 domain. **C)** The melting temperature of each construct at different temperatures, defined as the point of highest rate of fluorescence increase in the DSF curve. Error bars show ±SEM.

The T_m of each construct was determined by finding the point of greatest rate of fluorescence increase, which always occurred in the first transition, attributed to the Popeye domain based on the CD derived T_m. The change in T_m suggests a change in the stability of the Popeye domain when at different concentrations. The mechanism behind the change in melt curve shape is unclear. SEC-MALS confirmed the presence of dimeric complexes of each construct as discussed above. It is possible that the equilibrium between the monomeric and dimeric states of the construct were shifted across the protein concentration range tested. The equilibrium constant of construct dimerization is not known. The formation of a second state of the constructs could explain the appearance of a second transition in the DSF melt curves as the protein concentration is increased. However, it does not appear that a simple equilibrium between two states is occurring as the temperature of the first transition changes suggesting an additional destabilisation of the first state.

The impact of cAMP on the unfolding of the two constructs was then investigated. Both constructs were titrated with cAMP from 0.1 nM-10 mM. Surprisingly, neither construct showed a significant change in T_m over the full range of cAMP concentrations in either Buffer A or B (Figure 3.11B and E). The absence of a response from the GB1-E123-D266 construct contradicts previously reported results.[138] However, the fact that cAMP binding previously caused a destabilisation of GB1-E123-D266 suggests that it showed atypical activity. The large range of cAMP concentrations trialled mean it is unlikely that the K_D of the constructs was not covered by the titration.

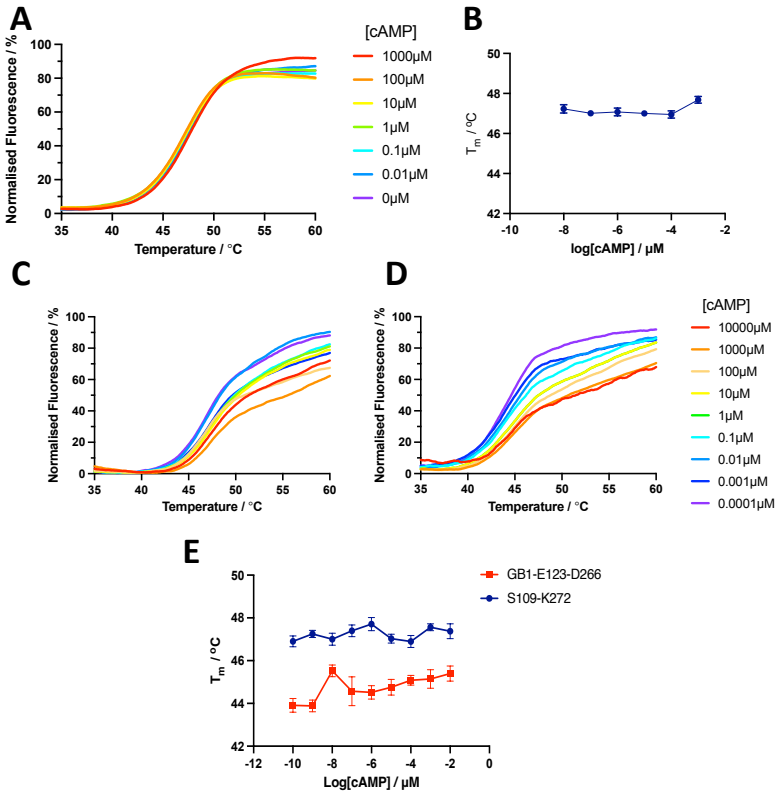


Figure 3.11: Differential Scanning Fluorimetry titration of cAMP with the S109-K272 and GB1-E123-K272 constructs. **A)** Normalised DSF melt curves of the S109-K272 construct in Buffer A in the presence of different concentrations of cAMP. Each curve represents the smoothed average of 7 replicates. **B)** The melting temperature of the S109-K272 construct in the presence of different cAMP concentrations, determined by the point of greatest rate of fluorescence change in **A**. Error bars show ±SEM, n = 7. **C)** Normalised DSF melt curves of the S109-K272 construct, and also GB1-E123-D266 **(D)** in Buffer B in the presence of different concentrations of cAMP. Each curve represents the smoothed average of 7 replicates. **E)** The melting temperature of the S109-K272 construct in the presence of different cAMP concentrations, determined by the point of greatest rate of fluorescence change in **C** and **D**. Error bars show ±SEM, n = 7.

Despite the lack of a shift in the point of greatest fluorescence change in the major transition, the T_m, a shift in the shapes of the curves was evident in Buffer B experiments. Inflection points in all curves were observed around 47-48 °C in both proteins, likely indicating the presence of a second transition. The normalised fluorescence level, which roughly corresponds to the total level of protein unfolding, at this inflection point differed between the cAMP concentrations. At low cAMP concentrations fluorescence had reached approximately 60% or 70% of the maximum fluorescence for the S109-K272

and GB1-E123-D266 constructs, respectively. At higher cAMP concentrations this had dropped to around 30-40%. The cause of this phenomenon is not clear but could indicate the formation of a separate cAMP bound state which is more resistant to unfolding. No change in the first transition T_m was seen suggesting this is distinct to the species present in the absence of cAMP. However, this trend continues to mM concentrations of cAMP which would be significantly lower than the 118 nM previously reported as the affinity of the Popeye domain for cAMP. If a fully functional CNBD was present it should be saturated with cAMP by this point and any cAMP-bound state to cAMP-unbound state equilibrium would be fully shifted to the bound state. The shift in curve shapes is similar to that observed when varying the concentration of the constructs. There could be a related mechanism that involves both cAMP and complexation. However, it is not clear what this could be, and this effect may be due to an unrelated process or confounding effect in the assay. This phenomenon was only seen in Buffer B and not when using Buffer A. This could be due to a change in stability between the two buffer systems. Given the unusual behaviour of the constructs with respect to changes cAMP and protein concentration, it could be that they are unstable or possess other non-ideal properties.

3.3.4.2 Microscale Thermophoresis

As an alternative cAMP binding assay to DSF, the constructs were subjected to MST to try and detect cAMP binding. MST involves the application of a thermal gradient to a capillary containing the target protein and ligand.[165] A point along the capillary is heated using a laser, which causes a reduction of protein concentration from the heated area compared to non-heated. The movement of the protein molecules away from the heat source, known as thermophoresis, is controlled by their charge, size and hydration shell.[166] Upon ligand binding to a protein, one or more of these parameters will likely change meaning that the level of thermophoresis will also change. The target protein is monitored through the use of fluorescent tags, or inherent fluorescence of the protein, so the induced concentration gradient can be followed by looking for a change in the rate of reduction of fluorescence at the point of heating.[165] This rate of fluorescence change can be plotted against the ligand concentration to detect binding that causes a change in thermophoretic properties of the target protein.

Given the uncertain DSF results, and the past issues with the GB1-E123-D266 construct, it was decided to also compare the S109-K272 construct to the previously reported GST-BVES construct.[71] The GST-BVES construct contains the entire cytoplasmic region of mouse Popdc1, along with an N-terminus GST tag. It was previously found to bind cAMP with an affinity of 118 nM using a radioligand assay.[71] While this construct has been reported to be difficult to handle, its previously reported cAMP binding perhaps made it a better control than the GB1-E123-D266 construct. The GST-BVES construct was expressed in BL21 Star *E. coli* in a similar way to the other constructs. Purification was achieved

through FPLC using a glutathione conjugated Sepharose column, which gave over 90% purity as judged by SDS-PAGE. Evidence of limited fragmentation was observed, but samples were deemed suitable for use in MST. The purified constructs were non-specifically labelled *via* primary amines using a succinimidyl ester functionalised Alex Fluor 647 dye. A labelling efficiency of approximately 0.35-0.5 was achieved and strong fluorescent signals were observed in the capillaries loaded with the labelled proteins. The constructs were assayed at a concentration of 200 nM in a buffer containing 20 mM phosphate, 250 mM NaCl at pH 7.5. cAMP was titrated from 0.6 nM-16.6 mM and mixed with the labelled protein before loading into the thermophoresis capillaries. As shown in Figure 3.12, no change in thermophoresis in relation to cAMP concentration was observed in the MST assay. This was the case for both the S109-K272, GB1-E123-D266 and GST-BVES construct. Good signal-to-noise was observed throughout the MST assays meaning it was unlikely cAMP response was not seen due to low signal to noise ratios.

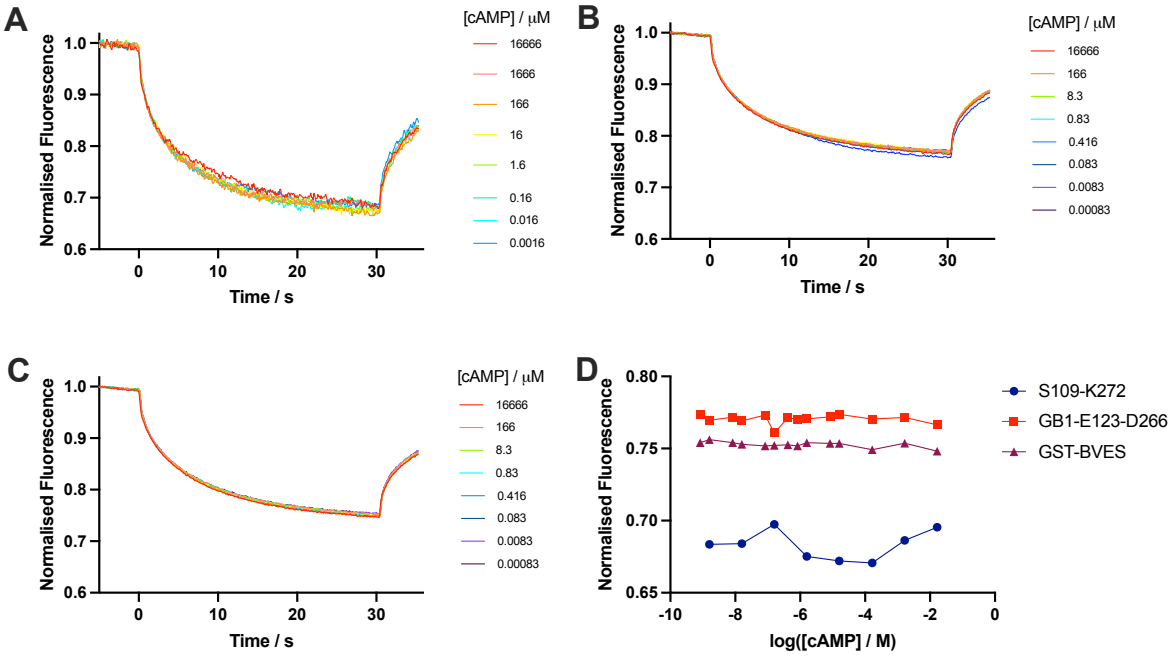


Figure 3.12: Microscale Thermophoresis Titration of cAMP with the S109-K272 and GST-BVES Constructs. The S109-K272 **(A)**, GB1-E123-D266 **(B)** and GST-BVES **(C)** constructs were subjected to MST in the presence of different cAMP concentrations and the change in fluorescence in response to the heating gradient was found. No clear cAMP dependent change in fluorescence changes was observed for any of the tested constructs **(D)**.

The lack of cAMP binding response in the S109-K272 seems to provide further evidence, along with the DSF assay, for this construct showing reduced or no cAMP binding activity. More surprising was the lack of response from the GST-BVES construct, which was intended to be used as a positive control for cAMP binding. The absence of cAMP binding to GST-BVES could have been due to a number of reasons. A tris-Cl buffer was used in the ^{3}H-cAMP binding study used to originally determine the cAMP

affinity of this construct, whereas a phosphate buffer was used for the MST binding experiments for both constructs. It is possible that the buffer impacts construct behaviour, possibly supported by the difference in DSF melt curves between the two buffers used in DSF. This was the first attempt at using the GST-BVES construct, and despite the construct appearing intact and well purified on an SDS-PAGE, it could be that expression on purification of this construct required further optimisation. However, the protocol used in this work closely matched the previously reported expression and purification of this construct.[71] It has been reported that this construct is difficult to use, particularly due to fragmentation of the construct.

3.3.4.3 cAMP-agarose affinity of control Popeye domain constructs

The issues with detecting cAMP binding to the GB1-E123-D266 and GST-BVES constructs, both of which have been reported to be active, albeit with some difficulties, was a clear cause for concern. Both the GB1-E123-D266 and GST-BVES constructs were therefore tested to see if they possessed any affinity for cAMP-agarose. Approximately 2 μmol of C8-conjugated cAMP was used in each incubation, along with 1-10 nmol of purified protein construct, ensuring an excess of binding sites was present. The cAMP-agarose beads were loosely packed into a column and equilibrated in buffer. Protein constructs were then added to the column and incubated for 1 hour before the elution of the loading sample. Three washes with buffer were performed before a 1 hour incubation with 50 mM cAMP. After incubation with the cAMP the final elution was collected, and all fractions were analysed on an SDS-PAGE gel, as shown in Figure 3.13. Both constructs seemed to display a non-specific affinity for the agarose beads. While a significant proportion of the GB1-E123-D266 remained bound to the cAMP-agarose after flowthrough of the loaded sample, it eluted steadily during the washes with minimal increase in concentration after the cAMP incubation. A major proportion of the GST-BVES construct was present in the initial flowthrough after the first incubation, suggesting minimal affinity for the cAMP-agarose. There was an unexplained upward shift in apparent molecular weight in the flowthrough fraction of the, presumed, GST-BVES construct. The GST-BVES construct also eluted steadily over the washes without a clear increase in elution in the presence of cAMP.

It was planned to examine the affinity of the S109-K272 construct to the cAMP-agarose but this was prevented by the closure of laboratory facilities as a result of the Covid-19 restrictions. This also prevented the running of a number of other planned experiments.

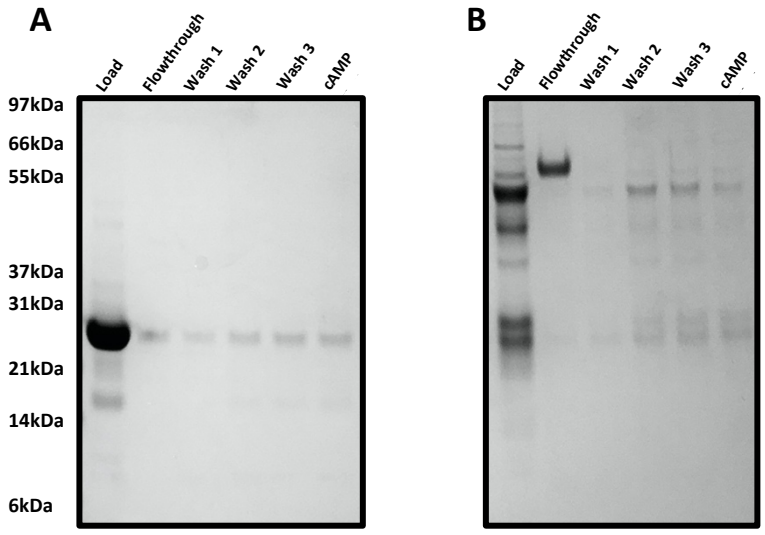


Figure 3.13: cAMP-Agarose Precipitation of the GB1-E123-D266 and GST-BVES Constructs. Purified GB1-E123-D266 (**A)** and GST-BVES **(B)** was added to a column containing cAMP-conjugated agarose and incubated for 1 hour before the loaded sample was allowed to flow through the column. Three washes were followed by addition of 50 mM cAMP and incubation for a further hour. Eluted fractions were collected and run on an SDS-PAGE. Only non-specific affinity for the cAMP-agarose was observed for both constructs.

3.3.5 Co-Expression of POPDC1 and POPDC2 Popeye Domain Constructs

After access to the protein production facilities at Kings College London were restored once the Covid-19 restrictions were lifted there was minimal time to further investigate the issues with the Popeye domain constructs or trial possible solutions. One factor that may influence Popeye domain stability and function could be intermolecular interactions with other Popeye domains. It had already been found that the S109-K272 and GB1-E123-D266 constructs dimerised through SEC-MALS. Unusual behaviour during DSF may also have been influenced by intermolecular Popeye domain interactions. This project also uncovered the possible role of heteromeric Popeye domain interactions in the function of full-length POPDC proteins in cells (see Chapter 6). Given the possibility that Popeye domains of POPDC1 and POPDC2 favourably interact in cells, and that this interaction is important for proper POPDC function, it was hypothesised that this interaction may enhance the activity of isolated Popeye domains. It could be that heteromeric interactions between isolated Popeye domains could be favourable to homomeric dimerization. To test this idea an analogous construct to GB1-S109-K272, formed of the Popeye domain of Popdc2 was created (Figure 3.14B). This construct consisted of residues Q94-K255 of Popdc2 with an N-terminus GB1 tag with a 6XHis tag linker, mimicking the GB1-S109-K272 construct. The Popeye domain residues were chosen through alignment with the sequence of Popdc1 to mimic the S109-K272 sequence. In the absence of a more detailed understanding of the solubility properties of the constructs, the nearest polar residues in Popdc2 aligned to S109 and K272 in Popdc1, which are the shown in Figure 3.14A, were chosen to form the N- and C-termini of the GB1-Q94-K255 construct. The new construct was inserted into the pRSFDUET plasmid, which contains an ampicillin resistance gene distinct from the kanamycin resistance gene found in the pLEICS-91 plasmid

to allow for double selection of co-transformed *E. coli*. No TEV cleavage site was included in this construct as it was planned to retain the GB1 tag to remove the need for solubility screening given the minimal time available for this investigation.

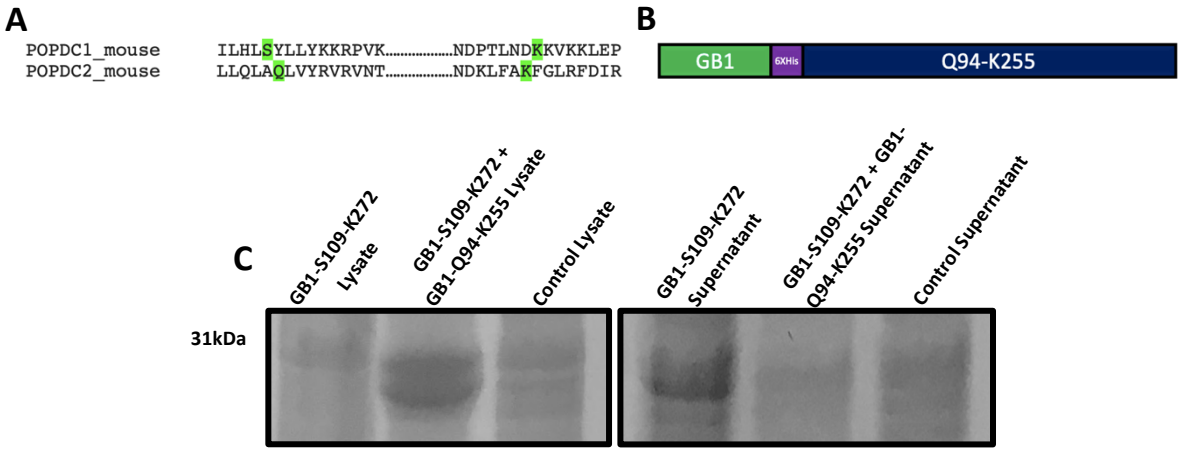


Figure 3.14: Expression Levels in *E. coli* of the GB1-S109-K272 Construct alone and with a POPDC2 derived Analogue GB1-Q94-K255. A) Partial alignment of the amino acid sequence of mouse Popdc1 and Popdc2. Highlighted residues show the terminal residues in the Popdc1 GB1-S109-K272 and Popdc2 GB1-Q94-K255 constructs. **B)** A schematic of the GB1-Q94-K255 construct. A N-terminus GB1 tag via a 6XHis tag linker is fused to the Popeye domain sequence, mimicking the GB1-S109-K272 construct. **C)** The GB1-S109-K272 construct was expressed alone as before alone, or with the Popdc2 derived GB1-Q94-K255 construct using double transformation. SDS-PAGE was used to assess the expression of the different constructs. The modest expression of GB1-S109-K272 was upregulated when co-expressed with GB1-Q94-K255, with both constructs present in large quantities at the expected positions of 27.7kDa and 26.6kDa. However, centrifugation removed both the GB1-S109-K272 and GB1-Q94-K255 constructs when co-expressed, whereas GB1-S109-K272 alone remained in the supernatant as usual.

BL21 (DE3) Star *E. coli* were co-transformed with both constructs, with single transformants acting as controls. It was found that co-expressing the Popdc1 GB1-S109-K272 and Popdc2 GB1-Q94-K255 constructs together led to a large increase in the concentration of GB1-S109-K272 in crude cell lysates compared to expression of the construct by itself (Figure 3.14C). Unfortunately, poor growth of the GB1-Q94-K255 only transformants prevented comparison to the Popdc2 construct only expression, with no opportunity to repeat this experiment. It was noted that expression of GB1-Q94-K255 in the double transformant bacteria was substantially greater than had been previously observed for the GB1-S109-K272 construct alone. This suggests that the two constructs are interacting and favourably influence each other's expression. This provides further evidence for heteromeric Popeye domain interactions between POPDC1 and POPDC2, as discussed in detail in Chapter 6. However, it was found that after centrifugation of the crude cell lysate containing both the tagged GB1-S109-K272 and GB1-Q94-K255 construct that they were each found in the pellet and not in the supernatant. This is in contrast to the normal behaviour of the GB1-S109-K272 construct alone which was robustly soluble with and without its GB1 tag. This suggests that while the two constructs interact with each other and

mutually enhance their expression levels, this interaction, or some other indirect effect, led to a large reduction in their solubility.

The reason for the increase in expression levels of the constructs when co-expressed, but reduction in solubility, is unclear. Perhaps some form of co-translational interaction is present which is able to enhance expression of the proteins.[167] This could then be countered by an unfavourable interaction between the mature proteins in terms of solubility. Significant optimisation of the sequence of the Popdc1 Popeye domain construct was needed to enhance its expression and solubility. Perhaps trialling different N- and C-termini positions in the Popdc2 construct would improve solubility when co-expressed with Popdc1 Popeye domain. However, it was decided there was insufficient time remaining in the project to pursue this further.

3.4 Discussion

3.4.1 The Properties of the Novel Popeye Domain Construct

The number of attempts to develop a construct of the Popeye domain which could be used in structural, or compound binding, studies reflects the high impact that successful preparation of such a construct would have on the study of POPDC proteins.[71,79,138] Throughout the different projects that have been carried out, difficulties with expression, purification, solubility and activity of the Popeye domain containing constructs have been a consistent challenge. Perhaps unsurprisingly, this work encountered the same set of issues. The sensitivity of expression levels in bacteria to minor extensions to the N- and C- termini of the Popeye constructs was unpredictable and hindered early exploration of potential new constructs. Switching the solubility protein tag to NusA, as opposed to GB1, also seemed to hinder expression. This project built upon progress that had been made in the study of the GB1-E123-D266 construct, which had been found to be expressed in *E. coli* and remain in solution after purification. Continuing with an N-terminus GB1 tag, and a similar range of Popdc1 residues, was convenient as it allowed the knowledge from the previous GB1-E123-D266 study to be used in the production of the GB1-S109-K272 construct. The finding that the Popdc1 sequence between S109-K272 remained in solution without the presence of a solubility tag in a standard phosphate buffer at a concentration of at least 100 μM led to hope that this construct represented a significant step forward compared to previous attempts. However, the S109-K272 and GB1-E123-D266 constructs were found to have similar thermal stability and secondary structure content in CD experiments. The additional residues in the S109-K272 construct seem to increase solubility without greatly altering the structure of the Popeye domain, although this is not conclusive given the low-resolution techniques used in this work.

There was difficulty in producing an effective purification protocol for the Popeye domain constructs given the endogenous affinity of the Popeye domain for the Ni-NTA columns used in FPLC. While this was partially explained by the activity of the H188 residue, mutation of this residue did not abolish affinity to the column. This could be related to the non-specific affinity of the GB1-E123-D266 to the cAMP-agarose beads seen in the cAMP precipitation assay. While another affinity tag, instead of 6XHis, could have been used to avoid this problem it was decided to use a modified FPLC protocol and SEC given the unpredictable expression levels seen when altering tags in this and previous work. The Ni-NTA FPLC purification was acceptable for the work carried out in this project, although a more effective purification protocol could have permitted x-ray crystallography attempts.

3.4.2 The Lack of cAMP Affinity to Novel and Known POPDC Constructs

Out of the three constructs tested in this work for cAMP binding affinity, S109-K272, GB1-E123-D266 and GST-BVES, all were tested in two of DSF, MST and cAMP-agarose precipitation. In all cases no clear affinity for cAMP was found. This is particularly troubling given the previous reports of cAMP affinity for the GB1-E123-D266 and GST-BVES constructs, albeit with some caveats.[71,138] The cause of the failure to reproduce the reported cAMP affinity is not clear. Both proteins were previously reported to be difficult to work with, and the issues experienced could just be due to minor changes in the construct preparation protocols, despite best efforts to follow previous work. The reduction in the proportion of α-helix within the S109-K272 construct compared to the corresponding region in the AlphaFold structure of Popdc1 could be due to the unfolding of the αC-helix of the Popeye domain, which, if it resembles the C-helix found in classical CNBDs,[94] could provide an explanation of the lack of cAMP affinity. It is possible that post translational modifications or chaperone assisted folding required for Popeye domain function does not occur in prokaryotic cells and other expression systems should be explored.[168]

A well characterised cAMP-binding positive control would have been useful in determining if any procedural errors in the cAMP-affinity assays were contributing to the lack of observed cAMP binding to the constructs. It was planned to use the CNBD of EPAC1 and EPAC2,[169] kindly provided by the Yarwood group, Herriot-Watt University in the MST and DSF assays to allow comparison with the Popeye domain constructs. Unfortunately, access to the laboratory at Kings College London, where all protein expression experiments in this project were performed, was blocked before the arrival of this construct as a result of the Covid-19 pandemic restrictions. Access to the protein production facilities at Kings College London was only restored for a limited time at the end of the project, at which point there was a focus on other areas of the project, which were given priority. This meant that the problems with cAMP binding affinity were not fully explored, and uncertainty remains as to why such issues were faced with all constructs used in this work.

The issues faced here in the development of a novel Popeye domain construct meant that it was not possible to gain empirical data on the structure of the Popeye domain using protein-NMR as planned. While the secondary structure estimates determined using CD do provide some clues about the true structure of the Popeye domain, this is not sufficient for significantly furthering the understanding of Popeye domain structure and behaviour. Unfortunately, other NMR-based aims such as using backbone assignment of peaks and ligand-observed techniques to run compound binding studies were also not completed. The lack of a high performing Popeye domain construct meant that it was decided not to proceed with plans to design further Popeye domain ligands based on those identified in the previous screen.[138] No new compound screening assays were validated because of the issues with cAMP binding, which meant any compound development would have suffered from the same issues as the previous screen, as discussed above. Overall, the aims of this part of the project were not met.

A separate attempt at producing a Popeye domain construct was recently carried out by another research group.[170] It was found that a construct containing residues L111-H279 of human POPDC1 with only a 6XHis tag and TEV cleavage site could be expressed and purified in *E. coli* .[206] However, this construct showed a tendency to aggregate. No clear cAMP affinity was detected in tests using cAMP-conjugated agarose, with non-specific affinity to the agarose beads found instead, correlating with the behaviour of the GB1-E123-D266 and GST-BVES construct in this work. The difference in solubility between the S109-K272 and 6XHis-L111-H279 construct demonstrates the high sensitivity of Popeye domain to minor changes in residues at the N- and C-termini. This highlights the difficulties in producing isolated Popeye domain, with problems with solubility and maintaining cAMP affinity once again being limiting factors.

3.4.3 Future Attempts at Studying POPDC Structure and Ligand Binding

Further work on isolated Popeye domain constructs could be carried out, but alternative approaches may be required. If the size of the constructs is one of the main factors in the poor performance in protein-NMR experiments, the focus could be shifted to obtaining x-ray crystallography derived structures, which are less sensitive to size but also have additional limitations regarding sample preparation.[1] The expression of POPDC protein constructs in eukaryotic cells could be utilised in future work, which may also enable the use of full length POPDC proteins in structural studies.[168] This may negate the apparent instability of truncated POPDC derived constructs.

The homo-dimerization of Popeye domains was demonstrated in both the S109-K272 and E123-D266 constructs, primarily through the results of the SEC-MALS experiments. Interactions between Popeye domains may be involved in modulating the behaviour of full-length POPDC proteins in cells (see Chapter 5 and 6). Instead of detailed structural studies, constructs similar to S109-K272 could be used

to study the impact of mutations or other modifications to the Popeye domain on dimerization. SEC-MALS is limited in its quantitative study of interactions due to the dilution of samples as they move through the SEC column, making determination of affinities and other parameters difficult.[7] Isothermal calorimetry (ITC), MST and CD, or other techniques, could be employed to focus on the study of Popeye domain interactions.[43] As well as yielding information on the affinity Popeye domains possess for each other, this may provide mechanistic insight into the effect of various Popeye domain mutations on POPDC interactions (see Chapter 6). The lack of cAMP binding to the constructs does mean that the constructs likely show changes in folding compared to native Popeye domain, and this would limit confidence in the relevance of any Popeye domain construct-based results.

For compound binding studies alternative techniques could be used to avoid problems with isolated Popeye domain constructs. Targeting full length POPDC proteins in cells, perhaps using thermal profiling assays such as CETSA, is one possibility.[171,172] This exploits changes in thermal stability of full-length proteins in cellular environments upon ligand binding, allowing proteins to be sorted based on the temperature at which their unfolding, and resulting precipitation, occurs. This would use expression of full-length POPDC proteins in eukaryotic cells, such as HEK293 cells, in the study of compound binding. This may provide a method of progressing the search for effective pharmacological modulators of POPDC protein behaviour in the absence of reliable and robust *in vitro* compound screening tools. The use of inter- or intramolecular BRET assays within cells to detect cAMP and hit compound binding to the Popeye domain is explored in Chapter 4.

4 Attempts to Develop Popeye Domain-Based cAMP Sensitive BRET Sensors for use in Ligand Binding Studies

4.1 Introduction

4.1.1 The Optical Sensing of cAMP in Cells

Optical cAMP sensors are a key tool in the interrogation of cAMP signalling.[139] These generally take the form of recombinant cAMP effector proteins that have been modified to contain fluorescent reporters that show a change in signal, usually *via* FRET, upon binding of cAMP. The earliest examples utilised tagged versions of the PKA holoenzyme.[173] The regulatory and catalytic subunits of PKA dissociate, fully or partially, upon cAMP binding to the regulatory subunit.[85] By tagging these subunits with a FRET pair, this dissociation can be detected by a drop in FRET. Many PKA based optical cAMP sensors have now been developed.[174] In addition, the conformational changes that occur in the EPAC proteins have also been co-opted in the development of FRET/BRET cAMP sensors. EPAC1 and EPAC2 are autoinhibited in the absence of cAMP but undergo a conformational change that exposes the previously shielded catalytic domain upon cAMP binding.[96,97] This conformational shift can cause a change in the efficiency of RET between two FRET or BRET pairs fused to different positions of the EPAC protein, thus allowing detection of cAMP by a change in FRET/BRET signal.[139] These types of cAMP sensors have been used to uncover many of the complexities of the cAMP pathway.[174]

The POPDC proteins have been suggested as possible templates on which to base novel optical cAMP sensors.[139] At present the only optical assay capable of reporting cAMP binding to POPDC proteins in cells is a bimolecular FRET assay based on the interaction between POPDC1 and TREK-1 developed by Froese *et al*.[71] It was found that CFP-tagged POPDC1 and YFP-tagged TREK-1, when co-expressed in HEK293T cells, was able to detect acute increases in cytosolic concentrations of cAMP by a reduction in FRET signal between the two proteins. The reason for this change in FRET is not fully understood, although it can be assumed that the binding of cAMP to POPDC1 leads to a conformational change in the interaction with TREK-1. While this assay has been highly useful in establishing that POPDC proteins bind cAMP in cells, and that they may mediate ion channel activity, it has several issues which mean it is not well suited for use in compound screening projects. The assay has a low dynamic range, with a maximal change in FRET after an increase in cAMP concentration of around 4%.[71] This would make it difficult to reliably rank prospective ligands, through measuring the change in FRET they induce, and then carry out optimisation of hit compounds. The assay has also only been applied to single cells using a specialised FRET microscope, which makes it a low throughput assay unsuitable for extensive compound screening. The only other reported assay that can detect functional changes in POPDC activity due to the binding of cAMP also exploits the interaction of POPDC proteins with TREK-1 but within *Xenopus* oocytes.[71,93,105] A cAMP dependent change in the TREK-1 current can be observed

in response to co-expression with POPDC proteins, possibly due to changes in the trafficking of TREK-1 to the cell surface, and further modulation of the TREK-1 current as a result of cAMP binding to POPDC proteins. It is a relatively low throughput assay as it relies on carrying out voltage clamp experiments on single cells. Also, the dose-response relationship between cAMP concentration and changes in TREK-1 current has not been established, with only saturating concentrations of cAMP used to give maximum response.[71,93,105]

The lack of an effective biological assay with which to measure cAMP binding to the Popeye domain, and cAMP mediated modulation of POPDC protein activity, is a significant issue in the search for POPDC specific cAMP mimicking ligands.[74] The development of an assay that allows for effective screening of hit compounds binding to the Popeye domain, or the ability to alter the function of POPDC proteins in a cellular context, would be a highly useful tool. This could also be used to further understand the fundamental role of the POPDC proteins in the cAMP pathway. If useful Popeye domain selective compounds are to be developed it will be essential to determine their effect on POPDC function and the resulting effects on the cAMP pathway. In addition, compounds designed to mimic cAMP should be tested for off-target binding to other CNBDs.

4.1.2 Previous Attempts to use POPDC Proteins in Optical cAMP Sensing

During the MRes phase of this project a cellular screening assay based on the previously reported POPDC1-TREK-1 FRET assay, but modified to use the NanoBRET platform, was used to try to develop a new assay to detect cAMP binding to POPDC proteins in cells.[175] It was hoped that this new assay could be used to screen for cellular activity of any hit compounds identified in experimental/*in silico* binding/docking studies. The key difference between the FRET assay reported by Froese *et al* and the new assay was the switch from using FRET to BRET. BRET uses an *in situ* chemical reaction to generate the electronically excited, luminescent donor species; whereas FRET uses incident light to excite a fluorescent donor group.[37] FRET can suffer from bleaching of the donor group due to the incident, excitatory light, meaning the level of donor excitation cannot be increased without risking damage to the sample.[37] Using lower excitatory light intensities leads to lower absolute levels of RET from the donor, which also means lower emission from any acceptor group, reducing the sensitivity of the assay. The efficiency of RET can be raised by increasing the overlap between the emission and absorption spectra of the donor and acceptor groups, respectively, which is illustrated in Figure 4.1. However, narrowing the gap between the two spectra increases the amount of bleed through between the two emission channels used to determine the FRET/BRET ratio, thus increasing background signal. In Figure 4.1A the spectra have a large degree of overlap, leading to high efficiency of RET, but also large bleed through from the donor channel. This reduces the sensitivity of the assay. In Figure 4.1B the spectra show minimal bleed through due to the lesser overlap between the donor

and acceptor spectra. However, the assay could be limited by the low emission from the acceptor caused by the inefficient RET. The highly intense bioluminescence of the NanoLuc luciferase employed in NanoBRET can lead to high levels of RET even with a wide spectral separation between the BRET groups.[176] The use of a red-shifted acceptor group reduces background signal and improves the signal-to-noise ratio of the assay.[143] NanoBRET uses a genetically fused HaloTag protein tag, which is formed of a modified alkane dehalogenase enzyme, to which a range of small molecule dyes can be covalently bound.[177] The very bright NanoLuc allows a highly spectrally separated dye bound to the HaloTag to be used as a BRET acceptor, specifically the rhodamine derivative HaloTag-618 dye.[143]

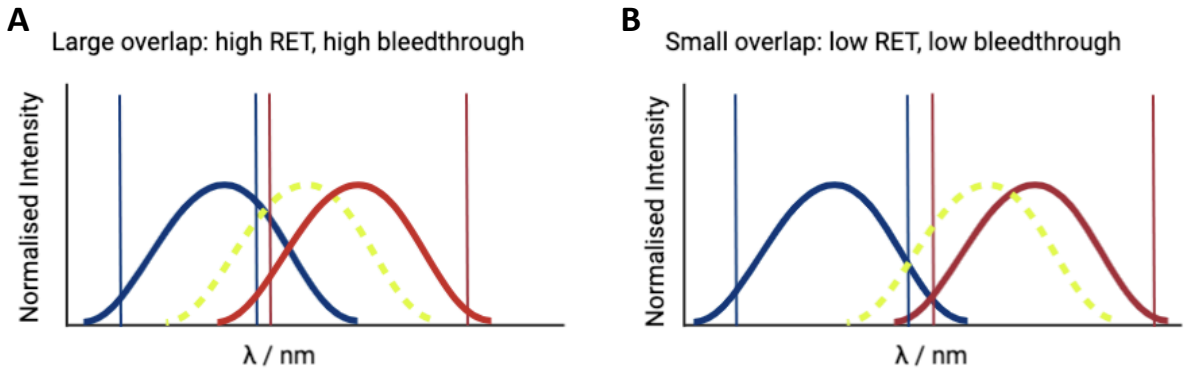


Figure 4.1: The Emission and Absorption Spectra of a BRET Donor and Acceptor Pair. A) The emission from a BRET donor (blue curve) overlaps with the absorption spectra of a BRET acceptor (yellow dashed curve). The greater the overlap between these two curves the more efficient RET between the two groups leading to a stronger emission (red curve) from the BRET acceptor. However, it will also lead to greater bleed through into the donor (blue vertical lines) and acceptor (red vertical lines) detection channels, giving a greater background signal. **B)** Reducing the overlap between the emission spectra of the donor and the absorption spectra will reduce the level of RET, leading to a weaker BRET acceptor emission signal but will reduce the background signal observed.

It was thought that the NanoBRET platform might improve on the 4% maximal change in FRET seen in the POPDC1 and TREK-1 FRET assay. This assay would be analogous to the FRET setup but with NanoLuc and HaloTag fusion tags instead of CFP and YFP FRET tags. It was hoped that an improvement in sensitivity might allow for signals to be recorded from populations of cell instead of having to focus on single cells to keep the background signal low. If an assay could be developed that allowed the detection of cAMP binding to the POPDC proteins within cells in a multi-well plate format it could be used for screening of potential Popeye domain ligands.

NanoLuc or HaloTag were fused to the C-terminus of mouse Popdc1 and the N-terminus of human TREK-1, which were co-expressed in HEK293 cells. A schematic of this assay is shown in Figure 4.2A. Cells were tested in a 96-well format in a BRET capable luminometer. Unfortunately, it was found that no consistent BRET response to increases to cellular cAMP concentrations, either through the addition of isoproterenol, forskolin or membrane permeable cAMP analogues, could be detected.[175]

Optimisation of the assay through changes to expression levels, cAMP stimulus and tag orientation did not lead to any significant improvements.

In addition, a trial to see if cAMP induced changes in the homomeric interactions between human POPDC1 could be detected using NanoBRET was also run (Figure 4.2B). POPDC1 tagged at the C-terminus with NanoLuc or HaloTag were co-expressed in HEK293 cells, as described for the POPDC1-TREK-1 assay. While a clear BRET signal was recorded, no significant change after incubation with forskolin or isoproterenol was found.[175] POPDC1-POPDC2 complexes are thought to form within cells and this heteromeric interaction may provide an alternative target for the development of BRET sensors. Although the mechanism of the interaction between these two proteins is uncertain, it is possible that cAMP binding influences this interaction. The probing of POPDC1-POPDC2 interactions within cells using the NanoBRET may also have applications outside of cAMP sensing (see Chapter 6).

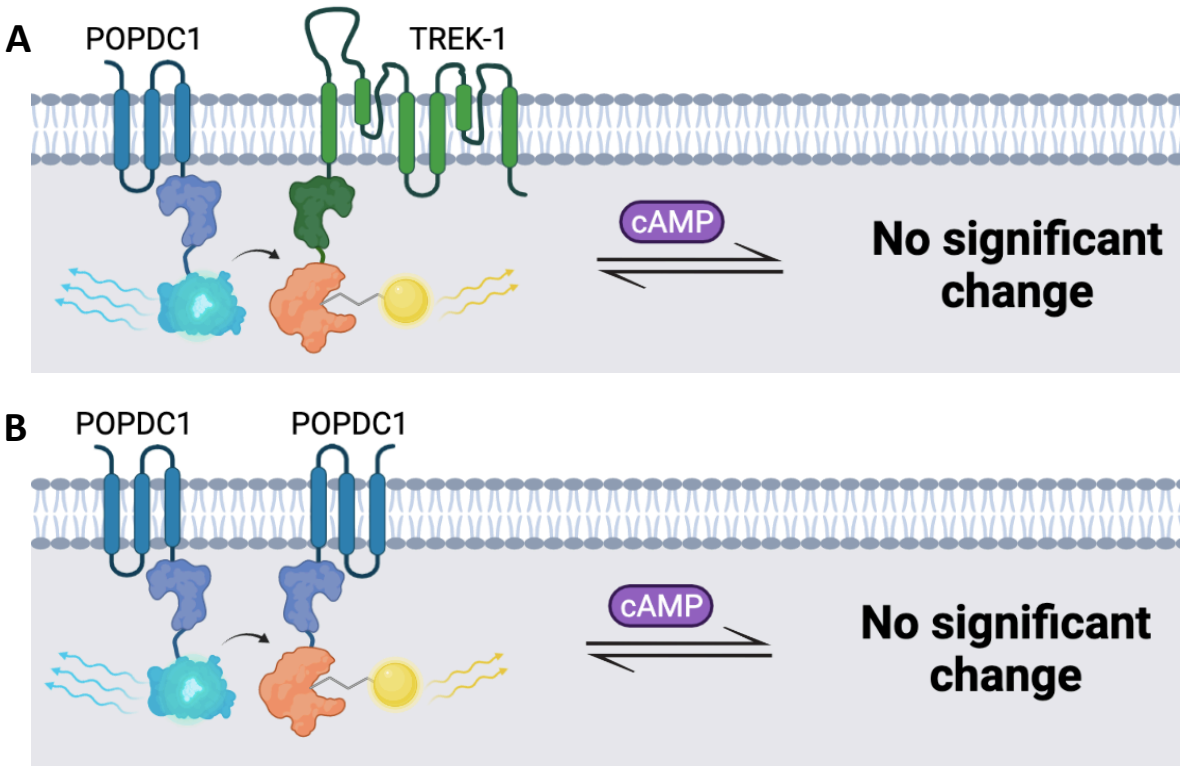


Figure 4.2: Schematic of the POPDC1-TREK-1 and POPDC1-POPDC1 NanoBRET Pairs Previously Trialled as cAMP Responsive BRET Reporters. A) NanoLuc or HaloTag were previously fused to the C-terminus of POPDC1 and N-terminus of TREK-1, respectively. POPDC1-NL and HT-TREK-1 pair are shown. **B)** POPDC1 was tagged at the C-terminus with NanoLuc and HaloTag on separate constructs. Both sets of NanoBRET pairs were co-expressed in HEK293 cells and cAMP concentrations in the cells were raised through addition of forskolin, isoproterenol or membrane permeable cAMP analogues. The BRET signal between the NanoLuc and HT-618 ligand covalently bound to HaloTag was measured at normal or raised cAMP concentrations. No significant changes in BRET were detected after the increase in cAMP concentrations.

An alternative approach would be to focus on the Popeye domain alone and try to detect conformational changes that occur upon cAMP binding directly. It is possible that an optical sensor based on the CNBD of POPDC proteins alone could be developed to measure cAMP binding to the

Popeye domain. However, given the lack of understanding of the allosteric shifts in the Popeye domain after cAMP binding this approach would be highly speculative.

4.2 Outline of Work and Aims

4.2.1 Description of this Work

This segment of work aimed to investigate if detectable changes, as measured by BRET, in the interaction between POPDC1 and POPDC2 could be stimulated by the addition of cAMP. This was to assess if such cAMP dependent changes could be exploited to develop a cell-based ligand activity assay. Based on the findings of Froese *et al*, and work performed in the MRes stage of the project, the NanoBRET platform was used to monitor the interaction of POPDC1 and POPDC2 in HEK293 cells. The level of cAMP in cells was raised and any changes in BRET signal recorded.

An attempt to develop an alternative compound screening assay using a cAMP sensitive BRET sensor based on the Popeye domain alone was also performed. The BRET2 platform was used by fusing GFP2 and a Renilla luciferase to the Popeye domain, which was then expressed in HEK293 cells, and changes in BRET signal upon raising the intracellular levels of cAMP.

In addition, the previously identified Popeye domain hit compounds were tested for their off-target activity on the classical cAMP-binding proteins PKA and EPAC1 using existing BRET2-based sensors.

4.2.2 Aims

1. Test if the interaction between POPDC1 and POPDC2 can be used to detect cAMP binding to POPDC proteins in cells.

2. Develop an optical cAMP sensor based on the Popeye domain.

3. Assess the level of off-target activity of the previously identified Popeye domain hit compounds.

4.3 Results

4.3.1 Examining cAMP Induced Changes in POPDC1-POPDC2 Interaction by NanoBRET

After the failure to develop a NanoBRET assay monitoring the interaction of POPDC1 and TREK-1, or the homomeric interaction of POPDC1 in the MRes phase of the project,[175] it was decided to examine if the interaction between human POPDC1 and POPDC2 would show a BRET response to changes in the concentration of cAMP. A schematic of this assay design in shown in Figure 4.3, where either NanoLuc or HaloTag was fused to the C-terminal end of full-length POPDC1 (POPDC1-NL and POPDC1-HT) or POPDC2 (POPDC2-NL and POPDC2-HT). These constructs were then co-expressed in HEK293 cells, and the BRET signal recorded under basal conditions or in the presence of raised cAMP

concentrations. HEK293 cells have previously been used to express POPDC constructs,[100,101] have extensively been used to in the study of transmembrane proteins,[178] and also endogenously express components of the cAMP pathway,[179] making them a suitable system in which to conduct the assay. The POPDC isoform to which the NanoLuc and HaloTag groups were added was changed to examine both combinations, which has been found to sometimes have a large effect on RET efficiency in the case of PKA based reporters.[180] Only the C-terminal of POPDC proteins were tagged to avoid issues with the membrane insertion of the N-terminal region. HEK293 cells were transiently transfected with the POPDC NanoBRET constructs and incubated for 48 hours, with the HaloTag-618 ligand added a day before measurement to allow full binding of the HaloTag-618 ligand to the HaloTag domains.

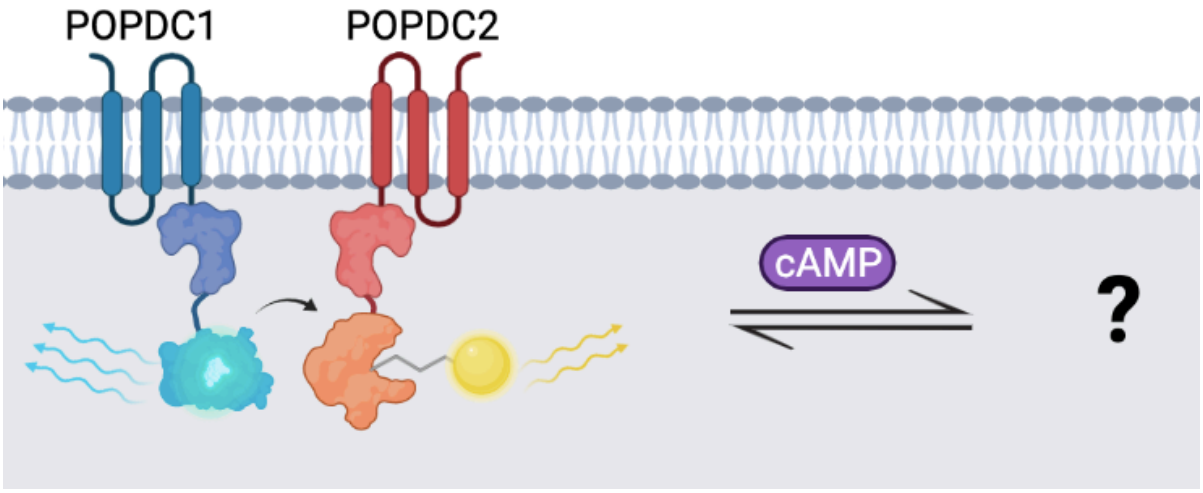


Figure 4.3: Schematic of the POPDC1 and POPDC2 NanoBRET Pairs Trialled as cAMP Responsive BRET Reporters. NanoLuc or HaloTag were fused to the C-terminal of POPDC1 or POPDC2 and expressed together in HEK293 cells. cAMP concentrations in the cells were raised through addition of forskolin and the BRET signal between the NanoLuc and the HaloTag-618 ligand measured at basal or raised cAMP concentrations.

Before BRET measurement, forskolin to a final concentration of 50 μM or vehicle was added to the cells and incubated for 20 minutes. Five minutes before measurement furimazine, the NanoLuc luciferase substrate, was added to the wells before the NanoLuc and HaloTag-618 emission was measured. As expected, a clear BRET signal was present showing that the tagged POPDC1 and POPDC2 proteins were interacting within the cells and RET was occurring. However, Figure 4.4 shows that there was no change in BRET between the POPDC1-HT and POPDC2-NL pair with the addition of forskolin, although there was a mild increase in BRET between POPDC1-NL and POPDC2-HT.

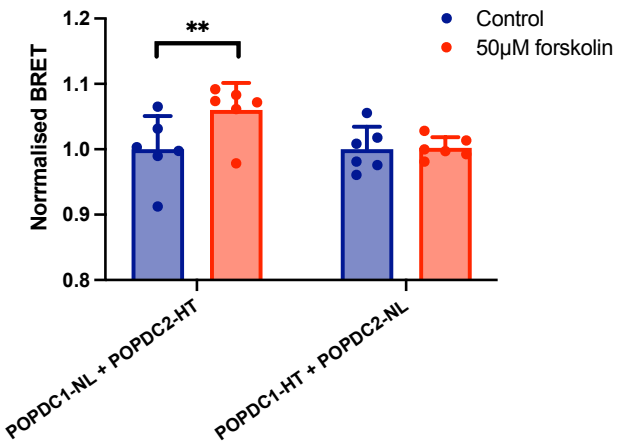


Figure 4.4: The Change in BRET between POPDC1 and POPDC2 NanoBRET Constructs after the Addition of Forskolin. Human POPDC1 and POPDC2 with either a NanoLuc or HaloTag C-terminus tag were co-expressed in HEK293 cells. The BRET signal between the constructs was measured after a 20 minute incubation with vehicle or 50 μM forskolin. The BRET signal between each POPDC pair was normalised to the vehicle control group and compared using student's t-test. A small change in BRET was found between POPDC1-NL and POPDC2-HT after the addition of forskolin (M = 1.060, SD = 0.0413) compared to the vehicle (M = 1.000, SD = 0.0510); t(5) = 5.60, p = 0.0025. No change was found between the POPDC1-HT and POPDC2-NL pairing with forskolin (M = 1.002, SD = 0.0166) or vehicle (M = 1.000, 0.0345); t(5) = 0.109, p = 0.917.

While the change in BRET between POPDC1-NL and POPDC2-HT after forskolin addition was found to be statistically significant, only a 6% increase was observed. This small rise in BRET means that this assay would possess a limited dynamic range for assessing the binding of cAMP or any other compounds to the POPDC1 and/or POPDC2. One parameter that can be used to assess the suitability of a screening assay is the Z factor, which uses the difference in the mean of a negative and positive control condition and their associated errors.[181] The determination of the Z factor is shown in Equation 4.1, where σ is the standard deviation and μ is the mean. This parameter accounts for the dynamic range and variation in signal from an assay. Z scores between 1-0.5 are generally taken to indicate an optimal assay. Scores between 0.5-0 may be acceptable depending on the intended use of the assay, but Z<0 means that the assay will not be able to be reliably used to assess potential hit compounds. The change in BRET between POPDC1-NL and POPDC2-HT yielded a Z score of -3.21, showing that this assay is highly unsuitable for use as a compound screening assay.

Equation 4.1:

$$Z = 1 - \frac{3(\sigma_{positive} + \sigma_{negative})}{|\mu_{positive} - \mu_{negative}|}$$

After the failure of the POPDC1-TREK-1, POPDC1-POPDC1,[175] and POPDC1-POPDC2 full-length NanoBRET assays, it was decided to cease attempts to make an alternative to the POPDC1-TREK-1 assay using BRET between full-length POPDC proteins in HEK293 cells.

4.3.2 Popeye Domain BRET Constructs

An alternative method to detect the presence of cAMP binding to the Popeye domain was proposed using isolated Popeye domain instead of full-length POPDC proteins with an interaction partner to form a unimolecular cAMP sensor. A FRET/BRET donor and acceptor could be placed at different points on the Popeye domain allowing RET to occur between them. If there was a sufficiently large conformational change in the Popeye domain upon cAMP binding, a change in the relative positions of the donor and acceptor groups may lead to a change in the observed FRET/BRET ratio. cAMP sensors usually rely on secondary allosteric conformational changes upon cAMP binding instead of the direct shifts in the CNBD itself.[139] Given that the Popeye domain is found between transmembrane domains and the C-terminal tail that is predicted to be highly disordered it is unlikely that large changes in the relative position of the Popeye domain and other areas of the protein occur. Although the C-terminal tail may obtain order upon binding to other proteins and have functions not yet known. What conformational changes occur within the Popeye domain upon cAMP binding are unknown.[74] This approach to designing a Popeye domain-based sensor is therefore highly speculative.

The putative αC-helix at the C-terminal end of the Popeye domain is proposed to act as a lid for the CNBD of the Popeye domain, which means it would be a likely place for conformational changes to occur. The relative placement of the BRET/FRET groups is of high importance in any sensor in order to effectively capture any conformational changes that occur. The function of any domain must also not be perturbed. The most practical approach was to tag the N- and C-terminal of the Popeye domain with a BRET donor and acceptor, truncating the full-length POPDC protein, as shown in Figure 4.5A. A series of different truncations were made to trial a range of donor-acceptor positions (Figure 4.5B). The series of constructs contained Popdc1 sequences between: E123-D266, E123-K272, E123-Q280, E123-S288, S109-D266, K114-D266 and K119-D266. These positions represent a reasonable range of tag positions, including around the C-terminal end of the predicted lid αC-helix of the Popeye domain. It was chosen to use the BRET2 platform which consists of a Rluc8 luciferase donor and a GFP2 acceptor.[182] The main reason to use BRET2, as opposed to NanoBRET, was the high cost of conducting NanoBRET assays, primarily due to price of the proprietary HT-618 ligand and furimazine NanoLuc substrate. GFP2 was fused to the N-terminal of the Popeye domain sequences and Rluc8 to the C-terminus, within the pGFP-N1 plasmid to allow expression in HEK293 cells.

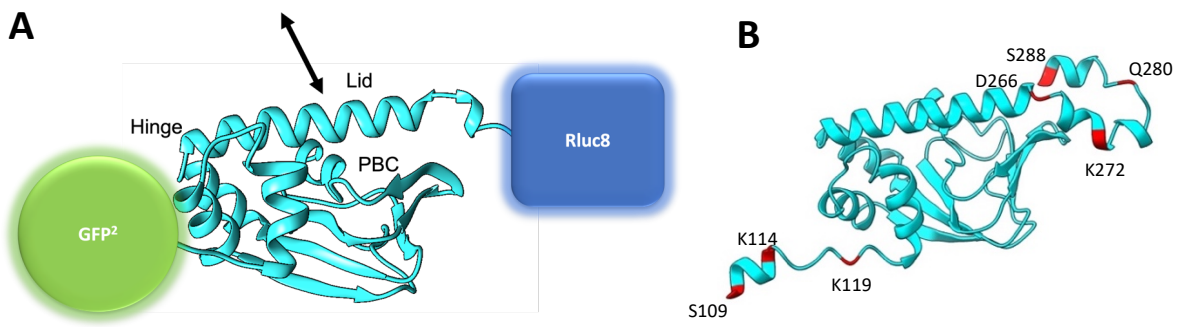


Figure 4.5: Schematic of the General Structure of the Proposed Unimolecular Popeye domain BRET cAMP Sensors. The unimolecular Popeye domain BRET cAMP sensors possessed a GFP2 tag on the N-terminus of the Popeye domain with a C-terminal Rluc8 tag. The AlphaFold structure of Popdc1 Popeye domain is shown as the core of the sensor. It was proposed that the αC-helix of the Popeye domain may undergo conformational changes upon cAMP binding, which may lead to a change in distance and/or orientation between the GFP2 and Rluc8 resulting in a change BRET efficiency **(A)**. The GFP2 and Rluc8 groups were placed at a variety of positions within the Popeye domain, with the terminal positions show in red: E123-D266, E123-K272, E123-Q280, E123-S288, S109-D266, K114-D266 and K119-D266 **(B).**

Each possible BRET sensor was expressed in HEK293 cells. Strong GFP2 and Rluc8 channel emission was recorded, with significant BRET efficiency of approximately 0.2-0.4 BU across the samples demonstrating efficient expression of the constructs and the close proximity of the BRET tags, likely indicating that Popeye domain sequence was folded. Upon addition of 50 μM forskolin to the cells, a small but significant increase in BRET was observed in three of the groups, E123-D266, E123-S288 and S109-D266 (Figure 4.6). Despite the changes in BRET in response to forskolin all three sensors that showed a statistically significant rise in BRET possessed Z factors below -1 meaning they were unsuitable for use in a screening assay. While it is possible that a specific cAMP induced conformational change in the Popeye domain was being detected, the small BRET change did not suggest this could be, at present, a viable method of forming a Popeye domain-based cAMP sensor. It was therefore decided to cease this avenue of work until more information about the mechanism of cAMP binding to the Popeye domain is known.

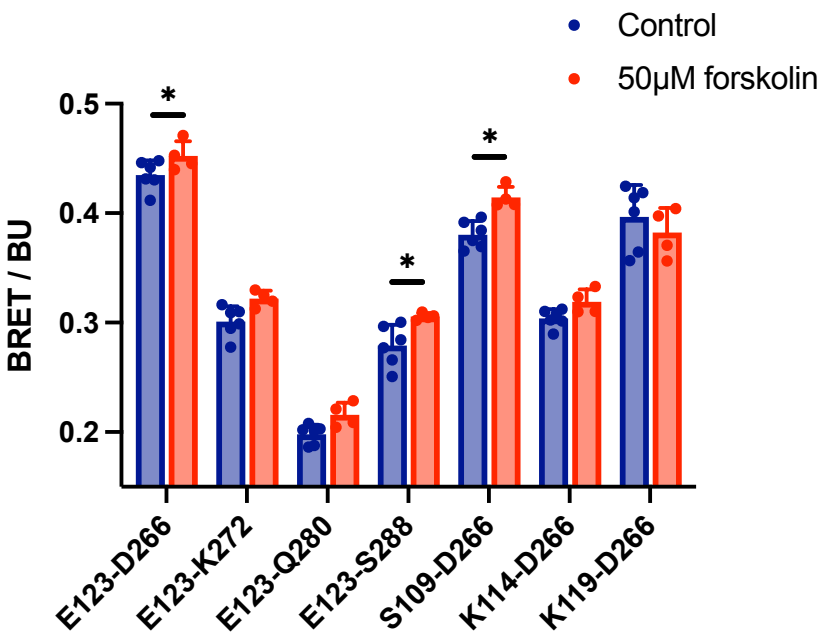


Figure 4.6: The Change in BRET Signal from a Series of Popeye Domain-Based cAMP Reporter Constructs within HEK293 Cells. A) The BRET signal from a series of Popeye domain constructs tagged with GFP2 and Rluc8 at the N and C terminals, respectively, when expressed in HEK293 cells. The BRET signal was measured after 20 minute incubation with 50µM forskolin or vehicle control. BRET signal was determined by the division of the GFP2 channel emission intensity by the Rluc8 channel. The control and forskolin groups (both n = 5) were compared by two tailed student's t-test. Three constructs were found to give significant changes in BRET after addition of 50µM forskolin: E123-D266, E123-S288 and S109-D266. A summary of data is shown in Appendix 10.1, Table 10.1. Z factors were determined for all BRET constructs that showed a significant change in BRET with forskolin addition and were found to be -2.94, -1.14 and -2.95 for the E123-D266, E123-S288 and S109-D266 constructs, respectively. * $p < 0.05$. Error bars = ±SD.

4.3.3 Hit Compound Off Target Screening

To further assess the properties of the seven hit compounds identified by the Domainex ligand screen (see Figure 3.1),[138] it was decided to test their activity towards the canonical cAMP effector proteins PKA and EPAC1. These compounds were designed in the previous screen to mimic cAMP binding to the Popeye domain. It will be important that any Popeye domain ligands developed are specific and do not bind to other CNBDs. Some initial screening for specificity against EPAC1 was previously conducted using an ELISA, although additional functional data would be useful. It was also desired to have an amenable specificity screening assay in hand in preparation for the further testing of possible Popeye domain ligands in the future. This work was conducted before the cessation of attempts to develop a Popeye domain-based construct for in vitro ligand binding studies (see Chapter 3) and cell-based BRET sensors, described above in this Chapter.

Two BRET-based cAMP sensors, based on PKA and EPAC1, were kindly provided by the Herberg group, University of Kassel.[183] The mechanism of each sensor is shown in a schematic in Figure 4.7A and B, respectively. These sensors exploit the same properties as other PKA and EPAC optical sensors, described above, and both use the BRET2 platform. The PKA sensor is formed by co-expression of the Cα and RIα subunits of human PKA, which interact to form the tetrameric PKA holoenzyme. The Cα

and RIα subunits are tagged with GFP2 and Rluc8, respectively, leading to RET between them in the holoenzyme form. Upon binding of cAMP to the RIα subunits, the Cα subunits are released leading to a drop in the BRET signal.[183] The unimolecular EPAC1 sensor contains a truncated version of human EPAC1 with an N-terminal GFP2 tag and a C-terminal fused Rluc8. In the non-cAMP bound form, an autoinhibitory interaction between the regulatory and catalytic regions of EPAC1 hold the GFP2 and Rluc8 groups in close proximity, leading to a high BRET signal. Binding of cAMP to the regulatory region releases this intramolecular interaction, increasing the distance between the GFP2 and Rluc8 tags. This leads to a cAMP-induced drop in BRET signal. If the identified hit compounds were leading to off-target activation of PKA or EPAC1 a drop in BRET signal would occur when incubated with the BRET sensors, mimicking the effect of cAMP.

The compounds were incubated with the BRET sensors in lysates of HEK293 cells expressing each sensor with the results shown in Figure 4.7C. Cell lysates were used to exclude any differences in cell permeability between the hit compounds, which had not been empirically determined. Cell lysates were incubated for 5 minutes with all compounds before measuring the BRET signal. Firstly, the cAMP analogues 8-Br-cAMP and 8-CPT-cAMP were titrated against each sensor to determine the maximal BRET change and allow comparison of the efficacy of hit compounds against the cAMP analogue positive controls (Figure 4.7C). The cAMP analogues led to a maximal 90% drop in BRET from the PKA sensor, with EC_{50}'s of 13.0 nM and 54.5 nM for 8-Br-cAMP and 8-CPT-cAMP, respectively. The EPAC1 sensor showed a smaller maximal drop in BRET signal, which is expected considering it is a unimolecular sensor, meaning the GFP2 and Rluc8 will remained tethered *via* the EPAC1 sequence even after cAMP binding. Here an approximate 40% drop in BRET was observed, with an EC_{50} of 311 nM and 3.36 μM for 8-CPT-cAMP and 8-Br-cAMP, respectively. When the seven hit compounds were added to the cell lysates no clear change in BRET signal was observed from either the PKA or EPAC1 sensor. This shows that no off-target activation of PKA and EPAC1 is occurring as a result of addition of the hit compounds, which would be required for any Popeye domain selective ligands. No competition experiments between the hit compounds and cAMP were conducted meaning that it is possible that the hit compounds bind to and antagonise the activation of PKA and EPAC1. This could be easily established by titrating cAMP against the BRET sensors in the presence of the hit compounds.

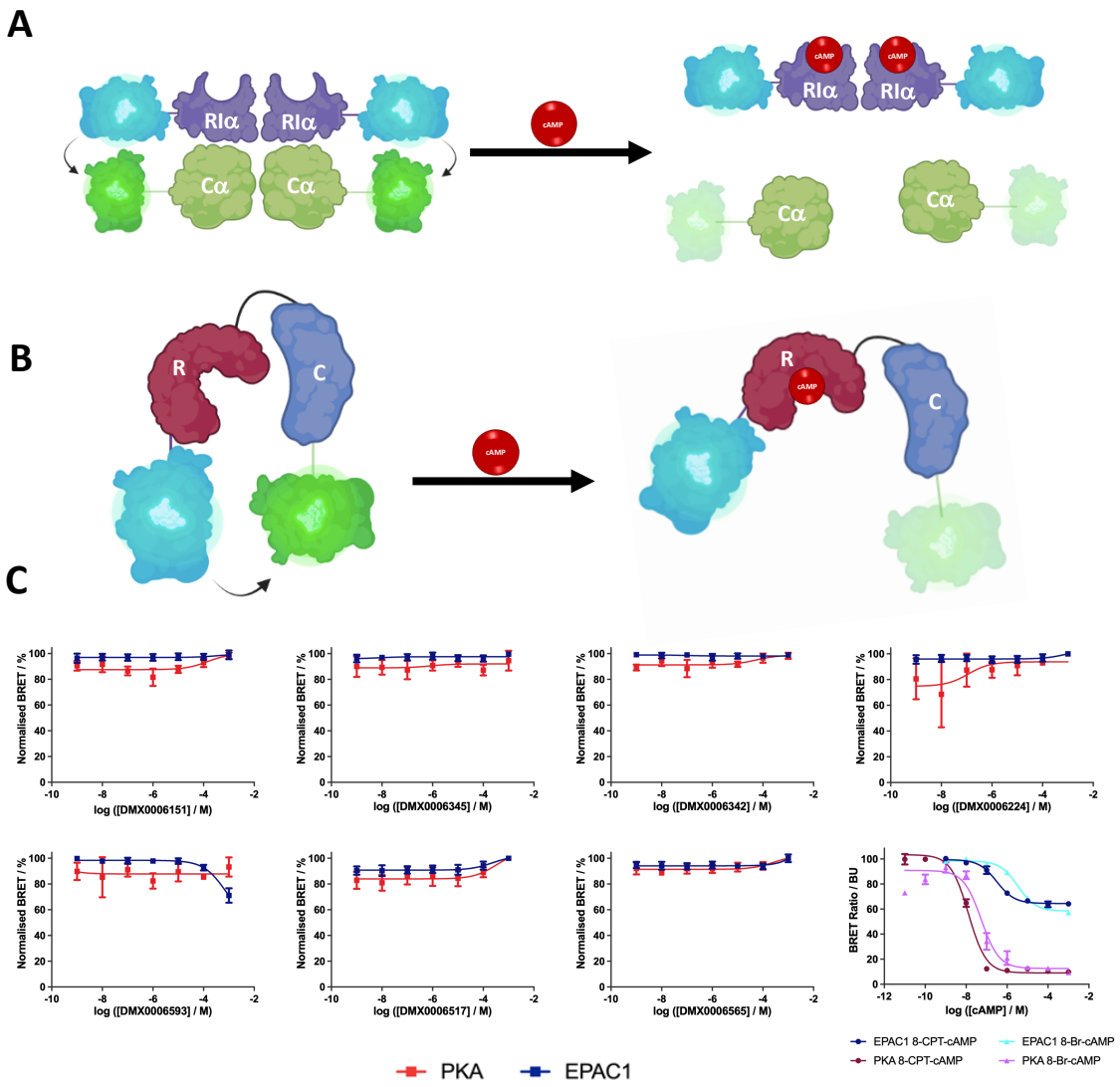


Figure 4.7: The Change in BRET Signal from a PKA and EPAC1 based BRET cAMP Reporter in Response to cAMP Analogues and the Popeye Domain Hit Compounds. A) Schematic of the PKA-based cAMP sensor. The RIα and Cα subunits of the tetrameric PKA holoenzyme are tagged with Rluc8 and GFP2. Dissociation of the holoenzyme upon cAMP binding leads to a drop in BRET. **B)** The EPAC1-based cAMP sensor contains GFP2 and Rluc8 groups fused to the catalytic region, C, and regulatory regions. Binding of cAMP leads to a dissociation of these domains, lowering the BRET signal. **C)** The change in BRET from HEK293 cell lysates containing the PKA or EPAC1 BRET reporters after addition of the previously identified Popeye domain hit compounds. No clear reduction in BRET, representing activation of PKA or EPAC1, was observed between 1 nM-1 mM. 8-CPT-cAMP and 8-Br-cAMP were used as positive controls which both led to clear dose-dependent reductions in BRET signals. Each point is formed of 9-16 replicates over 2-3 transfections. Error bars = ±SEM.

4.4 Discussion

It was hoped that modifying the POPDC1-TREK-1 FRET assay to use the NanoBRET platform would permit its use in compound screening efforts. The changes in BRET after an increase in cAMP concentration from one of the POPDC1-POPDC2 heteromeric pair reached 6%. This is comparable to the FRET assay of Froese *et al*,[71] which could mean that the assay was working in similar way. However, the increased error associated with measuring whole populations of cells in the 96-well plate, as opposed to measuring the signal from single cells, meant that the novel assay had a reduced signal-

to-noise than the original FRET assay. The extent of the BRET change was not suitable for assessing the activity of a range of hit compounds, as shown by the negative Z value for the assay.

The finding that neither the interaction between POPDC1-TREK-1, homomeric POPDC1,[175] or the heteromeric POPDC1-POPDC2 interaction formed the basis for a suitable BRET assay for compounds screening meant this area of the project did not progress. There are a number of reasons why these assays may have not work as hoped. The NanoLuc and HaloTag domains that are genetically fused to the proteins of interest in the NanoBRET platform are 19 kDa and 36 kDa, respectively.[143] The effect of appending these sequences to POPDC isoforms or TREK-1 is hard to predict. They may perturb the cellular localization of the proteins, alter the interaction between the proteins, or inhibit other important protein interactions.[36] Even if the normal function of the target proteins is maintained, it is possible that conformational changes upon ligand binding are not transduced to the tags in a way that leads to a change in RET efficiency between the donor and acceptor. RET is sensitive to the distance and orientation of the donor-acceptor pair. Predicting how this will change between the resting and active state of the bimolecular target protein pair is usually not possible unless the donor and acceptor are fused to inflexible regions of the proteins of interest and the interaction under observation is highly characterised.[36] Significant levels of trial and error are usually required to obtain optimal donor and acceptor positions on the proteins of interest. While the interface between POPDC1 and TREK-1, and POPDC1 and POPDC2 (see Chapter 6) have been approximately mapped to the Popeye domain,[71] no detailed structural information interaction site is available. The NanoBRET tags were fused to the C-terminus of the POPDC proteins. This is because the N-terminus of POPDC1 and POPDC2 is extracellular,[73] and the addition of a tag could have disrupted membrane insertion. Appending BRET groups to the Popeye domain, while closer to the possible interface, may have interfered with its function and other Popeye domain mediated interactions, making the C-terminal domain the most practical position to place the tags. However, the C-terminal tails of POPDC proteins are predicted to be disordered and are likely to be highly flexible.[184] The C-terminal domain could be truncated to bring the tags closer to the Popeye domain and putative interaction sites, perhaps making the distance between the donor and acceptor groups more sensitive to cAMP induced conformational changes. However, the role of the C-terminal domain is not understood and truncating this region risks disrupting normal POPDC function. The recently reported PPIs involving POPDC1 and PDE4A and AC9 were examined in different cAMP conditions.[100,101] These interactions could be exploited to examine the effect of binding of cAMP, or other compounds, specifically to the Popeye domain instead of global changes in cAMP concentration.

The brief attempt to develop a unimolecular, optical cAMP sensor based on the Popeye domain was also unsuccessful, despite some sensors showing statistically significant changes in BRET with raised cAMP. Further optimisation could have improved the dynamic range of the sensors, perhaps through BRET pair repositioning.[36] A change of approach to using small molecule dyes as FRET donor and acceptor groups, instead of relying on a bulky genetically encoded fluorescent protein and luciferase, could have improved responsiveness to small conformational changes, as well as lowering the risk of perturbing Popeye domain folding or function.[185] An empirically determined structure of the Popeye domain, preferably in the cAMP bound and unbound states, would aid the design of Popeye domain cAMP sensors. This could reveal what conformational changes, if any, are occurring in the Popeye domain upon cAMP binding. A unimolecular Popeye domain cAMP sensor would be an extremely useful tool, allowing the quick assessment of hit compound binding to the Popeye domain. It could also be used to quickly assess the impact of mutations in the Popeye domain on cAMP binding and help to investigate the binding mechanism of cAMP through mutagenesis studies. It may be possible to re-attempt the design of Popeye domain cAMP sensors when more detailed structural information is available to allow a more rational design process.

While it was useful to determine the extent of any off-target activity of the hit compounds on PKA and EPAC1, it will be difficult to further the development of Popeye domain binding ligands without an effective *in vitro* or cell-based assay for assessing their effects on the function of POPDC proteins. How cAMP binding changes the behaviour of POPDC proteins, and how this can be exploited to detect the binding of cAMP, is a major outstanding question and progress will be needed if the pharmacological modulation of POPDC proteins is going to be achieved.

5 Investigations into the Expression of Wildtype and Mutant POPDC1 and POPDC2 in Skeletal Muscle and HEK293 Cells

5.1 Introduction

5.1.1 POPDC Mutations are Associated with Mislocalisation of POPDC1 and POPDC2 in Patients

A number of mutations in POPDC genes have been identified in patients.[93,99,105,117,122-124,129] Patients carrying POPDC mutations tend to display muscular dystrophy and/or cardiac dysrhythmia phenotypes depending on the isoform affected. In several cases, skeletal muscle biopsy material from patients were taken and the expression pattern of POPDC1 and POPDC2 assessed. Immunohistochemical staining for POPDC1 and POPDC2 revealed that in many cases a mislocalisation or loss of expression of both proteins had occurred in the muscle fibres, regardless of which POPDC gene contained the mutation.[93,117,122] POPDC proteins are normally found at the plasma membrane of cells, and the loss of POPDC1 and POPDC2 at the plasma membrane is assumed to be related to the pathologies observed in affected patients. The clinically identified POPDC mutations have a varied effect at the protein level, from presumed total loss of POPDC1 expression in the case of *POPDC1* 1A>G,[122] nonsense mutations leading to large truncations of POPDC1 or POPDC2 such as POPDC1 p.R88X,[122] and POPDC2 p.W188X,[105] and also missense mutations such as POPDC1 p.S201F.[93] Despite the difference in the impact on protein structure, most mutations of *POPDC1* and *POPDC2*, for which patient biopsy material has become available, were found to affect both POPDC1 and POPDC2 expression patterns. Table 5.1 lists all currently identified POPDC mutations and their effect on POPDC1 and POPDC2 localisation in tissue if known. To date, POPDC localisation to the plasma membrane in the presence of mutations has only been studied in patient or animal model skeletal biopsy material. Patient biopsy material is often lacking given the rarity of individuals carrying POPDC mutations and the practical and ethical implications of performing biopsies on patients. This has meant that the behaviour of many known mutations on the protein level has not been investigated.[99,105,124,128,129] When *Popdc1* or *Popdc2* have been knocked out in mice, a loss of both POPDC1 and POPDC2 in the plasma membrane has been observed, with similar effects seen in zebrafish.[71,93] This mimics the effect on changes in expression and plasma membrane localisation in the case of nonsense or missense mutations of POPDC genes where the resulting mutant protein might still be translated and therefore at least theoretically be present. It appears that the mutations which lead to a loss in POPDC1 and POPDC2 localisation and/or expression at the plasma membrane, resemble the effect of total loss of one of the POPDC proteins. The reason for the double loss in POPDC protein expression at the plasma membrane is not known, but may be to do with an interaction between POPDC1 and POPDC2.[82]

Table 5.1: A table listing the known POPDC mutations identified in patients, as well as various animal models, and the effect of the mutation or knock out on the expression pattern or subcellular localisation of POPDC1 and POPDC2 in skeletal muscle fibres.

	Species	POPDC Protein Mutation	POPDC1 Loss or Mislocalisation	POPDC2 Loss or Mislocalisation	Reference
Animal Models	Mouse	*Popdc1*$^{-/-}$	N/A	Y	71
	Mouse	*Popdc1* (c.602CT>TC, p.S201F)	This work	This work	Unpublished
	Mouse	*Popdc2*$^{-/-}$	-	N/A	71
	Mouse	*Popdc2* (c.563G>A, p.W188X)	-	-	105
	Zebrafish	*popdc1*$^{-/-}$	N/A	Y	93
	Zebrafish	*Popdc1* (c.572CT>TC, p.S191F)	Y	Y	93
Patients	Human	*POPDC1* (c.1A>G, p.X)	Y	Y	122
	Human	*POPDC1* (c.262C>T, p.R88X)	Y	Y	122
	Human	*POPDC1* (c.275A>G, p.D92G)	-	-	128
	Human	*POPDC1* (c.427A>T, p.R143X)	-	-	129
	Human	*POPDC1* (c.457C>T, p.Q153X)	Y / This work	This work	117
	Human	*POPDC1* (c.515G>A, p.R172H)	This work	This work	Unpublished
	Human	*POPDC1* (c.547G>T, p.V183F)	This work	This work	Unpublished
	Human	POPDC1 (c.578T>G, p.I193S)	Y	-	117
	Human	*POPDC1* (c.602C>T, p.S201F)	Y	Y	93
	Human	*POPDC1* (c.816+2T>C, p.V217-K272del)	Y	Y	122
	Human	*POPDC1* (c.788C>A, p.S263X)	Y	Y	123
	Human	*POPDC2* (c.563G>A, p.W188X)	-	-	105
	Human	*POPDC3* (c.460A>G, p.K154E)	-	-	124
	Human	*POPDC3* (c.464T>A, p.L155H)	-	-	99
	Human	*POPDC3* (c.651A>T, p.L217F)	-	-	99
	Human	*POPDC3* (c.782>A, p.R261Q)	-	-	99

While mutations in the POPDC genes are rare, the increase in the use of exome sequencing in the diagnosis of unexplained disease states has led to an increase in the rate of pathogenic POPDC mutations being identified in patients suffering from muscular dystrophy and/or cardiac disease. One such newly reported *POPDC1* variant is the *POPDC1* (c.457C>T, p.Q153X) mutation, which was identified in a patient suffering from early onset sinus bradycardia and atrioventricular block, as well

as elevated creatine kinase concentrations in serum.[117] This nonsense mutation leads to a premature stop codon at residue Q153, causing a truncation of POPDC1 within the Popeye domain. POPDC1 plasma membrane expression appeared to be lost in biopsy material from the patient, although detailed quantitative measurements were not performed. The expression of POPDC2 was not investigated. It appears, at least from initial investigations, that this mutation is another example of a mutation which affects POPDC1 subcellular localisation and could possibly also have an effect on POPDC2. *POPDC1* (c.547G>T, p.V183F) is an unpublished novel variant found in two unrelated patients.[186] The effect of this variant on the expression and subcellular localisation of POPDC1 and POPDC2 has not been previously assessed. Skeletal muscle biopsies for both of these novel variants are examined below to look for changes in the expression and subcellular localisation of POPDC1 and POPDC2.

An unpublished *POPDC1* (c.515G>A, p.R172H) variant was recently found in a patient suffering from dilated cardiomyopathy. The R172H substitution affects a residue within a RLSILLK motif, which is implicated in the association of POPDC1 and PDE4A.[100] Sections from explanted heart were available for analysis of POPDC1 and POPDC2 expression and subcellular localisation within cardiomyocytes. Once again, detailed quantification of protein levels and localisation was not possible. However, it appears that no significant loss of either protein at the plasma membrane occurs. This would make the *POPDC1* (c.515G>A, p.R172H) mutation somewhat unusual in that the majority of pathogenic POPDC1 mutations have been found to show altered POPDC1 and POPDC2 expression patterns when examined. This effect has not been confirmed in skeletal muscle.

The reason for the combined loss of POPDC1 and POPDC2 expression in the presence of single *POPDC* mutations is not known, although a link to POPDC1-POPDC2 protein-protein interactions is suspected. The interaction of POPDC1 and POPDC2 is explored in Chapter 6. Given that this effect is a common phenotype of POPDC mutations, detailed analysis of the changes in expression level and subcellular localisation of POPDC1 and POPDC2 in the presence of novel and previously reported mutations would aid the understanding of the effects POPDC mutations in disease, as well as the basic workings of the POPDC proteins.[186] Being able to analyse biopsy samples so as to extract maximum information without relying on inefficient manual analysis of images permits more detailed analysis of samples. Consequently, there is much interest in automated image analysis tools for use on patient derived samples.[187] The use of such tools to be able to correlate changes in the expression of different proteins and morphological changes in muscle fibres has been applied to the study of muscle dystrophy.[188,189] Sections from patient and animal biopsy samples have previously been used to perform immunostaining with anti-POPDC antibodies, allowing the spatial distribution of the proteins to be

seen and their expression level estimated.[93,117,122] A sarcolemma marker, such as α-sarcoglycan, has typically been used to provide an independent outline of the plasma membrane. The intensity of fluorophore emission linked to anti-POPDC antibodies has previously been reported for the plasma membrane of single fibres within biopsy sections, although with relatively low numbers of fibres included.[93] Increasing the number of fibres that are analysed and also providing further information in addition to anti-POPDC fluorophore emission levels in the plasma membrane would permit a more detailed analysis of POPDC variant behaviour.

Adding the findings of analyses of POPDC expression patterns in biopsy material from previously unexamined variants to previous knowledge will help in the recognition of any patterns in the effect of different mutations. This may help determine the roles of the different domains of the POPDC proteins, and also the mechanism of different mutations' pathologies.

Studies into POPDC protein subcellular localisation have been hampered by the reliance on patient and animal biopsy material. In mature cardiomyocytes and skeletal muscle fibres both POPDC1 and POPDC2 are normally highly localised at the outer membranes of cells.[184] However, when POPDC1 or POPDC2 have previously been transiently transfected into COS-7 or HEK293 cells they were widely spread intracellularly (possibly retained in the ER) and largely absent from the plasma membrane of transfected cells. While some plasma membrane localisation of POPDC1 and POPDC2 is seen in transiently transfected cells, only a minor fraction of the expressed protein is correctly trafficked.[71,82,154] This has limited the use of cell models in the investigation of POPDC protein behaviour, particularly with respect to trafficking and subcellular localisation. Being able to utilise simple cell models would simplify the study of POPDC proteins by reducing the reliance on knock-in or knock-out animal models and tissue isolation.[186] The expression of POPDC proteins in HEK293 cells is investigated below and the links to the findings from biopsy material examined.

5.2 Outline of this Work and Aims

5.2.1 Description of this Work

Here, the change in POPDC1 and POPDC2 expression and localisation to the plasma membrane in skeletal muscle biopsy of patients possessing two novel *POPDC1* mutations, *POPDC1* (c.457C>T, p.Q153X) and *POPDC1* (c.547G>T, p.V183F), are quantified. In addition, the behaviour of POPDC1 and POPDC2 in the skeletal muscle and cardiac tissue of homozygous *Popdc1* (c.602CT>TC, p.S201F) mice are studied and compared to the previously reported effects in patients and zebrafish. To provide a greater insight into the changes in POPDC expression and subcellular localisation within skeletal muscle sections, a method to semi-automatically segment images containing immunohistochemically stained muscle fibres into areas of interest, particularly the plasma membrane and cytoplasm, was

developed. The relative concentrations of POPDC proteins in the different cellular compartments was then determined and analysed.

To further investigate the changes in POPDC trafficking as a result of the presence of pathogenic POPDC variants, a novel POPDC expression model using HEK293 cells was developed. This was used to model the subcellular location of POPDC proteins in HEK293 cells and the findings were compared to the clinical and animal model biopsy analysis reported here and in previous studies.

5.2.2 Aims

The aims of the studies described in this chapter were to:

1. Quantify the extent of POPDC1 and POPDC2 mislocalisation in patient and mouse tissue samples expressing the *POPDC1* (c.457C>T, p.Q153X), (c.547G>T, p.V183F) or (c.602CT>TC, p.S201F) variants.

2. Develop a HEK293 based cell model to investigate POPDC protein subcellular expression patterns in response to different POPDC mutations or the absence of a POPDC isoform.

5.3 Results

5.3.1 Analysis of POPDC1 and POPDC2 Plasma Membrane Localisation in Skeletal Muscle in the Presence of a Selection of POPDC Mutations

5.3.1.1 Development of a Semi-Automated Processing Method for Quantifying Plasma Membrane Enrichment of Proteins and other Parameters in Muscle Fibres

To achieve analysis of single muscle fibres in tissue sections in a time-efficient and non-biased manner, a custom image analysis script was written for use in the FIJI program.[142] This was designed to allow semi-automatic division of an image into separate muscle fibres and then further segment each fibre to produce different regions of interest (ROI), such as the whole fibre, intracellular region, cytoplasm and plasma membrane, as shown in Figure 5.1. This was achieved by using an α-sarcoglycan marker channel to produce outlines of the muscle fibres. A threshold was then applied to create individual regions containing each muscle fibre. Automated concurrent dilation and contraction of these areas was carried out to produce a region containing the sarcolemma of each fibre, and a separate ROI encompassing the sarcoplasm, as can be seen in Figure 5.1. The signal produced by anti-POPDC staining, as well as the α-sarcoglycan marker, could then be measured in each of the ROIs. The division of the image and fibres into distinct areas is automated, requiring manual input only for a final quality check, enabling non-biased measurements from an image using all muscle fibres present. The full macro is provided in the Methods Section in Figure 2.2.

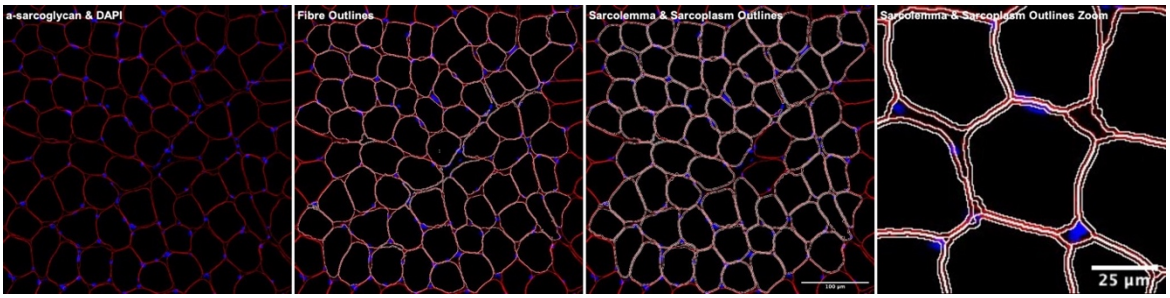


Figure 5.1: Outlines of Skeletal Muscle Fibres to allow Quantification of POPDC and α-Sarcoglycan Expression in the Sarcolemma and Sarcoplasm. The α-sarcoglycan marker was used to define the outline of each muscle fibre using an automated program within FIJI. These outlines were dilated and contracted to produce regions containing the sarcolemma of each muscle fibre, and a separate sarcoplasmic area. The intensity of the α-sarcoglycan and POPDC could then be measured from each area and the level of localisation to the sarcolemma determined.

To assess the changes in POPDC1 and POPDC2 protein expression and subcellular localisation the following outputs were calculated for each individual muscle fibre and were compared between control samples and those obtained from patients: 1) The relative concentration of POPDC protein in the plasma membrane; 2) the relative level of α-sarcoglycan in the plasma membrane; 3) The relative concentration of POPDC protein in the cytoplasm; 4) The relative concentration of α-sarcoglycan in the cytoplasm; 5) The ratio of POPDC protein to α-sarcoglycan concentration in the plasma membrane; 6) The ratio of POPDC concentration in the plasma membrane to POPDC concentration in the cytoplasm. In addition, the cross-sectional area of each fibre was measured to enable quantification of any hypertrophy of muscle fibres that may occur and also to relate any changes in protein behaviour to fibre size, which has previously been used to characterise muscular dystrophy phenotypes.[188] Fibres were analysed from multiple images and sections, although normalisation and comparison only occurred between sections that were concurrently stained and imaged to ensure comparability between samples. As such, separate control samples are used for comparisons against POPDC1 and POPDC2 stained samples, which were separately processed. Each measurement was then tested for statistically significant changes compared to control samples using a student's t-test. All sections of biopsy material were stained and imaged by Ursula Herbort-Brand.

5.3.1.2 The Effect of the *POPDC1* (c.457C>T, p.Q153X) Mutation on POPDC1 and POPDC2 Subcellular Expression in Skeletal Muscle Fibres

A qualitative analysis of POPDC1 staining of a skeletal muscle biopsy from a patient possessing the *POPDC1* (c.457C>T, p.Q153X) mutation, shortened to describe the protein level change alone (POPDC1 p.Q153X) was previously reported.[117] However, no analysis of POPDC2 was performed and detailed quantification of any differences in POPDC1 protein expression was also not completed. From the same set of biopsy material taken from the patient that was used in the previous analysis, new stains using anti-POPDC1 and anti-POPDC2, along with anti-α-sarcoglycan, antibodies were performed. Samples from an age and sex matched control patient were also identically processed to act as a

control. Multiple images were then taken using a confocal microscope to visualise the subcellular expression of POPDC1/POPDC2 and α-sarcoglycan. Example images of the staining results are shown in Figure 5.2. The α-sarcoglycan stain clearly shows the outline of muscle fibres in all samples, while DAPI was used to show the nuclei present. Clear expression of both POPDC1 (Figure 5.2A) and POPDC2 (Figure 5.2C) in the control sections was observed. However, it was evident that this clear plasma membrane enrichment was reduced in the patient for both POPDC1 (Figure 5.2B) and POPDC2 (Figure 5.2D). It also appeared that the cross-sectional area of muscle fibres was increased in the patient.

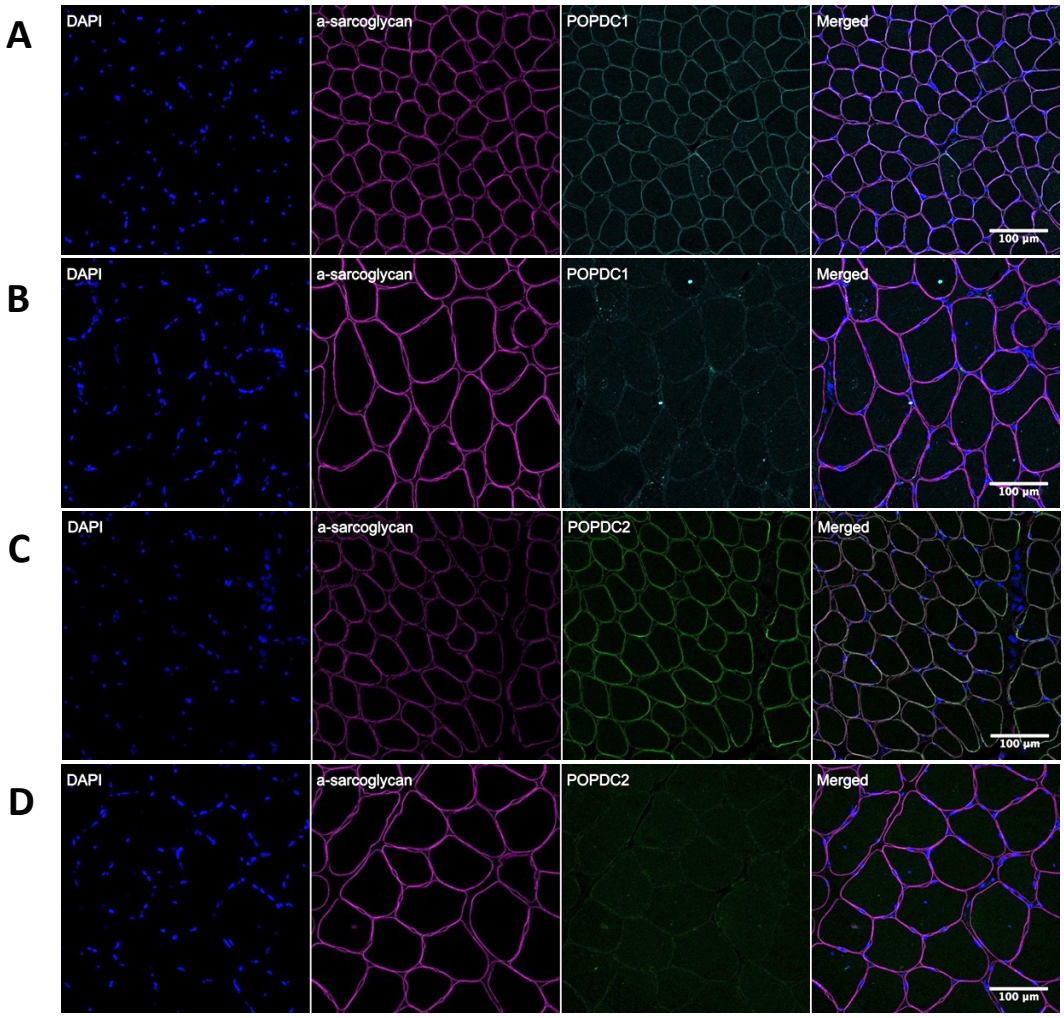


Figure 5.2: Immunostaining of POPDC1 and POPDC2 within Skeletal Muscle Fibres from a Patient possessing the POPDC1 p.Q153X Variant and a Control. Skeletal muscle biopsies were taken from a patient homozygous for *POPDC1 (c.457C>T, p.Q153X)* (**B** and **D**) and an age and sex-matched control (**A** and **C)**. Sections prepared from biopsies were immunostained with primary antibodies directed against α-sarcoglycan and either POPDC1 (**A** and **B**) or POPDC2 (**C** and **D**), while DAPI was used to mark the nuclei.

The images of these stained sections were then subjected to the new analysis method described above with the results shown in Figure 5.3. The behaviour of POPDC1, POPDC2 and α-sarcoglycan in the patient was normalised to the control samples, apart from the ratio of POPDC1 and POPDC2 in the plasma membrane compared to the cytoplasm so that the actual enrichment of POPDC proteins in the plasma membrane could be shown.

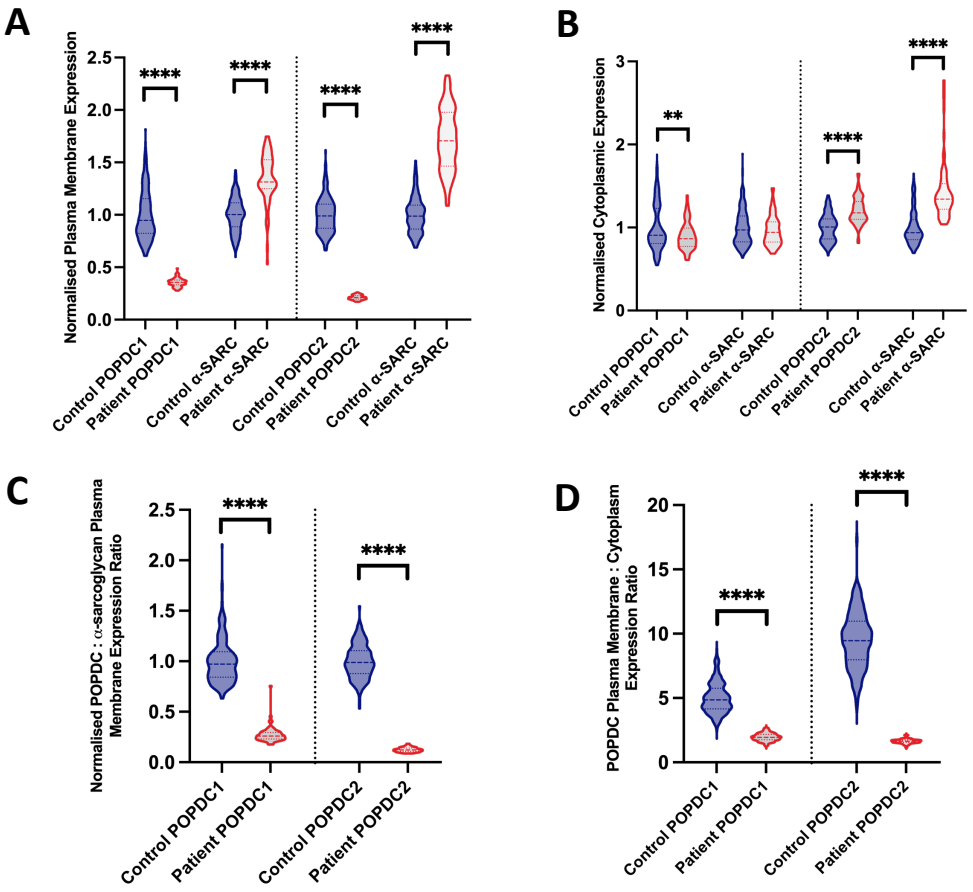


Figure 5.3: Quantification of the Changes in POPDC1 and POPDC2 Expression at the Plasma Membrane and Cytoplasm of Skeletal Muscle fibres of a Patient possessing the *POPDC1* p.Q153X Mutation. The levels of POPDC1 and POPDC2 in skeletal muscle biopsies from a patient possessing the *POPDC1 (c.457C>T, p.Q153X)* variant and a control were determined by analysing the intensity of anti-POPDC1 and anti-POPDC2 immunohistochemical staining of sections of skeletal muscle fibres (see Figure 5.2). Individual fibres were measured separately. α-sarcoglycan was used as a control sarcolemma marker protein and to provide an outline of the plasma membrane of fibres allowing measurement of POPDC concentration in the plasma membrane and cytoplasm. The normalised expression level of POPDC1 and POPDC2, as well as α-sarcoglycan, in the plasma membrane **(A)** and cytoplasm **(B)** was determined. POPDC1 and POPDC2 levels in the plasma membrane were further normalised to the concentration of α-sarcoglycan **(C).** The ratio POPDC1 and POPDC2 in the plasma membrane versus the cytoplasm was also determined **(D)**. Control and patient samples were compared by student's t-test, the total number of muscle fibres analysed was n = 65 for POPDC1 stained patient fibres and n = 238 for its associated control; n = 70 for POPDC2 stained patient fibres with n = 163 for associated control. ** p<0.005, **** p<0.0001. Summary data is provided in Appendix 10.2, Table 10.2.

It was found that the relative concentration of POPDC1 and POPDC2 in the plasma membrane significantly decreased compared to control sections by around 65% and 85%, respectively (Figure 5.3A). For both proteins there was also a clear narrowing in the range of plasma membrane expression of individual fibres, whereas control fibres displayed a wider spread of expression levels. It seemed that the drop in POPDC1 and POPDC2 plasma membrane expression was very consistent across all fibres from the patient biopsy. There was also an unexpected increase in the α-sarcoglycan plasma membrane levels of patient fibres (Figure 5.3A). The reduction in POPDC1 and POPDC2 plasma membrane levels were slightly increased after normalisation to the α-sarcoglycan plasma membrane marker, with a 73% reduction in POPDC1 and 88% in POPDC2, shown in Figure 5.3C. Only very small changes in the cytoplasmic concentration of POPDC1 and POPDC2 were detected (Figure 5.3B).

The ratio of POPDC protein in the plasma membrane compared to cytoplasm was used to quantify the extent of POPDC protein localisation to the plasma membrane. For both proteins there was a several fold reduction in the localisation to the plasma membrane in the presence of the POPDC1 p.Q153X mutation, shown in Figure 5.3D. Control fibres displayed 5-fold more POPDC1 in the membrane compared to the cytoplasm of fibres, with 9.5 times more POPDC2. This was reduced to a 1.9-fold and 1.6-fold increase, respectively, in the patient sample. The loss of POPDC proteins at the plasma membrane but without an increase in the cytoplasm suggests that overall expression was reduced, instead of the same amount of protein being present but mislocalised. Full results of the analysis are shown in Appendix 10.2, Table 10.2.

It was also noted that there was a large increase in the mean cross-sectional area of the muscle fibres in the patient sample, changing from 2009 μm^2 in the control to 5369 μm^2 in the patient fibres (Figure 5.4). This suggests that the POPDC1 p.Q153X mutation is associated with muscle fibre hypertrophy, which is likely involved in the muscular dystrophy phenotype seen in the patient.

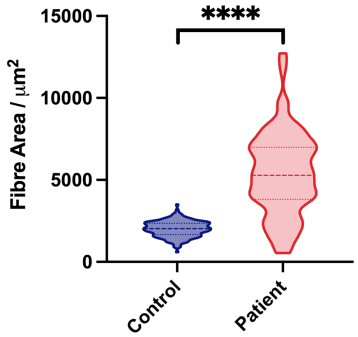


Figure 5.4: The Change in Cross-Sectional Area of Skeletal Muscle Fibres between a Patient Possessing the *POPDC1* p.Q153X Mutation and a Control. The area of each muscle fibre in each set of biopsy sections was determined. The cross-sectional area of fibres increased from the control (M = 2009, SD = 468 μm^2) to the patient (M = 5369, SD = 2507 μm^2). Control and patient samples were compared by student's t-test (t = 25.58, df = 534, p < 0.0001), n = 135 and n = 401 for patient and control fibres, respectively. **** p<0.0001.

The changes in POPDC protein subcellular expression were plotted against the area of each fibre to examine if the changes in fibre morphology bore any relation to POPDC behaviour, with the resulting plots shown in Figure 5.5. There was no clear relationship between fibre size and POPDC expression level or plasma membrane localisation in either the control or patient fibres. This can be seen by the lack of any clear positive or negative trend in POPDC expression results against the size of the fibres. Plotting the results of both sets of fibres against area reveal two distinct populations with minimal or no overlap. This demonstrates the consistency of the changes in POPDC expression and localisation in the POPDC1 p.Q153X expressing fibres.

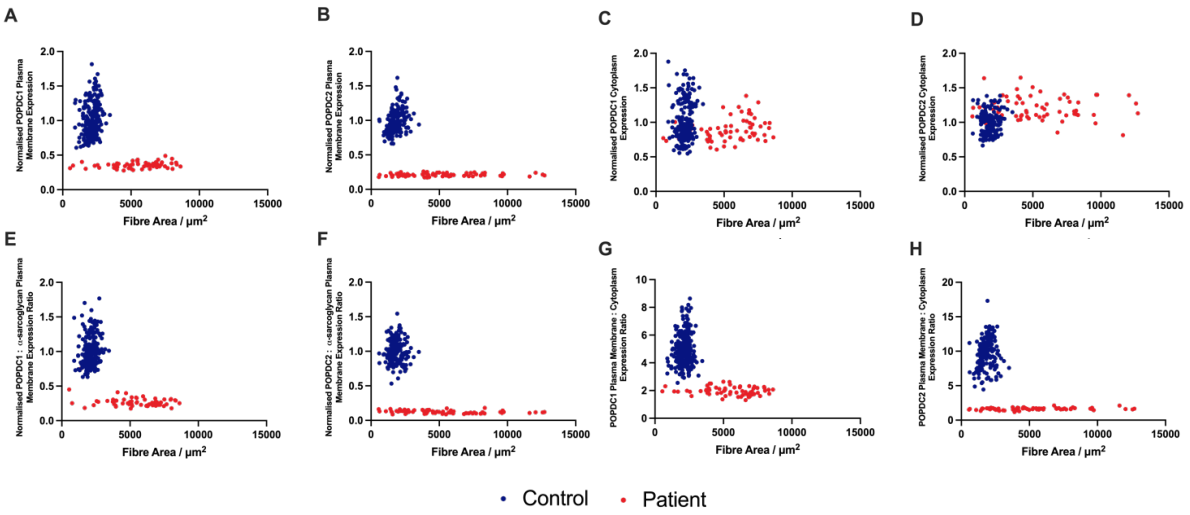


Figure 5.5: The Changes in POPDC1 and POPDC2 Subcellular Expression Plotted against the Cross-Sectional Area of Individual Skeletal Muscle Fibres of a patient possessing the *POPDC1* p.Q153X Variant and a Control. The normalised expression levels and localisation of POPDC1 and POPDC2 in individual muscle fibres of the *POPDC1* p.Q153X patient and control were plotted against the cross-sectional area of each fibre. Plots show the expression level of POPDC1 **(A)** and POPDC2 **(B)** at the plasma membrane and cytoplasm **(C)** and **(D)**, POPDC1 **(E)** and POPDC2 **(F)** plasma membrane expression relative to α-sarcoglycan. The ratio of POPDC1 **(G)** and POPDC2 **(H)** at the plasma membrane versus the cytoplasm is also shown.

5.3.1.3 The Effect of the *POPDC1* (c.547G>T, p.V183F) Mutation on POPDC1 and POPDC2 Subcellular Expression in Skeletal Muscle Fibres

No previous analysis of biopsy material from patients possessing the *POPDC1* (c.547G>T, p.V183F) (referred to on the protein level as POPDC1 p.V183F) variant has been performed. As such, it is not known if this variant leads to changes in POPDC protein subcellular expression in skeletal muscle fibres in a similar manner to other reported mutations. Skeletal muscle biopsy sections from a patient possessing the mutation in homozygous fashion and a matched control were stained for POPDC1 or POPDC2 as well as α-sarcoglycan, with example images shown in Figure 5.6. As expected, clear sarcolemma expression of α-sarcoglycan was seen in all samples, with strong POPDC1 and POPDC2 plasma membrane staining also seen in the control. The outlines of muscle can still be clearly observed in the POPDC1 and POPDC2 channels of the patient samples, perhaps indicating a lesser change in their expression level at the plasma membrane. Clear morphological changes in the fibres are evident. The same analysis method as that used for the POPDC1 p.Q153X samples was employed. It was found that there was an approximate 40% reduction in POPDC1 and POPDC2 expression at the plasma membrane (Figure 5.7A), which was a more modest loss compared to the POPDC1 p.Q153X mutation.

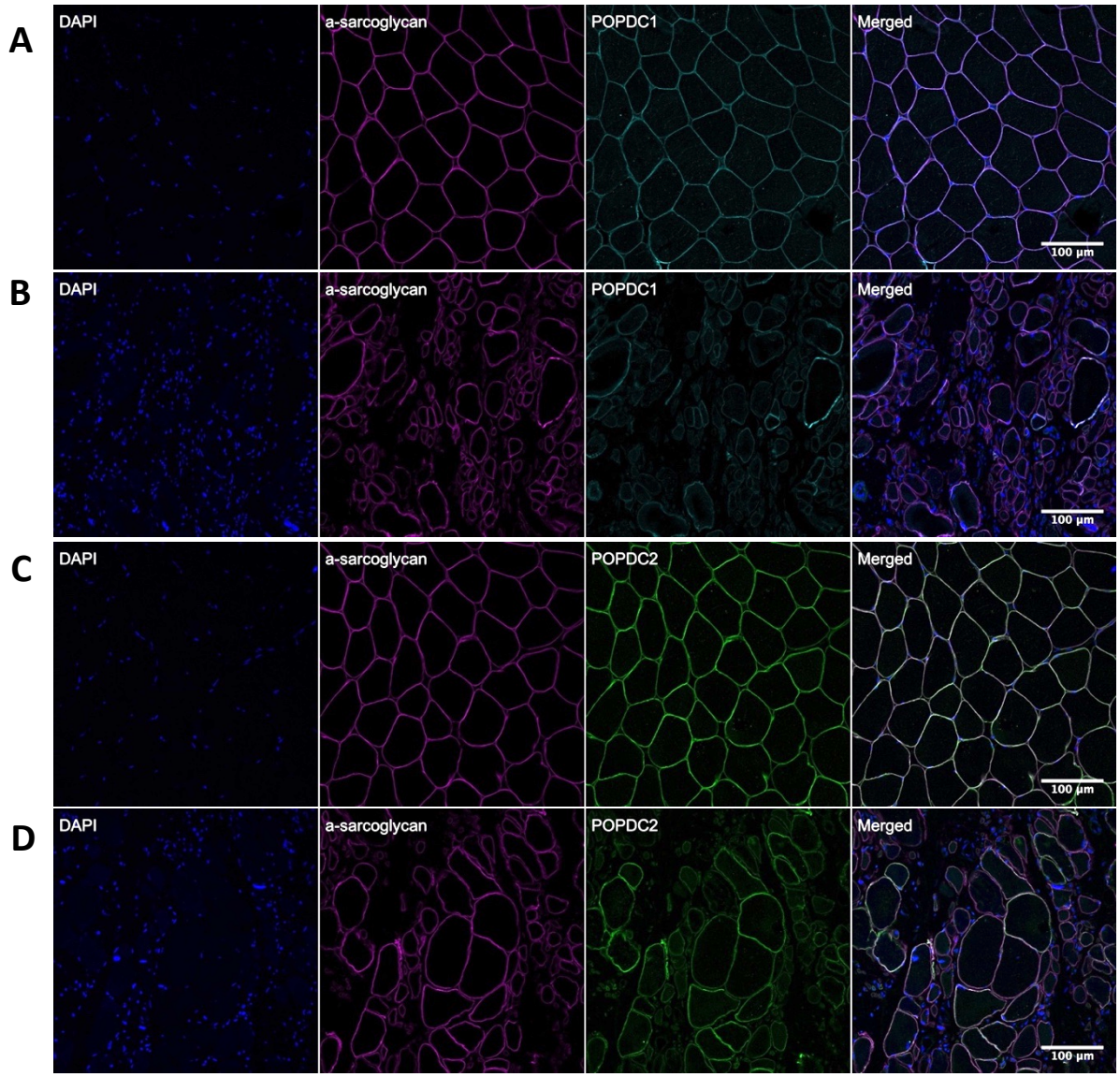


Figure 5.6: Immunostaining of POPDC1 and POPDC2 within Skeletal Muscle Fibres from a Patient possessing the *POPDC1* p.V183F Variant and a Control. Skeletal muscle biopsies were taken from a patient homozygous for *POPDC1* (c.547G>T, p.V183F) (**B** and **D**) and a matched control (**A** and **C**). Sections prepared from biopsies were immunostained with anti-α-sarcoglycan and either anti-POPDC1 (**A** and **B**) or anti-POPDC2 (**C** and **D**) primary antibodies, while DAPI was used to mark the nuclei. Multiple images were taken using a confocal microscope and analysed.

The levels of both POPDC proteins in the plasma membrane of many fibres in the patient samples overlapped with those of the control. This contrasts to the POPDC1 p.Q153X plasma membrane reduction, which was highly consistent across all patient fibres (Figure 5.3). A mild drop in α-sarcoglycan levels was also observed in the plasma membrane (Figure 5.7A). While the cytoplasmic levels of POPDC1 were unchanged, there was a two-fold average increase in the amount of POPDC2 in the cytoplasm of the patient samples, although this was highly variable between fibres (Figure 5.7B).

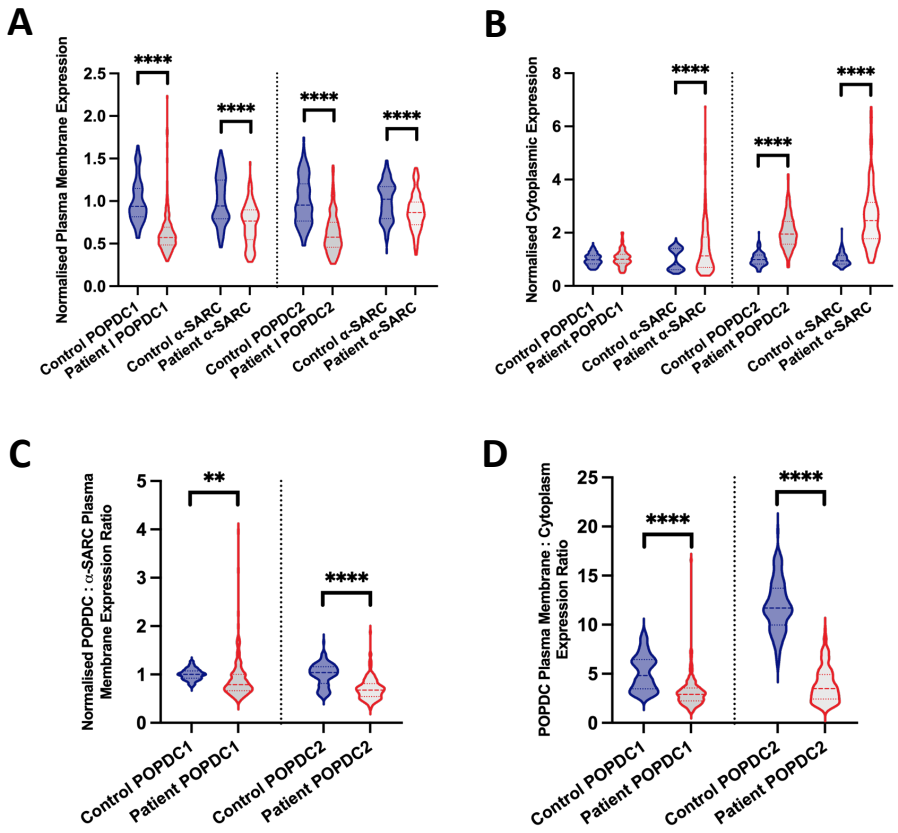


Figure 5.7: Quantification of the Changes in POPDC1 and POPDC2 Expression at the Plasma Membrane and Cytoplasm of Skeletal Muscle Fibres of a Patient possessing the *POPDC1* p.V183F Mutation. The levels of POPDC1 and POPDC2 in biopsies from a patient possessing the *POPDC1* p.V183F variant and control individual were determined by analysing the intensity of anti-POPDC1 and anti-POPDC2 stains in sections of skeletal muscle fibres. Individual fibres were measured separately. α-sarcoglycan was also measured as a control plasma membrane protein and to provide an outline of the plasma membrane of fibres allowing measurement of POPDC concentration in the plasma membrane and cytoplasm. The normalised expression level of POPDC1 and POPDC2, as well as α-sarcoglycan, in the plasma membrane **(A)** and cytoplasm **(B)** was measured. POPDC1 and POPDC2 levels in the plasma membrane were further normalised to the concentration of α-sarcoglycan **(C).** The ratio POPDC1 and POPDC2 in the plasma membrane versus the cytoplasm was also determined **(D)**. Control and patient samples were compared by student's t-test, n = 167 for POPDC1 stained patient fibres and n = 161 for associated control; n = 160 for POPDC2 stained patient fibres with n = 135 for associated control. ** p<0.005, **** p<0.0001. Summary data is provided in Appendix 10.2, Table 10.3.

When normalised to α-sarcoglycan levels there was still a slight drop in POPDC1 and POPDC2 at the plasma membrane, 9% and 30%, respectively (Figure 5.7C). The distribution of α-sarcoglycan normalised POPDC1 and POPDC2 plasma membrane expression showed a large upper tail, again showing the variability of the effects in the POPDC1 p.V183F patients. Figure 5.7D shows the ratio of both POPDC isoforms at the plasma membrane and cytoplasm dropped significantly compared to the control, from 5-fold to 3-fold for POPDC1 and 12-fold to 4-fold for POPDC2. Once again, there was significant overlap of POPDC localisation values between the two groups indicating inconsistent changes between individual muscle fibres.

It was found that a range of fibre sizes was present in the patient samples, with many smaller than the control fibres, although fibres comparable in size to wildtype fibres were also found (Figure 5.8). The average fibre cross-sectional area dropped to 899 μm^2 compared to 2933 μm^2 in the control. The

images in Figure 5.6 also display a clear change in shape of the fibres alongside the loss of fibre size consistency. This is a different pattern of fibre morphology compared to the POPDC1 p.Q153X case, which showed a consistent increase in the area of muscle fibres in the patient.

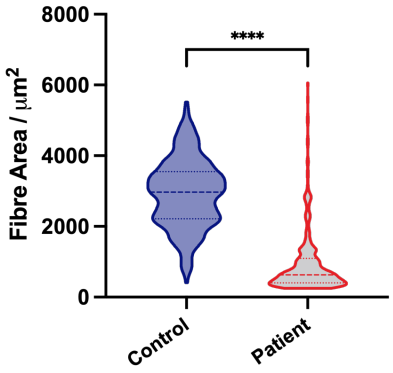


Figure 5.8: The Change in Cross-Sectional Area of Skeletal Muscle Fibres between a Patient possessing the *POPDC1* p.V183F Mutation and a Control. The area of each muscle fibre in each set of biopsy sections was determined. The cross-sectional area of fibres decreased from the control (M = 2933, SD = 957 μm²) to the patient (M = 940, SD = 899 μm²). Control and patient samples were compared by student's t-test (t = 26.80, df = 621, p < 0.0001), n = 327 and n = 296 for patient and control fibres, respectively, **** p<0.0001.

It was also noted that the changes in POPDC plasma membrane expression and localisation were correlated with fibre size. Smaller fibres tended to display a greater loss in POPDC plasma membrane expression (Figure 5.9A and B) including when normalised to α-sarcoglycan expression (Figure 5.9E and F), greater cytoplasmic concentrations (Figure 5.9C and D), and a reduced ratio of POPDC1 and POPDC2 at the plasma membrane to cytoplasm (Figure 5.9G and H). This trend was greater for POPDC2. The control and patient data points within each plot of Figure 5.9 show a reasonable level of overlap. When patient fibres were larger, and so comparable in size to control fibres, the changes in POPDC trafficking and expression behaviour were reduced and often comparable to control fibres.

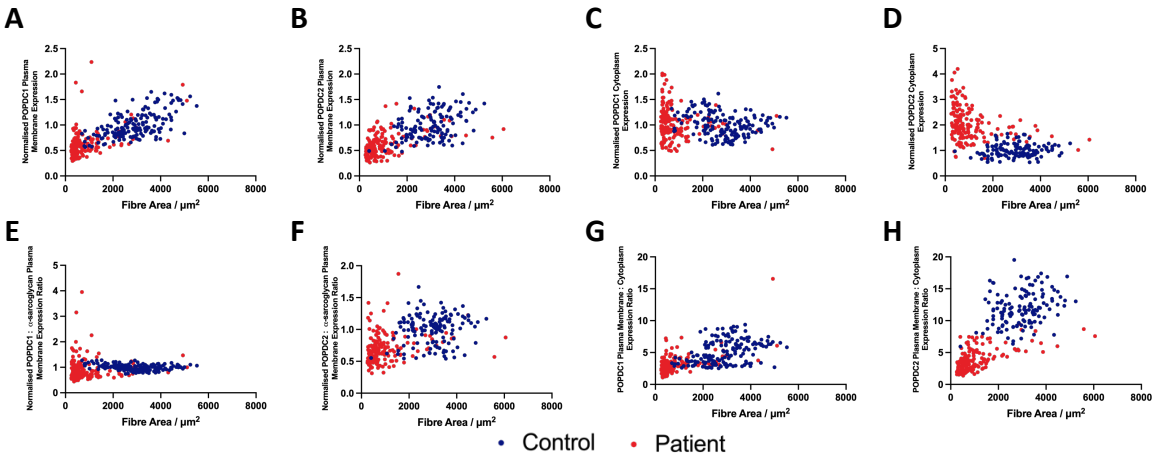


Figure 5.9: The Changes in POPDC1 And POPDC2 Expression Levels at the Plasma Membrane and Cytoplasm Plotted against the Cross-Sectional Area of Individual Skeletal Muscle Fibres of a Patient possessing the *POPDC1* P.V183F Variant and a Control. The normalised expression levels and localisation of POPDC1 and POPDC2 in individual muscle fibres of the *POPDC1* p.V183F patient and control were plotted against the cross-sectional area of each fibre. Plots show the expression level of POPDC1 **(A)** and POPDC2 **(B)** at the plasma membrane and cytoplasm **(C)** and **(D)**, POPDC1 **(E)** and POPDC2 **(F)** plasma membrane expression relative to α-sarcoglycan. The ratio of POPDC1 **(G)** and POPDC2 **(H)** at the plasma membrane versus the cytoplasm is also shown.

5.3.1.4 The Effect of the *POPDC1* (c.602CT>TC, p.S201F) Mutation on POPDC1 and POPDC2 Subcellular Expression in Mouse Skeletal Muscle Fibres

The immunostaining of skeletal muscle biopsy sections was previously used to investigate the changes in the plasma membrane concentration of POPDC1 and POPDC2 in patients possessing a *POPDC1* (c.602C>T, p.S201F) mutation.[93] It was found that POPDC1 and POPDC2 were reduced at the plasma membrane, although Western blot analysis of tissue indicated no clear overall loss of POPDC1 or POPDC2. This suggested that a disruption of trafficking of the POPDC proteins was responsible for the reduction in concentration at the plasma membrane. A homozygous Popdc1 (c.602CT>TC, p.S201F) model mouse line has recently been created by the Brand group.[190] It was thought to subject the skeletal muscle tissue of the mouse model to the analysis applied to the patient biopsies above to assess if the changes previously reported in the patient were also present in the mouse model. The more detailed analysis method employed here would also be able to provide additional information about the effect of the POPDC1 p.S201F variant. Skeletal muscle biopsies and subsequent staining was carried out as before, with typical images shown in Figure 5.10. As with the human samples, strong α-sarcoglycan staining was seen at the plasma membrane, along with POPDC1 and POPDC2 in the control mice. Clear drops in the localisation of the POPDC1 and POPDC2 signals to the sarcolemma of muscle fibres can be seen in the mutant mice.

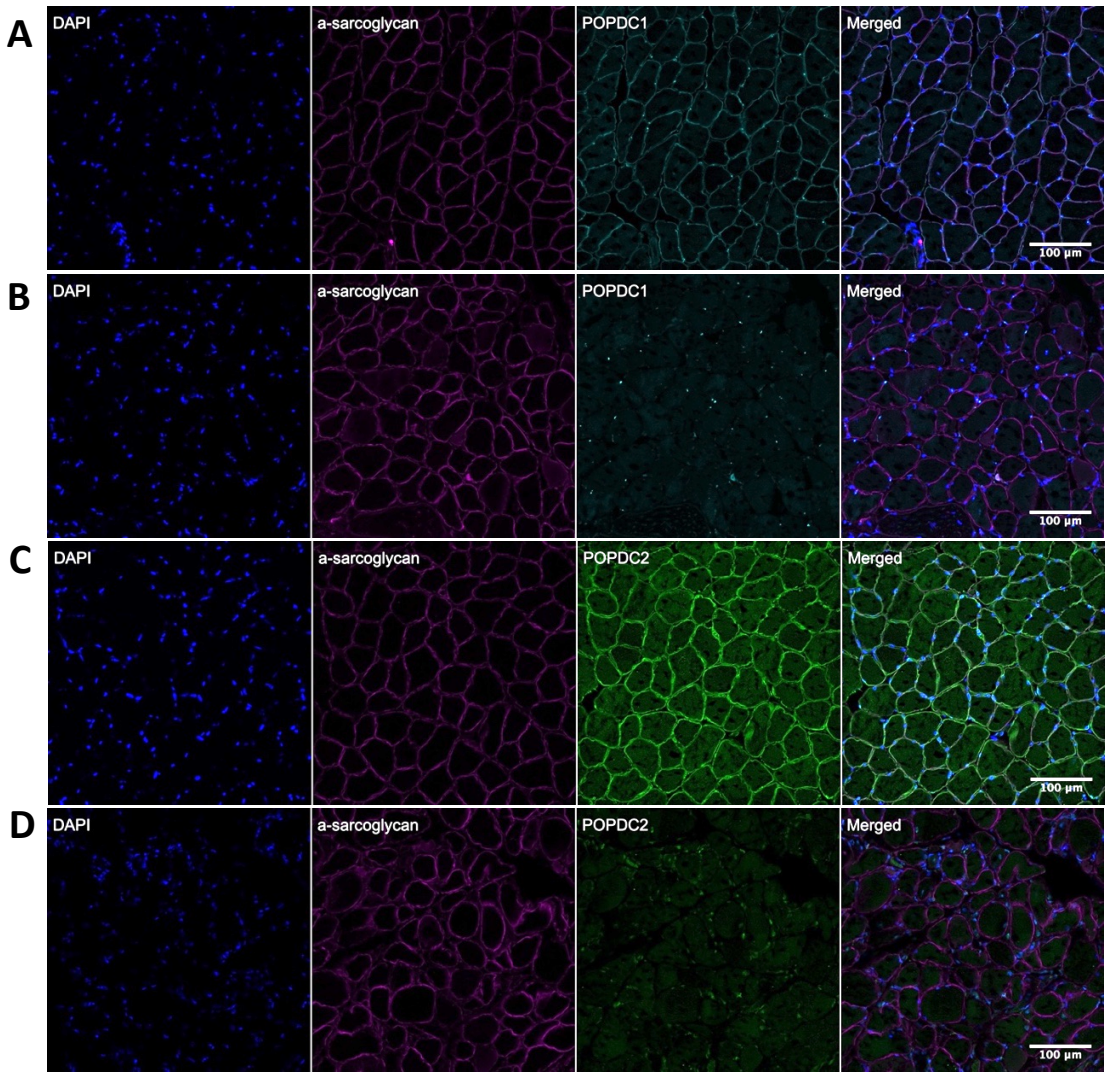


Figure 5.10: Immunostaining of POPDC1 and POPDC2 within Skeletal Muscle Fibres from a Homozygous *Popdc1* p.S201F Mouse and a Control. Skeletal muscle biopsies were taken from a mouse homozygous for *Popdc1* p.S201F (**B** and **D**) and a wildtype control mouse (**A** and **C)**. Sections prepared from biopsies were immunostained with anti-α-sarcoglycan and either anti-POPDC1 (**A** and **B**) or anti-POPDC2 (**C** and **D**) primary antibodies, while DAPI was used to mark the nuclei. Multiple images were taken using a confocal microscope and analysed, see Figure 5.11, with example images shown here.

Analysis of the images showed there was a large drop in the plasma membrane expression of both POPDC1 (75%) and POPDC2 (85%) in the mutant (Figure 5.11A). The result was similar when normalised to α-sarcoglycan levels in the plasma membrane (Figure 5.11C), while there were only minor changes in α-sarcoglycan signal (Figure 5.11A). Interestingly there was a very slight increase in the expression level of POPDC1 in the cytoplasm of the fibres, but a large decrease in POPDC2 (Figure 5.11B). The ratio of POPDC1 in the plasma membrane to cytoplasm fell from 4.5:1 in the control to 1:1 in the mutant, while the POPDC2 ratio dropped from 2.7:1 to 0.9:1 (Figure 5.11D). Full analysis results are provided in Appendix 10.2, Table 10.4.

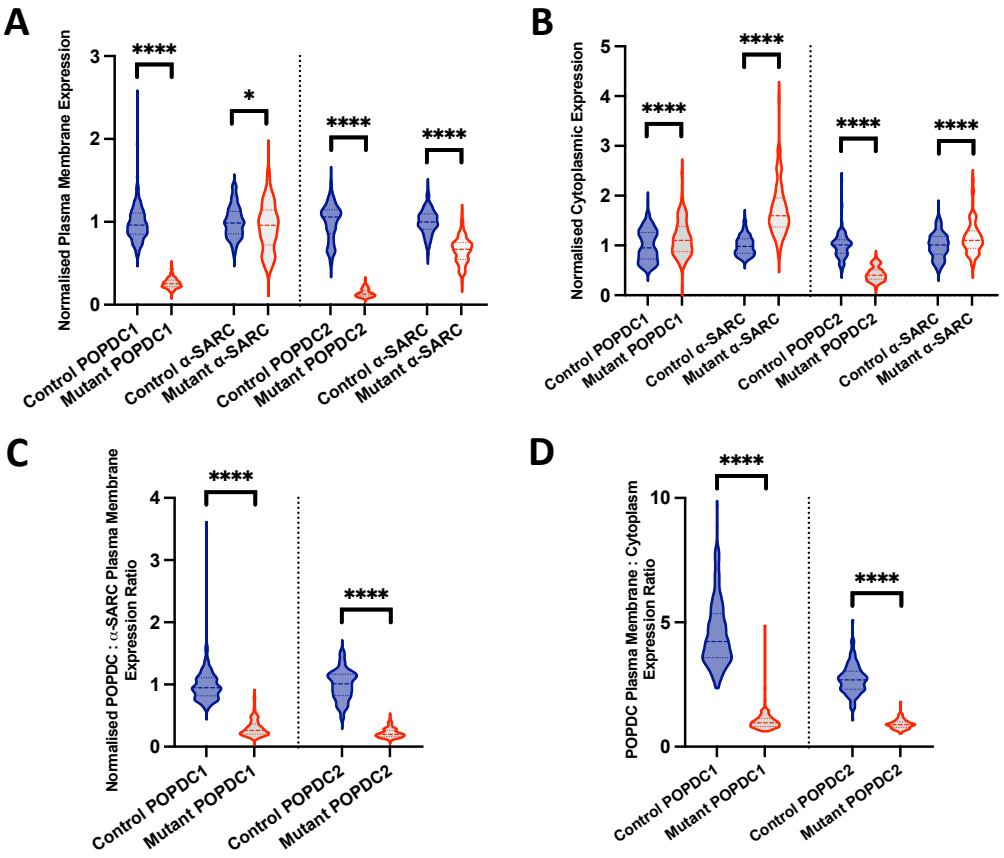


Figure 5.11: Quantification of the Changes in POPDC1 and POPDC2 Expression at the Plasma Membrane and Cytoplasm of Skeletal Muscle Fibres of a Homozygous *Popdc1* p.S201F Mouse Mutant. The levels of POPDC1 and POPDC2 in sections of mice expressing the *POPDC1* p.S201F variant in homozygous fashion and control mouse were determined by analysing the intensity of anti-POPDC1 and anti-POPDC2 stains in sections of skeletal muscle fibres. Individual fibres were measured separately. α-sarcoglycan was also measured as a control plasma membrane protein and to provide an outline of the plasma membrane of fibres allowing measurement of POPDC concentration in the plasma membrane and cytoplasm. The normalised expression level of POPDC1 and POPDC2, as well as α-sarcoglycan, in the plasma membrane **(A)** and cytoplasm **(B)** was measured. POPDC1 and POPDC2 levels in the plasma membrane were further normalised to the concentration of α-sarcoglycan **(C).** The ratio POPDC1 and POPDC2 in the plasma membrane versus the cytoplasm was also determined **(D)**. Control and patient samples were compared by student's t-test, n = 158 for POPDC1 stained mutant fibres and n = 270 for associated control; n = 118 POPDC2 stained mutant fibres with n = 148 for associated control. * p<0.05, **** p<0.0001. Summary data is provided in Appendix 10.2, Table 10.4.

There was only a very minor, although statistically significant, reduction in average fibre cross-sectional area from 1700 μm^2 to 1518 μm^2 in the mutant mice (Figure 5.12). This differs to the patient samples for the POPDC1 p.Q153X and V183F, which showed clear morphological changes of the muscle fibres.

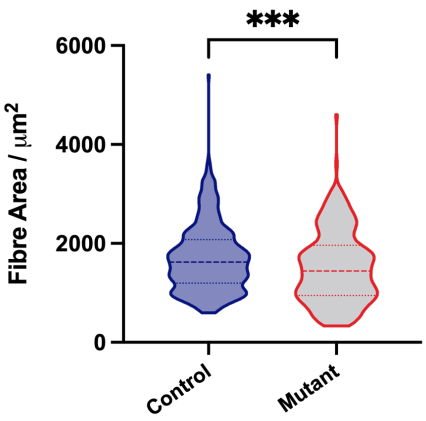


Figure 5.12: The Change in Cross-Sectional Area of Skeletal Muscle fibres between a Homozygous *Popdc1* p.S201F Mouse and a Control. The area of each muscle fibre in each set of biopsy sections was determined. The cross-sectional area of fibres slightly decreased from the control (M = 1700 SD = 673 μm²) to the patient (M = 1518, SD = 723 μm²). Control and patient samples were compared by student's t-test (t = 3.399, df = 692, p = 0.0007), n = 276 and n = 418 for mutant and control fibres, respectively, *** p<0.001.

Figure 5.13 shows there were no clear trends between the changes in POPDC plasma membrane levels and fibre size. There was a mild positive correlation between POPDC1 cytoplasmic levels and fibre area, as a related drop in the ratio of POPDC1 at the plasma membrane to cytoplasm. However, this was only evident in control fibres.

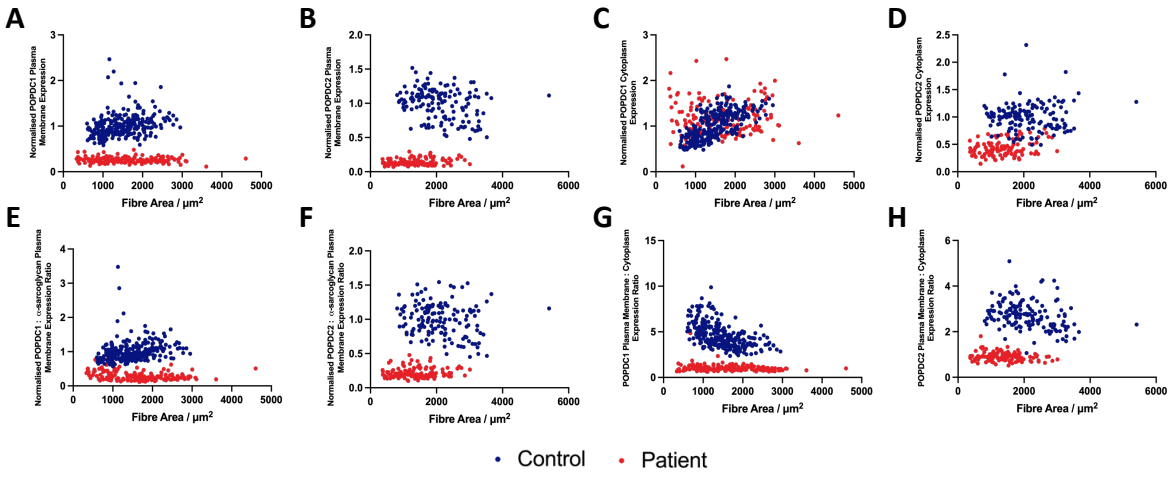


Figure 5.13: The Changes in POPDC1 and POPDC2 Expression Levels at the Plasma Membrane and Cytoplasm Plotted against the Cross-Sectional Area of Individual Skeletal Muscle Fibres of a Homozygous *Popdc1* p.S201F Mouse and a Control. The expression levels and localisation of POPDC1 and POPDC2 of individual fibres were plotted against the cross-sectional area of each fibre. Plotted values are normalised to control group for the expression level of POPDC1 **(A)** and POPDC2 **(B)** at the plasma membrane and cytoplasm **(C)** and **(D)**, POPDC1 **(E)** and POPDC2 **(F)** plasma membrane expression relative to α-sarcoglycan. The ratio of POPDC1 **(G)** and POPDC2 **(H)** at the plasma membrane versus the cytoplasm is also shown.

These results correlate with those reported in patient skeletal muscle biopsy where there were large reductions in POPDC1 and POPDC2 expression levels at the plasma membrane of fibres.[93] Similar effects have also been reported in muscle tissue of homozygous *popdc1* p.S201F zebrafish mutants.[93] More detail to the changes in POPDC protein expression patterns has been added here, along with the finding that only minimal muscle fibre morphological changes occur in the mutant mice. The close

resemblance of the human, mouse, and zebrafish pathologies, with respect to POPDC protein expression levels, gives confidence to the validity of the animal models and the conclusions taken from the clinical samples.

5.3.2 Development of a HEK293 Cell Model to Study the Subcellular Expression of POPDC Proteins

As discussed above, transfecting POPDC1 or POPDC2 into cell lines, such as HEK293 cells, leads to mostly intracellular expression, and not a plasma membrane localisation as seen in native tissue.[71,82,154] Inspired by the loss of plasma membrane expression seen in tissue biopsies expressing a mutant POPDC protein, and the similar effects seen in *Popdc1* or *Popdc2* null mutant mice and zebrafish,[71,93] it was hypothesised that normal subcellular expression of POPDC1 or POPDC2 alone in a cell model is suboptimal because they possess a co-dependence for correct subcellular localisation. It was thought that co-expressing POPDC1 and POPDC2 may lead to a closer replication of the native environment and permit correct trafficking of the proteins to the plasma membrane of the cells.

To assess the effects of single and double expression of POPDC1 and POPDC2 in cells, it was desired to obtain detailed information about POPDC protein expression in the different compartments of transiently transfected cells, as with the skeletal muscle biopsies analysed above. Full-length human POPDC1 and POPDC2, which were expressed as C-terminal ECFP or EYFP-fusion constructs, respectively, were used to directly visualise the subcellular protein localisation in fixed HEK293 cells using confocal microscopy. Tagging with GFP variants is an established method for monitoring subcellular location of membrane protein and has been widely used.[30,191] ECFP and EYFP fusion constructs were generated so that this system could possibly be used for FRET experiments to probe the interactions of the proteins, due to the partial overlap between the emission and absorption spectra of ECFP and EYFP, and is discussed further below.[192] HEK293 cells were chosen due to their use in POPDC protein expression,[100,101] along with their amenable culture and transfection properties.[178] To quantify the relative concentrations of POPDC protein in the cytoplasm and plasma membrane, images of cells expressing POPDC proteins were segmented into regions containing only the plasma membrane or the cytoplasm (intracellular area excluding the nucleus, indicated by Hoechst-33342 staining), as shown in Figure 5.14A. This method was adapted from the protocol developed for use in muscle fibre sections, discussed above. A plasma membrane marker 1,1'-dioctadecyl-3,3,3',3'-tetramethylindodicarbocyanine (DiD), a fluorescent dye possessing two C_{18} alkyl chains, which confer affinity for the plasma membrane of cells, was used to mark the plasma membrane of cells, which allowed the outline of transfected cells to be created. Extended incubation with DiD will result in labelling of intracellular membranes due to plasma membrane internalisation.[193] However, reduced incubation times followed by cell fixation results in selective plasma membrane

staining,[194] which was evident in the HEK293 cells shown below. While it was attempted to create an automated process to outline cells of interest, this was not possible due to the more variable plasma membrane staining efficiency of DiD compared to anti-α-sarcoglycan antibodies in skeletal muscle. Instead, manual tracing of cells using the DiD channel was used to provide the most consistent results. A custom script in FIJI was employed to systematically dilate and contract the outlines to create compartments containing the cytoplasm and an area containing only the plasma membrane. The full code of the FIJI script is shown in the Methods section in Figure 2.1. The intensity of ECFP and EYFP emission at the plasma membrane and cytoplasm were used to determine the different expression levels of each isoform, followed by the determination of the ratio of plasma membrane to cytoplasm expression, which was used as an indicator of POPDC trafficking/membrane localisation efficiency. Measurements after transfection of single proteins were compared to the results after POPDC1 and POPDC2 co-expression, thought to be a closer replicate for native tissue, using one-way ANOVA followed by Dunnett's test.

5.3.2.1 Changes in POPDC1 and POPDC2 Subcellular Expression in HEK293 Cells when Expressed Alone or in Combination

Single transfections of POPDC1 and POPDC2 were carried out to confirm the lack of plasma membrane association previously observed. It can be seen in Figure 5.14C and D that high levels of intracellular expression were observed for both proteins with minimal plasma membrane localisation when expressed alone. A high level of what appeared to be protein aggregates was also observed. Negligible signal was recorded in the EYFP channel in the case of single POPDC1-ECFP transfection, and likewise for the ECFP channel after expression of POPDC2-EYFP alone, indicating minimal bleed through between channels, allowing selective visualisation of each POPDC isoform. Meanwhile co-expression of POPDC1 and POPDC2 led to almost complete plasma membrane localisation of both proteins with two typical cells shown in Figure 5.14B. Minimal cytoplasmic or nuclear expression was observed, except for occasional and minor puncta. Instead, both POPDC1 and POPDC2 were confined to the plasma membrane of the cells. Such a subcellular expression pattern of POPDC1 and POPDC2 in transiently transfected cells has not been previously reported.

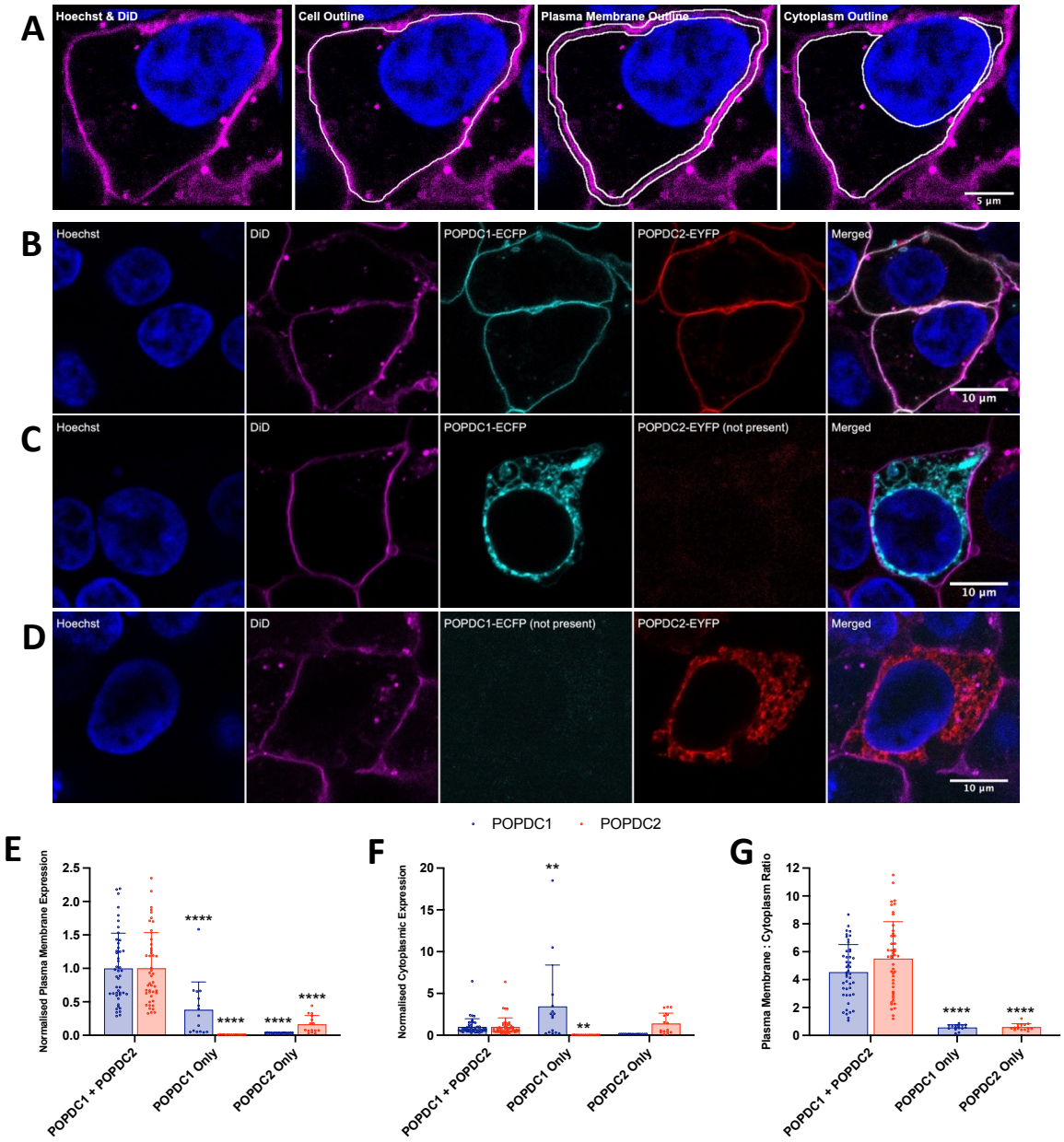


Figure 5.14: The Plasma Membrane and Cytoplasmic Expression of POPDC1 and POPDC2 when Transiently Expressed alone or Co-expressed in HEK293 Cells. A) HEK293 cells were segmented into areas containing the plasma membrane and cytoplasm using the Hoechst-33342 and DiD channels as a guide. An outline of the cell was manually created using the DiD stain, and then dilated and contracted by 0.4 µm to encapsulate the plasma membrane. The inner boundary of the plasma membrane outline and the nucleus, shown by the Hoechst-33342 channel, were used to define the cytoplasm of each cell. The intensity of ECFP and EYFP within these two areas were used to measure the subcellular expression of POPDC1 and POPDC2 constructs within the cells. POPDC1-ECFP and POPDC2-EYFP **(B)**, POPDC1-ECFP alone **(C)** or POPDC2-EYFP alone **(D)** were transiently expressed in HEK293 cells and imaged using confocal microscopy. The normalised level of plasma membrane **(E)** and normalised cytoplasmic **(F)** expression of POPDC1 and POPDC2 was determined for each transfected cells imaged. The plasma membrane to cytoplasm ratio for each isoform was also determined **(G)**. The number of cells analysed for POPDC1-ECFP + POPDC2-EYFP, POPDC1-ECFP only and POPDC2-EYFP only groups was n = 46, n = 15 and n = 15, respectively. Groups were compared using one-way ANOVA followed by Dunnett's post-hoc test using the double expression group as the control. Error bars show SD. ** p<0.005, **** p<0.0001.

Quantification of the level of ECFP and EYFP emission in the plasma membrane and cytoplasm was used to determine the changes in POPDC1 and POPDC2 subcellular localisation, respectively. The level of plasma membrane and cytoplasm expression when POPDC1 and POPDC2 were co-expressed was set to 1. It was found that there was a reduction in POPDC1 at the plasma membrane (M = 0.381, SD

= 0.417) but an increase in cytoplasmic levels (M = 3.447, SD = 4.944) when expressed alone. A similar trend was seen for POPDC2, with the relative plasma membrane level dropping (M = 0.163, SD = 0.132) and cytoplasmic concentrations increasing (M = 1.388, SD = 1.253) when expressed alone compared to co-expression (Figure 5.14E and F). The decrease in POPDC1 and POPDC2 at the plasma membrane, along with the concurrent increase in the cytoplasm, meant that the ratio of POPDC1 and POPDC2 concentration at the plasma membrane compared to the cytoplasm dropped in the presence of only one isoform, clearly seen in Figure 5.14G. The mean ratio of plasma membrane to cytoplasm levels of POPDC1 and POPDC2 in the co-expressing cells was 4.535, SD = 1.976 and 5.504, SD = 2.651, respectively. This dropped to 0.570, SD = 0.199 for POPDC1 and 0.599, SD = 0.236 for POPDC2 when expressed alone. This shows that the preference for plasma membrane localisation was lost, and in the absence of either POPDC1 or POPDC2, the majority of protein was found within the cell. The ECFP and EYFP channels are both included in the POPDC1 and POPDC2 only groups shown in Figure 5.14E and F. The low emission in the missing protein's channel confirms the minimal bleed through between the channels and the selective imaging of the POPDC1-ECFP and POPDC2-EYFP constructs.

It was also noted that the number of HEK293 cells which were clearly expressing POPDC1 and POPDC2 greatly increased after co-transfection compared to single transfections with the same amount of cDNA. This suggests that either enhanced cell survival, improved expression efficiency, or reduced degradation of POPDC1 and POPDC2 occurs during co-expression. However, this effect was not investigated further. During initial attempts to co-express POPDC1 and POPDC2, it was found that a greater number of POPDC1 and POPDC2 expressing cells were observed when an excess of *POPDC1* cDNA containing plasmid was used, compared to *POPDC2* coding plasmid. Cells transfected with a 5-fold excess of *POPDC1* cDNA appeared to show the most consistent expression pattern. While there were only mild changes in POPDC1 and POPDC2 plasma membrane localisation between different cells transfected with different plasmid ratios, shown in Appendix 10.3, Figures 10.1 and 10.2, the improved appearance of cells led to all experiments utilising a five-fold excess of *POPDC1* cDNA during transfection. Since both POPDC constructs were inserted into the same expression plasmid this effect is likely linked to the proteins themselves. It does not necessarily correspond to native expression levels in cardiomyocytes and muscle fibres but is more likely to be specific to the HEK293 expression system. In the heart, *POPDC2* is expressed at much higher levels than *POPDC1*, while in skeletal muscle *POPDC1* is expressed at slightly higher levels than *POPDC2*.[65,67] However, in future experiments with other cell types or expression plasmids it may be helpful to titrate *POPDC1* and *POPDC2* cDNAs to find the optimal conditions for each expression system.

5.3.2.2 The Changes in Cross-Sectional Expression Profiles of POPDC Proteins in HEK293 Cells in the Presence of POPDC1 and POPDC2 alone or when Co-Expressed

The change in fluorescence along cross sections of cells has been used to assess the degree of plasma membrane localisation of proteins.[195,196] To provide more detailed spatial information of the POPDC protein subcellular expression in the HEK293 cells, the changes in the concentration of POPDC1 and POPDC2 from the plasma membrane into the cytoplasm of HEK293 cells was determined by constructing cross-sectional expression profiles in the HEK293 cells. These were created by measuring the changes in relative ECFP/EYFP emission along an area perpendicular to the plasma membrane from outside the cell to the nucleus, at multiple points per cell, typically twelve. An example of the cross-section areas sampled in each cell is shown in Figure 5.15A. The multiple profiles from all cells were aligned by assigning the point of greatest DiD fluorescence as the location of the plasma membrane, allowing an average fluorescence plot for each POPDC isoform to be constructed. The peak of these plots represents the area where the highest concentration of POPDC1 and POPDC2 is found. For clarity and to account for the variable distance between the cell membrane and nuclei leading to a lower degree of averaging further inside the cell, profiles are shown up to 2 μm inside the cell. It should be noted that the width of the plasma membrane according to the peak of DiD emission is wider than the true width of a plasma membrane. This is due to non-perfect association of the DiD dye with the plasma membrane, the grouping of plasma membranes of cells that are in contact with each other, and an image pixel width of around 65 nm, which is wider than the plasma membrane. The averaging of all measured profiles also led to a reduction in apparent resolution of the expression profiles. As such, these plots are intended to show the trend in POPDC1 and POPDC2 concentration relative to the position of the plasma membrane and should not be thought to show the exact positions of the proteins within the cells. However, the shape of the constructed cross-sectional expression plots does provide an effective visualisation of the confinement of the proteins to the plasma membrane, and the extent of any cytoplasmic expression present. The emission profiles were further analysed by finding the Pearson correlation score of the POPDC1 and POPDC2 profile with that of the DiD plasma membrane marker. This provides a measure of how closely associated POPDC1 and POPDC2 expression was with the plasma membrane. A value of 1 indicates perfect correlation, whereas -1 shows an inverse correlation between the two variables. The correlation of POPDC1 with POPDC2 was also determined in cases where both proteins were present, acting in a similar way as a measure of colocalization but as a function of distance from the plasma membrane.

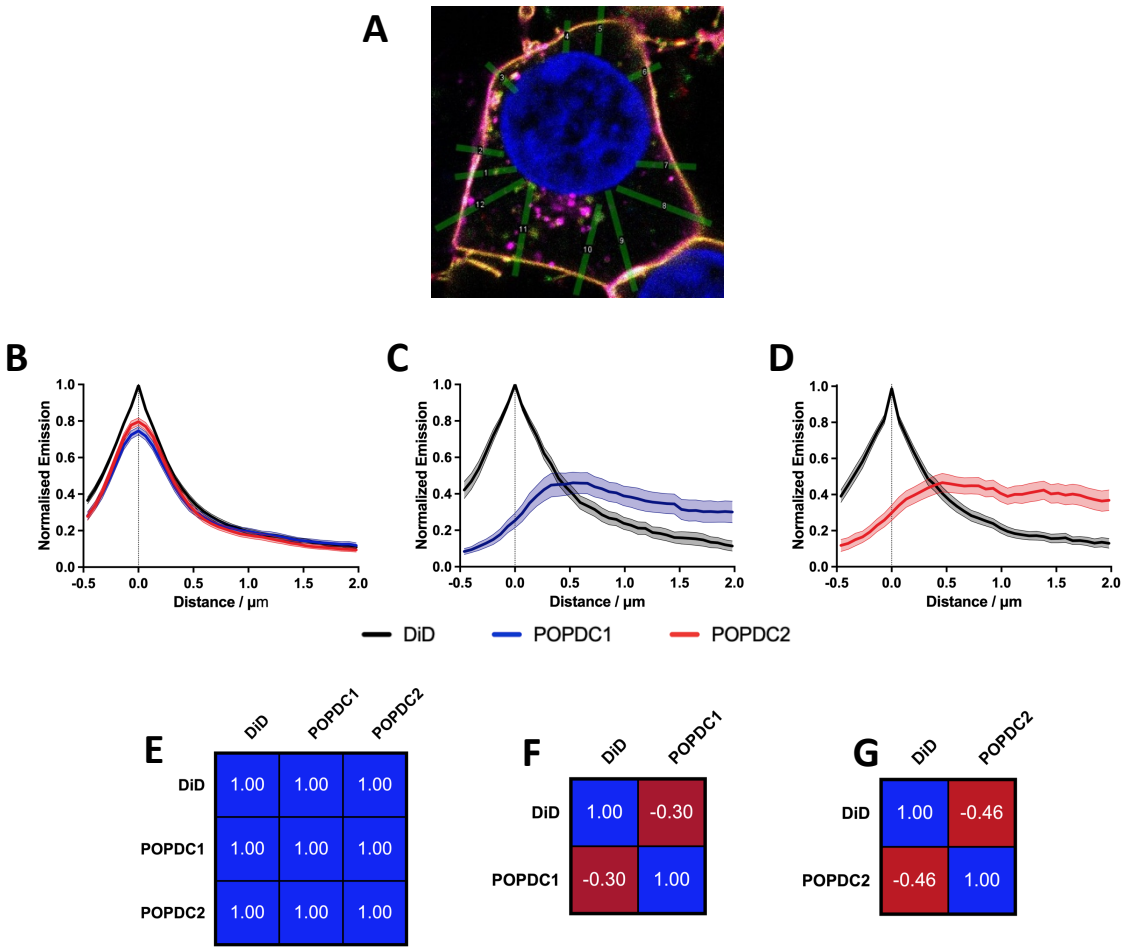


Figure 5.15: The Normalised Expression Profile of POPDC1 and POPDC2 Relative to Position of the Plasma Membrane of HEK293 Cells when Co-expressed or Expressed Alone. The level of POPDC1 and POPDC2, as determined by ECFP and EYFP emission, respectively, was measured along cross section of the cell, perpendicular to the plasma membrane, at multiple points of each HEK293 cell, as shown in **(A)**. The fluorescence profile of DiD was used to define the plasma membrane. The fluorescence profiles of the three fluorophores were normalised and averaged across all cross sections and centred about the plasma membrane. The changes in relative POPDC1 and POPDC2 concentrations from 0.5 µm outside to 2 µm inside a theoretical averaged HEK293 cell are shown for POPDC1-ECFP + POPDC2-EYFP (cells = 34, cross sections = 408) **(B)**, POPDC1-ECFP only (cells 7, cross sections 84) **(C)** and POPDC2-EYFP only (cells = 9, cross sections = 108) **(D)**. The shaded area of plots indicates the 95% confidence limits in the normalised mean expression level. The Pearson correlation score of the POPDC1 and POPDC2 expression profile with the plasma membrane (DiD), as well as each other, was found for POPDC1-ECFP + POPDC2-EYFP **(E)**, POPDC1-ECFP only **(F)** and POPDC2-EYFP only **(G)**.

Figure 5.15B shows that in the presence of both isoforms a clear peak in the concentration of POPDC1 and POPDC2 is found at the midpoint of the plasma membrane, which rapidly falls off when entering the cytoplasm. There is an almost exact correlation of both POPDC1 and POPDC2 expression with the DiD marker, with both isoforms yielding correlations values of 1.00, demonstrating the high preference of both isoforms for the plasma membrane (Figure 5.15E). There is also high correlation between POPDC1 and POPDC2 demonstrating a highly similar expression pattern of both proteins. When expressed alone both POPDC1 (-0.30) and POPDC2 (-0.46) show a negative correlation with the plasma membrane, indicating that their expression level increased moving away from the plasma membrane (Figure 5.15F and G). Small and broad peaks in the expression profiles of single POPDC1 or POPDC2 expression are found just within the plasma membrane, although there is a minimal decrease

in expression moving into the cytoplasm (Figure 5.15C and D). This indicates that POPDC1 and POPDC2, when expressed alone, were not specifically localised to the plasma membrane. The effect of the ratio of *POPDC1* and *POPDC2* coding plasmid DNA used during transfection on the POPDC cross section profiles is shown in Appendix 10.3, Figure 10.2.

5.3.2.3 Co-Expression of Wildtype and Mutant POPDC Proteins in HEK293 Cells

The demonstration that POPDC1 and POPDC2 subcellular expression in HEK293 cells is dependent on co-expression of both isoforms means the expression behaviour of the proteins in HEK293 cells is comparable to native tissue. It was hypothesised that this co-expression model could be used to investigate the effect of pathological *POPDC1/2* mutations identified in patients on POPDC protein subcellular localisation. A subset of mutations in *POPDC1* and *POPDC2* reported in patients was selected for co-expression with their wildtype partner in HEK293 cells following the same protocol as for the co-expression of POPDC1 + POPDC2 as shown above. The POPDC1 p.Q153X, p.V183F and p.S201F variants analysed in skeletal muscle above were chosen to allow comparison with their behaviour in biopsy samples.[93,117,186] In addition, the POPDC1 p.R172H variant, which has been suggested to not lead to any clear changes in the expression pattern of POPDC1 and POPDC2 in human cardiomyocytes, albeit in the absence of comprehensive quantification, was selected. Lastly, the previously reported POPDC2 p.W188X mutation, the only known pathogenic variant of POPDC2, was included.[105] The effect of this mutation on the subcellular expression of POPDC1 and POPDC2 is unknown. It was hypothesized that changes in POPDC1 and POPDC2 behaviour in HEK293 cells in the presence of the different variants would be reflective of the effects *in vivo*. These mutations include those for which the changes in POPDC expression in tissue are well characterised (POPDC1 p.Q153X, POPDC1 p.V183F, POPDC1 p.S201F), partially characterised (POPDC1 p.R172H) and unstudied (POPDC2 p.W188X). This should allow for the assay to hopefully be validated by comparison to native tissue for known mutations, but also be used in a predictive capacity to predict the behaviour of other mutations.

To determine if co-expressing this set of POPDC variants with their respective wildtype partners had an effect on the expression and plasma membrane localisation of POPDC1 or POPDC2, fusion constructs expressing ECFP or EYFP at the C-terminus were co-expressed in HEK293 cells. The full sequence of the constructs is shown in Appendix 10.9, Figure 10.9-13. Example images from each group are shown in Figure 5.16A-E. The concentration of POPDC1 and POPDC2 in the plasma membrane and cytoplasm analysed as before, with the results shown in Figure 5.14F and G. POPDC1 and POPDC2 expression values were compared using one-way ANOVA followed by Dunnett's test using the wildtype pair, shown in Figure 5.14, as the control group.

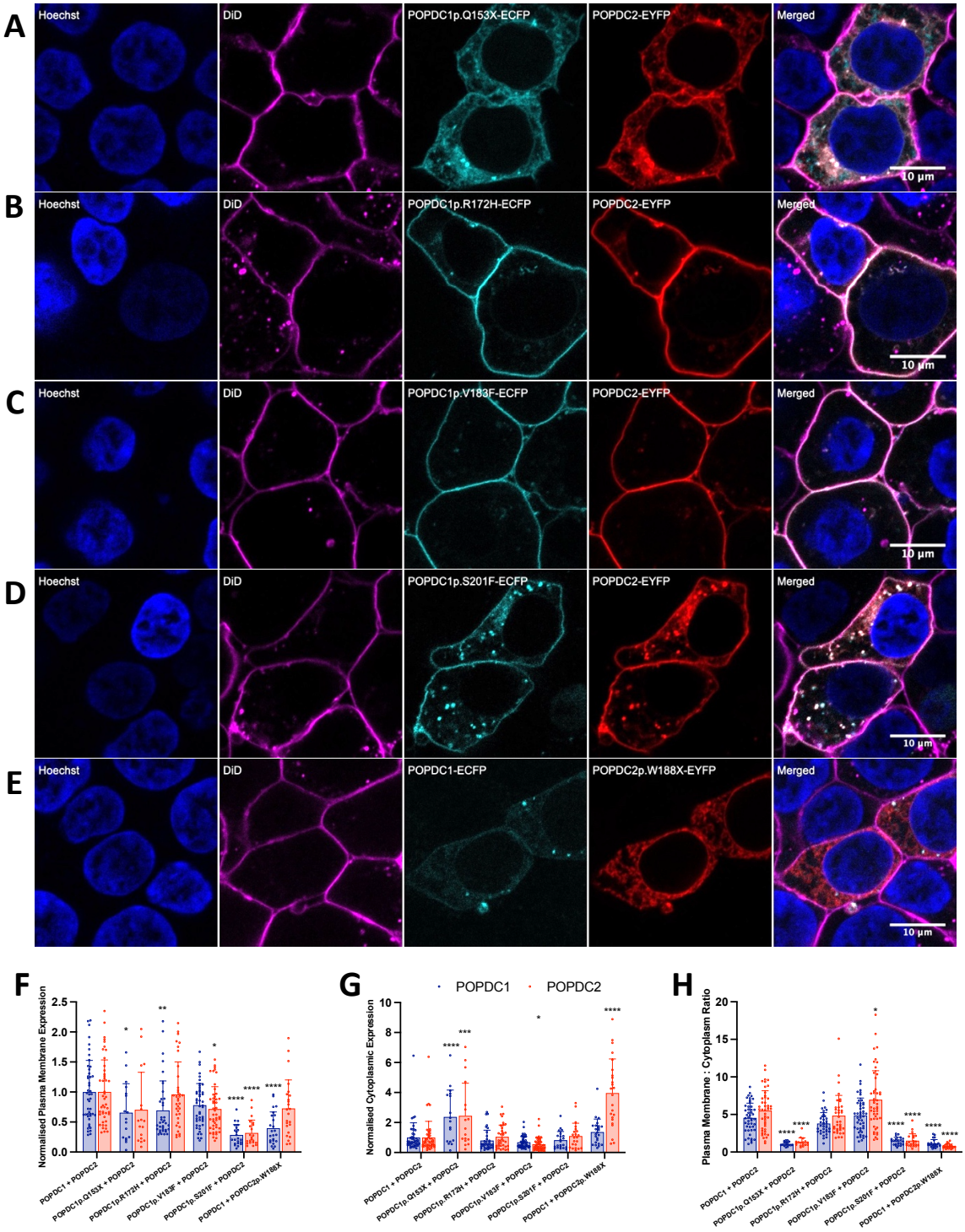


Figure 5.16: The Plasma Membrane and Cytoplasmic Expression of POPDC1 and POPDC2 in the Presence of Various POPDC Variants when Transiently Expressed in HEK293 Cells. HEK293 cells expressing POPDC1 p.Q153X-ECFP **(A)** (n = 17), POPDC1 p.R172H-ECFP **(B)** (n = 36), POPDC1 p.V183F-ECFP **(C)** (n = 47), POPDC1 p.S201F-ECFP **(D)** (n = 22) with POPDC2-EYFP, and POPDC2 p.W188X-EYFP with POPDC1-ECFP **(E)** (n = 24) were imaged using confocal microscopy. The plasma membrane of cells was marked using DiD. The normalised level of plasma membrane **(F)** and normalised cytoplasmic **(G)** expression of POPDC1 and POPDC2 was determined for each transfected cells imaged. The ratio of each isoform in the plasma membrane to cytoplasm was determined **(H)**. Groups were compared using one-way ANOVA followed by Dunnett's post-hoc test using the wildtype double expression group as the control. * p<0.05, ** p<0.005, *** p<0.001, **** p<0.0001. Error bars show SD. Summary data is provided in Appendix 10.3, Tables 10.5-16.

When POPDC1 p.Q153X-ECFP was co-expressed with POPDC2-EYFP it was seen that both isoforms were not strictly localised to the plasma membrane as in the case of wildtype POPDC1 and POPDC2

(Figure 5.16A). Instead, there was extensive intracellular expression and a high density of puncta suggesting aggregates of both isoforms had formed. It was found that there was an approximate 35% and 30% reduction in POPDC1 and POPDC2 expression levels at the plasma membrane, respectively, although this was only statistically significant in the case of POPDC1 (Figure 5.16F). This was coupled with a 2.5-fold increase in the average concentration of both isoforms within the cytoplasm of the cell (Figure 5.16G). These effects caused the ratio of both POPDC1 p.Q153X and POPDC2 in the plasma membrane versus the cytoplasm to fall to 1.1:1 and 1.3:1, respectively, significantly below wildtype levels of around 5:1 for both wildtype isoforms (Figure 5.16H). It would appear that some POPDC1 p.Q153X mutant protein and POPDC2 was able to reach the plasma membrane, with only a relatively mild drop compared to wildtype. The loss in the enrichment of POPDC1 p.Q153X and POPDC2 at the plasma membrane is mainly due to a large accumulation of both isoforms in the cytoplasm.

Cells expressing POPDC1 p.R172H-ECFP or POPDC1 p.V183F-ECFP with POPDC2-EYFP resembled each other in appearance, with both showing no obvious differences to cells expressing wildtype POPDC1 and POPDC2 upon visual inspection (Figure 5.16B and C). POPDC1 and POPDC2 channels showed clear plasma membrane outlines, with minimal intracellular expression. Quantification revealed that there had been a mild reduction in POPDC1 p.R172H expression at the plasma membrane to around 69% of wildtype cells, while there was no change in POPDC2 (Figure 5.16F). No significant changes in cytoplasmic expression levels were found (Figure 5.16G). Likewise, the ratio of POPDC1 p.R172H and POPDC2 within the plasma membrane and cytoplasm was not significantly changed compared to wildtype, at 3.8:1 and 4.9:1, respectively (Figure 5.16H). There was a minor reduction in the level of POPDC2 at the plasma membrane and cytoplasm when co-expressed with POPDC1 p.V183F. This led to a mild increase in the ratio of plasma membrane to cytoplasm levels of POPDC2 compared to wildtype. POPDC1 p.V183F itself was unchanged in all measures (Figure 5.16H).

In the case of co-expression of POPDC1 p.S201F with POPDC2 there was no significant increase in the overall intracellular expression of both proteins (Figure 5.16G). However, there appeared to be a higher rate of puncta within the cell indicating a higher tendency of the proteins to aggregate than in case of co-expression of wildtype isoforms. The outline of the cell was usually apparent in the cells when looking at the ECFP and EYFP channels, demonstrating that some protein was reaching the plasma membrane. It was found that there was around a 70% loss in POPDC1 and POPDC2 expression at the plasma membrane (Figure 5.16F). When the ratio of the concentration of both POPDC proteins in the plasma membrane compared to cytoplasm was determined it was found that both proteins showed a large reduction in the enrichment at the plasma membrane compared to wildtype cells, due to the loss of plasma membrane expression (Figure 5.16H). The fact that there was no significant

increase of POPDC1 p.S201F and POPDC2 localisation at the cytoplasm is suggestive of a mechanism distinct to the case of POPDC1 p.Q153X, which displayed extensive intracellular accumulation.

The one POPDC2 variant tested here, POPDC2 p.W188X, led to a serious mislocalisation of both proteins, with cells shown in Figure 5.16E. No increase in the cytoplasmic localisation of POPDC1 was seen but it was lost at the plasma membrane, leading to a 60% drop in POPDC1 signal. POPDC2 p.W188X in contrast was not significantly reduced at the plasma membrane but was found within the cytoplasm at an average level four-times greater than in case of cells co-expressing wildtype proteins (Figure 5.16F and G). There was a large reduction in the ratio of the plasma membrane to cytoplasm expression ratio of both proteins (Figure 5.16H). However, the reason for this seems to be different for each isoform, with POPDC1 not accumulated in the cell but found at a lower level at the plasma membrane, whereas POPDC2 p.W188X was at the plasma membrane at a level comparable to wildtype but greatly increased within the cell. POPDC2 p.W188X was the only variant that accumulated at higher concentrations within the cell compared to the plasma membrane, resembling the behaviour of the POPDC1/POPDC2 only cells shown in Figure 5.14.

There are clear differences between the groups, which suggests that the effect of each mutation on POPDC1 and POPDC2 is different. The two nonsense mutations, POPDC1 p.Q153X and POPDC2 p.W188X, which may produce mutant proteins with truncations show the greatest loss in plasma membrane localisation of both POPDC isoforms, followed by POPDC1 p.S201F. Apart from minor changes in POPDC1 or POPDC2 in the plasma membrane or cytoplasm, the POPDC1 p.R172H and POPDC1 p.V183F mutations have no effect on how effectively POPDC1 and POPDC2 are expressed and localised at the plasma membrane. Generally, the effects of the mutants were not as severe as complete removal of either isoform, shown in Figure 5.14C and D, with most cases still leading to favourable plasma membrane expression or at least parity with the cytoplasmic levels, suggesting some activity remained in the presence of the mutations. The exception to this is POPDC2 p.W188X.

5.3.2.4 The Changes in Cross-Sectional Expression Profiles of POPDC1 and POPDC2 in HEK293 Cells in the Presence of Various POPDC Variants

As before, the changes in the relative levels of both POPDC isoforms along cross sections of the cell were measured, with plots shown in Figure 5.17A-E. In all of the POPDC1 variants tested, a clear peak of POPDC1 and POPDC2 at the plasma membrane can be seen. This shows that plasma membrane association of POPDC1 and POPDC2 occurred in all these groups. This correlates with the finding that POPDC1 and POPDC2 were both more concentrated in the plasma membrane than the cytoplasm in all groups, albeit only slightly for POPDC1 p.Q153X. The Pearson correlation scores were determined for the relation of POPDC1 and POPDC2 levels to the DiD plasma membrane marker (Figure 5.17F-J).

POPDC1 p.Q153X (0.74) and POPDC2 (0.80) showed a drop in the correlation of both isoforms with the plasma membrane compared to wildtype (Figure 5.15), although both still showed a strong positive correlation. The POPDC1 p.R172H, p.V183F and p.S201F variants, along with their associated POPDC2 co-expression partner, all possessed correlation scores of 0.98-1.00, which are comparable with wildtype POPDC1 and POPDC2. In all of these cases the correlation between the POPDC1 and POPDC2 expression profiles showed Pearson scores of 0.99-1.00, indicating a high degree of colocalization between the proteins.

The POPDC2 p.W188X variant caused a more severe drop in correlation of POPDC1 and POPDC2 p.W188X with the plasma membrane to 0.63 and -0.22, respectively (Figure 5.17E). While there is slight peak of POPDC1 expression around the plasma membrane there is only a minimal drop off in expression moving into the cytoplasm. This is similar to the case of POPDC1 p.Q153X. However, no peak at plasma membrane is present for POPDC2 p.W188X, and in fact its expression was negatively correlated with the plasma membrane. It is also notable that the correlation between the POPDC1 and POPDC2 p.W188X expression profiles is only 0.62, so while the two proteins' expression is positively related it is greatly reduced compared to the other variants tested.

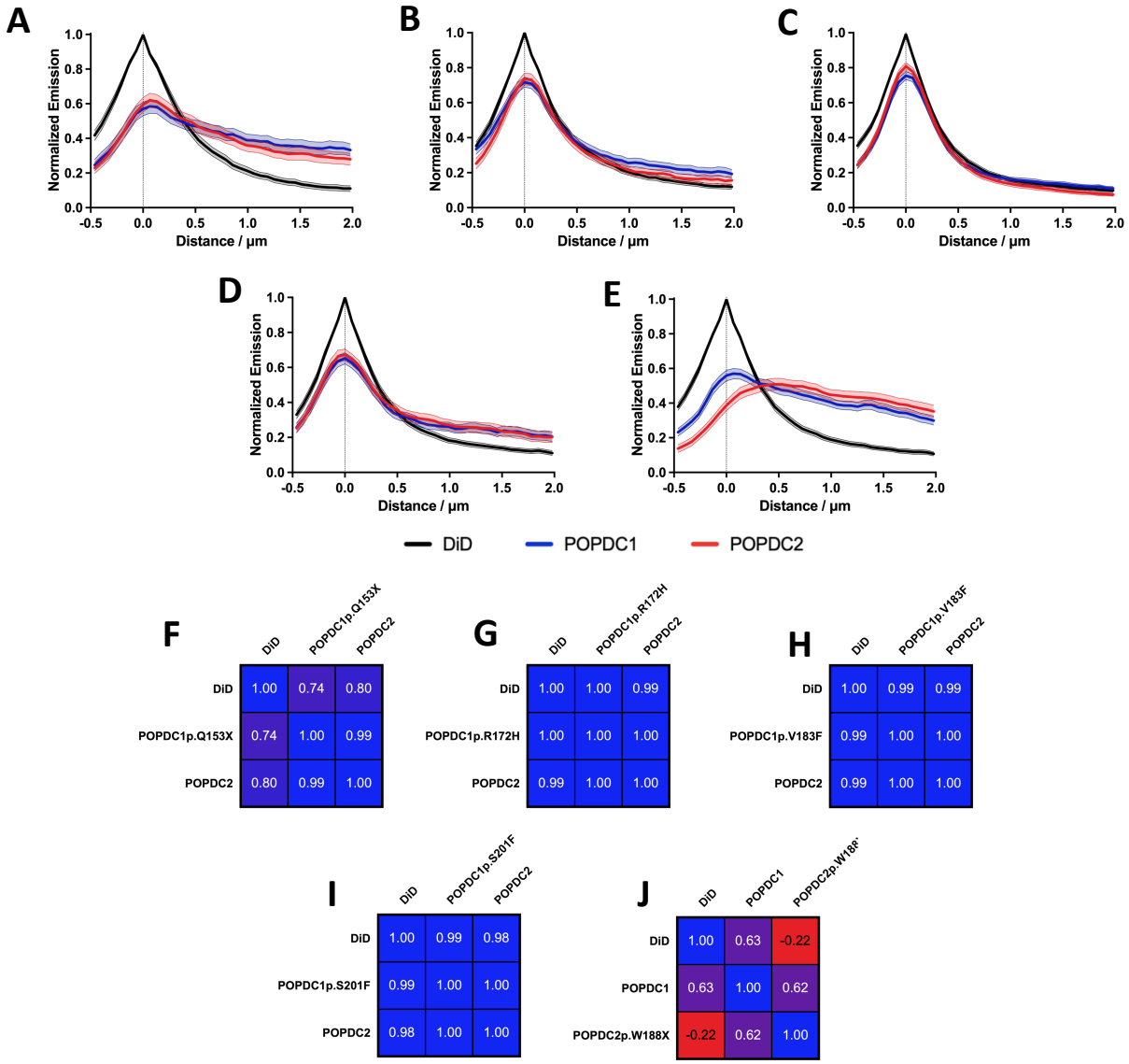


Figure 5.17: The Normalised Expression Profile of POPDC1 and POPDC2 Relative to the Position of the Plasma Membrane of HEK293 Cells in Presence of Various POPDC Variants. The level of POPDC1 and POPDC2 was measured along across cross sections of HEK293 cells perpendicular to the plasma membrane. The emission of DiD was used to define the plasma membrane. The intensities of the three fluorophores were normalised and averaged across all cross sections. The peak DiD emission was used to centre each profile at the plasma membrane. The changes in relative POPDC1 and POPDC2 concentrations from 0.5 µm outside to 2 µm inside a theoretical averaged cells are shown for POPDC1 p.Q153X-ECFP **(A)** (cells = 15, cross sections = 177), POPDC1 p.R172H-ECFP **(B)** (cells = 30, cross sections = 360), POPDC1 p.V183F-ECFP **(C)** (cells = 36, cross sections = 414), POPDC1 p.S201F-ECFP **(D)** (cells = 23, cross sections = 276) with POPDC2-EYFP, and POPDC2 p.W188X-EYFP with POPDC1-ECFP **(E)** (cells = 24, cross sections = 288). The shaded area of plots indicates the 95% confidence limits in the normalised mean expression level. The Pearson correlation scores between each POPDC isoform and DiD, as well as between the two POPDC isoforms were determined for each plot: POPDC1 p.Q153X-ECFP **(F)**, POPDC1 p.R172H-ECFP **(G)**, POPDC1 p.V183F-ECFP **(H),** POPDC1 p.S201F-ECFP **(I)** and POPDC2 p.W188X-EYFP **(J).**

5.4 Discussion

5.4.1 The Changes in POPDC Expression in Skeletal Muscle Fibres and Fibre Morphology in the Presence of Various POPDC Variants

The characterisation of the changes in POPDC1 and POPDC2 subcellular expression in biopsies from patients possessing the POPDC1p.Q153X and p.V183F mutations provides further examples of the dual change in POPDC protein changes previously reported for other variants.[93,117,122] The finding that the POPDC1 p.Q153X mutation leads to a reduction in POPDC1 p.Q153X protein levels at the plasma membrane of muscle fibres agrees with the non-quantitative analysis previously reported for POPDC1 alone.[117] POPDC2 showed a similar change in subcellular expression. There were no large changes in the level of either protein in the cytoplasm showing that a reduction of total expression appears to have occurred. The effect was highly consistent across all fibres. The change in POPDC2, in terms of the reduction in plasma membrane bias compared to control tissue, was greater than for POPDC1 p.Q153X. This highlights the tight link between POPDC1 and POPDC2 previously reported. A significant fibre hypertrophy was apparent in the patient biopsy, which is assumed to contribute to the muscular dystrophy pathology found in the patient.[117] The reason for this increase in fibre size is not known but could be a compensatory reaction of the muscle to mitigate the loss of POPDC1 and POPDC2 function in the fibres.

The analysis of the POPDC1 p.V183F mutant provides new evidence of another *POPDC1* mutation that causes changes in both POPDC1 and POPDC2 expression patterns. As with the POPDC1 p.Q153X, and other previously reported variants, a reduction in mean plasma membrane expression of both isoforms was found. A change in the relative concentrations in the plasma membrane and cytoplasm of fibres was also found. However, this sample shows a more complicated change in POPDC behaviour than other mutations. The changes in POPDC1 p.Q153X and p.S201F patient and mouse expressing fibres were highly consistent. In this case there was a large variation in the loss of normal POPDC subcellular expression between fibres which appeared to be related to the cross-sectional area of the fibres. There was also a severe change in the morphology in fibre shape and size compared to the control sample, which has not been seen in other pathological POPDC variants. This suggests a unique mechanism is behind the effects of the POPDC1 p.V183F mutation. Perhaps the V183F mutation leads to a change in a particular PPI, or other process. Other functions performed by other parts of the protein may be preserved, given that the rest of the amino acid sequence is not altered. This could explain the difference between this variant and the nonsense POPDC1 p.Q153X mutation.

The findings from the POPDC1 p.S201F mouse fibres support the conclusions made in the analysis of the patient biopsies.[93] This supports the use of this animal model in experiments to study the effect of the POPDC1 p.S201F variant *in vivo*.

The method of segmenting individual muscle fibres and recording the level of POPDC proteins in the plasma membrane and cytoplasm from each fibre allowed a detailed analysis of the changes between mutant and control fibres, not previously reported in the studies examining POPDC proteins. The numerous measures made helped to uncover the various subcellular expression patterns and the differences between the variant phenotypes. Relating the changes in fibre shape and POPDC expression revealed the difference in the POPDC1 p.V183F mutation behaviour compared to other variants, suggesting different mechanisms are at play, which can inform further study. It is recommended that future skeletal biopsy samples are analysed using similar methods so that any such trends can be uncovered.

α-sarcoglycan was stained to provide a marker for the sarcolemma and to enable normalisation of POPDC protein expression. It was noted that changes in α-sarcoglycan expression appeared to be present in the mutant samples. α-sarcoglycan is itself implicated in muscular dystrophies and changes in expression may provide evidence for the mechanism of POPDC mutant induced muscular dystrophy.[110]

5.4.2 Insights into the Mechanism of POPDC Mislocalisation

Studies into why a loss of both POPDC1 and POPDC2 expression is found in the case of single POPDC mutations has been limited by the reliance on finding novel POPDC mutations in patients and obtaining biopsy material to study. While these studies have provided evidence of this effect in some cases,[93,117,122] for many recorded POPDC mutations biopsy material is not available due to the practical and ethical constraints of performing biopsies on patients. Genetic knock-out and knock-in animal models have provided further methods of study,[71] such as the POPDC1 p.S201F mouse described above. However, production of genetic animal models for all known POPDC mutations would be impractical.

These experiments provided further evidence on the effects of POPDC1 and POPDC2 co-expression, and the effects of known mutations. The most severe effects on POPDC protein behaviour in HEK293 cells were found in the absence of either POPDC1 or POPDC2, matching the effects seen in *Popdc1* and *Popdc2* null mice.[71] It appeared that the behaviour of POPDC1 and POPDC2 in the HEK293 cell model correlated with the findings in native tissue. Large changes in subcellular expression were observed for the POPDC1 p.Q153X and p.S201F variants. This agrees with skeletal muscle analysis described above, as well as the previous report of the POPDC1 p.S201F mutation in patients.[93] This indicates that the effects seen in muscle do not require the complex environment of a muscle fibre to manifest, and are likely to be due to a direct effect between POPDC1 and POPDC2. The POPDC1 p.S201F mutation is unique because it has had its effect on cAMP binding affinity characterised.[93] The

drop in cAMP affinity reported likely influences the changes in POPDC1 and POPDC2 subcellular expression described here and previously in patients. This could provide a connection between cAMP binding to POPDC1 localisation, but also the relationship between POPDC1 and POPDC2, with POPDC2 apparently negatively affected by a change in the cAMP binding affinity of POPDC1. What mechanism underpins this effect is not known, although this is discussed further in Chapter 6.

While there were some changes in the subcellular expression of POPDC1 and POPDC2 in the presence of the POPDC1 p.V183F mutation in patient tissue, as described above, they were milder than those seen in the POPDC1 p.Q153X and p.S201F samples. In the HEK293 cells no large changes compared to wildtype were observed. This suggests that this mutation has an alternative effect on the protein compared to the others tested. It could be that the changes seen in skeletal muscle are due to a change in a tissue specific interaction or process that did not occur in the simple HEK293 cells. The POPDC1 p.R172H mutation was thought not to lead to large changes in POPDC expression in tissue, although there is limited evidence for this. In the HEK293 cells no large effects were seen, resembling the POPDC1 p.V183F mutation. This could perhaps inform the grouping of these two missense mutations into a common group based on their phenotype in HEK293 cells. The effect of the POPDC2 p.W188X on the subcellular expression of POPDC1 and POPDC2 in tissue is unknown. The severe effect of the mutation in the HEK293 cells would suggest that this variant would lead to mislocalisation of the POPDC proteins in native tissue. The confirmation that this occurs in patient or animal tissue would further validate the HEK293 cell model, allowing the model to be used to examine the effects on novel POPDC variants for which biopsy material is not available. An example of this is described in Chapter 7. This assay may reduce the dependence on patient and animal tissue samples, reducing the time, cost, and practical issues associated with the study of changes in POPDC protein trafficking. It would also be of interest to extend this model to the interplay between POPDC1 and POPDC3 which have been suggested to also interact with each other.[82]

The cross-sectional expression profiles showed that in all cases, apart from the POPDC2 p.W188X protein, the POPDC variants and their wildtype partner were able to associate with the plasma membrane. This demonstrates that the mutations do not totally abolish the membrane association of the POPDC proteins, although it may be disfavoured. This was even the case in the truncation POPDC1 p.Q153X mutant. This could be due to the presence of the unaltered transmembrane domains permitting some degree of membrane insertion and plasma membrane targeting,[47] even if some of the steps involved in the processing of the proteins is perturbed. The uncertainty about the function of each domain of the POPDC proteins makes conclusions about the specific effect of each mutation uncertain. However, these phenotypic measurements may help inform future attempts to

characterise the molecular mechanisms underlying the changes seen in each mutation, which is discussed further in Chapter 6.

POPDC proteins interact with many proteins found at the plasma membrane of striated muscle, such as Cav3, dysferlin and VAMP3.[71,72,118,119] Changes in the subcellular location of dysferlin has been linked to muscular dystrophy.[116] In addition, POPDC1 has been found to interact with PDE4A, AC9 and TREK-1.[71,100,101] The subcellular location of members of the cAMP pathway is essential for correct cAMP signalling due to the importance of the formation of cAMP nanodomains.[88] The POPDC proteins have been implicated in trafficking of other proteins to the plasma membrane and may also act as a scaffold for cAMP signalosomes.[101,119] The clear loss of normal POPDC subcellular localisation, as shown in skeletal muscle and HEK293 cells, as a result of mutations may lead to changes in the location or function of its interaction partners. If this is so, the changes in POPDC expression patterns observed here may be the cause of downstream effects that lead to muscular dystrophy in patients. Concurrent changes in the location of known and predicted POPDC interaction partners in tissue, or in the HEK293 model, should be examined to identify if other proteins are altered in a similar way to the POPDC proteins.

5.4.2.1 Limitations of the HEK293 POPDC Trafficking Model

There are some limitations to the HEK293 cell model which should be considered when interpreting results. This is a simplified model that does not provide a particularly close model of muscle cells.[197] The POPDC family has been found to interact with a large number of other proteins in striated muscle which are likely not present in HEK293 cells.[71,72,118,119] If any such interactions influence POPDC protein expression in native tissue this may reduce the accuracy of the model. The use of other cell lines could improve the comparison to native tissue. This could include the mouse myoblast C2C12 cell line, long used in the study of muscular dystrophy.[198] C2C12 cells are relatively amenable to transfection, endogenously express the POPDC proteins and have previously been used to study POPDC expression and protein-protein interactions.[73,118,199] This would allow the effects of POPDC mutations to be seen in differentiated muscle cells. An alternative would be the generation of induced pluripotent stem cells from patients carrying POPDC mutations, which could be used to generate differentiated muscle cells for *in vitro* studies.[200] Patient derived iPSCs have been used to model muscular dystrophies, and would provide a means of investigating specific mutations in the individual genetic environment of patients avoiding the limitations of obtaining biopsy material from patients.[201,202] This would raise the time and cost involved compared to the HEK293 cells.

In the HEK293 cells there was an almost binary change in trafficking between single POPDC1 or POPDC2 compared to co-expression. This provides evidence for an interaction between POPDC1 and

POPDC2 that is involved in the subcellular expression of both proteins. However, it is thought that POPDC1 and POPDC2 are expressed at different levels across tissues, with POPDC1 expressed strongly in cardiac and skeletal muscle, whereas POPDC2 is more favourably expressed in the heart.[65,67] It is unlikely that an equal ratio of POPDC1 and POPDC2 expression is maintained in all cell types. Mechanisms beyond only the formation of stoichiometric POPDC1-POPDC2 complexes are likely involved in the control of subcellular expression of POPDC proteins. It could be that other proteins are involved, and a variety of stimuli may influence the interactions of POPDC proteins, with such pathways perhaps also being tissue-specific. As with all transient transfection systems the actual expression levels of each protein in the cells would have been variable and at higher levels compared to native expression levels. Highly complex modulation of subunit stoichiometry usually occurs in cells to allow for the most efficient construction of protein complexes.[55] Such control is not possible in transiently transfected cell models.

Nonsense mediated decay (NMD) of mRNA acts as a means of preventing the production of C-terminally truncated proteins in eukaryotic cells through the detection and degradation of mRNA containing a premature termination codon.[203] The translation of non-mutant containing transcripts can also be regulated by NMD. The *POPDC1* (c.457C>T, p.Q153X) and *POPDC2* (c.563G>A, p.W188X) mutations identified in patients lead to truncation of the protein sequence by the introduction of a premature termination codons.[105,117] The role of NMD in the pathology of the known POPDC mutations is not fully understood. NMD was suggested as a possible reason for the reduction of POPDC1 protein levels in the patient possessing the *POPDC1* (c.457C>T, p.Q153X) mutation,[117] although Rinné *et al*. detected *POPDC2* (c.563G>A, p.W188X) coding mRNA and POPDC2 protein in patient leukocytes, suggesting that NMD did not totally prevent POPDC2 expression.[105] The use of cDNAs in the expression of the POPDC constructs means that NMD will not occur, as detection of premature termination codons usually requires the presence of exon junction complexes, which are positioned at exon-exon junctions during mRNA splicing.[204] Furthermore, the premature termination codons were removed from any POPDC constructs to permit the C-terminal fusion of the ECFP/EYFP domains. The lack of NMD mediated regulation of protein expression should be considered when interpreting the results of the HEK293 model. If mutant proteins are not expressed in native tissue, as a result of NMD or other mechanisms, HEK293 cells transfected only with a single POPDC isoform could be considered as an alternative model, representing conditions where effective translation of only non-mutated POPDC proteins occurs.

It is also possible that mutated POPDC proteins are degraded in native tissue, which would differ from the forced overexpression carried out in the HEK293 cells.[55] If mutated proteins are removed *in vivo*,

the findings from the single expression of POPDC1 or POPDC2 could be more relevant. In the case of the POPDC1 p.Q153X variant, skeletal muscle fibres showed a loss in expression of POPDC1 and POPDC2 at the plasma membrane but no large changes within the cytoplasm. In contrast, HEK293 cells exhibited significant accumulation of both isoforms within the cells. While the overall effect on POPDC plasma membrane localisation was similar, this was due to different effects in each system, perhaps indicating a difference in the mechanism between the two cell types.

In the case of the POPDC1 p.V183F mutation there was no negative effect on the localisation to the plasma membrane of POPDC1 or POPDC2 in HEK293 cells compared to wildtype. However, in the patient muscle biopsies modest decreases in POPDC1 and POPDC2 expression and localisation at the plasma membrane were observed, correlating with changes in the fibre size. It should therefore be noted that correct trafficking in the HEK293 cells does not necessarily mean that no changes will be seen in native tissue.

The presence of C-terminal ECFP/EYFP proteins to visualise the proteins within the cells may also affect the results. This method was chosen for reasons of experimental ease as well as the ability to conduct FRET analysis to investigate the putative interactions between POPDC1 and POPDC2 in the same system, described in Chapter 6. These tags are relatively large (28 kDa) compared to POPDC proteins (around 41 kDa) and may have influenced their behaviour.[32] However, these tags were present in all cases so their effect would have presumably been consistent across each group. The risks of interfering with POPDC function could be reduced by switching to other protein labelling techniques that do not require the fusion of large fluorescent proteins.[205] Antibody based labelling could also be employed, either by targeting POPDC proteins directly or through that use of small epitope tags. Fluorescence turn-on, or fluorophore complementation, techniques that are specific to the plasma membrane could also be used as an alternative.[206]

6 Investigations into the Mechanism and Function of the Interaction between POPDC1 and POPDC2

6.1 Introduction

6.1.1 POPDC1 Forms Homomeric Complexes

It is possible that the requirement for both POPDC1 and POPDC2 to be present in a functional form for normal POPDC protein subcellular expression to occur, examined in Chapter 5, is due to an interaction between POPDC1 and POPDC2. It is known that POPDC1 forms homomeric complexes, likely dimers. Homo-oligomerisation of POPDC1 was first identified by Knight *et al*.[73] It was found that Western blots assessing POPDC1 expression in COS-7 cells showed a significant amount of possible dimeric and higher order POPDC1 complexes as well as a minority amount of monomeric POPDC1. Subsequently, homodimer formation for POPDC1 was also described in cells with endogenous POPDC1 expression such as cardiac and skeletal myocytes.[73,77] Exposing the samples to reducing conditions led to a shift in favour of monomeric POPDC1. A homomeric interaction site was identified within the cytoplasmic region of POPDC1 through co-immunoprecipitation of full-length POPDC1 with a truncated POPDC1 construct containing only the cytoplasmic region.[73] This demonstrated that an interaction between POPDC1 proteins can occur within the cytoplasmic domain, which includes the Popeye domain and the C-terminal tail. Deletion analysis and peptide arrays were used to suggest that an interface was located between residues 251-284 at the C-terminal boundary of the Popeye domain.[81]

In Chapter 3 the dimerization of the S109-K272 and GB1-E123-D266 Popeye domain constructs was found using SEC-MALS. This shows that homomeric interactions between Popeye domains are possible. Residues 251-284, previously suggested to be particularly important for POPDC1 interactions, are only partially present in these two constructs, suggesting that other residues are involved in the formation of POPDC1 complexes. Although there is uncertainty about how closely the Popeye domain constructs resembled native protein, see Chapter 3, and the behaviour of isolated Popeye domains *in vitro* could differ from that of POPDC proteins in their native environment.

6.1.2 POPDC1 and POPDC2 Form Heteromeric Complexes

A direct interaction between POPDC1 and POPDC2 has recently been found.[82,186] When POPDC1 and POPDC2 were co-expressed in COS-7 cells, lysates analysed by Western blot showed that presumptive heterodimers could form alongside monomers. An interaction of POPDC1 and POPDC3 was also observed; no interaction between POPDC2 and POPDC3 could be detected with this method. A proximity ligation assay detected interactions between POPDC1 and POPDC2 in both atrial and ventricular sections from wildtype mice confirming the presence of POPDC1-POPDC2 complexes in their native environment.[186] To investigate the nature of the interaction between POPDC1 and

POPDC2, a series of deletion mutations of POPDC1 were created.[186] It was found that POPDC2 was co-precipitated with POPDC1 even after deletion of the entire intracellular domain. This suggested that the extracellular N-terminus and transmembrane domains of POPDC1 were sufficient to mediate POPDC1-POPDC2 interaction. It was also found that POPDC2 p.W188X is able to homodimerize as well as interact with wildtype POPDC2 and also heterodimerise with POPDC1.[82,186] As POPDC2 p.W188X lacks the second half of the cytoplasmic Popeye domain and the C-terminal tail, this is further evidence that the transmembrane domains and/or extracellular N-terminus is sufficient for an interaction between POPDC isoforms to occur. It was also found that the cytoplasmic region alone was sufficient to mediate specific POPDC heteromeric interaction, similar to previous reports for POPDC1.[73,82,186] This suggests that multiple interaction sites may be involved in mediating the homomeric and heteromeric interactions of POPDC proteins.

While it appears that multiple sites might be involved in homo- and heteromeric POPDC protein interactions, their individual roles are not known. POPDC1-POPDC2 complexes appear to be formed in the presence of only one interaction domain (N-terminus/transmembrane domain or cytoplasmic). However, it could be that multiple points of interaction are needed for fully functional complexes to form, which are able to achieve their proper subcellular localisation. The precise site of the POPDC monomer interfaces have not been determined. Despite the uncertainties in the mechanism and function of POPDC protein oligomerisation, it seems reasonable to hypothesise that disruption of the normal interactions between POPDC1 and POPDC2 contributes to the observed phenotypes of patients, and animal models, possessing POPDC mutations, such as those described in Chapter 5. It is suggestive of a role for POPDC protein oligomerisation in plasma membrane trafficking or upstream protein processing, although this has not been investigated in detail. The significance of homo-oligomerisation versus hetero-oligomerisation is also not known. An understanding of the role of POPDC protein family interactions would facilitate further study into the mechanism of diseases linked to POPDC mutations, as well as providing important information on the function of POPDC proteins in the cAMP pathway and other processes.

6.2 Outline of this Work and Aims

6.2.1 Description of this Work

The finding that POPDC1 and POPDC2 interact with each other, and the hypothesis that such interactions are perturbed as a result of POPDC mutations, was explored in transiently transfected HEK293 cells using quantitative BRET, acceptor-photobleaching FRET, BiFC and co-immunoprecipitation assays.

Finally, using the CAP protein family as a model for the Popeye domain of POPDC proteins, investigations into the specific mechanism of the POPDC protein interactions were performed. Mutagenesis of the POPDC proteins was carried out and the HEK293 trafficking model used to assess the role of specific amino acid residues in the Popeye domain in determining POPDC subcellular expression. These experiments were used to develop a working theory on the reason why POPDC1-POPDC2 interactions are required for normal POPDC localisation.

6.2.2 Aims

The aims of the studies described in this chapter were to:

1. Investigate the stoichiometry of POPDC1-POPDC2 interactions using quantitative BRET.
2. Determine if a change in the interaction between POPDC1 and POPDC2 is responsible for the protein trafficking defects seen in the presence of some *POPDC* mutations.
3. Investigate possible interaction domains of POPDC1 and POPDC2 and assess the importance of these putative interaction sites on POPDC protein trafficking.

6.3 Results

6.3.1 Investigations into the Stoichiometry of the Interaction Between POPDC1 and POPDC2 with Quantitative BRET

The hypothesised interaction between POPDC1 and POPDC2 is of significant interest given the mutual impact of POPDC mutations on the membrane localisation and expression of both POPDC1 and POPDC2, as demonstrated in Chapter 5. Understanding the interaction mechanism between these two proteins could provide an insight into the pathological mechanisms of known POPDC variants. It was desired to investigate the nature of the homo- and heteromeric-interactions between wildtype POPDC1 and POPDC2, before investigating the effects of specific POPDC mutations on the interactions between POPDC1 and POPDC2.

BRET is a similar technique to FRET which can be used to detect protein-protein interactions within cells.[36] The general mechanism of BRET, and the main differences from FRET, are discussed in Chapter 4. Quantitative BRET (qBRET) is a technique which has predominantly been used to study the oligomerisation of GPCRs.[207-209] In qBRET the relative concentrations of the proteins of interest expressed inside a cell, each fused to a BRET donor or acceptor, are varied and the dependence of the BRET signal on their relative concentrations is recorded, as shown in Figure 6.1A.

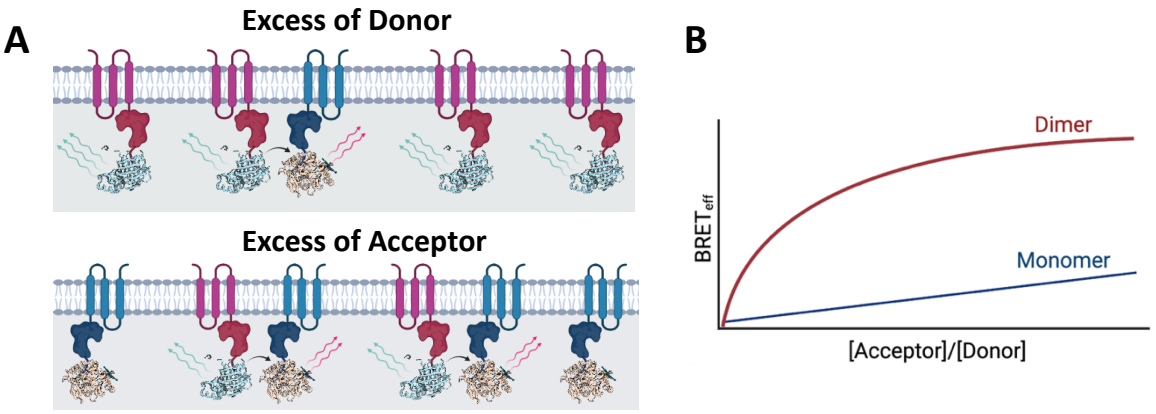


Figure 6.1: The Mechanism of a Type 1 Quantitative BRET Assay. A) In a type 1 quantitative BRET assay two proteins of interest are tagged with either a BRET donor (luciferase) or acceptor (fluorophore). These constructs are then expressed in cells. Any interactions between the proteins will enable RET to occur between the luciferase and the fluorophore. If there as an excess of donor fused protein most luciferase will not take part in RET, leading to high luminescence and minimal acceptor fluorophore emission. As the relative concentration of acceptor fused protein increases, more luciferase enzymes will be in close proximity to a BRET acceptor, leading to greater BRET signal, until this reaches a maximum. **B)** When the BRET signal is plotted against the relative acceptor to donor ratio, a hyperbolic increase in BRET will be seen if a specific interaction is occurring. Monomers will show a weak, linear increase in BRET due to diffusion-controlled interactions.

A type-1 qBRET assay keeps the overall protein expression within the cell constant, while varying the ratio of the interaction partners.[144] A specific binding interaction between proteins will produce a hyperbolic increase in BRET signal as the ratio of acceptor tagged protein to donor tagged protein increases, while if the tagged protein remain as monomers only a diffusion controlled linear increase in BRET will be seen (Figure 6.1B).[210] The stoichiometry of the interacting proteins can be determined by fitting BRET curves constructed by plotting the measured BRET against the expression ratio to Equation 6.1 (also shown in Equation 2.1), where $BRET_{eff}$ is the value of BRET at any measured point, $BRET_{max}$ is the saturating level of BRET at the maximum acceptor to donor ratio, f is the ratio of the acceptor tagged species to the donor tagged protein, and n is the stoichiometry of the interaction.[144]

Equation 6.1:

$$\frac{BRET_{eff}}{BRET_{max}} = 1 - \frac{1}{(1+f)^{n-1}}$$

It was thought that the stoichiometric information that can be gained from qBRET studies, and the high sensitivity of the NanoBRET platform, as discussed in Chapter 4, could be exploited to investigate the nature of POPDC1-POPDC2 complexes. In addition, the previously reported POPDC1 homomeric interactions and possible POPDC2 homomeric complexes were examined.[73,186] Human POPDC1 and POPDC2 sequences were tagged at the C-terminus with NanoLuc (POPDC-NL) or HaloTag (POPDC-HT), as shown in Chapter 4, Figure 4.3. These NanoBRET constructs were then transiently expressed in HEK293 cells which were plated into 96-well plates and the BRET signal was measured using a luminometer plate reader.

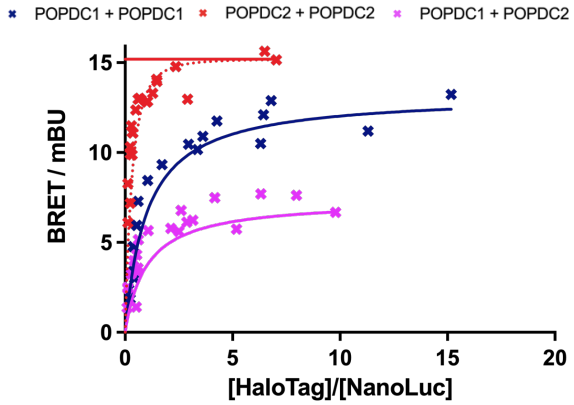
The relative expression levels of the interaction partners must be accurately known during qBRET to construct the BRET saturation curve and fit data points to Equation 6.1.[144] Approximate expression levels in transient transfections are nominally controlled by changing the amount of plasmid DNA used during transfection. Constant amounts of plasmid DNA containing the cDNA sequences for POPDC-NL and POPDC-HT were transfected into HEK293 cells with an increasing proportion of POPDC-HT containing plasmid. However, the amount of each plasmid transfected cannot be reliably used to determine protein expression levels due to the variation in transfection efficiency and protein expression levels.[144] Instead, the concentrations of the POPDC-NL and POPDC-HT in each set of cells were determined directly before the BRET measurement. The level of POPDC-NL was determined by measuring the total luminescence across all wavelengths from cells after luciferase substrate addition. The concentration of HaloTag-618, equivalent to the expression level of POPDC-HT, in the cells was found by the BRET independent stimulation of dye fluorescence. The respective luminescence and fluorescence values from these measurements were converted to a common unit through the use of a fusion protein formed of NanoLuc and HaloTag with a one-to-one stoichiometry of each species. The relationship between the fluorescence and luminescence of this construct was determined, which allowed the finding of a conversion factor to relate all luminescence and fluorescence values. This allowed the determination of the relative levels of POPDC-NL and POPDC-HT in each sample, to which the BRET signal was plotted against. The total expression of both POPDC constructs in each group used was also found to ensure changes in the total concentration of proteins did not skew results by increasing the chances of diffusion-controlled interactions occurring. No significant changes in total expression were found when changing the ratio of POPDC-NL and POPDC-HT expression (Appendix 10.3, Figure 10.3).

Analysis of the BRET saturation curves was carried out as previously reported by Felce *et al*.,[144] with further information provided in the Methods and Materials, Section 2.7.4). Briefly, the measured BRET saturation curves were either fitted to Equation 6.1 with a constraint of $n = 2$, for a dimer model, or $n = 1$ for a monomer model. Then non-linear least-squares regression was applied to the points to generate optimal curve fits for the two models. The difference between the absolute sum of squares for the dimer and the monomer model were determined and the ratio between them determined. The determined ratio was then subtracted from 1 to give an R^2 value, where positive values show a better fit to a dimer model, whereas a negative R^2 value indicated the presence of monomers.

Firstly, the co-expression of POPDC1-NL and POPDC1-HT at different ratios was performed. The BRET curves produced, along with the other POPDC combinations, are shown in Figure 6.2A. As expected, this pair produced a BRET curve that fitted best to a dimer model ($R^2 = 0.83$). This agrees with previous

reports of POPDC1 homodimers using co-immunoprecipitation and peptide array techniques.[73,77,81] The agreement with other techniques gave confidence that the qBRET protocol was functioning as required. In contrast, the co-expression of POPDC2-NL and POPDC2-HT produced BRET curves that did not match those expected for dimeric interactions (R^2 = -4.13). A very rapid increase in BRET was found as the POPDC2-HT:POPDC2-NL ratio increased, with a high $BRET_{max}$ value. However, it should be noted that type-1 BRET studies can be difficult to interpret in the case of higher order oligomer formation, with the appearance of false monomers.[144] This is due to the rapid saturation of the BRET signal as a result of BRET donors being in an environment with high BRET acceptor concentration, such as a multimeric complex, leading to highly efficient RET even at low relative acceptor concentrations. Points with acceptor to donor ratios below 2 were not used in curve fitting, to reduce the impact of diffusion controlled interactions.[144] However, by this point the BRET curve formed by the co-expression of POPDC2-NL and POPDC2-HT had almost reached saturation, meaning a pseudo-linear curve was produced. Although this form of BRET assay is not well suited to assessing higher order complexes,[144] constraining Equation 6.1 to n = 4, representing a tetramer, produced a good fit to the data points and is shown as a dashed line within Figure 6.2A. Higher order POPDC2 oligomers have previously been observed on Westerns blots.[82] In addition, the highest $BRET_{max}$ value was achieved by the POPDC2-NL POPDC2-HT pair. $BRET_{max}$ is not an indication of a strong or specific interaction by itself. It is dependent on the orientation of the BRET tags which may be independent of the strength of the protein-protein interaction.[36] However, particularly high $BRET_{max}$ values may indicate the presence of a specific interaction if supported by other evidence. In this case, it is likely that a higher order POPDC2 oligomer is forming, leading to the false monomer prediction in this assay.

A



B

POPDC Pair	R^2	$BRET_{max}$ / mBU
hPOPDC1-hPOPDC1	0.83	13.23
hPOPDC2-hPOPDC2*	-4.13	15.19
hPOPDC1-hPOPDC2	0.285	7.384

Figure 6.2: The Quantitative BRET Analysis of Homomeric and Heteromeric Interactions between POPDC1 and POPDC2. A) A graph showing the relationship between the BRET signal and the ratio of POPDC-HT and POPDC-NL constructs of when co-expressed in HEK293 cells. Points were fitted to Equation 6.1 considering only points with a POPDC-HT : POPDC-NL ratio between 2-15, although all measured data points are shown. POPDC1-POPDC1 homo-interactions and POPDC1-POPDC2 hetero-interactions are fitted to dimer BRET curves, POPDC2-POPDC2 is a fitted to a monomer curve (solid lines). However, a curve showing a tetramer fit for POPDC2-POPDC2 is also shown (dashed line), as this may be a false monomer result. **B)** A table showing the R^2 fit values to a dimer model for each POPDC combination, where positive values indicate dimers and negative values show monomer behaviour. The maximum BRET yielded from each interaction is also shown.

The saturation curve produced by the co-expression of POPDC1-HT and POPDC2-NL suggested the formation of dimers, $R^2 = 0.285$. If POPDC1 and POPDC2 homo-oligomers do indeed form, as suggested by the above results, the co-expression of POPDC1 and POPDC2 should theoretically permit the formation of both homo and hetero-oligomers. The robust hyperbolic saturation curve produced by POPDC1-HT and POPDC2-NL suggests that POPDC1-POPDC2 interactions are sufficiently favourable to overcome the formation of POPDC1 and POPDC2 homo-oligomers. It is therefore likely that POPDC1-POPDC2 heterodimers are the major species within systems where they are co-expressed. This assay, along with a previously conducted proximity ligation assay,[186] provides direct evidence of POPDC1-POPDC2 heteromers in a cellular environment with additional stoichiometric information.

6.3.1.1 Limitations of the qBRET Assay

The finding that plasma membrane localisation of both POPDC1 and POPDC2 within HEK293 cells is dependent on the presence of both of these proteins, as shown in Chapter 5, adds a caveat to the qBRET data obtained by transfection with POPDC1 or POPDC2 only. It can be assumed that when co-expressing POPDC1-NL and POPDC1-HT, or POPDC2-NL and POPDC2-HT, specific expression at the plasma membrane of cells was not achieved. Instead, it is likely that the interactions responsible for the observed BRET behaviour occurred intracellularly. This could mean that such interactions are not found in the normal plasma membrane environment of POPDC1 and POPDC2 and so may be less relevant to POPDC behaviour in native tissue.

There is uncertainty in the results of POPDC2 homomeric interactions. A type-3 BRET assay, where non-tagged competitor monomers are introduced to compete with BRET productive pairs, could have been used to determine if POPDC2 does form oligomers, as type-3 BRET is not as susceptible to producing pseudo monomer saturation curves.[144] It is, however, liable to falsely report the presence of oligomers. A type-3 BRET should ideally be completed to confirm the results of the type-1 assay run here.

A major drawback of this assay was the measurement of HaloTag-618 fluorescence to determine the levels of POPDC-HT in the cells. It was planned to use a plate reader to measure the fluorescence levels from the population of cells in each well of the 96-well plate. However, it was found that very low signal-to-noise was observed when measuring HaloTag-618 intensity from surface-attached cells within both white and black 96-well plates, particularly at low relative POPDC-HT concentrations. The protocol was modified to utilise cell suspensions instead of surface attached cells, which is common in qBRET protocols.[207-209] Cells were treated as before but, immediately before measurement, the cells were detached from tissue culture plates and seeded into 96-well plates in suspension at various cell

densities. This markedly improved the HaloTag-618 fluorescence signal and enabled a fully plate reader-based assay, which was time and cost efficient. However, it was found that the observed BRET saturation curves were of poor quality compared to those observed in cell-attached assays. It is known that POPDC proteins are involved in cell-cell contacts and are found at the plasma membrane in ideal conditions.[154,199] It has previously been reported that the formation of cell-cell contacts changes the plasma membrane localisation of endogenous POPDC1 in epithelial cells.[154] It was hypothesised that the detachment and resuspension of cells before BRET measurement may have led to changes in the localisation and/or intermolecular interactions of the POPDC proteins, compared to the confluent, surface attached cells used in the previous assay format. As an alternative method to measure the POPDC-HT concentrations in cells, aliquots of surface-attached cells were visualised under a widefield microscope, which was more sensitive to low emission levels than the plate reader, and the HaloTag-618 fluorescence measured from entire wells of microplates. This introduced the need for separate seeding of cells into microslides, fixing of cells and use of a widefield microscope. This significantly increased the time and cost of the assay, limiting its further use.

6.3.2 Changes in the POPDC1-POPDC2 Interaction in the Presence of Clinically Relevant POPDC Variants

6.3.2.1 AP-FRET

Changes in the interaction between POPDC1 and POPDC2 might be behind the changes in POPDC1 and POPDC2 subcellular expression seen in HEK293 cells and tissue in the presence of the subset of clinically identified POPDC mutants examined in Chapter 5. To try and detect any changes in the interaction of mutant POPDC proteins and their respective partner in HEK293 cells it was firstly decided to use FRET, specifically acceptor photo-bleaching FRET (AP-FRET). FRET was previously used by Froese *et al*. and Schindler *et al*. to measure changes in the POPDC1-TREK1 interaction upon addition of cAMP.[71,93] However, it has not been previously used to investigate POPDC-POPDC interactions. FRET follows the same principles as BRET, with the exception that incident light is used to excite the donor group instead of an *in situ* chemiluminescent reaction.[37] AP-FRET was chosen due to its relatively simple protocol,[192] which meant that the same cell preparation protocol and confocal microscope setup could be used as in the HEK293 cell trafficking assay described in Chapter 5 and further experiments below. AP-FRET has previously been used to study the interactions of transmembrane proteins, such as GPCRs.[211] qBRET could have been used again to provide detailed information on the changes in any interactions, including alterations in stoichiometry, but the higher cost and experimental time, in part due to the issues in measuring the HaloTag-618 signal on a plate reader, meant that AP-FRET was favoured. AP-FRET is a form of FRET that exploits changes in the quenching of the donor fluorophore by the acceptor before and after acceptor photobleaching, with

the mechanism outlined in Figure 6.3A, and an example of a cell subjected to AP-FRET also shown.[192] When RET occurs between a FRET donor and acceptor group the intensity of the donor fluorescence is reduced compared to a situation where it is in isolation, because the quantum yield of donor fluorescence drops due to the energy transferred to the acceptor. If the acceptor group is removed, or inactivated, then the donor quantum yield of fluorescence will increase due to the loss of the RET pathway, leading to an increase in donor fluorescence.[212] A baseline reading of the donor emission is made by exciting the donor group and measuring the emission from the donor before acceptor bleaching within a defined area of a cell. The same region of the cell is then exposed to a high level of incident light at the excitation wavelength of the acceptor to deliberately photobleach the acceptor group, inactivating it and removing the RET pathway. The donor fluorescence is then re-measured to detect if there has been any increase in donor emission as a result of the loss of RET to the acceptor.[212] If FRET was occurring in the initial conditions, an increase in donor fluorescence post acceptor photobleaching will be observed.

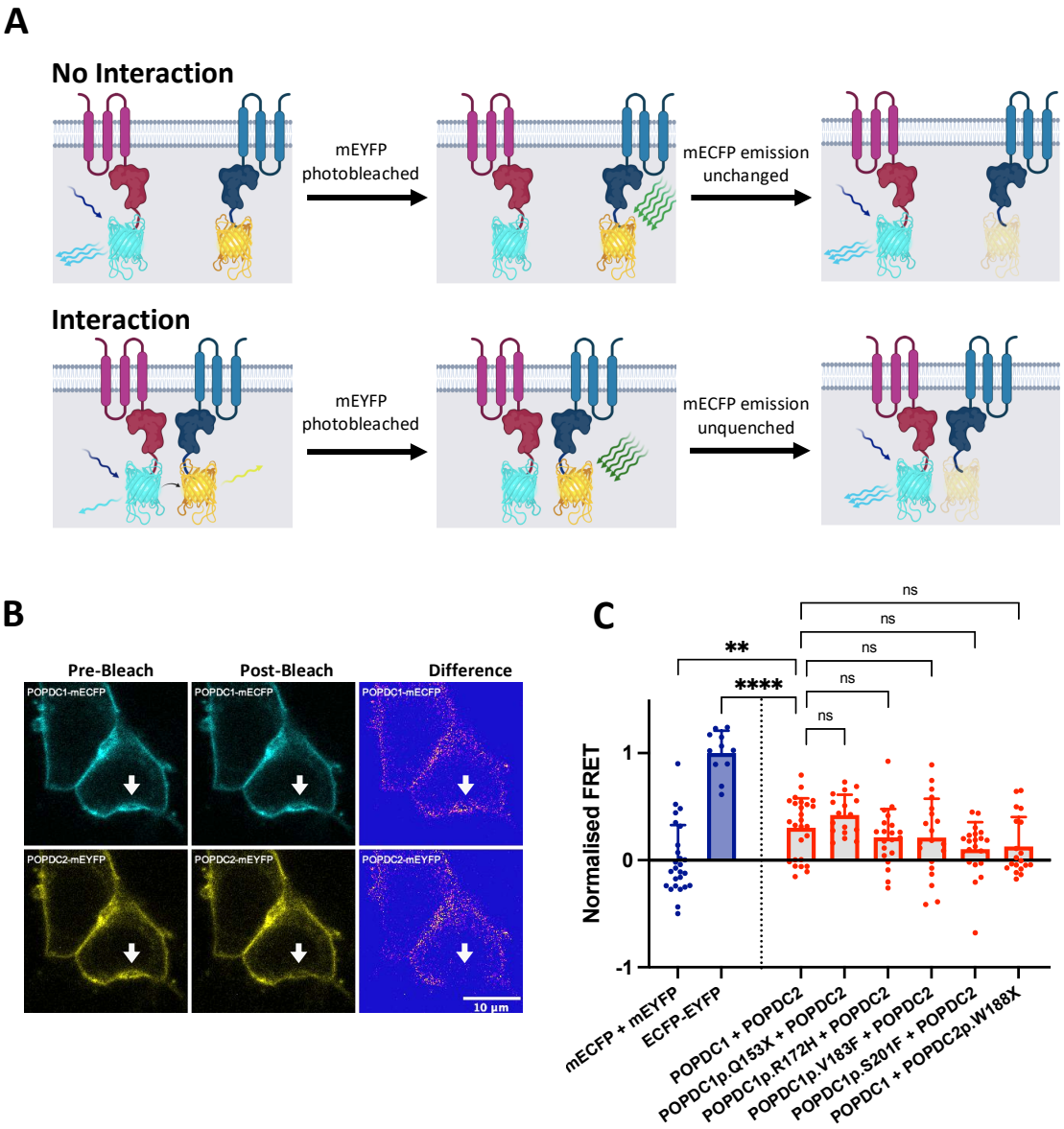


Figure 6.3: Acceptor-photobleaching FRET between POPDC1 and POPDC2 in the Presence of Various POPDC Mutants in HEK293 Cells. **A)** A schematic of the AP-FRET assay. If the FRET donor (mECFP) and acceptor (mEYFP) are in close contact, due to an interaction between the tagged proteins, the fluorescence of the mECFP will be quenched through RET. If the mEYFP is photobleached the level of mECFP fluorescence will increase due to the disruption of the RET pathway. If no interaction was occurring betweent the proteins of interest to which the mECFP and mEYFP groups are fused to, no change in mECFP emission will occur after mEYFP bleaching. **B)** The mECFP channel and mEYFP channel from cells expressing POPDC1-mECFP and POPDC2-mEYFP are shown pre- and post-photobleach. The difference in emission from each fluorophore between the two measurments is shown for each channel. The arrow indicates the position of the measurement area which was subjected to photobleaching of the mEYFP and from which mECFP levels were measured. **C)** The level of acceptor-photobleaching FRET was determined between free mECFP and mEYFP, as well as tethered ECFP-EYFP to determine the background and maximum FRET in system. FRET levels were normalised to the positive ECFP-EYFP control. The FRET signal between the different POPDC combinations were then measured. The difference between the wildtype POPDC pair and the mutant containing pairs were analysed using one-way ANOVA followed by Dunnett's method. ** p<0.01, **** p<0.0001. A summary of the data is provided in Appendix 10.7, Table 10.44 and 10.45.

The efficiency of FRET occurring in the baseline conditions is determined through the use of Equation 6.2, where E is the FRET efficiency, I_{pre} the level of mECFP fluorescence before photobleaching and I_{post} is the mECFP fluorescence after photobleaching of mEYFP.[212] To account for any incomplete bleaching

of the acceptor, the increase in donor emission can be scaled to the extent of the loss of acceptor emission. ROIs in which 70% of the initial mEYFP remained post-photobleaching were excluded.

Equation 6.2:

$$E = \frac{I_{post} + I_{pre}}{I_{post}}$$

The same protocol that was used to transfect and prepare cells for the analysis of POPDC protein expression and trafficking in HEK293 cells in Chapter 5 was used to prepare samples for AP-FRET. The same form of construct was used, with POPDC1 and POPDC2 fused at the C-terminus with ECFP or EYFP, respectively. However, it is known that GFP variants can weakly dimerise, which could lead to background FRET independent of specific POPDC interactions.[213] This endogenous dimerization can be abolished through the introduction of an A206K substitution to each GFP derivative, which introduces a repulsive, positive charge at the dimer interface.[214] The resulting GFP variants are designated as monomeric (mECFP and mEYFP). To remove the possibility that ECFP and EYFP may dimerise with each other, increasing the observed FRET levels, the previously used POPDC-ECFP/EYFP constructs were mutagenized through site-directed mutagenesis to introduce an A206K mutation to yield POPDC1-mECFP and POPDC2-mEYFP.

To assess the levels of background, diffusion-controlled FRET that could be expected within the cells, free mECFP and mEYFP were expressed in cells and used as negative controls (Figure 6.3C). The level of FRET recorded between these two free fluorophores was set as the zero FRET level for the POPDC pairs. In addition, ECFP and EYFP were tethered through an 11 amino acid linker to form a positive control (full sequence shown in Appendix 10.9, Figure 10.17), which was used to define the maximum possible FRET signal, set to equal one. Both the free fluorophores and the tethered positive control were expressed in the cytoplasm and nuclei of the HEK293 cells, with FRET measurements derived from cytoplasmic ROIs. A wide range of normalised FRET values were measured from the mECFP + mEYFP negative control (-0.498 to 0.900), suggesting that diffusion-controlled interactions could make a varied, but significant, contribution to FRET levels between the two fluorophores. However, the significantly higher level of FRET recorded from the ECFP-EYFP positive control does indicate that robust interactions will result in more efficient FRET, although a reasonable range of the FRET values (0.613 to 1.240) were found across the different ROIs despite the short 11 residue linker connecting the two fluorophores. This could suggest a more systematic issue with the precision of the FRET measurements using this protocol.

Wildtype POPDC1-mECFP and POPDC2-mEYFP were then co-expressed and the level of FRET between the two constructs was determined. Photobleaching and subsequent FRET measurements were

performed at ROIs about the plasma membrane, but which also encompassed the adjacent region of the cytoplasm. As would be expected if POPDC1 and POPDC2 were interacting, the FRET level was significantly greater than from the negative control, but less than that of the positive control, as determined by a one-way ANOVA followed by Dunnett's test using the POPDC wildtype pair as the control (Figure 6.3C). Substitution of one of the wildtype pair with either POPDC1 p.Q153X, p.R172H, p.V183F, p.S201F or POPDC2 p.W188X was then performed to attempt to determine the impact of each mutation on FRET, and so heteromeric POPDC interactions. It was found that no significant change in FRET occurred in the presence of any of the mutant POPDC species (Figure 6.3C). A summary of the results can be found in Appendix 10.7, Table 10.44 and 10.45.

This could mean that these mutations lead to no change in the interaction between POPDC1 and POPDC2. This would contradict the hypothesis that changes in expression and localisation of POPDC1 and POPDC2 in the skeletal muscle tissue of patients, as discussed in Chapter 5, was, in part at least, due to a change in heteromeric POPDC complex formation. While this may be the case, some caution should be applied when interpreting the results of this assay. As mentioned above, the negative and positive FRET controls displayed a wide range of FRET values between each measured ROI. This was also the case for the POPDC pairs, with the standard deviation of their FRET levels being between 44-243% of the mean. This high degree of variance means that only a very low confidence in the mean FRET values can be held, and as such this assay does not provide strong evidence on whether there is a change in the interaction of POPDC1 and POPDC2 in response to different mutations. The cause of this variance is not clear but, given the level of variance in FRET between the control constructs, it could be due to a systematic issue such as the confocal microscope protocol employed. It was noted that incomplete mEYFP photobleaching often occurred and extrapolation of the change in mECFP fluorescence was performed to account for this. This may have introduced increased error into the final mECFP fluorescence used to calculate the level of FRET. ROIs where over 70% of the mEYFP signal remained were excluded, however this threshold may have been insufficient and more stringent selection of ROIs may have reduced the variance in the final FRET values. More severe photobleaching could also have been applied but this would risk increased off-target bleaching of the mECFP or damage to cells. While attempts were made to minimise the bleed through between the mECFP and mEYFP channels, this may have also contributed the variable FRET levels. The range of FRET values from the free mECFP + mEYFP control also suggests that diffusion controlled interactions may have been contributing to FRET, and this may be greater for the membrane localised POPDC proteins. Low expression levels were desired for all transient transfection experiments performed in this work to reduce the effects of overexpression on the cells and POPDC behaviour. However, this was limited by the requirement for strong fluorescence signals from the constructs to allow for detection. It could be

that the concentrations of POPDC constructs, as well as the negative control fluorophores, was too high and resulted in non-native, diffusion-controlled interactions. The position of the mECFP and mEYFP tags at the C-terminus of the POPDC proteins, found at the end of the approximately 100 residue, disordered C-terminal tail may have further contributed to variable, poorly defined relative positions of the fluorophores, and so inconsistent FRET.

6.3.2.2 BiFC Study of POPDC Mutant Interactions

An alternative optical method to study the complexation of POPDC1 and POPDC2 in cells is BiFC. The schematic in Figure 6.4A demonstrates the principle of the assay, which utilises a split fluorophore where each fragment is fused to two different proteins of interest. If the two fragments, usually consisting of residues 1-154 (VN155) and 155-238 (VC155) of the Venus YFP derivative, are brought into contact by the interactions of the target proteins the Venus fluorophore may reform allowing fluorescence to occur.[38] The strength of the fluorescence from a sample provides a measurement of the efficiency of the interactions between the target proteins. POPDC1 variants were tagged at the C-terminus with VC155, while POPDC2 containing constructs possessed a VN155 domain at the C-terminus. Full sequences of these constructs are provided in Appendix 10.9, Figures 10.18-22. These were co-expressed in HEK293 cells and imaged using a confocal microscope. The signal from BiFC is an absolute value, not ratiometric as with FRET. This means that if greater amounts of a protein pair are expressed in a cell the fluorescence signal will increase, even if no change in their propensity to dimerise has occurred.[215] Transient transfections, which were used in all HEK293 based experiments in this work, can vary in efficiency between repeats, leading to changes in protein expression levels. A separate fluorescent protein can be co-transfected to act as an internal transfection control reporter.[216] Here mRFP was also transfected and expressed alongside the POPDC BiFC constructs in the cells and the measured Venus signal was then normalised to the mRFP fluorescence level. mRFP fluorescence was also used to define the areas of each image that contained cells that had been successfully transfected, by only selecting cells showing mRFP fluorescence above background levels. Measurements were only made from these cells, so the average Venus emission was not skewed by changes in the proportion of cells in each image that had been transfected. The median Venus signal from all transfected cells was then normalised to the median mRFP fluorescence from within the same area. An example of the different fluorescence channels used in the analysis of the cells is shown in Figure 6.4B. Co-expression of POPDC1-VN155 and POPDC2-VN155 was used as a negative control and to determine the levels of background fluorescence in cells. The level of Venus fluorescence in each group was compared using one-way ANOVA followed by a post-hoc Dunnett's test with the wildtype POPDC pair as a control.

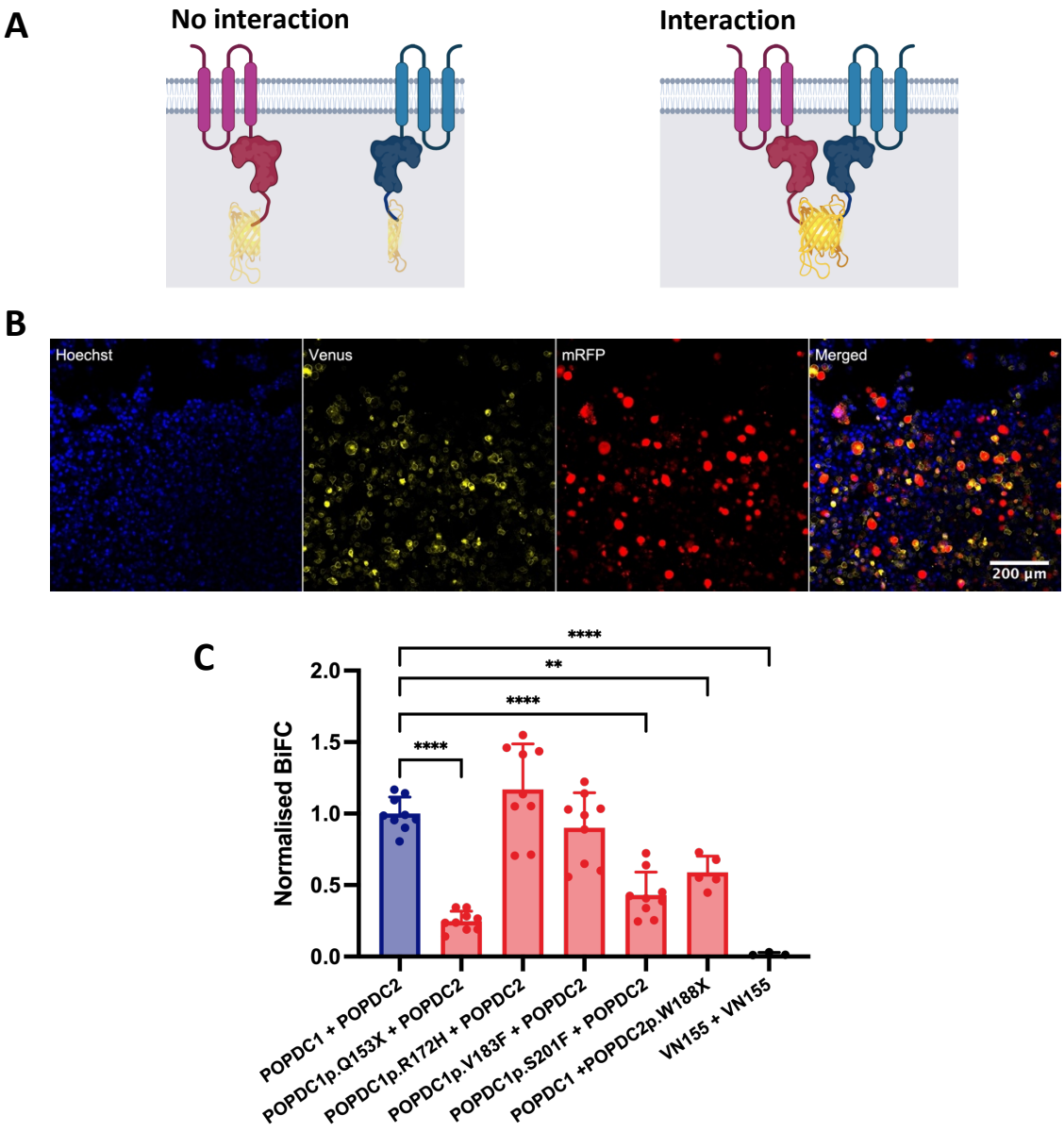


Figure 6.4: The Changes in BiFC Signal from the Co-expression of POPDC1 and POPDC2 Variants in HEK293 Cells. A) A cartoon showing the principle of the BiFC assay. The Venus fluorophore was split into two fragments and fused to the C-terminus of different POPDC protein variants. If an interaction occurred between the two POPDC protein when expressed in HEK293 cells, the Venus fragments would be brought together allowing the reformation of the fluorophore. **B)** An example image showing HEK293 cells expressing POPDC1-VC155 and POPDC2-VN155 as well as mRFP. The mRFP channel was used to define the areas of the image containing transfected cells from which the average Venus emission levels were found. Venus emission was normalised to mRFP levels to control for difference in transfection efficiency. **C)** The normalised BiFC signal from HEK293 cells expressing the different POPDC pairs. One-way Anova was performed followed by comparison to the wildtype POPDC1-VC155 and POPDC2-VN155 pair using Dunnett's method. ** P<0.005, **** P<0.0001. Summary data is provided in Appendix 10.6, Table 10.42 and 10.43.

The normalised Venus fluorescence levels from each group are shown in Figure 6.4C. It was found that all groups yielded Venus fluorescence above background levels. Wildtype POPDC1 and POPDC2, along with POPDC1 p.R172H and p.V183F, gave the highest levels of fluorescence, with the latter two not significantly different from the wildtype pair. Visual inspection of cells showed that these three groups also showed a clear increase in Venus emission at the plasma membrane of cells indicating that POPDC1-POPDC2 contacts were predominantly occurring at the plasma membrane, confirming the

observations from the HEK293 cells in Chapter 5. Meanwhile the introduction of POPDC1 p.Q153X, p.S201F and POPDC2 p.W188X led to an approximate 75%, 60% and 40% reduction in normalised Venus emission levels, respectively. The Venus emission from these groups were less localised to the plasma membrane compared to the rest of the cell. These results imply that the interaction between POPDC1 and POPDC2 was disrupted by the POPDC1 p.Q153X, p.S201F, and POPDC2 p.W188X mutations, but not fully abolished.

Unlike the AP-FRET assay, the different POPDC mutations caused an apparent change in POPDC1-POPDC2 complex formation. It is notable that the results of the BiFC assay correlate with those of the HEK293 trafficking assay in Chapter 5, where it was found that the subcellular expression of POPDC1 and POPDC2 was unaltered in the case of POPDC1 p.R172H and p.V183F compared to wildtype. In contrast, the POPDC1 p.Q153X, p.S201F and POPDC2 p.W188X variants led to a decrease in the plasma membrane localisation of POPDC1 and POPDC2. This supports the hypothesis that changes in POPDC1 and POPDC2 interactions are related to their expression at the plasma membrane.

Strong Venus emission was present in all groups suggesting that POPDC1-POPDC2 contacts were present in all cases. This suggests that the mutations did not totally abolish interactions between POPDC1 and POPDC2. It could be that a partial reduction in the affinity of the interaction occurred, shifting the equilibrium to non-complexed POPDC proteins. The mutations, particularly the nonsense POPDC1 p.Q153X and POPDC2 p.W188X mutations, are likely to have changed the relative positions of the Venus fragments relative to the wildtype partner whose C-terminal tail was intact. This could have led to changes in Venus reformation even if the two POPDC proteins were interacting and could reflect the altered nature of the POPDC1-POPDC2 complex in the case of these mutations. The reformation of the split Venus is usually thought to be irreversible, which means that BiFC will capture transient interactions between two target proteins.[38] This may lead to a summative effect where a small difference in the equilibrium between free and complexed POPDC proteins could cause an increase in the rate of Venus reformation and a large final difference in fluorescence over the protein expression time.

6.3.2.3 Co-Immunoprecipitation of POPDC2 and POPDC1 in the Presence of the POPDC Variants

Co-immunoprecipitation was next used as an orthogonal technique to probe any changes in the POPDC1-POPDC2 interaction as a result of the various POPDC mutations. This technique may be advantageous as it does not rely on the interaction of additional tags and any confounding effects from their position on the POPDC proteins. It was decided to use the same POPDC1-ECFP and POPDC2-EYFP constructs that had been used in the HEK293 cell trafficking assay, which are almost identical to those used in AP-FRET, as they already contained additional myc or HA epitope tags at the C-terminus

of their fluorescent protein domains. This would also control for any changes in the interaction induced by the presence of the fluorescent proteins that may have influenced the HEK293 cell data. The POPDC1-ECFP-myc and POPDC2-EYFP-HA constructs were co-expressed in HEK293 cells which were lysed approximately 48 hours after transfection. The soluble fraction of the lysate was then incubated with anti-myc conjugated agarose to precipitate POPDC1 constructs. Precipitated protein was analysed through a Western blot using an anti-HA primary antibody to detect co-precipitated POPDC2, shown in Figure 6.5. Cells expressing POPDC2-EYFP-HA only were used to assess non-specific co-precipitation of POPDC2 constructs.

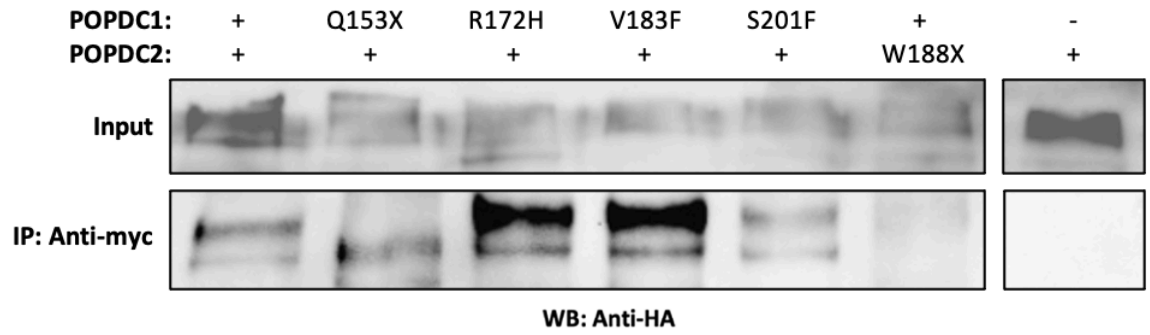


Figure 6.5: Co-Immunoprecipitation of POPDC2 with POPDC1 from HEK293 Cells in the Presence of Various POPDC Variants. POPDC1-ECFP-myc and POPDC2-EYFP-HA were co-expressed in HEK293 cells. POPDC variants of interest were each substituted in place of their wildtype equivalent. A negative control in which only POPDC2-EYFP-HA was expressed was used for comparison. Cell lysates were precipitated with an anti-myc antibody and subjected to Western blot analysis using an anti-HA tag antibody. Analysis was complicated by high levels of fragmentation and possible aggregation of the proteins. Note that all lanes shown are from the same blot, an additional lane containing an unrelated sample was removed between the main body of the blot and the POPDC2-EYFP-HA only control lane. An image of the full blot is shown in Appendix 10.5, Figure 10.4.

It was found that POPDC2 constructs were co-precipitated in all cases, but the level of co-precipitation varied. Negligible levels of POPDC2 were detected in the control sample showing that the co-precipitation was specific to POPDC1. Quantification of the level of co-precipitation in each group was complicated by the fact that the ECFP or EYFP containing regions of the constructs, which also contain the myc and HA epitopes, tended to be cleaved from the POPDC sequence during sample preparation. This meant that different bands were seen, including those corresponding to cleaved ECFP/EYFP only, full-length constructs and also complexed or aggregated protein which is commonly seen in Western blots of POPDC proteins.[82] Glycosylation is also known to shift POPDC bands in Western blots to various extents. Figure 6.5 shows bands corresponding to complexes or aggregates containing POPDC2. A full blot is shown in Appendix 10.5, Figure 10.4. Although detailed quantification was not possible, the co-precipitation assay suggested that POPDC1-POPDC2 interactions were preserved with all POPDC variants tested. However, they appeared to be significantly reduced in the case of POPDC2 p.W188X suggesting that interactions are disfavoured by the loss of the POPDC2 residues downstream

of W188. It appeared that the POPDC1 p.R172H and p.V183F showed higher levels of interaction, but this was not as clear in a repeat blot.

6.3.3 Investigations into a Putative Site of Interaction Between POPDC1 and POPDC2

As discussed above, previous co-immunoprecipitation experiments have found that POPDC1 and POPDC2 proteins are able to interact with each other through both their N-terminal extracellular or transmembrane domains, as well as their cytoplasmic regions.[82,186] Similar results were also obtained for the interaction of POPDC1 and POPDC3. The precise location or nature of the different proposed interaction sites is not known. A region between residues 268-274 of POPDC1, just downstream of the Popeye domain, has been proposed to be involved in the formation of POPDC1 homodimers.[81] In Chapter 3 it was found that isolated Popeye domain sequences from mouse Popdc1, containing residues S109-K272 and E123-D266, were able to form homodimers. This suggests that a homomeric, intermolecular interaction between POPDC1 monomers can form between two Popeye domains. Given the high degree of conservation of the Popeye domain across the POPDC protein family it is possible that homo- and heteromeric Popeye domain mediated interactions also occur through a common mechanism.[26]

It was decided to inspect the sequence and predicted structures of the POPDC family to try and identify possible common interaction domains, particularly within the Popeye domain. The absence of an empirical structure of any POPDC proteins means that structural investigations are highly reliant on models, meaning caution must be taken when interpreting findings. Figure 6.6A-C shows the structures of human POPDC1, POPDC2 and POPDC3 as predicted by the AlphaFold program.[23,24] One feature that is common to all structures is the αC-helix of the Popeye domain, highlighted in red in Figure 6.6. This was thought to be a possible candidate for an intermolecular Popeye domain interaction site. Alternative secondary structure predictions, such as the JPred4 server accessed from with the JalView application, agreed with the likely propensity for helix formation at these sites.[151] To assess the sequence of these putative α-helices and the level of conservation in this region, multispecies alignments of the three members of the POPDC family were created using the Clustal Omega alignment algorithm,[217] with the results shown in Figure 6.6D. It is known that Popeye domains show high levels of conservation, particularly around the proposed cAMP binding site. Previous alignments of the POPDC family have focused on the putative PBC, specifically the FL/IDSPEW/F and FQVT/S motifs.[71] The sequence of the predicted αC-helix was found to also be highly conserved in individual POPDC isoforms and across the POPDC family, shown in Figure 6.6D. It was noted that the residues which showed the highest level of conservation across the three POPDC isoforms were a set of hydrophobic residues spaced between 3-4 residues apart, highlighted in red in Figure 6.6D. The level of conservation of these αC-helix hydrophobic residues, as well as some others, was actually

greater than the FL/IDSPEW/F and FQVT/S, which are thought to be defining features of the Popeye domain.[71] The high level of conservation suggests that these residues perform a key function and is common in important protein interface sites.[29] Furthermore, α-helix interfaces are common in PPIs.[28]

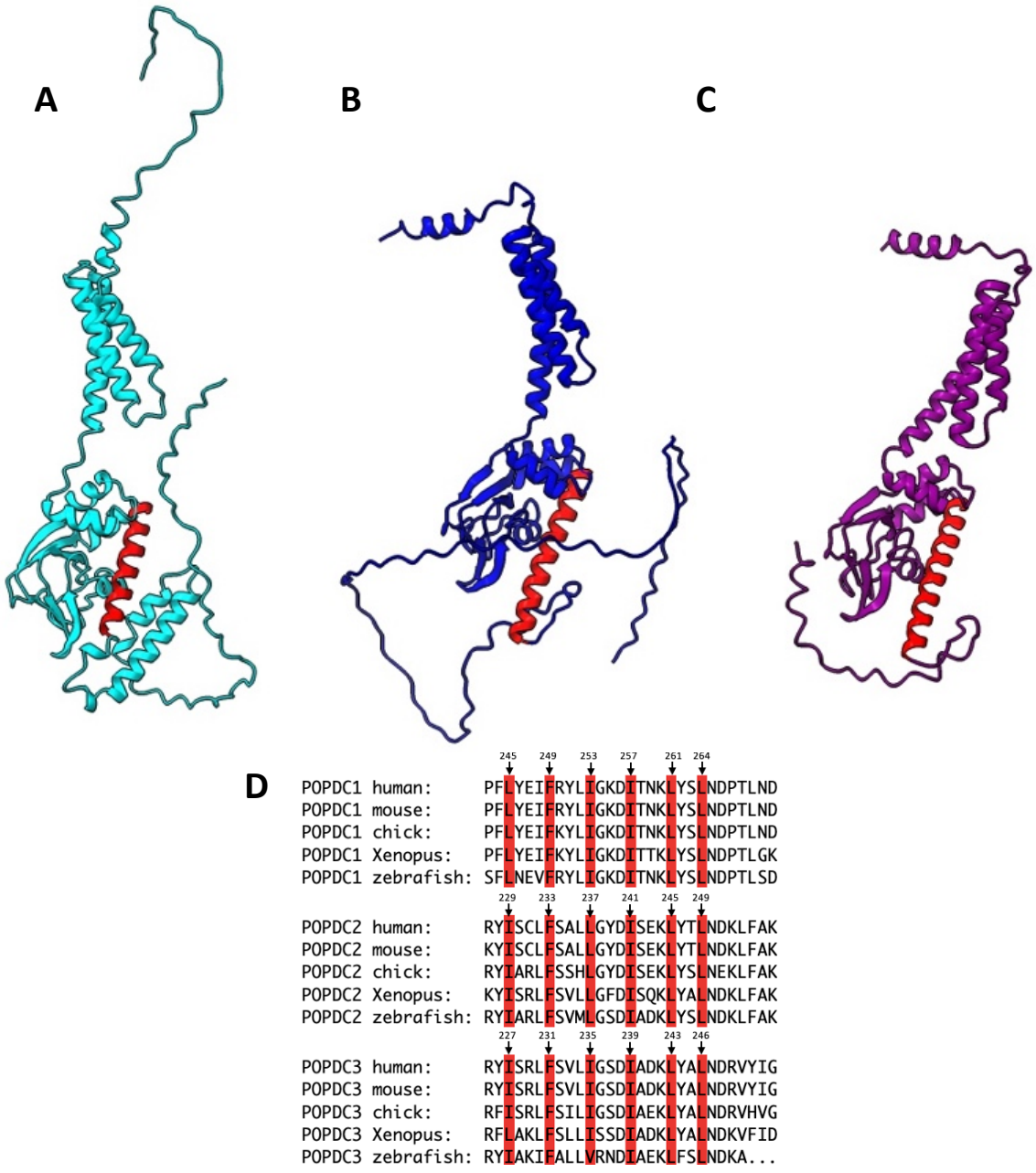


Figure 6.6: POPDC1, POPDC2 and POPDC3 all contain a Sequence of Highly Conserved Hydrophobic Residues with the Predicted αC-helix at the C-terminus of the Popeye Domain. The AlphaFold models of human POPDC1 **(A)**, POPDC2 **(B)** and POPDC3 **(C)**, with the predicted αC-helix highlighted in red. Aligning the amino acid sequences of POPDC1, POPDC2 and POPDC3 from multiple species shows high conservation and alignment of a set of hydrophobic amino acids within the αC-helix **(D)**. The highlighted residues in the human sequences are as follows: POPDC1 – L245, F249, I253, I257, L261 and L264; POPDC2 – I229, F233, L237, I241, L245 and L248; POPDC3 – I227, F231, I235, I239, L243 and L246.

Helix-helix interaction domains often show a heptad repeating pattern, with residues on the same face found at positions *i*, *i*+3 and *i*+7, due to the 3.7 residue per turn nature of α-helices.[218] The conserved αC-helix hydrophobic residues do not follow this typical pattern, mostly repeating every

four residues. This suggests that the face of the helix on which these residues will be found will shift along the sequence. Hydrophobic faces of helices are known to interact,[218] and it was proposed that some of these hydrophobic residues could be involved in the formation of a helix-helix interface between the Popeye domains of POPDC monomers.

The cAMP-binding CAP prokaryotic transcription factor, which possess just below 20% sequence identity to the Popeye domain, has been used as a template for the construction of Popeye domain homology models.[71,93] The relatively low sequence identity score of the CAP protein to Popeye domain significantly reduces the confidence in the accuracy of the models meaning caution should be exercised when interpreting any models produced.[18] CAP possesses an α-helix, known as the C-helix, at the C-terminal end of its CNBD, a classic feature of known CNBDs.[219] CAP monomers interact *via* the C-helix to form homodimers, with a roughly symmetric hydrophobic face of the C-helix forming the main interface (Figure 6.7A-C).[219,220] The C-helix is also involved in forming contacts with cAMP, which mediates an extension of the C-helix necessary for activation of CAP's DNA-binding function.[221] It was hypothesised that the Popeye domain could dimerise through a mechanism similar to CAP, in which the αC-helix of the Popeye domain would act in an analogous fashion to the C-helix of CAP.

Firstly, a partial alignment of the protein sequence of CAP and the Popeye domain of human POPDC1, POPDC2 and POPDC3 was created using the Clustal Omega algorithm (Figure 6.7G). This identified an alignment between the hydrophobic residues found in the C-helix of CAP, and those that are highly conserved in the αC-helix of the Popeye domain. A comparison between a previously reported crystal structure of CAP in its usual homo-dimeric form was then used as a template for Popeye domain monomers models from POPDC1 and POPDC2.[219] The AlphaFold structures of the Popeye domain of POPDC1 and POPDC2 were used, and each were fitted to one of the CAP monomers within the crystal structure using the Matchmaker tool within ChimeraX (Figure 6.7D). This created an artificial heteromeric Popeye domain dimer, with a pseudo symmetric alignment of the αC-helix in each Popeye domain monomer. The positions of the conserved hydrophobic residues highlighted in Figure 6.7E and F were examined. There was some overlap between the hydrophobic side chains of the CAP residues thought to be involved with dimerization and the Popeye domain hydrophobics. The *i*+4 pattern of the αC-helix hydrophobic residues suggests that not all of the conserved residues highlighted in Figure 6.7E and F will be involved in the interface, which is also thought to be the case in CAP.[219,221]

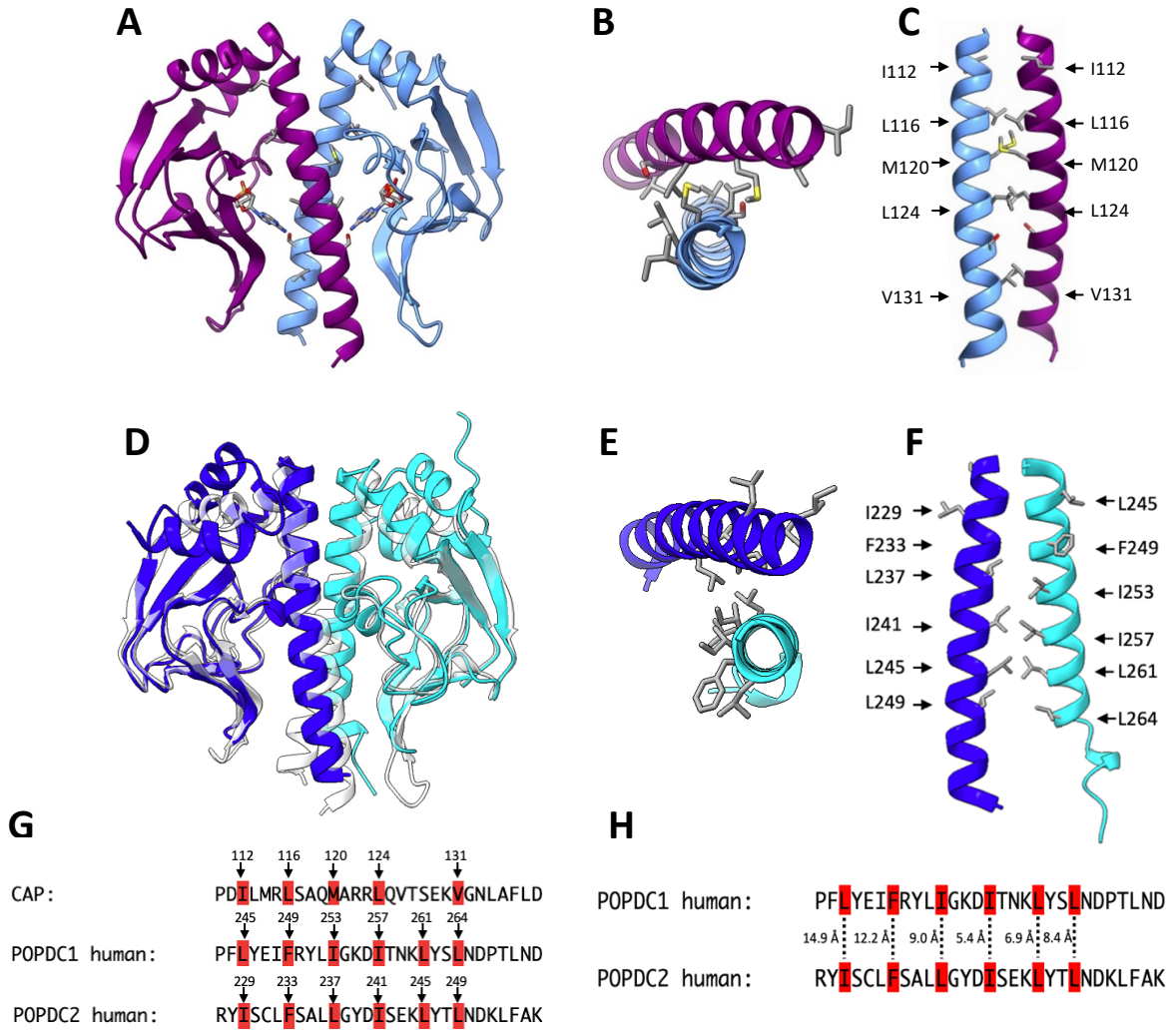


Figure 6.7: A Model POPDC1-POPDC2 Popeye Domain Dimer based on the Structure of CAP. A) The dimeric CNBD of CAP shown in the cAMP bound form (PDB: 1G6N). The C-helix, which mediates CAP monomer interactions as well as acting a lid for the cAMP binding site, is shown in **(B)** and **(C)**. The series of hydrophobic residues, aligned with those in the αC-helix of the Popeye domain are labelled in **(C)**. **D)** An overlay of the Popeye domain of POPDC1 and POPDC2 (taken from their respective AlphaFold structures) were overlayed with the CAP CNBD dimer, using the Matchmaker tool in ChimeraX, to produce an unrefined model of a heteromeric Popeye domain dimer. The artificial interface via the αC-helix is shown in **(E)** and **(F)**, with the highly conserved hydrophobic residues highlighted. **G)** An alignment of the C-helix and αC-helix of CAP (UniProt: P0ACJ8) and POPDC1 and POPDC2.The conserved and aligned hydrophobic residues are highlighted. **H)** The distance between the C_α atoms of the aligned hydrophobics in the artificial αC-helix interface.

The C_α atoms of the respective POPDC1 and POPDC2 aligned hydrophobics residues, were predicted to be closest to each other in the middle of the αC-helix sequences (Figure 6.7H). This suggests that residues in the middle of the proposed helix-helix interface are more likely to be important for dimer formation. This artificial dimer was only intended to be used as a rough guide and was not further optimised through minimisation or other techniques. Indeed, the side chains of the hydrophobic residues do not form an ideal interface, although they are within a reasonable proximity of each other. It should be noted that AlphaFold predicts the structure of proteins in the monomeric form and so this model dimer may not account for shifts in conformation that occur upon actual dimer formation. The hinge region immediately N-terminal to the αC-helix is normally highly flexible in CNBDs,[94] and

this may lead to greater uncertainty in the true orientation of the model helices. The reported confidence in the models of the Popeye domain also decreases significantly moving towards the C-terminal of the αC-helix. This could reflect an increased flexibility in the helix at the C-terminal end, which is seen in CAP until cAMP binding.[221] However, it appeared to be plausible that the side chains of some of the conserved hydrophobic residues could form an interface between Popeye domains. Such an interface would be almost symmetric, given the high level of conservation in the αC-helix region between POPDC1 and POPDC2. Proteins close in evolutionary space are known to be more likely to interact through analogous domains, which could be the case here.[26] It was decided to further investigate the importance of these residues and their possible role in POPDC1-POPDC2 complex formation.

6.3.4 Assessing the Importance of Conserved Hydrophobic Residues in the Popeye Domain for POPDC1 and POPDC2 Subcellular Expression in HEK293 Cells

If, as suggested in Chapter 5, an interaction between POPDC1 and POPDC2 is required for proper subcellular expression of both proteins to the plasma membrane, disrupting the proposed αC-helix interface could alter the localisation of POPDC proteins within cells. In the absence of methods with which to directly probe the Popeye domain structure and interfaces at the amino acid level, such as x-ray crystallography or protein-NMR, the HEK293 expression model could provide a proxy with which to test the effect of specific residues on the hypothesised Popeye domain interface. A series of mutations were made to the conserved αC-helix hydrophobic residues, highlighted in Figure 6.7, through site directed mutagenesis of the POPDC1-ECFP and POPDC2-EYFP used in HEK293 cells in Chapter 5. Each residue was switched in turn to an aspartic acid residue to introduce a repulsive negative charge into the putative hydrophobic core of the helix-helix interface. Insertion of aspartic acid has also been previously used to test the role of hydrophobic residues in helix-helix interfaces in other protein families.[60] To test the effect of the aspartic acid substitutions on POPDC1 and POPDC2 subcellular localisation, each αC-helix mutant protein was co-expressed with its wildtype partner in HEK293 cells and the expression and localisation of both proteins determined as before in Chapter 5. Each combination was compared to the result of the co-expression of wildtype POPDC1 and POPDC2 to assess if the specific mutations caused a change in POPDC1 or POPDC2 subcellular localisation.

A range of effects was found for each hydrophobic residue within POPDC1 and POPDC2. Within POPDC1 the L245D mutation, found at the N-terminal of the αC-helix, and L261D and L264D at the C-terminal end, showed no obvious visual changes in the distribution of the proteins in the cells (Figure 6.8A, E and F, respectively).

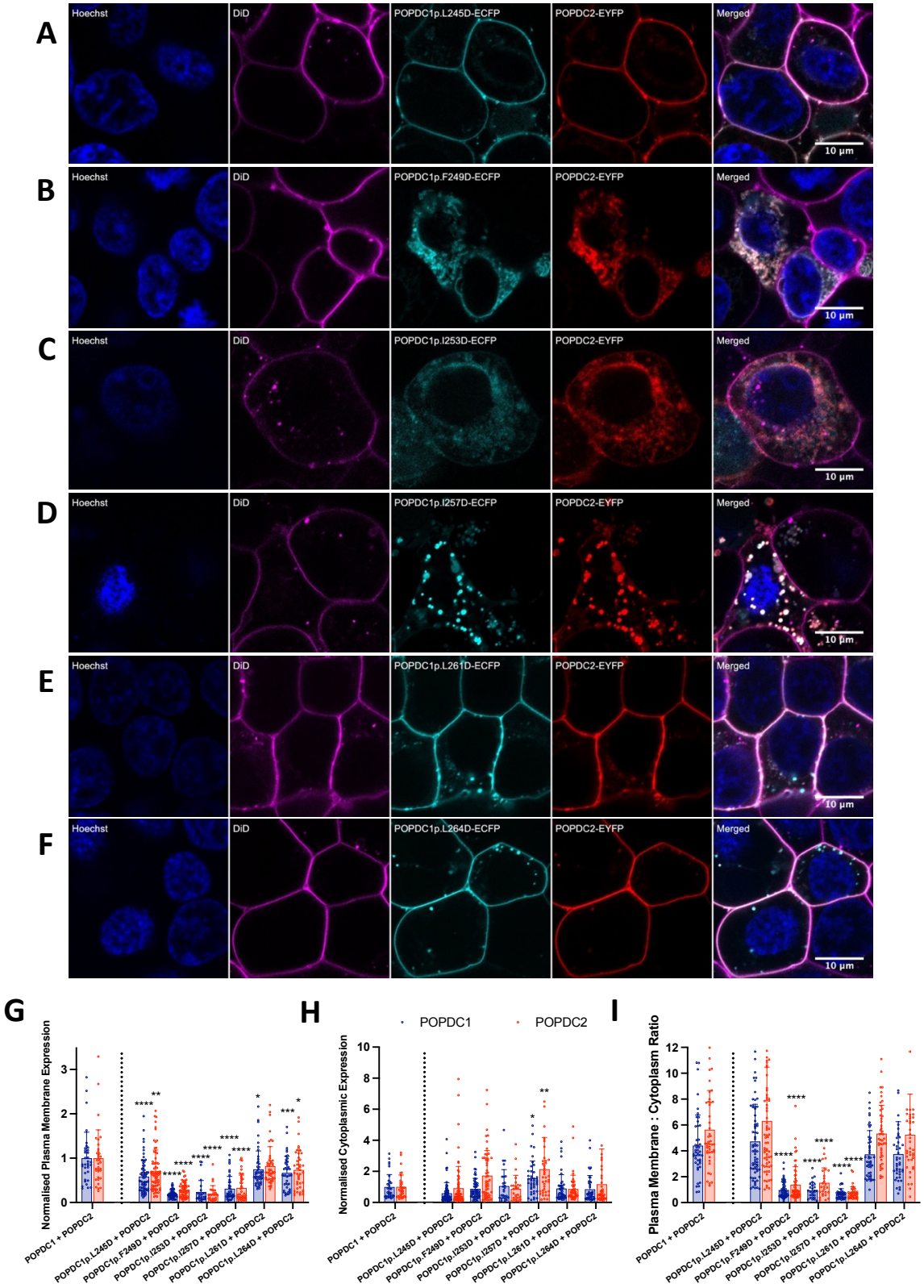


Figure 6.8: The Subcellular Expression of POPDC1 αC-helix Mutants and POPDC2 in HEK293 Cells. HEK293 cells expressing POPDC1 p.L245D-ECFP **(A)** (n = 71), POPDC1 p.F249D-ECFP **(B)** (n = 56), POPDC1 p.I253D-ECFP **(C)** (n = 27), POPDC1 p.I257D-ECFP **(D)** (n = 40), POPDC1 p.L261D-ECFP **(E)** (n = 47) and POPDC1 p.L264D-ECFP **(F)** (n = 42) with POPDC2-EYFP were imaged using confocal microscopy. The plasma membrane of cells was marked using DiD. The normalised level of plasma membrane **(G)** and cytoplasmic **(H)** expression of POPDC1 and POPDC2 was determined for each transfected cell imaged. The ratio of each isoform in the plasma membrane to cytoplasm was determined **(I)**. All values are shown normalised to wildtype POPDC1-ECFP + POPDC2-EYFP group. Groups were compared using one-way ANOVA followed by Dunnett's post-hoc test using the wildtype double expression group as the control. * p<0.05, ** p<0.005, *** p<0.001, **** p<0.0001. Error bars show SD. Summary data is provided in Appendix 10.3, Tables 10.17-28.

A clear plasma membrane signal from both proteins was observed, with minimal intracellular expression relative to the plasma membrane. No clear increase in the number of POPDC1 or POPDC2 aggregates was seen. Measurement of the ECFP and EYFP emission within the cells showed a mild drop in the plasma membrane levels of POPDC1 or POPDC2 of around 30-40% compared to wildtype, shown in Figure 6.8G. The cytoplasmic levels of both proteins were slightly reduced but not to a statistically significant extent (Figure 6.8H). The ratio of both proteins in the plasma membrane to cytoplasm, taken as a measure of the extent of localisation of each protein, was unchanged compared to the wildtype POPDC1 and POPDC2 pair (Figure 6.8I). In contrast, the aspartic acid substitutions within the middle of the helix, specifically F249D, I253D and I257D, showed a clear difference compared to wildtype expressing cells, as is evident from typical cells shown in Figure 6.8B, C and D, respectively. While some minimal plasma expression was retained there was a much stronger signal from within the cells. There was also a clear increase in the number of POPDC1 and POPDC2 puncta, particularly in the case of I257D, indicating a propensity for aggregation of both proteins. The drop in plasma membrane expression was found to be around 70-80% for both POPDC1 and POPDC2 (Figure 6.8G). Only minimal increases in the mean cytoplasmic concentration of POPDC1 and POPDC2 were observed, which were significant only for POPDC1 p.I257D (Figure 6.8H). However, the large drop in plasma membrane levels meant that the ratio of POPDC1 and POPDC2 at the plasma membrane to the cytoplasm was greatly reduced compared to wildtype cells (Figure 6.8I). Summary data is provided in Appendix 10.7, Tables 10.17-28.

The POPDC2 αC-helix mutations showed a similar pattern. The three middle residues in the sequence, F233, L237 and I241, showed the greatest changes in POPDC1 and POPDC2 after being substituted with aspartic acid, as shown in Figure 6.9B, C and D, respectively. Raised intracellular expression was seen with the three mutants, with a particular increase in puncta, presumed to show POPDC protein aggregates, as in the case of I241D. There was a drop in the levels of POPDC1 and POPDC2 at the plasma membrane after the insertion of aspartic acid at each of these positions, with a very large reduction for I241D (Figure 6.9G). Meanwhile there was a variety of effects on cytoplasmic levels for each mutation and between POPDC1 and POPDC2 (Figure 6.9H). Less clear changes in the expression pattern of the proteins were present when the N- and C-terminal αC-helix residues were mutated, with representative cells shown in Figure 6.9A, E and F, respectively. No change in the plasma membrane levels of POPDC1 or POPDC2 were observed and only a mild increase in cytoplasmic POPDC2 for I229D (Figure 6.9G and H). Reductions in the plasma membrane to cytoplasm ratio in both proteins were seen in all cases other than POPDC2 p.L245D, as shown in Figure 6.9I.

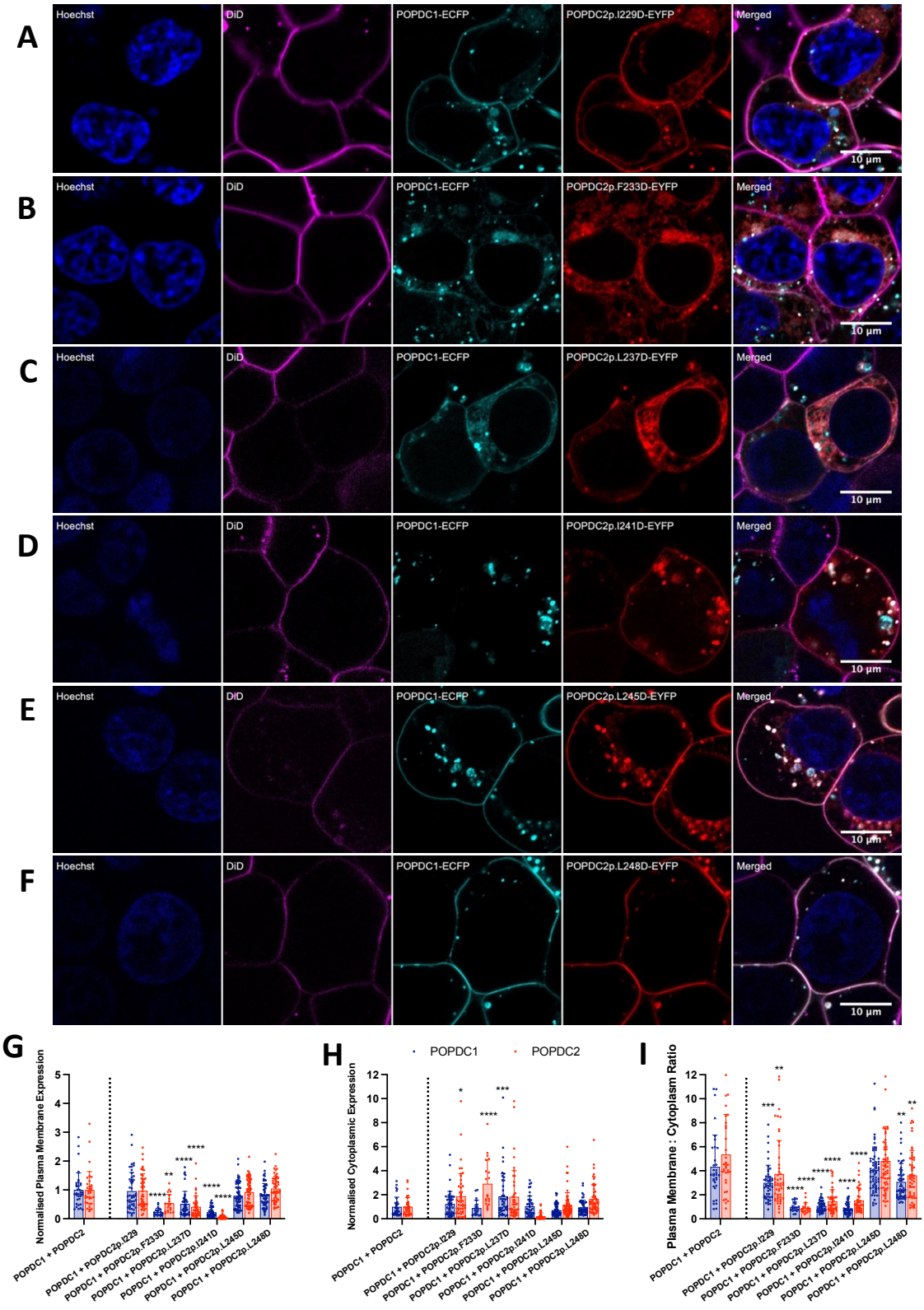


Figure 6.9: The Subcellular Expression of POPDC1 and POPDC2 αC-helix Mutants in HEK293 Cells. HEK293 cells expressing POPDC2 p.I229D-EYFP **(A)** (n = 48), POPDC2 p.F233D-EYFP **(B)** (n = 20), POPDC2 p.L237D-EYFP **(C)** (n = 45), POPDC2 p.I241D-EYFP **(D)** (n = 42), POPDC2 p.L245D-EYFP **(E)** (n = 63) and POPDC2 p.L248D-EYFP **(F)** (n = 56) with POPDC1-ECFP were imaged using confocal microscopy. The plasma membrane of cells was marked using DiD. The normalised level of plasma membrane **(G)** and cytoplasmic **(H)** expression of POPDC1 and POPDC2 was determined for each transfected cell imaged. The ratio of each isoform in the plasma membrane to cytoplasm was determined **(I)**. All values are shown normalised to wildtype POPDC1-ECFP + POPDC2-EYFP cells. Groups were compared using one-way ANOVA followed by Dunnett's post-hoc test using the wildtype double expression group as the control. * p<0.05, ** p<0.005, *** p<0.001, **** p<0.0001. Error bars show SD. Summary data is provided in Appendix 10.3, Tables 10.29-40.

However, the changes were much more severe for the F233D, L237D and I241D mutations. In this respect the results for POPDC1 and POPDC2 matched. The middle three of the conserved hydrophobic residues of the αC-helix were most sensitive to mutation (F249, I253 and I257 for POPDC1; F233, L237 and I241 for POPDC2), whereas peripheral residues were more tolerant of the aspartic acid substitution. The sensitivity of the residues to mutation correlates with their alignment in the sequences of POPDC1 and POPDC2 (Figure 6.6D). These residues are also spatially matched in the model of the Popeye domain dimeric interface based on the CAP protein dimer (Figure 6.7D, E and F). This suggests that these residues perform similar functions in both proteins. A symmetrical interaction between these residues that mediates POPDC1 and POPDC2 expression and/or trafficking would be consistent with this hypothesis. For some of mutations towards the termini of the helices, there was an apparent increase in intracellular puncta of POPDC1 and POPDC2 that was not shown in the mean changes in cytoplasmic expression levels, indicating that the introduction of aspartic acid at these sites was not completely tolerated.

6.3.5 A Possible Mechanism for how POPDC1-POPDC2 Complexation Controls Expression and Trafficking

The mutagenesis and modelling results provide a possible novel interface between POPDC1 and POPDC2. However, the reason why the formation of such an interface is required for normal localisation of both proteins is not clear. One possibility is that an interaction is required for the release of the proteins from the ER.[51] The distribution of POPDC1 and POPDC2 in the HEK293 cells in the presence of some of the clinical αC-helix mutations could be consistent with ER retention in some cases, although this was not examined through the use of ER markers. A different pattern was seen in some cases, which was more consistent with aggregation than endoplasmic reticulum localisation.

Inspection of the sequences of the POPDC proteins revealed a number of residues that may function as ER retention motifs. These included the KKXX motif, which can function as an endoplasmic retention signal when found in the cytoplasmic tails of transmembrane proteins.[222,223] The di-arginine motif RXR, also present in POPDC sequences, is known to function as an ER retention motif.[224] Additionally, a tyrosine based YXXϕ sequence, where ϕ is any bulky hydrophobic residue, associated with mediation of interactions with clathrin adapter proteins complexes, which are involved in regulating vesicular transport of transmembrane proteins,[225] is found at multiple points in the sequence of POPDC proteins. The sites of these three motifs within the monomeric AlphaFold models of POPDC1, POPDC2 and POPDC3 are shown in Figure 6.10A, B and C, respectively. Not all of the sequences that satisfy the general form of ER retention motifs will function as such. However, the models of POPDC proteins predict that some of these sequences are proximal to the proposed Popeye domain dimerization helical interface, as shown in Figure 6.10D-F. Two KKXX motifs in POPDC1 are found immediately C-

terminal of the αC-helix. A YXXL/M/V/I/F motif is found in close proximity to the N-terminus of the αC-helix of all three POPDC isoforms, part of a separate small α-helix. RXR motifs are also found within the Popeye domains of POPDC1 and POPDC2. It could be that when dimerization occurs through the αC-helix interface, it leads to shielding of these retention and trafficking signals. If this interaction is disrupted it could lead to retention of the proteins with the ER, followed by degradation.[55,63] This could explain the loss of normal POPDC expression in tissue and HEK293 cells expressing POPDC mutants.

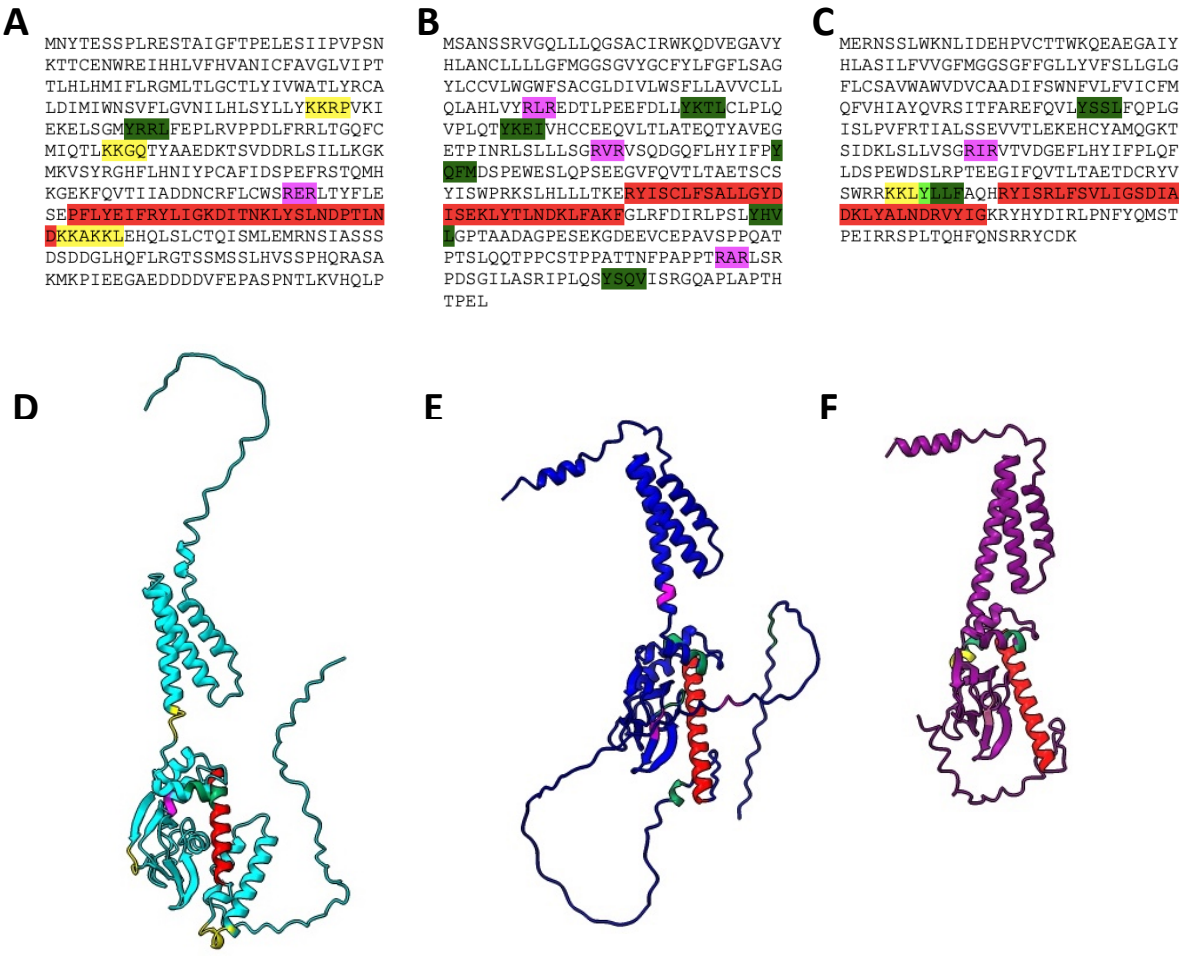


Figure 6.10: POPDC Protein Trafficking to the Plasma Membrane may be controlled by Endoplasmic Reticulum Retention and Adaptor Protein Interaction Signals. The sequence of human POPDC1 **(A)**, POPDC2 **(B)** and POPDC3 **(C)** contains a number of motifs that satisfy the general criteria of the RXR (pink) and KKXX (yellow) endoplasmic retention signals. In addition, several tyrosine containing YXXL/M/V/I/F motifs are present which may be involved in the interaction with adapter proteins. The sequence of the αC-helix is highlighted red. The AlphaFold structures of each protein, POPDC1 **(D)**, POPDC2 **(E)** and POPDC3 **(F)**, predict that a YXXL/M/V/I/F motif (green) is present in a small helical domain in close proximity to the αC-helix (red) that may be involved in Popeye domain interactions. In addition, two possible KKXX motifs (yellow) are found immediately downstream of this α-helix in POPDC1, with a further YXXL/M/V/I/F sequence downstream of the α-helix in POPDC2 (green). KXR motifs are shown in pink

6.3.6 The Putative αC-helix may also be involved in Popeye Domain cAMP Binding

As well as mediating dimerization of the CAP protein, the C-helix acts as a lid for the cAMP binding pocket,[221] a common feature of cyclic nucleotide binding domains.[94] The C-helix of CAP forms H-bonds with cAMP, possibly *via* water molecules, as well as forming hydrophobic interactions with the

adenine base.[219] In CAP, the binding of cAMP stabilises the C-terminal region of the C-helix. In the cAMP-unbound apo-CAP, this part of the helix is partly or fully unfolded, only gaining conformational stability in the presence of cAMP. This conformational change is responsible for the cAMP-dependent activation of CAP, leading to enhanced DNA binding. The C-helix does not need to be in the cAMP-bound state for dimerization to occur, which is mediated by residues upstream of the cAMP binding site of the C-helix.[221] It is possible that the αC-helix is involved in cAMP binding to the Popeye domain as well as POPDC interactions.

In CAP an adjacent threonine and serine (T127 and S128) within the C-helix each form one H-bond with one of the two cAMP molecules bound to the dimer, as shown in Figure 6.11B.[219] T127 in CAP is aligned with a super-conserved lysine residue in the POPDC proteins (K260, K244 in POPDC1 and POPDC2, respectively), whereas CAP S128 is aligned with L261 and L245 in POPDC1 and POPDC2, respectively, as shown in Figure 6.7A. This is the only place where the αC-helix hydrophobic residues do not align with another hydrophobic amino acid in CAP. This could suggest a distinct mode of cAMP binding between these two protein families, although a lysine could mimic the H-bond donor properties of T127 in CAP and so be performing a similar function. Models of the Popeye domain from the AlphaFold database or other modelling programs are monomeric. The Popeye domain artificial dimer shown in Figure 6.7D-F, if at all accurate, would be unable to replicate the conformational changes that occur in cAMP binding without detailed modelling. Determining the mode of cAMP binding from Popeye domain models alone is uncertain, especially if a dimeric binding mechanism is present such as in CAP. However, attempts to run docking experiments using homology models of the Popeye domain have been made.[71] Previous experiments focused on the identification of the PBC, those residues in the binding pocket that make contact with the phosphate group of cAMP. Minimal comment was made on any possible contribution of the αC-helix to cAMP binding. The AlphaFold structures of the POPDC proteins predict that K260 and K244 of POPDC1 and POPDC2, respectively, face into the putative cAMP binding pocket of the Popeye domain, shown in Figure 6.11D and E. This could mean that the lysine residue in each POPDC isoform mimics the function of T127 in CAP to form H-bonds with the adenine base of cAMP. A prediction of the cAMP binding mode to the Popeye domain of POPDC1 was made using the Phyre2 and 3DLigandSite servers, shown in Figure 6.11 C and D.[150,226] This prediction agreed with the previously proposed site of the PBC. It also suggested close contacts between K260 of the αC-helix, and also L264, with the adenine base. Both these residues are shown in Figure 6.11 C and D. While this model was not refined further it suggests that these side chains are involved in the formation H-bonds and hydrophobic interactions, respectively, with cAMP. Interestingly, the AlphaFold models of POPDC1 contain an H-bond between K260 and the hydroxyl group of S201 in the PBC, with equivalent interactions occurring in the POPDC2 and POPDC3 models.

In addition, the super conserved D256, found one turn above K260 in the αC-helix, forms a similar interaction. The predicted H-bond network is shown for POPDC1 in Figure 6.11E. The formation of such H-bonds could be involved in the positioning and stabilisation of the αC-helix and/or controlling the equilibrium between the cAMP-bound and unbound states. The uncertainty in the AlphaFold models, and its presentation in the cAMP unbound apo-form, means that detailed understanding of the mode of cAMP binding to the Popeye domain will require empirical studies, which are currently not yet available for POPDC proteins.

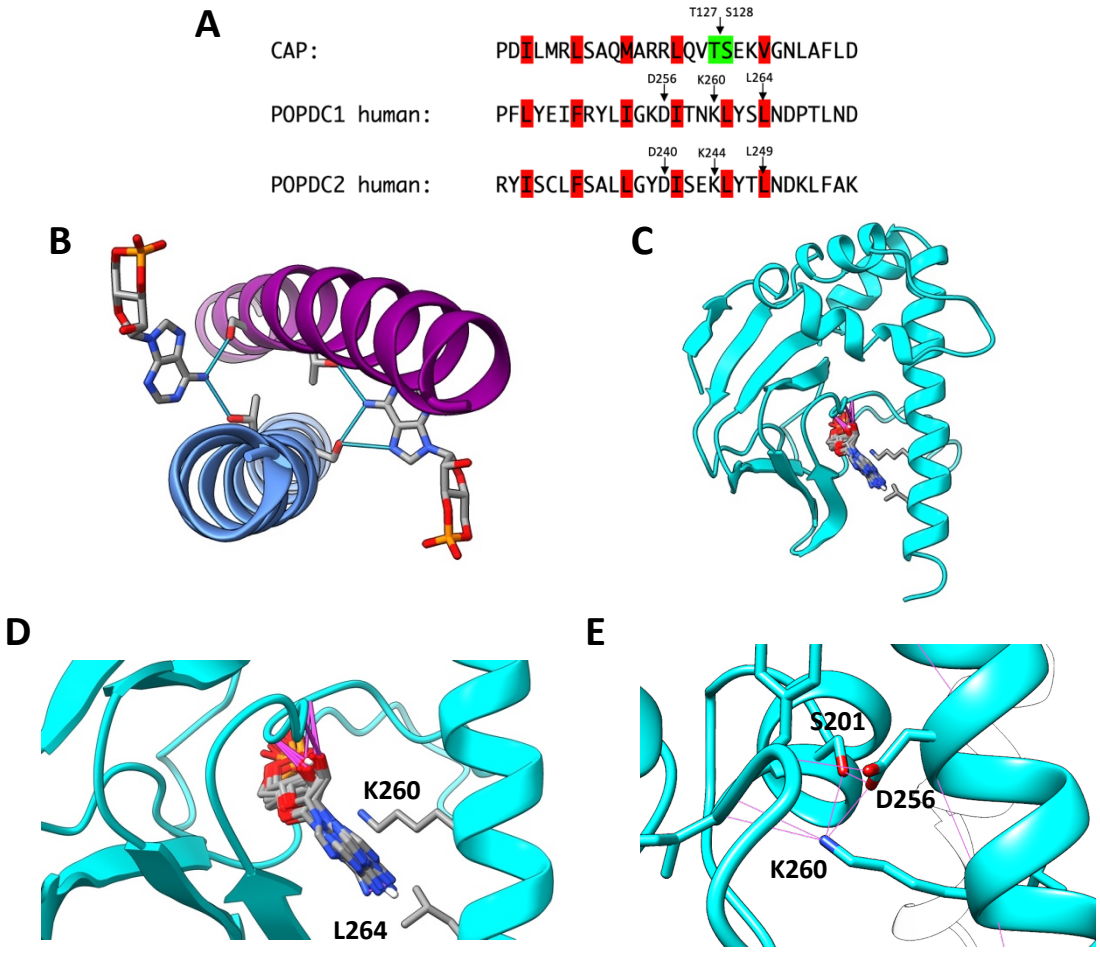


Figure 6.11: The Mode of cAMP Binding to CAP and a Possible Interactions between cAMP and the αC-helix of the Popeye Domain. **A)** An alignment of CAP and POPDC1 and POPDC2 sequences highlighting residues that may be involved in cAMP binding and/or intramolecular H-bonding. **B)** The binding of cAMP to the C-helices of a CAP dimer (PDB = 1G6N). **C)** The predicted bindings modes of cAMP to the Popeye domain of POPDC2 made by the Phyre2 and 3DLigandSite servers, with a zoomed version shown in **(D)**. The side chains of K260 and L264 are predicted to face into the cAMP binding pocket. **E)** The AlphaFold model of POPDC1, which has no cAMP present, predicts the formation of intramolecular H-bonds between the αC-helix and the PBC of the Popeye domain.

6.4 Discussion

6.4.1 POPDC1 and POPDC2 Form Heteromeric Complexes

It had previously been suggested that POPDC1 and POPDC2 form a complex.[82,186] The HEK293 cell expression experiments, reported in Chapter 5, provided evidence for the importance of the presumptive POPDC1-POPDC2 complexes. The qBRET experiments provided details on the stoichiometry of the interaction between POPDC1 and POPDC2, with POPDC1-POPDC2 dimers predicted to form in cells. Other higher order oligomeric complexes may be present in lower amounts, with some evidence previously reported from Western blots.[82] Here qBRET also found that POPDC1 is capable of forming homodimers, while the POPDC2 qBRET curves resembled higher order homomeric complexes, although this needs to be confirmed given the weaknesses of the type-1 qBRET protocol for detecting higher order complexes. The observed behaviour of POPDC1 and POPDC2 in HEK293 cells when expressed alone (see Chapter 5) also mean that the qBRET results seen in these cases may not resemble native interactions. If POPDC homomeric and heteromeric complexes are possible there will be an equilibrium between the different states when both proteins are expressed together. The robust heterodimer signal in the qBRET assay demonstrates that POPDC1 and POPDC2 can overcome the tendency to form homo-interactions and form significant levels of heterodimers. This preference for heteromeric interactions is supported by the almost complete rescue of plasma membrane trafficking upon co-expression of the two proteins witnessed in Chapter 5.

6.4.2 POPDC Proteins may Interact through their αC-Helix which could be required for Correct Subcellular Expression

This work provides evidence that POPDC proteins are able to interact *via* their Popeye domains, and that such interactions are required for normal processing. The finding that isolated Popeye domains were able to form dimers (see Chapter 3) directed the search for intermolecular interaction sites to this area. The absence of an empirical structure of monomeric or complexed POPDC proteins meant that the structure of the CAP protein, a previously used template for Popeye domain modelling,[71,93] was used to provide an initial template on which Popeye domain interactions could be modelled. Alignments of the sequences of the POPDC proteins revealed a set of super conserved hydrophobic residues within the αC-helix of the Popeye domain, which had not previously been examined in detail. It was found that there was a high degree of alignment between these residues and those involved in the hydrophobic interactions involved in CAP helix-helix dimerization. The hypothesis that these hydrophobic residues are involved in POPDC1-POPDC2 interactions was supported by the finding that mutating some of these residues removed the synergistic effect of co-expressing POPDC1 and POPDC2 in HEK293 cells. The rescue of plasma membrane localisation of both isoforms when expressed together in HEK293 cells was lost when several of these αC-helix residues in either POPDC1 or POPDC2 were substituted with aspartic acid.

The residues whose mutation was found to cause the most severe disruption of POPDC expression and trafficking were those in the core of the modelled αC-helix, with the residues towards the N- and C-termini more tolerant of the introduction of aspartic acid. This could be because these core residues are those that form the most important contacts with the opposing αC-helix and so are most important for dimerization. These residues are aligned with the region of the CAP C-helix that is in the helical form in both the cAMP-bound and unbound states, and so are responsible for CAP dimerization. Meanwhile the C-terminal residues found to be tolerant of mutation in the αC-helices are aligned to the region of the CAP C-helix containing T127 and S128, which is only stabilised once these residues bind to cAMP.[219] This could indicate a more important role for Popeye domain complexation in POPDC protein expression and trafficking, compared to cAMP binding. Changes in the POPDC1-POPDC2 interaction in response to raised cAMP concentrations in cells were not detected using qBRET experiments (Chapter 4). It could be that dimerization is a prerequisite of cAMP binding to Popeye domains, as the position and stability of the helices are likely to alter their performance as lids for the CNBD. This could explain the effects of the POPDC1 p.S201F mutation, known to show reduced cAMP affinity, shown in Chapter 5. In CAP, dimerization is required for proper cAMP binding due to the role of adjacent threonine and serine residues, although this may not be relevant for the Popeye domain.[219]

A more subtle site directed mutagenesis strategy using alanine scanning, without the introduction of the destructive negative charge of aspartic acid, might give more insight into the individual and summative contribution of each residue to the formation of the interface.[227] Other αC-helix residues should be examined through site directed mutagenesis as above, which could help uncover if the localisation defects are specific to changes in the hydrophobic residues. The changes in Popeye domain stability and structure in the presence of these mutations was not examined. It could be that the negative charges introduced through the aspartic acid substitutions caused a general destabilisation of the Popeye domain, which indirectly led to a loss of Popeye domain interactions and/or subcellular localisation. Mutations near interfaces are more likely to have allosteric effects on the protein.[228] A means of selectively disrupting POPDC oligomerisation within cells, without the unknown effects of the mutations, such as a disrupting peptide targeted to the αC-helix, or other domains, could be used instead of mutagenesis.[229] This approach has been applied to interaction of POPDC1 and PDE4A.[100]

The high degree of conservation of the αC-helix, and the symmetric effects of the aspartic acid mutations in aligned residues, could mean that αC-helix interfaces could form between Popeye domains from the same POPDC isoform. POPDC1 homo-dimerization has previously been reported,[81]

which this work confirmed along with the finding that POPDC2 may be able to form higher order complexes. In Chapter 3 Popdc1 Popeye domain constructs were found to dimerise. Perhaps this was due to the formation of a homomeric αC-helix interface. If this was the case, the preference for POPDC1-POPDC2 heteromers shown in the qBRET assay, and clear effects of POPDC1 and POPDC2 co-expression, may be influenced by other domains of the protein. It is thought that POPDC proteins can form interactions between both their extracellular N-termini and/or transmembrane domains as well as the cytoplasmic region where the Popeye domain is found.[73] [81,82] It could be that the preferential heteromeric complexes of POPDC proteins are favoured as a result of N-termini or transmembrane domain interactions, which is common in other transmembrane proteins.[230] The proposed Popeye domain interface may not dictate the preference for heteromeric interactions, but could instead be required for correct complex processing and localisation to the plasma membrane. This model of POPDC1-POPDC2 interactions is illustrated in Figure 6.12.

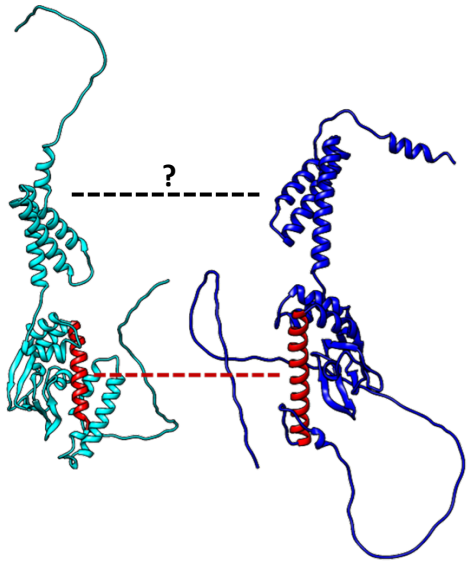


Figure 6.12: A Working Model for POPDC Protein Interactions. It is proposed that POPDC1 (cyan) and POPDC2 (blue) interact through their αC-helices, which controls their subcellular expression. In addition, an interaction(s) also likely occurs within the N-termini and/or transmembrane domains of the proteins.

Interactions between transmembrane domains can be required for trafficking of protein complexes. It has long been known that the T-cell antigen receptor complex, which contains eight transmembrane subunits from six different isoforms, is retained in the ER unless the complex is fully formed.[56] Interactions between the transmembrane subunits are essential for release from the ER. Retention of the complex in the ER leads to ER-associated degradation of the protein.[231] It could be that proper interactions between the transmembrane domains of the POPDC proteins are also required for normal processing, perhaps through the shielding of polar or charged residues, which are known to contribute to retention in the ER if exposed.[232] Extracellular domain interactions between the N-termini of POPDC

could also influence their localisation. These are known to be involved in the formation of the sarcoglycan complex, the construction of which is essential for correct trafficking of the different sarcoglycan subunits to the sarcolemma.[233]

From the evidence gathered above it appears that the interactions of the Popeye domain must be present to allow for correct trafficking of the POPDC1-POPDC2 complex. There is precedent for such a mechanism, for example the $GABA_B$ receptors require heterodimerisation of $GABA_B$ receptor 1 and $GABA_B$ receptor 2 for proper trafficking of both proteins from the ER to the plasma membrane.[57,58] These proteins interact through a cytoplasmic coiled-coiled helical interface formed of hydrophobic residues. Additional transmembrane interactions between the proteins are also present. An ER retention signal motif is positioned at the C-terminus of the interaction helix $GABA_B$ receptor 1. If this helix-helix interaction does not occur, $GABA_B$ receptor 1 is not trafficked to the plasma membrane. Formation of this interface leads to shielding of the retention motif, allowing proper trafficking of the heterodimer to the cell surface.[60] Substitution of hydrophobic residues in these helical domains with aspartic led to trafficking defects in $GABA_B$ receptor 1 in model cells. Given the proximity of the various candidate ER retention motifs to the proposed αC-helix interface, shown in Figure 6.10, this could provide a working model for the behaviour of POPDC proteins. The suggestion that intermolecular Popeye domain interactions are needed for trafficking to the plasma membrane due to the steric block of ER retention motifs could be tested in the HEK293 setup. Mutation of the possible retention motifs could be performed and their effects on the trafficking of POPDC1 and POPDC2 alone or together examined. This would provide empirical evidence that this working model is accurate. The retention of POPDC proteins in the ER may have led to some of the effects seen in the skeletal muscle, with retained protein being degraded within the ER.[55,63] In HEK293 cells, raised intracellular levels of protein were often seen, including aggregates. This may suggest that the overexpression of POPDC proteins unable to form the necessary interactions to allow trafficking to the plasma membrane led to an accumulation in the ER and were not efficiently cleared by the cell.[234] Such differences in the processing of dysfunctional protein is known between native tissue and overexpression systems.[235] The actual mechanisms behind the observed effects of the studied mutations on POPDC protein processing will need to be determined in the future.

The POPDC proteins are known to interact with a wide range of other protein types.[100 71,72,101,119] It is possible that these PPIs also influence the interactions between the members of the POPDC family in native tissue. This could provide an explanation of how POPDC proteins are normally expressed in different tissue despite the POPDC isoforms being expressed at different amounts.[65,67]

6.4.3 Some POPDC Mutations Identified in Patients may cause Partial Disruption of POPDC1-POPDC2 Complexes

This work aimed to establish whether the presence of clinically identified mutations of POPDC proteins led to a change in POPDC1-POPDC2 complex formation. This was tested through AP-FRET, BiFC and Co-IP assays. Unfortunately, the results of these assays were not fully conclusive. The poor performance of the AP-FRET, particularly the high variability in results across the POPDC and control groups, meant no firm conclusions could be drawn from this assay, despite no significant change between the wildtype POPDC pair and the mutants being detected. BiFC suggested that interactions are retained in all cases but vary in their favourability. The HEK293 trafficking competent variants showed high BiFC signals, alongside wildtype POPDC1 and POPDC2, while the trafficking deficient variants showed reduced signals. The BiFC results suggest that changes in the POPDC1-POPDC2 complex, but not a complete loss, occurred in response to some mutations and this correlated with subcellular expression behaviour. The Co-IP assay also showed changes in, but not full abolition of, the POPDC1-POPDC2 complex. However, the issues with fragmentation and aggregation of the POPDC constructs made interpretation of the results difficult.

The clinically relevant POPDC variants can be grouped according to the results of HEK293 trafficking model completed in Chapter 5: those that severally disrupted the subcellular expression of both POPDC proteins, and mutations that showed no or little difference to wildtype POPDC proteins. If the proposed αC-helix is the key interface site for controlling POPDC trafficking, the location of the mutations within each POPDC variant could explain the differing behaviour of the variants in HEK293 cells and native tissue. Figure 6.13 highlights the positions of all mutations in models of monomer POPDC1 and POPDC2 studied in this work, grouped by type and their observed behaviour.

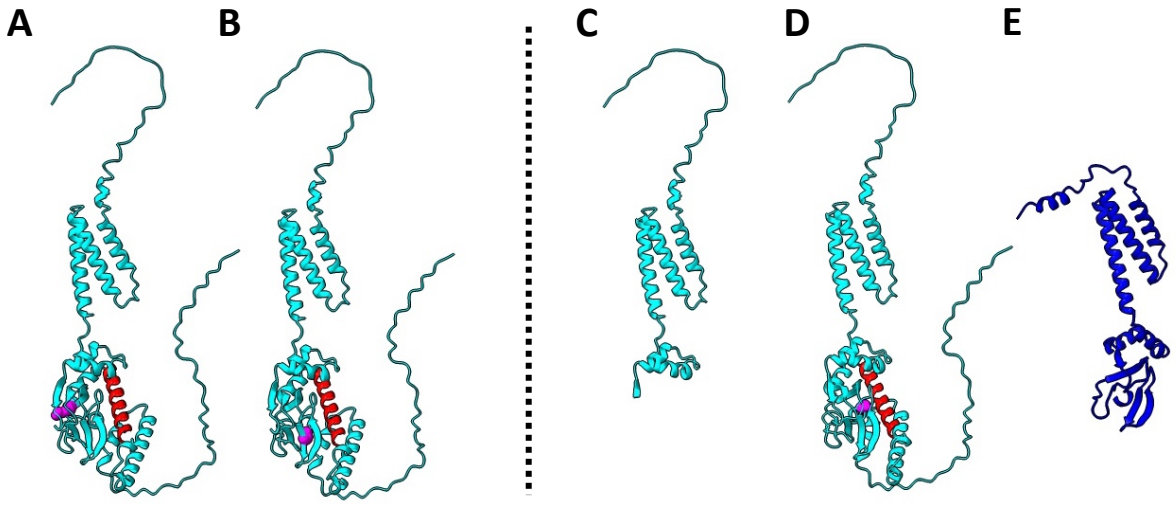


Figure 6.13: The Modified AlphaFold Structures of the Clinically Identified POPDC Mutations and their Relation to the αC-helix. The modelled structures of the POPDC1 p.R172H **(A)**, p.V183F **(B)**, p.Q153X **(C)**, p.S201F **(D)** and POPDC2 p.W188X **(E)** variants. The αC-helix is coloured red where present. The site of missense substitution mutations are highlighted in pink. The structures are grouped by their effect on POPDC1 and POPDC2 plasma membrane localisation in HEK293 cells.

Of the three variants that showed large changes in POPDC behaviour in HEK293 cells, two have a direct effect on the αC-helix, which is completely lost in the POPDC1 p.Q153X and POPDC2 p.W188X (Figure 6.13C and E). The other trafficking defective mutation, POPDC1 p.S201F, does not fall within αC-helix (Figure 6.18D). However, the affected residue is in very close proximity to this helix and is even predicted to form a H-bond with K260 of the αC-helix motif of the helix (Figure 6.11E). This variant has also been shown to reduce the affinity of cAMP binding to the Popeye domain. Based on the workings of the CAP proteins, binding of cAMP could influence the conformation and stability of the αC-helix.[219] The trafficking competent variants, POPDC1 p.R172H and p.V183F, contain point mutations at sites distal to the αC-helix (Figure 6.13A and B). The finding that these mutations do not directly interfere with the trafficking of both POPDC isoforms is consistent with a model in which the movement of POPDC1-POPDC2 complexes to the plasma membrane is mediated by an interface at the αC-helix.

This is only a subset of the known pathological POPDC protein mutations found in patients. Further investigations into the full set of known mutations, as well as those yet to be discovered, in patient biopsy material and the HEK293 model are required to determine if the trend between the location of mutations relative to the αC-helix and expression/trafficking behaviour is maintained. This will assist in the refinement of this model for the role of POPDC1-POPDC2 complex disruption in the pathology of POPDC mutations.

It should also be noted that the tested mutations may have caused a more general destabilisation of the structure of the Popeye domain, which could have led to the changes seen, instead of a specific

effect on POPDC1-POPDC2 complex formation. The effect of these mutations was only tested with respect to protein expression and trafficking in skeletal muscle and/or HEK293 cells, meaning that data on any changes in protein structure was not available.

7 POPDC2 is a Candidate Gene for Congenital Ectopic Tachycardia

7.1 Introduction

Junctional ectopic tachycardia (JET) is a form of tachycardia affecting the AV node and His bundle.[236] While the mechanism is not well understood, it is linked to increased automaticity of the AV node leading to very high heart rates and a dissociation of the electrical activation of the atrial and ventricular chambers. It is most often observed post-cardiac surgery, possibly due to damage around the AV node.[236] Congenital JET (cJET) is an extremely rare cardiac arrhythmia that is not caused by surgery, but is a genetic disease and usually occurs in infants within the first six months of life.[237] It used to be associated with a high mortality but recent progress in pharmacological treatment has improved the survival rate of affected patients. Mutations in the troponin I-interacting kinase gene, *TNNI3K*, have been linked to cJET.[238,239] However, it is uncertain how the disruption of these genes leads to JET and other factors may be involved.

Recently, a family was identified in which the father and three children displayed a cJET phenotype.[145] Exome sequencing across the family was carried out to try and identify a possible cJET causing gene variants using the Exomiser programme. Exomiser uses known associations of gene variants with disease, the predicted impact on the function of a protein, evolutionary conservation, known interactome, variant population frequencies, and any available animal model data to make predictions for the pathogenicity of gene variants across an individual's exome.[146] Identified variants were prioritised based on the value of the Exomiser generated score and the manual assessment of a gene's likely involvement in cJET. Interestingly, no variants in the *TNNI3K* gene were identified. However, a heterozygous *POPDC2* (c.734T>C; p.L245P) variant was found in all affected family members (Figure 7.1). Indeed, this variant was the only one identified that had an Exomiser score > 0.80, used as a priority cut-off score, and was present in all affected family members.[146] A pedigree of the family is shown in Figure 7.1.

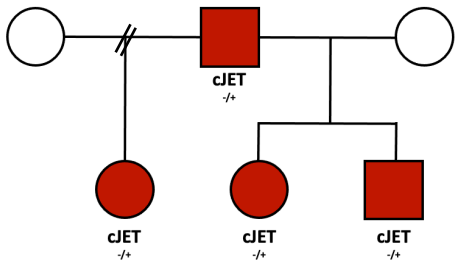


Figure 7.1: A Family Pedigree of a Family with Members who have displayed a cJET Phenotype, with respect to the *POPDC2* p.L245P Variant. Family pedigree of a family with members who have displayed a cJET phenotype. All affected patients, shown in red, possessed the heterozygous *POPDC2* p.L245P variant.

For some previously identified POPDC mutations, skeletal muscle or heart biopsy have been used to assess any changes in POPDC expression in tissue, including those mutations investigated in Chapter 5.[93,117,122] Biopsy material from the affected tissue, specifically the heart, was not available meaning that determination of any changes in expression or subcellular location of POPDC2 within cardiomyocytes was not possible. Although *POPDC2* has been suggested as a causative gene for cardiac conduction disorders,[105] a POPDC2 p.L245P mutation has not previously been reported in patients, nor been examined through the use of *in vitro* or *in vivo* animal models. In addition, cJET has not been previously linked with the POPDC genes. It was, therefore, desirable to obtain further empirical evidence to help determine if POPDC2 could be a cJET candidate gene and to specifically investigate the properties of the POPDC2 p.L245P variant.

7.2 Outline of Work and Aims

7.2.1 Description of this Work

After a family suffering from cJET was found to carry a heterozygous POPDC2 p.L245P mutation, attempts to characterise the behaviour of this POPDC2 protein variant in a cellular environment were performed. POPDC2 p.L245P, along with POPDC1, was co-expressed in HEK293 cells to assess the effect of the mutation on subcellular expression of the mutant protein and POPDC1. BiFC, AP-FRET and Co-IP assays were performed to determine if any changes in the interaction of POPDC1 and POPDC2 occur as a result of the mutation. The results of these assays and inferences from the modelled position of the L245 residues in POPDC2 were used to propose a possible mechanism underlying the dysfunction of POPDC2 in the presence of the L245P substitution.

7.2.2 Aims

The aims of the studies described in this chapter were to:

1. Examine the possible effects of the L245P substitution on the function of POPDC2 through the inspection of POPDC2 models.
2. Utilise the newly developed HEK293 cell expression model to investigate if the POPDC2 p.L245P variant causes mislocalisation of POPDC1 and/or POPDC2.
3. Use BiFC, AP-FRET and Co-IP to investigate if POPDC1 and POPDC2 interactions are altered in the presence of the POPDC2 p.L245P.

7.3 Results

7.3.1 Initial Assessment from Previous Investigations into POPDC2

Residue L245 in POPDC2 is found towards the C-terminus of the αC-helix (Figure 7.2B and C). The αC-helix is implicated in POPDC1-POPDC2 complex formation (see Chapter 6), and L245 is one of the highly conserved hydrophobic residues found within this helix, as shown in Figure 7.2. A very low frequency of this variant is found in general populations (gnomeAD frequency = 0.003%), suggesting it is not routinely tolerated.[145] When a POPDC2 p.L245D construct was co-expressed with POPDC1 in HEK293 cells, as part of the investigations into the role of the αC-helix on POPDC protein localisation, no significant changes in the localisation of either protein was observed (see Figure 6.9). A mild increase in the frequency of POPDC1/POPDC2 puncta was observed in the cells. This suggests that L245 is not essential for the proposed POPDC1-POPDC2 αC-helix interface that influences the subcellular expression of these proteins. The section of the αC-helix in which L245 resides may be involved in the binding of cAMP to the Popeye domain, based upon the structure of the CAP protein as discussed Chapter 6. L245 is bordered by lysine and tyrosine, forming a KLY motif that is highly conserved across all POPDC isoforms. The AlphaFold model of POPDC2 predicts that K244, within the KLY motif, faces into the cAMP binding pocket, along with L249. This could mean that these residues form contacts with cAMP. The formation of H-bonds to the PBC of the Popeye domain from K244 are predicted, which may have relevance for the stabilisation of the αC-helix and/or cAMP binding. Despite the low impact of the L245D mutation in the HEK293 cell model, the high conservation of L245 and its adjacent residues possibly involved in cAMP binding, mean that it is plausible that the POPDC2 p.L245P variant is pathogenic.

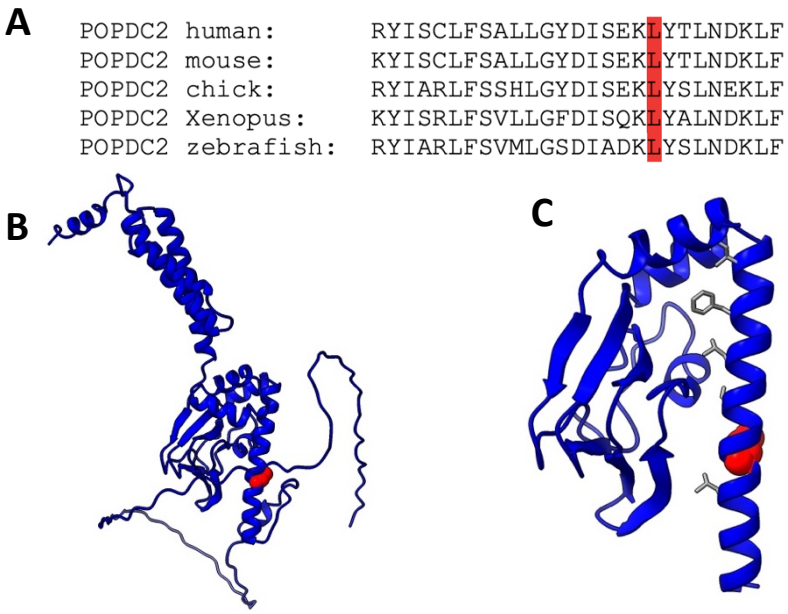


Figure 7.2: The Conservation of Residue L245 in POPDC2 and its Position in POPDC2. A) An alignment of POPDC2 from a selection of species with the position of L245P (human), and equivalent residues, highlighted in red. **B)** AlphaFold structure of full length POPDC2 with residue L245 highlighted in red. **C)** Zoomed view of the AlphaFold model of POPDC2 with L245 highlighted in red, with the side chains of the other conserved hydrophobic residues of the putative Popeye domain interaction domain also shown (see Chapter 6).

7.3.2 The Effect of the *POPDC2* p.L245P Mutation on POPDC1 and POPDC2 Protein Trafficking in HEK293 Cells

POPDC mutations have sometimes had their effects on POPDC protein expression assessed through the immunostaining of skeletal muscle or cardiac biopsies from patients or animal models.[93,117,122] Biopsy material was not available from any member of the affected family so the expression pattern of the POPDC2 p.L245P protein variant and wildtype POPDC1 in native tissue was not known. To test the effect of the POPDC2 p.L245P mutation on POPDC1 and POPDC2 subcellular expression, they were co-expressed in the HEK293 cell model, using an identical protocol to that performed for other tested POPDC mutants in Chapter 5 and 6. POPDC1 was tagged at the C-terminus with ECFP, while POPDC2 p.L245P was fused to EYFP at the same position (see Appendix 10.9, Figures 10.9 and 10.14 for the full construct sequences). After transient co-expression of both constructs in HEK293 cells, their position and expression level were determined by confocal microscopy. The plasma membrane of cells was marked using the DiD dye. Representative images of cells expressing POPDC1-ECFP and POPDC2p.L245-EYFP are displayed in Figure 7.3B, alongside cells expressing wildtype POPDC1-ECFP and POPDC2-EYPF (Figure 7.3A). This allowed a rapid assessment of POPDC2 p.L245P behaviour, without the need for taking a biopsy or the generation of a knock-in animal model. A clear mislocalisation of POPDC1 and POPDC2 p.L245P was observed in the HEK293 cells, with extensive intracellular expression and a high frequency of POPDC puncta. A small reduction in the expression level of POPDC1 at the plasma membrane was observed, while POPDC2 p.L245P was itself not altered at the plasma membrane, compared to cells expressing wildtype POPDC1 and POPDC2 (Figure 7.3C).

However, an accumulation of intracellular POPDC1 and POPDC2 p.L245P was observed as shown in Figure 7.3D. Quantification of plasma membrane localisation showed a clear reduction of both proteins at the membrane relative to the cytoplasm versus co-expression of both wildtype isoforms (Figure 7.3E). In terms of plasma membrane localisation, the POPDC2 p.L245P variant resembled the effects of the known pathogenic POPDC1 p.Q153X, p.S201F and POPDC2 p.W188X variants (see Chapter 5).

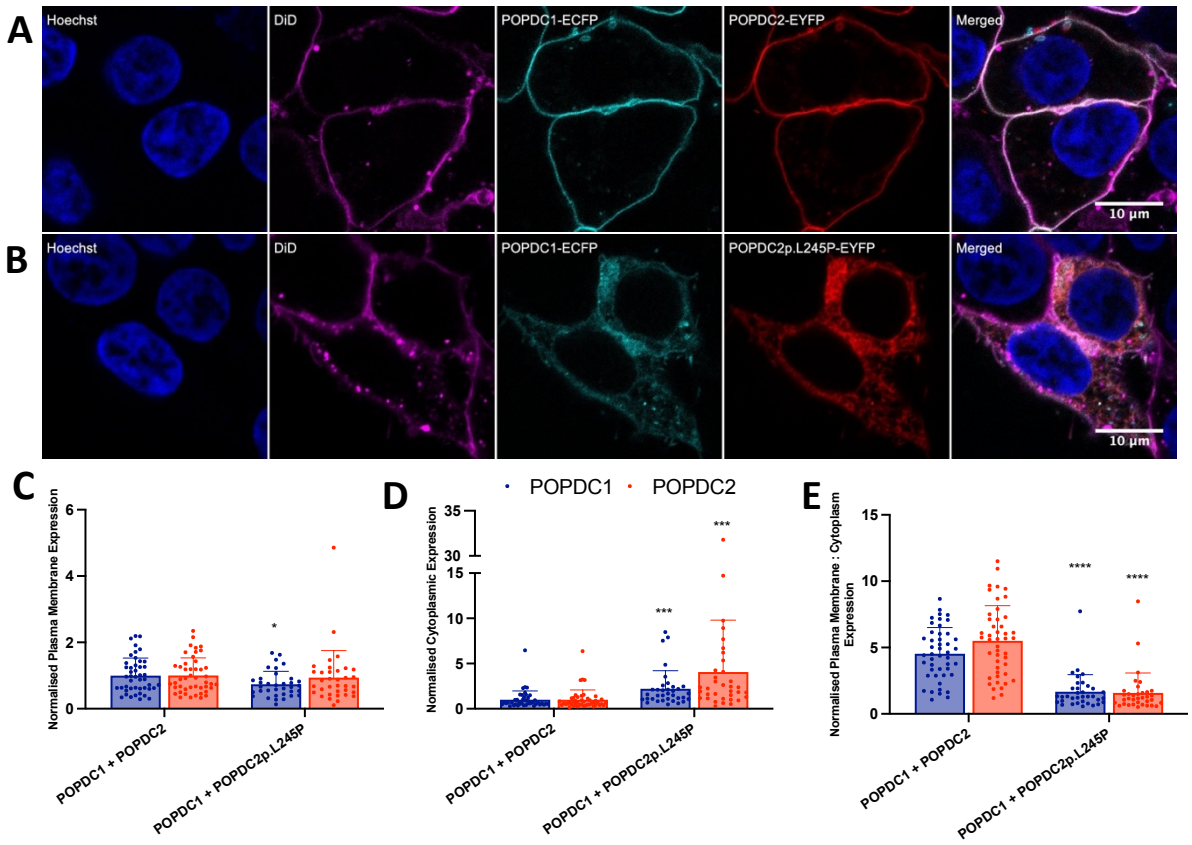


Figure 7.3: The Co-Expression of POPDC1 and POPDC2 p.L245P in HEK293 Cells. HEK293 cells were co-transfected with POPDC1-ECFP and POPDC2-EYFP (n = 46) **(A)** or POPDC2 p.L245P-EYFP (n = 35) **(A)** and imaged using confocal microscopy. The expression of each isoform, as determined by ECFP or EYFP emission, within the plasma membrane **(C)** and cytoplasm **(D)** of cells was determined and normalised to the wildtype pair. The ratio of POPDC1 and POPDC2 at the plasma membrane compared to the cytoplasm was also determined **(E)**. A summary of results is provided in Appendix 10.9, Table 10.46. Samples were compared using student's t-test; * p<0.05, *** p<0.0005, **** p<0.0001; error bars show SD.

The average cellular cross-sectional expression profiles of both isoforms also revealed a minor peak of expression about the plasma membrane, showing that both isoforms were able to reach the plasma membrane of the cell (Figure 7.4A and B). While POPDC1 and POPDC2, when co-expressed, show Pearson correlation scores of 1.00 with the plasma membrane this is reduced to 0.86 and 0.75 for POPDC1 and POPDC2 p.L245P, respectively, in the mutant containing cells (Figure 7.4C and D). There is still a preferable localisation of both isoforms to the plasma membrane compared to the cytoplasm, and the POPDC2 p.L245P variant does not totally abolish the ability of POPDC1 and POPDC2 to associate with the plasma membrane. However, it is clear that the high degree of specific plasma

membrane expression found in wildtype cells is lost. POPDC1 and POPDC2 p.L245P showed a correlation of 0.96 indicating that they maintain a highly similar spatial distribution across the cell.

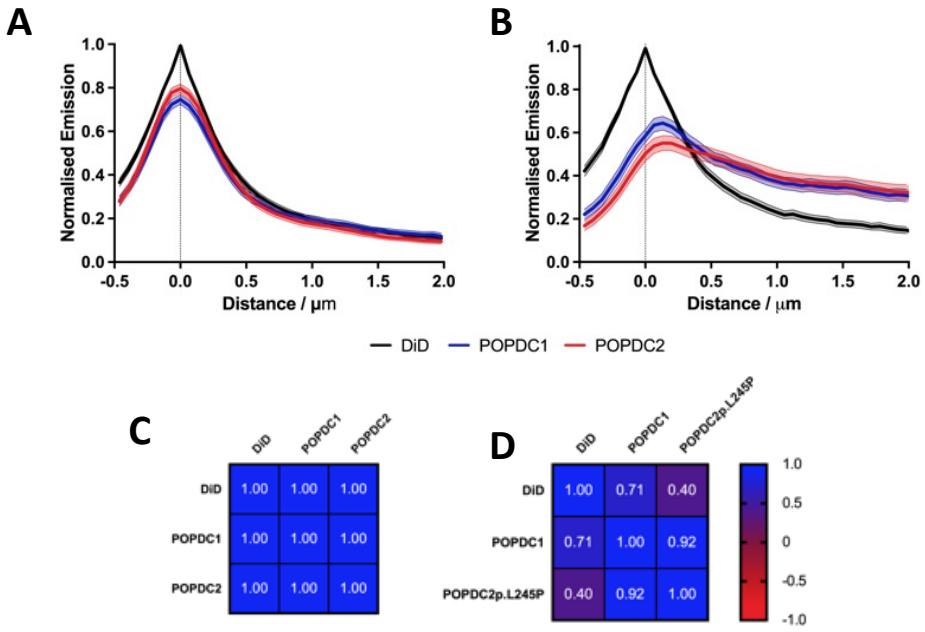


Figure 7.4: The Normalised Cellular Cross-Sectional Expression Profile of POPDC1 and POPDC2 Relative to the Position of the Plasma Membrane of HEK293 Cells in Presence of the POPDC2 p.L245P Variant. HEK293 cells were co-transfected with POPDC1-ECFP and POPDC2-EYFP or POPDC2 p.L245P-EYFP and imaged using confocal microscopy. The normalised average cross-sectional expression profile of each POPDC isoform, as well as the DiD plasma membrane marker, was measured across the radius of the cell from the plasma membrane to nucleus, at 12 non-overlapping points per cell. The region up to 2µm into each cell of each average expression profile is shown for wildtype POPDC1 + POPDC2 (cells = 34, cross sections = 408) **(A)** and POPDC1 + POPDC2 p.L245P (cells = 21, cross sections = 252) **(B)**. Area of lines show 95% confidence limit. The Pearson correlation score of each POPDC isoform with the plasma membrane marker other each other was determined for POPDC1 + POPDC2 **(C)** and POPDC1 + POPDC2 p.L245P **(D)**.

7.3.3 The Impact of the POPDC2 p.L245P Mutation on POPDC1-POPDC2 Interactions

7.3.3.1 Bimolecular Fluorescence Complementation

To investigate if POPDC2 p.L245P showed changes in its interaction with POPDC1 compared to wildtype POPDC2, a BiFC assay was performed in HEK293 cells. The protocol followed that used in the equivalent experiments for the other POPDC mutants reported in Chapter 6. POPDC1 was tagged at the C-terminus with VC155, while POPDC2 or POPDC2 p.L245P was tagged with C-terminal VN155. Free mRFP was also expressed in the cells to act as an internal control. Figure 7.5A shows the approximate 80% drop in normalised BiFC signal that was recorded after co-expression of the proteins in the presence of POPDC2 p.L245P compared to wildtype POPDC2. This implies that the interaction between POPDC1 and POPDC2 is disrupted by the presence of the L245P mutation in POPDC2.

7.3.3.2 Acceptor Photobleaching FRET

As well as BiFC, AP-FRET was also used to investigate the changes in interactions as a result of the L245P substitution following the protocol used for other mutants in Chapter 6. POPDC1 and POPDC2 or POPDC2 p.L245P were tagged at the C-terminus with monomerised mECFP or mEYFP, respectively, and co-expressed in HEK293 cells. The cells were imaged using confocal microscopy through which

AP-FRET was performed through measuring mECFP emission before and after bleaching of the mEYFP fluorophore. FRET values were normalised to a positive control construct containing tethered ECFP and EYFP. The high variability in AP-FRET results prevented the drawing of firm conclusions regarding the effect on POPDC1-POPDC2 interactions of the mutations tested in Chapter 6, and are discussed in Chapter 6.3.2.1. As such, caution should also be applied to these results. Indeed, a wide range of AP-FRET levels were recorded from the different ROIs examined in both the wildtype and POPDC1 and POPDC2 p.L245P groups. Despite this, it was found that the level of FRET between POPDC1-mECFP and POPDC2-mEYFP was significantly reduced after introduction of the POPDC2 p.L245P variant compared to the wildtype POPDC1 and POPDC2 pair (Figure 7.5B).

7.3.3.3 Co-Immunoprecipitation

To try and confirm any changes in the direct interaction of POPDC1 and POPDC2 as a result of the L245P mutation in POPDC2 a co-immunoprecipitation experiment was performed. POPDC1-ECFP-myc and POPDC2-EYFP-HA or POPDC2p.L245P-EYFP-HA were co-expressed in HEK293 cells before cell lysis. Cells expressing POPDC2-EYFP-HA only were used as a negative control. The cleared cell lysate was incubated with anti-myc agarose to perform immunoprecipitation of POPDC1-ECFP-myc. After release of precipitated protein, the sample was run on an SDS-PAGE gel and a Western blot performed using an anti-HA primary antibody, shown in Figure 7.5C, to detect the presence of POPDC2-EYFP-HA. It appeared that immunoprecipitation of POPDC2P.L245P with POPDC1 only occurred weakly compared to the wildtype pair, which suggests that the interaction between POPDC1 and POPDC2 is disrupted, although perhaps not totally abolished, by the POPDC2 p.L245P mutation.

The Co-IP assay was run concurrently with other POPDC mutants, shown in Chapter 6, where problems with the Co-IP assay are discussed. Briefly, aggregation of POPDC proteins in the sample buffer used to prepare proteins for SDS-PAGE meant that analysis of POPDC complexes by molecular weight analysis was not possible. Additional bands were also seen that corresponded with fragmentation products containing the EYFP-HA C-terminal tag. The full blot is shown in Appendix 10.5.

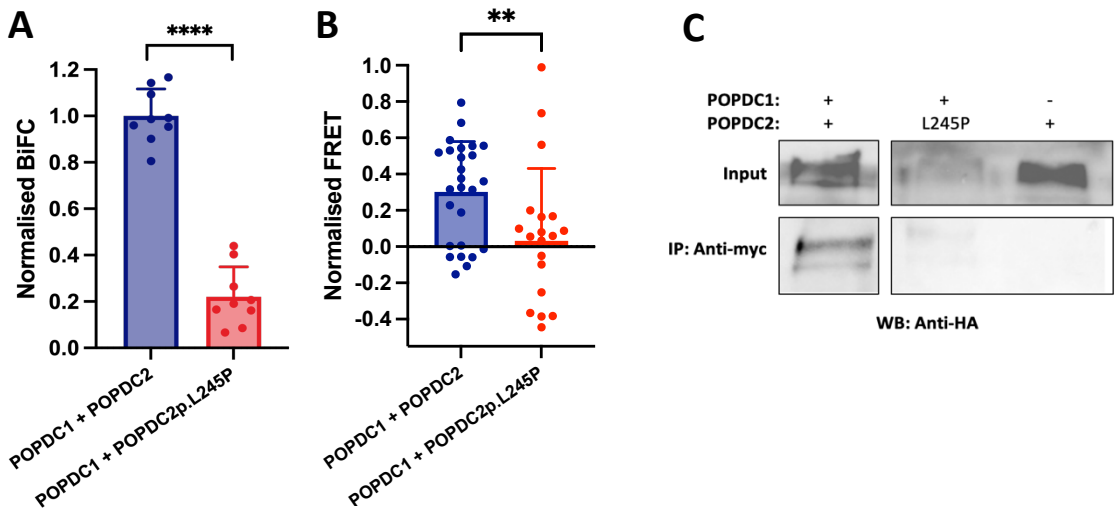


Figure 7.5: BiFC, AP-FRET and Co-IP Assays suggest the Interaction between POPDC1 and POPDC2 p.L245P is Impaired. (A) The normalised BiFC signal of the interaction of wildtype POPDC1 with POPDC2 and POPDC1 with POPDC2 p.L245P in HEK293 cells. The change in BiFC was analysed using student's t-test; $t(16) = 13.46$, $p < 0.0001$. **** $p<0.0001$; error bars show SD. A summary of results is provided in Appendix 10.8, Table 10.47. **(B)** The AP-FRET signal between POPDC1 and POPDC2 or POPDC1 and POPDC2 p.L245P in HEK293 cells. Changes in FRET were analysed with student's t-test; $t(44) = 2.715$, $p = 0.0094$ for POPDC FRET changes. ** $p < 0.01$. A summary of results is provided in Appendix 10.8, Table 10.48. **(C)** Co-IP of POPDC2-EYFP-HA with POPDC1-ECFP-myc from HEK293 cells. Western blot detected POPDC2-EYFP-HA using anti-HA primary antibody. Note that both input images and both immunprecipitation images shown are taken from the same respective blots, with other POPDC variants between the wildtype pair and POPDC1 with POPDC2 p.L245P and POPDC2 only lanes removed from each image. A full-size blot is shown in Appendix 10.5.

7.4 Discussion

7.4.1 POPDC2 p.L245P Resembles the Effect of POPDC Variants known to be Pathogenic, Supporting its Classification as a Candidate Gene for cJET

Testing of the POPDC2 p.L245P variant in the HEK293 cell trafficking model showed a clear mislocalisation of POPDC1 and POPDC2 p.L245P, with both proteins showing an accumulation in the cytoplasm. As with other POPDC mutations (e.g. POPDC1 p.Q153X, p.S201F and POPDC2 p.W188X), the subcellular localisation of both POPDC isoforms was altered. This suggests that these mutations have approximately similar effects on the interplay between POPDC1 and POPDC2, which was suggested to be required for proper trafficking in Chapter 6. If the mislocalisation of the POPDC1 and POPDC2 p.L245P proteins in the HEK293 cell model translates to the heart of patients carrying this mutation, the subcellular expression of both POPDC isoforms is likely also altered in cardiac myocytes. Such a correlation between muscle or heart tissue has been observed for the other POPDC mutations (see Chapter 5).

The BiFC, AP-FRET and Co-IP assay all suggest that the interaction between POPDC1 and POPDC2 is altered by the L245P substitution. This variant differs from other clinically relevant mutants tested (see Chapter 6) in that both BiFC and AP-FRET showed a significant change in the interaction. The weaknesses of both these approaches as applied to the POPDC proteins was discussed in Chapter 6 but the similar outcomes of both assays in the case of this mutation might represent a robust change in the interaction between POPDC1 and POPDC2.

Notwithstanding the caveats discussed in Chapter 5, the HEK293 model provides a novel method of testing for the potential pathogenicity of POPDC variants in the absence of other evidence. This was shown here in the case of the POPDC2 p.L245P mutation. This variant was detected through exome sequencing of patients suffering from cJET. It was not possible to obtain biopsy material to examine the effect of the POPDC2 p.L245P mutation on POPDC expression in native tissue. The HEK293 cell assay permitted rapid identification of any defects in POPDC1 and POPDC2 subcellular expression as a result of this mutation. While normal trafficking would not have ruled out the possibility that the POPDC2 p.L245P mutation is a disease-causing variant, the obvious loss of plasma membrane localisation of both POPDC isoforms provides early evidence that this is a plausible causative gene for these cases of cJET. While other assays have been developed to study the properties of POPDC mutations, such as a bimolecular POPDC1-TREK-1 FRET assay or the TREK-1 current assay in *Xenopus* oocytes these both rely on the interaction between POPDC proteins and TREK-1 to measure POPDC function.[71,93,105] It is beneficial to have an orthogonal assay with which to assess their behaviour, particularly addressing the changes in POPDC expression and localisation often observed to be affected in patients' biopsy material.[93,117,122] There are many other POPDC mutations linked to disease which could be examined with this assay to supplement, or in the absence of, biopsy or animal model data.

While additional evidence is required to confirm *POPDC2* as a cJET-related gene, these experiments justify further studies and can inform efforts to understand the phenotype of the affected patients. It would be interesting to confirm the change of POPDC localisation in biopsy material if this ever became available, or through the generation of a POPDC2 p.L245P knock-in animal model. The increasing use of exome sequencing in patients will provide further opportunities to detect changes in *POPDC2*, or other POPDC genes, in patients displaying similar disease phenotypes. This would provide further confidence in the classification of *POPDC2* as a candidate gene in cJET.

7.4.2 The Possible Mechanism of POPDC2 Functional Changes Caused by the L245P Mutation

The finding that the L245P mutation may lead to changes in POPDC protein expression, and consequently cJET, further suggests that the αC-helix plays a key role in POPDC protein function. However, it was shown in Chapter 6 that the POPDC2 p.L245D mutation had no significant impact on POPDC1 and POPDC2 trafficking or plasma membrane localisation in the HEK293 model. It would appear that the inclusion of proline, as opposed to aspartic acid, at position L245 is required for disruption of normal POPDC2 function. In Chapter 6 it was concluded that L245 was not essential for the αC-helix interface. However, L245 is highly conserved across POPDC2, as is its equivalent residue in POPDC1 (L261), making it likely that this residue serves an important purpose in both proteins (see

Figure 6.6). Prolines are known to lead to the destabilization of α-helices, due to their locked conformation of the N-C_α bond and the tertiary nature of the backbone N atom meaning no H-bonding is possible from the peptide bond nitrogen.[240] The inclusion of proline into α-helices can lead to kinks and other changes in conformation.[241] If the αC-helix is involved in POPDC intermolecular interactions *via* the Popeye domain, or acts as a form of lid to the cAMP binding domain (see Chapter 6), the introduction of the L245P mutation could lead to functional changes in the protein as a result of changes in the conformation of this helix. This may explain the difference in the behaviour of the POPDC2 p.L245D and POPDC2 p.L245P mutants in HEK293 cells. The αC-helix interface may be disrupted due to changes N- or C-terminal to the L245P residue. It should also be noted that L245 is positioned adjacent to K244, within the super conserved KLY motif (see Chapter 6), which is predicted to be involved in cAMP binding. If the helix was disrupted at this point, it could lead to changes in cAMP affinity and/or the position of the α-helix relative to the β-folds of the Popeye domain.

Structural studies of the Popeye domain with and without the L245P substitution would help to reveal the effect this substitution has on POPDC2 function. As discussed in Chapter 3, the failure to produce Popeye domain constructs suitable for protein-NMR or x-ray crystallography has prevented the collection of a detailed empirically derived, structure of the Popeye domain both in its unbound and cAMP bound state. This is another case where such information would be highly useful and further highlights the need to progress in this area.

8 Final Discussion

8.1 The Context of the Findings of this Work

This work aimed to address a number of questions in the study of the POPDC proteins. The POPDC proteins have been found to bind cAMP, and are emerging as an important mediator within cAMP signalling, although their full role remains unclear.[71,100,101] The POPDC proteins have been implicated in cardiac and muscular diseases, with a small number of patients possessing mutations in the POPDC genes identified.[242] Consequently there is an interest in furthering the understanding of the importance of cAMP binding to the POPDC proteins. The Popeye domain was revealed to bind to cAMP through a combination of structural modelling, a radioligand binding assay and cAMP-agarose precipitation techniques.[71] The highly divergent amino acid sequence of the Popeye domain CNBD compared to canonical CNBDs, mean that it would be advantageous to be able to directly determine the binding mode of cAMP to the Popeye domain.[71] For structural studies of the Popeye domain to occur a construct possessing the necessary properties required for the various structure determining techniques must be available.[8] Despite several attempts to produce such a construct, this has not been possible. This was due to poor expression, solubility, and conformational stability of candidate Popeye domain constructs.[79,80,138,170] Modelling and docking experiments are able to provide some insight, but the dearth of suitable templates for Popeye domain modelling limits these approaches,[18] although this problem may be partially overcome by newer, more accurate modelling techniques.[21,22] However, there remains a strong interest in empirically determining the structure of the Popeye domain. Understanding the binding mechanism of cAMP to the Popeye domain may also permit structure-based development of Popeye domain selective cAMP mimics. Such compounds would be highly useful in the study of the POPDC proteins' role in the cAMP pathway and may also provide the basis for novel therapeutics.[74,135] In addition, few cell-based assays are available to monitor POPDC protein function in response to cAMP, all of which rely on the interaction with the TREK-1 potassium channel, and are not suitable for compound screening studies due to their low dynamic range and/or throughput.[71,93,105]

Several patients suffering from muscular dystrophy and/or heart problems have been found to be carrying mutations in the POPDC genes. Changes in the subcellular expression of multiple POPDC proteins have been reported in the skeletal muscle fibres of a number of these patients.[93,117,122] The reason for this loss of POPDC proteins at the plasma membrane, including those which are not themselves mutated, is unknown. An interaction between POPDC1 and POPDC2 that is necessary for proper POPDC protein trafficking that is disrupted in the presence of mutations is one hypothesis. This effect is thought to be relevant to the phenotypes seen in patients and requires further study if the causes of the diseases in patients possessing POPDC mutations are to be uncovered.

It has also been noted that when POPDC1 or POPDC2 is transiently expressed in cell lines, they are mostly retained within the cell and do not effectively localise to the plasma membrane. This is in contrast to native tissue, where both POPDC1 and POPDC2 are found in the plasma membrane of cells.

8.2 Summary of the Main Findings of this Work

8.2.1 Attempts to Produce a Novel Popeye Domain Construct were Unsuccessful

To try and overcome the issues with solubility and stability in Popeye domain constructs, a series of extensions and truncations were made to a suboptimal Popeye domain construct previously developed, in the hope that this would lead to improvements in the behaviour of the construct. A novel construct, containing residues S109-K272 of murine Popdc1 and an N-terminal GB1 tag, was found to be reasonably well expressed in BL21 Star (DE3) *E. coli* and able to be purified, albeit with some difficulties due the construct's inherent affinity for the Ni-NTA columns used during FPLC purification. Notably, it was found that removing the GB1 tag to leave only Popeye domain derived residues did not lead to the precipitation of the protein. This is thought to be the first case of an untagged POPDC construct being soluble in standard buffer conditions.

This finding prompted initial structural characterisation of the construct using SEC-MALS and CD, which suggested it formed dimers and was folded. The thermal stability of the construct did not appear to have markedly increased compared to previous Popeye domain constructs. An initial ^{1}H-^{15}N HSQC-TROSY protein-NMR experiment showed some improvements in spectra quality. However, it was found that this construct did not show a clear ability to bind cAMP, suggesting it did not fully resemble a native Popeye domain. This prevented further use of this construct. It was intended to utilise this novel Popeye domain construct in the development of ligand screening assays such as DSF and MST to enable testing of potential Popeye domain ligands. The failure to produce a functional construct prevented this part of the project from being completed.

Some small-scale attempts were made to use uni- and bimolecular BRET based assays to detect cAMP binding to the Popeye domain. These attempt to develop novel assays within cells were also unsuccessful.

8.2.2 POPDC1 and POPDC2 Subcellular Expression is Dependent on Co-Expression

To investigate the observation that POPDC1 and POPDC2 can be lost from the plasma membrane of skeletal muscle in response to a mutation in only one of the respective proteins, skeletal muscle biopsy material from two patients carrying a *POPDC1* (c.457C>T, p.Q153X) mutation,[117] and *POPDC1* (c.547G>T, p.V183F) mutation,[186] respectively, were studied. The expression and subcellular location of POPDC1 and POPDC2, as well as the sarcolemma marker α-sarcoglycan, was determined in each

set of biopsies. It was found that the plasma membrane expression and localisation dropped in both cases, although this was much more consistent in the POPDC1 p.Q153X case, with only a mild change caused by p.V183F in both proteins. In addition, an increase in fibre cross-sectional area was found in the POPDC1 p.Q153X biopsy, with a highly variable average decrease in fibre area for POPDC1 p.V183F, suggesting different forms of muscular dystrophy. A loss of normal POPDC1 and POPDC2 plasma membrane expression was found in samples from a mutant mouse expressing the POPDC1 p.S201F mutant protein, confirming previously reported findings in a patient.[93]

POPDC1 or POPDC2 were each transiently expressed in HEK293 cells. As expected, both proteins were mostly found intracellularly, possibly within the ER, with a high rate of aggregation. However, co-expression of POPDC1 and POPDC2 led to almost complete rescue of plasma membrane localisation. This showed a co-dependency between POPDC1 and POPDC2 for correct trafficking. It was also shown that the mislocalisation of POPDC1 and POPDC2 in the presence of the POPDC1 p.Q153X and p.S201F mutations was replicated in HEK293 cells. Minimal changes were seen for POPDC1 p.V183F, suggesting a difference to the other mutations, as in native tissue. In addition, a POPDC1 p.R172H mutation was found to have minimal effect, while a POPDC2 p.W188X mutation,[105] was found to cause severe mislocalisation of both POPDC1 and POPDC2.

8.2.3 An Interaction through the αC-helix of the Popeye Domain may Modulate POPDC1-POPDC Subcellular Expression

After establishing that POPDC1 and POPDC2 require each other's presence to be normally expressed and localised in tissue and HEK293 cells, attention turned to the mechanism underpinning this effect. It was hypothesised that the recently identified interaction between POPDC1 and POPDC2 was responsible for mediating their trafficking to the plasma membrane.[82] qBRET further established the existence of POPDC1-POPDC2 dimers in cells, while also indicating that POPDC homo-complexes may also form. AP-FRET, BiFC and Co-IP were also used to try and detect changes in the POPDC1-POPDC2 complex that could be leading to the mislocalisation seen in the presence of the set of clinically identified variants. The results from these assays were not conclusive, partially due to the poor performance of the AP-FRET assay as well as the aggregation and fragmentation observed in the Co-IP Western blot. Taken together, there was some evidence for changes, or a reduction, in POPDC1-POPDC2 complex formation in the presence of some mutations, particularly those that caused large changes in subcellular expression in skeletal muscle and HEK293 cells.

Using the CAP proteins as a template,[219,220] a model was proposed on which POPDC1 and POPDC2 interacted through their predicted αC-helix within the Popeye domain, analogous to the C-helix of classical CNBDs.[94] This prediction was made mainly on the basis of the high degree of conservation

within the predicted αC-helix between POPDC1 and POPDC2, including a set of hydrophobic residues which aligned with those involved in CAP dimerization. A crude model of a Popeye domain dimer was constructed based on a CAP dimer. This model, and the alignment with CAP, guided the introduction of aspartic acid substitutions to the set of conserved hydrophobic residues within POPDC1 and POPDC2. These mutated constructs were then expressed in HEK293 cells, along with a wildtype partner, as was done for the clinical mutants. It was hypothesised that if POPDC1-POPDC2 complexes are required for optimal subcellular expression of both proteins, any mutations within the αC-helix that disrupted this complex would result in mislocalisation in the HEK293 cells. It was found that residues predicted to be within the core of the αC-helix were highly sensitive to the introduction of aspartic acid and led to severe mislocalisation of both POPDC1 and POPDC2. This provided strong evidence both for the existence of an αC-helix interface between POPDC1 and POPDC2, and also its importance to the subcellular localisation of both proteins.

Why such an interaction is required for proper POPDC protein processing was not determined. However, it was suggested that the formation of the αC-helix interface may lead to shielding of ER retention motifs within the cytoplasmic region of both proteins that prevent trafficking from the ER when uncovered.

8.3 Outlook and Future Work

8.3.1 Determining the Structure of the POPDC Proteins and Mode of cAMP Binding

The structure of the Popeye domain remains uncertain. This work heavily relied on models of the POPDC proteins, particularly those deposited in the AlphaFold database.[23,24] These models were useful in many cases, particularly in the development of the αC-helix POPDC1-POPDC2 interface hypothesis and the design of αC-helix mutagenesis experiments. However, all the conclusions based upon the model structures do need to be treated with caution. This is particularly true when considering the structure of POPDC dimers compared to the monomeric AlphaFold models, as these may not account for the shift in conformation that occur upon complex formation.[27] Therefore, there remains an incentive to produce an empirically determined structure of the Popeye domain and POPDC proteins.

Moving forward a number of strategies could be employed. The search for soluble and stable Popeye domain-based constructs could be continued, with the finding in this work that folded Popeye domain sequences can remain in solution suggesting that further improvements might be possible. However, the number of unsuccessful attempts could indicate that an alternative approach is required.[79,80,138,170] One option would be to use full length POPDC proteins expressed in eukaryotic cells followed by purification and stabilisation through the use of lipid systems. Solid-state NMR, or other techniques, could then be used to try and provide structural information.[243] The use of full-length proteins may

also permit attempts to determine the structures of complexes containing the POPDC proteins through cryo-EM, although this would likely be challenigng.[2] For now there remains no clear way of directly determining the structure of the POPDC proteins, likely meaning that the reliance on modelling will continue.

The search for recombinant POPDC constructs to use in structural studies is linked to the development of effective ligand binding assays. It was hoped that the construct produced in Chapter 3 would allow the use of simple assays such as DSF and MST in the assessment of compound binding to the Popeye domain, but this was not possible. While an *in vitro* binding assay will likely have to be established if Popeye domain ligands are to be optimised efficiently, ligand binding studies could also be switched to full length POPDC protein-based methods, such as CETSA which permits the binding of compounds to proteins within cells to be detected.[171]

There is also a need to be able to selectively alter the binding of cAMP to the POPDC proteins within cells without the possible wider changes of mutations or total removal of the proteins.[74] This project aimed to identify compounds that selectively bound to the POPDC proteins in a manner mimicking cAMP. However, the failure to find a method of assessing compound binding, *in vitro* or in cells, prevented this from being completed. Such compounds, if ever found, will provide a highly useful pharmacological tool for revealing the effect of cAMP binding to POPDC proteins. For example, the suggestion that POPDC proteins act as a sponge for cAMP,[74] mediating its diffusion in concert with PKA and PDEs,[91,92] could be tested by inhibiting cAMP binding with a Popeye domain selective, competitive cAMP antagonist. This would avoid the other changes in the cAMP signalling pathway that may be caused by the loss of POPDC protein PPIs in the case of using mutants or knock-outs.

8.3.2 The Importance of POPDC1-POPDC2 Interactions

While this and previous work provides strong evidence that POPDC1-POPDC2 interactions occur within cells, the exact nature of these interactions are uncertain. The HEK293 cell assay provided indirect evidence of disruption of these interactions and the resulting changes in POPDC protein subcellular expression. Modelling and mutagenesis studies suggested the formation of a hydrophobic residue mediated helix-helix interface between the αC-helices of POPDC1 and POPDC2. However, this model is highly dependent on the comparison of the Popeye domains to CAP, which only show very modest sequence similarity. Examining this proposed interface further is required to confirm this hypothesis. While the determination of the structure of this complex using direct methods, such as protein-NMR or cryo-EM would be ideal, this is unlikely to be achieved in the near future for the reasons discussed above. A number of other techniques could be employed instead. It was planned to use a peptide array to localise the interaction between POPDC1 and POPDC2, in a similar manner

to that used for early studies of POPDC1 homo-oligomerisation.[81] Unfortunately, time constraints and procedural difficulties meant this was not completed before the end of the project. The completion of such an experiment would be an obvious next step, although care should be taken that the secondary structures required for any interface to form are given the best chance of being present in the peptide sequences.[244] Cross-linking mass spectrometry could also be used to identify residues in POPDC1 and POPDC2 that are in close proximity.[42] This may be able to localise interactions between other areas of the proteins, which are thought to be present.

More sophisticated mutagenesis experiments could also be employed. Instead of introducing negative charges into the proposed hydrophobic core of the helix-helix interface, alanine scanning could be used. The introduction of unnatural charges are highly likely to lead to adverse effects on the protein.[245] Using neutral substitutions, such as alanine, may permit a more detailed determination of each residue's role in POPDC1-POPDC2 interactions.[246] It could also be seen if introducing opposite charges to equivalent positions within each αC-helix is able to rescue the interaction.

Why the POPDC1-POPDC2 complex must be formed for correct subcellular expression is still not clear. It was hypothesised that steric hindrance of ER retention motifs upon formation of the αC-helix interface may be responsible. While possible ER retention motifs are present in the sequences of the POPDC proteins, this needs to be established empirically. Mutating the candidate ER retention motifs and observing their effect on POPDC protein localisation in HEK293 cells would provide early evidence for or against this model.

The role of the POPDC proteins in the cAMP pathway was not examined in detail in this work, other than to provide context for the potential effects of the POPDC mutations studied and attempts to detect cAMP binding to the Popeye domain. However, the findings of this work may have a potentially significant impact on attempts to understand why POPDC proteins are required for normal cAMP signalling. The numerous PPIs that the POPDC proteins form with members of the cAMP pathway have provided an insight into their possible roles in cAMP signalling.[71,100,101] This work suggests that POPDC1 homo- and heterocomplex formation should be included when considering the role of POPDC PPIs in modulating cAMP signalling. POPDC proteins may act as scaffolds involved in the formation of cAMP signalosomes, known to be required for the selective activation of pathways downstream of cAMP pathway activation.[101] The finding here that the subcellular localisation of the POPDC proteins is controlled by inter-POPDC interactions gives them a potential role in cAMP signalling. If POPDC proteins are required to spatially organise other proteins at particular cellular locations, the loss of normal POPDC localisation will have downstream effects on cAMP signalosome organisation. For example, the disruption of PDE containing complexes are known to reshape cAMP nanodomains.[247]

As such, a loss in the previously reported POPDC1-PDE4A interaction, due to the disruption of POPDC1 localisation, may disrupt the compartmentation of cAMP. This could partially explain some of the phenotypes seen in patients and animal models. Changes in cAMP pathway member localisation in response to changes in POPDC1-POPDC2 interactions should be studied. This could be done through immunohistochemical analysis of tissue samples expressing mutant POPDC protein, or other proteins could be added to the HEK293 cell expression model alongside POPDC1 and POPDC2.

Similar conclusions can also be drawn for the importance of POPDC proteins in the proper function of muscle and heart specific proteins. Interactions between the POPDC proteins with dysferlin,[71] Cav3,[72] ANO5,[118] and other proteins normally found at the plasma membrane of muscle cells are known. The changes in POPDC plasma membrane expression in skeletal muscle, due to POPDC1 or POPDC2 mutations, could alter the subcellular location of their interaction partners. This has been confirmed in some cases, with dysferlin being found to be mislocalised in the presence of the *POPDC1* (c.457C>T, p.Q153X) mutation.[117] Determining the effects of the range of POPDC mutations on POPDC1-POPDC2 interactions, and subsequent trafficking to the plasma membrane, will form a large part of understanding their effects on the function of muscle cells and the consequent muscular dystrophy phenotypes. In addition, these findings may be of relevance to the study of the POPDC proteins' role in tumorigeneses.[98,135]

8.3.3 Further Testing of the Effects of POPDC Mutations

The greater prevalence of sequencing techniques in medical diagnosis has led to an increased rate of discovery of POPDC mutations associated with muscular and/or cardiac disease. The distribution of these mutations in the protein, and their associated phenotypes, will provide further information on the role of different domains of the protein. The HEK293 cell expression model was shown here to provide a method of testing the effect of POPDC mutations on the subcellular localisation of the POPDC proteins in the absence of biopsy material. This could enable rapid testing of possible disease causing POPDC variants, providing clues as to whether they could be causing disease in patients. This was shown in the case of the POPDC2 p.L245P variant, as described in Chapter 7. The mutation of the αC-helix hydrophobic residues showed how inferences about the role of individual residues could be made from the results of the HEK293 cell assay. Now that POPDC1 and POPDC2 can be localised to the plasma membrane of HEK293 cells, and possibly other cell types, other tests of POPDC function could be performed in cell lines with greater confidence in the relevance to native tissue.

POPDC3 was not studied in this work. Determining if POPDC3 is also able to modulate the subcellular expression other POPDC isoforms should be determined. This could be examined in the HEK293 cell model as done for POPDC1 and POPDC2. This would also enable the study of changes in POPDC protein

expression behaviour in response to POPDC3 mutations, which have not previously been studied in tissue or cell models.[99,124]

9 References

1 Papageorgiou, A. C., Poudel, N. & Mattsson, J. Protein Structure Analysis and Validation with X-Ray Crystallography. *Methods Mol Biol* **2178**, 377-404 (2021).

2 Costa, T. R. D., Ignatiou, A. & Orlova, E. V. Structural Analysis of Protein Complexes by Cryo Electron Microscopy. *Methods Mol Biol* **1615**, 377-413 (2017).

3 Howard, M. J. Protein NMR spectroscopy. *Curr Biol* **8**, R331-333 (1998).

4 Marion, D. An introduction to biological NMR spectroscopy. *Mol Cell Proteomics* **12**, 3006-3025 (2013).

5 Sugiki, T., Kobayashi, N. & Fujiwara, T. Modern Technologies of Solution Nuclear Magnetic Resonance Spectroscopy for Three-dimensional Structure Determination of Proteins Open Avenues for Life Scientists. *Comput Struct Biotechnol J* **15**, 328-339 (2017).

6 Greenfield, N. J. Using circular dichroism spectra to estimate protein secondary structure. *Nat Protoc* **1**, 2876-2890 (2006).

7 Some, D. Light-scattering-based analysis of biomolecular interactions. *Biophys Rev* **5**, 147-158 (2013).

8 Edavettal, S. C., Hunter, M. J. & Swanson, R. V. Genetic construct design and recombinant protein expression for structural biology. *Methods Mol Biol* **841**, 29-47 (2012).

9 Dreydoppel, M., Balbach, J. & Weininger, U. Monitoring protein unfolding transitions by NMR-spectroscopy. *J Biomol NMR* **76**, 3-15 (2022).

10 Raynal, B., Lenormand, P., Baron, B., Hoos, S. & England, P. Quality assessment and optimization of purified protein samples: why and how? *Microb Cell Fact* **13**, 180 (2014).

11 Kubicek, J., Block, H., Maertens, B., Spriestersbach, A. & Labahn, J. Expression and purification of membrane proteins. *Methods Enzymol* **541**, 117-140 (2014).

12 Gray, D. Overview of protein expression by mammalian cells. *Curr Protoc Protein Sci* **10**, 5.9.1-5.9.18 (2001).

13 Rosano, G. L. & Ceccarelli, E. A. Recombinant protein expression in Escherichia coli: advances and challenges. *Front Microbiol* **5**, 172 (2014).

14 Nilsson, J., Stahl, S., Lundeberg, J., Uhlen, M. & Nygren, P. A. Affinity fusion strategies for detection, purification, and immobilization of recombinant proteins. *Protein Expr Purif* **11**, 1-16 (1997).

15 Raran-Kurussi, S. & Waugh, D. S. Unrelated solubility-enhancing fusion partners MBP and NusA utilize a similar mode of action. *Biotechnol Bioeng* **111**, 2407-2411 (2014).

16 Raran-Kurussi, S. & Waugh, D. S. The ability to enhance the solubility of its fusion partners is an intrinsic property of maltose-binding protein but their folding is either spontaneous or chaperone-mediated. *PLoS One* **7**, e49589 (2012).

17 Booth, W. T., Schlachter, C. R., Pote, S., Ussin, N., Mank, N. J., Klapper, V., Offermann, L. R., Tang, C., Hurlburt, B. K. & Chruszcz, M. Impact of an N-terminal Polyhistidine Tag on Protein Thermal Stability. *ACS Omega* **3**, 760-768 (2018).

18 Jisna, V. A. & Jayaraj, P. B. Protein Structure Prediction: Conventional and Deep Learning Perspectives. *Protein J* **40**, 522-544 (2021).

19 Pearce, R. & Zhang, Y. Toward the solution of the protein structure prediction problem. *J Biol Chem* **297**, 100870 (2021).

20 Dhingra, S., Sowdhamini, R., Cadet, F. & Offmann, B. A glance into the evolution of template-free protein structure prediction methodologies. *Biochimie* **175**, 85-92 (2020).

21 Baek, M., DiMaio, F., Anishchenko, I., Dauparas, J., Ovchinnikov, S., Lee, G. R., Wang, J., Cong, Q., Kinch, L. N., Schaeffer, R. D., Millan, C., Park, H., Adams, C., Glassman, C. R., DeGiovanni, A., Pereira, J. H., Rodrigues, A. V., van Dijk, A. A., Ebrecht, A. C., Opperman, D. J., Sagmeister, T., Buhlheller, C., Pavkov-Keller, T., Rathinaswamy, M. K., Dalwadi, U., Yip, C. K., Burke, J. E., Garcia, K. C., Grishin, N. V., Adams, P. D., Read, R. J. & Baker, D. Accurate prediction of protein structures and interactions using a three-track neural network. *Science* **373**, 871-876 (2021).

22 Jumper, J., Evans, R., Pritzel, A., Green, T., Figurnov, M., Ronneberger, O., Tunyasuvunakool, K., Bates, R., Zidek, A., Potapenko, A., Bridgland, A., Meyer, C., Kohl, S. A. A., Ballard, A. J., Cowie, A., Romera-Paredes, B., Nikolov, S., Jain, R., Adler, J., Back, T., Petersen, S., Reiman, D., Clancy, E., Zielinski, M., Steinegger, M., Pacholska, M., Berghammer, T., Bodenstein, S., Silver, D., Vinyals, O., Senior, A. W., Kavukcuoglu, K., Kohli, P. & Hassabis, D. Highly accurate protein structure prediction with AlphaFold. *Nature* **596**, 583-589 (2021).

23 Varadi, M., Anyango, S., Deshpande, M., Nair, S., Natassia, C., Yordanova, G., Yuan, D., Stroe, O., Wood, G., Laydon, A., Zidek, A., Green, T., Tunyasuvunakool, K., Petersen, S., Jumper, J., Clancy, E., Green, R., Vora, A., Lutfi, M., Figurnov, M., Cowie, A., Hobbs, N., Kohli, P., Kleywegt, G., Birney, E., Hassabis, D. & Velankar, S. AlphaFold Protein Structure Database: massively expanding the structural coverage of protein-sequence space with high-accuracy models. *Nucleic Acids Res* **50**, D439-D444 (2022).

24 Tunyasuvunakool, K., Adler, J., Wu, Z., Green, T., Zielinski, M., Zidek, A., Bridgland, A., Cowie, A., Meyer, C., Laydon, A., Velankar, S., Kleywegt, G. J., Bateman, A., Evans, R., Pritzel, A., Figurnov, M., Ronneberger, O., Bates, R., Kohl, S. A. A., Potapenko, A., Ballard, A. J., Romera-Paredes, B., Nikolov, S., Jain, R., Clancy, E., Reiman, D., Petersen, S., Senior, A. W., Kavukcuoglu, K., Birney, E., Kohli, P., Jumper, J. & Hassabis, D. Highly accurate protein structure prediction for the human proteome. *Nature* **596**, 590-596 (2021).

25 Matthews, J. M. & Sunde, M. Dimers, oligomers, everywhere. *Adv Exp Med Biol* **747**, 1-18 (2012).

26 Zhang, Q. C., Petrey, D., Norel, R. & Honig, B. H. Protein interface conservation across structure space. *Proc Natl Acad Sci U S A* **107**, 10896-10901 (2010).

27 Poluri, K. M., Gulati, K. & Sarkar, S. Structural Aspects of Protein–Protein Interactions in *Protein-Protein Interactions*. 61-112 (Springer, Singapore, 2021).

28 Guharoy, M. & Chakrabarti, P. Secondary structure based analysis and classification of biological interfaces: identification of binding motifs in protein-protein interactions. *Bioinformatics* **23**, 1909-1918 (2007).

29 Guharoy, M. & Chakrabarti, P. Conserved residue clusters at protein-protein interfaces and their use in binding site identification. *BMC Bioinformatics* **11**, 286 (2010).

30 Chalfie, M., Tu, Y., Euskirchen, G., Ward, W. W. & Prasher, D. C. Green fluorescent protein as a marker for gene expression. *Science* **263**, 802-805 (1994).

31 Meissner, B., Rogalski, T., Viveiros, R., Warner, A., Plastino, L., Lorch, A., Granger, L., Segalat, L. & Moerman, D. G. Determining the sub-cellular localization of proteins within Caenorhabditis elegans body wall muscle. *PLoS One* **6**, e19937 (2011).

32 Spector, D. L. & Goldman, R. D. Transfection of mammalian cells with fluorescent protein fusions. *Cold Spring Harb Protoc* **2010**, 1233-1237 (2010).

33 Dunn, K. W., Kamocka, M. M. & McDonald, J. H. A practical guide to evaluating colocalization in biological microscopy. *Am J Physiol Cell Physiol* **300**, C723-742 (2011).

34 Clowsley, A. H., Kaufhold, W. T., Lutz, T., Meletiou, A., Di Michele, L. & Soeller, C. Detecting Nanoscale Distribution of Protein Pairs by Proximity-Dependent Super-resolution Microscopy. *J Am Chem Soc* **142**, 12069-12078 (2020).

35 Förster, T. Zwischenmolekulare Energiewanderung und Fluoreszenz. *Annalen der Physik* **437**, 55-75 (2006).

36 Pfleger, K. D. & Eidne, K. A. Illuminating insights into protein-protein interactions using bioluminescence resonance energy transfer (BRET). *Nat Methods* **3**, 165-174 (2006).

37 Boute, N., Jockers, R. & Issad, T. The use of resonance energy transfer in high-throughput screening: BRET versus FRET. *Trends in Pharmacological Sciences* **23**, 351-354 (2002).

38 Kerppola, T. K. Design and implementation of bimolecular fluorescence complementation (BiFC) assays for the visualization of protein interactions in living cells. *Nat Protoc* **1**, 1278-1286 (2006).

39 Dixon, A. S., Schwinn, M. K., Hall, M. P., Zimmerman, K., Otto, P., Lubben, T. H., Butler, B. L., Binkowski, B. F., Machleidt, T., Kirkland, T. A., Wood, M. G., Eggers, C. T., Encell, L. P. & Wood, K. V. NanoLuc Complementation Reporter Optimized for Accurate Measurement of Protein Interactions in Cells. *ACS Chem Biol* **11**, 400-408 (2016).

40 Lin, J. S. & Lai, E. M. Protein-Protein Interactions: Co-Immunoprecipitation. *Methods Mol Biol* **1615**, 211-219 (2017).

41 Alam, M. S. Proximity Ligation Assay (PLA). *Curr Protoc Immunol* **123**, e58 (2018).

42 Sinz, A. Cross-Linking/Mass Spectrometry for Studying Protein Structures and Protein-Protein Interactions: Where Are We Now and Where Should We Go from Here? *Angew Chem Int Ed Engl* **57**, 6390-6396 (2018).

43 Poluri, K. M., Gulati, K. & Sarkar, S. Experimental Methods for Determination of Protein–Protein Interactions in *Protein-Protein Interactions*. 197-264 (Springer Singapore, 2021).

44 Wallin, E. & von Heijne, G. Genome-wide analysis of integral membrane proteins from eubacterial, archaean, and eukaryotic organisms. *Protein Sci* **7**, 1029-1038 (1998).

45 Hegde, R. S. & Keenan, R. J. The mechanisms of integral membrane protein biogenesis. *Nat Rev Mol Cell Biol* **23**, 107-124 (2022).

46 Nyathi, Y., Wilkinson, B. M. & Pool, M. R. Co-translational targeting and translocation of proteins to the endoplasmic reticulum. *Biochim Biophys Acta* **1833**, 2392-2402 (2013).

47 Cosson, P., Perrin, J. & Bonifacino, J. S. Anchors aweigh: protein localization and transport mediated by transmembrane domains. *Trends Cell Biol* **23**, 511-517 (2013).

48 Sharpe, H. J., Stevens, T. J. & Munro, S. A comprehensive comparison of transmembrane domains reveals organelle-specific properties. *Cell* **142**, 158-169 (2010).

49 Herrmann, J. M. & Spang, A. Freight management in the cell: current aspects of intracellular membrane trafficking. *Methods Mol Biol* **457**, 3-12 (2008).

50 Jahn, R. & Scheller, R. H. SNAREs - engines for membrane fusion. *Nat Rev Mol Cell Biol* **7**, 631-643 (2006).

51 Pagny, S., Lerouge, P. & ronique Gomord, V. Signals and mechanisms for protein retention in the endoplasmic reticulum. *Journal of Experimental Botany* **50**, 157-164 (1999).

52 Ma, D., Zerangue, N., Lin, Y. F., Collins, A., Yu, M., Jan, Y. N. & Jan, L. Y. Role of ER export signals in controlling surface potassium channel numbers. *Science* **291**, 316-319 (2001).

53 Shikano, S. & Li, M. Membrane receptor trafficking: evidence of proximal and distal zones conferred by two independent endoplasmic reticulum localization signals. *Proc Natl Acad Sci U S A* **100**, 5783-5788 (2003).

54 Babu, M., Vlasblom, J., Pu, S., Guo, X., Graham, C., Bean, B. D., Burston, H. E., Vizeacoumar, F. J., Snider, J., Phanse, S., Fong, V., Tam, Y. Y., Davey, M., Hnatshak, O., Bajaj, N., Chandran, S., Punna, T., Christopolous, C., Wong, V., Yu, A., Zhong, G., Li, J., Stagljar, I., Conibear, E., Wodak, S. J., Emili, A. & Greenblatt, J. F. Interaction landscape of membrane-protein complexes in Saccharomyces cerevisiae. *Nature* **489**, 585-589 (2012).

55 Juszkiewicz, S. & Hegde, R. S. Quality Control of Orphaned Proteins. *Mol Cell* **71**, 443-457 (2018).

56 Lippincott-Schwartz, J., Bonifacino, J. S., Yuan, L. C. & Klausner, R. D. Degradation from the endoplasmic reticulum: disposing of newly synthesized proteins. *Cell* **54**, 209-220 (1988).

57 Kaupmann, K., Malitschek, B., Schuler, V., Heid, J., Froestl, W., Beck, P., Mosbacher, J., Bischoff, S., Kulik, A., Shigemoto, R., Karschin, A. & Bettler, B. GABA(B)-receptor subtypes assemble into functional heteromeric complexes. *Nature* **396**, 683-687 (1998).

58 Jones, K. A., Borowsky, B., Tamm, J. A., Craig, D. A., Durkin, M. M., Dai, M., Yao, W. J., Johnson, M., Gunwaldsen, C., Huang, L. Y., Tang, C., Shen, Q., Salon, J. A., Morse, K., Laz, T., Smith, K. E., Nagarathnam, D., Noble, S. A., Branchek, T. A. & Gerald, C. GABA(B) receptors function as a heteromeric assembly of the subunits GABA(B)R1 and GABA(B)R2. *Nature* **396**, 674-679 (1998).

59 Kuner, R., Kohr, G., Grunewald, S., Eisenhardt, G., Bach, A. & Kornau, H. C. Role of heteromer formation in GABAB receptor function. *Science* **283**, 74-77 (1999).

60 Burmakina, S., Geng, Y., Chen, Y. & Fan, Q. R. Heterodimeric coiled-coil interactions of human GABAB receptor. *Proc Natl Acad Sci U S A* **111**, 6958-6963 (2014).

61 Kikkert, M., Doolman, R., Dai, M., Avner, R., Hassink, G., van Voorden, S., Thanedar, S., Roitelman, J., Chau, V. & Wiertz, E. Human HRD1 is an E3 ubiquitin ligase involved in degradation of proteins from the endoplasmic reticulum. *J Biol Chem* **279**, 3525-3534 (2004).

62 Feige, M. J. & Hendershot, L. M. Quality control of integral membrane proteins by assembly-dependent membrane integration. *Mol Cell* **51**, 297-309 (2013).

63 Hessa, T., Sharma, A., Mariappan, M., Eshleman, H. D., Gutierrez, E. & Hegde, R. S. Protein targeting and degradation are coupled for elimination of mislocalized proteins. *Nature* **475**, 394-397 (2011).

64 Reese, D. E., Zavaljevski, M., Streiff, N. L. & Bader, D. bves: A novel gene expressed during coronary blood vessel development. *Dev Biol* **209**, 159-171 (1999).

65 Andree, B., Hillemann, T., Kessler-Icekson, G., Schmitt-John, T., Jockusch, H., Arnold, H. H. & Brand, T. Isolation and characterization of the novel popeye gene family expressed in skeletal muscle and heart. *Dev Biol* **223**, 371-382 (2000).

66 Breher, S. S., Mavridou, E., Brenneis, C., Froese, A., Arnold, H. H. & Brand, T. Popeye domain containing gene 2 (Popdc2) is a myocyte-specific differentiation marker during chick heart development. *Dev Dyn* **229**, 695-702 (2004).

67 Uhlen, M., Fagerberg, L., Hallstrom, B. M., Lindskog, C., Oksvold, P., Mardinoglu, A., Sivertsson, A., Kampf, C., Sjostedt, E., Asplund, A., Olsson, I., Edlund, K., Lundberg, E., Navani, S., Szigyarto, C. A., Odeberg, J., Djureinovic, D., Takanen, J. O., Hober, S., Alm, T., Edqvist, P. H., Berling, H., Tegel, H., Mulder, J., Rockberg, J., Nilsson, P., Schwenk, J. M., Hamsten, M., von Feilitzen, K., Forsberg, M., Persson, L., Johansson, F., Zwahlen, M., von Heijne, G., Nielsen, J. & Ponten, F. Proteomics. Tissue-based map of the human proteome. *Science* **347**, 1260419 (2015).

68 Andree, B., Fleige, A., Hillemann, T., Arnold, H. H., Kessler-Icekson, G. & Brand, T. Molecular and functional analysis of Popeye genes: A novel family of transmembrane proteins preferentially expressed in heart and skeletal muscle. *Exp Clin Cardiol* **7**, 99-103 (2002).

69 Ripley, A. N., Chang, M. S. & Bader, D. M. Bves is expressed in the epithelial components of the retina, lens, and cornea. *Invest Ophthalmol Vis Sci* **45**, 2475-2483 (2004).

70 Shetty, M. S., Ris, L., Schindler, R. F. R., Mizuno, K., Fedele, L., Giese, K. P., Brand, T. & Abel, T. Mice Lacking the cAMP Effector Protein POPDC1 Show Enhanced Hippocampal Synaptic Plasticity. *Cereb Cortex*, bhab426 (2021).

71 Froese, A., Breher, S. S., Waldeyer, C., Schindler, R. F., Nikolaev, V. O., Rinne, S., Wischmeyer, E., Schlueter, J., Becher, J., Simrick, S., Vauti, F., Kuhtz, J., Meister, P., Kreissl, S., Torlopp, A., Liebig, S. K., Laakmann, S., Muller, T. D., Neumann, J., Stieber, J., Ludwig, A., Maier, S. K., Decher, N., Arnold, H. H., Kirchhof, P., Fabritz, L. & Brand, T. Popeye domain containing proteins are essential for stress-mediated modulation of cardiac pacemaking in mice. *J Clin Invest* **122**, 1119-1130 (2012).

72 Alcalay, Y., Hochhauser, E., Kliminski, V., Dick, J., Zahalka, M. A., Parnes, D., Schlesinger, H., Abassi, Z., Shainberg, A., Schindler, R. F., Brand, T. & Kessler-Icekson, G. Popeye domain containing 1 (Popdc1/Bves) is a caveolae-associated protein involved in ischemia tolerance. *PLoS One* **8**, e71100 (2013).

73 Knight, R. F., Bader, D. M. & Backstrom, J. R. Membrane topology of Bves/Pop1A, a cell adhesion molecule that displays dynamic changes in cellular distribution during development. *J Biol Chem* **278**, 32872-32879 (2003).

74 Swan, A. H., Gruscheski, L., Boland, L. A. & Brand, T. The Popeye domain containing gene family encoding a family of cAMP-effector proteins with important functions in striated muscle and beyond. *J Muscle Res Cell Motil* **40**, 169-183 (2019).

75 Brand, T. The Popeye domain-containing gene family. *Cell Biochem Biophys* **43**, 95-103 (2005).

76 Ishida, T. & Kinoshita, K. PrDOS: prediction of disordered protein regions from amino acid sequence. *Nucleic Acids Res* **35**, W460-464 (2007).

77 Vasavada, T. K., DiAngelo, J. R. & Duncan, M. K. Developmental expression of Pop1/Bves. *J Histochem Cytochem* **52**, 371-377 (2004).

78 Lundby, A., Andersen, M. N., Steffensen, A. B., Horn, H., Kelstrup, C. D., Francavilla, C., Jensen, L. J., Schmitt, N., Thomsen, M. B. & Olsen, J. V. In vivo phosphoproteomics analysis reveals the cardiac targets of beta-adrenergic receptor signaling. *Sci Signal* **6**, rs11 (2013).

79 Popeye Expression Screen Results (Study Report). (Oxford Protein Production Facility, 2014).

80 Pfuhl, M. Unpublished (Kings College London, London, 2017).

81 Kawaguchi, M., Hager, H. A., Wada, A., Koyama, T., Chang, M. S. & Bader, D. M. Identification of a novel intracellular interaction domain essential for Bves function. *PLoS One* **3**, e2261 (2008).

82 Schindler, R. F. R. *Protein biochemistry of Popdc1 and -2 in heart and skeletal muscle.* PhD thesis, Imperial College London, (2013).

83 Sutherland, E. W., Rall, T. W. & Menon, T. Adenyl Cyclase. *Journal of Biological Chemistry* **237**, 1220-1227 (1962).

84 Neves, S. R., Ram, P. T. & Iyengar, R. G protein pathways. *Science* **296**, 1636-1639 (2002).

85 Gold, M. G. Swimming regulations for protein kinase A catalytic subunit. *Biochem Soc Trans* **47**, 1355-1366 (2019).

86 Conti, M., Mika, D. & Richter, W. Cyclic AMP compartments and signaling specificity: role of cyclic nucleotide phosphodiesterases. *J Gen Physiol* **143**, 29-38 (2014).

87 Baldwin, T. A. & Dessauer, C. W. Function of Adenylyl Cyclase in Heart: the AKAP Connection. *J Cardiovasc Dev Dis* **5**, 2 (2018).

88 Scott, J. D., Dessauer, C. W. & Tasken, K. Creating order from chaos: cellular regulation by kinase anchoring. *Annu Rev Pharmacol Toxicol* **53**, 187-210 (2013).

89 Anton, S. E., Kayser, C., Maiellaro, I., Nemec, K., Moller, J., Koschinski, A., Zaccolo, M., Annibale, P., Falcke, M., Lohse, M. J. & Bock, A. Receptor-associated independent cAMP nanodomains mediate spatiotemporal specificity of GPCR signaling. *Cell* **185**, 1130-1142 (2022).

90 Agarwal, S. R., Clancy, C. E. & Harvey, R. D. Mechanisms Restricting Diffusion of Intracellular cAMP. *Sci Rep* **6**, 19577 (2016).

91 Bock, A., Annibale, P., Konrad, C., Hannawacker, A., Anton, S. E., Maiellaro, I., Zabel, U., Sivaramakrishnan, S., Falcke, M. & Lohse, M. J. Optical Mapping of cAMP Signaling at the Nanometer Scale. *Cell* **182**, 1519-1530 (2020).

92 Zhang, J. Z., Lu, T. W., Stolerman, L. M., Tenner, B., Yang, J. R., Zhang, J. F., Falcke, M., Rangamani, P., Taylor, S. S., Mehta, S. & Zhang, J. Phase Separation of a PKA Regulatory Subunit Controls cAMP Compartmentation and Oncogenic Signaling. *Cell* **182**, 1531-1544 (2020).

93 Schindler, R. F., Scotton, C., Zhang, J., Passarelli, C., Ortiz-Bonnin, B., Simrick, S., Schwerte, T., Poon, K. L., Fang, M., Rinne, S., Froese, A., Nikolaev, V. O., Grunert, C., Muller, T., Tasca, G., Sarathchandra, P., Drago, F., Dallapiccola, B., Rapezzi, C., Arbustini, E., Di Raimo, F. R., Neri, M., Selvatici, R., Gualandi, F., Fattori, F., Pietrangelo, A., Li, W., Jiang, H., Xu, X., Bertini, E., Decher, N., Wang, J., Brand, T. & Ferlini, A. POPDC1(S201F) causes muscular dystrophy and arrhythmia by affecting protein trafficking. *J Clin Invest* **126**, 239-253 (2016).

94 Rehmann, H., Wittinghofer, A. & Bos, J. L. Capturing cyclic nucleotides in action: snapshots from crystallographic studies. *Nat Rev Mol Cell Biol* **8**, 63-73 (2007).

95 Berman, H. M., Ten Eyck, L. F., Goodsell, D. S., Haste, N. M., Kornev, A. & Taylor, S. S. The cAMP binding domain: an ancient signaling module. *Proc Natl Acad Sci U S A* **102**, 45-50 (2005).

96 Rehmann, H., Rueppel, A., Bos, J. L. & Wittinghofer, A. Communication between the regulatory and the catalytic region of the cAMP-responsive guanine nucleotide exchange factor Epac. *J Biol Chem* **278**, 23508-23514 (2003).

97 Rehmann, H., Prakash, B., Wolf, E., Rueppel, A., de Rooij, J., Bos, J. L. & Wittinghofer, A. Structure and regulation of the cAMP-binding domains of Epac2. *Nat Struct Biol* **10**, 26-32 (2003).

98 Amunjela, J. N., Swan, A. H. & Brand, T. The Role of the Popeye Domain Containing Gene Family in Organ Homeostasis. *Cells* **8**, 1594 (2019).

99 Vissing, J., Johnson, K., Topf, A., Nafissi, S., Diaz-Manera, J., French, V. M., Schindler, R. F., Sarathchandra, P., Lokken, N., Rinne, S., Freund, M., Decher, N., Muller, T., Duno, M., Krag, T., Brand, T. & Straub, V. POPDC3 Gene Variants Associate with a New Form of Limb Girdle Muscular Dystrophy. *Ann Neurol* **86**, 832-843 (2019).

100 Tibbo, A. J., Mika, D., Dobi, S., Ling, J., McFall, A., Tejeda, G. S., Blair, C., MacLeod, R., MacQuaide, N., Gok, C., Fuller, W., Smith, B. O., Smith, G. L., Vandecasteele, G., Brand, T. & Baillie, G. S. Phosphodiesterase type 4 anchoring regulates cAMP signaling to Popeye domain-containing proteins. *J Mol Cell Cardiol* **165**, 86-102 (2022).

101 Baldwin, T. A., Li, Y., Marsden, A., Schindler, R. F. R., Zhang, M., Carbajal, A. G., Garcia, M. A., Venna, V. R., Brand, T. & Dessauer, C. W. Popeye Domain-Containing Protein 1 Scaffolds a Complex of Adenylyl Cyclase 9 and the Two-Pore-Domain Potassium Channel TREK-1 in Heart. *bioRxiv*, 2021.2012.2021.473719 (2021).

102 Li, Y., Baldwin, T. A., Wang, Y., Subramaniam, J., Carbajal, A. G., Brand, C. S., Cunha, S. R. & Dessauer, C. W. Loss of type 9 adenylyl cyclase triggers reduced phosphorylation of Hsp20 and diastolic dysfunction. *Sci Rep* **7**, 5522 (2017).

103 Xian Tao, L., Dyachenko, V., Zuzarte, M., Putzke, C., Preisig-Muller, R., Isenberg, G. & Daut, J. The stretch-activated potassium channel TREK-1 in rat cardiac ventricular muscle. *Cardiovasc Res* **69**, 86-97 (2006).

104 Unudurthi, S. D., Wu, X., Qian, L., Amari, F., Onal, B., Li, N., Makara, M. A., Smith, S. A., Snyder, J., Fedorov, V. V., Coppola, V., Anderson, M. E., Mohler, P. J. & Hund, T. J. Two-Pore K+ Channel TREK-1 Regulates Sinoatrial Node Membrane Excitability. *J Am Heart Assoc* **5**, e002865 (2016).

105 Rinne, S., Ortiz-Bonnin, B., Stallmeyer, B., Kiper, A. K., Fortmuller, L., Schindler, R. F. R., Herbort-Brand, U., Kabir, N. S., Dittmann, S., Friedrich, C., Zumhagen, S., Gualandi, F., Selvatici, R., Rapezzi, C., Arbustini, E., Ferlini, A., Fabritz, L., Schulze-Bahr, E., Brand, T. & Decher, N. POPDC2 a novel susceptibility gene for conduction disorders. *J Mol Cell Cardiol* **145**, 74-83 (2020).

106 Sandoz, G., Thummler, S., Duprat, F., Feliciangeli, S., Vinh, J., Escoubas, P., Guy, N., Lazdunski, M. & Lesage, F. AKAP150, a switch to convert mechano-, pH- and arachidonic acid-sensitive TREK K(+) channels into open leak channels. *EMBO J* **25**, 5864-5872 (2006).

107 Frontera, W. R. & Ochala, J. Skeletal muscle: a brief review of structure and function. *Calcif Tissue Int* **96**, 183-195 (2015).

108 Bonnemann, C. G., Wang, C. H., Quijano-Roy, S., Deconinck, N., Bertini, E., Ferreiro, A., Muntoni, F., Sewry, C., Beroud, C., Mathews, K. D., Moore, S. A., Bellini, J., Rutkowski, A., North, K. N. & Members of International Standard of Care Committee for Congenital Muscular, D. Diagnostic approach to the congenital muscular dystrophies. *Neuromuscul Disord* **24**, 289-311 (2014).

109 Yoshida, M., Hama, H., Ishikawa-Sakurai, M., Imamura, M., Mizuno, Y., Araishi, K., Wakabayashi-Takai, E., Noguchi, S., Sasaoka, T. & Ozawa, E. Biochemical evidence for association of dystrobrevin with the sarcoglycan-sarcospan complex as a basis for understanding sarcoglycanopathy. *Hum Mol Genet* **9**, 1033-1040 (2000).

110 Tarakci, H. & Berger, J. The sarcoglycan complex in skeletal muscle. *Front Biosci* **21**, 744-756 (2016).

111 Widmaier, E. P., Hershel, R. & Strang, K. T. Cardiovascular Physiology in *Vander's Human Physiology*. 353-400 (McGraw Hill, 2011).

112 Setterberg, I. E., Le, C., Frisk, M., Li, J. & Louch, W. E. The Physiology and Pathophysiology of T-Tubules in the Heart. *Front Physiol* **12**, 718404 (2021).

113 de Lucia, C., Eguchi, A. & Koch, W. J. New Insights in Cardiac beta-Adrenergic Signaling During Heart Failure and Aging. *Front Pharmacol* **9**, 904 (2018).

114 Rudolf, R., Khan, M. M., Lustrino, D., Labeit, S., Kettelhut, I. C. & Navegantes, L. C. Alterations of cAMP-dependent signaling in dystrophic skeletal muscle. *Front Physiol* **4**, 290 (2013).

115 Bastiani, M. & Parton, R. G. Caveolae at a glance. *J Cell Sci* **123**, 3831-3836 (2010).

116 Bansal, D., Miyake, K., Vogel, S. S., Groh, S., Chen, C. C., Williamson, R., McNeil, P. L. & Campbell, K. P. Defective membrane repair in dysferlin-deficient muscular dystrophy. *Nature* **423**, 168-172 (2003).

117 Gangfuss, A., Hentschel, A., Heil, L., Gonzalez, M., Schonecker, A., Depienne, C., Nishimura, A., Zengeler, D., Kohlschmidt, N., Sickmann, A., Schara-Schmidt, U., Furst, D. O., van der Ven, P. F. M., Hahn, A., Roos, A. & Schanzer, A. Proteomic and morphological insights and clinical presentation of two young patients with novel mutations of BVES (POPDC1). *Mol Genet Metab* **136**, 226-237 (2022).

118 Li, H., Xu, L., Gao, Y., Zuo, Y., Yang, Z., Zhao, L., Chen, Z., Guo, S. & Han, R. BVES is a novel interactor of ANO5 and regulates myoblast differentiation. *Cell and Bioscience* **11**, 1-10 (2021).

119 Hager, H. A., Roberts, R. J., Cross, E. E., Proux-Gillardeaux, V. & Bader, D. M. Identification of a novel Bves function: regulation of vesicular transport. *EMBO J* **29**, 532-545 (2010).

120 Holt, I., Fuller, H. R., Schindler, R. F. R., Shirran, S. L., Brand, T. & Morris, G. E. An interaction of heart disease-associated proteins POPDC1/2 with XIRP1 in transverse tubules and intercalated discs. *BMC Mol Cell Biol* **21**, 88 (2020).

121 Kirchmaier, B. C., Poon, K. L., Schwerte, T., Huisken, J., Winkler, C., Jungblut, B., Stainier, D. Y. & Brand, T. The Popeye domain containing 2 (popdc2) gene in zebrafish is required for heart and skeletal muscle development. *Dev Biol* **363**, 438-450 (2012).

122 De Ridder, W., Nelson, I., Asselbergh, B., De Paepe, B., Beuvin, M., Ben Yaou, R., Masson, C., Boland, A., Deleuze, J. F., Maisonobe, T., Eymard, B., Symoens, S., Schindler, R., Brand, T., Johnson, K., Topf, A., Straub, V., De Jonghe, P., De Bleecker, J. L., Bonne, G. & Baets, J. Muscular dystrophy with arrhythmia caused by loss-of-function mutations in BVES. *Neurol Genet* **5**, e321 (2019).

123 Indrawati, L. A., Iida, A., Tanaka, Y., Honma, Y., Mizoguchi, K., Yamaguchi, T., Ikawa, M., Hayashi, S., Noguchi, S. & Nishino, I. Two Japanese LGMDR25 patients with a biallelic recurrent nonsense variant of BVES. *Neuromuscul Disord* **30**, 674-679 (2020).

124 Ullah, A., Lin, Z., Younus, M., Shafiq, S., Khan, S., Rasheed, M., Mahmood, A., Alqosaibi, A. I., Alshehri, M. A., Khan, A. & Umair, M. Homozygous missense variant in POPDC3 causes recessive limb-girdle muscular dystrophy type 26. *J Gene Med* **24**, e3412 (2022).

125 Gingold-Belfer, R., Bergman, M., Alcalay, Y., Schlesinger, H., Aravot, D., Berman, M., Salman, H., Brand, T. & Kessler-Icekson, G. Popeye domain-containing 1 is down-regulated in failing human hearts. *Int J Mol Med* **27**, 25-31 (2011).

126 Gingold-Belfer, R., Bergman, M., Schlsinger, H., Aravot, D., Berman, M., Salman, H., Brand, T. & Kessler-Icekson, G. Popeye domain containing (POPDC) genes are reprogrammed in failing human hearts. *Journal of Molecular and Cellular Cardiology* **44**, 721 (2008).

127 Tan, N., Chung, M. K., Smith, J. D., Hsu, J., Serre, D., Newton, D. W., Castel, L., Soltesz, E., Pettersson, G., Gillinov, A. M., Van Wagoner, D. R. & Barnard, J. Weighted gene coexpression network analysis of human left atrial tissue identifies gene modules associated with atrial fibrillation. *Circ Cardiovasc Genet* **6**, 362-371 (2013).

128 Meinke, P., Kerr, A. R. W., Czapiewski, R., de Las Heras, J. I., Dixon, C. R., Harris, E., Kolbel, H., Muntoni, F., Schara, U., Straub, V., Schoser, B., Wehnert, M. & Schirmer, E. C. A multistage sequencing strategy pinpoints novel candidate alleles for Emery-Dreifuss muscular dystrophy and supports gene misregulation as its pathomechanism. *EBioMedicine* **51**, 102587 (2020).

129 Beecher, G., Tang, C. & Liewluck, T. Severe adolescent-onset limb-girdle muscular dystrophy due to a novel homozygous nonsense BVES variant. *J Neurol Sci* **420**, 117259 (2021).

130 Han, P., Fu, Y., Liu, J., Wang, Y., He, J., Gong, J., Li, M., Tan, Q., Li, D., Luo, Y., Han, J., Liu, J., Tu, W., Wang, Y., Tian, D. & Yan, W. Netrin-1 promotes cell migration and invasion by down-regulation of BVES expression in human hepatocellular carcinoma. *Am J Cancer Res* **5**, 1396-1409 (2015).

131 Amunjela, J. N. & Tucker, S. J. POPDC1 is suppressed in human breast cancer tissues and is negatively regulated by EGFR in breast cancer cell lines. *Cancer Lett* **406**, 81-92 (2017).

132 Amunjela, J. N. & Tucker, S. J. Dysregulation of POPDC1 promotes breast cancer cell migration and proliferation. *Biosci Rep* **37**, BSR20171039 (2017).

133 He, X., Xu, H., Zhao, W., Zhan, M., Li, Y., Liu, H., Tan, L. & Lu, L. POPDC3 is a potential biomarker for prognosis and radioresistance in patients with head and neck squamous cell carcinoma. *Oncol Lett* **18**, 5468-5480 (2019).

134 Parang, B., Kaz, A. M., Barrett, C. W., Short, S. P., Ning, W., Keating, C. E., Mittal, M. K., Naik, R. D., Washington, M. K., Revetta, F. L., Smith, J. J., Chen, X., Wilson, K. T., Brand, T., Bader, D. M., Tansey, W. P., Chen, R., Brentnall, T. A., Grady, W. M. & Williams, C. S. BVES regulates c-Myc stability via PP2A and suppresses colitis-induced tumourigenesis. *Gut* **66**, 852-862 (2017).

135 Amunjela, J. N. & Tucker, S. J. POPDC proteins as potential novel therapeutic targets in cancer. *Drug Discov Today* **21**, 1920-1927 (2016).

136 Boukens, B. J. & Christoffels, V. M. Popeye proteins: muscle for the aging sinus node. *J Clin Invest* **122**, 810-813 (2012).

137 Firth-clark, S. Study to select a screening deck for the Popeye Domain of popdc1 using the Domainex LeadBuilder technology platform (Study Report). 1-9 (Domainex, 2016).

138 Chapman, K. & Brand, T. Identification of small molecule modulators that target POPDC1 - a hub gene essential in atrial fibrillation (Study Report). 1-17 (Domainex, Imperial College London, 2016).

139 Jiang, J. Y., Falcone, J. L., Curci, S. & Hofer, A. M. Interrogating cyclic AMP signaling using optical approaches. *Cell Calcium* **64**, 47-56 (2017).

140 Huth, J. R., Bewley, C. A., Jackson, B. M., Hinnebusch, A. G., Clore, G. M. & Gronenborn, A. M. Design of an expression system for detecting folded protein domains and mapping macromolecular interactions by NMR. *Protein Sci* **6**, 2359-2364 (1997).

141 Micsonai, A., Wien, F., Bulyaki, E., Kun, J., Moussong, E., Lee, Y. H., Goto, Y., Refregiers, M. & Kardos, J. BeStSel: a web server for accurate protein secondary structure prediction and fold recognition from the circular dichroism spectra. *Nucleic Acids Res* **46**, W315-W322 (2018).

142 Schindelin, J., Arganda-Carreras, I., Frise, E., Kaynig, V., Longair, M., Pietzsch, T., Preibisch, S., Rueden, C., Saalfeld, S., Schmid, B., Tinevez, J. Y., White, D. J., Hartenstein, V., Eliceiri, K., Tomancak, P. & Cardona, A. Fiji: an open-source platform for biological-image analysis. *Nat Methods* **9**, 676-682 (2012).

143 Machleidt, T., Woodroofe, C. C., Schwinn, M. K., Mendez, J., Robers, M. B., Zimmerman, K., Otto, P., Daniels, D. L., Kirkland, T. A. & Wood, K. V. NanoBRET--A Novel BRET Platform for the Analysis of Protein-Protein Interactions. *ACS Chem Biol* **10**, 1797-1804 (2015).

144 Felce, J. H., Latty, S. L., Knox, R. G., Mattick, S. R., Lui, Y., Lee, S. F., Klenerman, D. & Davis, S. J. Receptor Quaternary Organization Explains G Protein-Coupled Receptor Family Structure. *Cell Rep* **20**, 2654-2665 (2017).

145 Helm, B. M., Swan, A. H., Brand, T., Steinberg, L. A. & Kean, A. C. Using Exome Sequencing to Uncover A Popdc2 Variant as a Novel Candidate Cause of Familial Junctional Ectopic Tachycardia at *Heart Rhythm 2021.* S381 B-PO305-025 (Elsevier, Boston, MA, 2021).

146 Smedley, D., Jacobsen, J. O., Jager, M., Kohler, S., Holtgrewe, M., Schubach, M., Siragusa, E., Zemojtel, T., Buske, O. J., Washington, N. L., Bone, W. P., Haendel, M. A. & Robinson, P. N. Next-generation diagnostics and disease-gene discovery with the Exomiser. *Nat Protoc* **10**, 2004-2015 (2015).

147 Madeira, F., Pearce, M., Tivey, A. R. N., Basutkar, P., Lee, J., Edbali, O., Madhusoodanan, N., Kolesnikov, A. & Lopez, R. Search and sequence analysis tools services from EMBL-EBI in 2022. *Nucleic Acids Res*, gkac240-gkac240 (2022).

148 Waterhouse, A. M., Procter, J. B., Martin, D. M., Clamp, M. & Barton, G. J. Jalview Version 2--a multiple sequence alignment editor and analysis workbench. *Bioinformatics* **25**, 1189-1191 (2009).

149 Pettersen, E. F., Goddard, T. D., Huang, C. C., Meng, E. C., Couch, G. S., Croll, T. I., Morris, J. H. & Ferrin, T. E. UCSF ChimeraX: Structure visualization for researchers, educators, and developers. *Protein Sci* **30**, 70-82 (2021).

150 Kelley, L. A., Mezulis, S., Yates, C. M., Wass, M. N. & Sternberg, M. J. The Phyre2 web portal for protein modeling, prediction and analysis. *Nat Protoc* **10**, 845-858 (2015).

151 Drozdetskiy, A., Cole, C., Procter, J. & Barton, G. J. JPred4: a protein secondary structure prediction server. *Nucleic Acids Res* **43**, W389-394 (2015).

152 Cheng, Y. & Patel, D. J. An efficient system for small protein expression and refolding. *Biochem Biophys Res Commun* **317**, 401-405 (2004).

153 Frueh, D. P. Practical aspects of NMR signal assignment in larger and challenging proteins. *Prog Nucl Magn Reson Spectrosc* **78**, 47-75 (2014).

154 Osler, M. E., Chang, M. S. & Bader, D. M. Bves modulates epithelial integrity through an interaction at the tight junction. *J Cell Sci* **118**, 4667-4678 (2005).

155 Senisterra, G., Chau, I. & Vedadi, M. Thermal denaturation assays in chemical biology. *Assay Drug Dev Technol* **10**, 128-136 (2012).

156 Raimondi, D., Orlando, G., Fariselli, P. & Moreau, Y. Insight into the protein solubility driving forces with neural attention. *PLoS Comput Biol* **16**, e1007722 (2020).

157 Purification, A. & Protein, A. M. P. R. Ni Affinity Purification of Untagged cAMP Receptor Protein. *Biotechniques* **33**, 728-730 (2002).

158 Some, D., Amartely, H., Tsadok, A. & Lebendiker, M. Characterization of Proteins by Size-Exclusion Chromatography Coupled to Multi-Angle Light Scattering (SEC-MALS). *J Vis Exp* **2019**, e59615 (2019).

159 Lindman, S., Xue, W. F., Szczepankiewicz, O., Bauer, M. C., Nilsson, H. & Linse, S. Salting the charged surface: pH and salt dependence of protein G B1 stability. *Biophys J* **90**, 2911-2921 (2006).

160 Schmidt, H. L., Sperling, L. J., Gao, Y. G., Wylie, B. J., Boettcher, J. M., Wilson, S. R. & Rienstra, C. M. Crystal polymorphism of protein GB1 examined by solid-state NMR spectroscopy and X-ray diffraction. *J Phys Chem B* **111**, 14362-14369 (2007).

161 Walpole, S., Monaco, S., Nepravishta, R. & Angulo, J. STD NMR as a Technique for Ligand Screening and Structural Studies. *Methods Enzymol* **615**, 423-451 (2019).

162 Huang, R. & Leung, I. K. H. Protein-Small Molecule Interactions by WaterLOGSY. *Methods Enzymol* **615**, 477-500 (2019).

163 Pervushin, K., Riek, R., Wider, G. & Wuthrich, K. Attenuated T2 relaxation by mutual cancellation of dipole-dipole coupling and chemical shift anisotropy indicates an avenue to NMR structures of very large biological macromolecules in solution. *Proc Natl Acad Sci U S A* **94**, 12366-12371 (1997).

164 Niesen, F. H., Berglund, H. & Vedadi, M. The use of differential scanning fluorimetry to detect ligand interactions that promote protein stability. *Nat Protoc* **2**, 2212-2221 (2007).

165 Mueller, A. M., Breitsprecher, D., Duhr, S., Baaske, P., Schubert, T. & Langst, G. MicroScale Thermophoresis: A Rapid and Precise Method to Quantify Protein-Nucleic Acid Interactions in Solution. *Methods Mol Biol* **1654**, 151-164 (2017).

166 Duhr, S. & Braun, D. Why molecules move along a temperature gradient. *Proc Natl Acad Sci U S A* **103**, 19678-19682 (2006).

167 Koubek, J., Schmitt, J., Galmozzi, C. V. & Kramer, G. Mechanisms of Cotranslational Protein Maturation in Bacteria. *Front Mol Biosci* **8**, 689755 (2021).

168 Goehring, A., Lee, C. H., Wang, K. H., Michel, J. C., Claxton, D. P., Baconguis, I., Althoff, T., Fischer, S., Garcia, K. C. & Gouaux, E. Screening and large-scale expression of membrane proteins in mammalian cells for structural studies. *Nat Protoc* **9**, 2574-2585 (2014).

169 Parnell, E., McElroy, S. P., Wiejak, J., Baillie, G. L., Porter, A., Adams, D. R., Rehmann, H., Smith, B. O. & Yarwood, S. J. Identification of a Novel, Small Molecule Partial Agonist for the Cyclic AMP Sensor, EPAC1. *Sci Rep* **7**, 294 (2017).

170 Tibbo, A. J. *Compartmentalized cAMP Signaling via the PDE4-Popeye Protein Complex.* PhD thesis, University of Glasgow, (2020).

171 Jafari, R., Almqvist, H., Axelsson, H., Ignatushchenko, M., Lundback, T., Nordlund, P. & Martinez Molina, D. The cellular thermal shift assay for evaluating drug target interactions in cells. *Nat Protoc* **9**, 2100-2122 (2014).

172 Martinez Molina, D., Jafari, R., Ignatushchenko, M., Seki, T., Larsson, E. A., Dan, C., Sreekumar, L., Cao, Y. & Nordlund, P. Monitoring drug target engagement in cells and tissues using the cellular thermal shift assay. *Science* **341**, 84-87 (2013).

173 Zaccolo, M., De Giorgi, F., Cho, C. Y., Feng, L., Knapp, T., Negulescu, P. A., Taylor, S. S., Tsien, R. Y. & Pozzan, T. A genetically encoded, fluorescent indicator for cyclic AMP in living cells. *Nat Cell Biol* **2**, 25-29 (2000).

174 Paramonov, V. M., Mamaeva, V., Sahlgren, C. & Rivero-Muller, A. Genetically-encoded tools for cAMP probing and modulation in living systems. *Front Pharmacol* **6**, 196 (2015).

175 Swan, A. H. *Towards the Biophysical and Structural Characterization of the Interactions of POPDC1 and Small Molecule Ligands.* MRes thesis, Imperial College London, (2018).

176 Hall, M. P., Unch, J., Binkowski, B. F., Valley, M. P., Butler, B. L., Wood, M. G., Otto, P., Zimmerman, K., Vidugiris, G., Machleidt, T., Robers, M. B., Benink, H. A., Eggers, C. T., Slater, M. R., Meisenheimer, P. L., Klaubert, D. H., Fan, F., Encell, L. P. & Wood, K. V. Engineered luciferase reporter from a deep sea shrimp utilizing a novel imidazopyrazinone substrate. *ACS Chem Biol* **7**, 1848-1857 (2012).

177 Los, G. V., Encell, L. P., McDougall, M. G., Hartzell, D. D., Karassina, N., Zimprich, C., Wood, M. G., Learish, R., Ohana, R. F., Urh, M., Simpson, D., Mendez, J., Zimmerman, K., Otto, P., Vidugiris, G., Zhu, J., Darzins, A., Klaubert, D. H., Bulleit, R. F. & Wood, K. V. HaloTag: a novel protein labeling technology for cell imaging and protein analysis. *ACS Chem Biol* **3**, 373-382 (2008).

178 Thomas, P. & Smart, T. G. HEK293 cell line: a vehicle for the expression of recombinant proteins. *J Pharmacol Toxicol Methods* **51**, 187-200 (2005).

179 Atwood, B. K., Lopez, J., Wager-Miller, J., Mackie, K. & Straiker, A. Expression of G protein-coupled receptors and related proteins in HEK293, AtT20, BV2, and N18 cell lines as revealed by microarray analysis. *BMC Genomics* **12**, 14 (2011).

180 Ohta, Y., Kamagata, T., Mukai, A., Takada, S., Nagai, T. & Horikawa, K. Nontrivial Effect of the Color-Exchange of a Donor/Acceptor Pair in the Engineering of Forster Resonance Energy Transfer (FRET)-Based Indicators. *ACS Chem Biol* **11**, 1816-1822 (2016).

181 Zhang, J. H., Chung, T. D. & Oldenburg, K. R. A Simple Statistical Parameter for Use in Evaluation and Validation of High Throughput Screening Assays. *J Biomol Screen* **4**, 67-73 (1999).

182 Kocan, M., See, H. B., Seeber, R. M., Eidne, K. A. & Pfleger, K. D. Demonstration of improvements to the bioluminescence resonance energy transfer (BRET) technology for the monitoring of G protein-coupled receptors in live cells. *J Biomol Screen* **13**, 888-898 (2008).

183 Prinz, A., Diskar, M., Erlbruch, A. & Herberg, F. W. Novel, isotype-specific sensors for protein kinase A subunit interaction based on bioluminescence resonance energy transfer (BRET). *Cell Signal* **18**, 1616-1625 (2006).

184 Brand, T. POPDC proteins and cardiac function. *Biochem Soc Trans* **47**, 1393-1404 (2019).

185 Ko, W., Kim, S., Lee, S., Jo, K. & Lee, H. S. Genetically encoded FRET sensors using a fluorescent unnatural amino acid as a FRET donor. *RSC Advances* **6**, 78661-78668 (2016).

186 Swan, A. H., Schindler, R. F. R., Mayer, I., Davison, C., Fedele, L., Gruscheski, L., Susanne, R., Niels, D., Giorgio, T., Perna, F., Savarese, M., Udd, B., Hahn, A., Schanzer, A., Milting, H., Ferlini, A., Barton, P. J. R., Buchan, R., Walsh, R., Cook, S. A., Pfuhl, M., Chapman, K., Spivey, A. C. & Thomas, B. *Heteromeric interaction of POPDC1 and POPDC2 is essential for membrane trafficking.* Unpublished (2022).

187 Pell, R., Oien, K., Robinson, M., Pitman, H., Rajpoot, N., Rittscher, J., Snead, D., Verrill, C. & group, U. K. N. C. R. I. C.-M. P. q. a. w. The use of digital pathology and image analysis in clinical trials. *J Pathol Clin Res* **5**, 81-90 (2019).

188 Ripolone, M., Velardo, D., Mondello, S., Zanotti, S., Magri, F., Minuti, E., Cazzaniga, S., Fortunato, F., Ciscato, P., Tiberio, F., Sciacco, M., Moggio, M., Bettica, P. & Comi, G. P. Muscle histological changes in a large cohort of patients affected with Becker muscular dystrophy. *Acta Neuropathol Commun* **10**, 48 (2022).

189 Scaglioni, D., Ellis, M., Catapano, F., Torelli, S., Chambers, D., Feng, L., Sewry, C., Morgan, J., Muntoni, F. & Phadke, R. A high-throughput digital script for multiplexed immunofluorescent analysis and quantification of sarcolemmal and sarcomeric proteins in muscular dystrophies. *Acta Neuropathol Commun* **8**, 53 (2020).

190 Herbort-Brand, U. & Brand, T. Unpublished (Imperial College London, 2022).

191 Bastiaens, P. Observing proteins in their natural habitat: the living cell. *Trends in Biochemical Sciences* **25**, 631-637 (2000).

192 Zimmermann, T. Photobleaching and Sensitized Emission-Based Methods for the Detection of Forster Resonance Energy Transfer. *Methods Mol Biol* **2040**, 235-274 (2019).

193 Angelova, P. R., Choi, M. L., Berezhnov, A. V., Horrocks, M. H., Hughes, C. D., De, S., Rodrigues, M., Yapom, R., Little, D., Dolt, K. S., Kunath, T., Devine, M. J., Gissen, P., Shchepinov, M. S., Sylantyev, S., Pavlov, E. V., Klenerman, D., Abramov, A. Y. & Gandhi, S. Alpha synuclein aggregation drives ferroptosis: an interplay of iron, calcium and lipid peroxidation. *Cell Death Differ* **27**, 2781-2796 (2020).

194 Zhang, Y., Yan, Y., Xia, S., Wan, S., Steenwinkel, T. E., Medford, J., Durocher, E., Luck, R. L., Werner, T. & Liu, H. Cell Membrane-Specific Fluorescent Probe Featuring Dual and Aggregation-Induced Emissions. *ACS Appl Mater Interfaces* **12**, 20172-20179 (2020).

195 Jacob, R. S., Eichmann, C., Dema, A., Mercadante, D. & Selenko, P. alpha-Synuclein plasma membrane localization correlates with cellular phosphatidylinositol polyphosphate levels. *Elife* **10**, e61951 (2021).

196 van Unen, J., Botman, D., Yin, T., Wu, Y. I., Hink, M. A., Gadella, T. W. J., Jr., Postma, M. & Goedhart, J. The C-terminus of the oncoprotein TGAT is necessary for plasma membrane association and efficient RhoA-mediated signaling. *BMC Cell Biol* **19**, 6 (2018).

197 DeSimone, A. M., Cohen, J., Lek, M. & Lek, A. Cellular and animal models for facioscapulohumeral muscular dystrophy. *Dis Model Mech* **13** (2020).

198 Yaffe, D. & Saxel, O. Serial passaging and differentiation of myogenic cells isolated from dystrophic mouse muscle. *Nature* **270**, 725-727 (1977).

199 Smith, T. K. & Bader, D. M. Characterization of Bves expression during mouse development using newly generated immunoreagents. *Dev Dyn* **235**, 1701-1708 (2006).

200 Takahashi, K. & Yamanaka, S. Induction of pluripotent stem cells from mouse embryonic and adult fibroblast cultures by defined factors. *Cell* **126**, 663-676 (2006).

201 Miyagoe-Suzuki, Y. & Takeda, S. Skeletal muscle generated from induced pluripotent stem cells - induction and application. *World J Stem Cells* **9**, 89-97 (2017).

202 Valetdinova, K. R., Maretina, M. A., Vyatkin, Y. V., Perepelkina, M. P., Egorova, A. A., Baranov, V. S., Kiselev, A. V., Gershovich, P. M. & Zakian, S. M. Generation of three Duchenne muscular dystrophy patient-derived induced pluripotent stem cell (iPSC) lines ICGi002-A, ICGi002-B and ICGi002-C. *Stem Cell Res* **48**, 101941 (2020).

203 Hug, N., Longman, D. & Caceres, J. F. Mechanism and regulation of the nonsense-mediated decay pathway. *Nucleic Acids Res* **44**, 1483-1495 (2016).

204 Le Hir, H., Gatfield, D., Izaurralde, E. & Moore, M. J. The exon-exon junction complex provides a binding platform for factors involved in mRNA export and nonsense-mediated mRNA decay. *EMBO J* **20**, 4987-4997 (2001).

205 Wombacher, R. & Cornish, V. W. Chemical tags: applications in live cell fluorescence imaging. *J Biophotonics* **4**, 391-402 (2011).

206 FitzGerald, L. I., Aurelio, L., Chen, M., Yuen, D., Rennick, J. J., Graham, B. & Johnston, A. P. R. A molecular sensor to quantify the localization of proteins, DNA and nanoparticles in cells. *Nat Commun* **11**, 4482 (2020).

207 Kaczor, A. A., Makarska-Bialokoz, M., Selent, J., de la Fuente, R. A., Marti-Solano, M. & Castro, M. Application of BRET for studying G protein-coupled receptors. *Mini Rev Med Chem* **14**, 411-425 (2014).

208 Szalai, B., Hoffmann, P., Prokop, S., Erdelyi, L., Varnai, P. & Hunyady, L. Improved methodical approach for quantitative BRET analysis of G Protein Coupled Receptor dimerization. *PLoS One* **9**, e109503 (2014).

209 Achour, L., Kamal, M., Jockers, R. & Marullo, S. Using quantitative BRET to assess G protein-coupled receptor homo- and heterodimerization. *Methods Mol Biol* **756**, 183-200 (2011).

210 Felce, J. H. & Davis, S. J. Unraveling receptor stoichiometry using bret. *Front Endocrinol* **3**, 86 (2012).

211 Busnelli, M., Mauri, M., Parenti, M. & Chini, B. Analysis of GPCR dimerization using acceptor photobleaching resonance energy transfer techniques. *Methods Enzymol* **521**, 311-327 (2013).

212 Van Munster, E. B., Kremers, G. J., Adjobo-Hermans, M. J. & Gadella, T. W., Jr. Fluorescence resonance energy transfer (FRET) measurement by gradual acceptor photobleaching. *J Microsc* **218**, 253-262 (2005).

213 Pope, J. R., Johnson, R. L., Jamieson, W. D., Worthy, H. L., Kailasam, S., Ahmed, R. D., Taban, I., Auhim, H. S., Watkins, D. W., Rizkallah, P. J., Castell, O. K. & Jones, D. D. Association of Fluorescent Protein Pairs and Its Significant Impact on Fluorescence and Energy Transfer. *Adv Sci* **8**, 2003167 (2020).

214 von Stetten, D., Noirclerc-Savoye, M., Goedhart, J., Gadella, T. W., Jr. & Royant, A. Structure of a fluorescent protein from Aequorea victoria bearing the obligate-monomer mutation A206K. *Acta Crystallogr Sect F Struct Biol Cryst Commun* **68**, 878-882 (2012).

215 Kerppola, T. K. Bimolecular fluorescence complementation (BiFC) analysis as a probe of protein interactions in living cells. *Annu Rev Biophys* **37**, 465-487 (2008).

216 Waadt, R., Schlucking, K., Schroeder, J. I. & Kudla, J. Protein fragment bimolecular fluorescence complementation analyses for the in vivo study of protein-protein interactions and cellular protein complex localizations. *Methods Mol Biol* **1062**, 629-658 (2014).

217 Sievers, F., Wilm, A., Dineen, D., Gibson, T. J., Karplus, K., Li, W., Lopez, R., McWilliam, H., Remmert, M., Soding, J., Thompson, J. D. & Higgins, D. G. Fast, scalable generation of high-quality protein multiple sequence alignments using Clustal Omega. *Mol Syst Biol* **7**, 539 (2011).

218 Walshaw, J. & Woolfson, D. N. Open-and-shut cases in coiled-coil assembly: alpha-sheets and alpha-cylinders. *Protein Sci* **10**, 668-673 (2001).

219 Passner, J. M., Schultz, S. C. & Steitz, T. A. Modeling the cAMP-induced allosteric transition using the crystal structure of CAP-cAMP at 2.1 A resolution. *J Mol Biol* **304**, 847-859 (2000).

220 Popovych, N., Tzeng, S. R., Tonelli, M., Ebright, R. H. & Kalodimos, C. G. Structural basis for cAMP-mediated allosteric control of the catabolite activator protein. *Proc Natl Acad Sci U S A* **106**, 6927-6932 (2009).

221 Sharma, H., Yu, S., Kong, J., Wang, J. & Steitz, T. A. Structure of apo-CAP reveals that large conformational changes are necessary for DNA binding. *Proc Natl Acad Sci U S A* **106**, 16604-16609 (2009).

222 Jackson, M. R., Nilsson, T. & Peterson, P. A. Identification of a consensus motif for retention of transmembrane proteins in the endoplasmic reticulum. *EMBO J* **9**, 3153-3162 (1990).

223 Nilsson, T., Jackson, M. & Peterson, P. A. Short cytoplasmic sequences serve as retention signals for transmembrane proteins in the endoplasmic reticulum. *Cell* **58**, 707-718 (1989).

224 Zerangue, N., Schwappach, B., Jan, Y. N. & Jan, L. Y. A new ER trafficking signal regulates the subunit stoichiometry of plasma membrane K(ATP) channels. *Neuron* **22**, 537-548 (1999).

225 Ohno, H., Stewart, J., Fournier, M. C., Bosshart, H., Rhee, I., Miyatake, S., Saito, T., Gallusser, A., Kirchhausen, T. & Bonifacino, J. S. Interaction of tyrosine-based sorting signals with clathrin-associated proteins. *Science* **269**, 1872-1875 (1995).

226 Wass, M. N., Kelley, L. A. & Sternberg, M. J. 3DLigandSite: predicting ligand-binding sites using similar structures. *Nucleic Acids Res* **38**, W469-473 (2010).

227 Fleming, K. G. & Engelman, D. M. Specificity in transmembrane helix-helix interactions can define a hierarchy of stability for sequence variants. *Proc Natl Acad Sci U S A* **98**, 14340-14344 (2001).

228 Faure, A. J., Domingo, J., Schmiedel, J. M., Hidalgo-Carcedo, C., Diss, G. & Lehner, B. Mapping the energetic and allosteric landscapes of protein binding domains. *Nature* **604**, 175-183 (2022).

229 Wang, X., Ni, D., Liu, Y. & Lu, S. Rational Design of Peptide-Based Inhibitors Disrupting Protein-Protein Interactions. *Front Chem* **9**, 682675 (2021).

230 Li, E., Wimley, W. C. & Hristova, K. Transmembrane helix dimerization: beyond the search for sequence motifs. *Biochim Biophys Acta* **1818**, 183-193 (2012).

231 Bonifacino, J. S., Cosson, P. & Klausner, R. D. Colocalized transmembrane determinants for ER degradation and subunit assembly explain the intracellular fate of TCR chains. *Cell* **63**, 503-513 (1990).

232 Bonifacino, J. S., Cosson, P., Shah, N. & Klausner, R. D. Role of potentially charged transmembrane residues in targeting proteins for retention and degradation within the endoplasmic reticulum. *EMBO J* **10**, 2783-2793 (1991).

233 Chen, J., Shi, W., Zhang, Y., Sokol, R., Cai, H., Lun, M., Moore, B. F., Farber, M. J., Stepanchick, J. S., Bonnemann, C. G. & Chan, Y. M. Identification of functional domains in sarcoglycans essential for their interaction and plasma membrane targeting. *Exp Cell Res* **312**, 1610-1625 (2006).

234 Li, H. & Sun, S. Protein Aggregation in the ER: Calm behind the Storm. *Cells* **10**, 3337 (2021).

235 Di Blasi, R., Marbiah, M. M., Siciliano, V., Polizzi, K. & Ceroni, F. A call for caution in analysing mammalian co-transfection experiments and implications of resource competition in data misinterpretation. *Nature Communications* **12**, 2545 (2021).

236 Alasti, M., Mirzaee, S., Machado, C., Healy, S., Bittinger, L., Adam, D., Kotschet, E., Krafchek, J. & Alison, J. Junctional ectopic tachycardia (JET). *J Arrhythm* **36**, 837-844 (2020).

237 Tulino, D., Dattilo, G., Tulino, V., Marte, F. & Patane, S. A congenital form of junctional ectopic tachycardia. *Int J Cardiol* **145**, e54-e56 (2010).

238 Theis, J. L., Zimmermann, M. T., Larsen, B. T., Rybakova, I. N., Long, P. A., Evans, J. M., Middha, S., de Andrade, M., Moss, R. L., Wieben, E. D., Michels, V. V. & Olson, T. M. TNNI3K mutation in familial syndrome of conduction system disease, atrial tachyarrhythmia and dilated cardiomyopathy. *Hum Mol Genet* **23**, 5793-5804 (2014).

239 Xi, Y., Honeywell, C., Zhang, D., Schwartzentruber, J., Beaulieu, C. L., Tetreault, M., Hartley, T., Marton, J., Vidal, S. M., Majewski, J., Aravind, L., Care4Rare Canada, C., Gollob, M., Boycott, K. M. & Gow, R. M. Whole exome sequencing identifies the TNNI3K gene as a cause of familial conduction system disease and congenital junctional ectopic tachycardia. *Int J Cardiol* **185**, 114-116 (2015).

240 MacArthur, M. W. & Thornton, J. M. Influence of proline residues on protein conformation. *J Mol Biol* **218**, 397-412 (1991).

241 Schmidt, T., Situ, A. J. & Ulmer, T. S. Structural and thermodynamic basis of proline-induced transmembrane complex stabilization. *Sci Rep* **6**, 29809 (2016).

242 Brand, T. The Popeye Domain Containing Genes and Their Function as cAMP Effector Proteins in Striated Muscle. *Journal of Cardiovascular Development and Disease* **5**, 18 (2018).

243 Marassi, F. M., Das, B. B., Lu, G. J., Nothnagel, H. J., Park, S. H., Son, W. S., Tian, Y. & Opella, S. J. Structure determination of membrane proteins in five easy pieces. *Methods* **55**, 363-369 (2011).

244 Katz, C., Levy-Beladev, L., Rotem-Bamberger, S., Rito, T., Rüdiger, S. G. D., Friedler, A., Ru¨diger, S. G. D. R. d. & Friedler, A. Studying protein-protein interactions using peptide arrays. *Chemical Society Reviews* **40**, 2131-2145 (2011).

245 Gray, V. E., Hause, R. J. & Fowler, D. M. Analysis of Large-Scale Mutagenesis Data To Assess the Impact of Single Amino Acid Substitutions. *Genetics* **207**, 53-61 (2017).

246 Ibarra, A. A., Bartlett, G. J., Hegedüs, Z., Dutt, S., Hobor, F., Horner, K. A., Hetherington, K., Spence, K., Nelson, A., Edwards, T. A., Woolfson, D. N., Sessions, R. B. & Wilson, A. J. Predicting and Experimentally Validating Hot-Spot Residues at Protein–Protein Interfaces. *ACS Chemical Biology* **14**, 2252-2263 (2019).

247 Blair, C. M. & Baillie, G. S. Reshaping cAMP nanodomains through targeted disruption of compartmentalised phosphodiesterase signalosomes. *Biochemical Society Transactions*, BST20190252 (2019).

10 Appendix

10.1 Popeye Domain-Based cAMP BRET Sensor Data

Table 10.1: Table summarising the cAMP dependent change in BRET signal from the Popeye domain sensors. See Figure 4.6.

N-Terminus	C-Terminus	Control / 50 μM Forskolin	Replicates	Mean BRET / BU	SD	t*	df*	p*
E123	D266	Control	5	0.432	0.013	2.401	8	0.043
		50 μM Forskolin	5	0.451	0.012			
E123	K272	Control	5	0.302	0.016	1.178	8	0.113
		50 μM Forskolin	5	0.317	0.012			
E123	Q280	Control	5	0.197	0.010	2.292	8	0.051
		50 μM Forskolin	5	0.213	0.012			
E123	S288	Control	5	0.275	0.018	3.710	8	0.006
		50 μM Forskolin	5	0.305	0.004			
S109	D266	Control	5	0.381	0.014	2.359	8	0.046
		50 μM Forskolin	5	0.407	0.020			
K114	D266	Control	5	0.304	0.009	1.695	8	0.129
		50 μM Forskolin	5	0.316	0.122			
K119	D266	Control	5	0.396	0.033	0.565	8	0.590
		50 μM Forskolin	5	0.386	0.021			

* t, df and p values refer to the results of student's t-test comparing each control and 50 μM forskolin group.

10.2 Skeletal Muscle Biopsy Image Analysis Supplementary Results

Table 10.2: Table summarising the data for skeletal muscle biopsy Staining for POPDC1, POPDC2 and α-sarcoglycan in control and POPDC1 p.Q153X patient.

Normalised Protein Expression Levels

Protein	Region	Control/Patient	Fibres Analysed	Normalised Mean	SD	t*	df*	p*	Figure
POPDC1	Plasma Membrane	Patient	65	0.356	0.042	21.88	301	<0.0001	5.3A
		Control	238	1	0.236				
α-sarcoglycan (POPDC1 control)	Plasma Membrane	Patient	65	1.347	0.236	13.87	301	<0.0001	
		Control	238	1	0.160				
POPDC2	Plasma Membrane	Patient	70	0.211	0.021	38.79	231	<0.0001	
		Control	163	1	0.169				
α-sarcoglycan (POPDC2 control)	Plasma Membrane	Patient	70	1.719	0.293	23.57	231	<0.0001	
		Control	163	1	0.169				
POPDC1	Cytoplasm	Patient	65	0.896	0.165	2.89	301	0.004	5.3B
		Control	238	1	0.278				
α-sarcoglycan (POPDC1 control)	Cytoplasm	Patient	65	0.963	0.181	1.26	301	0.209	
		Control	238	1	0.214				
POPDC2	Cytoplasm	Patient	70	1.206	0.162	8.97	231	<0.0001	
		Control	163	1	0.161				
α-sarcoglycan (POPDC2 control)	Cytoplasm	Patient	70	1.437	0.361	11.71	231	<0.0001	
		Control	163	1	0.204				
Normalised POPDC Expression Relative to α-sarcoglycan									
POPDC1 / α-sarcoglycan	Plasma Membrane	Patient	65	0.273	0.080	26.33	301	<0.0001	5.3C
		Control	238	1	0.218				
POPDC2 / α-sarcoglycan	Plasma Membrane	Patient	70	0.124	0.022	43.49	231	<0.0001	
		Control	163	1	0.170				
Ratio of POPDC in the Plasma Membrane to Cytoplasm									
POPDC1	Plasma Membrane / Cytoplasm	Patient	65	1.961	0.294	20.98	301	<0.0001	5.3D
		Control	238	5.005	1.158				
POPDC2	Plasma Membrane / Cytoplasm	Patient	70	1.636	0.163	30.85	231	<0.0001	
		Control	163	9.501	2.127				

* t, df and p values refer to the results of student's t-test comparing the patient to the control.

Table 10.3: Table summarising the data for skeletal muscle biopsy staining for POPDC1, POPDC2 and α-sarcoglycan in control and POPDC1 p.V183F patient.

Normalised Protein Expression Levels

Protein	Region	Control/Patient	Fibres Analysed	Normalised Mean	SD	t*	df*	p*	Figure
POPDC1	Plasma Membrane	Mutant	167	0.629	0.268	12.89	326	<0.0001	5.7A
		Control	161	1	0.252				
α-sarcoglycan (POPDC1 control)	Plasma Membrane	Mutant	167	0.730	0.238	9.47	326	<0.0001	
		Control	161	1	0.277				
POPDC2	Plasma Membrane	Mutant	160	0.62	0.229	12.92	293	<0.0001	
		Control	135	1	0.276				
α-sarcoglycan (POPDC2 control)	Plasma Membrane	Mutant	160	0.874	0.216	4.88	293	<0.0001	
		Control	135	1	0.225				
POPDC1	Cytoplasm	Mutant	167	1.040	0.306	1.34	326	0.181	5.7B
		Control	161	1	0.219				
α-sarcoglycan (POPDC1 control)	Cytoplasm	Mutant	167	1.417	1.034	4.78	326	<0.0001	
		Control	161	1	0.402				
POPDC2	Cytoplasm	Mutant	160	2.044	0.635	17.99	293	<0.0001	
		Control	135	1	0.246				
α-sarcoglycan (POPDC2 control)	Cytoplasm	Mutant	160	2.598	1.171	15.58	293	<0.0001	
		Control	135	1	0.239				
Normalised POPDC Expression Relative to α-sarcoglycan									
POPDC1 / α-sarcoglycan	Plasma Membrane	Mutant	167	0.908	0.426	2.66	326	0.008	5.7C
		Control	161	1	0.114				
POPDC2 / α-sarcoglycan	Plasma Membrane	Mutant	160	0.706	0.225	11.06	293	<0.0001	
		Control	135	1	0.23				
Ratio of POPDC in the Plasma Membrane to Cytoplasm									
POPDC1	Plasma Membrane / Cytoplasm	Mutant	167	3.119	1.554	10.79	326	<0.0001	5.7D
		Control	161	5.135	1.824				
POPDC2	Plasma Membrane / Cytoplasm	Mutant	160	3.868	1.781	31.27	293	<0.0001	
		Control	135	11.89	2.604				

* t, df and p values refer to the results of student's t-test comparing the patient to the control.

Table 10.4: Table summarising the data for skeletal muscle biopsy staining for POPDC1, POPDC2 and α-sarcoglycan in control and POPDC1 p.S201F mouse.

Normalised Protein Expression Levels

Protein	Region	Control/Patient	Fibres Analysed	Normalised Mean	SD	t*	df*	p*	Figure
POPDC1	Plasma Membrane	Mutant	158	0.259	0.061	36.91	426	<0.0001	5.11A
		Control	270	1	0.248				
α-sarcoglycan (POPDC1 control)	Plasma Membrane	Mutant	158	0.943	0.294	2.45	426	0.015	
		Control	270	1	0.189				
POPDC2	Plasma Membrane	Mutant	118	0.142	0.048	41.41	264	<0.0001	
		Control	148	1	0.221				
α-sarcoglycan (POPDC2 control)	Plasma Membrane	Mutant	118	0.659	0.155	18.17	264	<0.0001	
		Control	148	1	0.150				
POPDC1	Cytoplasm	Mutant	158	1.155	0.375	4.61	426	<0.0001	5.11B
		Control	270	1	0.312				
α-sarcoglycan (POPDC1 control)	Cytoplasm	Mutant	158	1.724	0.537	20.09	426	<0.0001	
		Control	270	1	0.192				
POPDC2	Cytoplasm	Mutant	118	0.428	0.143	22.38	264	<0.0001	
		Control	148	1	0.246				
α-sarcoglycan (POPDC2 control)	Cytoplasm	Mutant	118	1.158	0.336	4.35	264	<0.0001	
		Control	148	1	0.257				
Normalised POPDC Expression Relative to α-sarcoglycan									
POPDC1 / α-sarcoglycan	Plasma Membrane	Mutant	158	0.3	0.138	27.99	426	<0.0001	5.11C
		Control	270	1	0.296				
POPDC2 / α-sarcoglycan	Plasma Membrane	Mutant	118	0.219	0.0745	34.22	264	<0.0001	
		Control	148	1	0.239				
Ratio of POPDC in the Plasma Membrane to Cytoplasm									
POPDC1	Plasma Membrane / Cytoplasm	Mutant	158	1.027	0.401	32.63	426	<0.0001	5.11D
		Control	270	4.554	1.323				
POPDC2	Plasma Membrane / Cytoplasm	Mutant	118	0.9004	0.189	31.83	264	<0.0001	
		Control	148	2.718	0.597				

* t, df and p values refer to the results of student's t-test comparing the mutant mouse to the control.

10.3 HEK293 POPDC1 and POPDC2 HEK293 Cells Co-Expression Supplementary Results

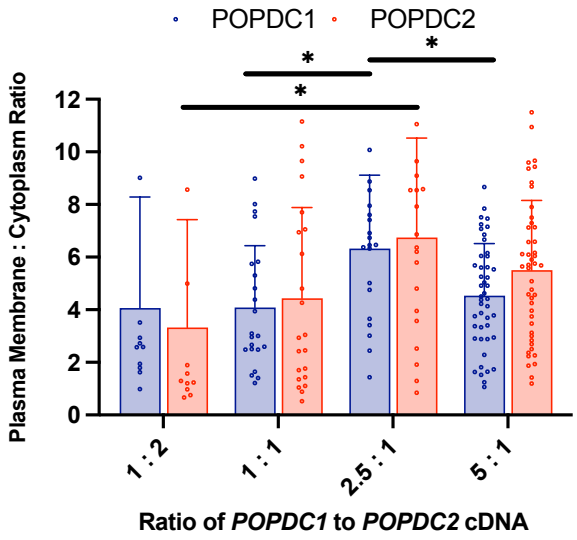


Figure 10.1: The plasma Membrane Localisation of POPDC1 and POPDC2 in HEK293 cells when Co-Transfected at differing Ratios. HEK293 cells were segmented into areas representing the plasma membrane and cytoplasm. The intensity of ECFP and EYFP within these two areas were used to measure the subcellular localisation of POPDC1 and POPDC2 constructs within the cells. POPDC1-ECFP and POPDC2-EYFP were transiently expressed in HEK293 cells using different ratios of plasmid and imaged using confocal microscopy. The plasma membrane to cytoplasm expression ratio for each isoform was then determined. Groups were compared using one-way ANOVA followed by Tukey's multiple comparison, * p<0.05.

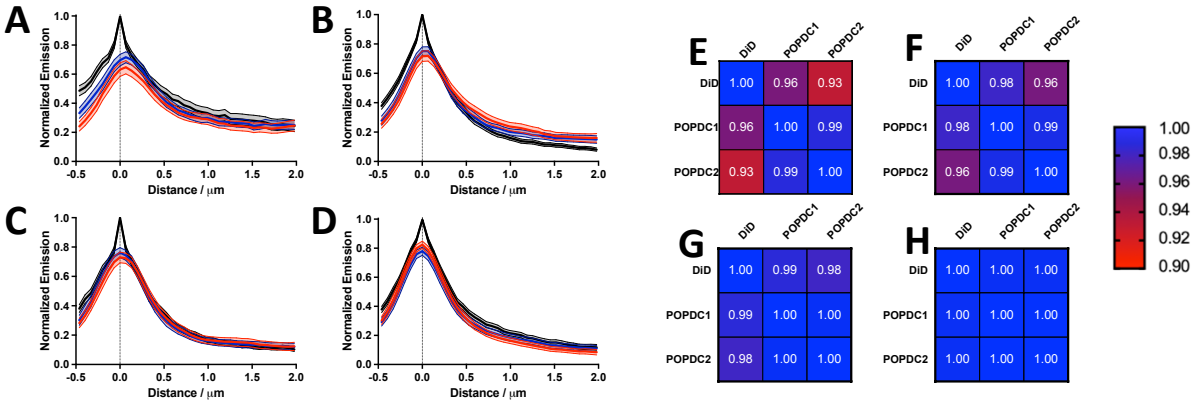


Figure 10.2: The Normalised Expression Profile of POPDC1 and POPDC2 Relative to Position of the Plasma Membrane of HEK293 Cells when Transfected a different Ratios. The level of POPDC1 and POPDC2, as determined by ECFP and EYFP emission, respectively, was measured across the plasma membrane and cytoplasm at multiple points of HEK293 cells. Differing ratios of POPDC1 and POPDC2 construct containing plasmids were used in the transfection. The average change in the relative POPDC1 and POPDC2 concentrations from 0.5 mm outside to 2 mm inside a theoretical averaged cell are shown for POPDC1-ECFP + POPDC2-EYFP at transfections ratios of 1:2 **(A)**, 1:1 **(B)** 2.5:1 **(C)** and 5:1 **(D)**. The Pearson correlation score of POPDC1 and POPDC2 expression profile with the plasma membrane (DiD), as well as each other, was found for each group and shown for 1:2 **(E)**, 1:1 **(F)** 2.5:1 **(G)** and 5:1 **(H)**.

Table 10.5: Table summarising the normalised POPDC1 plasma membrane expression in HEK293 cells in the presence of the clinical POPDC mutations. See Figure 5.16F.

POPDC1 Variant	POPDC2 Variant	Cells Analysed	Mean Expression	SD	Cell Mean Difference to Control	95.00% CI of diff	p*
POPDC1	POPDC2	46	1	0.526	-	-	-
POPDC1p.Q153X	POPDC2	17	0.656	0.482	0.344	0.038 to 0.649	0.020
POPDC1p.R172H	POPDC2	36	0.694	0.491	0.306	0.067 to 0.550	0.006
POPDC1p.V183F	POPDC2	47	0.780	0.360	0.220	-0.003 to 0.443	0.055
POPDC1p.S201F	POPDC2	22	0.285	0.169	0.715	0.436 to 0.994	<0.0001
POPDC1	POPDC2p.W188X	24	0.398	0.269	0.602	0.331 to 0.873	<0.0001

* p values relate to Dunnett's post hoc test after one-way ANOVA using the wildtype pair as the control.

Table 10.6: ANOVA table summarising the comparisons of the normalised POPDC1 plasma membrane expression in HEK293 cells in the presence of the clinical POPDC mutations (see Table 10.5).

ANOVA table	SS	DF	MS	F (DFn, DFd)	p
Treatment (between columns)	10.45	5	2.09	F (5, 186) = 11.84	P<0.0001
Residual (within columns)	32.82	186	0.177		
Total	43.27	191			

Table 10.7: Table summarising the normalised POPDC2 plasma membrane expression in HEK293 cells in the presence of the clinical POPDC mutations. See Figure 5.16F.

POPDC1 Variant	POPDC2 Variant	Cells Analysed	Mean Expression	SD	Cell Mean Difference to Control	95.00% CI of diff	p*
POPDC1	POPDC2	46	1	0.534	-	-	-
POPDC1p.Q153X	POPDC2	17	0.702	0.626	0.298	-0.048 to 0.643	0.120
POPDC1p.R172H	POPDC2	36	0.960	0.541	0.040	-0.231 to 0.311	0.996
POPDC1p.V183F	POPDC2	47	0.715	0.374	0.285	0.033 to 0.537	0.020
POPDC1p.S201F	POPDC2	22	0.318	0.215	0.682	0.367 to 0.998	<0.0001
POPDC1	POPDC2p.W188X	24	0.725	0.475	0.275	-0.031 to 0.581	0.097

* p values relate to Dunnett's post hoc test after one-way ANOVA using the wildtype pair as the control.

Table 10.8: ANOVA table summarising the comparisons of the normalised POPDC2 plasma membrane expression in HEK293 cells in the presence of the clinical POPDC mutations (see Table 10.7).

ANOVA table	SS	DF	MS	F (DFn, DFd)	P value
Treatment (between columns)	8.47	5	1.694	F (5, 186) = 7.511	P<0.0001
Residual (within columns)	41.94	186	0.226		
Total	50.41	191			

Table 10.9: Table summarising the normalised POPDC1 cytoplasm expression in HEK293 cells in the presence of the clinical POPDC mutations. See Figure 5.16G.

POPDC1 Variant	POPDC2 Variant	Cells Analysed	Mean Expression	SD	Cell Mean Difference to Control	95.00% CI of diff	p*
POPDC1	POPDC2	46	1	0.979	-	-	-
POPDC1p.Q153X	POPDC2	17	2.374	1.791	-1.374	-2.010 to -0.738	<0.0001
POPDC1p.R172H	POPDC2	36	0.797	0.689	0.203	-0.296 to 0.701	0.783
POPDC1p.V183F	POPDC2	47	0.676	0.388	0.324	-0.140 to 0.789	0.285
POPDC1p.S201F	POPDC2	22	0.819	0.578	0.181	-0.400 to 0.762	0.912
POPDC1	POPDC2p.W188X	24	1.361	0.866	-0.361	-0.925 to 0.203	0.369

* p values relate to Dunnett's post hoc test after one-way ANOVA using the wildtype pair as the control.

Table 10.10: ANOVA table summarising the comparisons of the normalised POPDC1 cytoplasm expression in HEK293 cells in the presence of the clinical POPDC mutations (see Table 10.9).

ANOVA table	SS	DF	MS	F (DFn, DFd)	P value
Treatment (between columns)	42.23	5	8.445	F (5, 186) = 11.04	P<0.0001
Residual (within columns)	142.20	186	0.765		
Total	184.50	191			

Table 10.11: Table summarising the normalised POPDC2 cytoplasm expression in HEK293 cells in the presence of the clinical POPDC mutations. See Figure 5.16G.

POPDC1 Variant	POPDC2 Variant	Cells Analysed	Mean Expression	SD	Cell Mean Difference to Control	95.00% CI of diff	p*
POPDC1	POPDC2	46	1	1.079	-	-	-
POPDC1p.Q153X	POPDC2	17	2.447	2.176	-1.448	-2.359 to -0.536	0.0003
POPDC1p.R172H	POPDC2	36	1.046	0.787	-0.046	-0.761 to 0.669	0.999
POPDC1p.V183F	POPDC2	47	0.544	0.422	0.456	-0.210 to 1.122	0.304
POPDC1p.S201F	POPDC2	22	1.098	0.858	-0.098	-0.930 to 0.735	0.999
POPDC1	POPDC2p.W188X	24	3.965	2.271	-2.965	-3.774 to -2.157	<0.0001

* p values relate to Dunnett's post hoc test after one-way ANOVA using the wildtype pair as the control.

Table 10.12: ANOVA table summarising the comparisons of the normalised POPDC2 cytoplasm expression in HEK293 cells in the presence of the clinical POPDC mutations (see Table 10.11).

ANOVA table	SS	DF	MS	F (DFn, DFd)	P value
Treatment (between columns)	224.9	5	44.98	F (5, 186) = 28.64	P<0.0001
Residual (within columns)	292.1	186	1.57		
Total	517	191			

Table 10.13: Table summarising the normalised ratio of POPDC1 in the plasma membrane and cytoplasm in HEK293 cells in the presence of the clinical POPDC mutations. See Figure 5.16H.

POPDC1 Variant	POPDC2 Variant	Cells Analysed	Ratio of Plasma Membrane : Cytoplasm Expression	SD	Cell Mean Difference to Control	95.00% CI of diff	p*
POPDC1	POPDC2	46	4.535	1.976	-	-	-
POPDC1p.Q153X	POPDC2	17	1.080	0.289	3.455	2.249 to 4.661	<0.0001
POPDC1p.R172H	POPDC2	36	3.783	1.465	0.751	-0.195 to 1.697	0.175
POPDC1p.V183F	POPDC2	47	4.877	2.319	-0.342	-1.224 to 0.539	0.812
POPDC1p.S201F	POPDC2	22	1.449	0.512	3.086	1.984 to 4.188	<0.0001
POPDC1	POPDC2p.W188X	24	1.115	0.539	3.419	2.349 to 4.490	<0.0001

* p values relate to Dunnett's post hoc test after one-way ANOVA using the wildtype pair as the control.

Table 10.14: ANOVA table summarising the comparisons of the normalised POPDC1 ratio in the plasma membrane and cytoplasm in HEK293 cells in the presence of the clinical POPDC mutations (see Table 10.13).

ANOVA table	SS	DF	MS	F (DFn, DFd)	P value
Treatment (between columns)	467.6	5	93.51	F (5, 186) = 33.99	P<0.0001
Residual (within columns)	511.7	186	2.75		
Total	979.3	191			

Table 10.15: Table summarising the normalised ratio of POPDC2 in the plasma membrane and cytoplasm in HEK293 cells in the presence of the clinical POPDC mutations. See Figure 5.16H.

POPDC1 Variant	POPDC2 Variant	Cells Analysed	Ratio of Plasma Membrane : Cytoplasm Expression	SD	Cell Mean Difference to Control	95.00% CI of diff	p*
POPDC1	POPDC2	46	5.504	2.651	-	-	<0.0001
POPDC1p.Q153X	POPDC2	17	1.302	0.587	4.202	2.290 to 6.114	0.726
POPDC1p.R172H	POPDC2	36	4.845	2.697	0.660	-0.839 to 2.159	0.039
POPDC1p.V183F	POPDC2	47	6.953	3.873	-1.448	-2.846 to -0.051	<0.0001
POPDC1p.S201F	POPDC2	22	1.516	0.903	3.989	2.243 to 5.735	<0.0001
POPDC1	POPDC2p.W188X	24	0.773	0.287	4.731	3.035 to 6.427	<0.0001

* p values relate to Dunnett's post hoc test after one-way ANOVA using the wildtype pair as the control.

Table 10.16: ANOVA table summarising the comparisons of the normalised POPDC1 ratio in the plasma membrane and cytoplasm in HEK293 cells in the presence of the clinical POPDC mutations (see Table 10.15).

ANOVA table	SS	DF	MS	F (DFn, DFd)	P value
Treatment (between columns)	1030	5	206	F (5, 186) = 29.81	P<0.0001
Residual (within columns)	1285	186	6.911		
Total	2315	191			

Table 10.17: Table summarising the normalised POPDC1 plasma membrane expression in HEK293 cells in the presence of the αC-helix POPDC1 mutations. See Figure 6.8G.

POPDC1 Variant	POPDC2 Variant	Cells Analysed	Mean Expression	SD	Cell Mean Difference to Control	95.00% CI of diff	p*
POPDC1	POPDC2	34	1	0.586	-	-	-
POPDC1p.L245D	POPDC2	71	0.584	0.369	0.416	0.224 to 0.607	<0.0001
POPDC1p.F249D	POPDC2	56	0.189	0.090	0.811	0.611 to 1.010	<0.0001
POPDC1p.I253D	POPDC2	27	0.237	0.258	0.763	0.526 to 0.999	<0.0001
POPDC1p.I257D	POPDC2	40	0.310	0.278	0.690	0.476 to 0.904	<0.0001
POPDC1p.L261D	POPDC2	47	0.748	0.415	0.252	0.045 to 0.458	0.010
POPDC1p.L264D	POPDC2	42	0.668	0.379	0.333	0.121 to 0.544	0.0004

* p values relate to Dunnett's post hoc test after one-way ANOVA using the wildtype pair as the control.

Table 10.18: ANOVA table summarising the comparisons of the normalised POPDC1 plasma membrane expression in HEK293 cells in the presence of the αC-helix POPDC1 mutations (see Table 10.17).

ANOVA table	SS	DF	MS	F (DFn, DFd)	P value
Treatment (between columns)	21.52	6	3.586	F (6, 310) = 27.88	P<0.0001
Residual (within columns)	39.88	310	0.1286		
Total	61.4	316			

Table 10.19: Table summarising the normalised POPDC2 plasma membrane expression in HEK293 cells in the presence of the αC-helix POPDC1 mutations. See Figure 6.8G.

POPDC1 Variant	POPDC2 Variant	Cells Analysed	Mean Expression	SD	Cell Mean Difference to Control	95.00% CI of diff	p*
POPDC1	POPDC2	34	1	0.637	-	-	-
POPDC1p.L245D	POPDC2	71	0.713	0.470	0.288	0.070 to 0.505	0.004
POPDC1p.F249D	POPDC2	56	0.289	0.166	0.711	0.485 to 0.938	<0.0001
POPDC1p.I253D	POPDC2	27	0.198	0.182	0.802	0.534 to 1.071	<0.0001
POPDC1p.I257D	POPDC2	40	0.329	0.289	0.671	0.428 to 0.914	<0.0001
POPDC1p.L261D	POPDC2	47	0.820	0.438	0.180	-0.054 to 0.415	0.193
POPDC1p.L264D	POPDC2	42	0.733	0.443	0.267	0.027 to 0.508	0.023

* p values relate to Dunnett's post hoc test after one-way ANOVA using the wildtype pair as the control.

Table 10.20: ANOVA table summarising the comparisons of the normalised POPDC2 plasma membrane expression in HEK293 cells in the presence of the αC-helix POPDC1 mutations (see Table 10.19).

ANOVA table	SS	DF	MS	F (DFn, DFd)	P value
Treatment (between columns)	22.07	6	3.679	F (6, 310) = 22.20	P<0.0001
Residual (within columns)	51.37	310	0.1657		
Total	73.44	316			

Table 10.21: Table summarising the normalised POPDC1 cytoplasm expression in HEK293 cells in the presence of the αC-helix POPDC1 mutations. See Figure 6.8H.

POPDC1 Variant	POPDC2 Variant	Cells Analysed	Mean Expression	SD	Cell Mean Difference to Control	95.00% CI of diff	p*
POPDC1	POPDC2	34	1	0.799	-	-	-
POPDC1p.L245D	POPDC2	71	0.591	0.692	0.409	-0.045 to 0.864	0.094
POPDC1p.F249D	POPDC2	56	0.873	0.675	0.127	-0.347 to 0.601	0.952
POPDC1p.I253D	POPDC2	27	1.051	1.062	-0.051	-0.613 to 0.511	0.999
POPDC1p.I257D	POPDC2	40	1.554	1.109	-0.554	-1.063 to -0.046	0.027
POPDC1p.L261D	POPDC2	47	0.900	0.889	0.100	-0.390 to 0.591	0.987
POPDC1p.L264D	POPDC2	42	0.849	0.882	0.151	-0.352 to 0.654	0.922

* p values relate to Dunnett's post hoc test after one-way ANOVA using the wildtype pair as the control.

Table 10.22: ANOVA table summarising the comparisons of the normalised POPDC1 cytoplasm expression in HEK293 cells in the presence of the αC-helix POPDC1 mutations (see Table 10.21).

ANOVA table	SS	DF	MS	F (DFn, DFd)	P value
Treatment (between columns)	24.82	6	4.137	F (6, 310) = 5.695	P<0.0001
Residual (within columns)	225.2	310	0.7264		
Total	250	316			

Table 10.23: Table summarising the normalised POPDC2 cytoplasm expression in HEK293 cells in the presence of the αC-helix POPDC1 mutations. See Figure 6.8H.

POPDC1 Variant	POPDC2 Variant	Cells Analysed	Mean Expression	SD	Cell Mean Difference to Control	95.00% CI of diff	p*
POPDC1	POPDC2	34	1	0.765	-	-	-
POPDC1p.L245D	POPDC2	71	0.912	1.406	0.088	-0.731 to 0.908	0.999
POPDC1p.F249D	POPDC2	56	1.730	1.603	-0.730	-1.584 to 0.124	0.122
POPDC1p.I253D	POPDC2	27	0.867	0.876	0.133	-0.880 to 1.146	0.998
POPDC1p.I257D	POPDC2	40	2.136	2.051	-1.136	-2.053 to -0.220	0.009
POPDC1p.L261D	POPDC2	47	0.860	0.896	0.140	-0.745 to 1.025	0.996
POPDC1p.L264D	POPDC2	42	1.167	2.272	-0.167	-1.073 to 0.740	0.992

* p values relate to Dunnett's post hoc test after one-way ANOVA using the wildtype pair as the control.

Table 10.24: ANOVA table summarising the comparisons of the normalised POPDC2 cytoplasm expression in HEK293 cells in the presence of the αC-helix POPDC1 mutations (see Table 10.23).

ANOVA table	SS	DF	MS	F (DFn, DFd)	P value
Treatment (between columns)	65.95	6	10.99	F (6, 310) = 4.657	P=0.0001
Residual (within columns)	731.7	310	2.36		
Total	797.7	316			

Table 10.25: Table summarising the normalised ratio of POPDC1 in the plasma membrane and cytoplasm in HEK293 cells in the presence of the αC-helix POPDC1 mutations. See Figure 6.8I.

POPDC1 Variant	POPDC2 Variant	Cells Analysed	Ratio of Plasma Membrane : Cytoplasm Expression	SD	Cell Mean Difference to Control	95.00% CI of diff	p
POPDC1	POPDC2	34	4.325	2.651	-	-	-
POPDC1p.L245D	POPDC2	71	4.723	2.880	-0.398	-1.474 to 0.678	0.828
POPDC1p.F249D	POPDC2	56	0.975	0.613	3.350	2.229 to 4.472	<0.0001
POPDC1p.I253D	POPDC2	27	0.944	0.613	3.382	2.052 to 4.711	<0.0001
POPDC1p.I257D	POPDC2	40	0.672	0.405	3.654	2.450 to 4.857	<0.0001
POPDC1p.L261D	POPDC2	47	3.728	1.836	0.597	-0.564 to 1.759	0.567
POPDC1p.L264D	POPDC2	42	3.754	2.504	0.572	-0.619 to 1.762	0.631

* p values relate to Dunnett's post hoc test after one-way ANOVA using the wildtype pair as the control.

Table 10.26: ANOVA table summarising the comparisons of the normalised POPDC1 ratio in the plasma membrane and cytoplasm in HEK293 cells in the presence of the αC-helix POPDC1 mutations (see Table 10.25).

ANOVA table	SS	DF	MS	F (DFn, DFd)	P value
Treatment (between columns)	877.4	6	146.2	F (6, 310) = 35.94	P<0.0001
Residual (within columns)	1261	310	4.069		
Total	2139	316			

Table 10.27: Table summarising the normalised ratio of POPDC2 in the plasma membrane and cytoplasm in HEK293 cells in the presence of the αC-helix POPDC1 mutations. See Figure 6.8I.

POPDC1 Variant	POPDC2 Variant	Cells Analysed	Ratio of Plasma Membrane : Cytoplasm Expression	SD	Cell Mean Difference to Control	95.00% CI of diff	p*
POPDC1	POPDC2	34	5.490	3.291	-	-	-
POPDC1p.L245D	POPDC2	71	6.318	4.162	-0.828	-2.294 to 0.638	0.476
POPDC1p.F249D	POPDC2	56	1.386	1.391	4.104	2.575 to 5.632	<0.0001
POPDC1p.I253D	POPDC2	27	1.538	1.144	3.951	2.139 to 5.764	<0.0001
POPDC1p.I257D	POPDC2	40	0.743	0.486	4.746	3.106 to 6.386	<0.0001
POPDC1p.L261D	POPDC2	47	5.338	2.190	0.152	-1.431 to 1.734	0.999
POPDC1p.L264D	POPDC2	42	5.247	3.135	0.243	-1.379 to 1.865	0.997

* p values relate to Dunnett's post hoc test after one-way ANOVA using the wildtype pair as the control.

Table 10.28: ANOVA table summarising the comparisons of the normalised POPDC2 ratio in the plasma membrane and cytoplasm in HEK293 cells in the presence of the αC-helix POPDC1 mutations (see Table 10.27).

ANOVA table	SS	DF	MS	F (DFn, DFd)	P value
Treatment (between columns)	1576	6	262.7	F (6, 310) = 34.76	P<0.0001
Residual (within columns)	2343	310	7.559		
Total	3919	316			

Table 10.29: Table summarising the normalised POPDC1 plasma membrane expression in HEK293 cells in the presence of the αC-helix POPDC2 mutations. See Figure 6.9G.

POPDC1 Variant	POPDC2 Variant	Cells Analysed	Mean Expression	SD	Cell Mean Difference to Control	95.00% CI of diff	p
POPDC1	POPDC2	34	1	0.5860	0.04266	-0.2184 to 0.3037	-
POPDC1	POPDC2p.I229D	48	0.957	0.647	0.7652	0.4370 to 1.093	0.9954
POPDC1	POPDC2p.F233D	20	0.235	0.128	0.4866	0.2219 to 0.7512	<0.0001
POPDC1	POPDC2p.L237D	45	0.513	0.433	0.7778	0.5091 to 1.047	<0.0001
POPDC1	POPDC2p.I241D	42	0.222	0.168	0.2056	-0.04223 to 0.4534	<0.0001
POPDC1	POPDC2p.L245D	63	0.795	0.446	0.1926	-0.06058 to 0.4458	0.1408
POPDC1	POPDC2p.L248D	56	0.807	0.410	0.04266	-0.2184 to 0.3037	0.2027

* p values relate to Dunnett's post hoc test after one-way ANOVA using the wildtype pair as the control.

Table 10.30: ANOVA table summarising the comparisons of the normalised POPDC1 plasma membrane expression in HEK293 cells in the presence of the αC-helix POPDC2 mutations (see Table 10.29).

ANOVA table	SS	DF	MS	F (DFn, DFd)	P value
Treatment (between columns)	22.89	6	3.816	F (6, 301) = 18.46	P<0.0001
Residual (within columns)	62.22	301	0.2067		
Total	85.12	307			

Table 10.31: Table summarising the normalised POPDC2 plasma membrane expression in HEK293 cells in the presence of the αC-helix POPDC2 mutations. See Figure 6.9G.

POPDC1 Variant	POPDC2 Variant	Cells Analysed	Mean Expression	SD	Cell Mean Difference to Control	95.00% CI of diff	p*
POPDC1	POPDC2	34	1	0.637	-	-	-
POPDC1	POPDC2p.I229D	48	0.970	0.587	0.030	-0.229 to 0.289	0.999
POPDC1	POPDC2p.F233D	20	0.534	0.308	0.467	0.141 to 0.792	0.002
POPDC1	POPDC2p.L237D	45	0.414	0.374	0.586	0.324 to 0.849	<0.0001
POPDC1	POPDC2p.I241D	42	0.062	0.074	0.938	0.672 to 1.205	<0.0001
POPDC1	POPDC2p.L245D	63	0.924	0.462	0.076	-0.169 to 0.322	0.912
POPDC1	POPDC2p.L248D	56	1.042	0.431	-0.042	-0.294 to 0.209	0.995

* p values relate to Dunnett's post hoc test after one-way ANOVA using the wildtype pair as the control.

Table 10.32: ANOVA table summarising the comparisons of the normalised POPDC2 plasma membrane expression in HEK293 cells in the presence of the αC-helix POPDC2 mutations (see Table 10.31).

ANOVA table	SS	DF	MS	F (DFn, DFd)	P value
Treatment (between columns)	37.05	6	6.175	F (6, 301) = 30.36	P<0.0001
Residual (within columns)	61.22	301	0.2034		
Total	98.27	307			

Table 10.33: Table summarising the normalised POPDC1 cytoplasm expression in HEK293 cells in the presence of the αC-helix POPDC2 mutations. See Figure 6.9H.

POPDC1 Variant	POPDC2 Variant	Cells Analysed	Mean Expression	SD	Cell Mean Difference to Control	95.00% CI of diff	p*
POPDC1	POPDC2	34	1	0.799	-	-	-
POPDC1	POPDC2p.I229D	48	1.232	1.040	-0.232	-0.805 to 0.341	0.773
POPDC1	POPDC2p.F233D	20	0.897	0.651	0.103	-0.617 to 0.823	0.998
POPDC1	POPDC2p.L237D	45	1.860	1.881	-0.861	-1.441 to -0.280	0.001
POPDC1	POPDC2p.I241D	42	1.032	0.862	-0.032	-0.621 to 0.557	0.999
POPDC1	POPDC2p.L245D	63	0.718	0.478	0.282	-0.262 to 0.825	0.564
POPDC1	POPDC2p.L248D	56	0.949	0.592	0.051	-0.505 to 0.606	0.999

* p values relate to Dunnett's post hoc test after one-way ANOVA using the wildtype pair as the control.

Table 10.34: ANOVA table summarising the comparisons of the normalised POPDC1 cytoplasm expression in HEK293 cells in the presence of the αC-helix POPDC2 mutations (see Table 10.33).

ANOVA table	SS	DF	MS	F (DFn, DFd)	P value
Treatment (between columns)	38.66	6	6.443	F (6, 301) = 6.477	P<0.0001
Residual (within columns)	299.4	301	0.9948		
Total	338.1	307			

Table 10.35: Table summarising the normalised POPDC2 cytoplasm expression in HEK293 cells in the presence of the αC-helix POPDC2 mutations. See Figure 6.9H.

POPDC1 Variant	POPDC2 Variant	Cells Analysed	Mean Expression	SD	Cell Mean Difference to Control	95.00% CI of diff	p*
POPDC1	POPDC2	34	1	0.765	-	-	-
POPDC1	POPDC2p.I229D	48	1.871	1.877	-0.871	-1.700 to -0.046	0.034
POPDC1	POPDC2p.F233D	20	2.913	1.980	-1.910	-2.95 to -0.876	<0.0001
POPDC1	POPDC2p.L237D	45	1.828	2.170	-0.827	-1.660 to 0.009	0.054
POPDC1	POPDC2p.I241D	42	0.207	0.288	0.794	-0.056 to 1.640	0.076
POPDC1	POPDC2p.L245D	63	1.112	1.060	-0.112	-0.895 to 0.672	0.998
POPDC1	POPDC2p.L248D	56	1.654	1.220	-0.654	-1.450 to 0.146	0.151

* p values relate to Dunnett's post hoc test after one-way ANOVA using the wildtype pair as the control.

Table 10.36: ANOVA table summarising the comparisons of the normalised POPDC2 cytoplasm expression in HEK293 cells in the presence of the αC-helix POPDC2 mutations (see Table 10.35).

ANOVA table	SS	DF	MS	F (DFn, DFd)	P value
Treatment (between columns)	139	6	23.1	F (6, 301) = 11.20	P<0.0001
Residual (within columns)	622	301	2.06		
Total	760	307			

Table 10.37: Table summarising the normalised ratio of POPDC1 in the plasma membrane and cytoplasm in HEK293 cells in the presence of the αC-helix POPDC2 mutations. See Figure 6.9I.

POPDC1 Variant	POPDC2 Variant	Cells Analysed	Ratio of Plasma Membrane : Cytoplasm Expression	SD	Cell Mean Difference to Control	95.00% CI of diff	p*
POPDC1	POPDC2	34	4.325	2.651	-	-	-
POPDC1	POPDC2p.I229D	48	3.000	1.469	1.326	0.440 to 2.211	0.0009
POPDC1	POPDC2p.F233D	20	0.998	0.407	3.328	2.214 to 4.441	<0.0001
POPDC1	POPDC2p.L237D	45	1.071	0.493	3.254	2.356 to 4.152	<0.0001
POPDC1	POPDC2p.I241D	42	0.875	0.520	3.450	2.539 to 4.362	<0.0001
POPDC1	POPDC2p.L245D	63	4.054	1.926	0.271	-0.570 to 1.112	0.898
POPDC1	POPDC2p.L248D	56	3.077	1.525	1.248	0.389 to 2.108	0.0013

* p values relate to Dunnett's post hoc test after one-way ANOVA using the wildtype pair as the control.

Table 10.38: ANOVA table summarising the comparisons of the normalised POPDC1 ratio in the plasma membrane and cytoplasm in HEK293 cells in the presence of the αC-helix POPDC2 mutations (see Table 10.37).

ANOVA table	SS	DF	MS	F (DFn, DFd)	P value
Treatment (between columns)	534.6	6	89.1	F (6, 301) = 37.44	P<0.0001
Residual (within columns)	716.3	301	2.38		
Total	1251	307			

Table 10.39: Table summarising the normalised ratio of POPDC2 in the plasma membrane and cytoplasm in HEK293 cells in the presence of the αC-helix POPDC2 mutations. See Figure 6.9I.

POPDC1 Variant	POPDC2 Variant	Cells Analysed	Ratio of Plasma Membrane : Cytoplasm Expression	SD	Cell Mean Difference to Control	95.00% CI of diff	p*
POPDC1	POPDC2	34	5.49	3.291	-	-	-
POPDC1	POPDC2p.I229D	48	3.733	2.796	1.756	0.450 to 3.063	0.004
POPDC1	POPDC2p.F233D	20	0.903	0.437	4.587	2.945 to 6.229	<0.0001
POPDC1	POPDC2p.L237D	45	1.443	0.971	4.046	2.722 to 5.371	<0.0001
POPDC1	POPDC2p.I241D	42	1.533	1.009	3.957	2.613 to 5.302	<0.0001
POPDC1	POPDC2p.L245D	63	4.814	2.862	0.676	-0.565 to 1.916	0.515
POPDC1	POPDC2p.L248D	56	3.617	2.083	1.873	0.606 to 3.140	0.001

* p values relate to Dunnett's post hoc test after one-way ANOVA using the wildtype pair as the control.

Table 10.40: ANOVA table summarising the comparisons of the normalised POPDC2 ratio in the plasma membrane and cytoplasm in HEK293 cells in the presence of the αC-helix POPDC2 mutations (see Table 10.39).

ANOVA table	SS	DF	MS	F (DFn, DFd)	P value
Treatment (between columns)	723.3	6	120.6	F (6, 301) = 23.29	P<0.0001
Residual (within columns)	1558	301	5.176		
Total	2281	307			

10.4 Quantitative BRET Summary Data

Table 10.41: Table summarising the parameters determined for the different POPDC combinations in the qBRET assay.

POPDC Pair	Dimer model / R^2	$BRET_{max}$ / mBU	Expression Ratio vs Total Expression / *p*
hPOPDC1-hPOPDC1	0.83	13.23	0.1453
hPOPDC2-hPOPDC2*	-4.13	15.19	0.9871
hPOPDC1-hPOPDC2	0.285	7.384	0.1725

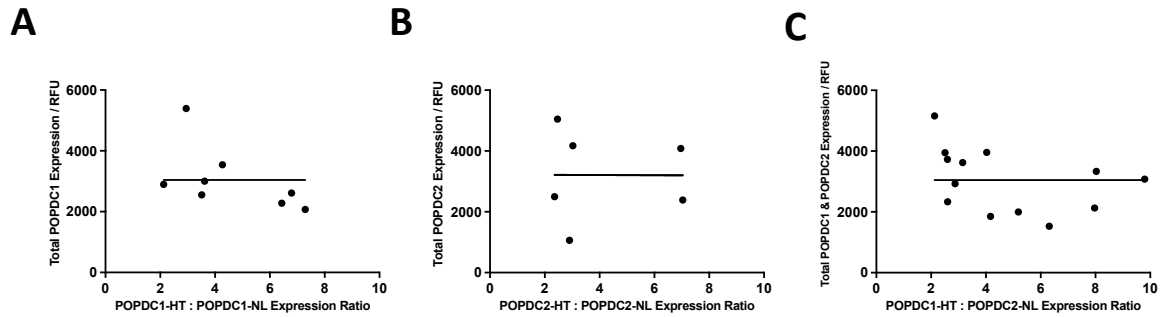


Figure 10.3: Plots showing the Total Expression Level of POPDC-NL and POPDC-HT at different Expression Ratios. The total expression of POPDC-NL and POPDC-HT constructs in HEK293 cells were determined for each expression ratio. This was determined by summing the total HaloTag-618 fluorescence and NanoLuc luminescence (after conversion to RFU). POPDC1-NL + POPDC1-HT **(A)**, POPDC2-NL + POPDC2-HT **(B)**, POPDC1-HT + POPDC2-NL **(C)**. No significant difference to a horizontal line was found in the relationship between expression ratio and total expression, as determined by an F test with the p values shown in Table 10.42.

10.5 POPDC1 + POPDC2 Clinical Mutant Co-Immunoprecipitation Full Blots

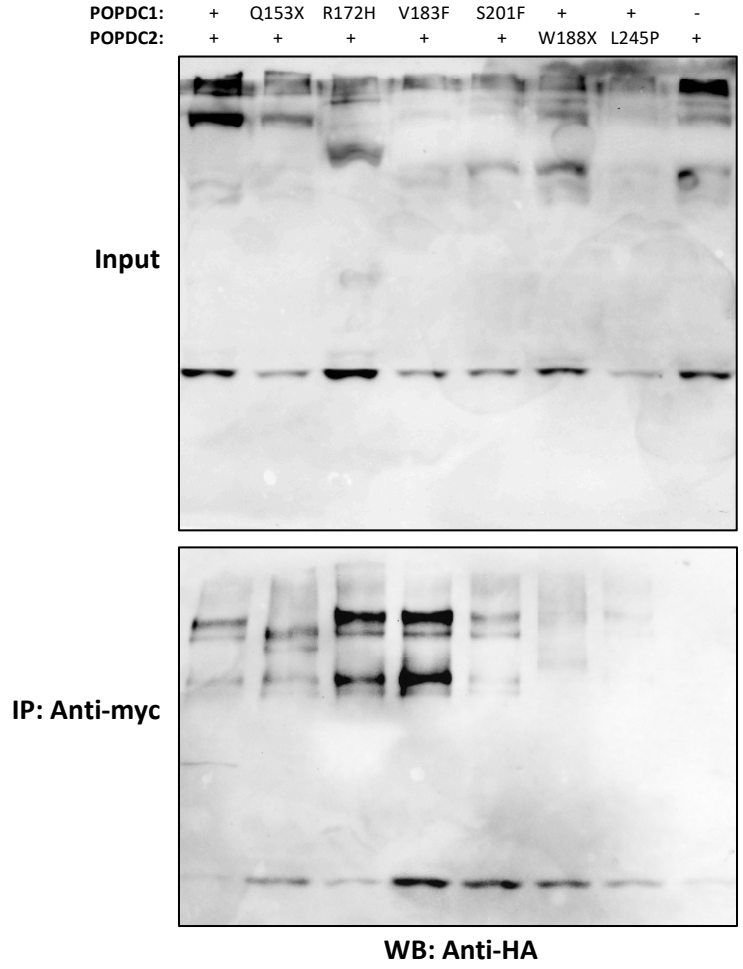


Figure 10.4: Co-Immunoprecipitation of POPDC2 with POPDC1 from HEK293 Cells in the Presence of Various POPDC Variants Full Blots. POPDC1-ECFP-myc and POPDC2-EYFP-HA were co-expressed in HEK293 cells. POPDC variants of interest were each substituted in place of their wildtype equivalent. A negative control in which only POPDC2-EYFP-HA was expressed was used for comparison. Cell lysates were precipitated with an anti-myc antibody and subjected to Western blot analysis using an anti-HA tag antibody. Segments of each blot are shown in Figure 6.5.

10.6 POPDC1 + POPDC2 Clinical Mutants Bimolecular Fluorescence Complementation Summary Data

Table 10.42: Table summarising the normalised BiFC signal produced by co-expression of POPDC1 and POPDC2 with different clinically identified mutations. See Figure 6.4C.

POPDC1-VC155 Variant	POPDC2-VN155 Variant	Images	Median Normalised Venus Emission	SD	Mean Difference to Control	95.00% CI of diff	p*
POPDC1	POPDC2	9	1	0.116	-	-	-
POPDC1p.Q153X	POPDC2	9	0.248	0.069	0.752	0.509 to 0.995	<0.0001
POPDC1p.R172H	POPDC2	9	1.168	0.319	-0.169	-0.411 to 0.074	0.282
POPDC1p.V183F	POPDC2	9	0.901	0.244	0.099	-0.144 to 0.341	0.785
POPDC1p.S201F	POPDC2	9	0.430	0.160	0.570	0.327 to 0.813	<0.0001
POPDC1	POPDC2p.W188X	5	0.590	0.113	0.410	0.123 to 0.698	0.002
POPDC1-VN155	POPDC2	3	0.018	0.0109	0.982	0.639 to 1.325	<0.0001

* p values relate to Dunnett's post hoc test after one-way ANOVA using the wildtype pair as the control.

Table 10.43: ANOVA table summarising the comparisons of the normalised BiFC signal produced by co-expression of POPDC1 and POPDC2 with different clinically identified mutations (see Table 10.42).

ANOVA table	SS	DF	MS	F (DFn, DFd)	P value
Treatment (between columns)	7.097	6	1.183	F (6, 46) = 32.18	P<0.0001
Residual (within columns)	1.691	46	0.03676		
Total	8.788	52			

10.7 POPDC1 + POPDC2 Clinical Mutants Acceptor Photobleaching FRET Summary Data

Table 10.44: Table summarising the normalised AP-FRET signal produced by co-expression of POPDC1 and POPDC2 with different clinically identified mutations. See Figure 6.3C.

mECFP-Tagged Species	mEYFP-Tagged Species	ROIs Analysed	Normalised Mean FRET	SD	Mean Difference to Control	95.00% CI of diff	p*
POPDC1	POPDC2	26	0.302	0.277	-	-	-
POPDC1p.Q153X	POPDC2	17	0.423	0.188	-0.121	-0.355 to 0.114	0.638
POPDC1p.R172H	POPDC2	20	0.213	0.265	0.0891	-0.135 to 0.313	0.848
POPDC1p.V183F	POPDC2	20	0.212	0.362	0.0904	-0.133 to 0.314	0.839
POPDC1p.S201F	POPDC2	20	0.103	0.251	0.199	-0.0247 to 0.422	0.105
POPDC1	POPDC2p.W188X	19	0.128	0.275	0.174	0.0530 to 0.401	0.215
mECFP	mEYFP	26	0	0.0.327	0.302	0.0938 to 0.511	0.0011
ECFP-EYFP		11	1	0.208	-0.698	-0.968 to -0.427	<0.0001

* p values relate to Dunnett's post hoc test after one-way ANOVA using the wildtype POPDC1 and POPDC2 co-expression group as the control.

Table 10.45: ANOVA table summarising the comparisons of the normalised AP-FRET signal produced by co-expression of POPDC1 and POPDC2 with different clinically identified mutations (see Table 10.44).

ANOVA table	SS	DF	MS	F (DFn, DFd)	P value
Treatment (between columns)	9.156	7	1.308	F (7, 151) = 16.48	P<0.0001
Residual (within columns)	11.98	151	0.07935		
Total	21.14	158			

10.8 Summary of Assays used to Characterise the POPDC2p.L245P Variant

Table 10.46: Table summarising the normalised expression and plasma membrane localisation of POPDC1 and POPDC2 in HEK293 cells in the presence of the POPDC1 p.L245P mutation.

Normalised POPDC1 Plasma Membrane Expression Levels

POPDC1 Variant	POPDC2 Variant	Cells Analysed	Mean Expression	SD	t*	df*	p*	Figure
POPDC1	POPDC2	46	1	0.526	2.479	79	0.015	7.3C
POPDC1	POPDC2p.L245P	35	0.738	0.388				

Normalised POPDC2 Plasma Membrane Expression Levels

POPDC1 Variant	POPDC2 Variant	Cells Analysed	Mean Expression	SD	t*	df*	p*	Figure
POPDC1	POPDC2	46	1	0.534	0.421	79	0.068	7.3C
POPDC1	POPDC2p.L245P	35	0.937	0.816				

Normalised POPDC1 Cytoplasmic Expression Levels

POPDC1 Variant	POPDC2 Variant	Cells Analysed	Mean Expression	SD	t*	df*	p*	Figure
POPDC1	POPDC2	46	1	0.979	3.603	79	0.0005	7.3D
POPDC1	POPDC2p.L245P	35	2.216	1.998				

Normalised POPDC2 Cytoplasmic Expression Levels

POPDC1 Variant	POPDC2 Variant	Cells Analysed	Mean Expression	SD	t*	df*	p*	Figure
POPDC1	POPDC2	46	1	1.079	3.542	79	0.0007	7.3D
POPDC1	POPDC2p.L245P	35	4.061	5.739				

Ratio of POPDC1 Expression in Plasma Membrane to Cytoplasm

POPDC1 Variant	POPDC2 Variant	Cells Analysed	Ratio of Plasma Membrane : Cytoplasm Expression	SD	t*	df*	p*	Figure
POPDC1	POPDC2	46	4.535	1.976	7.449	79	<0.0001	7.3E
POPDC1	POPDC2p.L245P	35	1.670	1.290				

Ratio of POPDC2 Expression in Plasma Membrane to Cytoplasm

POPDC1 Variant	POPDC2 Variant	Cells Analysed	Ratio of Plasma Membrane : Cytoplasm Expression	SD	t	df	p	Figure
POPDC1	POPDC2	46	5.504	2.651	7.849	79	<0.0001	7.3E
POPDC1	POPDC2p.L245P	35	1.575	1.506				

* t, df and p values refer to the results of student's t-test comparing the mutant mouse to the control.

Table 10.47: Table summarising the normalised BiFC signal produced by co-expression of POPDC1/POPDC1 p.L245P and POPDC2. See Figure 7.5A.

POPDC1 Variant	POPDC2 Variant	Images	Median Normalised Venus Emission	SD	t*	df*	p*
POPDC1	POPDC2	9	1	0.116	13.46	16	<0.0001
POPDC1	POPDC2p.L245P	9	0.221	0.129			

* t, df and p values refer to the results of student's t-test comparing the mutant mouse to the control.

Table 10.48: Table summarising the normalised AP-FRET signal produced by co-expression of POPDC1/POPDC1 p.L245P and POPDC2. See Figure 7.5B.

POPDC1 Variant	POPDC2 Variant	ROIs Analysed	Mean FRET	SD	t	df	p
POPDC1	POPDC2	26	0.302	0.278	2.715	44	0.0094
POPDC1	POPDC2p.L245P	20	0.0316	0.399			

* t, df and p values refer to the results of student's t-test comparing the mutant mouse to the control.

10.9 Full Oligonucleotide Sequences of Protein Constructs

ATGCAGTACAAACTGATCCTGAACGGTAAAACCCTGAAAGGTGAAACCACCACCGAAGCTGTTGACGCTGCTACCGCGGAAAAAGTTTTCAAACAGTACG
CTAACGACAACGGTGTTGACGGTGAATGGACCTACGACGACGCTACCAAAACCTTCACCGTTACCGAAGGATCTCATCATCATCATCATCATGGATCCGA
AAACCTGTATTTTCAGGGCGCCTCATATCTTTTGTACAAGAAAAGACCGGTCAAAATTGAAAAGGAGCTGGGTGGTGTCTACCATCGGTTGTTTGAACCA
CTCCGAGTCCCTCCGGATTTGTTTAGAAGGTTAACCGGACAGTTTTGTATGATCCAGACCTTGAAAAGGGGCCAGGTTTACGCCACAGAGGACAAAACCT
CAGTTGATGATCGTCTTAGTATTCTCCTAAAAGGAAGAATGAAGGTCTCCTATCGAGGACATTTTCTGCATAACATTTACCCGTGTGCCTTTATAGATTC
TCCCGAATTCAGATCAACGCAGATGCACAAAGGCGAAAAATTCCAGGTCACCATTGTTGCAGATGATAACTGCAGGTTCTTATGCTGGTCAAGAGAAAGA
CTGACTTACTTTCTGGAGTCAGAGCCTTTTCTGTATGAAATTTTTAGGTACCTTATAGGAAAAGACATTACAAATAAGCTGTACTCACTGAATGACCCTA
CTTTAAATGATAAGTAA

Figure 10.5: The cDNA Oligonucleotide Sequence of the GB1-S109-K272 Popeye Domain Construct.

ATGCAGTACAAACTGATCCTGAACGGTAAAACCCTGAAAGGTGAAACCACCACCGAAGCTGTTGACGCTGCTACCGCGGAAAAAGTTTTCAAACAGTACG
CTAACGACAACGGTGTTGACGGTGAATGGACCTACGACGACGCTACCAAAACCTTCACCGTTACCGAAGGATCTCATCATCATCATCATCATGGATCCGA
AAACCTGTATTTTCAGGGCGCCGAGCTGGGTGGTGTCTACCATCGGTTGTTTGAACCACTCCGAGTCCCTCCGGATTTGTTTAGAAGGTTAACCGGACAG
TTTTGTATGATCCAGACCTTGAAAAGGGGCCAGGTTTACGCCACAGAGGACAAAACCTCAGTTGATGATCGTCTTAGTATTCTCCTAAAAGGAAGAATGA
AGGTCTCCTATCGAGGACATTTTCTGCATAACATTTACCCGTGTGCCTTTATAGATTCTCCCGAATTCAGATCAACGCAGATGCACAAAGGCGAAAAATT
CCAGGTCACCATTGTTGCAGATGATAACTGCAGGTTCTTATGCTGGTCAAGAGAAAGACTGACTTACTTTCTGGAGTCAGAGCCTTTTCTGTATGAAATT
TTTAGGTACCTTATAGGAAAAGACATTACAAATAAGCTGTACTCACTGAATGACTAG

Figure 10.6: The cDNA Oligonucleotide Sequence of the GB1-E123-D266 Popeye Domain Construct.

ATGTCCCCTATACTAGGTTATTGGAAAATTAAGGGCCTTGTGCAACCCACTCGACTTCTTTTGGAATATCTTGAAGAAAAATATGAAGAGCATTTGTATG
AGCGCGATGAAGGTGATAAATGGCGAAACAAAAAGTTTGAATTGGGTTTGGAGTTTCCCAATCTTCCTTATTATATTGATGGTGATGTTAAATTAACACA
GTCTATGGCCATCATACGTTATATAGCTGACAAGCACAACATGTTGGGTGGTTGTCCAAAAGAGCGTGCAGAGATTTCAATGCTTGAAGGAGCGGTTTTG
GATATTAGATACGGTGTTTCGAGAATTGCATATAGTAAAGACTTTGAAACTCTCAAAGTTGATTTTCTTAGCAAGCTACCTGAAATGCTGAAAATGTTCG
AAGATCGTTTATGTCATAAAACATATTTAAATGGTGATCATGTAACCCATCCTGACTTCATGTTGTATGACGCTCTTGATGTTGTTTTATACATGGACCC
AATGTGCCTGGATGCGTTCCCAAAATTAGTTTGTTTTAAAAAACGTATTGAAGCTATCCCACAAATTGATAAGTACTTGAAATCCAGCAAGTATATAGCA
TGGCCTTTGCAGGGCTGGCAAGCCACGTTTGGTGGTGGCGACCATCCTCCAAAATCCGGATCTGATCGAGGTCGTGGGATCCCCGAATTCCCGGGTCGAC
TCGAGATGAAGAAAAGACCGGTCAAAATTGAAAAGGAGCTGGGTGGTGTCTACCATCGGTTGTTTGAACCACTCCGAGTCCCTCCGGATTTGTTTAGAAG
GTTAACCGGACAGTTTTGTATGATCCAGACCTTGAAAAGGGGCCAGGTTTACGCCACAGAGGACAAAACCTCAGTTGATGATCGTCTTAGTATTCTCCTA
AAAGGAAGAATGAAGGTCTCCTATCGAGGACATTTTCTGCATAACATTTACCCGTGTGCCTTTATAGATTCTCCCGAATTCAGATCAACGCAGATGCACA
AAGGCGAAAAATTCCAGGTCACCATTGTTGCAGATGATAACTGCAGGTTCTTATGCTGGTCAAGAGAAAGACTGACTTACTTTCTGGAGTCAGAGCCTTT
TCTGTATGAAATTTTTAGGTACCTTATAGGAAAAGACATTACAAATAAGCTGTACTCACTGAATGACCCTACTTTAAATGATAAGAAAGTTAAGAAGCTG
GAGCCCCAGATGAGCCTCTGCACACAGATCTCCATGCTGGAGATGAGGAACAGTATCACCAGCTCCAGCGACGGCGAGGACGGCCTGCACCACTTTCTGC
GGGGCTCCTCCAGCACGGCGTCTCTCCCCATGTCCTCCCCGCAGCAGCGAGCCTCTGCCAAGATGAAGCCAATCGAGGAAGGGGTAGAAGATGACGATGA
GGTCTTTGTGTCTCCAGACGCACTCAAAGTCCATCAGTTGCTATTGAACAGAAACTCATCAGCGAAGAGGATCTGTGA

Figure 10.7: The cDNA Oligonucleotide Sequence of the GST-BVES Popeye Domain Construct.

ATGCAGTACAAACTGATCCTGAACGGTAAAACCCTGAAAGGTGAAACCACCACCGAAGCTGTTGACGCTGCTACCGCGGAAAAAGTTTTCAAACAGTACG
CTAACGACAACGGTGTTGACGGTGAATGGACCTACGACGACGCTACCAAAACCTTCACCGTTACCGAAGGATCTCATCATCATCATCATGGATCCAT
GCAGCTGGTCTATCGTGTCCGGGTGAATACCCTCCCGGAGGAATTCAATCTCCTCTACAGGACACTGTGCCTGCCCCTGCAGGTGCCCCTGCAGGTCTAC
AAGGAGATTGTCCACTGCTGCCATGAGCAGGTCTTGACGCTGGCCACAGAGCAGACCTACGCTGTGGAGGGGGAGACCCCCATCAATCGCCTGTCCCTGC
TCCTCTCAGGCCGGGTTCGAGTGAGCCAAGACGGGCAGTTTCTGCACTACATCTTTCCGTATCAGTTCATGGACTCTCCTGAATGGGAATCACTGCATCC
TTCTGAAGAGGGGACCTTCCAGGTGACGCTGACTGCGGAGACCGAATGTAGCTACATTTCCTGGCCCCGGAAAAATCTTTACCTTCTTCTGAACAGAGAG
CGATACATCTCCCGCCTCTTCTCAGCCCTGCTGGGCTATGACATCTCGGAGAAGCTCTATACCCTCAATGACAAGCTGTTTGCCAAGTAA

Figure 10.8: The cDNA Oligonucleotide Sequence of the GB1-Q94-K255 POPDC2 Popeye Domain Construct.

ATGAATTATACAGAGTCCAGCCCATTGAGAGAATCAACTGCCATAGGTTTTACACCTGAGTTAGAAAGTATCATACCTGTGCCTTCCAATAAGACCACTT
GTGAAAACTGGAGAGAGATACATCATCTGGTTTTTCATGTAGCAAATATTTGTTTTGCAGTTGGGTTGGTTATTCCAACTACTCTTCACCTTCATATGAT
ATTTCTTAGGGGAATGTTAACTCTAGGATGTACCCTTTATATCGTCTGGGCCACTCTCTACCGATGTGCCTTGGATATAATGATCTGGAACTCTGTGTTC
TTGGGTGTCAACATTTTGCATCTGTCGTATCTTTTATACAAGAAGAGACCGGTAAAGATTGAAAAGGAACTCAGTGGCATGTACCGGCGATTGTTTGAAC
CACTCCGTGTGCCTCCAGATTTGTTCAGAAGACTAACTGGACAGTTTTGCATGATCCAAACCTTGAAAAAGGGCCAAACTTATGCTGCAGAGGATAAAAC
CTCAGTTGATGACCGTCTGAGTATTCTCTTGAAGGGAAAAATGAAGGTCTCCTATCGAGGACATTTTCTGCATAACATTTACCCCTGTGCCTTTATAGAT
TCTCCTGAATTTAGATCAACTCAGATGCACAAAGGTGAAAAATTCCAGGTCACCATTATTGCAGATGATAACTGCAGATTTTTATGCTGGTCAAGAGAAA
GATTAACATACTTTCTGGAATCAGAACCTTTCTTGTATGAAATCTTTAGGTATCTTATTGGAAAAGACATCACAAATAAGCTCTACTCATTGAATGATCC
CACCTTAAATGATAAAAAAGCCAAAAAGCTGGAACATCAGCTCAGCCTCTGCACACAGATCTCCATGTTGGAAATGAGGAACAGTATAGCCAGCTCCAGT
GACAGTGACGACGGCTTGCACCAGTTTCTTCGGGGTACCTCCAGCATGTCCTCTCTTCATGTGTCATCCCCACACCAGCGAGCCTCTGCCAAGATGAAAC
CGATAGAAGAAGGAGCAGAAGATGATGATGACGTTTTTGAACCGGCATCTCCAAATACATTGAAAGTCCATCAGCTGCCTCGGGATCCACCGGTCGCCAC
CATGGTGAGCAAGGGCGAGGAGCTGTTCACCGGGGTGGTGCCCATCCTGGTCGAGCTGGACGGCGACGTAAACGGCCACAAGTTCAGCGTGTCCGGCGAG
GGCGAGGGCGATGCCACCTACGGCAAGCTGACCCTGAAGTTCATCTGCACCACCGGCAAGCTGCCCGTGCCCTGGCCCACCCTCGTGACCACCCTGACCT
GGGGCGTGCAGTGCTTCAGCCGCTACCCCGACCACATGAAGCAGCACGACTTCTTCAAGTCCGCCATGCCCGAAGGCTACGTCCAGGAGCGCACCATCTT
CTTCAAGGACGACGGCAACTACAAGACCCGCGCCGAGGTGAAGTTCGAGGGCGACACCCTGGTGAACCGCATCGAGCTGAAGGGCATCGACTTCAAGGAG
GACGGCAACATCCTGGGGCACAAGCTGGAGTACAACTACATCAGCCACAACGTCTATATCACCGCCGACAAGCAGAAGAACGGCATCAAGGCCAACTTCA
AGATCCGCCACAACATCGAGGACGGCAGCGTGCAGCTCGCCGACCACTACCAGCAGAACACCCCCATCGGCGACGGCCCCGTGCTGCTGCCCGACAACCA
CTACCTGAGCACCCAGTCCGCCCTGAGCAAAGACCCCAACGAGAAGCGCGATCACATGGTCCTGCTGGAGTTCGTGACCGCCGCCGGGATCACTCTCGGC
ATGGACGAGCTGTACAAGGGAGGAAGCGGAGAGCAGAAACTCATCTCTGAAGAGGATCTGTAA

Figure 10.9: The cDNA Oligonucleotide Sequence of the POPDC1-ECFP Construct.

ATGAGCGCCAACAGCAGCAGAGTGGGCCAGCTTCTCTTGCAGGGTTCAGCGTGCATTAGGTGGAAGCAGGATGTGGAAGGGGCTGTCTACCACCTAGCCA
ACTGCCTCTTACTCCTGGGCTTCATGGGGGGCAGTGGGGTGTATGGATGCTTCTATCTTTTTGGCTTCCTGAGTGCAGGTTACCTGTGCTGCGTGCTGTG
GGGCTGGTTCAGTGCCTGTGGCCTGGACATTGTTCTTTGGAGCTTCCTGCTGGCTGTGGTCTGCCTGCTCCAGCTGGCACACCTGGTATACCGCCTGCGT
GAGGACACCCTCCCTGAGGAGTTTGACCTCCTCTACAAGACGCTGTGCCTGCCCTTGCAGGTGCCCCTACAGACATACAAGGAGATTGTTCACTGCTGCG
AGGAGCAGGTCTTAACTCTGGCCACTGAACAGACCTATGCTGTGGAGGGTGAGACACCCATCAACCGCCTGTCCCTGCTGCTCTCTGGCCGGGTTCGTGT
GAGCCAGGATGGGCAGTTTCTGCACTACATCTTTCCATACCAGTTCATGGACTCTCCTGAGTGGGAATCACTACAGCCTTCTGAGGAGGGGGTGTTCCAG
GTCACTCTGACTGCTGAGACCTCATGTAGCTACATTTCCTGGCCCCGGAAAAGTCTCCATCTTCTTCTGACCAAAGAGCGATACATCTCCTGCCTCTTCT
CGGCTCTGCTGGGATATGACATCTCGGAGAAGCTCTACACTCTCAATGACAAGCTCTTTGCTAAGTTTGGGCTGCGCTTTGACATCCGCCTTCCCAGCCT
CTACCATGTCCTGGGTCCCACTGCTGCAGATGCTGGACCAGAGTCCGAGAAGGGTGATGAGGAAGTCTGTGAGCCAGCTGTGTCCCCTCCTCAGGCCACA
CCCACCTCTCTCCAGCAAACACCCCCTTGTTCTACCCCTCCAGCTACCACCAACTTTCCTGCACCTCCTACCCGGGCCAGGTTGTCCAGGCCAGACAGTG
GCATACTGGCTTCTAGAATTCCTCTCCAGAGCTACTCTCAAGTTATATCCAGGGGACAGGCCCCTTTGGCTCCAACCCACACGCCTGAACTTCGGGATCC
ACCGGTCGCCACCATGGTGAGCAAGGGCGAGGAGCTGTTCACCGGGGTGGTGCCCATCCTGGTCGAGCTGGACGGCGACGTAAACGGCCACAAGTTCAGC
GTGTCCGGCGAGGGCGAGGGCGATGCCACCTACGGCAAGCTGACCCTGAAGTTCATCTGCACCACCGGCAAGCTGCCCGTGCCCTGGCCCACCCTCGTGA
CCACCTTCGGCTACGGCCTGCAGTGCTTCGCCCGCTACCCCGACCACATGAAGCAGCACGACTTCTTCAAGTCCGCCATGCCCGAAGGCTACGTCCAGGA
GCGCACCATCTTCTTCAAGGACGACGGCAACTACAAGACCCGCGCCGAGGTGAAGTTCGAGGGCGACACCCTGGTGAACCGCATCGAGCTGAAGGGCATC
GACTTCAAGGAGGACGGCAACATCCTGGGGCACAAGCTGGAGTACAACTACAACAGCCACAACGTCTATATCATGGCCGACAAGCAGAAGAACGGCATCA
AGGTGAACTTCAAGATCCGCCACAACATCGAGGACGGCAGCGTGCAGCTCGCCGACCACTACCAGCAGAACACCCCCATCGGCGACGGCCCCGTGCTGCT
GCCCGACAACCACTACCTGAGCTACCAGTCCGCCCTGAGCAAAGACCCCAACGAGAAGCGCGATCACATGGTCCTGCTGGAGTTCGTGACCGCCGCCGGG
ATCACTCTCGGCATGGACGAGCTGTACAAGGGAGGAAGCGGATACCCATACGATGTTCCAGATTACGCTTAA

Figure 10.10: The cDNA Oligonucleotide Sequence of the POPDC2-EYFP Construct.

ATGAATTATACAGAGTCCAGCCCATTGAGAGAATCAACTGCCATAGGTTTTACACCTGAGTTAGAAAGTATCATACCTGTGCCTTCCAATAAGACCACTT
GTGAAAACTGGAGAGAGATACATCATCTGGTTTTTCATGTAGCAAATATTTGTTTTGCAGTTGGGTTGGTTATTCCAACTACTCTTCACCTTCATATGAT
ATTTCTTAGGGGAATGTTAACTCTAGGATGTACCCTTTATATCGTCTGGGCCACTCTCTACCGATGTGCCTTGGATATAATGATCTGGAACTCTGTGTTC
TTGGGTGTCAACATTTTGCATCTGTCGTATCTTTTATACAAGAAGAGACCGGTAAAGATTGAAAAGGAACTCAGTGGCATGTACCGGCGATTGTTTGAAC
CACTCCGTGTGCCTCCAGATTTGTTCAGAAGACTAACTGGACAGTTTTGCATGATCCGGGATCCACCGGTCGCCACCATGGTGAGCAAGGGCGAGGAGCT
GTTCACCGGGGTGGTGCCCATCCTGGTCGAGCTGGACGGCGACGTAAACGGCCACAAGTTCAGCGTGTCCGGCGAGGGCGAGGGCGATGCCACCTACGGC
AAGCTGACCCTGAAGTTCATCTGCACCACCGGCAAGCTGCCCGTGCCCTGGCCCACCCTCGTGACCACCCTGACCTGGGGCGTGCAGTGCTTCAGCCGCT
ACCCCGACCACATGAAGCAGCACGACTTCTTCAAGTCCGCCATGCCCGAAGGCTACGTCCAGGAGCGCACCATCTTCTTCAAGGACGACGGCAACTACAA
GACCCGCGCCGAGGTGAAGTTCGAGGGCGACACCCTGGTGAACCGCATCGAGCTGAAGGGCATCGACTTCAAGGAGGACGGCAACATCCTGGGGCACAAG
CTGGAGTACAACTACATCAGCCACAACGTCTATATCACCGCCGACAAGCAGAAGAACGGCATCAAGGCCAACTTCAAGATCCGCCACAACATCGAGGACG
GCAGCGTGCAGCTCGCCGACCACTACCAGCAGAACACCCCCATCGGCGACGGCCCCGTGCTGCTGCCCGACAACCACTACCTGAGCACCCAGTCCGCCCT
GAGCAAAGACCCCAACGAGAAGCGCGATCACATGGTCCTGCTGGAGTTCGTGACCGCCGCCGGGATCACTCTCGGCATGGACGAGCTGTACAAGGGAGGA
AGCGGAGAGCAGAAACTCATCTCTGAAGAGGATCTGTAA

Figure 10.11: The cDNA Oligonucleotide Sequence of the POPDC1p.Q153X-ECFP Construct.

ATGAATTATACAGAGTCCAGCCCATTGAGAGAATCAACTGCCATAGGTTTTACACCTGAGTTAGAAAGTATCATACCTGTGCCTTCCAATAAGACCACTT
GTGAAAACTGGAGAGAGATACATCATCTGGTTTTTCATGTAGCAAATATTTGTTTTGCAGTTGGGTTGGTTATTCCAACTACTCTTCACCTTCATATGAT
ATTTCTTAGGGGAATGTTAACTCTAGGATGTACCCTTTATATCGTCTGGGCCACTCTCTACCGATGTGCCTTGGATATAATGATCTGGAACTCTGTGTTC
TTGGGTGTCAACATTTTGCATCTGTCGTATCTTTTATACAAGAAGAGACCGGTAAAGATTGAAAAGGAACTCAGTGGCATGTACCGGCGATTGTTTGAAC
CACTCCGTGTGCCTCCAGATTTGTTCAGAAGACTAACTGGACAGTTTTGCATGATCCAAACCTTGAAAAAGGGCCAAACTTATGCTGCAGAGGATAAAAC
CTCAGTTGATGAC**CGT**CTGAGTATTCTCTTGAAGGGAAAAATGAAG**GTC**TCCTATCGAGGACATTTTCTGCATAACATTTACCCCTGTGCCTTTATAGAT
TCTCCTGAATTTAGATCAACTCAGATGCACAAAGGTGAAAAATTCCAGGTCACCATTATTGCAGATGATAACTGCAGATTTTTATGCTGGTCAAGAGAAA
GATTAACATACTTTCTGGAATCAGAACCTTTCTTGTATGAAATCTTTAGGTATCTTATTGGAAAAGACATCACAAATAAGCTCTACTCATTGAATGATCC
CACCTTAAATGATAAAAAAGCCAAAAAGCTGGAACATCAGCTCAGCCTCTGCACACAGATCTCCATGTTGGAAATGAGGAACAGTATAGCCAGCTCCAGT
GACAGTGACGACGGCTTGCACCAGTTTCTTCGGGGTACCTCCAGCATGTCCTCTCTTCATGTGTCATCCCCACACCAGCGAGCCTCTGCCAAGATGAAAC
CGATAGAAGAAGGAGCAGAAGATGATGATGACGTTTTTGAACCGGCATCTCCAAATACATTGAAAGTCCATCAGCTGCCTCGGGATCCACCGGTCGCCAC
CATGGTGAGCAAGGGCGAGGAGCTGTTCACCGGGGTGGTGCCCATCCTGGTCGAGCTGGACGGCGACGTAAACGGCCACAAGTTCAGCGTGTCCGGCGAG
GGCGAGGGCGATGCCACCTACGGCAAGCTGACCCTGAAGTTCATCTGCACCACCGGCAAGCTGCCCGTGCCCTGGCCCACCCTCGTGACCACCCTGACCT
GGGGCGTGCAGTGCTTCAGCCGCTACCCCGACCACATGAAGCAGCACGACTTCTTCAAGTCCGCCATGCCCGAAGGCTACGTCCAGGAGCGCACCATCTT
CTTCAAGGACGACGGCAACTACAAGACCCGCGCCGAGGTGAAGTTCGAGGGCGACACCCTGGTGAACCGCATCGAGCTGAAGGGCATCGACTTCAAGGAG
GACGGCAACATCCTGGGGCACAAGCTGGAGTACAACTACATCAGCCACAACGTCTATATCACCGCCGACAAGCAGAAGAACGGCATCAAGGCCAACTTCA
AGATCCGCCACAACATCGAGGACGGCAGCGTGCAGCTCGCCGACCACTACCAGCAGAACACCCCCATCGGCGACGGCCCCGTGCTGCTGCCCGACAACCA
CTACCTGAGCACCCAGTCCGCCCTGAGCAAAGACCCCAACGAGAAGCGCGATCACATGGTCCTGCTGGAGTTCGTGACCGCCGCCGGGATCACTCTCGGC
ATGGACGAGCTGTACAAGGGAGGAAGCGGAGAGCAGAAACTCATCTCTGAAGAGGATCTGTAA

Figure 10.12: The cDNA Oligonucleotide Sequence of the POPDC1p.R172H/p.V183F/p.S201F-ECFP Constructs. Highlighted codons code for residues R172, V183 and S201, respectively. Each codon was mutated to introduce the respective mutations (c.515G>A, p.R172H; c.547G>T, p.V183F; and c.602C>T, p.S201F) at each position in the respective POPDC1-ECFP mutants.

ATGAGCGCCAACAGCAGCAGAGTGGGCCAGCTTCTCTTGCAGGGTTCAGCGTGCATTAGGTGGAAGCAGGATGTGGAAGGGGCTGTCTACCACCTAGCCA
ACTGCCTCTTACTCCTGGGCTTCATGGGGGGCAGTGGGGTGTATGGATGCTTCTATCTTTTTGGCTTCCTGAGTGCAGGTTACCTGTGCTGCGTGCTGTG
GGGCTGGTTCAGTGCCTGTGGCCTGGACATTGTTCTTTGGAGCTTCCTGCTGGCTGTGGTCTGCCTGCTCCAGCTGGCACACCTGGTATACCGCCTGCGT
GAGGACACCCTCCCTGAGGAGTTTGACCTCCTCTACAAGACGCTGTGCCTGCCCTTGCAGGTGCCCCTACAGACATACAAGGAGATTGTTCACTGCTGCG
AGGAGCAGGTCTTAACTCTGGCCACTGAACAGACCTATGCTGTGGAGGGTGAGACACCCATCAACCGCCTGTCCCTGCTGCTCTCTGGCCGGGTTCGTGT
GAGCCAGGATGGGCAGTTTCTGCACTACATCTTTCCATACCAGTTCATGGACTCTCCTGAGCGGGATCCACCGGTCGCCACCATGGTGAGCAAGGGCGAG
GAGCTGTTCACCGGGGTGGTGCCCATCCTGGTCGAGCTGGACGGCGACGTAAACGGCCACAAGTTCAGCGTGTCCGGCGAGGGCGAGGGCGATGCCACCT
ACGGCAAGCTGACCCTGAAGTTCATCTGCACCACCGGCAAGCTGCCCGTGCCCTGGCCCACCCTCGTGACCACCTTCGGCTACGGCCTGCAGTGCTTCGC
CCGCTACCCCGACCACATGAAGCAGCACGACTTCTTCAAGTCCGCCATGCCCGAAGGCTACGTCCAGGAGCGCACCATCTTCTTCAAGGACGACGGCAAC
TACAAGACCCGCGCCGAGGTGAAGTTCGAGGGCGACACCCTGGTGAACCGCATCGAGCTGAAGGGCATCGACTTCAAGGAGGACGGCAACATCCTGGGGC
ACAAGCTGGAGTACAACTACAACAGCCACAACGTCTATATCATGGCCGACAAGCAGAAGAACGGCATCAAGGTGAACTTCAAGATCCGCCACAACATCGA
GGACGGCAGCGTGCAGCTCGCCGACCACTACCAGCAGAACACCCCCATCGGCGACGGCCCCGTGCTGCTGCCCGACAACCACTACCTGAGCTACCAGTCC
GCCCTGAGCAAAGACCCCAACGAGAAGCGCGATCACATGGTCCTGCTGGAGTTCGTGACCGCCGCCGGGATCACTCTCGGCATGGACGAGCTGTACAAGG
GAGGAAGCGGATACCCATACGATGTTCCAGATTACGCTTAA

Figure 10.13: The cDNA Oligonucleotide Sequence of the POPDC2p.W188X-EYFP Construct

ATGAGCGCCAACAGCAGCAGAGTGGGCCAGCTTCTCTTGCAGGGTTCAGCGTGCATTAGGTGGAAGCAGGATGTGGAAGGGGCTGTCTACCACCTAGCCA
ACTGCCTCTTACTCCTGGGCTTCATGGGGGGCAGTGGGGTGTATGGATGCTTCTATCTTTTTGGCTTCCTGAGTGCAGGTTACCTGTGCTGCGTGCTGTG
GGGCTGGTTCAGTGCCTGTGGCCTGGACATTGTTCTTTGGAGCTTCCTGCTGGCTGTGGTCTGCCTGCTCCAGCTGGCACACCTGGTATACCGCCTGCGT
GAGGACACCCTCCCTGAGGAGTTTGACCTCCTCTACAAGACGCTGTGCCTGCCCTTGCAGGTGCCCCTACAGACATACAAGGAGATTGTTCACTGCTGCG
AGGAGCAGGTCTTAACTCTGGCCACTGAACAGACCTATGCTGTGGAGGGTGAGACACCCATCAACCGCCTGTCCCTGCTGCTCTCTGGCCGGGTTCGTGT
GAGCCAGGATGGGCAGTTTCTGCACTACATCTTTCCATACCAGTTCATGGACTCTCCTGAGTGGGAATCACTACAGCCTTCTGAGGAGGGGGTGTTCCAG
GTCACTCTGACTGCTGAGACCTCATGTAGCTACATTTCCTGGCCCCGGAAAAGTCTCCATCTTCTTCTGACCAAAGAGCGATACATCTCCTGCCTCTTCT
CGGCTCTGCTGGGATATGACATCTCGGAGAAGCCCTACACTCTCAATGACAAGCTCTTTGCTAAGTTTGGGCTGCGCTTTGACATCCGCCTTCCCAGCCT
CTACCATGTCCTGGGTCCCACTGCTGCAGATGCTGGACCAGAGTCCGAGAAGGGTGATGAGGAAGTCTGTGAGCCAGCTGTGTCCCCTCCTCAGGCCACA
CCCACCTCTCTCCAGCAAACACCCCCTTGTTCTACCCCTCCAGCTACCACCAACTTTCCTGCACCTCCTACCCGGGCCAGGTTGTCCAGGCCAGACAGTG
GCATACTGGCTTCTAGAATTCCTCTCCAGAGCTACTCTCAAGTTATATCCAGGGGACAGGCCCCTTTGGCTCCAACCCACACGCCTGAACTTCGGGATCC
ACCGGTCGCCACCATGGTGAGCAAGGGCGAGGAGCTGTTCACCGGGGTGGTGCCCATCCTGGTCGAGCTGGACGGCGACGTAAACGGCCACAAGTTCAGC
GTGTCCGGCGAGGGCGAGGGCGATGCCACCTACGGCAAGCTGACCCTGAAGTTCATCTGCACCACCGGCAAGCTGCCCGTGCCCTGGCCCACCCTCGTGA
CCACCTTCGGCTACGGCCTGCAGTGCTTCGCCCGCTACCCCGACCACATGAAGCAGCACGACTTCTTCAAGTCCGCCATGCCCGAAGGCTACGTCCAGGA
GCGCACCATCTTCTTCAAGGACGACGGCAACTACAAGACCCGCGCCGAGGTGAAGTTCGAGGGCGACACCCTGGTGAACCGCATCGAGCTGAAGGGCATC
GACTTCAAGGAGGACGGCAACATCCTGGGGCACAAGCTGGAGTACAACTACAACAGCCACAACGTCTATATCATGGCCGACAAGCAGAAGAACGGCATCA
AGGTGAACTTCAAGATCCGCCACAACATCGAGGACGGCAGCGTGCAGCTCGCCGACCACTACCAGCAGAACACCCCCATCGGCGACGGCCCCGTGCTGCT
GCCCGACAACCACTACCTGAGCTACCAGTCCGCCCTGAGCAAAGACCCCAACGAGAAGCGCGATCACATGGTCCTGCTGGAGTTCGTGACCGCCGCCGGG
ATCACTCTCGGCATGGACGAGCTGTACAAGGGAGGAAGCGGATACCCATACGATGTTCCAGATTACGCTTAA

Figure 10.14: The cDNA Oligonucleotide Sequence of the POPDC2p.L245P-EYFP Construct

ATGAATTATACAGAGTCCAGCCCATTGAGAGAATCAACTGCCATAGGTTTTACACCTGAGTTAGAAAGTATCATACCTGTGCCTTCCAATAAGACCACTT
GTGAAAACTGGAGAGAGATACATCATCTGGTTTTTCATGTAGCAAATATTTGTTTTGCAGTTGGGTTGGTTATTCCAACTACTCTTCACCTTCATATGAT
ATTTCTTAGGGGAATGTTAACTCTAGGATGTACCCTTTATATCGTCTGGGCCACTCTCTACCGATGTGCCTTGGATATAATGATCTGGAACTCTGTGTTC
TTGGGTGTCAACATTTTGCATCTGTCGTATCTTTTATACAAGAAGAGACCGGTAAAGATTGAAAAGGAACTCAGTGGCATGTACCGGCGATTGTTTGAAC
CACTCCGTGTGCCTCCAGATTTGTTCAGAAGACTAACTGGACAGTTTTGCATGATCCAAACCTTGAAAAAGGGCCAAACTTATGCTGCAGAGGATAAAAC
CTCAGTTGATGACCGTCTGAGTATTCTCTTGAAGGGAAAAATGAAGGTCTCCTATCGAGGACATTTTCTGCATAACATTTACCCCTGTGCCTTTATAGAT
TCTCCTGAATTTAGATCAACTCAGATGCACAAAGGTGAAAAATTCCAGGTCACCATTATTGCAGATGATAACTGCAGATTTTTATGCTGGTCAAGAGAAA
GATTAACATACTTTCTGGAATCAGAACCTTTC**TTG**TATGAAATC**TTT**AGGTATCTT**ATT**GGAAAAGAC**ATC**ACAAATAAG**CTC**TACTCA**TTG**AATGATCC
CACCTTAAATGATAAAAAAGCCAAAAAGCTGGAACATCAGCTCAGCCTCTGCACACAGATCTCCATGTTGGAAATGAGGAACAGTATAGCCAGCTCCAGT
GACAGTGACGACGGCTTGCACCAGTTTCTTCGGGGTACCTCCAGCATGTCCTCTCTTCATGTGTCATCCCCACACCAGCGAGCCTCTGCCAAGATGAAAC
CGATAGAAGAAGGAGCAGAAGATGATGATGACGTTTTTGAACCGGCATCTCCAAATACATTGAAAGTCCATCAGCTGCCTCGGGATCCACCGGTCGCCAC
CATGGTGAGCAAGGGCGAGGAGCTGTTCACCGGGGTGGTGCCCATCCTGGTCGAGCTGGACGGCGACGTAAACGGCCACAAGTTCAGCGTGTCCGGCGAG
GGCGAGGGCGATGCCACCTACGGCAAGCTGACCCTGAAGTTCATCTGCACCACCGGCAAGCTGCCCGTGCCCTGGCCCACCCTCGTGACCACCCTGACCT
GGGGCGTGCAGTGCTTCAGCCGCTACCCCGACCACATGAAGCAGCACGACTTCTTCAAGTCCGCCATGCCCGAAGGCTACGTCCAGGAGCGCACCATCTT
CTTCAAGGACGACGGCAACTACAAGACCCGCGCCGAGGTGAAGTTCGAGGGCGACACCCTGGTGAACCGCATCGAGCTGAAGGGCATCGACTTCAAGGAG
GACGGCAACATCCTGGGGCACAAGCTGGAGTACAACTACATCAGCCACAACGTCTATATCACCGCCGACAAGCAGAAGAACGGCATCAAGGCCAACTTCA
AGATCCGCCACAACATCGAGGACGGCAGCGTGCAGCTCGCCGACCACTACCAGCAGAACACCCCCATCGGCGACGGCCCCGTGCTGCTGCCCGACAACCA
CTACCTGAGCACCCAGTCCGCCCTGAGCAAAGACCCCAACGAGAAGCGCGATCACATGGTCCTGCTGGAGTTCGTGACCGCCGCCGGGATCACTCTCGGC
ATGGACGAGCTGTACAAGGGAGGAAGCGGAGAGCAGAAACTCATCTCTGAAGAGGATCTGTAA

Figure 10.15: The cDNA Oligonucleotide Sequence of the αC-helix Mutant POPDC1-ECFP Constructs. Highlighted codons code for residues L245, F249, I253, I257, L261 and L264. Each codon was mutated to GAC through directed mutagenesis to introduce an aspartic acid at each position in the respective POPDC1-ECFP mutants.

ATGAGCGCCAACAGCAGCAGAGTGGGCCAGCTTCTCTTGCAGGGTTCAGCGTGCATTAGGTGGAAGCAGGATGTGGAAGGGGCTGTCTACCACCTAGCCA
ACTGCCTCTTACTCCTGGGCTTCATGGGGGGCAGTGGGGTGTATGGATGCTTCTATCTTTTTGGCTTCCTGAGTGCAGGTTACCTGTGCTGCGTGCTGTG
GGGCTGGTTCAGTGCCTGTGGCCTGGACATTGTTCTTTGGAGCTTCCTGCTGGCTGTGGTCTGCCTGCTCCAGCTGGCACACCTGGTATACCGCCTGCGT
GAGGACACCCTCCCTGAGGAGTTTGACCTCCTCTACAAGACGCTGTGCCTGCCCTTGCAGGTGCCCCTACAGACATACAAGGAGATTGTTCACTGCTGCG
AGGAGCAGGTCTTAACTCTGGCCACTGAACAGACCTATGCTGTGGAGGGTGAGACACCCATCAACCGCCTGTCCCTGCTGCTCTCTGGCCGGGTTCGTGT
GAGCCAGGATGGGCAGTTTCTGCACTACATCTTTCCATACCAGTTCATGGACTCTCCTGAGTGGGAATCACTACAGCCTTCTGAGGAGGGGGTGTTCCAG
GTCACTCTGACTGCTGAGACCTCATGTAGCTACATTTCCTGGCCCCGGAAAAGTCTCCATCTTCTTCTGACCAAAGAGCGATAC**ATC**TCCTGCCTC**TTC**T
CGGCTCTG**CTG**GGATATGAC**ATC**TCGGAGAAG**CTC**TACACT**CTC**AATGACAAGCTCTTTGCTAAGTTTGGGCTGCGCTTTGACATCCGCCTTCCCAGCCT
CTACCATGTCCTGGGTCCCACTGCTGCAGATGCTGGACCAGAGTCCGAGAAGGGTGATGAGGAAGTCTGTGAGCCAGCTGTGTCCCCTCCTCAGGCCACA
CCCACCTCTCTCCAGCAAACACCCCCTTGTTCTACCCCTCCAGCTACCACCAACTTTCCTGCACCTCCTACCCGGGCCAGGTTGTCCAGGCCAGACAGTG
GCATACTGGCTTCTAGAATTCCTCTCCAGAGCTACTCTCAAGTTATATCCAGGGGACAGGCCCCTTTGGCTCCAACCCACACGCCTGAACTTCGGGATCC
ACCGGTCGCCACCATGGTGAGCAAGGGCGAGGAGCTGTTCACCGGGGTGGTGCCCATCCTGGTCGAGCTGGACGGCGACGTAAACGGCCACAAGTTCAGC
GTGTCCGGCGAGGGCGAGGGCGATGCCACCTACGGCAAGCTGACCCTGAAGTTCATCTGCACCACCGGCAAGCTGCCCGTGCCCTGGCCCACCCTCGTGA
CCACCTTCGGCTACGGCCTGCAGTGCTTCGCCCGCTACCCCGACCACATGAAGCAGCACGACTTCTTCAAGTCCGCCATGCCCGAAGGCTACGTCCAGGA
GCGCACCATCTTCTTCAAGGACGACGGCAACTACAAGACCCGCGCCGAGGTGAAGTTCGAGGGCGACACCCTGGTGAACCGCATCGAGCTGAAGGGCATC
GACTTCAAGGAGGACGGCAACATCCTGGGGCACAAGCTGGAGTACAACTACAACAGCCACAACGTCTATATCATGGCCGACAAGCAGAAGAACGGCATCA
AGGTGAACTTCAAGATCCGCCACAACATCGAGGACGGCAGCGTGCAGCTCGCCGACCACTACCAGCAGAACACCCCCATCGGCGACGGCCCCGTGCTGCT
GCCCGACAACCACTACCTGAGCTACCAGTCCGCCCTGAGCAAAGACCCCAACGAGAAGCGCGATCACATGGTCCTGCTGGAGTTCGTGACCGCCGCCGGG
ATCACTCTCGGCATGGACGAGCTGTACAAGGGAGGAAGCGGATACCCATACGATGTTCCAGATTACGCTTAA

Figure 10.16: The cDNA Oligonucleotide Sequence of the αC-helix Mutant POPDC2-EYFP Constructs. Highlighted codons code for residues L245, F249, I253, I257, L261 and L264. Each codon was mutated to GAC through directed mutagenesis to introduce an aspartic acid at each position in the respective POPDC2-EYFP mutants.

ATGGTGAGCAAGGGCGAGGAGCTGTTCACCGGGGTGGTGCCCATCCTGGTCGAGCTGGACGGCGACGTAAACGGCCACAAGTTCAGCGTGTCCGGCGAGG
GCGAGGGCGATGCCACCTACGGCAAGCTGACCCTGAAGTTCATCTGCACCACCGGCAAGCTGCCCGTGCCCTGGCCCACCCTCGTGACCACCCTGACCTG
GGGCGTGCAGTGCTTCAGCCGCTACCCCGACCACATGAAGCAGCACGACTTCTTCAAGTCCGCCATGCCCGAAGGCTACGTCCAGGAGCGCACCATCTTC
TTCAAGGACGACGGCAACTACAAGACCCGCGCCGAGGTGAAGTTCGAGGGCGACACCCTGGTGAACCGCATCGAGCTGAAGGGCATCGACTTCAAGGAGG
ACGGCAACATCCTGGGGCACAAGCTGGAGTACAACTACATCAGCCACAACGTCTATATCACCGCCGACAAGCAGAAGAACGGCATCAAGGCCAACTTCAA
GATCCGCCACAACATCGAGGACGGCAGCGTGCAGCTCGCCGACCACTACCAGCAGAACACCCCCATCGGCGACGGCCCCGTGCTGCTGCCCGACAACCAC
TACCTGAGCACCCAGTCCGCCCTGAGCAAAGACCCCAACGAGAAGCGCGATCACATGGTCCTGCTGGAGTTCGTGACCGCCGCCGGGATCACTCTCGGCA
TGGACGAGCTGTACAAGGGAGGAAGCGGAATGGATCCACCGGTCGCCACCATGGTGAGCAAGGGCGAGGAGCTGTTCACCGGGGTGGTGCCCATCCTGGT
CGAGCTGGACGGCGACGTAAACGGCCACAAGTTCAGCGTGTCCGGCGAGGGCGAGGGCGATGCCACCTACGGCAAGCTGACCCTGAAGTTCATCTGCACC
ACCGGCAAGCTGCCCGTGCCCTGGCCCACCCTCGTGACCACCTTCGGCTACGGCCTGCAGTGCTTCGCCCGCTACCCCGACCACATGAAGCAGCACGACT
TCTTCAAGTCCGCCATGCCCGAAGGCTACGTCCAGGAGCGCACCATCTTCTTCAAGGACGACGGCAACTACAAGACCCGCGCCGAGGTGAAGTTCGAGGG
CGACACCCTGGTGAACCGCATCGAGCTGAAGGGCATCGACTTCAAGGAGGACGGCAACATCCTGGGGCACAAGCTGGAGTACAACTACAACAGCCACAAC
GTCTATATCATGGCCGACAAGCAGAAGAACGGCATCAAGGTGAACTTCAAGATCCGCCACAACATCGAGGACGGCAGCGTGCAGCTCGCCGACCACTACC
AGCAGAACACCCCCATCGGCGACGGCCCCGTGCTGCTGCCCGACAACCACTACCTGAGCTACCAGTCCGCCCTGAGCAAAGACCCCAACGAGAAGCGCGA
TCACATGGTCCTGCTGGAGTTCGTGACCGCCGCCGGGATCACTCTCGGCATGGACGAGCTGTACAAGTAA

Figure 10.17: The cDNA Oligonucleotide Sequence of the ECFP-EYFP AP-FRET Positive Control Construct

ATGAATTATACAGAGTCCAGCCCATTGAGAGAATCAACTGCCATAGGTTTTACACCTGAGTTAGAAAGTATCATACCTGTGCCTTCCAATAAGACCACTT
GTGAAAACTGGAGAGAGATACATCATCTGGTTTTTCATGTAGCAAATATTTGTTTTGCAGTTGGGTTGGTTATTCCAACTACTCTTCACCTTCATATGAT
ATTTCTTAGGGGAATGTTAACTCTAGGATGTACCCTTTATATCGTCTGGGCCACTCTCTACCGATGTGCCTTGGATATAATGATCTGGAACTCTGTGTTC
TTGGGTGTCAACATTTTGCATCTGTCGTATCTTTTATACAAGAAGAGACCGGTAAAGATTGAAAAGGAACTCAGTGGCATGTACCGGCGATTGTTTGAAC
CACTCCGTGTGCCTCCAGATTTGTTCAGAAGACTAACTGGACAGTTTTGCATGATCCAAACCTTGAAAAAGGGCCAAACTTATGCTGCAGAGGATAAAAC
CTCAGTTGATGACCGTCTGAGTATTCTCTTGAAGGGAAAAATGAAGGTCTCCTATCGAGGACATTTTCTGCATAACATTTACCCCTGTGCCTTTATAGAT
TCTCCTGAATTTAGATCAACTCAGATGCACAAAGGTGAAAAATTCCAGGTCACCATTATTGCAGATGATAACTGCAGATTTTTATGCTGGTCAAGAGAAA
GATTAACATACTTTCTGGAATCAGAACCTTTCTTGTATGAAATCTTTAGGTATCTTATTGGAAAAGACATCACAAATAAGCTCTACTCATTGAATGATCC
CACCTTAAATGATAAAAAAGCCAAAAAGCTGGAACATCAGCTCAGCCTCTGCACACAGATCTCCATGTTGGAAATGAGGAACAGTATAGCCAGCTCCAGT
GACAGTGACGACGGCTTGCACCAGTTTCTTCGGGGTACCTCCAGCATGTCCTCTCTTCATGTGTCATCCCCACACCAGCGAGCCTCTGCCAAGATGAAAC
CGATAGAAGAAGGAGCAGAAGATGATGATGACGTTTTTGAACCGGCATCTCCAAATACATTGAAAGTCCATCAGCTGCGGGCCCGGGATCCAGGAGGTGG
CGACAAGCAGAAGAACGGCATCAAGGCCAACTTCAAGATCCGCCACAACATCGAGGACGGCGGCGTGCAGCTCGCCGACCACTACCAGCAGAACACCCCC
ATCGGCGACGGCCCCGTGCTGCTGCCCGACAACCACTACCTGAGCTACCAGTCCAAACTGAGCAAAGACCCCAACGAGAAGCGCGATCACATGGTCCTGC
TGGAGTTCGTGACCGCCGCCGGGATCACTCTCGGCATGGACGAGCTGTACAAGGGAGGAAGCGGAGAGCAGAAACTCATCTCTGAAGAGGATCTGTAA

Figure 10.18: The cDNA Oligonucleotide Sequence of the POPDC1-VC155 Construct

ATGAGCGCCAACAGCAGCAGAGTGGGCCAGCTTCTCTTGCAGGGTTCAGCGTGCATTAGGTGGAAGCAGGATGTGGAAGGGGCTGTCTACCACCTAGCCA
ACTGCCTCTTACTCCTGGGCTTCATGGGGGGCAGTGGGGTGTATGGATGCTTCTATCTTTTTGGCTTCCTGAGTGCAGGTTACCTGTGCTGCGTGCTGTG
GGGCTGGTTCAGTGCCTGTGGCCTGGACATTGTTCTTTGGAGCTTCCTGCTGGCTGTGGTCTGCCTGCTCCAGCTGGCACACCTGGTATACCGCCTGCGT
GAGGACACCCTCCCTGAGGAGTTTGACCTCCTCTACAAGACGCTGTGCCTGCCCTTGCAGGTGCCCCTACAGACATACAAGGAGATTGTTCACTGCTGCG
AGGAGCAGGTCTTAACTCTGGCCACTGAACAGACCTATGCTGTGGAGGGTGAGACACCCATCAACCGCCTGTCCCTGCTGCTCTCTGGCCGGGTTCGTGT
GAGCCAGGATGGGCAGTTTCTGCACTACATCTTTCCATACCAGTTCATGGACTCTCCTGAGTGGGAATCACTACAGCCTTCTGAGGAGGGGGTGTTCCAG
GTCACTCTGACTGCTGAGACCTCATGTAGCTACATTTCCTGGCCCCGGAAAAGTCTCCATCTTCTTCTGACCAAAGAGCGATACATCTCCTGCCTCTTCT
CGGCTCTGCTGGGATATGACATCTCGGAGAAGCTCTACACTCTCAATGACAAGCTCTTTGCTAAGTTTGGGCTGCGCTTTGACATCCGCCTTCCCAGCCT
CTACCATGTCCTGGGTCCCACTGCTGCAGATGCTGGACCAGAGTCCGAGAAGGGTGATGAGGAAGTCTGTGAGCCAGCTGTGTCCCCTCCTCAGGCCACA
CCCACCTCTCTCCAGCAAACACCCCCTTGTTCTACCCCTCCAGCTACCACCAACTTTCCTGCACCTCCTACCCGGGCCAGGTTGTCCAGGCCAGACAGTG
GCATACTGGCTTCTAGAATTCCTCTCCAGAGCTACTCTCAAGTTATATCCAGGGGACAGGCCCCTTTGGCTCCAACCCACACGCCTGAACTTCGGGATCC
AGGAGGTGGCGGGAGCGGAGGTGGCGGGAGTATGGTGAGCAAGGGCGAGGAGCTGTTCACCGGGGTGGTGCCCATCCTGGTCGAGCTGGACGGCGACGTA
AACGGCCACAAGTTCAGCGTGTCCGGCGAGGGCGAGGGCGATGCCACCTACGGCAAGCTGACCCTGAAGCTGATCTGCACCACCGGCAAGCTGCCCGTGC
CCTGGCCCACCCTCGTGACCACCCTGGGCTACGGCCTGCAGTGCTTCGCCCGCTACCCCGACCACATGAAGCAGCACGACTTCTTCAAGTCCGCCATGCC
CGAAGGCTACGTCCAGGAGCGCACCATCTTCTTCAAGGACGACGGCAACTACAAGACCCGCGCCGAGGTGAAGTTCGAGGGCGACACCCTGGTGAACCGC
ATCGAGCTGAAGGGCATCGACTTCAAGGAGGACGGCAACATCCTGGGGCACAAGCTGGAGTACAACTACAACAGCCACAACGTCTATCTCACCGCCGGAG
GAAGCGGATACCCATACGATGTTCCAGATTACGCTTGA

Figure 10.19: The cDNA Oligonucleotide Sequence of the POPDC2-VN155 Construct

ATGAATTATACAGAGTCCAGCCCATTGAGAGAATCAACTGCCATAGGTTTTACACCTGAGTTAGAAAGTATCATACCTGTGCCTTCCAATAAGACCACTT
GTGAAAACTGGAGAGAGATACATCATCTGGTTTTTCATGTAGCAAATATTTGTTTTGCAGTTGGGTTGGTTATTCCAACTACTCTTCACCTTCATATGAT
ATTTCTTAGGGGAATGTTAACTCTAGGATGTACCCTTTATATCGTCTGGGCCACTCTCTACCGATGTGCCTTGGATATAATGATCTGGAACTCTGTGTTC
TTGGGTGTCAACATTTTGCATCTGTCGTATCTTTTATACAAGAAGAGACCGGTAAAGATTGAAAAGGAACTCAGTGGCATGTACCGGCGATTGTTTGAAC
CACTCCGTGTGCCTCCAGATTTGTTCAGAAGACTAACTGGACAGTTTTGCATGATCCGGGATCCAGGAGGTGGCGACAAGCAGAAGAACGGCATCAAGGC
CAACTTCAAGATCCGCCACAACATCGAGGACGGCGGCGTGCAGCTCGCCGACCACTACCAGCAGAACACCCCCATCGGCGACGGCCCCGTGCTGCTGCCC
GACAACCACTACCTGAGCTACCAGTCCAAACTGAGCAAAGACCCCAACGAGAAGCGCGATCACATGGTCCTGCTGGAGTTCGTGACCGCCGCCGGGATCA
CTCTCGGCATGGACGAGCTGTACAAGGGAGGAAGCGGAGAGCAGAAACTCATCTCTGAAGAGGATCTGTAA

Figure 10.20: The cDNA Oligonucleotide Sequence of the POPDC1p.Q153X-VC155 Construct

ATGAATTATACAGAGTCCAGCCCATTGAGAGAATCAACTGCCATAGGTTTTACACCTGAGTTAGAAAGTATCATACCTGTGCCTTCCAATAAGACCACTT
GTGAAAACTGGAGAGAGATACATCATCTGGTTTTTCATGTAGCAAATATTTGTTTTGCAGTTGGGTTGGTTATTCCAACTACTCTTCACCTTCATATGAT
ATTTCTTAGGGGAATGTTAACTCTAGGATGTACCCTTTATATCGTCTGGGCCACTCTCTACCGATGTGCCTTGGATATAATGATCTGGAACTCTGTGTTC
TTGGGTGTCAACATTTTGCATCTGTCGTATCTTTTATACAAGAAGAGACCGGTAAAGATTGAAAAGGAACTCAGTGGCATGTACCGGCGATTGTTTGAAC
CACTCCGTGTGCCTCCAGATTTGTTCAGAAGACTAACTGGACAGTTTTGCATGATCCAAACCTTGAAAAAGGGCCAAACTTATGCTGCAGAGGATAAAAC
CTCAGTTGATGAC**CGT**CTGAGTATTCTCTTGAAGGGAAAAATGAAG**GTC**TCCTATCGAGGACATTTTCTGCATAACATTTACCCCTGTGCCTTTATAGAT
TCTCCTGAATTTAGATCAACTCAGATGCACAAAGGTGAAAAATTCCAGGTCACCATTATTGCAGATGATAACTGCAGATTTTTATGCTGGTCAAGAGAAA
GATTAACATACTTTCTGGAATCAGAACCTTTCTTGTATGAAATCTTTAGGTATCTTATTGGAAAAGACATCACAAATAAGCTCTACTCATTGAATGATCC
CACCTTAAATGATAAAAAAGCCAAAAAGCTGGAACATCAGCTCAGCCTCTGCACACAGATCTCCATGTTGGAAATGAGGAACAGTATAGCCAGCTCCAGT
GACAGTGACGACGGCTTGCACCAGTTTCTTCGGGGTACCTCCAGCATGTCCTCTCTTCATGTGTCATCCCCACACCAGCGAGCCTCTGCCAAGATGAAAC
CGATAGAAGAAGGAGCAGAAGATGATGATGACGTTTTTGAACCGGCATCTCCAAATACATTGAAAGTCCATCAGCTGCGGGCCCGGGATCCAGGAGGTGG
CGACAAGCAGAAGAACGGCATCAAGGCCAACTTCAAGATCCGCCACAACATCGAGGACGGCGGCGTGCAGCTCGCCGACCACTACCAGCAGAACACCCCC
ATCGGCGACGGCCCCGTGCTGCTGCCCGACAACCACTACCTGAGCTACCAGTCCAAACTGAGCAAAGACCCCAACGAGAAGCGCGATCACATGGTCCTGC
TGGAGTTCGTGACCGCCGCCGGGATCACTCTCGGCATGGACGAGCTGTACAAGGGAGGAAGCGGAGAGCAGAAACTCATCTCTGAAGAGGATCTGTAA

Figure 10.21: The cDNA Oligonucleotide Sequence of the POPDC1p.R172H/p.V183F/p.S201F-VC155 Constructs. Codons highlighted in red code for residues R172, V183 and S201. Each codon had previously been mutated to introduce the respective mutations (c.515G>A, p.R172H; c.547G>T, p.V183F; and c.602C>T, p.S201F) at each position.

ATGAGCGCCAACAGCAGCAGAGTGGGCCAGCTTCTCTTGCAGGGTTCAGCGTGCATTAGGTGGAAGCAGGATGTGGAAGGGGCTGTCTACCACCTAGCCA
ACTGCCTCTTACTCCTGGGCTTCATGGGGGGCAGTGGGGTGTATGGATGCTTCTATCTTTTTGGCTTCCTGAGTGCAGGTTACCTGTGCTGCGTGCTGTG
GGGCTGGTTCAGTGCCTGTGGCCTGGACATTGTTCTTTGGAGCTTCCTGCTGGCTGTGGTCTGCCTGCTCCAGCTGGCACACCTGGTATACCGCCTGCGT
GAGGACACCCTCCCTGAGGAGTTTGACCTCCTCTACAAGACGCTGTGCCTGCCCTTGCAGGTGCCCCTACAGACATACAAGGAGATTGTTCACTGCTGCG
AGGAGCAGGTCTTAACTCTGGCCACTGAACAGACCTATGCTGTGGAGGGTGAGACACCCATCAACCGCCTGTCCCTGCTGCTCTCTGGCCGGGTTCGTGT
GAGCCAGGATGGGCAGTTTCTGCACTACATCTTTCCATACCAGTTCATGGACTCTCCTGAGCGGGATCCAGGAGGTGGCGGGAGCGGAGGTGGCGGGAGT
ATGGTGAGCAAGGGCGAGGAGCTGTTCACCGGGGTGGTGCCCATCCTGGTCGAGCTGGACGGCGACGTAAACGGCCACAAGTTCAGCGTGTCCGGCGAGG
GCGAGGGCGATGCCACCTACGGCAAGCTGACCCTGAAGCTGATCTGCACCACCGGCAAGCTGCCCGTGCCCTGGCCCACCCTCGTGACCACCCTGGGCTA
CGGCCTGCAGTGCTTCGCCCGCTACCCCGACCACATGAAGCAGCACGACTTCTTCAAGTCCGCCATGCCCGAAGGCTACGTCCAGGAGCGCACCATCTTC
TTCAAGGACGACGGCAACTACAAGACCCGCGCCGAGGTGAAGTTCGAGGGCGACACCCTGGTGAACCGCATCGAGCTGAAGGGCATCGACTTCAAGGAGG
ACGGCAACATCCTGGGGCACAAGCTGGAGTACAACTACAACAGCCACAACGTCTATCTCACCGCCGGAGGAAGCGGATACCCATACGATGTTCCAGATTA
CGCTTGA

Figure 10.22: The cDNA Oligonucleotide Sequence of the POPDC2p.W188X-VN155 Construct

ATGAGCGCCAACAGCAGCAGAGTGGGCCAGCTTCTCTTGCAGGGTTCAGCGTGCATTAGGTGGAAGCAGGATGTGGAAGGGGCTGTCTACCACCTAGCCA
ACTGCCTCTTACTCCTGGGCTTCATGGGGGGCAGTGGGGTGTATGGATGCTTCTATCTTTTTGGCTTCCTGAGTGCAGGTTACCTGTGCTGCGTGCTGTG
GGGCTGGTTCAGTGCCTGTGGCCTGGACATTGTTCTTTGGAGCTTCCTGCTGGCTGTGGTCTGCCTGCTCCAGCTGGCACACCTGGTATACCGCCTGCGT
GAGGACACCCTCCCTGAGGAGTTTGACCTCCTCTACAAGACGCTGTGCCTGCCCTTGCAGGTGCCCCTACAGACATACAAGGAGATTGTTCACTGCTGCG
AGGAGCAGGTCTTAACTCTGGCCACTGAACAGACCTATGCTGTGGAGGGTGAGACACCCATCAACCGCCTGTCCCTGCTGCTCTCTGGCCGGGTTCGTGT
GAGCCAGGATGGGCAGTTTCTGCACTACATCTTTCCATACCAGTTCATGGACTCTCCTGAGTGGGAATCACTACAGCCTTCTGAGGAGGGGGTGTTCCAG
GTCACTCTGACTGCTGAGACCTCATGTAGCTACATTTCCTGGCCCCGGAAAAGTCTCCATCTTCTTCTGACCAAAGAGCGATACATCTCCTGCCTCTTCT
CGGCTCTGCTGGGATATGACATCTCGGAGAAGCCCTACACTCTCAATGACAAGCTCTTTGCTAAGTTTGGGCTGCGCTTTGACATCCGCCTTCCCAGCCT
CTACCATGTCCTGGGTCCCACTGCTGCAGATGCTGGACCAGAGTCCGAGAAGGGTGATGAGGAAGTCTGTGAGCCAGCTGTGTCCCCTCCTCAGGCCACA
CCCACCTCTCTCCAGCAAACACCCCCTTGTTCTACCCCTCCAGCTACCACCAACTTTCCTGCACCTCCTACCCGGGCCAGGTTGTCCAGGCCAGACAGTG
GCATACTGGCTTCTAGAATTCCTCTCCAGAGCTACTCTCAAGTTATATCCAGGGGACAGGCCCCTTTGGCTCCAACCCACACGCCTGAACTTCGGGATCC
AGGAGGTGGCGGGAGCGGAGGTGGCGGGAGTATGGTGAGCAAGGGCGAGGAGCTGTTCACCGGGGTGGTGCCCATCCTGGTCGAGCTGGACGGCGACGTA
AACGGCCACAAGTTCAGCGTGTCCGGCGAGGGCGAGGGCGATGCCACCTACGGCAAGCTGACCCTGAAGCTGATCTGCACCACCGGCAAGCTGCCCGTGC
CCTGGCCCACCCTCGTGACCACCCTGGGCTACGGCCTGCAGTGCTTCGCCCGCTACCCCGACCACATGAAGCAGCACGACTTCTTCAAGTCCGCCATGCC
CGAAGGCTACGTCCAGGAGCGCACCATCTTCTTCAAGGACGACGGCAACTACAAGACCCGCGCCGAGGTGAAGTTCGAGGGCGACACCCTGGTGAACCGC
ATCGAGCTGAAGGGCATCGACTTCAAGGAGGACGGCAACATCCTGGGGCACAAGCTGGAGTACAACTACAACAGCCACAACGTCTATCTCACCGCCGGAG
GAAGCGGATACCCATACGATGTTCCAGATTACGCTTGA

Figure 10.23: The cDNA Oligonucleotide Sequence of the POPDC2p.L245P-VN155 Construct

10.9.1 Site Directed Mutagenesis Sanger Sequencing Results

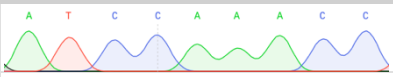
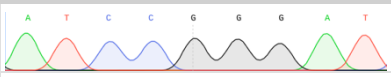
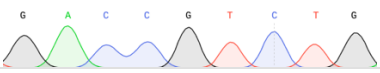
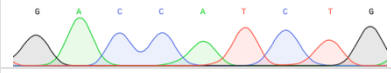
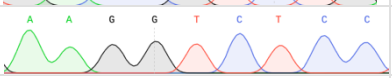
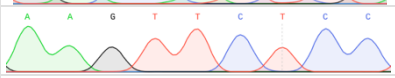
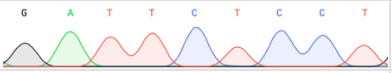
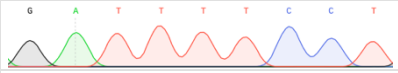
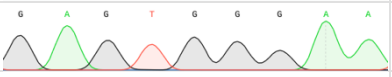
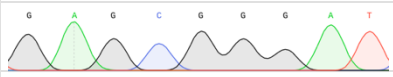
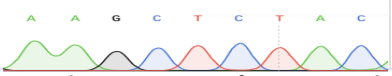
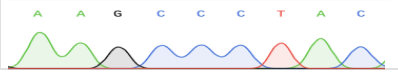
Mutation	Wildtype Sequence	Mutant Sequence
POPDC1-ECFP (c.465_1081del; p.Q153X)		
POPDC1-ECFP (c.515G>A; p.R172H)		
POPDC1-ECFP (c.547G>T; p.V183F)		
POPDC1-ECFP (c.602C>T; p.S201F)		
POPDC2-EYFP (c.561_1093del; p.W188X)		
POPDC2-EYFP (c.734T>C; p.L245P)		

Figure 10.24: The Forward Sanger Sequencing Chromatograms of Site Directed Mutagenesis of POPDC1 and POPDC2 to Introduce Clinically Identified Mutations. Chromatograms showing the results of Sanger sequencing of POPDC constructs used in the HEK293 trafficking experiments. The target codon is shown, flanked by a 5' and 3' codon, in the wildtype template sequence and the mutagenized product.

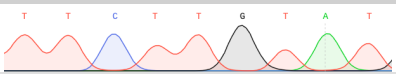
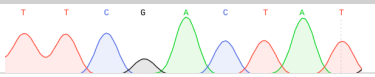
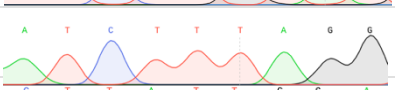
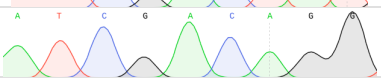
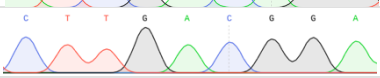
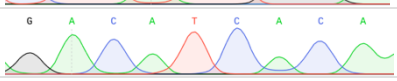
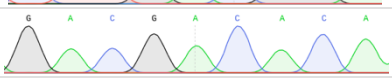
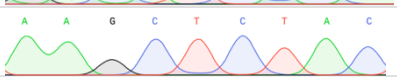
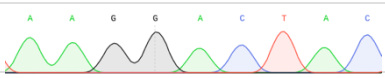
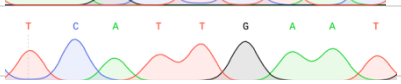
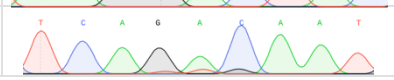
Mutation	Wildtype Sequence	Mutant Sequence
POPDC1-ECFP (c.733TTG>GAC; p.L245D)		
POPDC1-ECFP (c.745TTT>GAC; P.F249D)		
POPDC1-ECFP (c.757ATT>GAC; p.I253D)		
POPDC1-ECFP (c.769ATC>GAC; p.I257D)		
POPDC1-ECFP (c.781CTC>GAC; p.L261D)		
POPDC1-ECFP (c.790TTG>GAC; p.L264D)		

Figure 10.25: The Forward Sanger Sequencing Chromatograms of Site Directed Mutagenesis of αC-helix POPDC1 Mutants. Chromatograms showing the results of Sanger sequencing of POPDC constructs used in the HEK293 trafficking experiments. The target codon is shown, flanked by a 5' and 3' codon, in the wildtype template sequence and the mutagenized product.

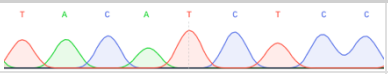
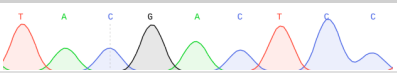
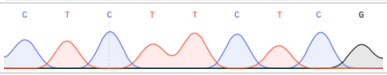
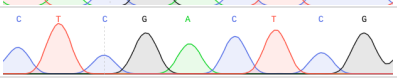
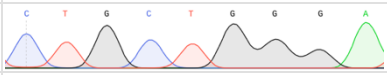
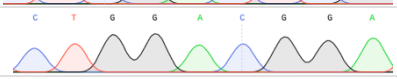
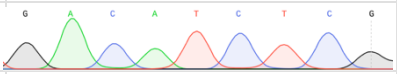
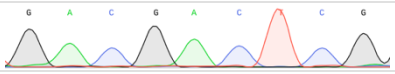
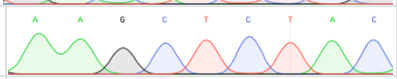
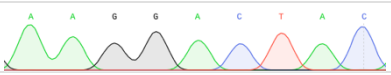
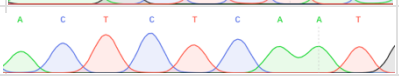
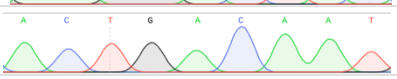
Mutation	Wildtype Sequence	Mutant Sequence
POPDC2-EYFP (c.685ATC>GAC; p.I229D)		
POPDC2-EYFP (c.697TTC>GAC; p.F233D)		
POPDC2-EYFP (c.709CTG>GAC; p.L237D)		
POPDC2-EYFP (c.721ATC>GAC; p.I241D)		
POPDC2-EYFP (c.733CTC>GAC; p.L245D)		
POPDC2-EYFP (c.742CTC>GAC; p.L248D)		

Figure 10.26: The Forward Sanger Sequencing Chromatograms of Site Directed Mutagenesis of αC-helix POPDC2 Mutants. Chromatograms showing the results of Sanger sequencing of POPDC constructs used in the HEK293 trafficking experiments. The target codon is shown, flanked by a 5' and 3' codon, in the wildtype template sequence and the mutagenized product.